Edited by D. L. Buchanan and M. J. Jones

Sulphide deposits in mafic and ultramafic rocks

The Institution of Mining and Metallurgy

Sulphide deposits in mafic and ultramafic rocks

Proceedings of IGCP Projects 161 and 91, Third Nickel Sulphide Field Conference, Perth, Western Australia, 23–25 May, 1982

Edited by D. L. Buchanan and M. J. Jones

The Institution of Mining and Metallurgy

ISBN 0 900488 71 9

UDC 553.27:553.661.2:553.482

Published at the offices of The Institution of Mining and Metallurgy
44 Portland Place
London W1
England

Printed in England by Stephen Austin/Hertford

Introduction

In May, 1982, the University of Western Australia in Perth hosted a three-day international conference on nickel sulphides, followed by a ten-day field excursion to the Western Australian nickel sulphide deposits. The conference was arranged by Professor D. I. Groves, C. M. Lesher and Dr. R. E. T. Hill under the auspices of the International Geological Correlation Programme's Projects 161 ('Sulphide deposits in mafic and ultramafic rocks') and 91 ('Metallogeny of the Precambrian'). This volume contains a selection of the papers that were presented at the Perth conference. Most of the papers are related to the nickel sulphide deposits of Western Australia, but contributions with settings in North America, Finland, Vietnam and Southern Africa have also been included.

Groves, Lesher and Gee's paper headed the list of Australian contributions with a review of the tectonic setting of the komatiitic-hosted nickel sulphide deposits of the Western Australian Shield and established a framework for the other papers. In the following paper Hill provides an outline of the results of experimental work designed to model iron, nickel and copper sulphides typical of the Western Australian occurrences. In this study the importance of copper in modifying the stability field of the monosulphide solid solution is demonstrated. The roles of geophysics and geochemistry in exploration for nickel sulphide deposits in Western Australia are dealt with by Pridmore *et al.* and Smith, respectively. The deep laterite cover and poor outcrop require heavy reliance to be placed on these techniques during exploration and the fundamental constraints of the different methods are critically reviewed by the authors.

Six papers describe specific aspects of the Agnew, Kambalda and Windarra nickel deposits. Little information is available in the literature on the Agnew and Windarra deposits and the contributions by Billington and Schmulian, respectively, provide concise reviews of the geology of these areas. In contrast to Agnew and Windarra, the broad geological characteristics of the Kambalda nickel deposits have been extensively reported. By drawing on this work the four papers on Kambalda are able to focus on more detailed aspects of the ore setting. Hudson and Donaldson report the preliminary results of research undertaken on the platinum-group elements. They describe the laboratory techniques that are used to concentrate platinum-group minerals from ores with very low platinum-group element concentrations and demonstrate the importance of not assuming that these elements are present in solid solution in other minerals. Palladium–iridium ratios are used by Lesher and Keays to support their model for the origin of mobilized sulphides at Kambalda. They provide evidence to suggest that metamorphism and hydrothermal fluids played an important role in the redistribution of the original magmatic sulphides. The origin of the magmatic sulphides at Kambalda is discussed by Lesher, Arndt and Groves, who propose answers to the problem of producing a very high proportion of sulphides in relation to the volume of host unit by suggesting a mechanism of flow-through of magma. In addition, the view is supported that sulphur from sediments played an important role in controlling the distribution of the ores. Paterson *et al.*, in a study of sediment-associated ores at Kambalda, conclude that, for the nickel-rich sulphides at least, the ultramafic-hosted ores were the original source of the mineralization. In their model tectonic factors, together with metamorphic and hydrothermal processes, contributed to the remobilization of the magmatic ores.

Contributions on magmatic sulphides associated with mafic intrusions located in the Appalachian belt of North America by Thompson and Naldrett (Moxie Pluton and Katahdin Gabbro, central Maine) and Wrightson and Misra (Lick Fork prospect, Virginia) provide insights into controls present during the segregation of immiscible sulphides. Sulphur isotope data demonstrated the importance of sulphur assimilation from floor rocks in the formation of the sulphide mineralization in the Maine intrusions. The problems that are associated with studying rocks where the primary magmatic textures have been changed by subsequent metamorphism are described in the second paper with reference to the Lick Fork prospect.

Alapieti and Piirainen describe the Koillismaa layered complex of Finland, where copper, nickel and platinum-group element sulphide mineralization is associated with a zone in which the original magma appears to have been contaminated with salic material from the floor. In a short contribution Le Thac Xinh and Nguyen Van Chu describe some Vietnamese mafic intrusions hosting sulphide mineralization.

The three papers that cover sulphide deposits in mafic and ultramafic rocks in Southern Africa include a contribution by Hammerbeck, in which he proposes a classification based both on geological environment and host rocks. In their paper Buchanan and Rouse describe the results of carbon and sulphur isotope studies used to demonstrate the role of contamination in the genesis of the platinum-group element, nickel and copper sulphide mineralization associated with the Platreef of the Bushveld Complex. The volume concludes with a return to komatiitic-hosted nickel sulphides, Chimimba giving an account of the geological characteristics of the Trojan Nickel mine, Zimbabwe.

If we may end on a personal note, we should like to express appreciation of the efforts of all the contributors and of the assistance of the referees in our very agreeable editorial role.

D. L. Buchanan
M. J. Jones
January, 1984

Contents

Cover photograph shows finely laminated nickeliferous sediment, Juan shoot, Kambalda, Western Australia

Tectonic setting of the sulphide nickel deposits of the Western Australian Shield

D. I. Groves B.Sc.(Hons.), Ph.D., A.M.Aus.I.M.M.
Department of Geology, University of Western Australia, Nedlands, Western Australia
C. M. Lesher B.Sc., A.M.
Formerly Department of Geology, University of Western Australia, Nedlands, Western Australia (now J. Tuzo Wilson Research Laboratories, University of Toronto-Erindale, Mississauga, Ontario, Canada)
R. D. Gee B.Sc.(Hons.), Ph.D., A.M.Aus.I.M.M.
Geological Survey of Western Australia, Perth, Western Australia

Synopsis

The sulphide nickel resources of Australia are concentrated in the Western Australian Shield. This shield is considered to have developed by extensive, but incomplete, Proterozoic reworking of once-continuous Archaean crust. It now constitutes relic Archaean cratons and intervening orogenic mobile belts transected by narrow, curvilinear tectono-thermal mobile belts of younger Proterozoic age. Remnants of the Archaean cratons are exposed in the Yilgarn and Pilbara Blocks. In the former an ancient (to *ca* 3600 m.y.) high-grade gneiss terrain (Western Gneiss Terrain) occurs along the western margin of the block and is interpreted to flank younger (*ca* 3000–2800 m.y.) greenstone belts to the east. Ancient (to *ca* 3500 m.y.) granitoid–greenstone terrains dominate the Pilbara Block.

Proterozoic mobile belts contain only traces of nickel mineralization, except for one locality in the Halls Creek Province. The Archaean high-grade gneiss terrains contain no important mineralization, and the Pilbara granitoid–greenstone terrains contain only scattered examples of less important types of mineralization.

The important deposits (e.g. Kambalda, Windarra, Agnew, Mt Keith) are all of komatiitic affinity and are best developed in the youngest greenstone belts of the eastern part of the Yilgarn Block. In particular, they are concentrated within, and adjacent to, the Norseman–Wiluna Belt, which contrasts in age, lithofacies and structural style with all other greenstone belts in the shield. It is interpreted to have been a rift zone. Within this belt the two main deposit types—the volcanic peridotite-associated and intrusive dunite-associated deposits—are concentrated into spatially separate zones. Precise controls on this heterogeneous distribution cannot be determined unequivocally from available data. One possibility is that the major volcanic peridotite-associated deposits were developed selectively in the actively subsiding axial part of the rift zone during the early extensional phase, whereas intrusive dunite-associated deposits were formed during a subsequent (less active?) stage of volcanic basin development. Distinctive sub-types (facies) of the volcanic peridotite-associated deposits form clusters that are generally within the rift zone. These may represent deposits related to discrete eruption centres, and at least part of their variation is due to relative position within extensive, topographically confined, linear flows.

In the past fifteen years or so the discovery of a number of nickel deposits in the Western Australian Shield has led to the recognition of a new class of deposits associated with both extrusive and intrusive ultramafic rocks of komatiitic affinity and has stimulated research on these ores and their host rocks. Several papers in this volume discuss such ores or their komatiitic hosts. It is therefore appropriate in this introductory paper to present a classification of these deposits and to attempt to place them in regional perspective, as presently understood, within the framework of the Western Australian Shield.

The evolution of the Western Australian Shield is summarized with emphasis on the Archaean terrains that host all sulphide nickel deposits mined to date in Australia. The nature of nickel deposits within the major tectonic provinces of the shield is outlined and, in particular, the distribution of major deposits within the Yilgarn Block is discussed. Although definitive data are not available, alternative tectonic models are considered. Other publications provide more exhaustive reviews of the Western Australian Shield[1] and recent reviews and comprehensive bibliographies of the nickel deposits,[2,3] and discussions of these within the broader framework of Archaean metallogeny.[4,5]

Classification of nickel deposits

The nickel deposits of Western Australia (Fig. 1) have been classified into five types on the basis of their host rocks and geologic setting.[2] Their classification, with the major examples and abbreviated comments on host rocks, ores and setting, is shown in Table 1. These deposits currently contribute about 12% of world mine production of sulphide nickel and contain about 14.5% of total identified resources of nickel in sulphide ores with grades in excess of 0.8% Ni.[6]

Most deposits consist of massive, matrix, disseminated and/or breccia sulphide ores that comprise, dominantly, pyrrhotite, pentlandite, chalcopyrite and magnetite with variable amounts of pyrite and chromite and minor quantities of other Fe–Ni sulphides, sulpharsenides and arsenides. The ores are normally closely related to ultramafic and/or mafic rocks. There is consensus that they are mainly magmatic concentrations derived from immiscible sulphide liquids that separated from parental magmas, but they have been variably modified by deformation, metamorphism and weathering.[2] From an economic viewpoint the deposit types that are associated with ultramafic rocks of komatiitic affinity—the volcanic peridotite-associated and intrusive dunite-associated deposits—are of prime importance, having provided virtually all nickel production from Western Australia to date.[6] It has been suggested that these two types of deposit formed from similar magmas by similar magmatic processes, but had different cooling histories,[7] perhaps reflecting different environments of magma emplacement (this is further discussed below).

Tectonic framework of Western Australian Shield

Overview

The major tectonic elements of the Precambrian crust of Western Australia are Archaean cratons with intervening tectonothermal mobile belts and orogenic mobile belts of Proterozoic age.[1] These are overlain by, or in tectonic contact with, exten-

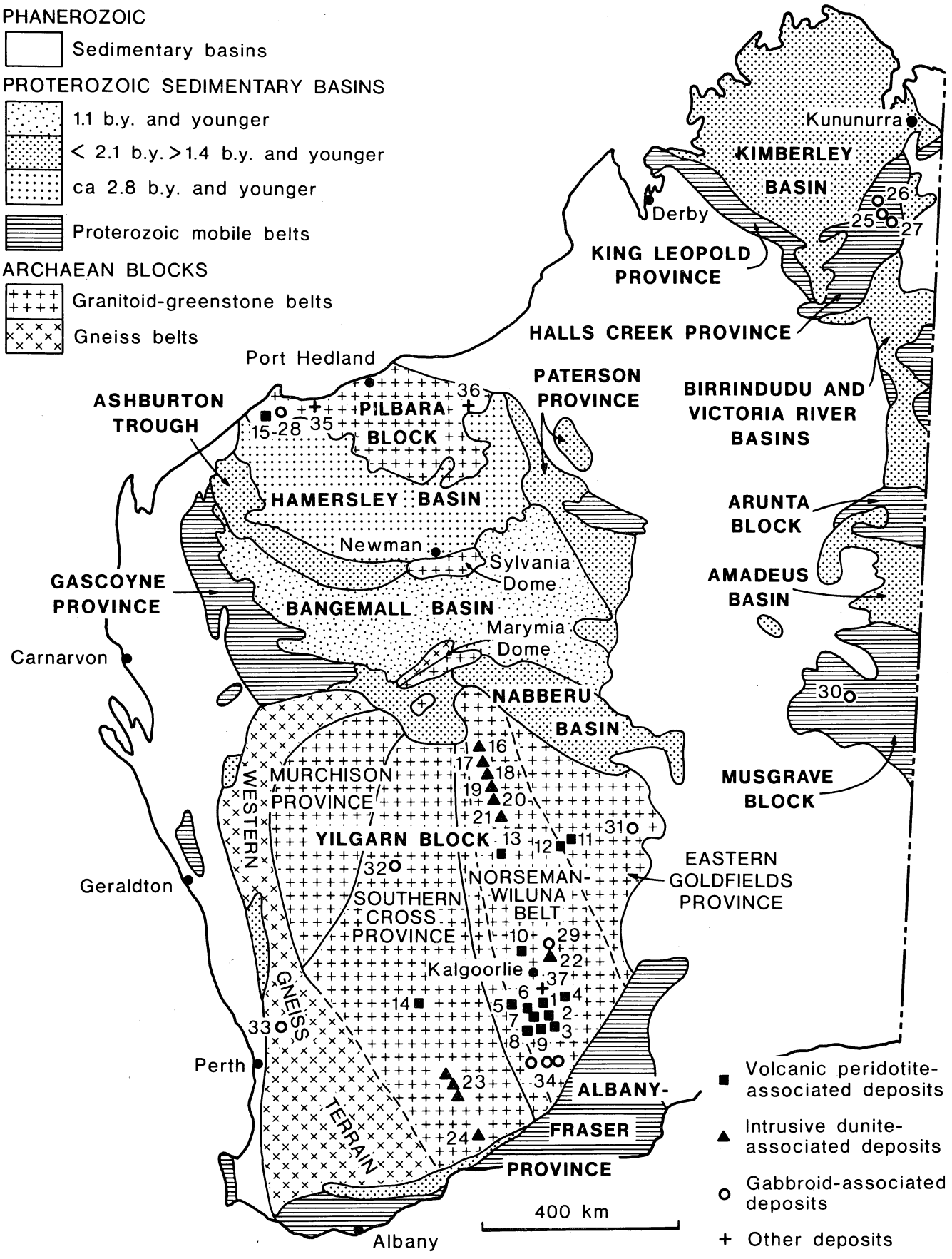

Fig. 1 Major tectonic units of Western Australia (adapted from 1:1 000 000 map of Geological Survey of Western Australia, 1979). Deposits shown are: *Volcanic peridotite-associated deposits:* 1, Kambalda; 2, St Ives; 3, Tramways; 4, Carnilya; 5, Nepean; 6, Spargoville; 7, Mt Edwards; 8, Wannaway; 9, Redross; 10, Scotia; 11, Windarra; 12, South Windarra; 13, Marriott; 14, Trough Well; 15, Ruth Well. *Intrusive dunite-associated deposits:* 16, Honeymoon Well; 17, Mt Keith; 18, Six-Mile; 19, Sir Samuel; 20, Agnew; 21, Weebo Bore; 22, Black Swan; 23, Forrestania (including Mt Hope, Flying Fox, New Morning, Cosmic Boy and Digger Rocks); 24, Ravensthorpe; 25, Sally Malay; 26, Keller Creek; 27, Corkwood; 28, Mt Sholl; 29, Carr Boyd; 30, Giles Complex; 31, Mt Venn; 32, Youangarra; 33, New Norcia; 34, deposits associated with Jimberlana Dyke. *Layered sedimentary-associated deposits:* 35, Sherlock Bay. *Vein-type arsenical deposits:* 36, Bamboo; 37, Mt Martin

Table 1 Classification of nickel sulphide deposits in Western Australia (adapted and abbreviated from Marston *et al.* [2])

Deposit type and setting	Host rocks	Sulphide ores	Examples	Tectonic province
Intrusive dunite-associated deposits Narrow fold belts with major faults that parallel dunite lenses	Subconcordant lenses 0.5–10 km long, 50–1100 m thick of komatiitic dunite* (45–51%MgO) some with less magnesian margins. Country rocks variable, komatiite flow sequences commonly in hanging-wall	Lenticular shoots of massive, matrix and breccia ore near margin, disseminated ore above and in lens cores, Ni/Cu = 19–70+, Ni/Co = 30–70	Agnew, Mount Keith–Betheno, Six Mile, Goliath, Cliffs–Charterhall Honeymoon Well, Sir Samuel, Forrestania Group (Cosmic Boy, Digger Rocks, Flying Fox, New Morning, Mt Hope)	Northeastern margin of Norseman–Wiluna Belt, Eastern Goldfields Province Southeastern part of Southern Cross Province
Volcanic peridotite-associated deposits Base of stratigraphically low, thick komatiite piles, commonly exposed around granitoid-cored domes	Altered flows 25–75 m thick and several hundred metres long of cumulate komatiite (36–45%MgO) at or near base of komatiitic volcanic pile. Mineralized flows differentiated and olivine-enriched. Commonly basalt footwall and flanking sulphidic sediments	Lenticular shoots of massive, matrix and disseminated ores at base of flow and confined to embayments or troughs in footwall. Ni/Cu = 7–19, Ni/Co = 40–60	Kambalda deposits, St Ives–Tramways deposits, Carnilya deposits, Widgiemooltha deposits, Spargoville deposits, Mt Edwards, Nepean, Scotia Windarra–South Windarra Trough Well Ruth Well	Central part of southern Norseman–Wiluna Belt, Eastern Goldfields Province Northeastern Eastern Goldfields Province Southern Cross Province West Pilbara Block
Gabbroid-associated deposits Variable occurrence	Layered or composite igneous complexes of gabbro-norite, pyroxenite and peridotite, generally less than 100 km² in original area	Layer or pipe-like bodies of mainly disseminated ore. Ni/Cu <7, Ni/Co *ca* 25	Carr Boyd Mt Sholl, Radio Hill Sally Malay	Norseman–Wiluna Belt West Pilbara Block Halls Creek Province, Kimberley Block
Layered sedimentary-associated deposits Variable occurrence	Banded sulphidic metasediment up to a few metres thick or tens of metres thick in ultramafic, mafic or mafic–felsic sequences	Thin layers of disseminated sulphides with variable Ni/Cu, Ni/Co	Sherlock Bay Relatively minor shoots at Kambalda (e.g. Jan Shoot) Small shoots at Windarra	West Pilbara Block Norseman–Wiluna Belt Northeastern Eastern Golfields Province
Vein-type arsenical deposits	Associated with faulted or strongly deformed host rocks, country rocks include carbonated ultramafics	Quartz–carbonate–Fe sulphide–Ni arsenide–gold veinlets	Mount Martin (isolated occurrences at Kambalda) Bamboo	Southern, central part of Norseman–Wiluna Belt East Pilbara Block

* Nomenclature of ultramafic rocks of komatiitic affinity from Groves and Lesher.[3]

sive Proterozoic sedimentary basins and are partly covered by Phanerozoic sequences deposited in continental grabens and shallow intracratonic basins (Fig. 1).

It is suspected that continuous, but heterogeneous, Archaean crust that consisted of granitoid–greenstone and high-grade gneiss terrains initially extended over the whole shield. This terrain has, however, been disrupted by Proterozoic mobile belts of various ages that transect the shield, leaving large, equant relic Archaean blocks, some of which are exposed and some buried (Fig. 2). The mobile belts appear to have developed selectively over high-grade gneiss terrains, whereas granitoid–greenstone terrains at the same structural level largely escaped imposed Proterozoic reworking.[1] The older mobile belts (*ca* 2000 to 1600 m.y.) were characterized by crustal rifting, major sedimentation and variable tectono-metamorphic events.[1] Longer-lived mobile belts (*ca* 1600–1000 m.y.) were characterized by intense metamorphism, basement reworking and plutonism without associated trough sedimentation.[1] Cratonic cover sequences appear to have developed more or less continuously throughout the late Archaean and Proterozoic. They formed on the oldest stable areas prior to 2700 m.y., whereas major tectono-magmatic events were occurring in younger Archaean granitoid–greenstone terrains (the Archaean–Proterozoic boundary is used in a tectonic sense in this paper). Mafic dykes, including the Widgiemooltha dyke suite of the Yilgarn Block, intruded the Archaean gneiss belt and granitoid–greenstone terrains soon after cratonization.

All sulphide nickel deposits occur in the Archaean cratons or Proterozoic mobile belts, and these are briefly reviewed below.

Archaean cratons

The most ancient tectonic units in the Western Australian Shield are the Archaean Pilbara and Yilgarn Blocks (Fig. 1), which are dominated by granitoid–greenstone terrains that range from *ca* 3500 to *ca* 2800 m.y. in age. Gravity data indicate that these are the exposed segments of more extensive, but nevertheless finite, cratons, partly covered by Proterozoic sedimentary basins (cf. Figs. 1 and 2). Although the precursors to the granitoid–greenstone terrains of both terrains are interpreted to be large discrete volcanic basins or platforms that developed on pre-existing crust,[1,5] the two cratons differ in (1) crustal thickness and structure, (2) relative heterogeneity, (3) distribution of high-grade gneiss terrains and (4) age, stratigraphic continuity, gross tectonic pattern and metallogeny of their granitoid–greenstone terrains. They appear to have developed independently of each other, though they have been in the same relative position since *ca* 2400 m.y.[8] The existence of an Archaean craton beneath the Kimberley Basin (Fig. 1) has been proposed, but data are equivocal[9] and the age of the basement in this area is not known with certainty.

Although restricted areas of the dominantly granitoid–greenstone terrains of the east Pilbara Block appear transitional to high-grade gneiss terrains,[10] the only major exposed area of high-grade gneisses is the Western Gneiss Terrain along the western margin of the Yilgarn Block.[11] This terrain consists of repeatedly deformed and metamorphosed shelf to trough sediments, intruded by mafic and ultramafic rocks, and intercalated with sheets of orthogneiss. These rocks date back to at least 3600 m.y. and have a protracted tectonic and metamorphic history that is not yet fully understood. There is evidence[11,12] that the Western Gneiss Terrain forms a basement to the significantly younger (<3000 m.y.) greenstones immediately to the east, though direct evidence of the basement elsewhere is lacking. Similarly, formation of the Pilbara greenstones on stable basement is also inferred from indirect evidence,[5,13] but no older sequences (cf. Western Gneiss Terrain) have yet been recognized in the block: the oldest recognized granitoids and derived gneisses appear equivalent in age to the oldest volcanic sequences.[14]

Despite significant differences between greenstone belts (see below), they all show a broadly similar evolution that characterizes such belts on a global scale. They developed through an early volcanic stage dominated by widespread mafic (± ultramafic) volcanism and more restricted felsic volcanism and associated sedimentation. Some intrusive granitoids (granodiorites to tonalites), subsequently largely strongly deformed gneisses, were synchronous with early volcanism. The subsequent history of the greenstone belts was dominated by clastic sedimentation that involved both greenstone and granitoid detritus in more restricted depositional basins. Early sub-horizontal deformation that involved thrusting, recumbent folding and crustal thickening occurred at least locally[10] and was followed by one or more phases of ubiquitous upright folding.[10,11,12] The latter events were accompanied by low- to moderate-pressure metamorphism, widespread crustal melting and granitoid emplacement and diapiric uprise of granitoid and gneiss diapirs.[12] Large strike–slip displacements accompanied the later events in some areas.[10]

Greenstone basins

From the viewpoint of the regional distribution of nickel mineralization, contrasts in age, lithofacies, structural patterns and interpreted basin development between greenstone belts appear of prime importance. At one extreme the stratigraphically relatively coherent volcanic sequences of the *ca* 3500 m.y. Pilbara greenstone belts appear to have been deposited in an extensive shallow-water basin or basins. Shallow-water sediments, including evaporitic sequences, are widespread in the basaltic sequences[15,16] that interfinger with subaerial to shallow-water felsic volcanics and derived epiclastic sediments[15] that contain no significant mafic/ultramafic detritus. Basalts dominate the volcanic sequences and extrusive ultramafics are relatively rare, particularly in the lower sequences.[13] In the Yilgarn Block the probably 3000 m.y. greenstones[17] of the Murchison and Southern Cross Provinces appear to represent similar, but discrete, greenstone depositories[11] that resemble in several respects the Pilbara basin(s). Their volcanic sequences are correlated on a regional basis, basalts dominate the volcanic sequences and extensive komatiites are rare in most areas.[11] The silicified shallow-water clastic and evaporitic sediments that typify the volcanic sequences in the Pilbara are absent, however, and greater water depths are inferred, though detailed sedimentological analysis has not been undertaken. When allowance is made for superimposed deformations the gross tectonic pattern of all these provinces is of more or less equally spaced ovoid granitoid–gneiss domes with intervening arcuate to stellate greenstone belts, probably largely controlled by diapiric uprise of low-density granitoid-dominated crust through tabular greenstone slabs of more or less constant thickness.[5]

The *ca* 2800 m.y. greenstones[19] of the Norseman–Wiluna Belt of the Eastern Goldfields Province contrast in lithofacies and structural pattern with the other greenstone provinces. This belt represents a distinctive segment of the Western Australian Shield and, significantly, is exceptionally well mineralized, containing most of the major nickel deposits. It appears to have been a fault-bounded graben or rift zone up to 200 km wide and at least 800 km long, bounded on both the east and west by more stable basins characterized by BIF. It is typified by an abundance of extrusive komatiites, numerous felsic volcanic centres, paucity of BIF and corresponding abundance of sulphidic shales and cherts, and a complex stratigraphy. Clastic sediments within the volcanic pile contain both felsic and mafic/ultramafic detritus suggestive of fault reactivation of submarine mafic/ultramafic sequences.[18] The gross structural and metamorphic pattern is markedly linear, particularly for

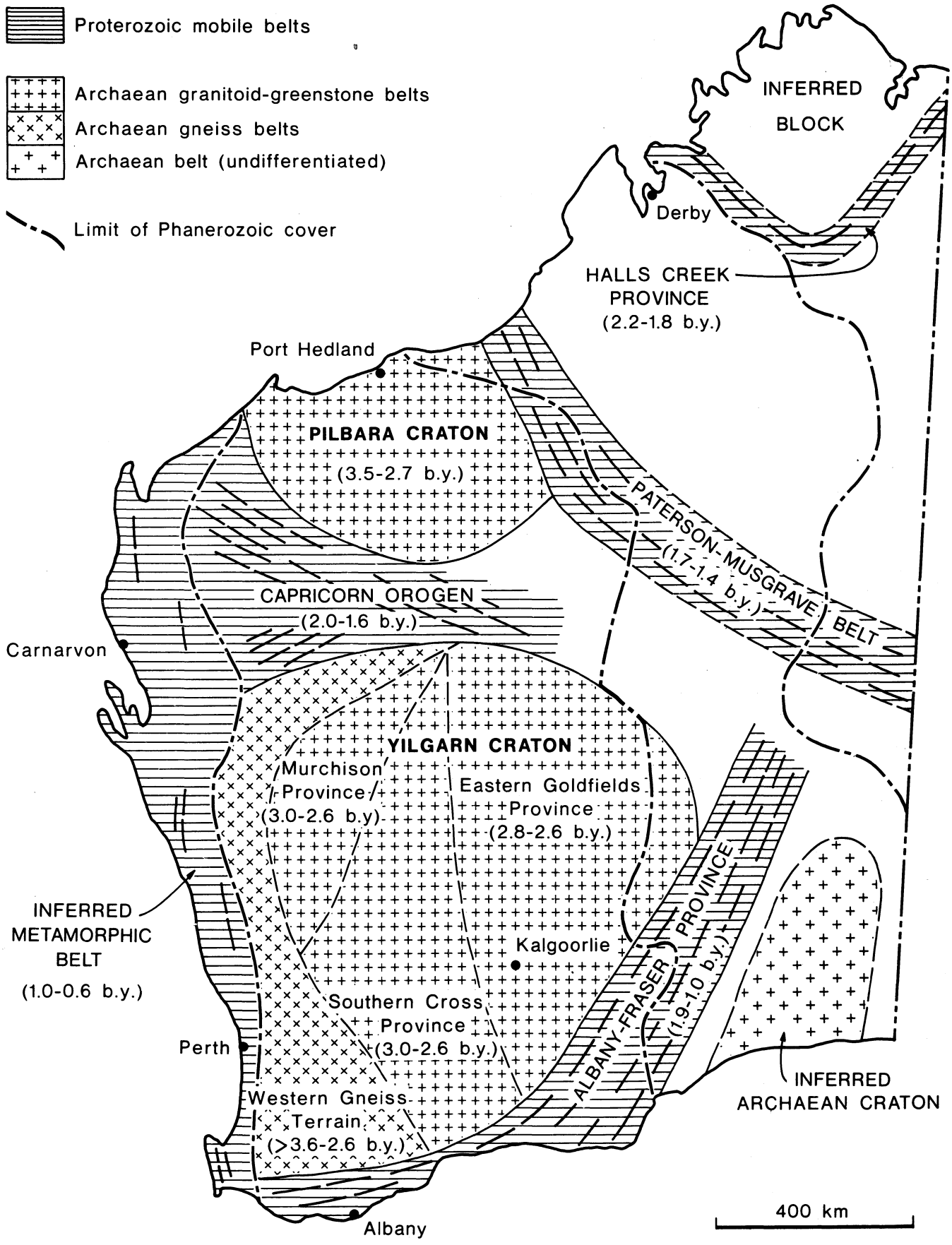

Fig. 2 Reconstruction of major Archaean and Proterozoic tectonic units of Western Australian Shield. After Gee[1]

the higher metamorphic grade domains, and though ovoid granitoid domes are present, these are also commonly elongate parallel to the elongation of other structural elements (Fig. 3). Tectonic reactivation along major faults with the same trend has disrupted the zone into tectonic slices, and elongate zones of small diapirs are probably due to edge effects that relate to initial fault contacts between gneiss basement and greenstones.[12]

The broad contrasts in style of the volcanic basins have been interpreted to reflect variations in their tectonic setting. The *ca*

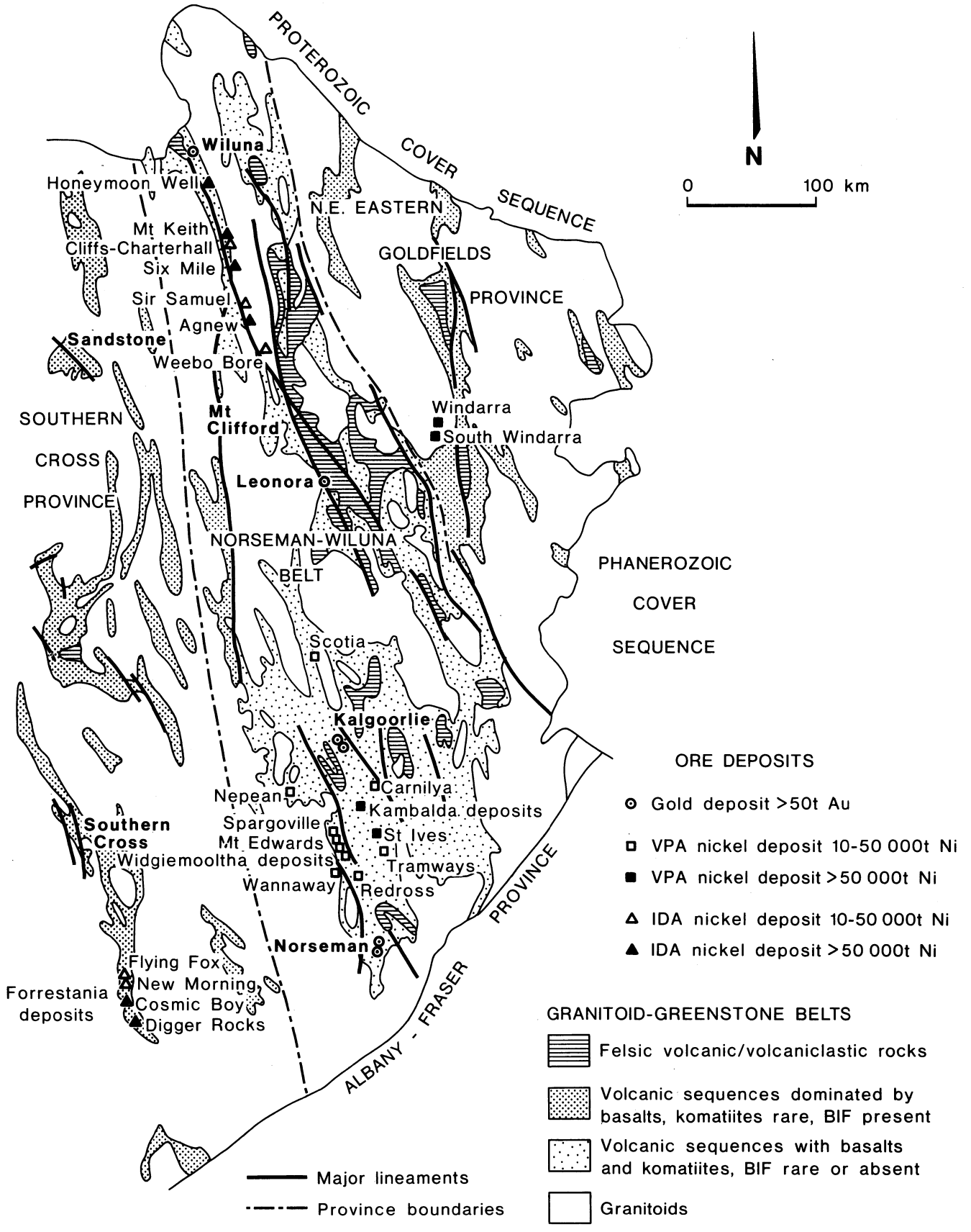

Fig. 3 Solid geology of eastern part of the Yilgarn Block illustrating setting of major nickel deposits in terms of lithofacies, structure and major tectonic subdivisions of granitoid–greenstone terrains. Base map adapted from 1:1 000 000 map of Geological Survey of Western Australia

3500 m.y. east Pilbara basin and the *ca* 3000 m.y. Murchison and Southern Cross basins have been interpreted as volcanically active, but relatively stable non-fault controlled 'platforms' with negative marginal relief in which the major (possibly only) source of sedimentary detritus was local felsic volcanic centres.[18] In contrast, several authors[1-5,11,12,18] have considered the younger (2800 m.y.[19]) Norseman–Wiluna Belt to be a rift zone in which volcanism and sedimentation were controlled by major crustal faults in a more extensional regime.[5]

Proterozoic mobile belts

The major orogenic mobile belts of the shield are the Capricorn

Orogen and the Halls Creek Province (Fig. 2). Part of the Musgrave Block is also exposed near the South Australian border (Fig. 1).

The Capricorn Orogen represents a major zone of trough sedimentation, deformation, metamorphism, basement reworking and granitoid emplacement that developed between the Pilbara and Yilgarn Cratons between 2000 and 1600 m.y.[1] It comprises the Ashburton Trough, Gascoyne Province, the western part of the Nabberu Basin and basement rocks beneath the marine shelf cover sequence of the Bangemall Basin (Fig. 1). Proterozoic reworking of high-grade gneisses of the Western Gneiss Terrain in the southern transitional part of the Gascoyne Province and the occurrence of reactivated Archaean gneiss domes (e.g. Marymia Dome; Fig. 1) within the Nabberu Basin support the interpretation that the orogen developed in an ensialic setting over a high-grade gneiss terrain.[1] Significant mafic magmatism, including dolerite sills and basaltic volcanism, accompanied the development of this orogen on its southern margin. Some of these lavas are more magnesian than normal tholeiites, but no komatiites have been recorded.

The Halls Creek Province also represents a zone of trough sedimentation, tectono-metamorphism and granitoid emplacement that may include inliers of reworked Archaean basement. It had a complex history that extended from at least 2200 to *ca* 1800 m.y. with major deformation/metamorphic events in the interval *ca* 2000 to 1800 m.y.[20] The structure is complex with at least three phases of folding[21] and metamorphic grade varies along the province from greenschist to granulite facies.[22] Mafic and ultramafic bodies of various ages intrude the province, particularly in the northeastern section.

The western part of the Musgrave Block (Fig. 1) is part of the Gawler Province,[9] which is typified by strong deformation, high metamorphic grade and relatively thin Proterozoic platform sequences. The Musgrave Block is mentioned briefly here because it includes the Giles Complex, which contains minor nickel sulphide mineralization. Large lateritic nickel deposits are also developed at Wingelinna over pyroxenitic to dunitic portions of the Complex.[23]

Available exposure combined with gravity data indicates that the Archaean cratons and Proterozoic orogenic mobile belts are enveloped by Proterozoic tectono-thermal mobile belts. These involved extensive basement reworking and voluminous granitoid emplacement without the trough sedimentation that typified the earlier Proterozoic mobile belts.[1] Tectono-thermal mobile belts include the Albany–Fraser Province (1900–1000 m.y.), the Paterson–Musgrave Belt (1700–1400 m.y.) and a belt inferred to have developed along the western margin of the Western Gneiss Terrain between 1000 and 600 m.y.; their development has been compared with arrested rifts in a continental setting.[1] Large mafic to ultramafic intrusive bodies are present in these belts.[24]

Regional distribution of nickel deposits

Yilgarn Block

Although minor nickel occurrences have been recorded from gabbroids and ultramafic intrusives in the Western Gneiss Terrain and gabbroids in the Murchison Province, 96% of the pre-mining resources of contained nickel (>0.8% Ni) in Western Australia occur in the eastern half of the Yilgarn Block, the majority of this resource being in the Norseman–Wiluna Belt.[2,6]

To date, *volcanic peridotite-associated deposits*[2,3,25–29] have provided most nickel production. These deposits are best developed in the southern third of the Norseman–Wiluna Belt between Scotia and Redross (Figs. 1, 3 and 4), where about 87% of the pre-mining nickel resource for this deposit type is concentrated.[2] The geographic concentration is even more pronounced in the Kambalda–St Ives area (about 70% of pre-mining resources), which lies in the axial zone of the rift postulated for the Norseman–Wiluna Belt. Outside of the southern part of the belt the other important deposits occur in the Windarra area (Figs. 1 and 3), where BIF is abundant. The occurrence at Trough Well (Fig. 1(14)) represents the only example of this deposit type in the Southern Cross Province.

On the regional scale deposits are clustered around anticlinal structures that, in places, are demonstrably granitoid-cored domes that form segments of elongate, fault-bounded structural highs to expose stratigraphically low mafic–ultramafic sequences[2] (Fig. 4). The deposits occur in greenschist–amphibolite transition or amphibolite-facies metamorphic domains that, at least in part, reflect the low stratigraphic position of mineralized sequences.[30] Stratigraphic control on the deposits in the southern part of the Norseman–Wiluna Belt has been suggested by several authors[31] and concentration of the larger deposits in the lowermost komatiite formations within the mafic–ultramafic sequences[26,27] suggests a finer-scale stratigraphic control. Available data, summarized by Groves and Lesher,[3] suggest that most of the deposits are localized in elongate depressions parallel to the dominant structural trend of the greenstone belts, which provides further evidence that the present stratigraphic-structural pattern reflects original basin features.

Intrusive dunite-associated deposits[2,3,32,33,34] account for more than 40% of the total sulphide nickel resource for deposits with grades above 0.8% Ni, and 95% of the resource for deposits with lower grades. All major deposits are concentrated along the northeastern margin of the Norseman–Wiluna Belt or in the southern part of the Southern Cross Province in the Forrestania area (Fig.3). Both groups of deposits show a marked linear trend and are confined to narrow, elongate greenstone belts the shape of which is, at least in part, fault-controlled by major strike faults.

The deposits along the northeastern margin of the Norseman–Wiluna Belt show a remarkable degree of tectonic control, extending for more than 100 km along, or adjacent to, a major lineament that sub-parallels the edge of the proposed rift. The deposits along this zone are associated with discontinuous, probably tectonically disrupted ultramafic (mainly serpentinite) lenses that are largely komatiitic dunite with some peripheral peridotite. The largest lens at Agnew is up to 6000 m long, 700 m thick and more than 1000 m deep. Similar host rocks occur at Forrestania, but tectonic control is less evident as nickel deposits occur on both limbs of a tight syncline.[33] An important feature of the deposits is the occurrence of predominantly marginal massive to breccia ores, overlain by disseminated sulphides in amphibolite-facies metamorphic domains, whereas centrally disposed disseminated mineralization typifies greenschist-facies domains. An exception is provided by the Cliffs–Charterhall deposit, where massive sulphides do occur in an upper greenschist facies domain only a few kilometres south of the disseminated Mt Keith deposit. More or less centrally located disseminated sulphides do also occur in some dunites at Forrestania in a high-grade domain.[33]

Although most authors agree that the host komatiitic dunites are intrusive[2,32,33] or at least subvolcanic,[7] it has still not been established unequivocally whether they were intruded as sills or dykes; definitive relationships are obscured by largely tectonic contacts between dunite lenses and country rocks, but available evidence summarized by Marston *et al.*[2] favours the sill hypothesis. Several authors have suggested that the intrusives represent the residue of olivine fractionation in zones that fed komatiite lava piles that now overlie the dunite pods in some areas.[32] Significantly, these komatiites are generally less magnesian than those which host volcanic peridotite-associated deposits (cf. Kambalda and Mt Clifford data[35]). The apparent variation

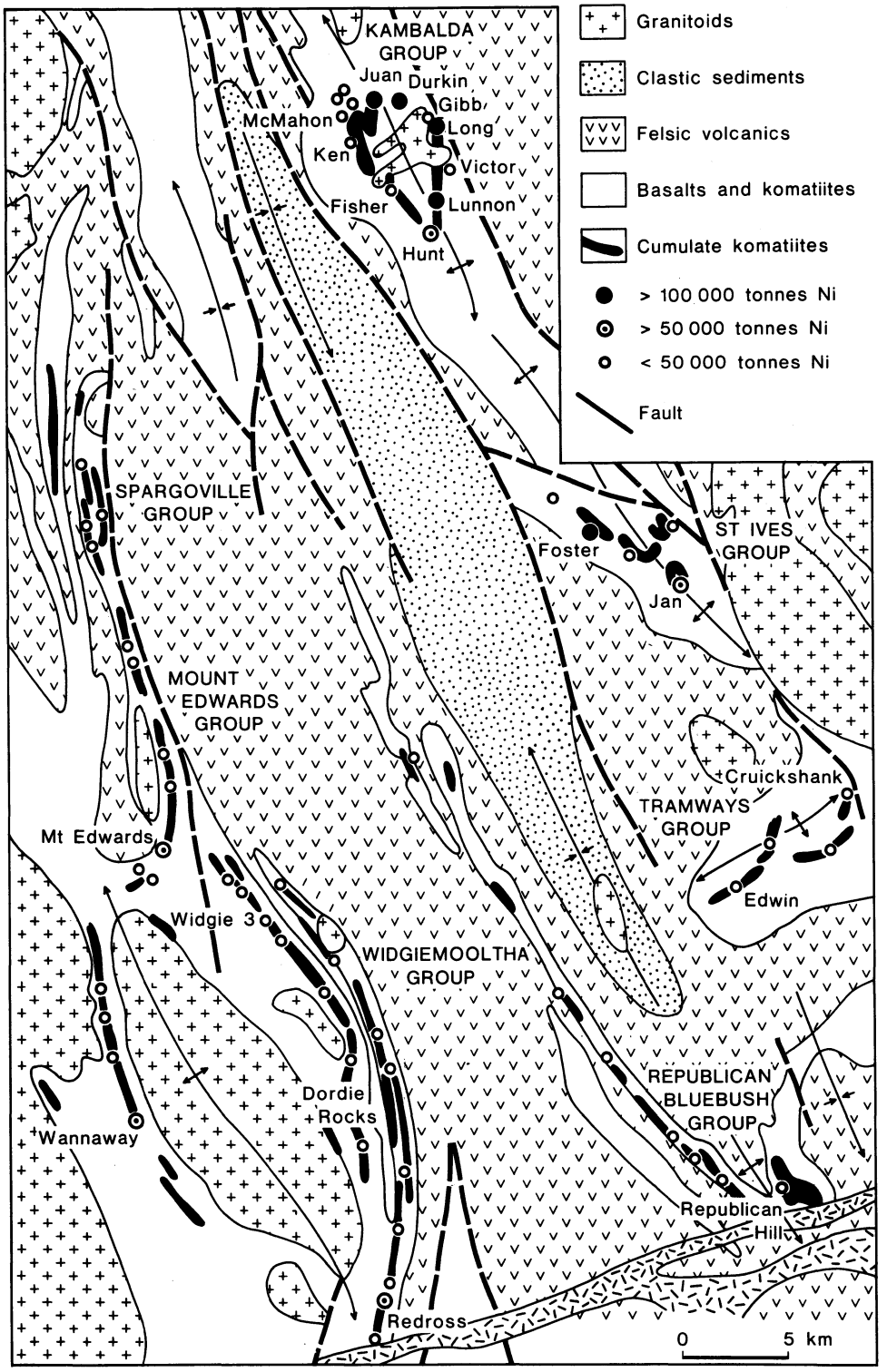

Fig. 4 Regional setting of volcanic peridotite-associated nickel deposits of Kambalda–St Ives–Tramways–Widgiemooltha area showing important structural and lithological associations. Adapted from Marston *et al.*[2]

in mineralization style with metamorphic grade is one feature that is difficult to reconcile with the sill hypothesis. Proponents of the dyke hypothesis suggest, however, that the higher metamorphic grade may coincide with deeper levels of the intrusives,[36] where gravity concentration of magmatic sulphides occurred during emplacement.

There is only one significant *gabbroid-associated deposit* in the Yilgarn Block. This occurs at Carr Boyd (Fig. 1), where intrusive breccia pipes of bronzite–sulphide pegmatoid occur within a troctolite–olivine anorthosite unit of a mafic–ultramafic layered intrusion emplaced into tholeiitic metabasalts.[37] The parent magma is thought to be a high-alumina tholeiite—in contrast to the komatiitic affinities of the major deposits described above. Other deposits of this type (e.g. at New Norcia and Youangarra) are very small. Deposits of this type also occur in the Proterozoic dykes of the Widgiemooltha Suite—for example, in the Jimberlana Dyke[38] and at Cowarna Rocks.[39]

Small *layered sedimentary-associated deposits* occur at Windarra and Kambalda in association with volcanic perido-

tite-associated deposits.[40] Small *vein-type arsenical deposits* occur at Mt Martin near Kalgoorlie and isolated occurrences occur at Kambalda.[2]

Pilbara Block

The Pilbara Block is sparsely mineralized. No systematic groups or metallogenic provinces of nickel are evident. One small volcanic peridotite-associated deposit at Ruth Well (West Pilbara) in a thick komatiite and komatiitic basalt pile[41] may represent the only deposit of this class older than 3000 m.y.[25] Several small nickel occurrences are associated with mafic–ultramafic intrusions south of Ruth Well, the major deposit being that at Mt Sholl.[42] This deposit, unlike that at Carr Boyd, is inferred to have formed from a magma of komatiitic affinity. Ruth Well, Mt Sholl and other small deposits occur adjacent to one of the major strike faults in the Pilbara.[4] The largest of the layered sedimentary-associated deposits occurs at Sherlock Bay to the east of Ruth Well and Mt Sholl. Here disseminated nickel and copper sulphides occur in a metamorphosed carbonate-facies iron formation within mainly felsic volcanics.[43] One small vein-type arsenical deposit occurs at Bamboo in the east Pilbara and traces of nickel sulphides are known from ultramafic intrusions, but no significant komatiite-associated deposits are present.

The paucity of nickel mineralization in the older (*ca* 3500 m.y.) volcanics of the Pilbara Block appears to be characteristic of greenstone belts of this age throughout the world.[4,25] The aluminium-depleted komatiites that characterize these terrains are largely barren of sulphide nickel deposits, whereas younger aluminium-undepleted komatiites are commonly well mineralized. Various models have been presented to explain temporal changes in komatiite magma,[44] but no satisfactory explanation for the increased abundance of sulphides has yet been presented.

Proterozoic orogenic mobile belts

The only significant nickel deposits in this setting occur in the Halls Creek Province in the Kimberley area. Here nickel and copper sulphides are associated with gabbroid intrusions that vary in age relative to the major deformation and metamorphic events in the belt.[21] The major deposit at Sally Malay represents the only significant sulphide nickel resource (grades greater than 1% Ni+Cu) outside the eastern part of the Yilgarn Block.

The deposit lies at the base of a small layered intrusion within the granulite-facies domain of the Province. The intrusion postdates peak metamorphism and the sulphides occur in a norite that represents the chilled border zone of the intrusion, which comprises peridotite, troctolite, olivine norite to olivine gabbro, norite–gabbro and micronorite from the base upwards.[21] There is strong evidence that salic contamination occurred and this may have induced sulphide separation from the silicate magma.[21]

No nickel sulphide mineralization has been recorded from the Capricorn Orogen.

Proterozoic tectono-thermal mobile belts

There are no significant nickel deposits within such belts, but in the Fraser Range disseminated sulphides occur in granoblastic pyroxene granulites that have been interpreted as parts of premetamorphic layered intrusions that comprise peridotite–pyroxenite and anorthositic norite.[45] Post-orogenic norites in the same belt are unmineralized.

Summary

Although nickel deposits, particularly those of gabbroid-associated type, are widely distributed in the various tectonic units of the Western Australian Shield, there is a major concentration of deposits of komatiitic affinity in the eastern part of the Yilgarn Block. Of these, the most important deposits are confined to the Norseman–Wiluna Belt, which represents a distinctive greenstone setting within the Archaean cratons. On the basis of worldwide occurrences of nickel deposits of komatiitic affinity[25] the young age (*ca* 2800 m.y.)[19] of the greenstones of this area is important. There are also, however, other, probably largely tectonic, controls on the deposits and these are discussed below.

Regional controls of nickel mineralization in Yilgarn Block

The nickel deposits of the Yilgarn Block show a markedly heterogeneous distribution that is apparent on three scales. (1) A concentration of all deposit types in the eastern part of the Yilgarn Block, particularly within the Norseman–Wiluna Belt, and an absence of significant deposits in the Western Gneiss Terrain, Murchison Province and northern part of the Southern Cross Province (Fig. 1). (2) A marked geographic separation of volcanic peridotite-associated deposits from intrusive dunite-associated deposits. Most volcanic peridotite-associated deposits cluster between the western margin and axial zone of the Norseman–Wiluna Belt, whereas the intrusive dunite-associated deposits occur in flanking linear zones close to the northeast margin of the Norseman–Wiluna Belt and in the Southern Cross Province (Fig. 3). (3) The volcanic peridotite-associated deposits occur in groups within discrete structural highs, commonly around granitoid-cored domes. The two major concentrations of deposits—Kambalda and Widgiemooltha (Fig. 5)—differ in size and critical geological features, which suggests that they may represent different sub-types within the volcanic peridotite-associated class of deposits. The Scotia and Windarra deposits also show important differences in lithofacies.

Distribution in Yilgarn Block

The absence of nickel deposits from the Western Gneiss Terrain is not surprising in view of the lack of thick mafic–ultramafic sequences and large intrusives with a significant ultramafic component. Such high-grade gneiss terrains in other parts of the world are similarly poorly mineralized, though tectonically reworked, probable gabbroid-associated nickel deposits do occur at Pikwe–Selebi in the Limpopo Mobile Belt.[46]

The paucity of nickel mineralization in the granitoid–greenstone terrains of the Murchison and Southern Cross Provinces almost certainly relates to the paucity of komatiites—more particularly, thick cumulate komatiites and komatiitic dunites—in those provinces relative to the well-mineralized Norseman–Wiluna Belt. This, in turn, appears dependent on the tectonic setting of the Norseman–Wiluna Belt relative to the other Provinces. Clearly, the active rift environment envisaged for the Norseman–Wiluna Belt was more conducive to komatiite eruption than the 'platform-style'[18] relatively more stable basins of greenstone deposition represented by the east Pilbara Block and Murchison and Southern Cross Provinces.

Spatial separation of major deposits of komatiitic affinity

The spatial separation of the volcanic peridotite-associated and intrusive dunite-associated deposits within the Norseman–Wiluna Belt is an intriguing problem. If a rift model is valid, three possible explanations for the spatial separation of the two deposit types should be explored. (1) As a result of variations in the degree of crustal extension along the length of the graben because of variations in the tension in and/or competence of the crust[47] komatiites were erupted in the rift valley and dunites were intruded in the longitudinally equivalent unrifted plateau (Fig. 6*A*). (2) Komatiites were erupted in the deep central part of a symmetrical rift and dunites were intruded in the marginal zones as a result of differences in elevation and the relative

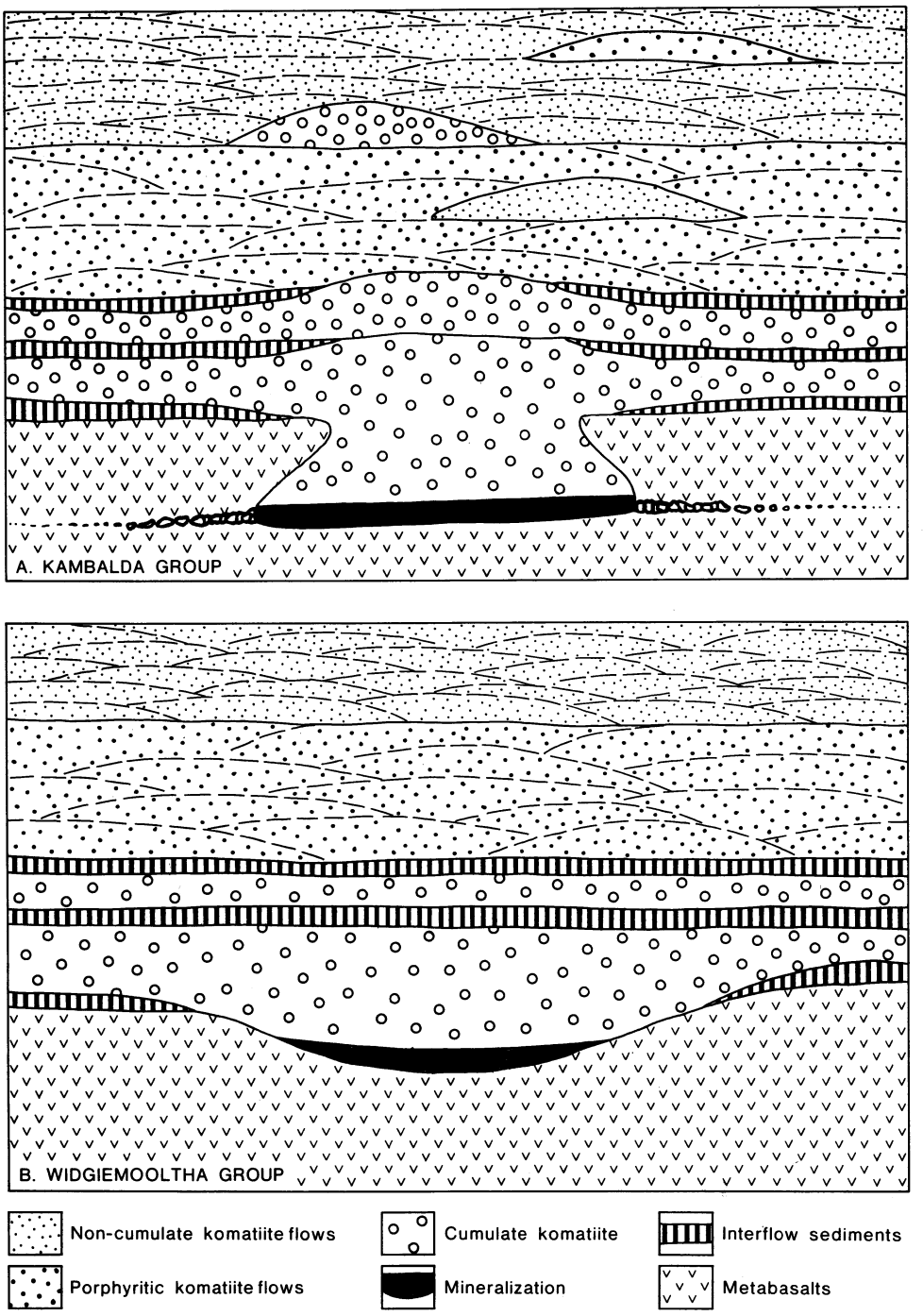

Fig. 5 Schematic cross-sections of deposits of Kambalda Group *(A)* and Widgiemooltha Group *(B)* showing contrasts in nature of 'trough' structures, sediment–nickel ore relationships and nature of overlying ultramafic sequences. Fig. 5*A* adapted from Gresham and Loftus-Hills[26] and Lesher *et al.*[35] Fig. 5*B* adapted from McQueen[27]

thicknesses of crust and lithosphere[48] (Fig. 6*B*). (3) Komatiites were erupted during the initial stretching phase of rifting and dunites were intruded during the subsequent thermal subsidence phase of basin formation[49] (Fig. 6*C*).

Distinction between these models is restricted by uncertainties concerning tectonic setting and age relationships of sequences that enclose nickel deposits in different segments of the greenstone belts, and by uncertainties concerning depositional environments of host rocks. Clearly, further research is required, but it is relevant to review the available data here.

Although there is no compelling evidence that the volcanic deposits do lie in deep-water grabens, available evidence is at least consistent with this hypothesis. For example, the most important deposits of the Kambalda area are considered to be in the axial zone of the rift (Fig. 3). Here interflow sediments within the mafic–ultramafic sequences are typically sulphidic shales or cherts with a distal clastic component[50] and vesicles are absent from basaltic lavas. The Widgiemooltha area, on the western margin of the proposed rift zone, is less well characterized, but is dominated by similar sulphidic shales and cherts, although amygdaloidal metabasalts do occur in parts of the sequence. The marked elongation of Kambalda nickel ores within synvolcanic depressions parallel to the predicted orientation of faults that delineate the rift zone and the absence of evidence for local feeders also suggest topographic gradients along fault troughs.[51] The available evidence is thus consistent with the hypothesis that the volcanic peridotite-associated deposits formed within an active rift zone, the most important mineralization being concentrated in the axial zone.

The depositional environment of the sequences in which the

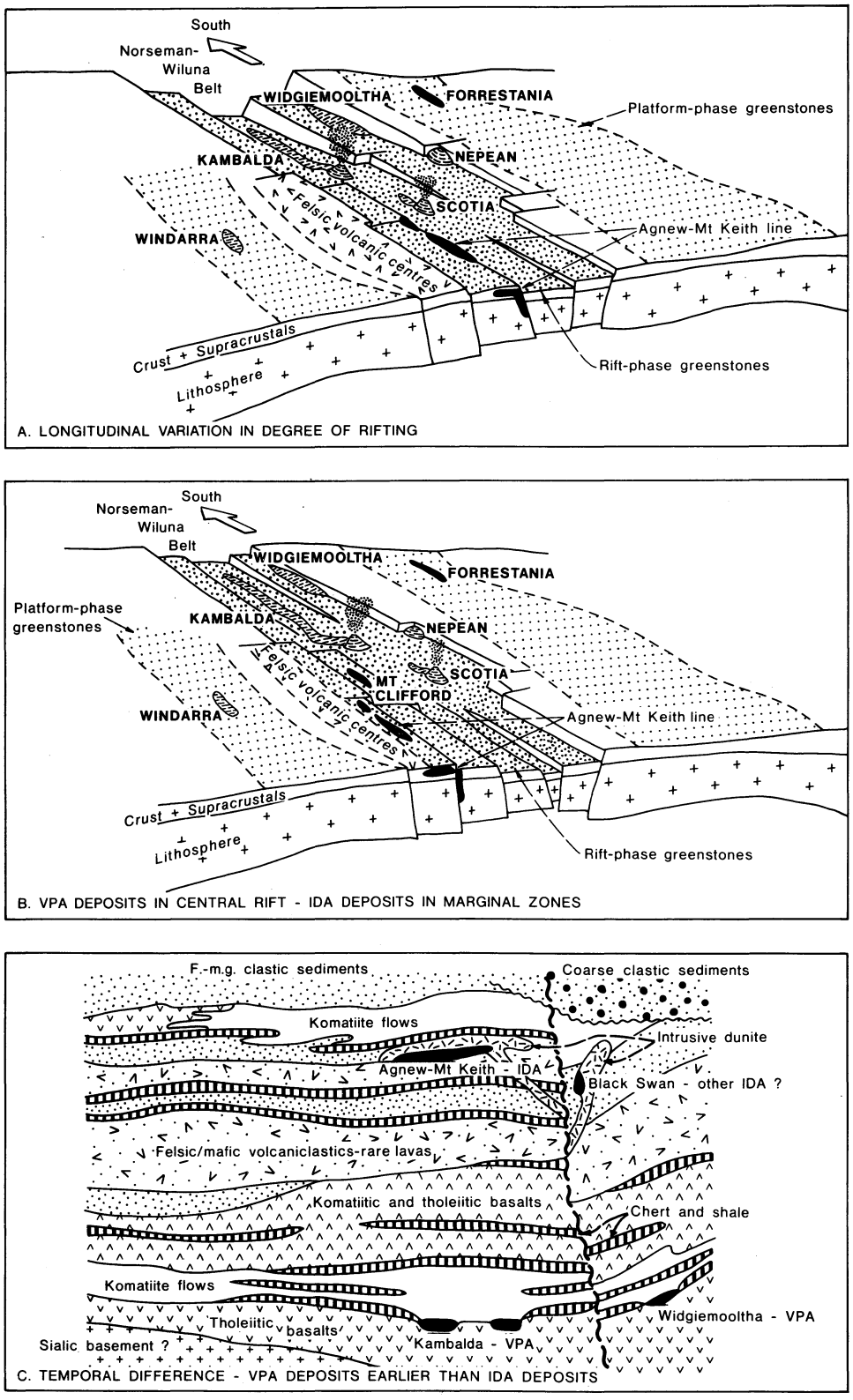

Fig. 6 Possible models for spatial separation of volcanic peridotite-associated and intrusive dunite-associated deposits in Norseman–Wiluna Belt: *A*, variation in degree of extension along length of the rift with komatiites erupted in rift valley and dunites intruded in longitudinally equivalent unrifted plateau; *B*, komatiites erupted in deep central part of rift and dunites intruded in marginal zones; *C*, komatiites erupted during initial stretching phase of rifting and dunites intruded during subsequent subsidence phase. Cross-section showing temporal relationship adapted from Marston and Groves[4]

intrusive dunite-associated deposits occur is even less well constrained and this, together with the possibility that some tectonic transport has been involved in final emplacement of host dunite bodies, severely limits tectonic reconstructions. Currently, the data required to differentiate between models 1 and 2 are not available;[5] detailed sedimentological and volcanological data in conjunction with structural studies are essential in the future. Similarly, the possibility of allochthonous emplacement and difficulties in establishing stratigraphic correlations between the southern and northeastern segments of the Eastern Goldfields Province make unequivocal interpretation of temporal relationships between important dunite-associated

deposits and major volcanic peridotite-associated deposits difficult (this is compounded for the Forrestania deposits, where inter-province correlation is required). Despite these problems, there is general consensus that the mineralized dunites, at least in the Norseman–Wiluna Belt, were emplaced at a higher stratigraphic level than the hosts to volcanic peridotite-associated deposits,[2] which indicates the potential importance of temporal variations in degree of extension across the evolving basin (model 3, Fig. 6*C*).

It must be concluded that available data are insufficient to establish precise tectonic controls on the distribution of komatiite-associated nickel deposits. This is one of the major outstanding problems in understanding the genesis of these deposits.

Facies distribution of volcanic peridotite-associated deposits

Although the volcanic peridotite-associated deposits exhibit many important common features,[3,4] there are also important differences between groups of deposits.[51]

The Kambalda (excluding St Ives–Tramways) deposits occur in a discrete, thick pile of komatiite lava flows. Individual deposits are typified by distinctive re-entrant ore-confining 'troughs', a complex komatiite stratigraphy and lack of interflow sediments above the trough zones[26] (Fig. 5), and hosting cumulate komatiite units that show strong evidence for longitudinal emplacement.[3,51] The deposits are large relative to other deposits of this type, several oreshoots containing in excess of 100 000 t of nickel metal.[26] The Widgiemooltha deposits occur within a regional mafic–ultramafic association that contains three major ultramafic sequences, the upper two being mineralized;[27] each discrete ultramafic sequence is thinner than that at Kambalda and no deposit reaches 100 000 t of nickel metal.[2] Although deposits are confined by shallow, open embayments in the footwall rocks, these are not as prominent as those at Kambalda, sediments may occur above the ore zone and the complexities in the komatiite sequence above the ore zone evident at Kambalda[26] do not appear to be present[27] (Fig. 5). There is no field evidence for feeders to the ultramafic sequence in the Kambalda or Widgiemooltha groups. At Scotia, however, there are dunite dykes and ultramafic pyroclastic breccias in the ore environment and marked lateral variation of the basal ultramafic unit away from this zone.[28]

On the basis of these observations the Scotia deposit is considered as a proximal deposit adjacent to a volcanic vent. The Kambalda deposits are considered to occur in longitudinally emplaced flows at some distance from a vent. It is possible that eruption was controlled by cross fractures that intersected the rift zone and that longitudinal flow down regional pitchlines parallel to the rift resulted in the present distribution of host komatiites and ores at Kambalda (Fig. 4). The Widgiemooltha deposits may be related to fissure eruption adjacent to the bounding faults of the rift zone in situations where regional gradients and longitudinal flow were less important. Alternatively, they may represent the most distal sections of a Scotia–Kambalda facies trend.

Conclusions

All important sulphide nickel deposits of Australia occur in the Western Australian Shield. This shield appears to have developed as a result of extensive but incomplete Proterozoic reworking of once-continuous Archaean crust that was cratonized by *ca* 2600 m.y. Earliest Proterozoic intrusive activity is recorded by dyke swarms that intruded this stable crust; some nickel–copper sulphide mineralization was associated with these intrusions (e.g. Jimberlana Dyke).

Orogenic mobile belts (*ca* 2200–1600 m.y.), involving thick trough sedimentation, developed at least in part over high-grade gneissic crust. In the Halls Creek Province of this type mafic intrusions of various ages contain traces of nickel–copper sulphides and one significant gabbroid-associated deposit occurs at Sally Malay in a post-metamorphism layered gabbro–norite body. Relics of Archaean crust and the older mobile belts are transected by younger, long-lived (*ca* 1900–1000 m.y.) tectono-thermal mobile belts, including the Albany–Fraser Province, which contains traces of nickel sulphides in mafic intrusions that have been metamorphosed to granulite facies.

Remnants of the Archaean crust are preserved in the Pilbara and Yilgarn Blocks, which are the exposed portions of more extensive but discrete cratons now partly covered by Proterozoic cover sequences. An old (*ca* 3600 m.y.) high-grade gneiss terrain, the Western Gneiss Terrain, occurs along the western margin of the Yilgarn Block and is interpreted to flank younger (<3000 m.y.) granitoid–greenstone terrains to the east. It, like most other Archaean high-grade gneiss terrains, contains no significant nickel deposits. The older Pilbara granitoid–greenstone terrain (to 3500 m.y.) is also poorly mineralized. Only a number of small, low-grade deposits of variable type occur in the western part of the block.

Within the younger greenstone belts of the Yilgarn Block the majority of important nickel deposits of komatiitic affinity occur within, or adjacent to, the Norseman–Wiluna Belt in the eastern part of the block. This belt contrasts in age, lithofacies and structural style with other greenstone belts in the Yilgarn Block and with those of the Pilbara Block. It is interpreted as a young (*ca* 2800 m.y.) major fault-controlled rift zone superimposed on other, more stable basins ('platforms') of greenstone deposition. Within, and adjacent to, this belt there is a marked spatial separation of volcanic peridotite-hosted deposits and intrusive dunite-hosted deposits—the two major classes of Archaean nickel deposits. The reasons for this separation are not yet clear, but it is suggested that most vigorous komatiite eruption in the axial zone of the rift basin during the early extensional volcanic stage of basin evolution was conducive to the formation of the most important volcanic peridotite-associated deposits in this zone. The intrusive dunite-associated deposits are considered to have been emplaced under conditions of lower extension, perhaps later in the volcanic stage of basin evolution, but their precise tectonic setting is presently unclear. Within the rift zone, clustering of sub-types of volcanic peridotite-associated deposits was related to different eruption conditions and/or to relative position with respect to eruptive centres within rift-parallel, longitudinally differentiated komatiite flows.

Acknowledgement

This paper represents a summary of research work on the evolution of the Western Australian Shield and the genesis of nickel deposits carried out mainly by geologists from the Geological Survey of Western Australia, University of Western Australia, C.S.I.R.O. Division of Mineralogy and exploration companies, particularly Western Mining Corporation, Ltd. We are indebted to our colleagues in these institutions for this information. In particular, we have drawn heavily on the work of R. J. Marston, D. R. Hudson and J. R. Ross, and we are indebted to R. J. Marston for his constructive criticism of an early draft of this paper. One author (R.D.G.) publishes with the permission of the Director of the Geological Survey of Western Australia.

References

1. Gee R. D. Structure and tectonic style of the Western Australian Shield. *Tectonophys.*, **58**, 1979, 327–69.
2. Marston R. J. *et al.* Nickel sulfide deposits in Western Australia: a review. *Econ. Geol.*, **76**, 1981, 1330–63.
3. Groves D. I. and Lesher C. M. eds. Regional geology and nickel deposits of the Norseman–Wiluna Belt, Western Australia. *Univ. West Aust. geol. Dep. Extension Service Publ.* no. 7, 1982, 234 p.

4. Marston R. J. and Groves D. I. The metallogenesis of Archaean base-metal deposits in Western Australia. In *Archaean geology* Glover J. E. and Groves D. I. eds. *Spec. Publ. geol. Soc. Aust.* no. 7, 1981, 409–20.
5. Groves D. I. The Archaean and earliest Proterozoic evolution and metallogeny of Australia. *Revta bras. Geoscências*, **12**, 1982, 135–48.
6. Ross J. R. and Travis G. A. The nickel sulfide deposits of Western Australia in global perspective. *Econ. Geol.*, **76**, 1981, 1291–329.
7. Donaldson M. J. and Lesher C. M. Intrusive dunite and extrusive peridotite: analogous products of komatiitic magmas resulting from different cooling rates. In *Nickel sulphide field conference III, Abstr. volume*, 1982, 31–2.
8. Embleton B. J. J. The palaeomagnetism of 2400 m.y. old rocks from the Australian Pilbara craton and its relation to Archaean–Proterozoic tectonics. *Precamb. Res.*, **6**, 1978, 275–91.
9. Rutland R. W. R. Structural framework of the Australian Precambrian. In *Precambrian of the southern hemisphere* Hunter D. R. ed. (Amsterdam: Elsevier, 1981), 1–32. *(Developments in Precambrian geology* 2)
10. Bickle M. J. *et al.* Horizontal tectonic interaction of an Archean gneiss belt and greenstones, Pilbara Block, Western Australia. *Geology*, **8**, 1980, 525–9.
11. Gee R. D. *et al.* Crustal development in the Archaean Yilgarn Block, Western Australia. In *Archaean geology* Glover J. E. and Groves D. I. eds. *Spec. Publ. geol. Soc. Aust.* no. 7, 1981, 43–56.
12. Archibald N. J. *et al.* Evolution of Archaean crust in the Eastern Goldfields Province of the Yilgarn Block, Western Australia. In *Archaean geology* Glover J. E. and Groves D. I. eds. *Spec. Publ. geol. Soc. Aust.* no. 7, 1981, 491–504.
13. Hickman A. H. Crustal evolution of the Pilbara Block, Western Australia. In *Archaean geology* Glover J. E. and Groves D. I. eds. *Spec. Publ. geol. Soc. Aust.* no.7, 1981, 57–69.
14. Bickle M. J. *et al.* Archaean tectonics in the 3500 Ma Pilbara Block: structural and metamorphic tests of the batholith concept. *Proc. geol. Ass. Can. — Mineralog. Ass. Can. joint ann. Meeting, Winnipeg, 1982*, in press.
15. Barley M. E. *et al.* Sedimentary evidence for an Archaean shallow-water volcanic-sedimentary facies, eastern Pilbara Block, Western Australia. *Earth Planet. Sci. Lett.*, **43**, 1979, 74–84.
16. Lowe D. R. Comparative sedimentology of the principal volcanic sequences of Archean greenstone belts in South Africa, Western Australia and Canada: implications for crustal evolution. *Precamb. Res.*, **17**, 1982, 1–29.
17. Fletcher I. R. *et al.* Variability of E^{i}_{Nd} in greenstone belts in the Archaean of Western Australia. In *Fifth Int. Conf. Geochron. Cosmochron. Isotope Geol., Nikko, Japan Abstr.*, 1982.
18. Groves D. I. and Batt W. D. Spatial and temporal variations of Archaean metallogenic associations in terms of evolution of granitoid–greenstone terrains. In *Archaean geochemistry* (Berlin, etc.: Springer-Verlag), in press.
19. McCulloch M. T. and Compston W. Sm–Nd age of Kambalda and Kanowna greenstones and heterogeneity in the Archaean mantle. *Nature, Lond.*, **294**, 1981, 322–7.
20. Plumb K. A. The tectonic evolution of Australia. *Earth-Sci. Rev.*, **14**, 1979, 205–49.
21. Thornett J. R. The Sally Malay deposit: gabbroid-associated nickel–copper sulfide mineralization in the Halls Creek mobile zone, Western Australia. *Econ. Geol.*, **76**, 1981, 1565–80.
22. Dow D. B. and Gemuts I. Geology of the Kimberley region, Western Australia: the East Kimberley. *Bull. geol. Surv. West. Aust.* 120, 1969, 135 p.
23. Sprigg R. C. and Rochow K. Nickeliferous ochres in the Hinckley (W.A.) and Tominson (S.A.) Ranges ('Daisy Bates'—Wingelinna field). In *Economic geology of Australia and Papua New Guinea 1. Metals* Knight C. L. ed. (Parkville, Victoria: Australasian Institute of Mining and Metallurgy , 1975), 1008–9. (*Monograph series* no. 5)
24. Daniels J. L. The geology of the Blackstone Region, Western Australia. *Bull. geol. Surv. West. Aust.* 123, 1974, 257 p.
25. Groves D. I. and Hudson D. R. The nature and origin of Archaean strata-bound volcanic-associated nickel–iron–copper sulphide deposits. In *Handbook of strata-bound and stratiform ore deposits, volume 9* Wolf K. H. ed. (Amsterdam: Elsevier, 1981), 305–410.
26. Gresham J. J. and Loftus-Hills G. D. The geology of the Kambalda nickel field, Western Australia. *Econ. Geol.*, **76**, 1981, 1373–416.
27. McQueen K. G. Volcanic-associated nickel deposits from around the Widgiemooltha dome, Western Australia. *Econ. Geol.*, **76**, 1981, 1417–43.
28. Page M. L. and Schmulian M. L. The proximal volcanic environment of the Scotia nickel deposit. *Econ. Geol.*, **76**, 1981, 1469–79.
29. Stolz G. W. and Nesbitt R. W. The komatiite nickel sulfide association at Scotia: a petrochemical investigation of the ore environment. *Econ. Geol.*, **76**, 1981, 1480–502.
30. Binns R. A. Gunthorpe R. J. and Groves D. I. Metamorphic patterns and development of greenstone belts in the eastern Yilgarn Block, Western Australia. In *The early history of the earth* Windley B. F. ed. (New York: Wiley, 1976), 303–13.
31. Gemuts I. and Theron A. The Archaean between Coolgardie and Norseman—stratigraphy and mineralization. Reference 23, 66–74.
32. Naldrett A. J. and Turner A. R. The geology and petrogenesis of a greenstone belt and related nickel sulfide mineralization at Yakabindie, Western Australia. *Precamb. Res.*, **5**, 1977, 43–103.
33. Porter D. J. and McKay K. G. The nickel sulfide mineralization and metamorphic setting of the Forrestania area, Western Australia. *Econ. Geol.*, **76**, 1981, 1524–49.
34. Donaldson M. J. and Bromley G. J. The Honeymoon Well nickel sulfide deposits, Western Australia. *Econ. Geol.*, **76**, 1981, 1550–64.
35. Lesher C. M. *et al.* Geochemistry of komatiites from Kambalda, Western Australia: I. Chalcophile element depletion—a consequence of sulfide liquid separation from komatiitic magmas. *Econ. Geol.*, **76**, 1981, 1714–28.
36. Binns R. A. Groves D. I. and Gunthorpe R. J. Nickel sulphides in Archaean ultramafic rocks of Western Australia. In *Correlation of the Precambrian* Sidorenko A. V. ed. (Moscow: Nauka, 1977), 349–80; *Referat. Zh., Geol.*, no. 1 1978, V222.
37. Purvis A. C. Nesbitt R. W. and Hallberg J. A. The geology of part of the Carr Boyd Rocks Complex and its associated nickel mineralization, Western Australia. *Econ. Geol.*, **67**, 1972, 1093–113.
38. Travis G. A. Nickel–copper sulphide mineralization in the Jimberlana intrusion. Reference 23, 75–8.
39. Purvis A. C. and Moeskops P. G. Nickel–copper sulfide-rich Proterozoic dykes at Cowarna Rocks, Western Australia. *Econ. Geol.*, **76**, 1981, 1597–605.
40. Paterson H. L. *et al.* Nickeliferous sediments and sediment-associated nickel ores at Kambalda, Western Australia. In *Sulphide deposits in mafic and ultramafic rocks* Buchanan D. L. and Jones M. J. eds (London: IMM, 1984), 81–94.
41. Nisbet E. G. and Chinner G. A. Controls of the eruption of mafic and ultramafic lavas, Ruth Well Ni–Cu prospect, West Pilbara. *Econ. Geol.*, **76**, 1981, 1729–35.
42. Mathison C. I. and Marshall A. E. Ni–Cu sulfides and their host mafic-ultramafic rocks in the Mt. Sholl intrusion, Pilbara region, Western Australia. *Econ. Geol.*, **76**, 1981, 1581–96.
43. Keays R. R. *et al.* Iridium and palladium as discriminants of volcanic-exhalative, hydrothermal, and magmatic nickel sulfide mineralization. *Econ. Geol.*, **77**, 1982, 1535–47.
44. Weaver B. L. and Tarney J. Thermal aspects of komatiite generation and greenstone belt models. *Nature, Lond.*, **279**, 1979, 689–92.
45. Tyrwhitt D. S. and Orridge G. R. Regional geology and mineralization of the Fraser Range orogenic belt, Western Australia. Reference 23, 405–8.
46. Wakefield J. The structural and metamorphic evolution of the Pikwe Ni–Cu sulfide deposit, Selebi–Pikwe, Eastern Botswana. *Econ. Geol.*, **71**, 1976, 988–1055.
47. Illies J. H. Graben formation—the Maltese islands—a case history. *Tectonophys.*, **73**, 1981, 151–68.
48. Le Pichon X. and Francheteau J. A plate-tectonic analysis of the Red Sea–Gulf of Aden area. *Tectonophys.*, **46**, 1978, 369–406.
49. McKenzie D. Some remarks on the development of sedimentary basins. *Earth planet. Sci. Lett.*, **40**, 1978, 25–32.
50. Bavinton O. A. The nature of sulfidic metasediments at Kambalda and their broad relationships with associated ultramafic rocks and nickel ores. *Econ. Geol.*, **76**, 1981, 1606–28.
51. Lesher C. M. and Groves D. I. Localization of volcanic peridotite-associated Ni-sulphide mineralization at Kambalda, Western Australia, and implications for ore emplacement. In *Nickel sulphide field conference III, Abstract vol.* 1982, 31–2.

Experimental study of phase relations at 600°C in a portion of the Fe–Ni–Cu–S system and its application to natural sulphide assemblages

R. E. T. Hill B.(app)Sc., Ph.D.
CSIRO, Division of Mineralogy, Wembley, Western Australia

Synopsis

A laboratory study was undertaken to determine the condensed equilibrium phase relations at 600°C in that portion of the quaternary Fe–Ni–Cu–S system which lies in the neighbourhood of the monosulphide solid solution (MSS). The study sought to determine to what extent copper affects the temperatures of stability and compositions of iron–nickel sulphides in bulk compositions similar to those of massive Fe–Ni–Cu ores. Experimental data, including stable phase assemblages and phase compositions, are presented.

In the quaternary system at 600°C MSS forms stable phase assemblages with pentlandite, chalcopyrite solid solution, pyrite and vaesite. Over the range of bulk compositions displayed by natural ores copper as well as metal/sulphur ratio have a significant effect on the thermal stability of pyrite and pentlandite. Errors therefore accompany the widespread practice of ignoring copper or chalcopyrite when the mineralogical and compositional changes that have accompanied the initial cooling of primary magmatic sulphides or their subsequent homogenization during isochemical metamorphism are being deciphered. These errors are most significant for ores the bulk compositions of which lie toward the sulphur-deficient side of the cupriferous MSS. Temperatures as much as 300°C above the copper-absent value are possible for the interpreted upper stability limits of pentlandite in these ores.

The experimental data show that up to 2.0 at% copper can occur in pentlandite stable at 600°C in a bulk composition equivalent to natural magmatic ores. This is equivalent to nearly 10 vol% chalcopyrite. Pentlandite contains more copper than coexisting MSS and the copper content of both phases increases with increasing iron.

The major sulphide minerals that are associated with mineralized ultramafic–mafic rocks are pyrrhotite, pentlandite, chalcopyrite and pyrite. These minerals fall within the chemical confines of the Fe–Ni–Cu–S system and knowledge of its phase relations is, thus, significant to an understanding of the processes that affect the mineralogy of iron–nickel–copper sulphide ores.

It has become customary to apply phase relations to unravel the mineralogical changes that accompanied the cooling of magmatic sulphide accumulations or their subsolidus reconstitution during subsequent metamorphic or metasomatic events. The relative thermal stability of major phases in the system is, therefore, used to explain the present distribution of sulphide phases in massive ores.

Chemical and mineralogical heterogeneity is a property that is common to most of these massive ores. This heterogeneity varies from regular fine- or medium-scale mineralogical layering to irregularly disposed zones of relative enrichment of one or more sulphide phases and is usually reflected in significant variations in the concentration of copper relative to nickel.

Enrichment of either copper or nickel by liquid fractionation at high temperatures is possible in the Fe–Ni–Cu–S system[1] and fractionation of natural sulphide–oxide liquids has, thus, been proposed by many authors as a process that is responsible for the gross heterogeneity that is exhibited by some massive ores.

Apart from these high-temperature effects there are, however, three main postulated and feasible subsolidus processes that may have effected the heterogeneity in nickel ores: stress-induced heterogeneous nucleation of phases exsolving from homogeneous sulphide solid solution, ductility-contrast mobilization induced by postmagmatic tectonism and chemical alteration to equilibrate with an imposed postmagmatic environment. An interpretation of the heterogeneity based on these processes relies on a knowledge of subsolidus phase relations in the Fe–Ni–Cu–S system. Of particular significance is the relative thermal stabilities or order of crystallization of chalcopyrite, pentlandite and pyrite from bulk compositions similar to those of massive ores.

It has been usual practice in the past for research workers to neglect copper in any consideration of the order of crystallization of iron–nickel sulphides from massive ore accumulations and their relative stabilities at subsequent metamorphic temperatures. This practice was based on the belief that copper does not affect the temperatures of stability of pentlandite and pyrite in bulk compositions similar to those of the ores. This paper presents the results of a research programme on subsolidus phase relations in part of the Fe–Ni–Cu–S system at 600°C and shows that there is a considerable difference between the interpreted relative thermal stabilities of pentlandite, pyrite and chalcopyrite in natural ore bulk compositions depending on whether the stabilities are determined with or without consideration of copper. Data have been obtained on the solubility of copper in pentlandite and in monosulphide solid solution at its sulphur-rich and sulphur-poor limits in equilibrium with a copper-rich phase.

These analytical data aid interpretation of the distribution of nickel and copper in an iron–nickel–copper massive sulphide assemblage caused by cooling or metamorphic homogenization.

Previous work

Numerous experimental studies have been conducted and published by previous authors on aspects of phase relations in the quaternary Fe–Ni–Cu–S system and, more specifically, in the ternary boundary systems Fe–Ni–S, Cu–Ni–S and Cu–Fe–S and the basic binary systems. A complete review of these is not necessary in this paper. The results of many of these studies have been summarized adequately by Kullerud, Yund and Moh,[2] Craig and Kullerud[1] and Barker.[3] These previous phase relation studies have covered a wide range of temperatures and provide a basis for our understanding of the cooling of magmatic Fe–Ni–Cu sulphide–oxide liquids and the formation of nickel ores.

Such recent developments as the use of the electron microprobe to determine the compositions of equilibrated phases and methods to monitor and measure sulphur fugacities over equili-

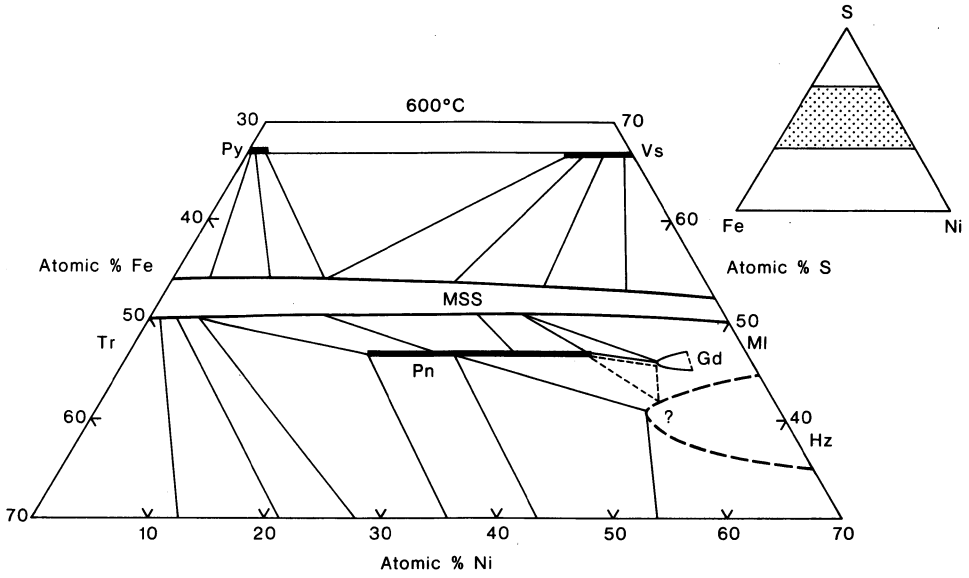

Fig. 1 Phase relations in central portion of Fe–Ni–S system at 600°C. Data adapted from Barker.[3] All phases and phase assemblages coexist with vapour

brated assemblages have resulted in modifications and additions to earlier work. This paper falls within this category.

Equilibrium phase relations in the central portion of the condensed ternary Fe–Ni–S system at 600°C are shown in Fig. 1, which has been adapted from a review[3] of previously published data. At this temperature the system is dominated by monosulphide solid solution (MSS) and pentlandite. The pentlandite exhibits a wide range in composition and coexists with MSS and iron-rich godlevskite at its nickel-rich limit and MSS and taenite (Fe–Ni alloy) at its iron-rich extremity.[4] The MSS is stable with pentlandite over the entire range of the pentlandite composition. Pyrite and/or vaesite form stable assemblages with the MSS along its sulphur-rich boundary.[5]

In this system the pentlandite is stabilized by a reaction between MSS and heazlewoodite at 610°C.[6] Below 610°C the pentlandite expands in composition from a singular point situated at an iron/nickel ratio of 1:1 towards more iron- and nickel-rich compositions. By 600°C the final breakdown of tie-lines between MSS and heazlewoodite at both the nickel- and iron-rich extremities of the pentlandite has occurred. This permits the coexistence of pentlandite, godlevskite and MSS, and of pentlandite, taenite and MSS in these regions of the diagram (Fig. 1).

The field of MSS narrows as temperature falls. The sulphur-rich and sulphur-poor limits of this MSS solvus were studied by Naldrett and Kullerud[7] and the isotherms that limit the solvus over part of the MSS compositional range are portrayed in Fig. 2. The stable coexistence of pyrite and pentlandite in this system depends on the temperature of breakdown of MSS, which does not take place above 300°C or even possibly 260°C.[9] This low-temperature places upper limits on the temperatures of formation of coexisting pyrite and pentlandite in natural ores.

If copper is removed as either the element or as chalcopyrite from the primary bulk compositions of most massive nickel–copper ores, the compositions plot within the confines of the MSS field in the Fe–Ni–S system, even at temperatures as low as 500°C or lower.[8,10] The orders of appearance of pentlandite and pyrite in these adjusted ore compositions are governed by the relative shrinkage rates of the sulphur-poor and sulphur-rich limits of the MSS with temperature and the positions of the bulk compositions between these limits of the MSS stability field. For example, the bulk composition, chalcopyrite-free, of the Lunnon Shoot ore at Kambalda, Western Australia,[11] plots to the sulphur-rich side of the MSS at 500°C (Fig. 2). The phase relationships show that at about 475°C pyrite would begin to exsolve from this ore and pentlandite would not be a stable phase until pyrite–pentlandite tie-lines are established at a temperature below the breakdown of MSS.

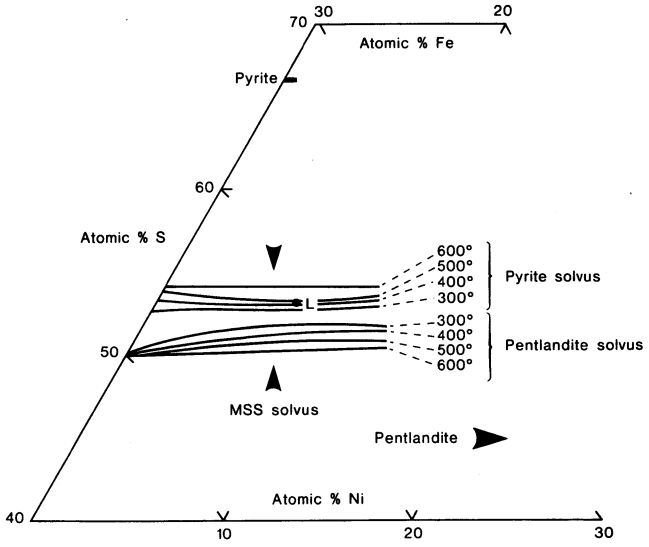

Fig. 2 Central portion of Fe–Ni–S system showing isotherms limiting solvus of iron-rich portion of MSS. After Naldrett and Kullerud.[8] L = bulk composition of Lunnon Shoot massive sulphide, chalcopyrite-free after Ewers and Hudson[11]

This procedure of adjusting the bulk compositions of nickel–copper massive ores to determine temperatures of stability of pentlandite and pyrite is widespread and presupposes that copper has negligible effect on these temperatures. Details of phase relations in the Fe–Ni–Cu–S quaternary system are insufficiently known at present to allow this supposition. Experiments with a composition equivalent to that of the massive footwall ore of the Strathcona deposit, Sudbury, were conducted by Craig,[10] the results indicating that copper had little effect on the thermal stability of pentlandite in the ore. These data do not assess the combined effects of copper and metal/sulphur ratio on pyrite and pentlandite stability, which could be applicable to a variety of ore compositions.

Phase relations in the Fe–Ni–Cu–S system were presented by Craig and Kullerud.[1,12] A schematic chemographic presentation of the condensed subsolidus equilibrium phase assemblages at 650°C and 550°C were portrayed in Figs. 4 and 5 by

Craig and Kullerud[1] and are not reproduced here: certain features of this work are, however, relevant to this discussion.

The authors related that copper does not increase the upper temperature limit of stability of pentlandite in the quaternary system above that derived for the Fe–Ni–S system (610°C).[1] They indicated that pentlandite and bornite solid solution (BnSS) become stable together at 590°C after the final breakdown of cupriferous MSS–heazlewoodite tie-lines and that the stable coexistence of pentlandite and chalcopyrite solid solution (cpy SS or ISS)* does not occur in this system above 575°C, at which temperature tie-lines between copper-bearing MSS and BnSS begin to break down. Thus, these data place an upper limit of 575°C on an equilibrium assemblage that contains pentlandite and chalcopyrite or their co-exsolution from MSS in natural ore compositions.

The experimental studies of Craig and Kullerud[1,12] have shown that several phases within the quaternary system exhibit quaternary extensions of their solid solution into the Fe–Ni–Cu–S system. The MSS is particularly significant in this regard, as the compositions of most of the pyrrhotite-rich nickel–copper ores plot within or in close proximity to the quaternary limits of the monosulphide solution. It is therefore important to determine details of the quaternary equilibrium phase relations in the neighbourhood of the monosulphide solution. This paper reports the results of a study that was undertaken to quantify these features.

Present study

The data reported here were from eight experiments that were conducted at 600°C: they constitute two series that span the MSS from iron- to nickel-rich compositions at around 49 and 53 at% sulphur. All charges contained near 5 at% copper, which is sufficient to saturate all stable Fe–Ni sulphides with copper and render a stable copper-rich phase also. The bulk compositions of the reacted charges are listed in Table 1. The sulphur contents of the charges were specifically chosen such that one series was to lie between MSS and pentlandite and the other just beyond the sulphur-rich limit of the MSS. Furthermore, bulk compositions of the charges were chosen so that the compositions of the MSS phases at equilibrium would closely match in Fe/Fe+Ni ratio for four pairs of runs on opposite sides of the MSS. Previously published data[4] were used as a guide. This procedure was used to facilitate graphical presentation of the results.

Table 1 Bulk compositions of experimental charges equilibrated at 600°C (analysis by AAS)

Run number	Bulk compositions, at% Fe	Ni	Cu	S
136*A*	9.72	36.59	5.18	48.51
136*B*	17.70	28.79	4.75	48.76
136*C*	26.65	19.85	4.68	48.82
136*D*	35.35	10.93	4.53	49.19
181*A*	8.94	33.00	5.00	53.04
181*B*	17.91	24.21	5.02	52.87
181*C*	26.81	15.19	5.00	53.00
181*D*	35.74	6.26	5.00	53.00

Experimental method

The experimental charges were prepared and equilibrated at elevated temperature by use of a technique that was developed by A. Fletcher at the CSIRO laboratories. The usual silica-tube technique[14] has been modified by Fletcher to include an initial reaction stage, and subsequent homogenization, pelletization and sintering for a short period at elevated temperatures under hydrostatic pressure prior to extended annealing in evacuated silica tubes. This preparation prior to annealing produces a pre-reacted dense sulphide pellet the high percentage of grain surface contact of which facilitates subsequent equilibration, produces good equilibrium textures and yields a grain size that is sufficiently large for accurate electron-probe phase analysis.

In this study the dense pellets (approximately 250 mg in weight) were annealed in horizontal tube furnaces for a period of at least 800 h at 600°C. This time was deemed sufficient to establish as near to true equilibrium as possible among the phases (cf. Vaughan and Craig[15]). On rapid cooling a portion of each of the equilibrated pellets was analysed by AAS to determine accurate bulk compositions. The remainder of each pellet was used for optical and X-ray phase identification and phase analysis by the electron-probe. The electron-probe analyses were obtained by the wavelength-dispersive method and were corrected by use of the MAGIC program of Colby.[16] Metal standards were used for the iron, nickel and copper determinations and a pyrite standard was used for sulphur. The electron-probe is a M.A.C. 400S model and was operated at 19.3 kV with sample current around 10 nA.

Starting materials for the experimental charges were pre-reduced ultrapure Roc Ric iron and nickel powder, Koch Light copper metal powder and BDH sulphur purified by the method of Bacon and Fanelli.[17]

Results

The experimental data, including the phase assemblage and phase compositions in each experimental product, are listed in Table 2. The spatial disposition of the stable assemblages in the Fe–Ni–Cu–S system is portrayed schematically in Fig. 3. For ease of presentation the phase assemblages are depicted in pairs with similar MSS phase compositions that range across the system from the iron- to the nickel-rich portion of the diagram.

Pentlandite and MSS coexist in all the 600°C run products in the series of experiments with bulk compositions beyond the sulphur-deficient boundary of copper-free MSS, i.e. runs 136*A*–*D* (Fig. 3). In the most nickeliferous of these runs (136*A*) the stable condensed phase assemblage is pentlandite–MSS–godlevskite–BnSS, which forms a univariant four-phase volume in the condensed quaternary system at 600°C (Fig. 3*A*). The stability of this assemblage at 600°C was reported also by Gill.[18] The stable coexistence of pentlandite and BnSS results from the final breakdown of cupriferous MSS–heazlewoodite tie-lines in the quaternary system below 610°C. The presence of the assemblage at 600°C, as indicated in this study and that of Gill,[18] places the temperature of this cupriferous MSS–heazlewoodite breakdown at least 10°C above that reported by Craig and Kullerud.[1] The pentlandite in these run products is believed to be present as a stable phase at 600°C and not to have resulted from the rapid destabilization during cooling of high temperature non-quenchable MSS–heazlewoodite that was found to occur under certain conditions in earlier studies of the Fe–Ni–S system by Kullerud[6] and others. This conclusion is based on the chemical homogeneity of the phase and on textural evidence, including grain size, shape and phase distribution.

Pentlandite coexists with chalcopyrite solid solution (ISS) in the remaining three run products of the low-sulphur series. The stable assemblage in run 136*B* is pentlandite–MSS–ISS–BnSS. This wedge-shaped volume formed by the four coexisting sulphides (Fig. 3*B*) separates on its nickel-rich side the three-dimensional field formed by the three-phase planes of stable divariant pentlandite–MSS–BnSS assemblages from divariant pentlandite–MSS–ISS assemblages such as those identi-

*ISS, 'intermediate solid solution', refers to the extensive field of 'chalcopyrite solid solution' in the central portion of the Cu–Fe–S system.[13]

Table 2 Equilibrium condensed phase assemblages and electron-probe analyses of phases in experimental run products quenched from 600°C

Run number	Phases present	Phase compositions, at% Fe	Ni	Cu	S
136*A*	Pn	—	—	—	—
	MSS	8.90	39.90	0.25	51.00
	Gd	4.70	47.30	0.60	47.50
	BnSS	8.60	2.00	49.00	40.00
136*B*	Pn	19.50	32.00	1.00	47.50
	MSS	17.10	30.50	0.40	52.00
	ISS	22.00	2.00	27.60	48.50
	BnSS	10.85	1.20	45.50	42.50
136*C*	Pn	24.10	27.10	1.00	47.80
	MSS	27.80	19.70	0.40	52.10
	ISS	31.64	2.63	15.53	50.20
136*D*	Pn	28.50	22.70	2.00	46.90
	MSS	40.30	7.60	0.80	51.40
	ISS	34.20	1.40	15.00	49.40
181*A*	MSS	8.00	39.70	0.25	52.10
	ISS	24.10	2.70	23.40	49.90
	Vs	1.00	32.20	0.45	66.40
181*B*	MSS	16.80	30.00	0.22	53.00
	ISS	27.50	1.40	21.00	50.00
	Vs	2.20	30.90	0.48	66.50
181*C*	MSS	27.40	19.10	0.15	53.30
	ISS	29.60	1.40	18.60	50.40
	Vs	6.00	27.00	0.48	66.50
181*D*	MSS	37.80	8.70	0.27	53.20
	ISS	31.50	0.93	17.65	50.00
	Py	32.20	1.15	0.10	66.60

Pn = pentlandite, MSS = Fe–Ni monosulphide solid solution, BnSS = bornite solid solution, ISS = chalcopyrite solid solution, Py = pyrite, Vs = vaesite, Gd = godlevskite. ($\bar{s}$ for major metals up to ±0.5%, sulphur up to ± 1%; trace metals <2 at% ±5–20% of amounts present.)

fied in the more iron-rich experimental charges (136*C* and 136*D*, Fig. 3*C* and *D*). This stable coexistence of pentlandite and a chalcopyrite solid solution over a wide compositional range in the quaternary system at 600°C is not in agreement with the previously summarized work of Craig and Kullerud.[1] Gill[18] also noted the stability of the four-phase assemblage pentlandite–MSS–ISS–BnSS at 600°C, thus implying the existence of the field formed by the planes of coexistence of divariant pentlandite, MSS and ISS. His data, however, appear not to be consistent with the extensive field of coexistence of these phases as shown in this study. Gill's data imply a more restricted compositional range for pentlandite—ISS coexistence and indicate an extensive field of coexistence of BnSS with pentlandite and MSS for compositions in the quaternary more iron-rich than the univariant four-phase volume.

The condensed phase assemblages stable at 600°C in the four runs of the sulphur-rich series are all divariant and consist of MSS, ISS and either vaesite or pyrite (Fig. 3). Pyrite is the stable disulphide in the most iron-rich of the bulk compositions (181*D*).

Tie-lines that join the analysed coexisting cupriferous Fe–Ni sulphides from this study are shown in Fig. 4. The relevant phase and bulk compositions that are depicted are projections on to the Fe–Ni–S boundary of the quaternary system from the coexisting ISS in all cases, except those for run 136*A*, for which the projection point is the coexisting BnSS.

The phase relations and the gross compositions of the coexisting cupriferous quaternary iron–nickel sulphides, not unexpectedly, bear close resemblance to those of the copper-free Fe–Ni–S system at 600°C (Fig. 1). The grain size of the pentlandite in assemblage 136*A* was of insufficient size to produce reliable chemical analyses. The composition plotted for this pentlandite in Fig. 4 is taken from Gill,[18] whose 600°C data on run G-70 include compositions of godlevskite and MSS comparable with those of this study. The slope of pentlandite–MSS tie-lines in the nickel-rich region is dissimilar to those of Misra and Fleet,[4] which are plotted in Fig. 1.

It is particularly significant that at 600°C the sulphur-rich and sulphur-poor limits of MSS in equilibrium with disulphide and pentlandite, respectively, outline a much narrower field of MSS if a copper-rich phase is present relative to the copper-free system (Fig. 4).

The extent of copper solubility in the iron–nickel phases and the compositions of the copper-rich phases in the respective assemblages are portrayed in Fig. 5. In this figure the compositions of coexisting cupriferous iron–nickel sulphides are projected at constant copper content, and constant metal/sulphur ratios on to the Fe–S join of the Cu–Fe–S system. The compositions thus projected are joined to their coexisting cupriferous phase or phases to outline the stable phase assemblages. The compositions of the BnSS and ISS phases are represented as projections at constant metal/sulphur ratio from the Ni–S join of the quaternary. The fields of stability of BnSS and ISS at 600°C are taken from Cabri.[13] For ease in presentation and interpretation each diagram depicts the assemblages stable in those pairs of runs the MSS compositions of which have similar Fe/Fe+Ni ratios. The sulphur-rich and sulphur-poor compositional limits of copper-free MSS on the projections are from sections through the Fe–Ni–S ternary at Fe/Fe+Ni atomic ratios of 0.18, 0.36, 0.60 and 0.83 (Fig. 5 *A*—*D*), which pass through as near as possible the similar MSS compositions from the pairs of experimental runs portrayed on each diagram.

In all of the analysed assemblages BnSS and ISS compositions lie close to the sulphur-rich limit of their solid solution fields in the Cu–Fe–S system at 600°C (Fig. 5). With reference to the ISS phases, in particular, this helps to place restricted metal/sulphur compositional limits on the field of stability of the two-condensed phase assemblage MSS–ISS, which is of particular significance to natural ores. As would be expected, the BnSS and ISS phases are richest in copper in the nickel-rich assemblages and the ISS phase approaches the compositions of cubanite in the iron-rich assemblages (Fig. 5*C* and *D*). The nickel content of the BnSS and ISS in all run products is less than 3 at% (Table 2). There are insufficient data, however, to determine any relationship between gross composition and the nickel content.

The copper content of MSS in equilibrium with pentlandite is less than that in the coexisting pentlandite in all of the relevant experimental runs (Fig. 5). Copper in MSS increases with increasing iron content from 0.24 to 0.76 at% over the compositional range of the experiments, whereas the coexisting pentlandite shows a concomitant increase from 1.00 at% in run 136*B* to 2.00 at% in run 136*D* (Table 2). A similar relationship was observed by Gill,[18] whose data show a maximum of 2.4 wt% at 600°C copper in pentlandite for the assemblage pentlandite–MSS–BnSS. The copper content of sulphur-rich MSS in equilibrium with ISS and disulphide is very low and shows little variation over the range of MSS compositions covered by the experiments (Table 2). Vaesite is much richer in copper than pyrite in these assemblages (0.48 at% as opposed to 0.10 at%).

In this study no experimental charges were equilibrated within the two-condensed phase region MSS–ISS. Nevertheless, the disposition of points of known MSS compositions on each of the projections in Fig. 5 enables accurate sections of

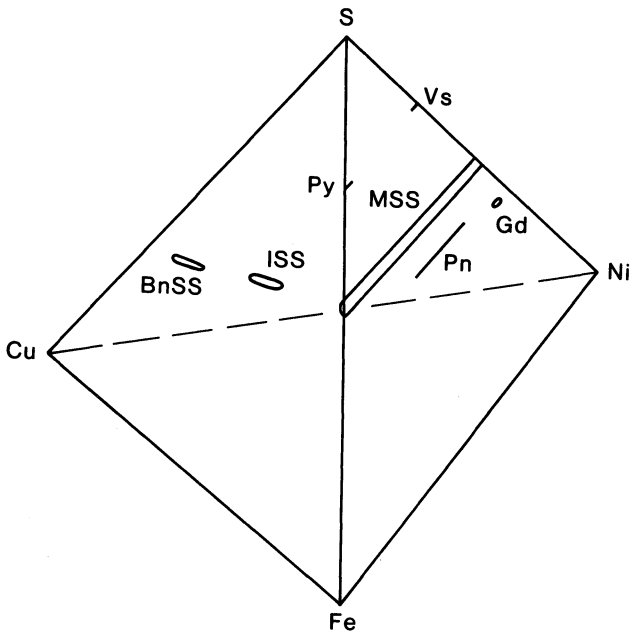

Fig. 3 Diagrams showing schematically condensed phase assemblages stable in experimental runs at 600°C. Each diagram depicts stable phase relations in pair of labelled run products with similar MSS compositions. Phase assemblages for each run listed in Table 2, as is explanation of phase abbreviations

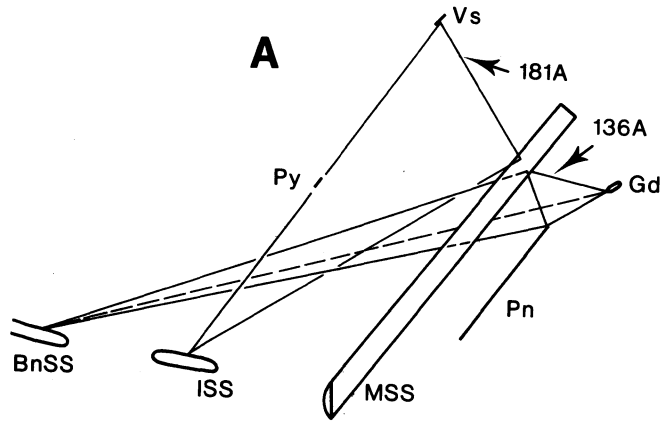

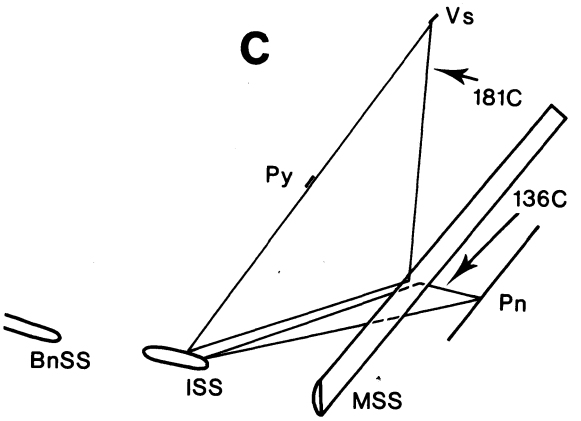

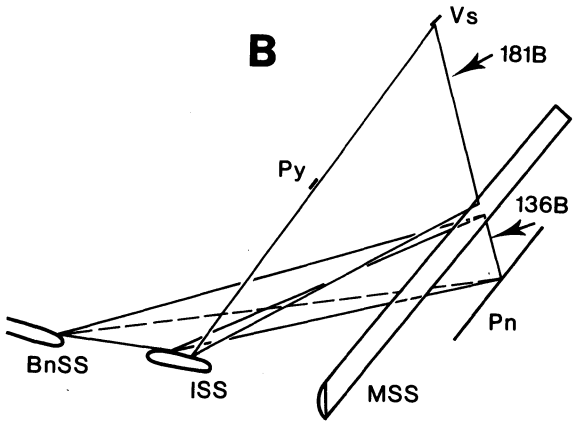

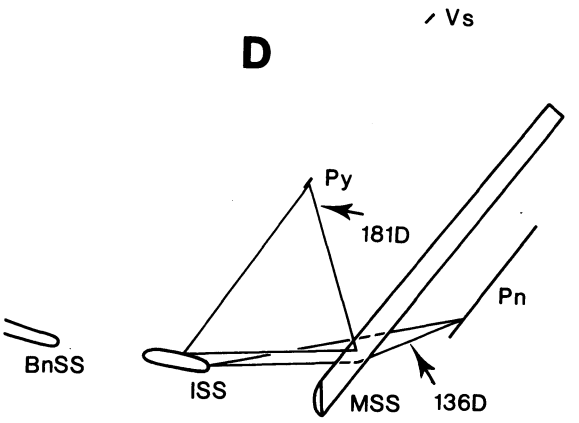

the extensions of MSS into the quaternary system to be constructed. On each section the composition of the MSS phase in equilibrium with pentlandite lies very near the maximum extension of the MSS into the quaternary system and these compositions together represent a close approximation to the locus of maximum solubility of copper in MSS at 600°C.

Pentlandite in the Fe–Ni–S system exhibits very limited variation in metal/sulphur ratio at 600°C and in this respect can be considered essentially as a line phase.[4] It is not unreasonable, therefore, to expect that copper-bearing pentlandite exhibits a similar property and extends into the quaternary system as an essentially planar phase. Phase relations in the quaternary system are such that tie-lines that join this cupriferous pentlandite and BnSS that coexist in assemblages with one or both of the phases MSS and ISS limit the extension of pentlandite into the system. Thus, the pentlandite compositions in the assemblages pentlandite–MSS–godlevskite–BnSS and pentlandite–MSS–ISS–BnSS (Fig. 5 *A* and *B*) lie on the limit of copper solubility in pentlandite at 600°C. Conversely, the pentlandite stable in run products 136*C* and 136*D* may not have compositions at the

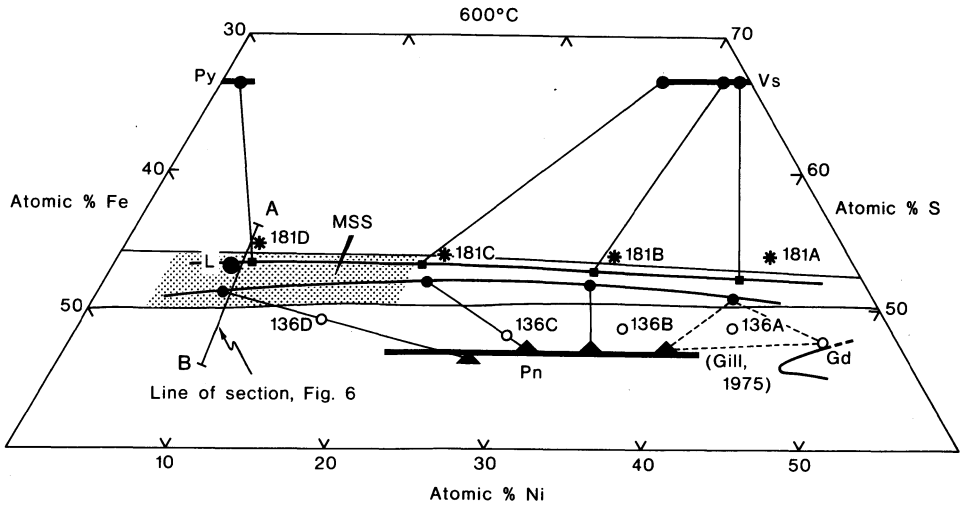

Fig. 4 Diagram showing tie-lines joining compositions of coexisting cupriferous Fe–Ni sulphides stable in experimental runs at 600°C projected on to Fe–Ni–S system. Positions of projections of bulk compositions of experimental charges also shown. Composition of pentlandite shown for run 136*A* taken from Gill.[18] Diagram shows projected position of sulphur-rich and sulphur-poor limits of MSS in equilibrium with disulphide and pentlandite, respectively, and accepted position of 600°C solvus of copper-free MSS. Shaded area outlines range of compositions expressed by chalcopyrite-free bulk compositions of natural primary ores (see text for explanation of projection of data). Phase abbreviations as for Table 2. L = chalcopyrite-free bulk composition of Lunnon Shoot massive sulphide[11]

limit of extension of pentlandite into the quaternary field (Fig. 5*C* and *D*). These pentlandites are in equilibrium with MSS and ISS and possible phase relations permit the coexistence of more cupriferous pentlandite with ISS and/or BnSS in more sulphur-deficient assemblages. The phase compositions expressed in these assemblages do, nevertheless, have significant application to the mineralogy of natural coexisting iron–nickel–copper sulphides.

Geological significance

The phase relationships that have been outlined in this study permit accurate evaluation of the relative thermal stability and compositions of iron–nickel sulphides in bulk compositions equivalent to those of most magmatic iron–nickel–copper ores. In this vein the data show that potential inaccuracies accompany the technique of ignoring copper or chalcopyrite when the mineralogical and compositional changes that have accompanied the initial cooling of these primary magmatic sulphides or their subsequent metamorphic recrystallization are being deciphered.

The estimated primary chalcopyrite-free bulk compositions of most of the magmatic ores lie within the metal/sulphur limits of the MSS stability field at 600°C over the range of iron–nickel values outlined in Fig. 4. The results of this study of the quaternary system show that sulphides that may be stable at 600°C in ores the bulk compositions of which plot within this range include MSS, pentlandite, pyrite, vaesite and chalcopyrite solid solution (ISS). For any bulk composition the stable assemblage at this temperature depends largely on the copper content and the metal/sulphur ratio.

To illustrate and emphasize the effect of copper as well as the metal/sulphur ratio it is enlightening to consider details of the phase relationships in the neighbourhood of the MSS as expressed in Fig. 5*D* and reproduced with additions in Fig. 6. The phase assemblages and compositions portrayed are those from the pair of experimental runs 136*D* and 181*D*. The MSS compositions in these run products contain similar Fe/Fe+Ni ratios and lie on the section through the MSS expressed in the figure. This section lies within the compositional limits expressed by the natural ores and, in particular, can be considered to contain the bulk composition of the Lunnon Shoot massive sulphide[11] (Fig. 4). The positions of the isotherms outlining the quaternary MSS solvus (Fig. 6) are inferred from the 600°C limit established in this study and the data of Naldrett and co-workers[8] on the copper-free system.

The Lunnon Shoot bulk sulphide composition is relatively sulphur-rich (53 at%) and it includes 0.6 at% copper, which is sufficient for it to plot outside the quaternary solid solution field of MSS at 600°C. The composition lies on the sulphur-rich boundary of the two-phase field MSS–ISS and these phases would form a stable assemblage with pyrite at a temperature just below 600°C. This temperature is about 150°C higher than that indicated for the upper limit of stability of pyrite in the ore if consideration is given to the chalcopyrite-free bulk composition (projection point *A* in Fig. 6) and the isotherms of the ternary solvus of MSS as previously described. The ore would thus contain stable pyrite at all temperatures below 600°C during initial magmatic cooling or subsequent isochemical reheating.

This effect by what have normally been considered as insignificant amounts of copper on the interpreted thermal stabilities of the iron–nickel sulphides in the ores is much more pronounced for bulk compositions toward the sulphur-deficient side of the MSS field. For example, an ore with a bulk composition equivalent to that of the MSS phase stable at 600°C in run product 136*D* (*X* in Fig. 6) would be exsolving a chalcopyrite phase (ISS) and cupriferous pentlandite at 600°C. If this composition were projected from either copper or chalcopyrite on to the Fe–Ni–S face to points *Y* and *Z* (Fig. 6), respectively, the interpreted upper temperature limits of stability of pentlandite in the 'ore' would be *ca* 300°C and 350°C—some 300° below the correct value.

The pentlandite stable at 600°C in 'ore' *X* (Fig. 6) contains 2.00 at% copper, which represents near 10 vol% dissolved chalcopyrite. Furthermore, the data from this study indicate that similar copper values in excess of 1.0 at% are possible in pentlandites stable at 600°C over the compositional range of natural sulphide 'ores' shown in Fig. 4. Thus, early relatively high-temperature pentlandite exsolved from cooling MSS contains significant dissolved copper and may be ultimately associated with zones of chalcopyrite enrichment in the 'ores'. This study does not reveal how the solubility of copper in pentlandite

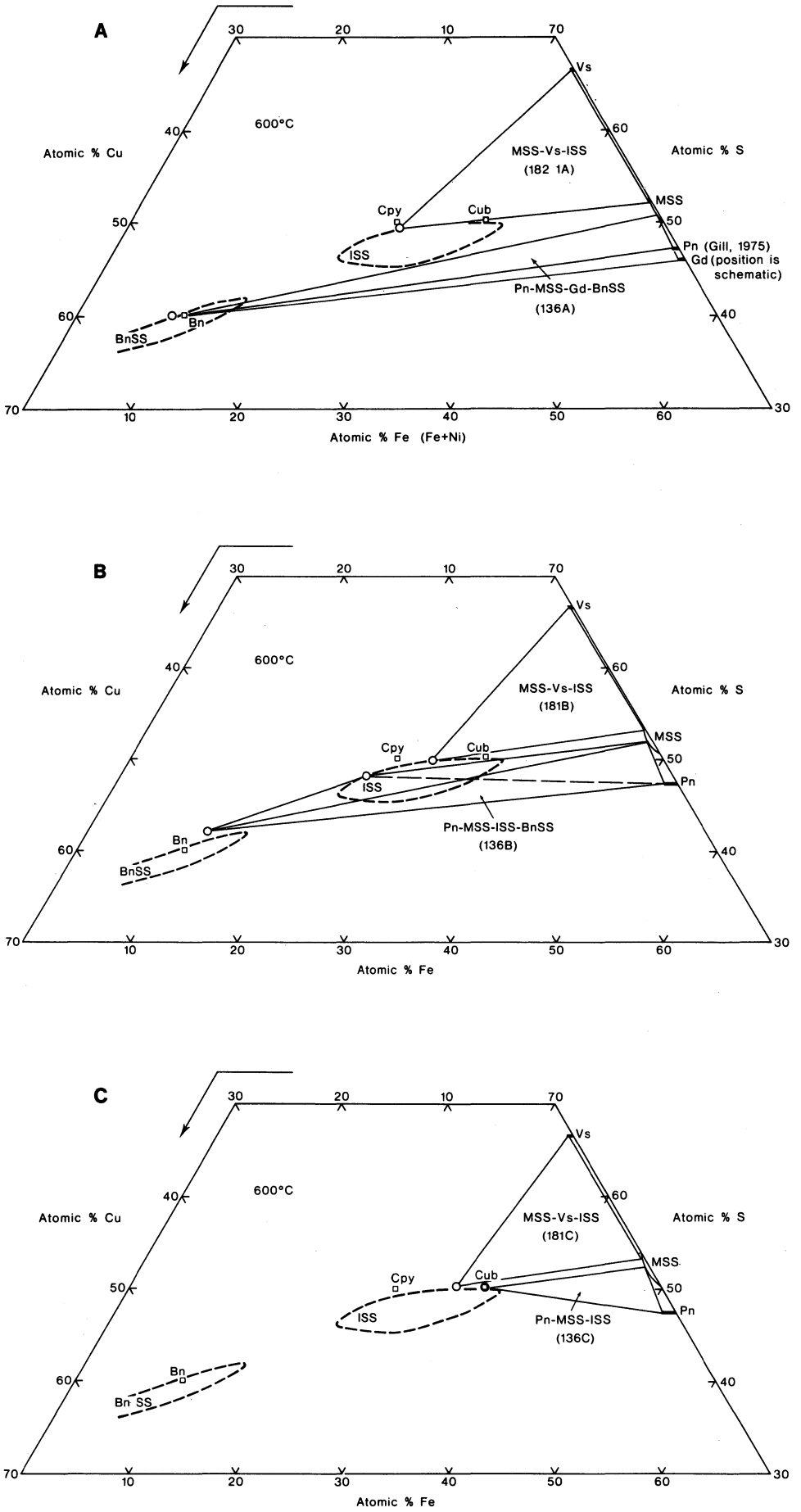

Fig. 5 Projections of phase relations stable in experimental runs at 600°C on to Cu–Fe–S face of Fe–Ni–Cu–S quaternary system (*see also facing page*). Explanation of method of projection given in text. All phases and phase assemblages in equilibrium with vapour. Phase abbreviations as for Table 2. Solid solution limits of ISS and BnSS after Cabri.[13] Composition of pentlandite shown in *A* (run 136*A*) taken from Gill.[18] Sections through MSS depicted in *A*–*D* are at (Fe/Fe+Ni) atomic ratios of 0.18, 0.36, 0.60 and 0.83, respectively

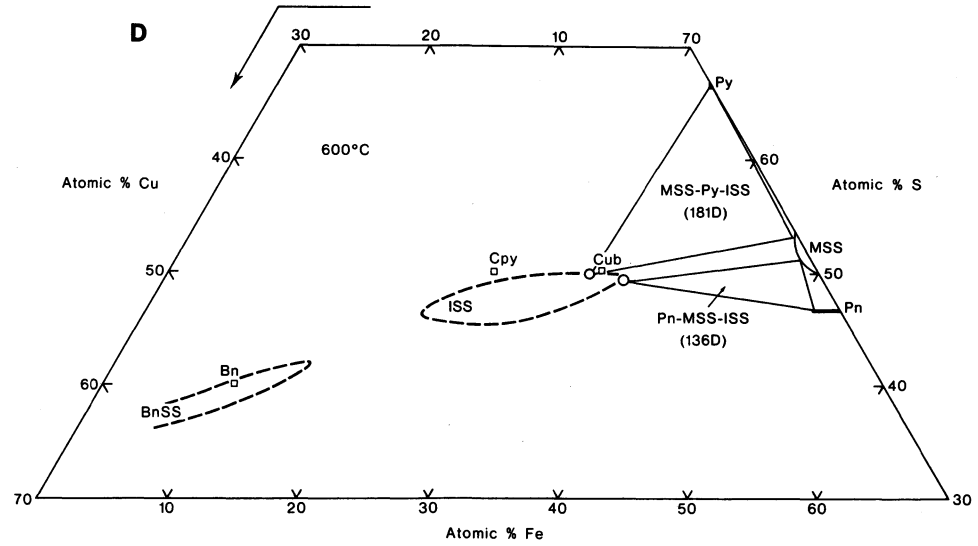

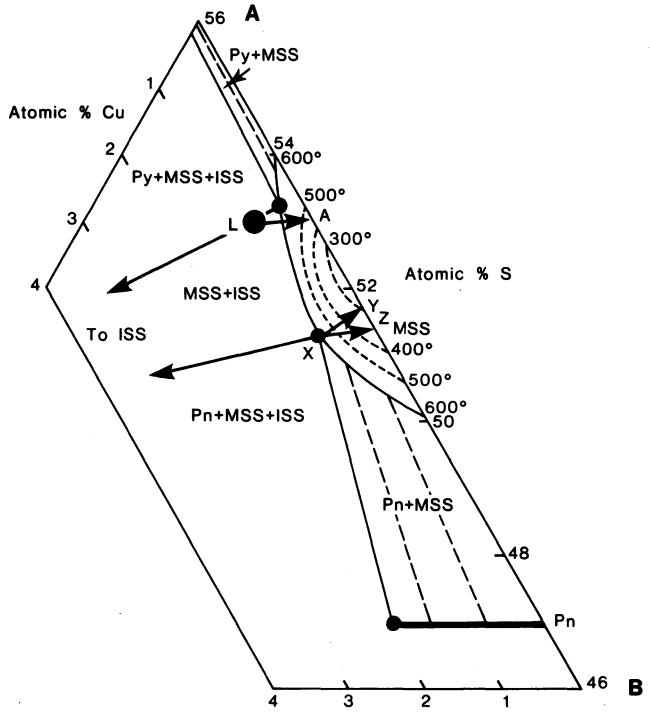

Fig. 6 Quaternary phase relations in neighbourhood of MSS as expressed in experimental run products 136*D* and 181*D*. Assemblages projected at constant copper content and metal/sulphur ratio on to section *A*–*B* through MSS shown in Fig. 4. All phases and phase assemblages in equilibrium with vapour. *L* = bulk composition of Lunnon Shoot massive sulphide.[11] See text for discussion of points *A*, *X*, *Y* and Z

varies as a function of temperature, but the 600°C data indicate that pentlandite will harbour significant copper and hence chalcopyrite during isochemical reheating and partial homogenization associated with subsequent metamorphism at this temperature and retain this copper during any concomitant relative phase mobilization induced by such properties as ductility contrasts during deformation.

Acknowledgement

The author wishes to gratefully acknowledge Professor G. Kullerud's constructive criticisms of the manuscript. Special thanks are also expressed to members of the CSIRO staff: A. Fletcher for the experimental runs, C. Steel and Mrs. A. Lawford for drafting the diagrams and Ms. I. Piercy for typing the manuscript.

References

1. Craig J. R. and Kullerud G. Phase relations in the Cu–Fe–Ni–S system and their application to magmatic ore deposits. In *Magmatic ore deposits* Wilson H. D. B. ed. *Econ. Geol. Monograph* 4, 1969, 344–58.
2. Kullerud G. Yund R. A. and Moh G. H. Phase relations in the Cu–Fe–S, Cu–Ni–S and Fe–Ni–S systems. Reference 1, 323–43.
3. Barker W. W. The Fe–Ni–S system + (Co, Cu). *CSIRO Aust. FP Rep.* 26, 1983, 23 p.
4. Misra K. C. and Fleet M. E. The chemical composition of synthetic and natural pentlandite assemblages. *Econ. Geol.*, **68,** 1973, 518–39.
5. Clark L. A. and Kullerud G. The sulfur-rich portion of the Fe–Ni–S system. *Econ. Geol.*, **58,** 1963, 853–85.
6. Kullerud G. Thermal stability of pentlandite. *Can. Mineralogist*, **7,** 1963, 353–66.
7. Naldrett A. J. and Kullerud G. The Fe–Ni–S system—limits of the Fe_{1-x}–$Ni_{1-x}S$ solid solution between 600 and 250°C. *Yb. Carnegie Instn Wash.*, **65,** 1965–66, 1967, 320–6.
8. Naldrett A. J. Craig J. R. and Kullerud G. The central portion of the Fe–Ni–S system and its bearing on pentlandite exsolution in iron–nickel ores. *Econ. Geol.*, **62,** 1967, 826–47.
9. Craig J. R. Pyrite–pentlandite assemblages and other low temperature relations in the Fe–Ni–S system. *Am. J. Sci.*, **273A,** 1973, 496–510.
10. Craig J. R. Appearance of phases during cooling of pyrrhotite-rich Ni–Cu ores. *Yb. Carnegie Instn Wash.*, **65,** 1965–66, 1967, 335–6.
11. Ewers W. E. and Hudson D. R. An interpretive study of a nickel–iron sulfide ore intersection, Lunnon Shoot, Kambalda, Western Australia. *Econ. Geol.*, **67,** 1972, 1075–92.
12. Craig J. R. and Kullerud G. The Cu–Fe–Ni–S system. *Yb. Carnegie Instn Wash.*, **65,** 1965–66, 1967, 329–35.
13. Cabri L. J. New data on phase relations in the Cu–Fe–S system. *Econ. Geol.*, **68,** 1973, 443–54.
14. Kullerud G. Experimental techniques in dry sulfide research. In *Research techniques for high pressure and high temperature* Ulmer G. C. ed. (Berlin, etc.: Springer, 1971), 289–315.
15. Vaughan D. J. and Craig J. R. *Mineral chemistry of metal sulfides* (London, etc.: Cambridge University Press, 1978), 493 p.
16. Colby J. W. MAGIC IV—a new improved version of MAGIC. Paper presented to sixth national conference on electron probe analysis, 1971.
17. Bacon R. F. and Fanelli R. Purification of sulfur. *Ind. Engng Chem.*, **34,** 1942, 1043–8.
18. Gill J. W. Pentlandite phase relations in the Cu–Fe–Ni–S system. M.Sc. thesis, McGill University, Montreal, 1975.

Geophysical exploration for nickel sulphide deposits in the Yilgarn Block, Western Australia*

D. F. Pridmore Ph.D.
Western Mining Corporation, Ltd., Exploration Division, Kalgoorlie, Western Australia
J. H. Coggon Ph.D.
Western Australian School of Mines, Kalgoorlie, Western Australia
D. J. Esdale B.Sc., Dip.Appl.Geophys., Dip.Educ.
Western Mining Corporation, Ltd., Exploration Division, Kalgoorlie, Western Australia
F. W. Lindeman B.A.(Earth Sci.)
Western Mining Corporation, Ltd., Exploration Division, Kalgoorlie, Western Australia

Synopsis

Almost all the presently viable nickel reserves in the Yilgarn Block contain nickel in a sulphide phase. Both volcanic peridotite-associated (VPA) deposits and intrusive dunite-associated (IDA) deposits are characterized by massive, matrix and disseminated sulphides (typically, pyrrhotite, pentlandite, pyrite, chalcopyrite, magnetite and other spinels), though in the IDA deposits the volume of disseminated sulphides is far greater than that in the VPA deposits.

Potentially all geophysical techniques have application in the direct detection of these deposits—gravity for the detection of the dense massive and matrix ore; magnetics for the detection of magnetite and pyrrhotite in the ores; electromagnetics for the detection of the massive and matrix ore; and induced polarization for the detection of disseminated and to some extent matrix and massive ore. In practice the application of geophysical techniques is limited to a varying extent by (1) the relatively small size of an economic accumulation of sulphides, particularly the VPA deposits, (2) the extreme depth of weathering and lack of outcrop on the Yilgarn Block and (3) the abundance of geological noise or anomalous responses caused by sources other than economic mineralization.

Western Australia is the third largest producer of sulphide nickel in the world with 12% of mine production and 14.5% of total identified resources of nickel in ores with greater than 0.8% Ni. More than 95% of the nickel metal resource is found in the Yilgarn Block (Fig. 1).[1,2]

The initial discovery of nickel sulphides in Western Australia was made in 1966 at Kambalda when Western Mining Corporation drilled a gossan with a coincident induced polarization (IP) anomaly at the base of an ultramafic unit.[3] The success at Kambalda triggered an exploration boom that resulted in the discovery of further significant accumulations of nickel sulphides. Although geophysics, particularly magnetics and IP, played an important role in the discovery of some other deposits, geophysical methods were promoted by contractors and operators of varying competence and, consequently, earned a poor reputation. In retrospect, it is clear that geophysical techniques were imported from other nickel-rich provinces, notably Canada, and were applied on the Yilgarn Block without the necessary modification and adaptation required for the vastly different near-surface conditions. The deep oxidation and weathering that characterize much of the Yilgarn Block increase the depth to the top of the target, short-circuit electrical and electromagnetic energy, making it more difficult both to excite the target and to detect the response of the target, and generate magnetic noise in lateritic terrains.

Following a brief review of the geology of the environments that host nickel sulphide mineralization, the application of the different geophysical techniques is discussed and illustrated with examples over economic nickel sulphide mineralization.

Geology

Detailed descriptions of the geology of the nickel sulphide deposits as well as the mineralogy and geometry of the deposits themselves were presented in an excellent special issue of the journal *Economic Geology* on nickel deposits in Western Australia. Only material relevant to the discussion of geophysical exploration, taken principally from Marston *et al.*,[1] is summarized here.

Almost all the nickel sulphide deposits are hosted by volcanic or intrusive high MgO ultramafics within folded narrow and arcuate greenstone belts of Archaean age. Two important styles of mineralization occur. The intrusive dunite-associated (IDA) deposits occur as lenticular shoots of massive (>80%) sulphide, matrix (40–80%) sulphide and disseminated (5–40%) sulphide in sub-concordant, thick lenses of meta-dunite. Pyrrhotite and pentlandite are the dominant sulphide phases in such sulphide-rich systems as the Agnew deposit, with minor magnetite, chromite, pyrite and chalcopyrite. Low-grade (0.4–1.0% Ni) disseminated mineralization is dominant in most deposits, forming zones 500–2000 m long and 25–320 m thick. High-grade (1–4% Ni) disseminated sulphides, which account for most of the ore reserves at Agnew, may be associated with lower-grade disseminations and also with zones of massive and brecciated sulphides. Generally, the more extensive zones of mineralization occur within the thickest portions of the largest ultramafic lenses.

Most of the nickel that has been produced from the Yilgarn Block (95% to 1981) has come from the volcanic peridotite-associated deposits (VPA), of which the ores at Kambalda are the type example. The ores occur as massive, matrix or disseminated sulphides at or close to the basal contact of the lowermost olivine peridotite unit in an ultramafic sequence, often within local structural depressions.[4] Only 17% of the metal reserve is found in hanging-wall positions. A typical cross-section is massive sulphide ore in direct contact with footwall basalt, overlain by a thicker more extensive zone of matrix ore, which is, in turn, overlain by disseminated sulphides within the silicate matrix. A typical ore environment is illustrated schematically in Fig. 2. The massive ore is typically less than 1 m thick, though in areas of structural complexity significantly greater thicknesses occur. The oreshoots are ribbon-like with the plunge extent as the greatest dimension. The width or strike extent varies from 50 to 300 m, the length or plunge extent of the larger shoots from 1000 to 2300 m and the thickness from 1 to 5 m in shoots with more than 2% Ni to 5–20 m in lower-grade shoots (1–2% Ni). Most shoots contain less than 1 500 000 t at 1.5–3.5% Ni. Sulphides and spinels in order of abundance are pyrrhotite, pentlandite, pyrite, chalcopyrite,

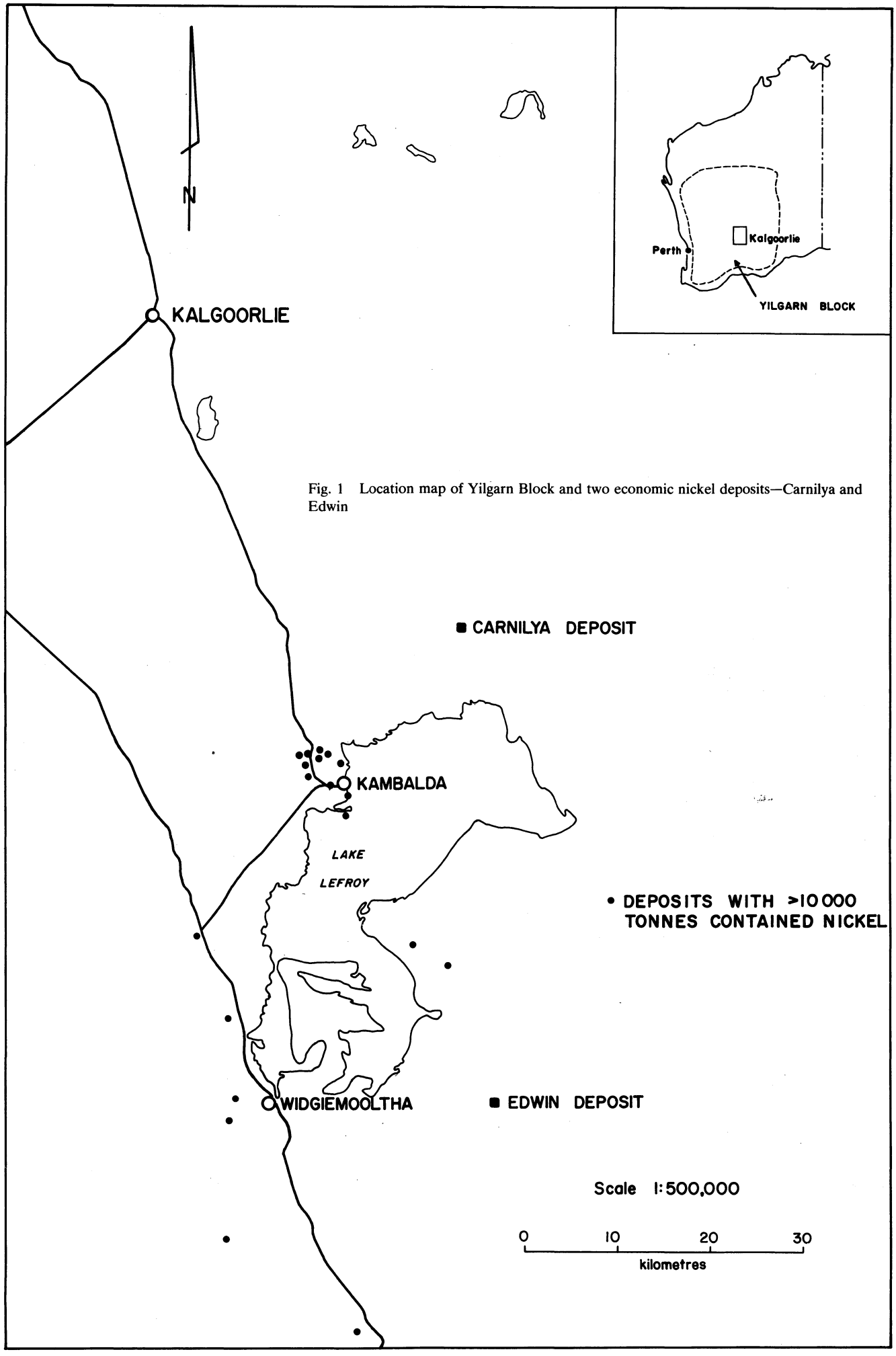

Fig. 1 Location map of Yilgarn Block and two economic nickel deposits—Carnilya and Edwin

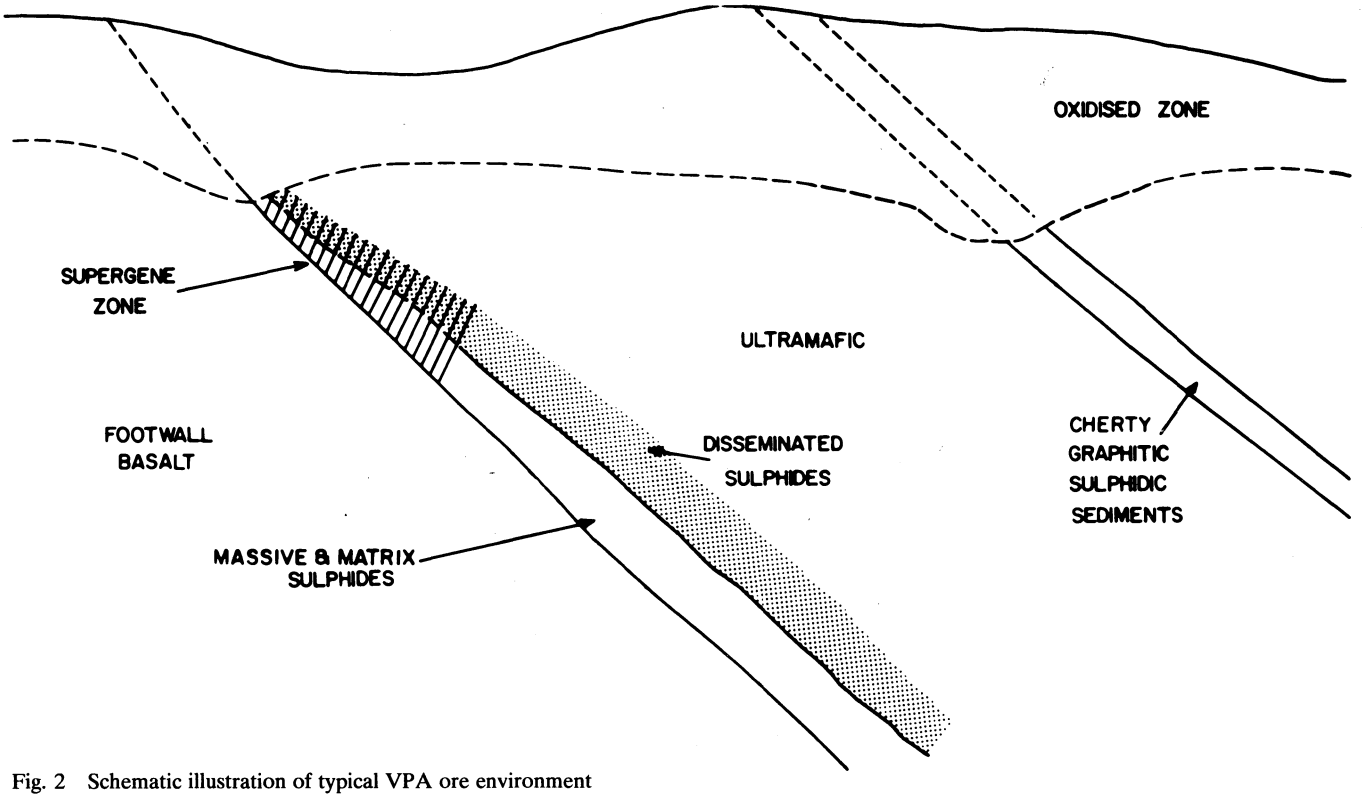

Fig. 2 Schematic illustration of typical VPA ore environment

magnetite and chromite.

The host ultramafic sequence is typically composed of numerous ultramafic lava flows of total thickness up to 800 m, with thin (1–10 m) interbedded, variably albitic, sulphidic and carbonaceous sediments. The basal flows tend to have the highest MgO content and greatest thickness. Footwall and hanging-wall units to the ultramafic unit are typically basalts, with sediments of similar nature to the interbedded sediments often occupying the contact between the footwall basalt and ultramafic unit. The present mineralogy of the ultramafic host rock reflects the degree of serpentinization, talc–carbonate alteration and grade of metamorphism to which the unit has been subjected. At typical intermediate metamorphic grades, antigorite, chlorite and tremolite grading to talc, magnesite, dolomite and chlorite are common assemblages.

The Yilgarn Block has undergone a complex weathering cycle from at least mid-Tertiary times to the present, resulting in zones 15–125 m deep where the sulphides have been altered to hydrated oxides of iron above the water-table. Below the water-table complete supergene alteration of pyrrhotite and pentlandite to pyrite and violarite, respectively, can extend to depths of 200–300 m, and partial alteration has been observed to depths of 400 m. Alluvium in the form of transported silts and clays and saline evaporative deposits (salinas) are found in the palaeo-drainage systems. Laterite profiles have been developed over both alluvial deposits and oxidized bedrock. Subsequent erosion has left etch surfaces where alluvium or oxidized rock is exposed. About 70–80% of the Yilgarn Block is covered by laterite and salina surfaces and virtually all known mineral deposits occur in or adjacent to the etch surfaces.[5]

Geophysical techniques

Theoretically, all geophysical techniques have some application in the direct detection of the VPA deposits: the gravity method for the detection of the dense massive and matrix nickeliferous sulphides; the magnetic method for the detection of pyrrhotite and magnetic associated with the ore; the electromagnetic method for the detection of matrix and massive ore; and the induced polarization method for the detection of disseminated, matrix and massive sulphides. Gravity and electromagnetic techniques potentially have less application in the search for IDA deposits because of the smaller volumes of massive ore. In practice the application of geophysical techniques is limited by the relatively small 'detectable' size of economic accumulations of sulphide (not only are the total tonnages relatively small (cf. stratiform copper–zinc sulphide deposits) but the tonnage per vertical metre is often small as these deposits typically have a large plunge extent), the extreme depth of weathering on the Yilgarn Block, which has the effect of increasing the distance between the target and sensor and isolating the target from the sensor through losses in the overburden, and abundant geologic noise or anomalies produced by sources other than economic mineralization.

The following examples and discussion of the application of each of the four geophysical techniques are centred around exploration for VPA deposits, as most of our experience has been with this class of deposit.

Gravity method

The range of densities for rock types common in a nickel ore environment is given in Table 1. Although massive pentlandite–pyrrhotite ore has a contrast in excess of 1 t/m^3 from the host silicates, the relatively small size and deep oxidation of the deposits often reduce the size of the anomaly from the target to less than those produced by structural complexities in the hanging-wall–footwall contact and by the uneven depth of weathering and thickness of alluvium. In special situations, such as areas covered by salinas or alluvium, the gravity method can

Table 1 Density of geological units common in nickel ore environment

	Density, t/m^3
Alluvium	1.5–2.0
Oxidized rock	2–3.0
Ultramafic	2.7–3.2
Basalt	2.7–3.2
Shales	1.8–3.2
Matrix–massive ore	3.0–5.0

be used for the mapping of units of different density; the more dense mafic and ultramafic units follow the gravity highs and the less dense sediments and felsic volcanic units are mapped by the gravity lows.

Magnetic method

Although pyrrhotite is the most abundant sulphide in the VPA deposits, its magnetic susceptibility is usually less than that of magnetite (and associated magnetic spinels), and the amount of magnetite in the ore is generally insufficient to produce a distinct signature within the normally complex magnetic patterns producd by the host ultramafics and to a lesser extent the mafic units in the stratigraphy. The basal portion of the ultramafic unit, which has the highest MgO content, tends to be the most magnetic, though the amount of magnetite present depends on the degree of serpentinization and talc–carbonate alteration present. With increasing serpentinization and addition of CO_2 the number of alternative phases in which iron coexists increases (e.g. ankerite, chlorite) and the amount of magnetite tends to decrease. Some high MgO units have no magnetic signature. Although of limited use for the direct detection of nickel sulphide mineralization, the magnetic method is extremely useful as a cheap reconnaissance mapping tool and, in some instances, for the detection of the high MgO units that host nickel mineralization.

The usefulness of a detailed magnetic survey can be gauged by comparing contours of the total magnetic field in the vicinity of the Tramways ultramafic (Fig. 3) with the geologic plan of the area at the same scale (Fig. 4), taken from Gresham and Loftus-Hills.[4] The aeromagnetic data were gathered at a sensor height of 30 m and at a line spacing of approximately 150 m. An area of strong magnetic relief is generally coincident with the known distribution of ultramafic rocks, though the correspondence is not exact. Crosscutting dykes, exhibiting both normal and reverse magnetization, are the prominent sub-linear features on the contour map. Although the contours are useful as an aid to geologic mapping, it can be seen that there is no distinct magnetic signature associated with the known mineralization. Close inspection reveals a weak high spatially associated with the Edwin shoot at 513 550N, 388 875E. Pridmore,[6] on the basis of magnetic susceptibility measurements of drill core, concluded that the anomaly was due to a concentration of magnetite in ultramafic occupying the hinge zone of a fold in the contact between the footwall basalt and ultramafic rather than magnetite and pyrrhotite in the ore zone.

The effectiveness of the ground magnetic method is often severely reduced by the presence of an irregular distribution near the surface of intensely magnetized iron oxides, notably maghemite and other less cation-deficient species of magnetite, originally present as pisolites in the ferruginous and mottled

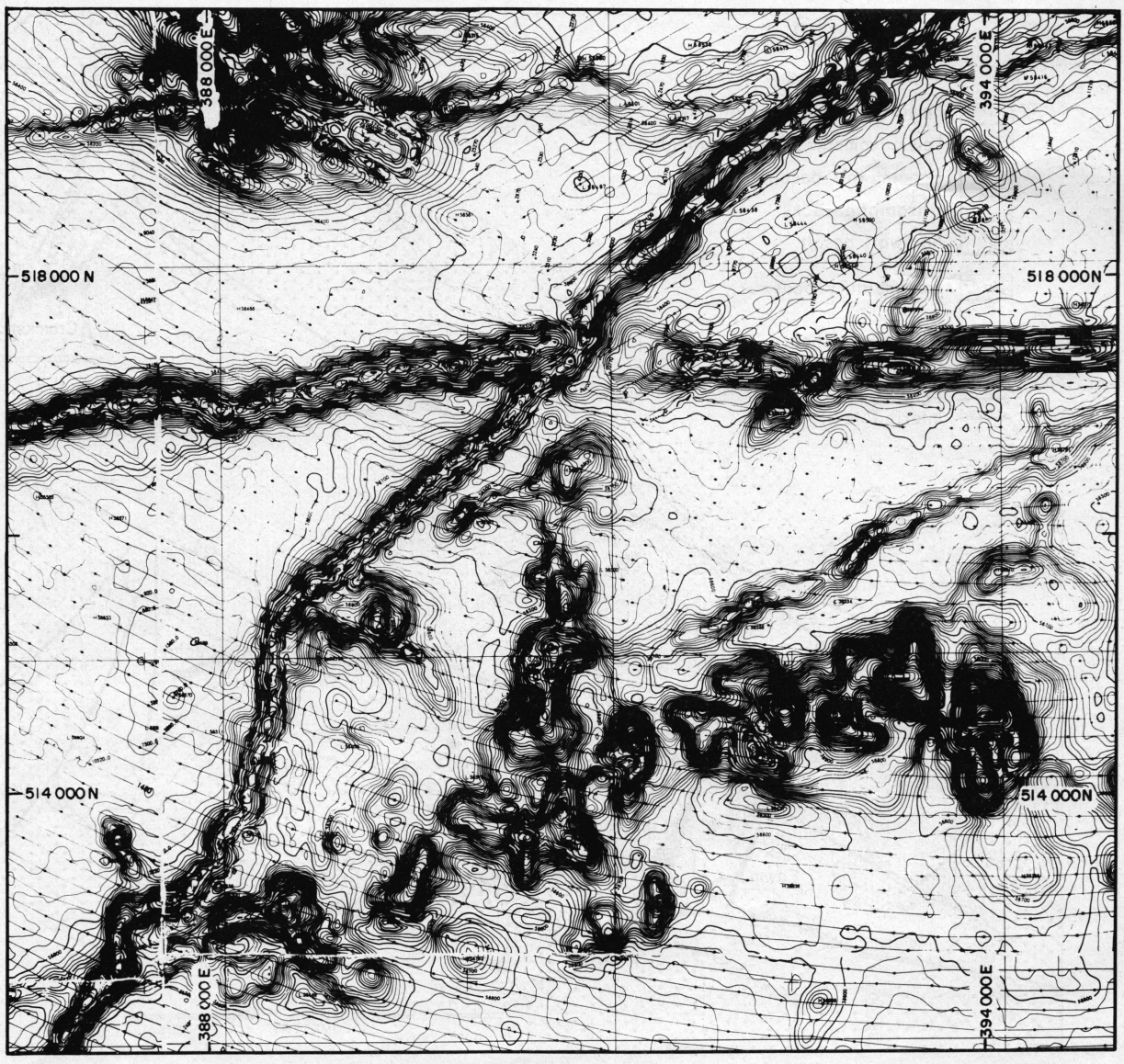

Fig. 3 Contoured aeromagnetic data in vicinity of Tramways ultramafic (contour interval, 20 nanoteslas)

zones of the laterite profile.[7] Such material gives a 'spiky' appearance to the results, with spike amplitudes often in excess of several hundred nanoteslas. This effect attenuates with elevation more rapidly than does the response from non-surficial features and acceptable data can often be obtained by taking readings with the sensor on a pole, typically 3–6 m in length. Alternatively, an ultra-detail low-level aeromagnetic survey is flown over the area of interest.

A ground magnetic profile of the vertical magnetic field where some of the results are affected by surficial magnetic material is shown in Fig. 5. The data were collected with the sensor about 1 m above the ground over the anomaly coincident with the Edwin shoot. Although the noise does not obscure the anomaly, it renders the interpretation of the geometry of the magnetic body unreliable. The same anomaly detected by the airborne survey discussed above is also shown in Fig. 5. The shape of the anomaly is slightly different from that of the ground profile as the flight line is at an angle of about 45° to the ground traverse and because total magnetic field was measured in the airborne survey. Although the amplitude of the aeromagnetic anomaly is smaller than that recorded on the ground, the data are not affected by the surficial material.

Electrical and electromagnetic (EM) methods

The electrical resistivity (ρ) and electrical polarizability of geological units common in a nickel ore environment are listed in Table 2. The resistivity of the nickel sulphides is quite variable,

Table 2 Electrical resistivity and electrical polarizability of geological units common in nickel ore environment

	Electrical resistivity, Ω m	Electrical polarizability
Alluvium	0.2–50	Weak
Oxidized rock	2–50	Weak
Unweathered silicates	100–10 000	Weak–moderate
Graphitic–sulphidic sediments	0.001–20	Strong
Ni sulphides	0.001–20	Strong

ranging from 10^{-3} to greater than 10 Ω m, depending on the amount of massive sulphides present and the degree of connexion between the sulphides. The resistivity of graphitic/sulphidic sediments spans the same range. A resistivity log through a massive nickel sulphide intersection is shown in Fig. 6. In this instance no ultramafic is present in the hole. For targets where the thickness of the body is significantly less than the other dimensions, the quotient t/ρ, where t is the thickness and ρ is the resistivity, rather than ρ controls the amplitude of the electromagnetic response.[8] Similarly, the product of thickness and electrical polarizability, α, tends to control the amplitude of the IP response. The range in the properties t/ρ and $t\alpha$ for nickel sulphide mineralization is very similar to the range for graphitic/sulphidic sediments and discrimination between targets on this basis is a dangerous practice. Although con-

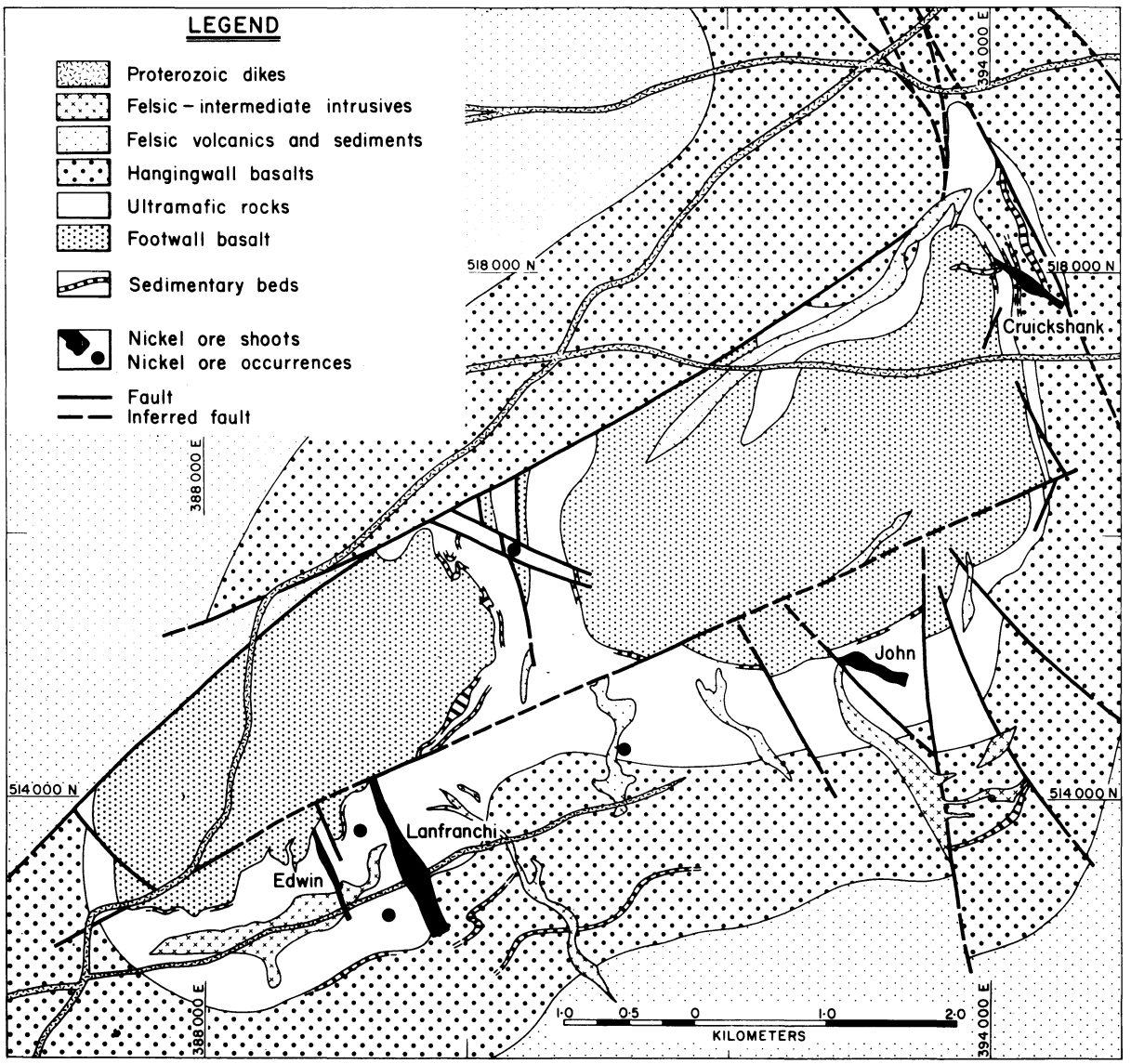

Fig. 4 Geologic plan of Tramways

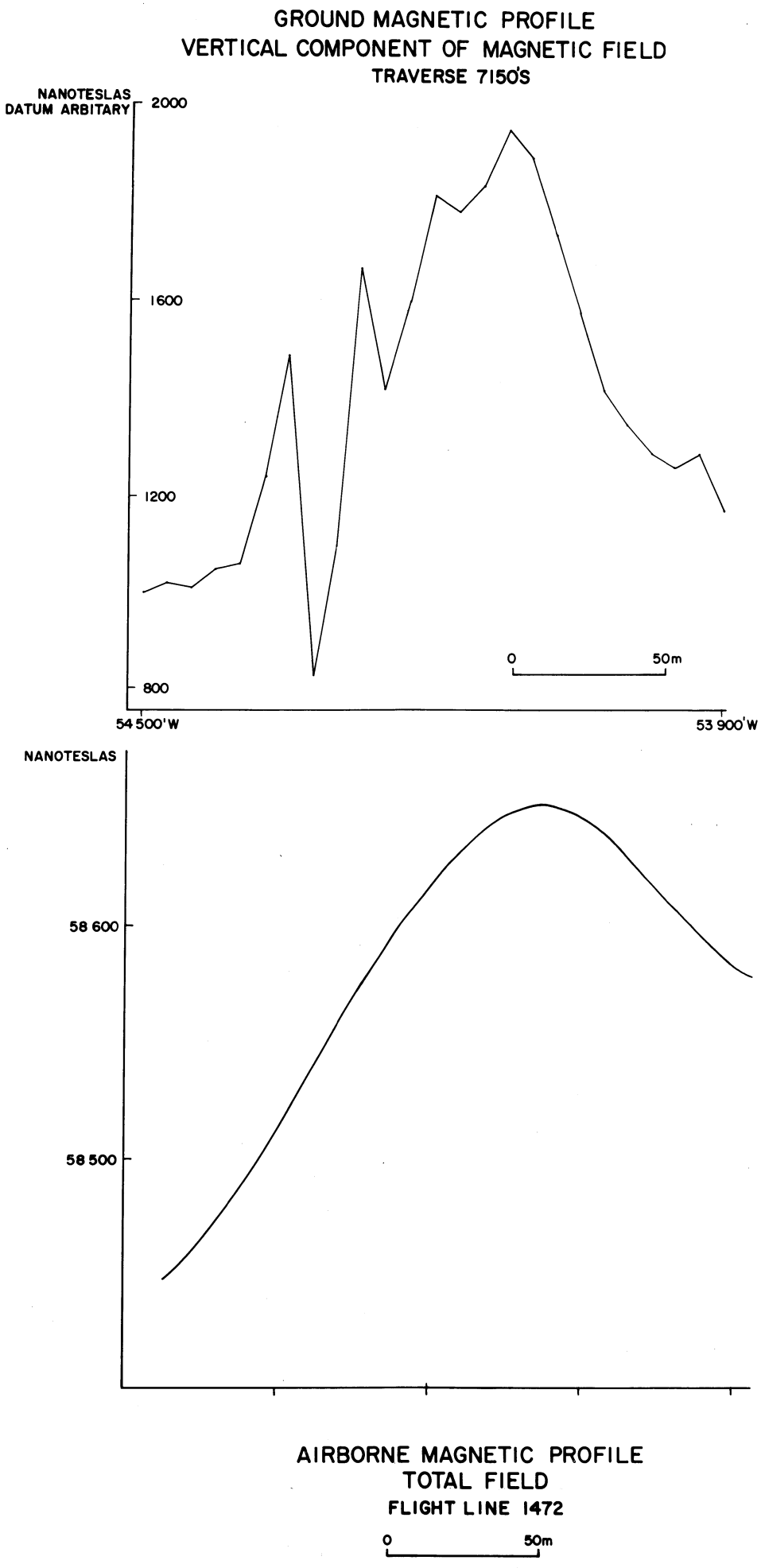

Fig. 5 Comparison of ground magnetic and aeromagnetic traverses over Edwin shoot

ductors with a very long strike length can be dismissed as sediments, many sediments are conductive for strike lengths of the same order as economic mineralization, either through facies changes, structural control or original stratigraphy. Since sediments often occur in the same stratigraphic position as nickeliferous sulphides, the decision to drill EM or IP anomalies is rarely taken without support from geochemistry and geology. A further source of geological noise for the IP technique is the presence of shear zones in ultramafic rocks that have been partially or completely serpentinized.[9]

Weathered material and alluvium is less resistive (0.2–50 Ω m) than the fresh bedrock because of increased porosity, the pore space being partially saturated with saline (and thus conductive) groundwater, and because of the increase in clay mineral content. The most conductive elements in the overburden in Western Australia are the salinas or (usually dry) salt lakes, with resistivities in the range 0.2–0.5 Ω m. Less spectacular in terms of absolute resistivities, but at least as significant, are palaeo-drainage channels where thick sequences of alluvium and oxidized material extend for depths of 50–100 m with

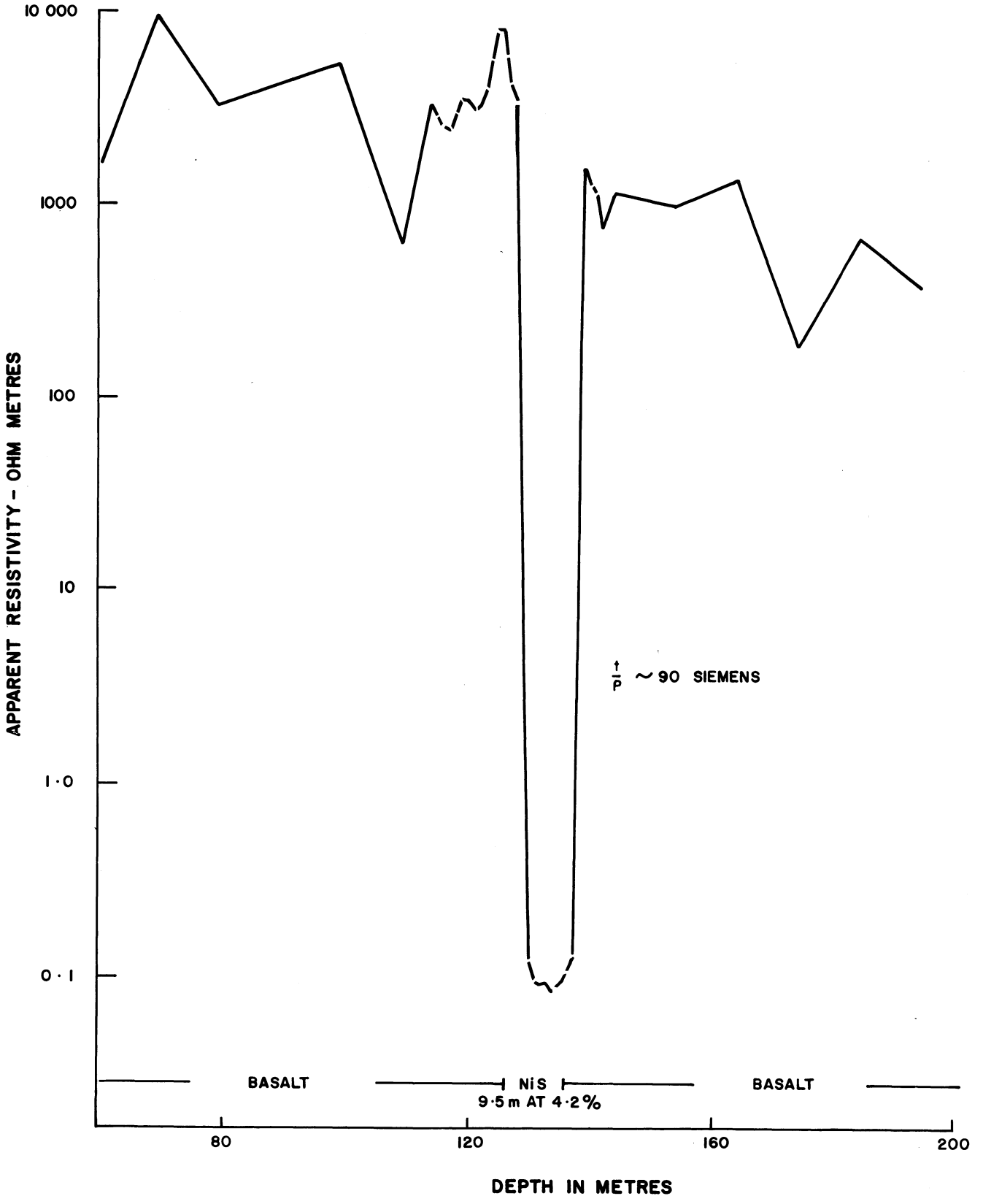

Fig. 6 Downhole resistivity log through massive sulphide intersection

average resistivities of 1–2 Ω m.

The overburden reduces the coupling between the geophysical sensing system and the target both geometrically, since the two are further separated, and electrically, in that energy is dissipated in the conductive overburden. For both IP and EM methods the effect of the overburden is to reduce the sensitivity and resolution of the technique.

Each method has advantages and limitations. The volume of the target is larger for the IP technique as the massive nickeliferous sulphides are invariably associated with larger volumes of matrix and disseminated ore: in fact, in some VPA-type deposits (and many IDA-type deposits) massive sulphides form such a small portion of the orebody that they would not respond to low-frequency EM techniques. On the other hand, many sediments contain sufficient sulphides and/or graphite to respond to an IP survey but do not have a sufficiently low resistivity to respond to a low-frequency EM survey. The IP technique, particularly when used in dipole–dipole mode, is not as sensitive to the dip of a thin target as some EM techniques. Fig. 7 illustrates the apparent resistivity and per cent frequency effect pseudo-sections that would be observed over the thin, two-dimensional body dipping at 60° illustrated at the bottom of Fig. 7. The asymmetry in the p.f.e. pseudo-section is very subtle and could result, without independent information on

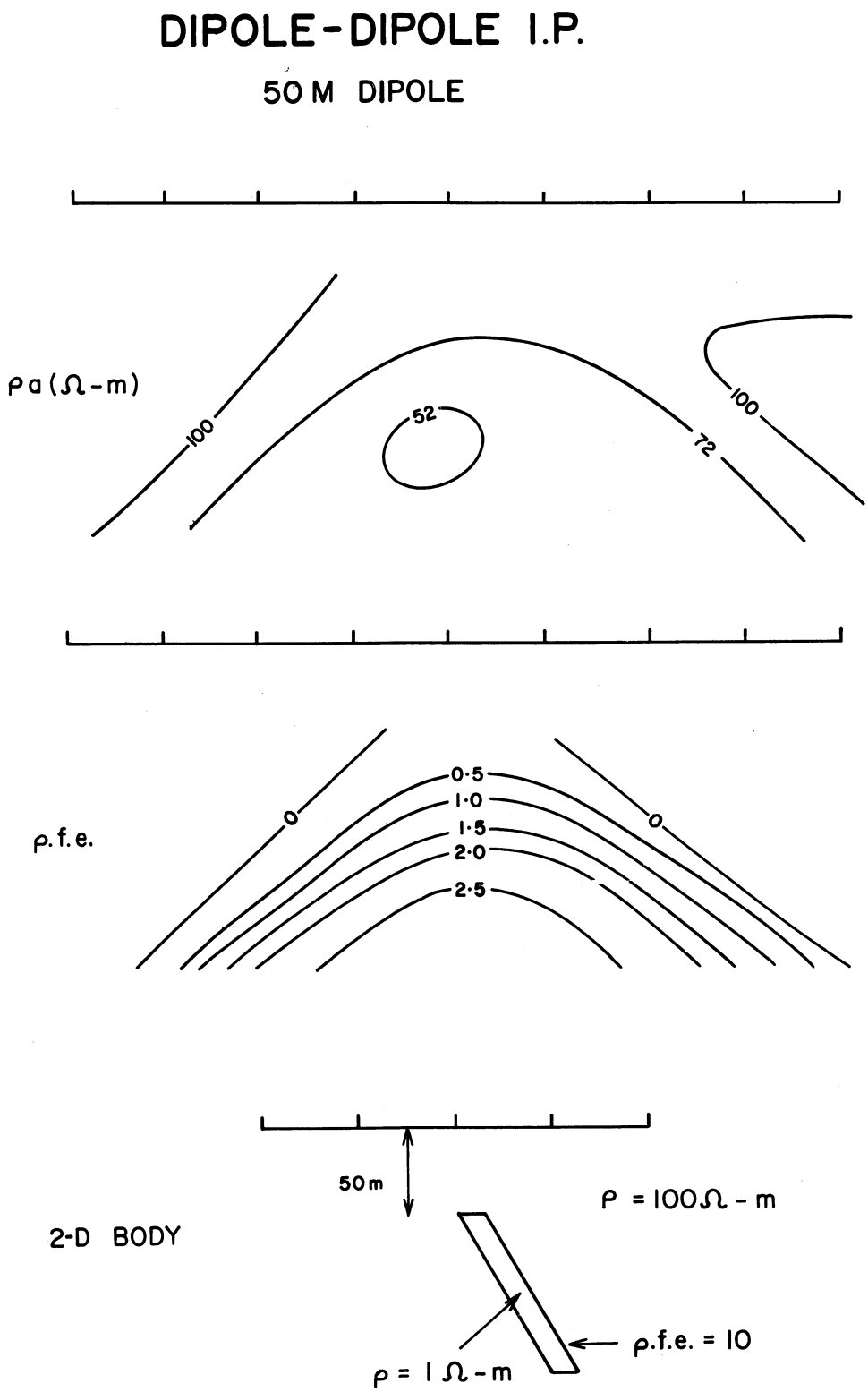

Fig. 7 Apparent resistivity and per cent frequency effect pseudo-sections that would be obtained over two-dimensional body illustrated at bottom. Results obtained numerically with finite-element technique

the dip, in the anomaly being tested ineffectively. Further discussion on the application of the IP method in the Kambalda environment may be found in Coggon.[10]

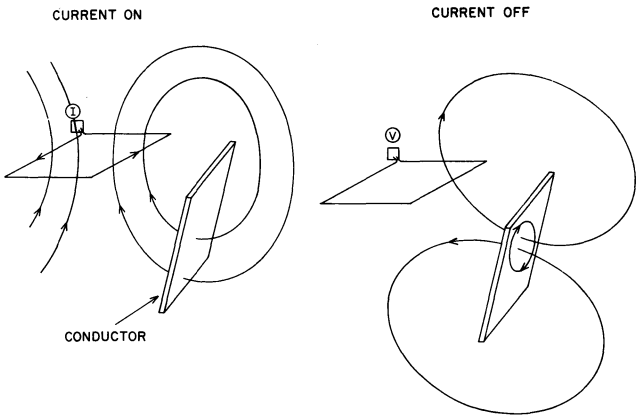

Fig. 8 Schematic illustration of principles of TEM technique depicting magnetic field lines associated with primary current flowing through loop on left and field lines associated with induced current in conductor on right

A single-loop transient electromagnetic system (TEM) developed in Russia in the 1960s and imported to Australia in 1971 by Western Mining Corporation and others has proved to be effective in areas of irregular conductive overburden. The Commonwealth Scientific and Industrial Research Organisation (CSIRO) subsequently developed a modified version of the TEM unit that is marketed under the name SIROTEM. A brief description of the system is included as background for the results to be presented in the next section. Further information is available elsewhere.[11,12] Measurements are taken of the decaying voltage induced in a large square loop of wire following the termination of current flow in the wire. Fig. 8 illustrates the principles involved. When current is flowing in the wire the magnetic field produced by the current cuts any nearby conductor. After the loop current is switched off, currents are induced in the conductor that try to maintain the primary magnetic field (Faraday's law). The secondary magnetic field caused by the induced current is detected in the loop as a decaying voltage. The voltage, normalized by the current flowing in the loop, is expressed as microvolts/ampère at a certain time after the loop current is switched off. Typical profiles of the voltage at a given delay over the centre of a sheet-like conductor are given in Fig. 9. The asymmetry in the profile, once the dip of the body becomes less than 90°, is quite distinct (cf. Fig. 7).

Other advantages of the TEM technique are the large source dimensions, which give good penetration in conductive overburden, and the multichannel capability, which aids in the discrimination of bedrock conductors from overburden response. The data in Fig. 10, derived from scale modelling results, illustrate how the decay of the secondary voltage after primary current turn-off can be used to discriminate between overburden and bedrock conductor response. The overburden response, though large at early delay times, decays away more quickly than the response from the buried bedrock conductors. In this example the bedrock conductors were modelled by thin sheets with a t/ρ quotient of 130 siemens, a dip of 60°, depth of burial of 50 m, depth extent of 450 m and strike lengths of 100 and 200 m—approximations to a medium- and large-tonnage VPA deposit. The t/ρ quotient of the overburden is 10 siemens, a moderate overburden and the loop size is 100 m. The results in Fig. 10 also show the dramatic effect of strike length on the peak amplitude of the response of a bedrock conductor. After about 3 ms the response from the conductor of strike length 200 m is greater than that of the overburden, whereas the response from the smaller conductor never exceeds that of the overburden.

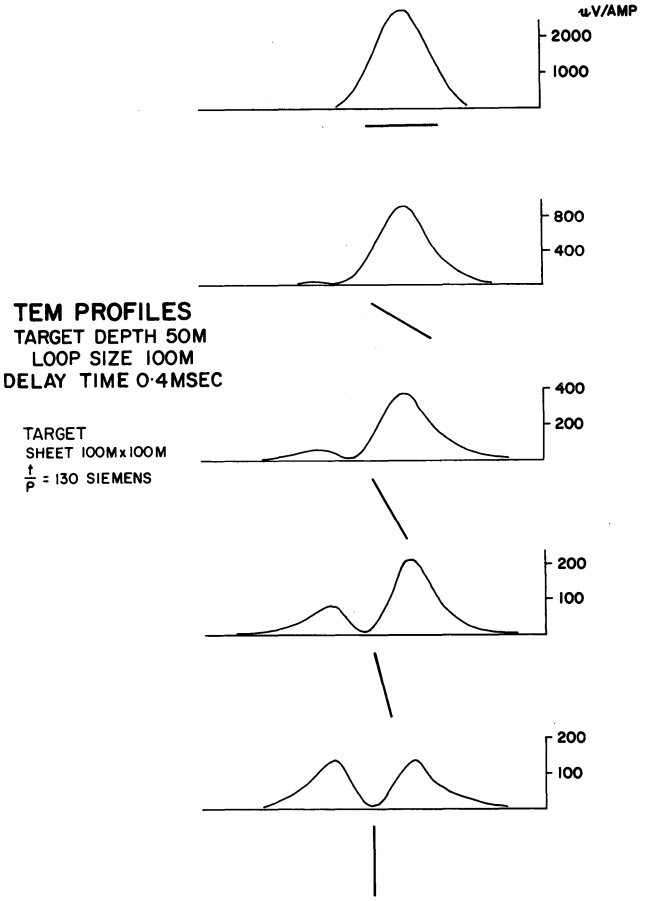

Fig. 9 Profiles of voltage in microvolt/amp obtained with TEM system over small body at different dips. Data obtained from scale models

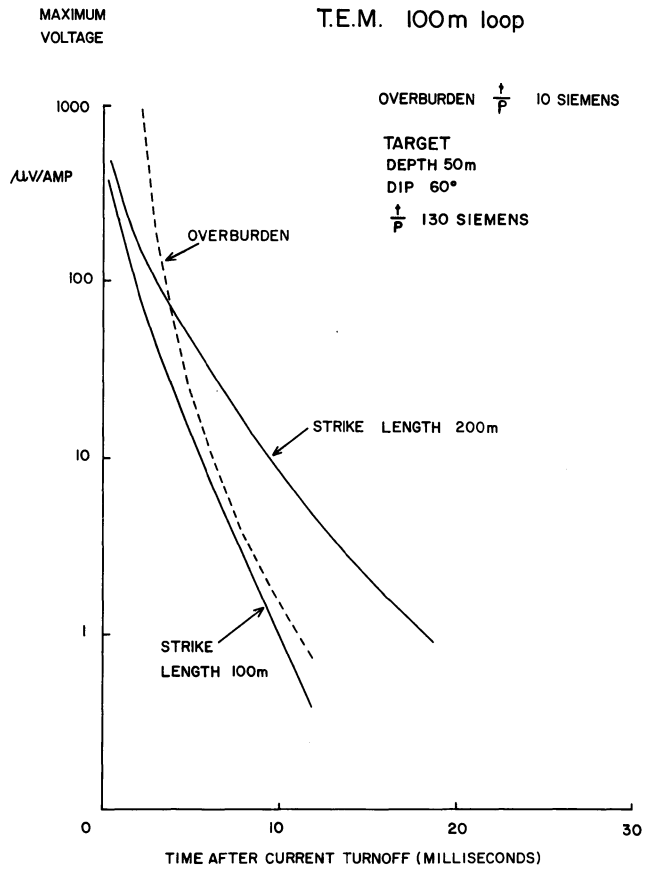

Fig. 10 Plot of voltage as a function of delay time for thin bedrock conductor targets of strike length 100 and 200 m together with response of overburden with common thickness resistivity quotient (loop size, 100 m). Data obtained from scale models

The decays shown are for the overburden and conductor responses alone and do not reflect the interaction when both are present.

Two case histories illustrate many of the points that have been discussed.

Case histories—electrical and electromagnetic methods

Edwin shoot

The Edwin shoot is a relatively small massive and matrix sulphide position at the base of the Tramways ultramafic unit (Fig. 4). The mineralization plunges at about 25–30° to the southeast. Numerous interflow sediments are present in the ultramafic and at the basal contact of the ultramafic with footwall basalt. The depth of oxidation is about 30 m and supergene alteration extends to a depth of about 80 m (more information can be found in Gresham and Loftus-Hills[4]). The 60-m loop TEM response, together with a geological cross-section, is shown in Fig. 11. The Edwin shoot, located at about 54300'W on line 7300'S, gives a good response at delays out to about 4 ms. The shape of the anomaly is consistent with the flat dip of the mineralization on line 7300'S (cf. Fig. 9). The overburden over the footwall basalt gives a large response at an early delay, but decays away more quickly than the response from the Edwin shoot. There is very little response from the hanging-wall sediments and nickel mineralization to the east of the shoot. Dipole–dipole IP results on line 7300'S are shown in pseudo-section form in Fig. 12. The per cent frequency effect was measured at frequencies of 0.3 and 3 Hz. The apparent resistivity data indicate increasing conductive overburden to the west and east of the Edwin shoot—a reflection of the outcrop of the ultramafic sequence above the mineralization and slightly to the north of the line. The variation in near-surface resistivity is sufficient to mask the presence of the buried massive sulphides. The p.f.e. data are anomalous over the Edwin shoot, but the hanging-wall sediments to the east of the mineralization also give a response.

Carnilya Hill

At Carnilya the sequence hosting the massive sulphides is overturned (Fig. 13). The massive nickeliferous sulphides occur again at the contact between the ultramafic and basalt units. The basaltic unit structurally below the host ultramafic contains a carbonaceous sulphidic sediment. The depth of weathering is about 30 m and supergene alteration extends to a depth of 120 m. In this case the sediment gives a larger TEM response than the mineralization at early delay times, probably reflecting the shallower depth of weathering of the sediment (Fig. 13). At later delay times the response of the massive sulphides is a little larger than that of the sediment, which indicates either greater dimensions or better t/ρ quotient. Results from adjacent lines indicate

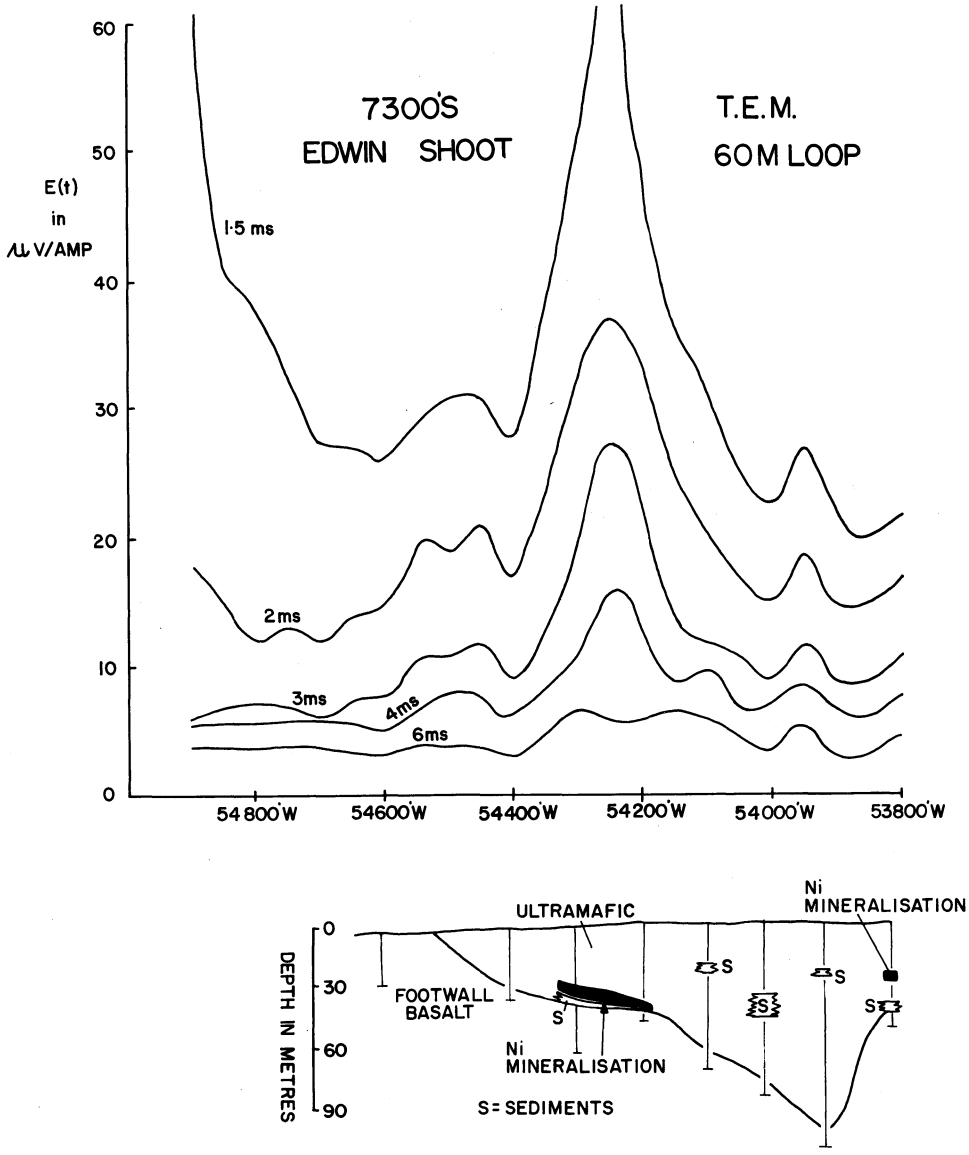

Fig. 11 Profiles of TEM voltage measured at different delay times on line 7300'S, Edwin shoot, with geologic cross-section

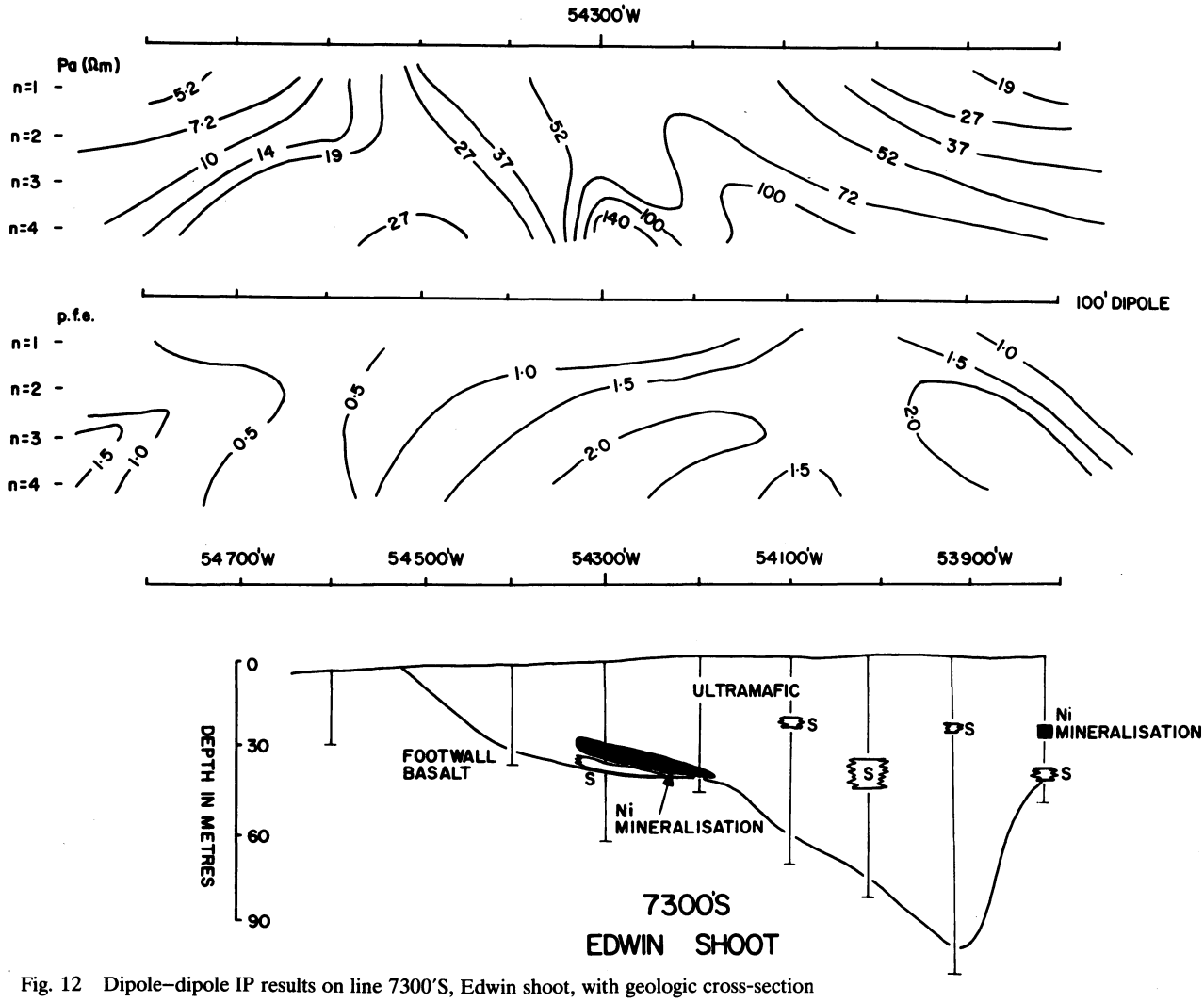

Fig. 12 Dipole–dipole IP results on line 7300'S, Edwin shoot, with geologic cross-section

that the sediment has the longer strike length, which suggests that the nickeliferous sulphides have the better t/ρ quotient. Dipole–dipole IP data with a dipole size of 50 m are shown in Fig. 14. Measurements were made at frequencies of 0.3 and 3 Hz. The apparent resistivity pseudo-section is dominated by the resistivity low caused by the sediment. Values below 2 Ω m were recorded. Again there is no indication of the massive nickel sulphides, which outcrop as gossanous material close to 14000'S. Although the sediment is thicker than the massive sulphides and can be expected to give a larger response, it must be concluded that the conductive carbon graphite and sulphides in the sediment are not oxidized as deeply as the massive sulphides. This conclusion is supported by observations elsewhere in the Yilgarn.

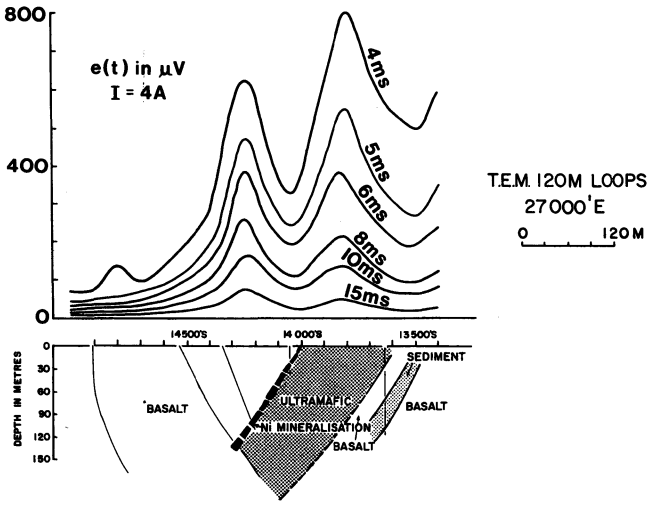

Fig. 13 Profiles of TEM voltage measured at different delay times on line 27000'E, Carnilya deposit, with geologic cross-section

A small positive p.f.e. response is associated with the massive nickel mineralization, but again the pseudo-section is dominated by a large diffuse negative response, reflecting electromagnetic coupling produced by the conductive sediments. Electromagnetic coupling is produced when the alternating currents, which are injected into the ground to measure IP effects, induce further currents to flow in conductive regions. These currents give voltages that are not in phase with the transmitted current and are electromagnetically coupled to the transmitter as opposed to the galvanic coupling used to measure IP effects. The p.f.e. can be of the same sign as that usually produced by IP effects, or may be of opposite sign, such as those illustrated in Fig. 14. Negative EM coupling effects are produced by lateral inhomogeneities, whereas positive effects are produced by layered environments. Although it is not obvious, broad-band measurements indicate that positive coupling effects are present at the deeper separations to the south of the massive sulphides. The negative effects associated with the sediment extend to low frequency (less than 0.125 Hz). In this instance, however, broad-band low-frequency information did not change, significantly, the interpretation based on the data in Fig. 14. EM coupling effects, both positive and negative, are exacerbated by conducting overburden and render conventional interpretational aids useless. Electromagnetic coupling is reduced by lowering the frequency at which data are gathered in the frequency domain or measuring over later delays in the time domain.

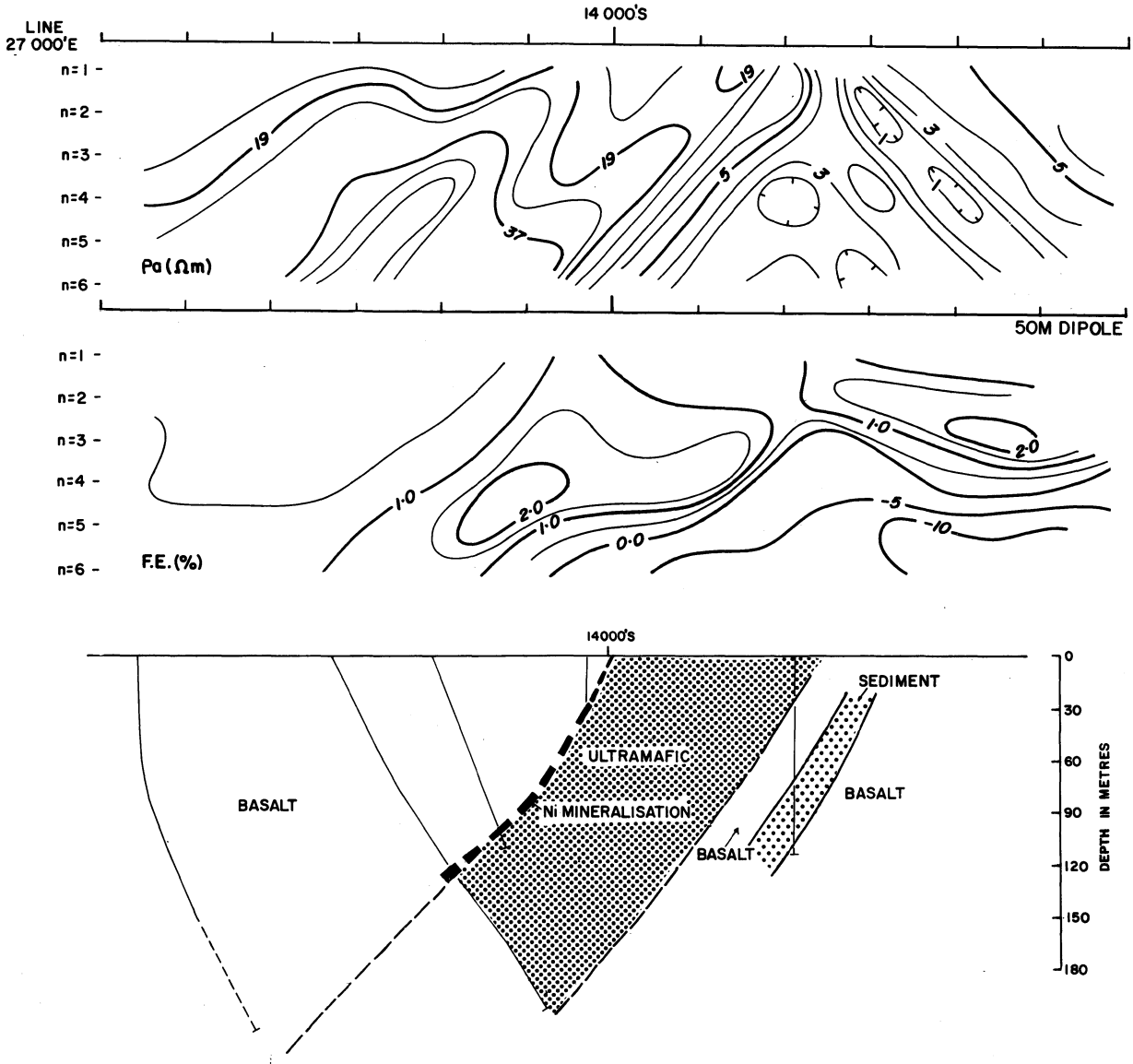

Fig. 14 Dipole–dipole IP results on line 27000'E, Carnilya deposit, with geologic cross-section

Conclusions

The deep oxidation and weathering on the Yilgarn Block limit the application of geophysics in the search for nickel sulphides. The magnetic method is the most commonly used geophysical technique, both as a cheap reconnaissance geological mapping tool and in some cases for the detection of the high MgO lava flows and intrusives that host the mineralization. The magnetite and pyrrhotite associated with economic accumulations of nickel sulphides rarely produce a distinct magnetic signature, given that the host ultramafic rocks usually give rise to complex magnetic patterns. The presence of intensely and irregularly magnetized oxides of iron in the oxidized zone significantly reduces the effectiveness of ground magnetic surveys. Normally, a ground survey would be carried out with the sensor on a 3- or 6-m pole. Ultra-detail aeromagnetic surveys (sensor height less than 50 m, line spacing less than 200 m) have replaced, to a significant extent, ground magnetic surveys.

IP and EM techniques find some application in the direct detection of nickeliferous sulphides, but the ubiquitous presence of graphitic/sulphidic sediments in ore environments, the small size of economic accumulations of ore and the presence of conductive overburden limit their effectiveness. Although nickel sulphide deposits form a larger target for the IP method relative to the EM method, and some IDA deposits may not respond to EM techniques, more sediments are responsive to IP than to EM techniques. Discrimination between economic and non-economic IP and EM responses is rarely based on physical properties of the target. Low-frequency or time-domain IP and EM measurements and large-loop EM systems must be used to penetrate the conductive overburden.

The gravity method is of little use for the direct detection of massive nickeliferous sulphides because of the deep weathering and relatively small size of the target. The method finds some application in the mapping of broad stratigraphy beneath cover.

Acknowledgement

The Director of Exploration, Western Mining Corporation, kindly granted permission for this material to be published. The Broken Hill Proprietary Company agreed to the release of data from the Carnilya deposit.

The ideas presented here have evolved over a period of time during discussions with other geoscientists in Western Mining Corporation and their contribution is acknowledged. Jeff Gresham critically reviewed the manuscript. Uwe Sinn and Graham Fraser were responsible for collecting much of the early field data; Mary Monaco typed the manuscript; and Ron Graham, Karen O'Malley and Greg Dutkiewicz drafted the figures.

References

1. Marston R. J. *et al.* Nickel sulfide deposits in Western Australia: a review. *Econ. Geol.*, **76**, 1981, 1330–63.

2. Groves D. I. *et al.* A special issue on nickel deposits and their host rocks in Western Australia: preface. *Econ. Geol.*, **76,** 1981, 1289–90.
3. Woodall R. and Travis G. A. The Kambalda nickel deposits, Western Australia. In *Mining and petroleum geology* Jones M. J. ed. (London: IMM, 1970), 517–33. (*Proc. 9th Commonw. Min. Metall. Congr., 1969* vol. 2)
4. Gresham J. J. and Loftus-Hills G. D. The geology of the Kambalda nickel field, Western Australia. *Econ. Geol.*, **76,** 1981, 1373–416.
5. Perriam R. Western Mining Corporation Internal Report K/2436, 1979.
6. Pridmore D. F. The Edwin nickel shoot—results of geophysical investigations. B.Sc.Hons. thesis, University of Adelaide, 1970.
7. Wilkes P. G. Characteristics of magnetic sources and guidelines for exploration in the Cobar area N.S.W. *Bull. Aust. Soc. Explor. Geophys.*, **10,** 1979, 34–41.
8. Grant F. S. and West G. F. *Interpretation theory in applied geophysics* (New York, etc.: McGraw-Hill, 1965), 584 p.
9. Moeskops P. G. and Quick D. H. Field and laboratory studies of the induced electrical polarization of serpentinized ultramafic rocks from the Western Australian Archaean nickel belt. *Trans. Instn Min. Metall. (Sect. B: Appl. earth sci.),* **80,** 1971, B85–94.
10. Coggon J. H. Induced polarisation anomalies. Ph.D. thesis, University of California, Berkeley, 1971.
11. Buselli G. and O'Neill B. SIROTEM: a new portable instrument for multichannel transient electromagnetic measurements. *Bull. Aust. Soc. Explor. Geophys.*, **8,** 1977, 82–7.
12. Spies B. R. The application of the transient electromagnetic method in Australian conditions—field examples and model studies. Ph.D. thesis, Macquarie University, 1980.

Geochemical exploration for nickel sulphides in lateritic terrain in Western Australia

B. H. Smith B.Agric.Sci., Ph.D.
Western Mining Corporation, Ltd., Perth, Western Australia

Synopsis

Most of the discoveries of nickel sulphide deposits in Western Australia have followed the search for gossans. The chances of further discoveries depend on improving our understanding of the cover of strongly leached and transported materials that obscure approximately 85% of the area of the Yilgarn Block that has nickel sulphide mineralization potential.

The lateritic profiles that are observed on the Yilgarn Block today were formed over a period of more than 100 m.y. of warm and humid climates. This lateritized land surface has been preserved by induration during subsequent arid climates as well as by the structural stability of the Yilgarn Block.

In geochemical surveys of lateritized terrain samples have to be taken from at least the saprolite zone usually by drilling so that confident predictions can be made of the significance of analytical data. Account must be taken of the mineralogy of samples, as well as the nature of the horizon of a laterite profile that is being sampled, owing to the concentrating effects on trace elements of Fe and Mn oxides.

Multivariate techniques have been applied successfully to analytical data in gossan recognition when textural evidence is ambiguous. Pathfinder geochemistry has also been used in gossan recognition and the most significant recent advance has come from studies of platinum group metals in nickel sulphides and their dispersion during weathering.

The Eastern Goldfields Province of the Yilgarn Block (Fig. 1) has been the principal area of nickel sulphide discoveries in Western Australia, the first discovery in 1966 being the major mineralized environment at Kambalda. The find was the catalyst for considerable exploration activity for nickel sulphides in Western Australia (Fig. 2) and this activity continued into the early 1970s. Discoveries of viable orebodies—Mt. Edwards, Redcross, Spargoville, Nepean, Scotia, Carr Boyd, Mt. Windarra, Carnilya, South Windarra and Agnew—were made in quick succession. Most of these finds were the result of prospecting for the oxidized exposures of mineralization in which the approach was guided by intuition as much as by careful geological assessment. The significance of 'gossanous' brown rocks was simply tested by analysing for Ni and sometimes Cu owing to the association of small amounts of chalcopyrite with nickel sulphide mineralization. Following the discovery of a gossan, drill targets were often defined by use of conventional geochemical techniques and sampling of surface materials on regular grid patterns.

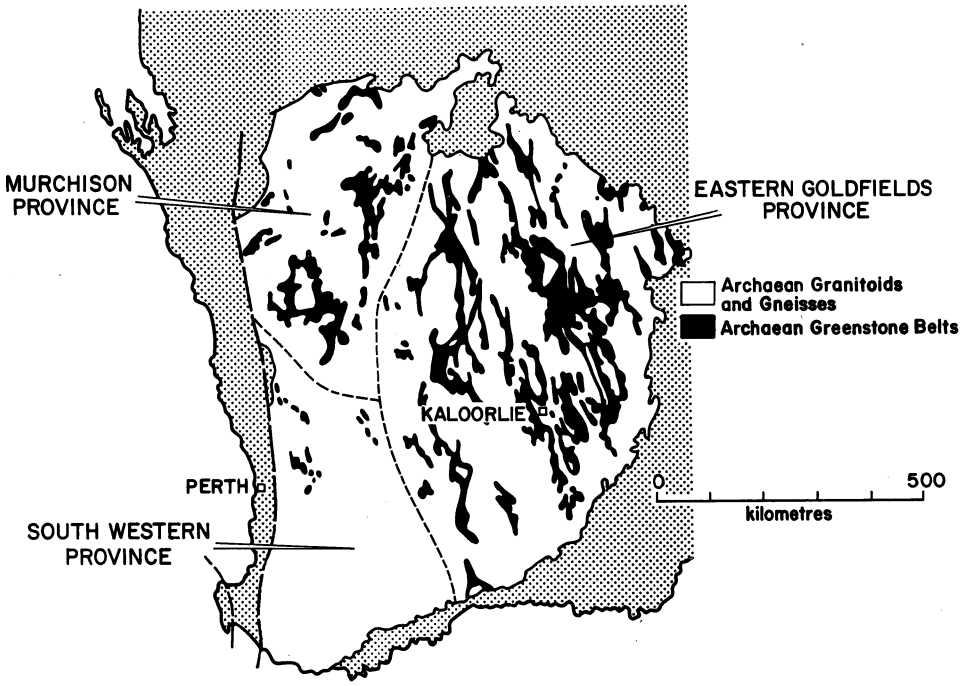

Fig. 1 Geology of Yilgarn Block, Western Australia

In the heady days of the 'nickel boom' in Western Australia from the late 1960s to the early 1970s exploration activity was intense and surface sampling programmes were usually carried out with little thought to the nature of the material that was collected. Samples were taken from deeply weathered and transported materials as well as responsive residual soils, so the results had variable relevance. Recent studies in geomorphology[1-4] and the chemistry and mineralogy[5-9] of the weathered zone of the Archaean Shield have increased our understanding of the secondary dispersion of elements in highly weathered materials. Approximately 85%[10] of the area of the Archaean Block with potential for nickel sulphide mineralization is covered by strongly leached or transported materials (Fig. 3), so these studies have particular relevance for future exploration geochemistry in these terrains.

Geology

Nickel sulphide mineralization in the Eastern Goldfields Province[11] of the Yilgarn Block is associated with Archaean basic

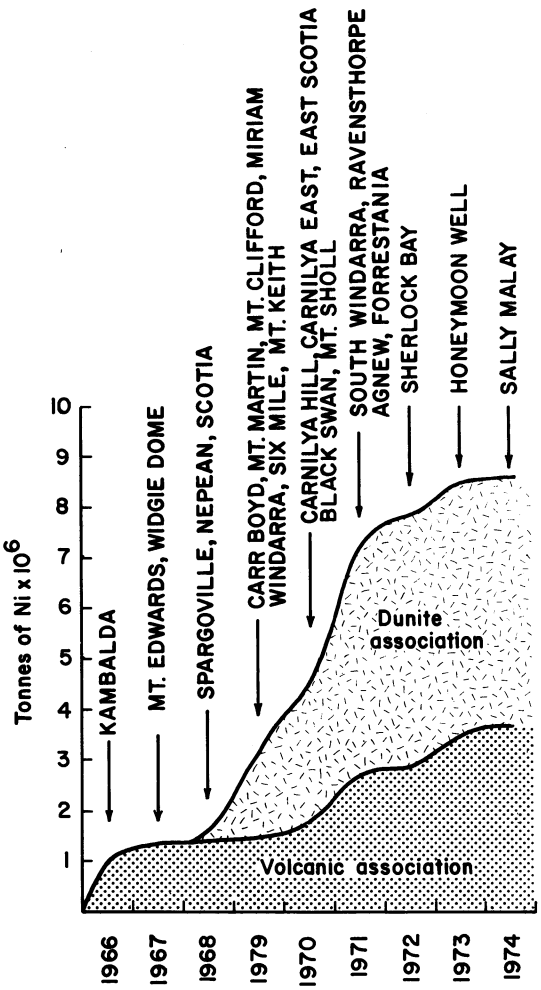

Fig. 2 Discovery of nickel sulphide resources in Western Australia

and ultrabasic extrusive and intrusive rocks[12,13] (Fig. 1). These rocks are usually steeply dipping and form part of NNW-trending belts of metamorphosed igneous and sedimentary rocks. These greenstone belts constitute about 30% of the Eastern Goldfields Province and are separated by ovoid granitoid plutons with marginal facies of gneiss and migmatite, which are the altered remnants of the original basement.

Igneous rocks predominate in the layered successions of the greenstone belts and nickel sulphides hosted by ultrabasic rocks mainly occur as two ore types. In one major type massive to disseminated nickel sulphide mineralization occurs in the lowest flow units of ultrabasic lava piles as a pyrrhotite–pentlandite–(chalcopyrite) assemblage. In the second major type intrusive rocks of dunitic composition host disseminated nickel sulphides in a pyrrhotite–pentlandite assemblage. Small quantities of platinum group metals, as well as Co, Se, Te, As and Au, may be incorporated in both types of mineralization.

Palaeoclimates

The weathering events that produced the highly leached profiles that we observe now occurred in the period from the early Cretaceous to the mid-Miocene. The factors that affected climate during that period differed greatly from those which control climate today.[14] There was a small temperature gradient from the poles to the equator and sea temperatures were higher. As a result, warm and moist weather conditions influenced the Australian continent. In the late Paleocene the land mass of Tasmania was located at about 70°S latitude (present position, 42°S) and sea temperatures in the vicinity were as high as 18–20°C. Tropical and sub-tropical rain forests extended well inland from coastal areas from the Cretaceous and the climates of the mid-Eocene were particularly humid and a cover of luxuriant rain forest developed over most of the continent.

Rifting of Australia and Antarctica commenced in the mid-Paleocene[1,2,14] as the Australian continent began its slow northward drift. Sea temperatures in higher latitudes began to decline and by the late Eocene the sea temperatures around Tasmania were in the range 8–10°C. An Antarctic ice cap did not appear until the mid-Eocene and major expansion of this cap occurred during the late Miocene, when sea temperatures declined further. Dry anticyclonic weather patterns developed[1,14] and affected most of the Australian continent. The dominant vegetation changed to dry sclerophyll woodland and grassland, and the rain forest cover retracted to coastal areas. Arid climates have predominated since the late Miocene.

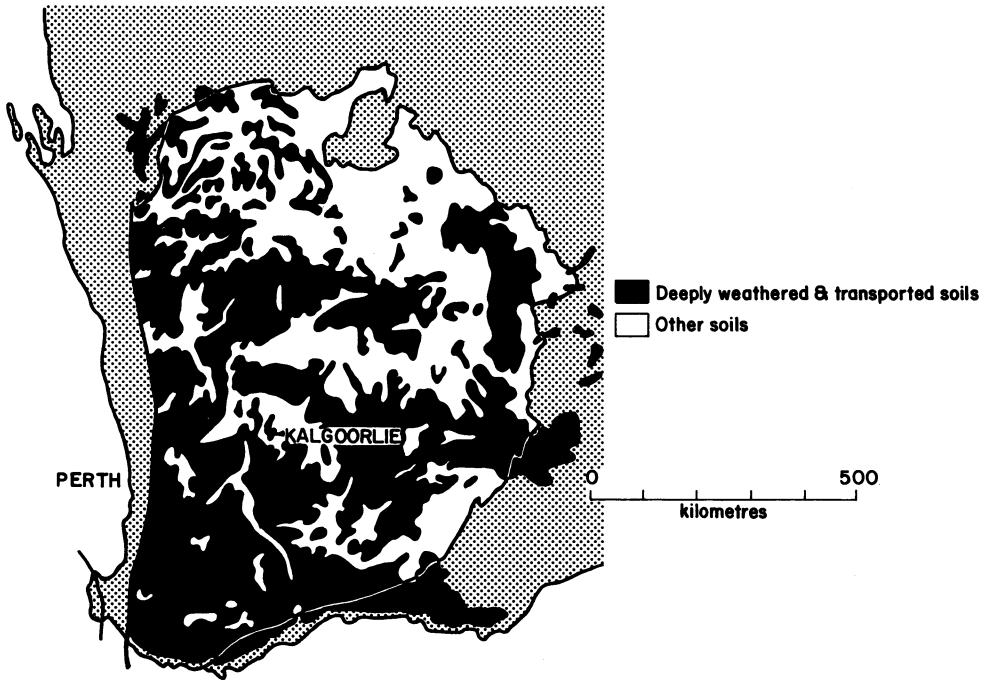

Fig. 3 Areal extent of deeply weathered and transported soils on Yilgarn Block, Western Australia

Weathering history and geomorphology

The Archaean rocks of the Yilgarn Block have been subjected to extended periods of weathering since the surface was stripped by glaciation in the Permian.[2,15] The results of these weathering events can be observed over wide areas today as the Yilgarn Block has only been affected by minor epeirogenic movements since the Permian glaciation, and marine incursions have only occurred over the southern and southeastern margins of the Yilgarn Block.

The warm and humid climates from the early Cretaceous to the late Eocene produced deeply weathered profiles on the gently undulating surface left after glaciation. The drainage systems were predominantly west to the Indian Ocean and east and southeast to the ancient Great Australian Bight.[1] These were active prior to the rifting of the Antarctic and the Australian continents, which was well advanced by the mid-Eocene. Some of these drainages probably formed on pre-existing glacial valleys. From stratigraphic evidence[1] external flow from the major continental drainage systems diminished in the late Eocene and had ceased altogether by the late Miocene. The courses of these ancient drainages are still discernible today as broad valleys and they are also marked by chains of playa lakes and salinas, as well as by deposits of calcretes and terrestrial limestones.

chromite, magnetite, rutile, ilmenite and zircon.[18] Profiles dominated by kaolinite, quartz and secondary silica minerals have developed over granitoids, whereas secondary iron minerals have more prominence in profiles developed on greenstones. Iron and manganese oxides have concentrated at the ancient water-table (Fig. 5) and are indicative of climatic fluctuations that produced oxidizing and reducing conditions that favoured concretionary deposition. On the more felsic rocks of the layered greenstone sequences only incipient ferruginous layers developed as a consequence of their lower initial iron content. Also, the low aluminium content of olivine-rich ultramafic rocks inhibited the formation of clay minerals during weathering[19] and silica from these rocks was deposited as cristobalite, tridymite and opaline silica. Lag deposits of secondary forms of silica are usually obvious on eroded laterite surfaces over olivine-rich ultramafic rocks.

Longer-term cycles in climate caused induration of ferruginous zones during arid phases[16] and weak ferrruginous zones formed at the newly established water-tables at lower levels in the original saprolite zone of some weathered profiles.[18] With the subsequent return of humid conditions the indurated layers were able to resist erosional forces and an etched land surface developed.[2,20] The lower clay-rich horizons of the weathered profiles were exposed at breakaways (Fig. 4) and the erosional

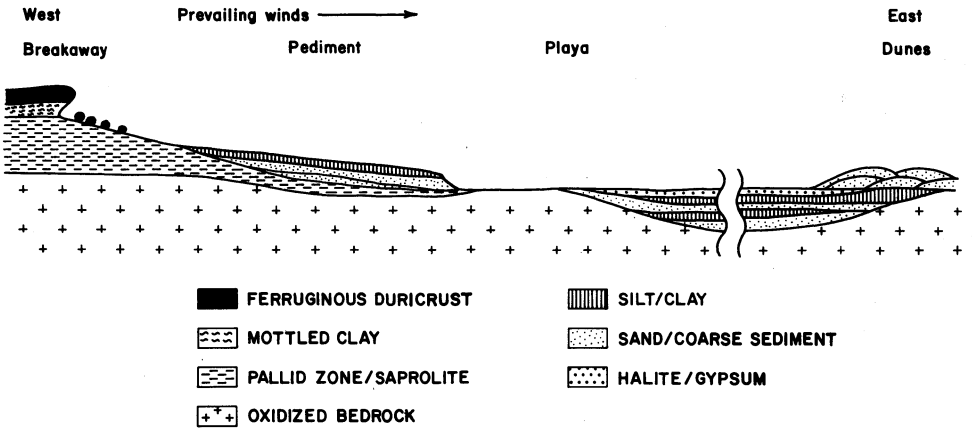

Fig. 4 Simplified geomorphology of deeply weathered and partly eroded surface of Yilgarn Block, Western Australia

The palaeo-weathering front generally parallels the ancient land surface, which has been partly eroded and partly obscured by the deposition of erosional products[16,17] (Fig. 4). There can be considerable local variation in the depth of weathering as a result of lithological differences. Within the greenstone belts such sediments as cherts and iron formations stand out as pronounced ridges. Metamorphosed rocks—for example, serpentinites and talc carbonate rocks—are also resistant to weathering. As a general feature, however, the greenstones have been weathered to a greater extent than the granitic plutons: often, therefore, the areas of weathered granitoids have a slightly higher relief than that of the surrounding greenstones.[16]

Water-tables were close to the surface (Fig. 5) during the warm and humid climatic phases and leaching was intense. In the present arid climate water-tables are much lower than when the laterite profiles were forming during the humid phases and are generally at the level of the original saprolite zone (Fig. 5). The term 'laterite' is used in many contexts in the literature: here it is used in reference to a complete profile of strongly leached material. As the laterite profiles formed, soluble elements were transported out of the profiles and there was a relative enrichment of such less soluble elements as Fe, Al, Si and Mn as secondary minerals and of such resistant minerals as

products were deposited on pediments. In the interior of the continent most of the weakly indurated and deeply weathered profiles that developed on granitoids have been severely eroded and many of the products are present today as aeolian deposits.[16] These obscure a significant proportion of the lithologies of inland areas. By contrast, in areas of granitoids nearer to the coast—for example, the Darling Ranges—weathered profiles are largely intact.[21] These profiles are usually shallower than the few remnant intact profiles of the interior and the changes in the depth of weathering of these near-coastal profiles are broadly related to present-day climatic patterns.[1] Thus, by inference, these profiles are more recent than those of the interior.

The gradual onset of arid conditions from the late Eocene produced pervasive deposition of silica from groundwater.[16,18,22] The slowing in the lateral movement of groundwater caused by the lowering of relief by erosional processes during the humid phases was accentuated by the diminishing rainfall. The silica-rich layers became indurated as the arid conditions became more severe. Deposition of silica was favoured in coarse sediments in the lower parts of drainage channels. Some of these indurated silica-rich layers were exposed by later erosional events. These silicified layers may be massive and up to 5 m in thickness.[16] Silica-cemented hardpans of more recent

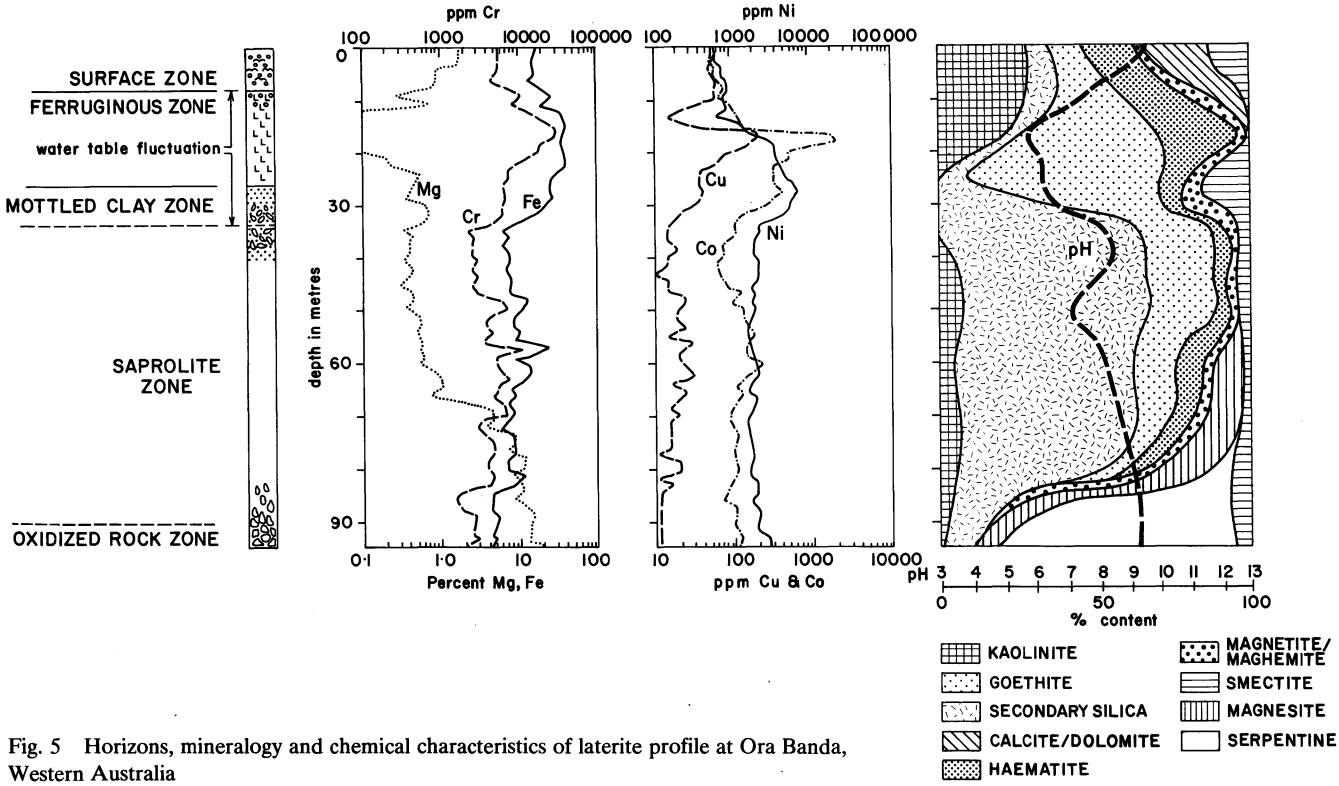

Fig. 5 Horizons, mineralogy and chemical characteristics of laterite profile at Ora Banda, Western Australia

origin such as the Wiluna hardpan[23,24] have also formed over some parts of the Yilgarn Block. These hardpans are usually less than 0.5 m in thickness and their formation is related to cyclical inundation and desiccation.

Thus, the geomorphology of the Yilgarn Block is the product of many factors that have been operative during a weathering history of more than 100 m.y. An understanding of these factors is essential for geochemists engaged in the search for nickel sulphides in Western Australia.

Mineralogy and geochemistry of a laterite profile formed on ultramafic rocks

The main mineralogical and geochemical features of a laterite profile formed on ultramafic rocks of the Yilgarn Block are discussed briefly, a high proportion of the area of nickel sulphide potential being covered by such material[10] (Fig. 3). The horizons, mineralogical and geochemical characteristics of a laterite profile formed on ultramafic rocks at Ora Banda are shown in Fig. 5. The depth of weathered profiles varies considerably and is usually greatest on olivine-rich rocks, sometimes exceeding 100 m on these types.

Weathered bedrock and saprolite horizons

The boundary between these two horizons is gradational. In the saprolite zone of the example (Fig. 5) serpentine minerals have been weathered to secondary silica, smectite (mostly nontronite), kaolinite and goethite. The aluminium content of the serpentinite is less than 0.5% and the formation of kaolinite and smectite has been inhibited.[19] Silica has deposited mainly as chalcedony and opaline silica, some magnesium having deposited as magnesite. The increase in silica concentration in the saprolite zone is absolute owing to contributions from overlying horizons.

The concentration of magnesium shows a marked depletion through the saprolite zone, whereas nickel remains steady and copper shows an increase. Nickel and copper have been incorporated into a variety of minerals in this horizon. Nickel can replace magnesium in serpentine minerals and smectites and may also be combined in goethite and some of the chlorites.[18,19,25,26,27] Copper has a stronger affinity for goethite than serpentine.[18] Magnetite and chromite are residual.

Mottled clay horizon

The mottled clay horizon varies considerably in thickness and may even be absent. The boundary with the saprolite zone is gradational and the horizon is visually distinct as a result of the mottling caused by the differences in the oxidation states of iron. The horizon is also marked by the absence of any pseudomorphing of the original rock-forming minerals by the textures of the clay aggregates. Serpentine and magnesite have been completely weathered from this horizon and there is an increase in goethite and smectite contents and a marked decrease in secondary silica content toward the top of the horizon. The alternating oxidizing and reducing conditions in the mottled clay zone caused precipitation and solution of iron and manganese oxides and these conditions were conducive to the coprecipitation of nickel and copper, as well as trace elements such as cobalt, and zinc.[28-32] These elements are also combined in smectite in this horizon. Manganese oxides are particularly efficient collectors and have highly specific reactions with cobalt.[28] High values of Co and Ni have been reported from electron-microprobe analyses of manganese nodules[26] (K. Norrish, personal communication). The leaching and concentration of nickel and copper in laterite profiles make the assessment of geochemical data difficult in the absence of information on both the horizon and the nature of the material sampled.

Ferruginous horizon

The boundary between the mottled clay horizon and this horizon is sharp. The increase in iron and aluminium contents follows in response to losses of mobile components. The lower part of this horizon is often friable and dominated by disordered goethite. These goethites have a high aluminium content[8,33] and high surface areas, so they are important sinks for trace metals.[34] The stronger affinity of copper for goethite in comparison to nickel[6,9,18] is reflected in Fig. 5. Copper values peak at a higher level of the horizon than those of nickel. In the upper parts of the ferruginous horizon the goethite crystal structure is more ordered[8] (K. Norrish, personal communication). Impurity elements have been expelled from the crystal lattices of the

iron oxides and trace metals lost from the horizon. Some of the liberated aluminium has been incorporated in kaolinite. Kaolinite crystals are commonly finely intergrown with goethite in this horizon.[8,26] Hematite has formed in the upper levels of the ferruginous horizon by dehydrolysis of goethite, and chromite and magnetite contents have remained relatively constant despite absolute losses during weathering. The near-surface section of this horizon exhibits some modifications as a result of arid climates subsequent to the warm and humid climates that were responsible for lateritization.[18] Carbonates have formed coatings on soil aggregates and nodules. Carbonate was initially deposited at the surface by deflation from playas, and the clays of colluvial veneers were mostly transported during intermittent periods of high rainfall that have occurred mainly as summer thunderstorms.

pH profile

The pH values show a steady decrease through the saprolite zone from the oxidized rock zone with perturbations at the lower limit of the ancient water-table owing to fluctuating oxidizing and reducing conditions[8,18] (Fig. 5). Higher in the profile the pH drops sharply as a result of the prolonged leaching, whereas closer to the surface the pH increases again because of carbonates. At the surface the pH is poised between pH 8 and 9 by carbonate–bicarbonate buffering.

Accounting for weathering

Observations on nature and field relationships of material collected during routine surface-sampling programmes

The geomorphology of an area that is to be explored for nickel sulphides by use of geochemical techniques requires careful assessment. The landform units that can be reliably tested by surface sampling need to be defined precisely. This is usually carried out by use of colour air photography. Infrared photography can accentuate spectral differences of surface cover. The area over which surface geochemistry may be usefully applied can be extended by subdividing analytical data according to soil type. The value of this technique was demonstrated at the Digger Rocks prospect at Forrestania.[35] Three soil types were defined and the analytical data for nickel and copper from samples taken at a depth of 0.5 m with a hand auger were subdivided accordingly. Within each data set of soil type four different populations of nickel and copper were defined by statistical analysis. The results (Fig. 6) improved the definition of the mineralized zone by eliminating variations in element dispersion caused by differences in soil type.

The usefulness of surface geochemistry may also be extended by taking into account the concentrating effects that are produced by the coprecipitation of elements with iron and manganese oxides. Correction may be achieved by plotting the divergence of the value of a particular element in each sample from that predicted by regression analysis of all the sample results for the same element versus iron and manganese content.

The effect of iron content on element concentration is erratic for samples that contain $<5\%$ iron. At higher percentages it is found that the line of best fit is often curvilinear, the element values tending toward a plateau with increase in iron content. For samples in the lower range of iron concentrations a higher proportion of the total iron is present as coatings on other soil minerals rather than as discrete iron oxides. These surface coatings are more effective adsorbers than the discrete forms of the iron oxides and, thus, the efficiency of adsorption decreases with increase in iron content.

Subsurface sampling in areas covered by intact laterite profiles and transported materials

When drill samples are taken from these areas complete information is required on texture and mineralogy owing to the depletion and concentration of elements within different horizons of a laterite profile (Fig. 5). As a general rule samples have to be taken from at least the saprolite zone so that valid assessments can be made of the data. Element values may, however, be considerably depleted in the upper part of the saprolite zone. Thus, the reliability of the assessment of element data increases with depth, but there are concomitant increases in the cost of sampling. Therefore exploration programmes in deeply weathered terrain have to be a compromise of several factors.

The secondary haloes of nickel and copper dispersed from the sheet-like bodies of nickel sulphide mineralization on basal contacts are usually of limited dimensions. At East Scotia, northeast of Kalgoorlie, the halo for copper was only 10 m across strike, whereas that for nickel was 20 m.[18] In practice geochemical drill-holes are usually spaced at 20 m across strike and 200 m along strike when lateritized terrain is being explored. This spacing also takes into account the minimum size for a viable ore position under normal economic conditions applicable to Western Australia. Significant economies can be gained by accurately placing drill traverses, thereby limiting the number of holes that are required to straddle the basal contact of an ultramafic sequence. Drill traverses are usually sited from an interpretation of magnetic data and the locations may be confirmed by use of the geochemical signatures of the parent rocks in the drill samples when definite mineralogical or textural evidence has been obliterated by weathering. Drilling costs can also be contained by developing skills in data assessment to allow recognition of the subtle anomalies of mineralization in strongly weathered material as high as possible in the saprolite zone.

Multivariate analysis of element data

Facilities for the simultaneous analysis of several elements in a single sample are becoming more readily available, particularly with the advent of the plasma-source optical emission spectrograph. Few geochemists, however, fully exploit the opportunity to utilize multi-element data on samples—a notable failure on the part of those who are involved in assessing data from strongly weathered terrain. The comments that were made by Marshall in 1970 on the lack of application of the geostatistical approach to geochemical exploration are still relevant nearly one and a half decades later.[36]

In exploration most gossanous samples are screened by analysis of microtextures by use of polished sections. Many samples of gossanous appearance in hand specimen, however, have their microtextures partly or completely obliterated by the growth of secondary minerals. Thus, the relationship of these samples to mineralization from polished sections is often ambiguous and multi-element data may be used as the key to their significance. Empirical subdivisions of various combinations and ratios of analytical data for Cu, Ni, Zn, Pb, Mn and Cr have been used to distinguish true from false gossans.[37] Principal component analysis has also been applied to the same data[38] and 42% of the variability could be accounted for by a factor almost wholly dependent on Ni and Cu values, an additional 26% of the variability being accounted for by a factor determined mainly by Cr values. This method of separating gossans from non-gossans was simplified for field use by devising log/log plots of Cr versus Cu × Ni showing the fields of significance. Also, true and false gossans have been successfully classified by use of a triangular diagram of Ni, Cu and Zn concentrations.[39] Discriminant function analysis has also been applied to gossanous material and data for Ni, Cu, Co, Cr and Zn on samples of known parentage have been used.[40] Six subdivisions were created for sample parentage and a graphical classification was then devised for samples of unknown origin. The use of multivariate analysis is of considerable benefit when large numbers

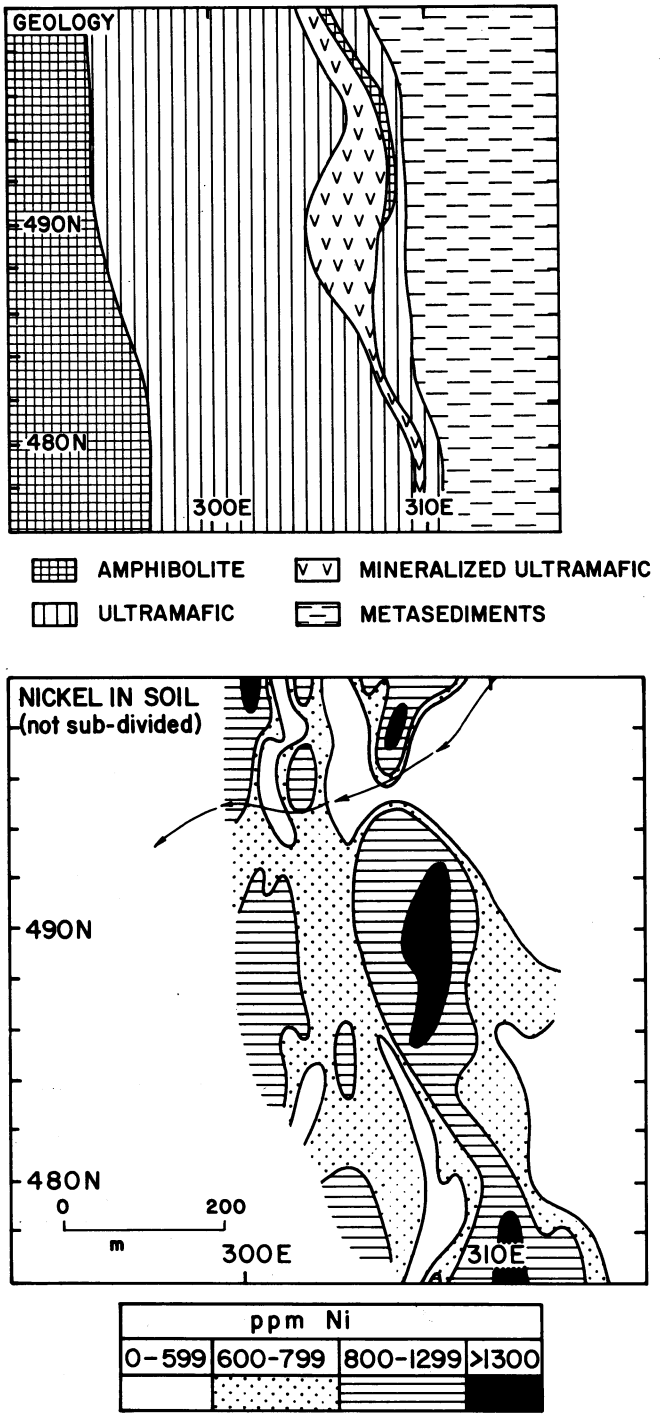

Fig. 6 Soil types and Ni and Cu contours of Digger Rocks prospect, Western Australia. From Leggo and McKay[35]

of samples have to be screened and the significance of borderline cases can be defined by such other techniques as textural analysis or analysis of pathfinder elements.

Pathfinders

Copper

Copper as chalcopyrite is associated with the various styles of nickel sulphide mineralization.[13] Copper is particularly valuable as a pathfinder and commonly used because analysis is simple—in contrast to analysis of the other pathfinder elements discussed below. Also, copper is strongly bound by iron oxides[30,31] and is thus retained well up into the weathering zone (Fig. 5).

Platinum group metals

The platinum group metals (PGM) are combined in nickel sulphide mineralization at the ppb level of concentration.[41] Analysis is usually carried out by neutron activation analysis (NAA) after preconcentration by fire assay. Pairs of the PGM of contrasting chemistry, such as Pd and Ir, are usually analysed to overcome variability as a result of fractionating effects at the time of emplacement of nickel sulphide mineralization, possible redistribution during metamorphism or fractionation during weathering.[42] The PGM may exist in primary form as discrete mineral phases and concentrations vary considerably in

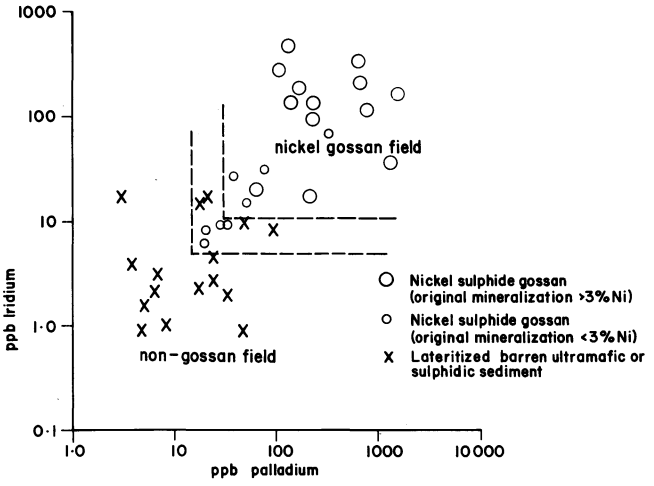

Fig. 7 Iridium and palladium values for nickel gossans, lateritized barren ultramafic rocks and sulphidic sediments with ambiguous nickel and copper geochemistry. From Travis and co-workers[42]

nickel sulphide deposits. A broad relationship can, however, be recognized between Ir concentration and the Ni grade of a deposit[41,42] (Fig. 7). The PGM are inert in the weathering zone as is demonstrated by the maintenance of concentrations in Si-enriched horizons, which are the zones of intense leaching[9,42] and also by the relative concentration of PGM in the ferruginous zone of laterite profiles.[42,43] Thus, gossanous samples that cannot be classified on the basis of their nickel and copper geochemistry can often be evaluated successfully by consideration of their Pd and Ir values[42] (Fig. 7). The value of PGM as pathfinders has also been demonstrated by other workers.[9,39] Despite these encouraging results, the analysis of PGM in gossanous samples is not commonly used in geochemical programmes in Western Australia because of constraints of cost and availability of analytical services.

Selenium

Selenium is of interest because of its association with sulphides[44] and its relative immobility during weathering. Anomalous selenium is only indicative of the presence of sulphides and is not definitive for nickel sulphide mineralization. Selenium combines with iron during weathering[43] and concentrates in the ferruginous zone of laterites. Selenium values of 10–20 ppm have been reported for nickel gossans and values of <2 ppm for ferruginous material of gossanous appearance from barren environments.[39]

Tellurium

Tellurium is also often associated with sulphides. Tellurides are inert in the weathering zone.[45] A range of 0.15–10 ppm Te has been reported for nickel sulphide gossans and 0.005–0.10 ppm Te for non-gossan samples.[40]

Conclusions

The high proportion of weathered and transported cover over potentially mineralized ground of the Yilgarn Block of Western Australia poses a considerable challenge for exploration geochemistry in the search for nickel sulphides. Recent studies have gone a long way towards increasing our understanding of the geomorphology, mineralogy and chemistry of this cover and further studies of these subjects will ensure that the best possible use is made of exploration resources. The improvements in the availability and ease of manipulation of multivariate data will undoubtedly bring rewards, and similar rewards could be available from a wider use of pathfinder techniques, particularly those which involve the PGM.

References

1. Van de Graaff W. J. E. *et al.* Relict early Cainozoic drainages in arid Western Australia. *Z. Geomorph.*, **21,** 1977, 379–400.
2. Finkl C. W. Jr. and Fairbridge R. W. Paleogeographic evolution of a rifted cratonic margin: S.W. Australia. *Palaeogeogr. Palaeoclim. Palaeoecology,* **26,** 1979, 221–52.
3. Mulcahy M. J. Landscapes, laterites and soils in southwestern Australia. In *Landform studies from Australia and New Guinea* Jennings J. N. and Mabbutt J. A. eds (Canberra: Australian National University Press, 1967), 211–30.
4. Mulcahy M. J. Churchward H. M. and Dimmock G. M. Landforms and soils on an uplifted peneplain in the Darling Range, Western Australia. *Aust. J. Soil Res.*, **10,** 1972, 1–14.
5. Nickel E. H. *et al.* Supergene alteration at the Perseverance nickel deposit, Agnew, Western Australia. *Econ. Geol.*, **72,** 1977, 184–203.
6. Butt C. R. M. and Sheppy N. R. Geochemical exploration problems in Western Australia exemplified by the Mt. Keith area. In *Geochemical exploration 1974* Elliott I. L. and Fletcher W. K. eds (Amsterdam: Elsevier, 1975), 391–415.
7. Thornber M. R. Supergene alteration of sulphides, V. Laboratory studies on the dispersion of Ni, Cu, Co and Fe. *Chem. Geol.*, **26,** 1979, 135–49.
8. Butt C. R. M. and Nickel E. H. Mineralogy and geochemistry of the weathering of the disseminated nickel sulfide deposit at Mt. Keith, Western Australia. *Econ. Geol.*, **76,** 1981, 1736–51.
9. Wilmshurst J. R. The weathering products of nickeliferous sulphides and their associated rocks in Western Australia. Reference 6, 417–36.
10. Brodie-Hall *Sir* Laurence chairman. *Understanding the near-surface environment of the Kalgoorlie region to aid mineral exploration and water management* (Perth, W.A.: State Committee of C.S.I.R.O., 1975), 24 p.
11. Williams I. R. Structural subdivision of the Eastern Goldfields Province, Yilgarn Block, Western Australia. *Ann. Rep. geol. Surv. West. Aust. 1973,* 1974, 53–9.
12. Gee R. D. Regional geology of the Archaean nuclei of the Western Australian Shield. In *Economic geology of Australia and Papua New Guinea 1. Metals* Knight C. L. ed. (Parkville, Victoria: Australasian Institute of Mining and Metallurgy, 1975), 43–55. (*Monograph series* no. 5)
13. Marston R. J. *et al.* Nickel sulfide deposits in Western Australia: a review. *Econ. Geol.*, **76,** 1981, 1330–63.
14. Kemp E. M. Tertiary climatic evolution and vegetation history in the southeast Indian Ocean region. *Palaeogeogr. Palaeoclim. Palaeoecology,* **24,** 1978, 169–208.
15. Playford P. E. Cope R. N. and Cockbain A. E. Palaeogeographic development of Western Australia. Phanerozoic. In *The geology of Western Australia. Mem. geol. Surv. West. Aust.* 2, 1975, 451–60.
16. Mabbutt J. A. Weathering history and landform development. In *Conceptual models in exploration geochemistry* Butt C. R. M. and Smith R. E. eds. *Special Issue J. geochem. Explor.*, **12,** 1980, 96–116.
17. Butt C. R. M. The nature and origin of the lateritic weathering mantle, with particular reference to Western Australia. In *Geophysical prospecting in deeply weathered terrains. Univ. West. Aust. Geol. Dep. Extension Service Publ.* no. 6, 1981, 11–29.
18. Smith B. H. Some aspects of the use of geochemistry in the search for nickel sulphides in lateritic terrain in Western Australia. *J. geochem. Explor.*, **8,** 1977, 259–81.
19. Fardon R. S. H. The genesis of lateritic nickel deposits. Ph.D. thesis, Harvard University., 1967, 132p.
20. Finkl C. W. Jr. and Churchward H. M. The etched land surfaces of southwestern Australia. *J. geol. Soc. Aust.*, **20,** 1973, 295–307.
21. Davy R. A study of laterite profiles in relation to bed rock in the Darling Range near Perth, W.A. *Rep. geol. Surv. West. Aust.* 8, 1979, 87 p.
22. Nickel E. H. and Thornber M. R. Chemical constraints on the weathering of serpentinites containing nickel–iron sulphides. *J. geochem. Explor.*, **8,** 1977, 235–45.
23. Litchfield W. H. and Mabbutt J. A. Hardpan in soils of semi-arid Western Australia. *J. Soil Sci.*, **13,** 1962, 148–59.
24. Bettenay E. and Churchward H. M. Morphology and stratigraphic relationships of the Wiluna hardpan in arid Western Australia. *J. geol. Soc. Aust.*, **21,** 1974, 73–80.
25. Canterford J. H. Nickel—some recent developments. *2. Nickel mineralogy re-examined* (Melbourne: C.S.I.R.O. Division of Mineral

Chemistry, 1974), 34 p.
26. Elias M. Donaldson M. J. and Giorgetta N. Geology, mineralogy, and chemistry of lateritic nickel–cobalt deposits near Kalgoorlie, Western Australia. *Econ. Geol.*, **76,** 1981, 1775–83.
27. Golightly J. P. Nickeliferous laterites: a general description. In *International laterite symposium* Evans D. J. I. Shoemaker R. S. and Veltman H. eds (New York: AIME, 1979), 3–23.
28. McKenzie R. M. The sorption of cobalt by manganese minerals in soils. *Aust. J. Soil Res.*, **5,** 1967, 235–46.
29. McKenzie R. M. The sorption of some heavy metals by the lower oxides of manganese. *Geoderma,* **8,** 1972, 29–35.
30. Forbes E. A. Posner A. M. and Quirk J. P. The specific adsorption of divalent Cd, Co, Cu, Pb and Zn on goethite. *J. Soil Sci.*, **27,** 1976, 154–66.
31. Grimme H. Die Adsorption von Mn, Co, Cu und Zn durch Goethit aus verdünnten Lösungen, *Z. Pflanzenernähr. Bodenkd.*, **121,** 1968, 58–65.
32. Thornber M. R. Allchurch P. D. and Nickel E. H. Variations in gossan geochemistry at the Perseverance nickel sulfide deposit, Western Australia: a descriptive and experimental study. *Econ. Geol.*, **76,** 1981, 1764–74.
33. Zeissink H. E. The mineralogy and geochemistry of a nickeliferous laterite profile (Greenvale, Queensland, Australia). *Mineral. Deposita,* **4,** 1969, 132–52.
34. Zeissink H. E. Trace element behavior in two nickeliferous laterite profiles. *Chem. Geol.*, **7,** 1971, 25–36.
35. Leggo M. D. and McKay K. G. Forrestania nickel deposits, Yilgarn Block, W. A. Reference 16, 178–83.
36. Marshall N. J. Geostatistics in geochemical exploration—a review. In *Proceedings of the second seminar on geochemical prospecting methods and techniques:* (New York: United Nations, 1970), 314–40. (*Miner. Resour. Development Series* no. 38)
37. Clema J. M. and Stevens-Hoare N. P. A method of distinguishing nickel gossans from other ironstones of the Yilgarn Shield, Western Australia. *J. geochem. Explor.*, **2,** 1973, 393–402.
38. Joyce A. S. and Clema J. M. An application of statistics to the chemical recognition of nickel gossans in the Yilgarn Block, Western Australia. *Proc. Australas. Inst. Min. Metall.* no. 252, 1974, 21–4.
39. Moeskops P. G. Yilgarn nickel gossan geochemistry—a review, with new data. *J. geochem. Explor.*, **8,** 1977, 247–58.
40. Bull A. J. and Mazzucchelli R. H. Application of discriminant analysis to the geochemical evaluation of gossans. Reference 6, 221–6.
41. Keays R. R. and Davison R. M. Palladium, iridium and gold in the ores and host rocks of nickel sulfide deposits in Western Australia. *Econ. Geol.*, **71,** 1976, 1214–28.
42. Travis G. A. Keays R. R. and Davison R. M. Palladium and iridium in the evaluation of nickel gossans in Western Australia. *Econ. Geol.*, **71,** 1976, 1229–43.
43. McGoldrick P. J. and Keays R. R. Precious and volatile metals in the Perseverance nickel deposit gossan: implications for exploration in weathered terrains. *Econ. Geol.*, **76,** 1981, 1752–63.
44. Stanton R. L. *Ore petrology* (New York: McGraw-Hill, 1972), 713 p.
45. Leutwein F. Tellurium: behavior during weathering and alteration of rocks. In *Handbook of geochemistry* Wedepohl K. H. ed. (Berlin: Springer-Verlag, 1978), **II–4,** 52–G–I.

Geological review of the Agnew nickel deposit, Western Australia

L. G. Billington B.A., M.Sc., A.M.Aus.I.M.M.
Agnew Mining Company Pty., Ltd., Leinster, Western Australia

Synopsis

The Agnew nickel deposit occurs in a major linear greenstone belt in the Archaean Eastern Goldfields Province of Western Australia, and has been subjected to mid-amphibolite facies metamorphism of dynamic style. The largest dunitic ultramafic body in the Perseverance Block is host to the bulk of the nickel mineralization. The Perseverance Ultramafic is mineralogically zoned and has an embayed western margin against a mixed metasedimentary–metavolcanic wallrock sequence.

Three categories of nickel sulphide mineralization are concentrated on this western margin at the thickest part of the ultramafic exposure. Massive sulphides characteristically occur as contact mineralization, internal mineralization and as remobilized concentrations in vein form structures.

Disseminated ore constitutes the largest volume of mineralized materials in the deposit and occurs in three separate shoots in *en-échelon* relation. Weakly mineralized 'cloud sulphide' zones surround and envelop the shoots and persist much further along strike. In the upper mine levels the shoots are truncated by a shear or crush zone, which inhibits geological knowledge to the south but marks a major fundamental structural break.

Most of the ore types have suffered supergene alteration and there is a complex variable distribution of the mineralogical facies. The ore types have been metamorphically retextured, but the oreshoots can be characterized by their Ni tenor and some chemical ratios. S/Se values, PGE and precious metal values are distinctly different from those of other nickel sulphide ores extracted.

Despite intense structural and metamorphic modification of the mineralizations, some features support an original magmatic derivation for the sulphides. These include the localization of massive sulphide ore types on one marginal contact within an embayment structure, the general distribution of disseminated mineralizations located immediately above the massive sulphides and the Ni/Cu, Ni/Co, Fe/Ni ratios of the oreshoots being similar to those of deposits that typify the intrusive dunite-associated class of nickel sulphide deposit. Varying S/Ni ratios between different shoots suggest a revision of the single magmatic intrusion model in favour of a changing composition between successive magmatic episodes.

Agnew nickel mine is situated 330 km north of Kalgoorlie, Western Australia (Fig. 1). The deposit (previously named the Perseverance nickel deposit) occurs within the same greenstone belt that also contains the Honeymoon Well and Mt Keith nickel prospects and was discovered in April, 1971, when gossanous outcrops were recognized in a favourable structure initially demarcated by aeromagnetics, geological mapping and ground magnetics.

By March, 1974, an *in-situ* geological reserve that totalled 45 000 000 t of ore at an average grade of 2.05% Ni and 0.10% Cu, and with minor cobalt, had been delineated by diamond drilling. This represents 69% of the identified Western Australian nickel resource contained within the intrusive dunite-associated class of deposit type,[25] with a grade of 1.0% or more, and Agnew mine is the first of this class to have been mined in Western Australia.

Ore production by a joint venture between Seltrust Mining Corporation Pty., Ltd., and Mount Isa Mines, Ltd., commenced in September, 1977, and has proceeded continuously since that date. To 31 December, 1982, a total of 1 564 000 t of ore at an average grade of 2.82% Ni had been delivered to a concentrator at the mine site. This ore had been extracted from the upper levels of a decline mine by mechanized cut and fill mining methods. Mining to 290-m vertical depth has concentrated on the extraction of multiple massive sulphide vein structures supplemented by lower-grade disseminated sulphide materials. Total payable nickel produced to 31 December, 1982, was 70 237 000 lb nickel metal in matte.

Regional geological setting

The Agnew Fe–Ni–Cu sulphide deposit is situated within a major greenstone belt in the Archaean Eastern Goldfields Province.[31] This Province has been subdivided into three north-trending zones[30] on the basis of rock associations and regional structural characteristics. The Norseman–Wiluna zone comprises dominantly metavolcanics and metasediments, and trends NNW from Leonora to north of Wiluna, where the greenstone belt is overlapped by Proterozoic sediments (Fig. 1). The Agnew supracrustal belt (Fig. 2) constitutes part of this zone and is characterized by relatively abundant mafic igneous rocks, minor basic volcanics, a lack of banded iron formation and large-scale NNW-trending faults and folds.[30,31]

The major structures of the Agnew area are the Agnew Anticline, the Mt White Sycline and the Leinster Anticline. Further northeast and isolated from these by an unnamed fault is the Perseverance Block (Fig. 3), which contains the Perseverance Ultramafic body and the Agnew nickel deposit (Fig. 4).

The Perseverance Block comprises five ultramafic units (Seltrust Mining Corporation data), which were each explored for economic sulphide mineralization: only the two easternmost, termed the '60A' Ultramafic and the Perseverance Ultramafic, have offered sufficient potential for the concentration of mineralization. These ultramafic units are foliated and folded in places with pervasive development of talc–carbonate and serpentine–chlorite mineralogies. Locally, the ultramafics have been interpreted to be transgressive, suggestive of intrusion,[1,17] but poor exposure and intensive surface weathering render establishment of field relationships of the units difficult. Between the '60A' fault and the Perseverance Fault the strata dip steeply west, and are considered to form the overturned limb of an anticline, based on the extrapolation of regional fold axes into this immediate area and the orientation of sulphide distribution in the ultramafic units. Attitude and displacement of the major faults are not known.

Metamorphism

The greenstone belt that extends from Leonora to Wiluna (Fig. 1) is transected by the regional metamorphic isograds, which results in considerable mineralogical variation within the ultramafic rock types from lizardite serpentinites at Wiluna to olivine–talc metadunites at Agnew (Fig. 5). Progressively deeper levels of the one host intrusion may be exposed in a

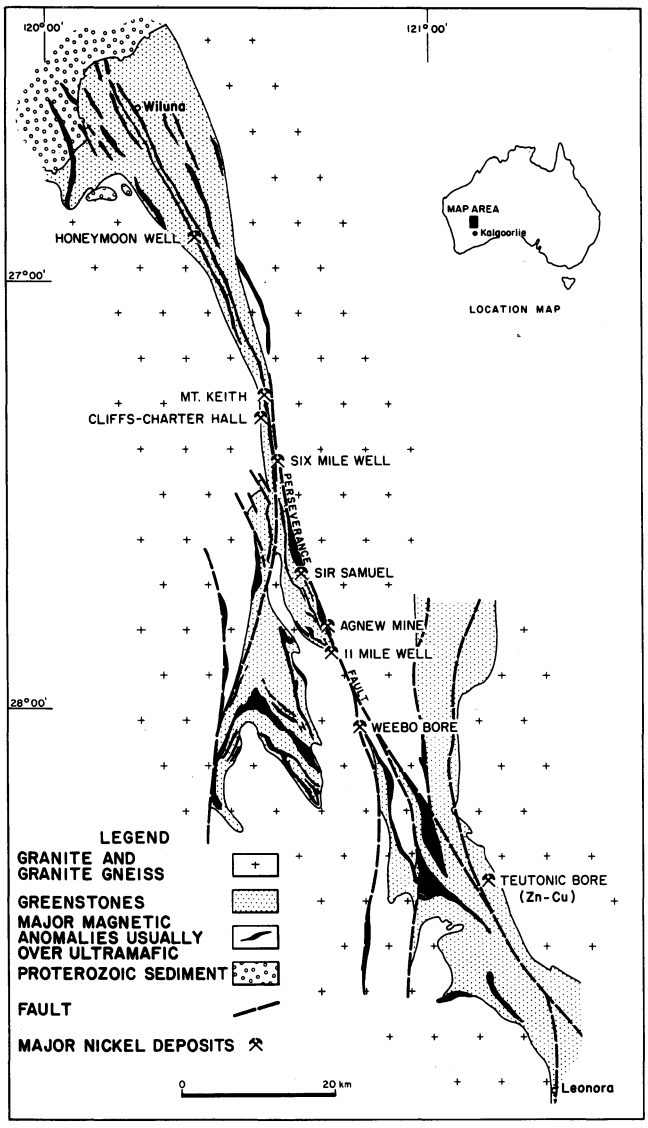

Fig. 1 Location map showing Agnew nickel mine in terms of regional geology of northern part of Leonora–Wiluna belt

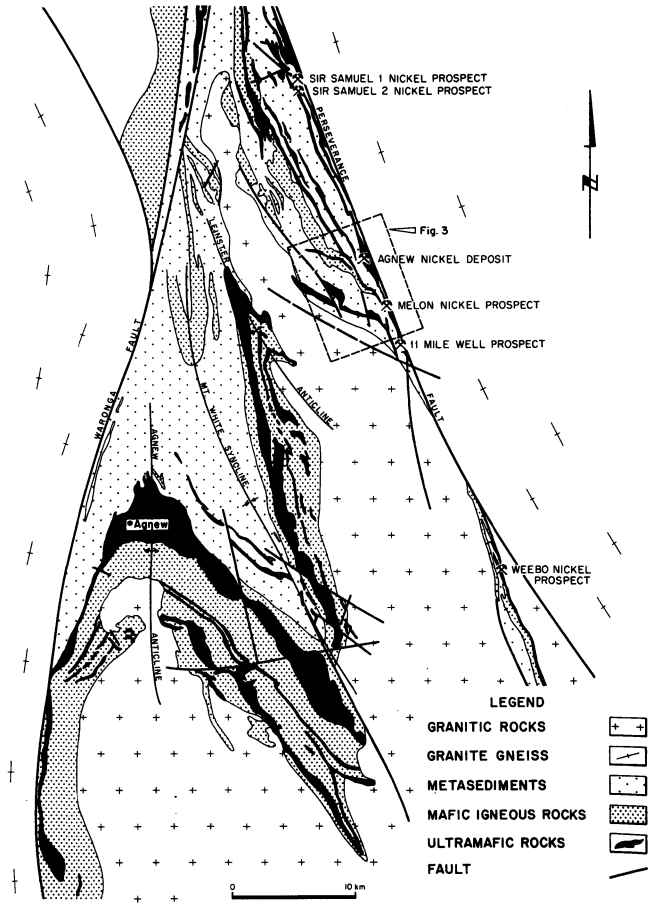

Fig. 2 Geological surface plan of Agnew supracrustal belt based on Seltrust Mining Corporation Pty., Ltd., data

southerly direction to reveal an increase in metamorphic grade from Wiluna to Agnew.[6] The regional setting of rock types that bear diagnostic mineral assemblages in the south near Agnew nickel mine suggests mid-amphibolite facies metamorphism, and peak conditions are reasonably well established at 600 ± 50°C and 3 to 5 kbar.[5]

Retrograde metamorphism has not been of significance in the evolvement of rocks in the Agnew area.

Local deposit setting

In the immediate vicinity of the Agnew nickel deposit, and between the Perseverance and '60A' faults, the stratigraphic sequence is termed the Perseverance Sequence. An informal lithological succession is recorded in Table 1 from west to east and surface distribution is illustrated in Fig. 4. The extent of this sequence to present knowledge is shown in Fig. 3. The arcuate shape of the contact between the Upper Metasediment Series and the Perseverance Ultramafic portrays at surface an east-facing embayment (Fig. 4) close to which is localized the bulk of the nickel sulphide mineralization. At this apex of the embayment the sequence has a true thickness of 1200 m, but this varies to the north and south because of the divergent orientation of the two limiting faults. The sequence exceeds 3 km in true thickness north of the Perseverance Bore (Fig. 3), where further ultramafic units enter the succession.

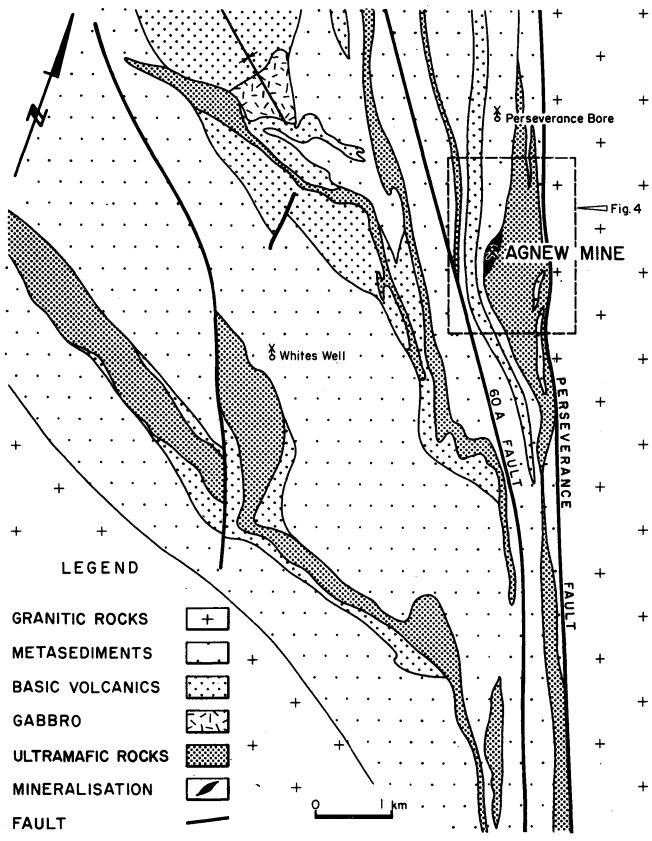

Fig. 3 Geological surface plan of Perseverance Block in vicinity of Agnew mine based on Seltrust Mining Corporation Pty., Ltd., data. Area of Fig. 3 shown in Fig. 2

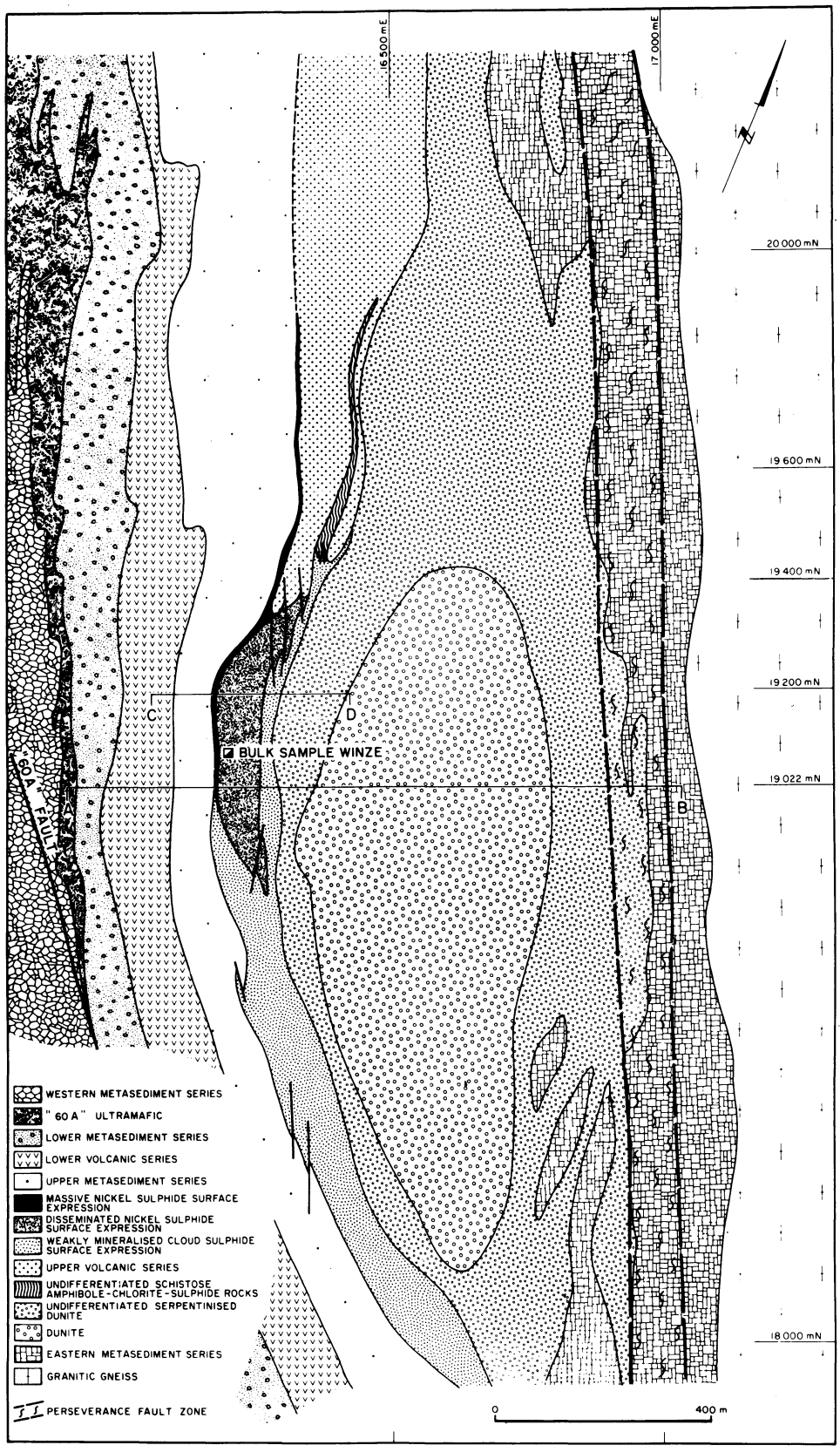

Fig. 4 Geological surface plan of Agnew embayment area based on surface mapping by Seltrust Mining Corporation Pty., Ltd., and diamond drill interpretation. Area of Fig. 4 shown in Fig. 3

Petrology of Perseverance Sequence

Perseverance Ultramafic

The Perseverance Ultramafic unit is the thickest unit in the Perseverance Sequence and is host to the bulk of the nickel sulphide mineralization. It forms an assymetric lens 10 km in length, varying in width from a few metres only at its extremities to a maximum of 800 m at its centre (Fig. 3). The eastern margin is irregular and difficult to delineate owing to much faulting and intercalation of metasediments and granitic gneiss due to the influence of the Perseverance Fault zone (Fig. 4). The western contact is arcuate (convex west) in plan, but not in cross-section at the point of convex apex (Fig. 6).

Northeast, and possibly southeast, of this embayment structure the contact with the Upper Volcanic Series and the Upper Metasediment Series is serrated and complex owing to the local

Table 1 Perseverance Sequence from west to east as identified close to Agnew nickel deposit and bounded by '60A' and Perseverance faults

Rock unit name	Thickness, m	Lithology members
Western Metasediment Series	10–500	Psammite and pelite
'60A' Ultramafic	10–130	Predominantly serpentinized ultramafic with minor talc–carbonate rock and black shale
Lower Metasediment Series	50–140	Predominantly interbedded psammite and pelite with minor basic meta-tuff
Lower Volcanic Series	0.2–130	Metagabbro, metabasalt and basic meta-tuff
Upper Metasediment Series	70–400	Predominantly interbedded psammite and pelite with minor thin felsic volcanics
Shoot 1A Massive Sulphide	0.2–8	Massive Fe–Ni–Cu sulphides with breccia fragments of wallrocks
Upper Volcanic Series	0–250	Felsic metavolcanics, thin intercalated metabasalt, cherty siliceous exhalative lenses and bedded sulphidic sediments
Perseverance Ultramafic	20–800	Dunite, serpentinized dunite and serpentinite with local concentrations of sulphide-rich zones
Eastern Metasediment Series	0–400	Psammite, felsic metavolcanics, mylonitized sediments and intercalated granitic gneiss

steeply dipping strike–slip and dip–slip faults (Fig. 4).

The thick elliptical Perseverance Ultramafic is internally comprised of concentric zones in plan of serpentinite, serpentinized dunite and talc–carbonate–serpentine derivatives that enclose an ovoid core of dunite (Fig. 4). The dunite consists of a tightly interlocked mosaic of primary magmatic subhedral, equigranular cumulate olivines, up to 1 cm in diameter, light brown in thin-section colour with colourless rims. A complete chemical analysis of the dunite is not available, but olivine composition has been reported to be Fo_{92} to Fo_{94}.[15]

An irregular enveloping transitional zone of partially serpentinized dunite with talc and carbonate separates the dunite from the serpentinized dunite. Olivine analyses of Fo_{89} to Fo_{93} have been recorded for partially serpentinized olivines of this zone,[5] but these latter values are only for colourless olivine granules of metamorphic generation.

In the upper portion of the deposit the zones of economic grade mineralization are contained within the massive serpentinite, but lower in the deposit the broader mineralized zones are distributed through the serpentinite, the serpentinized dunite and the dunite. Massive sulphide commonly occurs on the western contact with wallrocks, but where it is absent, a selvedge of higher alumina rocks, as talc–tremolite–biotite assemblages, occurs on the contact.

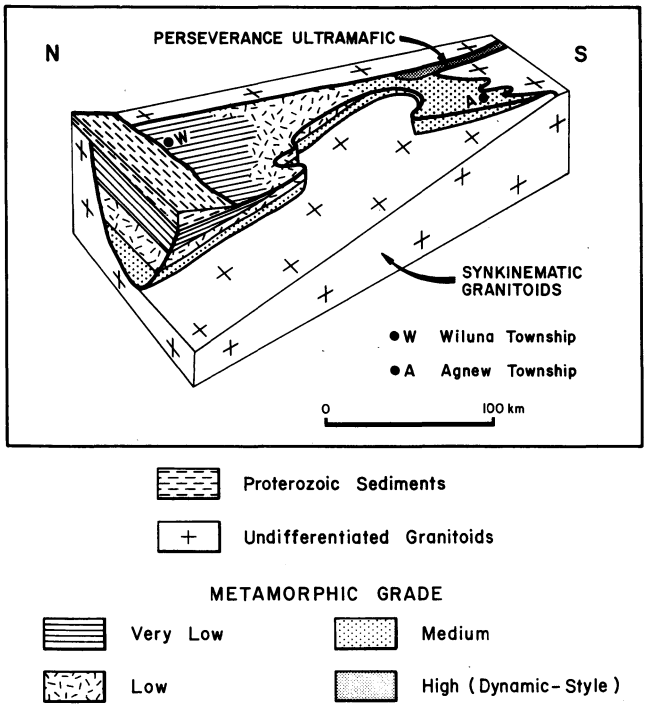

Fig. 5 Schematic block diagram (adapted from Archibald and co-workers[2]) of distribution of metamorphic facies in vicinity of Agnew mine. Published with permission of Elsevier Scientific Publishing Co.

Metasedimentary rocks

Metasedimentary rocks are represented in each of the units in the Perseverance Sequence and lithological character and proportional abundance vary both between units and within units. These variations are too diverse to consider here, but the members comprise psammite, pelite, graphitic black shales and cherts and siliceous-albitic chemical (exhalative ?) sediments that bear minor stratiform sulphides.

All of these rock types are well foliated and finely interbedded and only isolated instances of sedimentary younging features can be found in drill core. The spectrum of rock types present at Agnew is similar to that which comprises the greenstone sequences throughout the Yilgarn Block.

Metabasic rocks

Three basic volcanic rock types constitute the metabasic rocks of the sequence, and these are not only confined to the Lower and Upper Volcanic Series units of the sequence. Basic tuffs and low magnesian (0–10% MgO) metabasalts form stratabound members intercalated with the metasedimentary members. Locally intrusive metagabbroic rocks with thin contact thermal aureoles dominate the Lower Volcanic Series unit, and also occupy grossly discordant positions elsewhere in the sequence.

Felsic volcanic rocks

Metamorphosed acid volcanic rocks, the most abundant rock type in the Perseverance Sequence, occur in each of the Lower Metasediment Series, the Lower Volcanic Series, the Upper Metasediment Series, the Upper Volcanic Series and the Eastern Metasediment Series in variable proportions. They are essentially rhyolitic-dacitic acid crystal tuffs and other felsic pyroclastics.

Granitic pegmatites form discordant dykes and veins in late-formed fractures.

Types of mineralization

Three categories of nickel sulphide mineralization are distinguishable by assay within the deposit. This division into three sub-populations is confirmed by statistical analyses of assay data.[16]

The categories recognized are (1) massive sulphides with more than 4% Ni content and S/Ni ratio close to 5.0, (2) stongly disseminated sulphides, ranging from 1.0 to 3.0% Ni with S/Ni ratio close to 3.0 and (3) weakly disseminated sulphides with $<1\%$ Ni content and S/Ni ratio less than 1.8. Interfaces between these types are usually sharp and distinct.

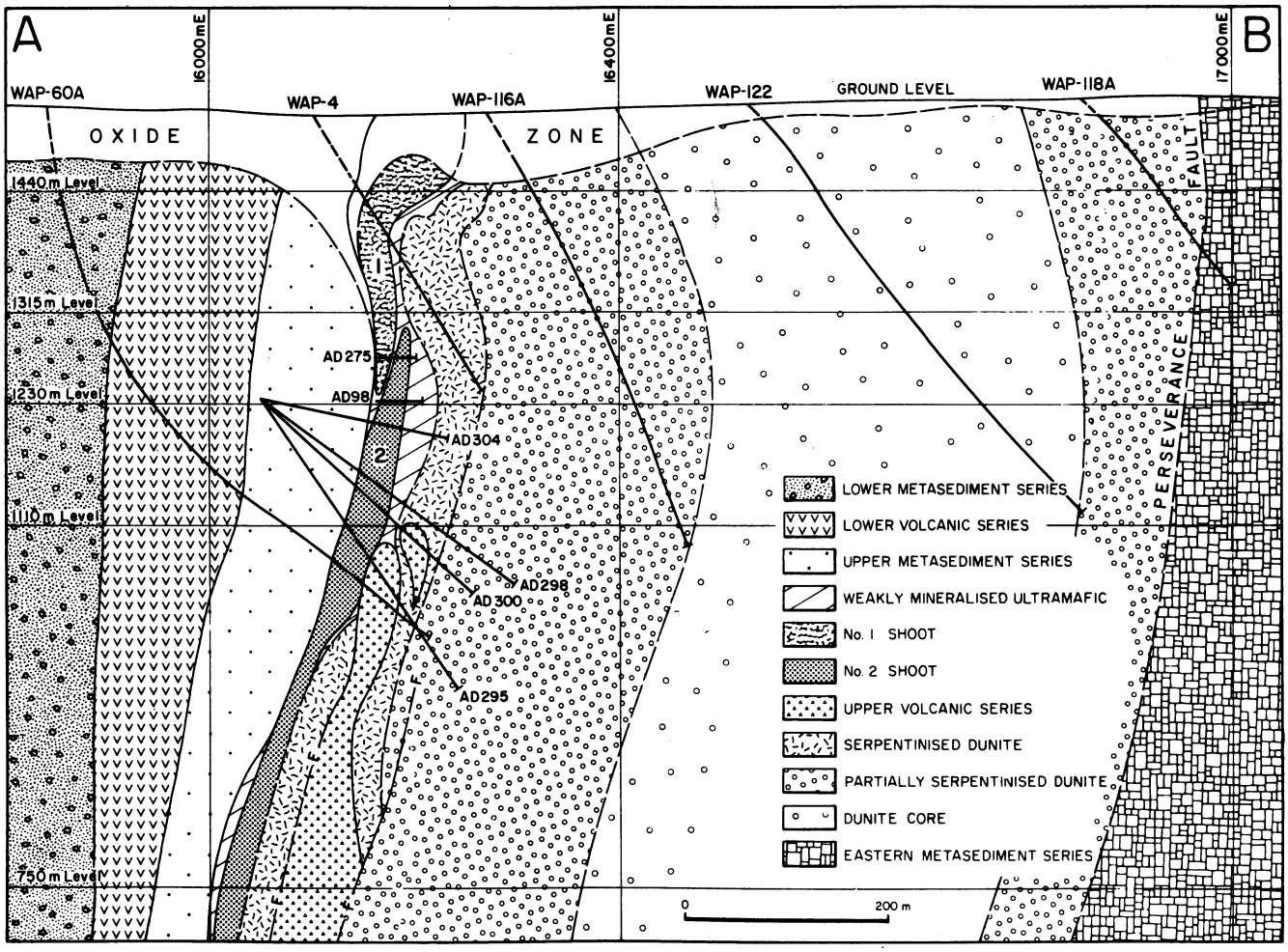

Fig. 6 East–west cross-section through Agnew mine at 19022 m N. Mine openings are not shown, for clarity, but some diamond drill paths, on which interpretation is based, are shown

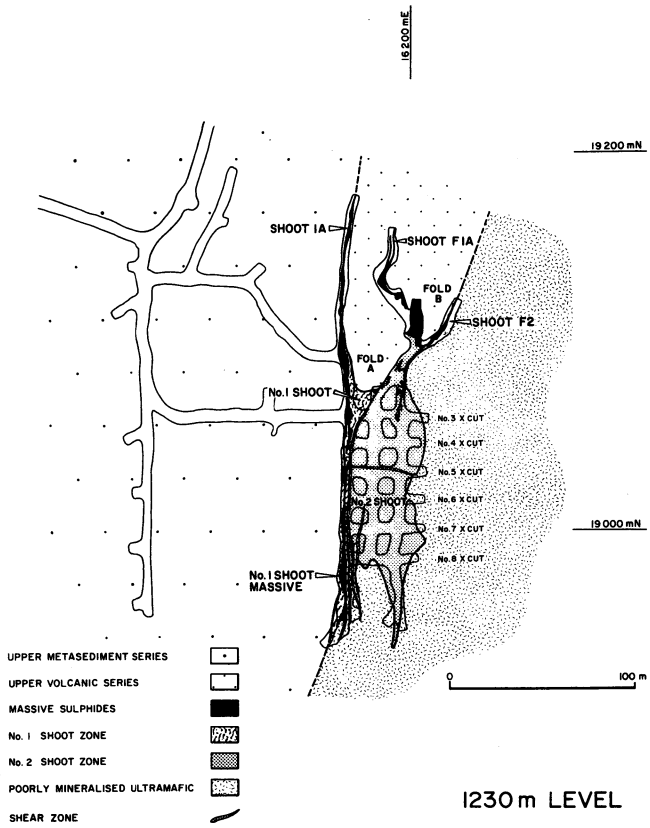

Fig. 7 Geological plan of 1230-m level, Agnew mine, based on exposures underground (shown) and diamond drill cores (not shown)

Shoot distribution

Disseminated ore

The bulk of the mineralization in the Agnew deposit is comprised of strongly disseminated sulphides, localized on the western margin of the Perseverance Ultramafic (Fig. 4). Three large, discrete, elliptical zones of strongly disseminated sulphides known as 'disseminated ore' have been outlined for the purposes of mining—No. 1 Shoot, No. 2 Shoot and No. 3 Shoot (Fig. 6).

No. 1 Shoot has surface expression above the deposit (Fig. 4) and No. 2 Shoot occurs in *en-échelon* relation to No. 1 Shoot, downdip to the east. No. 3 Shoot occurs further downdip and *en échelon* to the east, but is not present in areas of mining to date. It has an undefined lower limit and its own morphology and distribution with relationship to No. 2 Shoot are inadequately defined.

Cloud sulphides

Weakly disseminated sulphides separate and envelop the shoots, and form continuous zones along strike beyond the limits of the shoots. These persistent zones are locally referred to as 'cloud sulphide' zones (Fig. 4) and are coincident with the distribution of massive serpentinite in the upper parts of the deposit. This association is not constant throughout the deposit, however, and for clarity all further discussion of ultramafic materials outside the shoots themselves will be termed 'poorly mineralized ultramafic'.

Massive sulphide

Massive sulphide forms discrete sheets within the deposit as

either contact ore to the disseminated mineralization or vein form structures internal to the disseminated shoots and also within the wallrocks. The largest concentration of contact massive sulphide in the deposit is that named No. 1 Shoot Massive, which occurs immediately adjacent to No. 1 Shoot and the wallrocks of the Upper Metasediment Series unit (Figs. 7 and 8).

Several veins of massive sulphide named Shoot F2, Shoot F1A and Shoot 1A occur north of that body and are in most cases geologically continuous from one to the other. Thus, the change in name of a continuous massive sulphide sheet is applied at arbitrarily chosen positions. The change in name from No. 1 Shoot Massive to Shoot 1A is applied at the position where the contact massive sulphide departs from the ultramafic–metasediment contact and becomes vein form in struc-

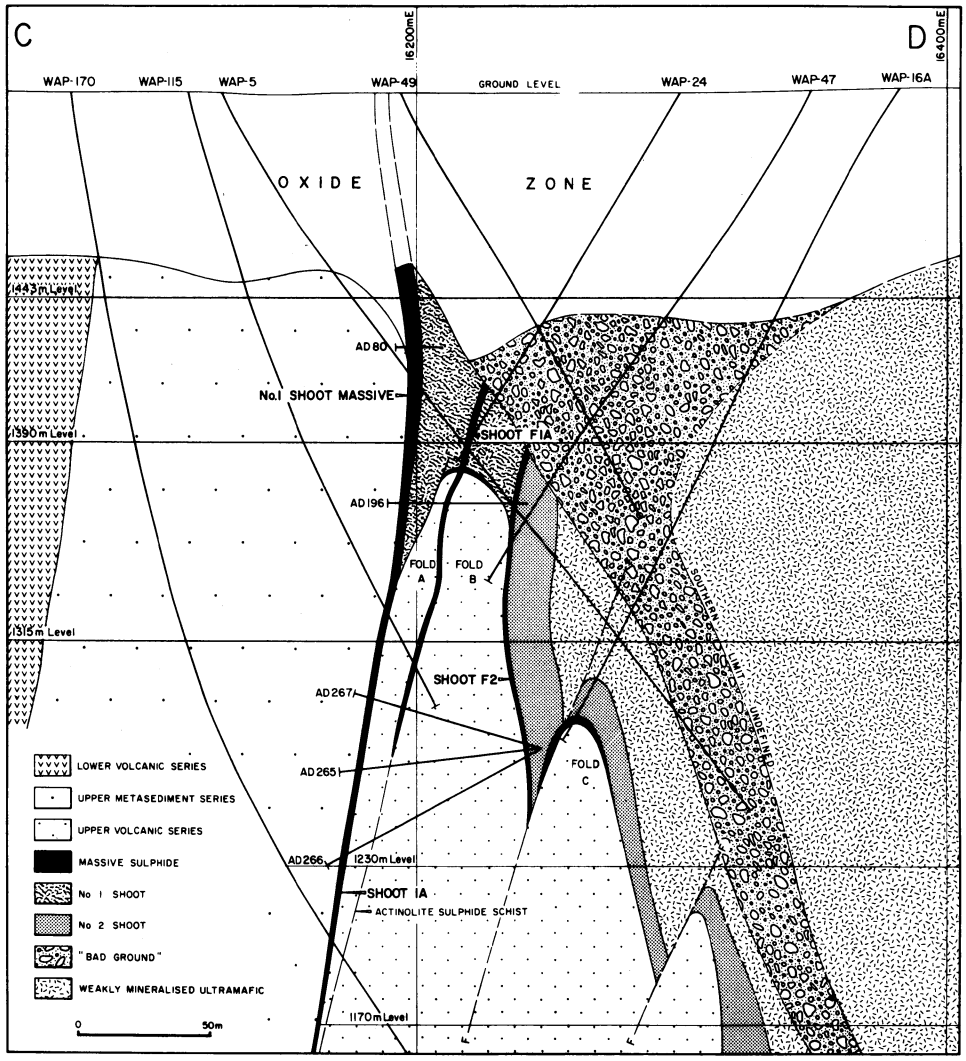

Fig. 8 East–west cross-section through Agnew mine at 19200 m N. Mine openings are not shown, for clarity, but some diamond drill paths are shown

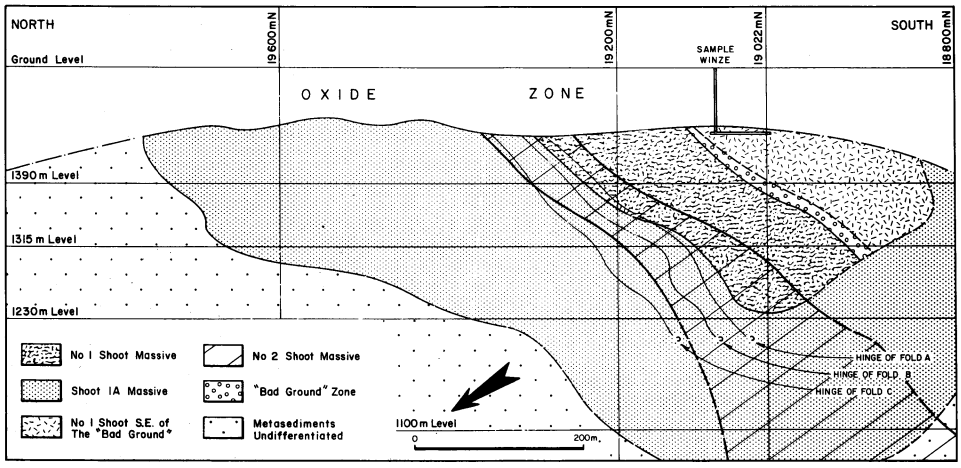

Fig. 9 North–south longitudinal section through Agnew mine at a composite position. No. 1 Shoot Massive and Shoot 1A Massive lie in same plane, but No. 2 Shoot Massive lies in a second plane east of the former. Arrowhead indicates average vector of decreasing average massive sulphide thickness in Shoot 1A only

ture, internal to the wallrocks (Fig. 7).

Some massive sulphide concentrations remain without name; one other is referred to as the *En Echelon* Vein and 'O' Shoot is a remote sheet of massive sulphide to the northeast of the disseminated shoots occurring internal to poorly mineralized ultramafic.

In-situ geological reserves of disseminated ore and massive sulphide ore to 1160-m vertical depth and a cutoff grade at the 1.0% total Ni isograd are presented in Table 2.

Table 2 Published reserves[27] of individual shoots in Agnew mine as calculated from surface diamond drilling to 1160-m vertical depth (Data for Shoot F1A, Shoot F2 and No. 1 Shoot Massive are included as No. 1 Shoot reserves and for No. 2 Shoot Massive as No. 2 Shoot; 'other' includes 'O' Shoot and those sulphide concentrations without name)

Shoot name	t×10⁶	Ni,%	Cu,%
Shoot 1A	1.7	4.36	0.18
No. 1 Shoot	7.5	2.22	0.11
No. 2 Shoot	19.3	1.92	0.09
No. 3 Shoot	16.1	1.89	0.10
Other	0.6	1.45	0.08
Total/average	45.2	2.05	0.10

Deposit structure

Massive sulphide shoots

Shoot 1A is the most extensive vein form mineralization in the deposit. It occupies a concordant position within the stratigraphic succession (Table 1) and diamond drilling has indicated that this unit extends in excess of 600 m along strike north of its junction with No. 1 Shoot Massive, and beyond the limit of that body in depth (Fig. 9). Shallow rotary drilling from surface indicates anomalous geochemistry further north still at the along-strike position.

Massive sulphide thicknesses in Shoot 1A vary considerably over short distances, exhibiting a highly variable distribution in plan. Local pinch and swell produces sulphide thicknesses of between 0 and 12 m. On a gross scale the average massive sulphide thickness appears to decrease with increased distance from the ultramafic body. The arrowhead in Fig. 9 indicates the average vector of decreasing massive sulphide thickness in Shoot 1A. Shoot 1A is offset by local faulting in some places, and in one position the massive sulphide shows a repetition in *en-échelon* arrangement, with no evidence of faulting.

The greatest concentrations of massive sulphide ore type occur at the junctions of planes of contact mineralization with planes of vein form mineralization. These are most commonly positions of structural dilatation at the hinge positions of fold crests in the adjacent wallrock. Three fold crests (folds *A*, *B* and *C*, Figs. 7, 8 and 9) are present above the 1230-m level and bear massive sulphide concentrations in the hinge position. All three folds plunge southerly at variable, undulating plunge angles, but they maintain a general sub-parallel attitude, which is similar to that of the limits to contact mineralization (Fig. 9). Massive sulphides continue down plunge in these dilatant zones, but vary in shape and thickness from level to level in areas mined to date.

Shoot F1A and Shoot F2 are massive sulphide concentrations in contact positions involved with complex structural dislocation and modification. The relationship between Shoot 1A, Shoot F1A, Shoot F2 and No. 1 Shoot Massive is sufficiently complex that on each of five mine levels exposed to date the distribution of these units has been different.

No 1 Shoot

The No. 1 Shoot zone is the predominant disseminated ore in the upper mine levels. It occurs immediately adjacent to the northwest ultramafic contact with wallrocks, and has a maximum horizontal width of 50 m at its top, where it is truncated by surface. The shoot tapers in width to a few metres at a depth of 290 m below surface (1230-m level), where contact and internal massive sulphide become proportionately more abundant (Fig. 7).

The northwest ultramafic contact of No. 1 Shoot, which dips southeast on average, is disrupted and serrated in the upper mine levels by a sub-parallel series of northwest–southeast-orientated dip-slip faults (Fig. 4). These structural dislocations have produced a complex distribution and pattern of massive sulphide internal to the disseminated ore.

Footwall shear

At the 1230-m level the No. 1 Shoot and No. 2 Shoot zones come into contact, at their point of overlap, and a prominent north–south-orientated shear plane ('the Footwall Shear') marks their separation. Other significant shears occur in both longitudinal and transverse orientation at this and other levels, but 'the Footwall Shear' is a major sub-vertical handicap to mining activities.

No. 2 Shoot

The area of disseminated ore available for mining is greatest in the lowermost of the levels exposed to date (1230-m level, Fig. 7), where the No. 2 Shoot is well defined as a broad ellipse in plan abutting the base of No. 1 Shoot. Some massive sulphides occur irregularly internally to the disseminated ore of No. 2 Shoot, but these are not as volumetrically important as those in contact or vein positions.

The area of disseminated ore amenable to extraction decreases with each successive higher level in the mine as a result of the progressive encroachment of the 'bad ground' zone upon the shoots.

Bad ground

The 'bad ground' is a prominent structural zone in the upper mine levels intersected on all developed levels other than the 1230-m level (Fig. 8). It has a sharp contact with the 'disseminated ore' of the shoots, which dips shallowly southeast, and it has an undefined width or lateral extent. The zone has not been fully breached by mining or drill-hole intersections and its southern limit is undefined, other than to know that the bulk sample winze (Fig. 9) is in unaltered mineralized (No. 1 Shoot?) ultramafic-hosted material.

The 'bad ground' is comprised of brecciated white quartz, grey quartz, chalcedony and pale green silicified ultramafic fragments cemented by red-brown-yellow iron oxide–clay based matrix. The brecciation varies in intensity and any pre-existing fabric is totally obliterated. The 'bad ground' resembles a crush or shear zone fill and the material creates mining and metallurgical problems. The zone bears some high Ni contents, which are manifest as millerite, polydymite and other secondary nickel-enriched species.

Ore mineralogy zonation

The distinct vertical sulphide mineral zonation within the deposit is related to weathering and processes of secondary supergene alteration. Distinguishable zones classified after Nickel *et al.*[20] as also recognized at Kambalda[19] are:

ca 0– 50 m in vertical depth	Oxide zones; base coincident with water-table
ca 50–200 m in vertical depth	Violarite–pyrite zone; irregular base

ca 200–400 m in vertical depth	Transition zone; irregular base
Below *ca* 400 m in vertical depth	Primary zone

Boundaries between these zones are gradational and very irregular, particularly in the instance of the oxide zone, because water has percolated down shears and fractures, which localized resultant deep oxidation and silicification. Supergene alteration of the primary sulphides is extensive and the mineralogical changes involve complex chemistry. Mineralogical changes between one zone and another, although irregularly developed, are broadly consistent with an increase in oxidation potential toward the surface (described in detail by Nickel *et al.*[20]).

The transition zone, the violarite–pyrite zone and the oxide zone constitute the supergene profile, and the term primary sulphide is used here to indicate that it predates supergene alteration, and does not necessarily presume a primary magmatic origin.

Mine development off the bulk sample winze (Fig. 9) has provided previous documentation of the geology of the upper parts of this deposit[20] and no further mining has occurred in the vicinity of that bulk sample winze since 1973.

Petrology of ore types

Massive sulphide ore

Massive sulphide ores are the dominant ore type extracted in the upper levels of the mine. This ore type consists nominally of between 80 and 100% by volume iron–nickel–copper–cobalt sulphide minerals, the remainder being alteration derivatives and silicate-rich and oxide-bearing 'breccia' inclusions. Massive sulphides consist predominantly of monoclinic pyrrhotite and pentlandite in primary sulphide ore, or violarite and pyrite in the supergene profile with accessory chalcopyrite–pyrite. Chrome spinel is erratic in occurrence, but is more concentrated in the massive sulphides than in other ore types. Patchy and variable alteration of the iron–nickel sulphide phases to iron oxides is common in the upper levels of the mine, where the violarite–pyrite zone and the transition zone prevail (Fig. 10).

Disseminated sulphide ore

The identification of this ore type is defined by Ni content rather than by petrological features, since all varieties of mineralized rock types bearing Ni content between 1.0 and 4.0% are characterized as 'disseminated ore'. The ore type is commonly comprised of a primary assemblage of pentlandite and hexagonal pyrrhotite within serpentinite converted to disseminated blebs and stringers of violarite and pyrite between adcumulate serpentine after olivine (Fig. 10) upon supergene alteration. Minor chalcopyrite, pyrite and magnetite occur dispersed throughout.

Triangular-textured ore

A textural variant of disseminated ore, which occurs in many structural positions in the deposit, is triangular-textured ore. This ore type conforms to the general definition of matrix ore as applied by Marston and co-workers[14] in having 40–80% sulphides, but it is not necessarily equivalent to the special textures in sulphide aggregates otherwise commonly ascribed

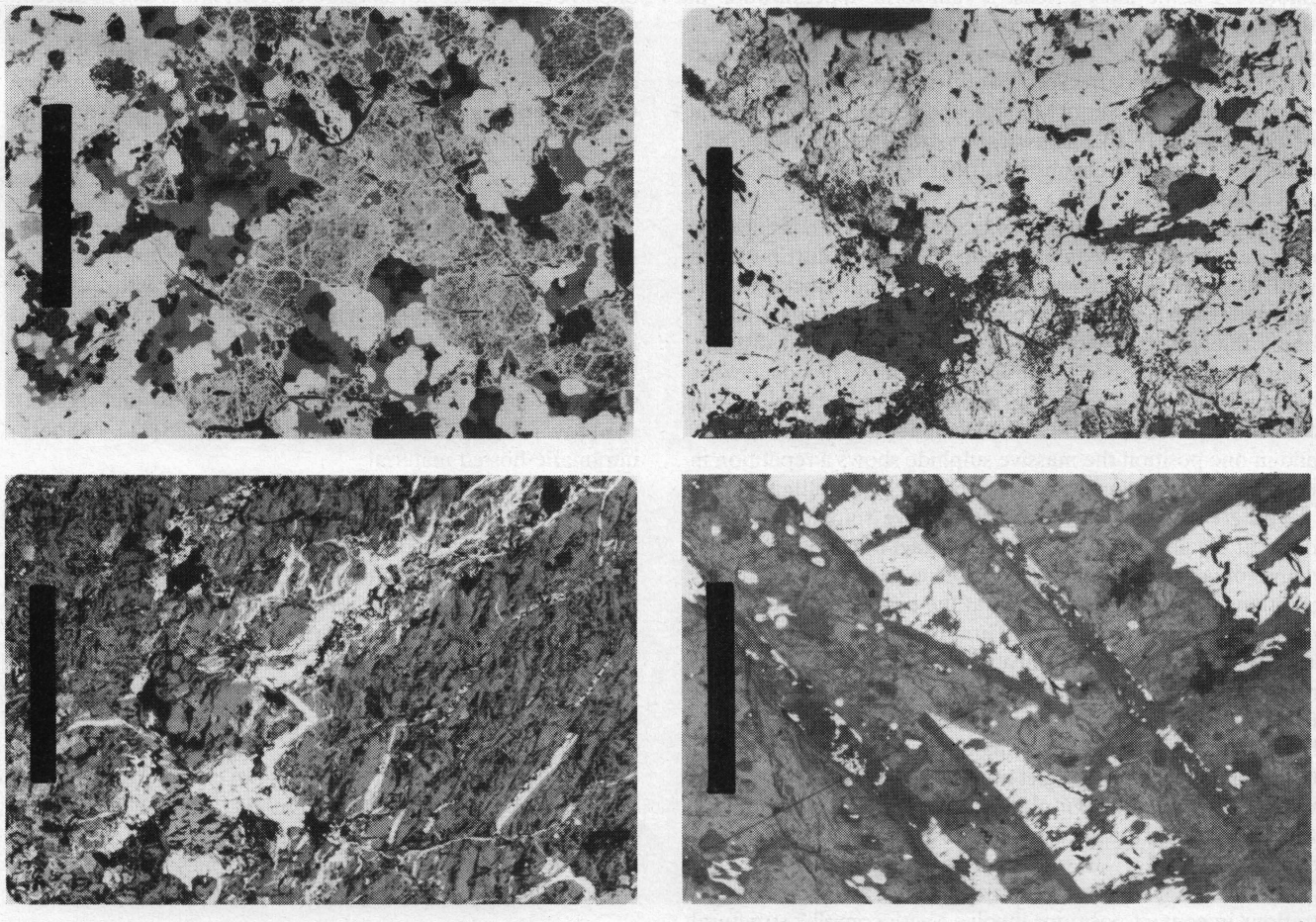

Fig. 10 Agnew ore aggregates: (*a*) (*top left*), massive sulphide ore type with supergene mineral assemblage (black bar 1.0 mm; sample no. LAG-8606); (*b*) (*top right*), massive sulphide ore type with primary sulphide mineral assemblage (black bar 1.0 mm; sample no. LAG-8709); (*c*) (*bottom left*), stringered and blebby pyrite and violarite in disseminated ore within serpentine–magnetite matrix host, violarite–pyrite zone (black bar 1.0 mm; sample no. LAG-8876A); (*d*) (*bottom right*), triangular-textured ore type in transition zone with pyrite–pyrrhotite–violarite–pentlandite aggregates between elongate laths of serpentine (black bar 1.0 mm; sample no. LAG-8708)

to this collective label.[3,4,11,21,22] Although markedly different texturally from the normal disseminated ore texture (Fig. 10), this ore type still bears similar metal grades and constituent mineralogy.

Deposit geochemistry

A suite of Agnew rock and ore types has been sampled for minor-element contents (Table 3), which vary widely between the shoots. Ratios of the major metals are more uniform, and are similar to those quoted for other nickel sulphide deposits of Western Australia.

The oreshoots exposed by mining within 290 m of the surface are each characterized by the average values of some particular metal to metal and sulphur to metal ratios (Table 4). Ni/Cu, Ni/Co and Fe/Ni values of the oreshoots are relatively consistent and are similar to the range of values of ores of the intrusive dunite-associated class of deposit. The Fe/Ni and S/Ni values are particularly distinctive for each of the shoots in this deposit and the S/Ni values for the massive sulphide shoots at Agnew are at variance with those presented for similar massive ores elsewhere in Western Australia.[24]

Geochemical profiles through ore zones intersected by diamond drilling have been compiled from assay data (Figs. 11 and 12). These profiles confirm mineralogical observations and trends shown by geochemical analyses of ores. Nickel shows a maximum concentration at the basal massive sulphide layer, and then decreases eastward, interrupted only by internal positions of massive sulphide layers.

Copper and cobalt both correlate well with nickel, and Pb and Zn levels are low in general, except at positions of concentration of spinel bands.

Sub-parallel massive sulphide veins and overlapping disseminated oreshoots are readily identified by marked increases in Ni content, but intermittent changes in the other minor ele-

Table 3 Minor-element content of some Agnew rock types

Element*	Sample number† 1	2	3	4	5	6	7	8	9	10
Ni,%	6.43	5.83	4.48	4.47	3.58	2.20	1.85	1.94	2.85	0.52
Cu	1712	1550	2625	1300	570	980	920	850	980	575
Co	1589	1480	980	1250	950	520	390	340	740	161
Cr	1440	2000	1920	1560	1402	956	580	206	1300	127
Ti	163	790	450	530	1150	540	780	550	860	2840
V	40	30	52	24	44	14	15	9	30	91
W	<10	< 10	<10	75	<10	140	151	156	92	<10
Zr	43	64	30	18	81	5	25	16	40	146
Nb	< 5	13	5	15	16	23	25	12	22	6
Pb	nd	19	nd	22	16	14	16	12	16	nd
Zn	nd	333	nd	230	140	176	173	137	154	nd
Ag	nd	2	nd	< 1	1	< 1	< 1	< 1	< 1	nd
Pt, ppb	<50	<100	50	<50	<50	<50	<50	<50	<50	nd
Pd, ppb	92	< 10	96	< 5	35	< 5	84	100	< 5	nd
Au, ppb	7	54	16	< 3	< 5	< 3	22	21	< 3	< 5
Ratios										
Ni/Cu	37.56	37.61	17.07	34.38	62.81	22.45	20.11	22.82	29.08	9.04
Ni/Co	40.46	39.39	45.71	35.76	37.68	42.31	47.44	57.06	38.51	32.30
Ni/Cr	44.65	29.15	23.33	28.65	25.53	23.01	31.90	94.17	21.92	40.94

Analyses by Pilbara Laboratories Pty., Ltd., Perth, Western Australia.
nd, not determined; Pt, Pd, Au by fire assay; Ni by wet chemistry assay; all others by ICP analysis.

*ppm unless otherwise indicated.
†1, Shoot 1A massive sulphide, 1315-m level; 2, Shoot 1A from extreme north end massive sulphide, 1365-m level; 3, No. 1 Shoot Massive massive sulphide, 1230-m level; 4, Shoot F1A massive sulphide near junction with Shoot F2, 1275-m level; 5, Shoot F2 massive sulphide, 1390-m level; 6, No. 2 Shoot Massive massive sulphide, 1200-m level; 7, No. 2 Shoot strongly disseminated mineralization, 1200-m level; 8, No. 2 Shoot strongly disseminated mineralization, 1190-m level; 9, actinolite sulphide schist along strike from Shoot F1A massive sulphide, 1275-m level; 10, actinolite sulphide schist along strike from Shoot 1A massive sulphide, 1315-m level.

Table 4 Geochemical characterization of oreshoots in upper levels of Agnew mine, shown by range in mean value of data sets (stoping areas), where $n > 500$ per stoping area for % Ni and Ni/Cu, and where $n > 100$ per stoping area for Fe/Ni and S/Ni. Ore grades are averages based on sampling of ores and grade data were not recalculated to 100% sulphides

Shoot Name	Character	% Ni	Ni/Cu	Ni/Co	Fe_{tot}/Ni	S/Ni
No. 1 Shoot Massive		6.4–6.6	50–55	40–45	6.0–7.0	4.0–5.0
Shoot 1A		5.5–6.5	40–50	40–55	5.0–6.5	4.5–6.5
Shoot F1A		6.0–6.5	35–45	40–55	7.5–8.5	5.5–7.5
Shoot F2		5.8–6.5	35–50	35–43	3.0–6.0	5.0–6.0
No. 1 Shoot		1.6–2.2	20–30	45–55	10.0–13.0	1.8–3.0
No. 2 Shoot		1.5–2.1	26–36	55–70	6.0–9.0	3.0–5.0

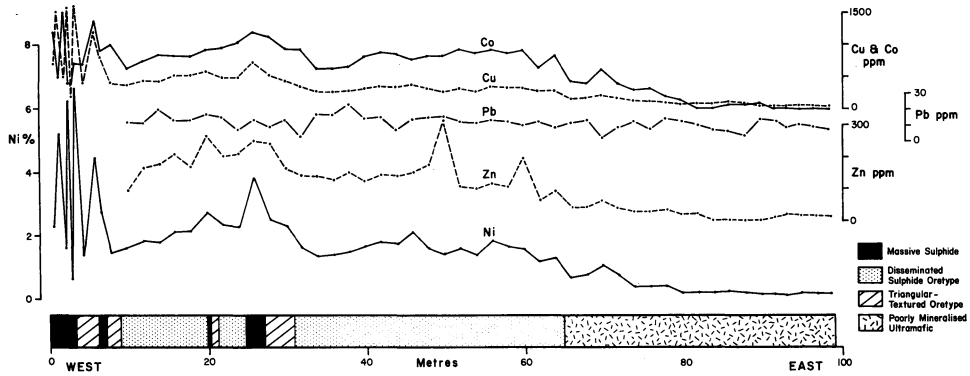

Fig. 11 West–east geochemical profile (Ni, Cu, Co, Pb, Zn) across diamond drill hole AD304

ments and S/Ni reflect the variable abundance of silicate inclusions in the massive sulphide breccia ore.

Contacts between massive sulphide and disseminated ore, within the supergene profile, are sharp and distinct, with marked change in Ni content (Fig. 12), but recognition of the change from a disseminated oreshoot to poorly mineralized ultramafic is less distinct and dependent on assay control (Fig. 11). The wallrocks to the oreshoots are barren of Ni content (Fig. 12).

Some unpublished S/Se data from drill core samples collected from primary sulphide, well below the areas being mined (Table 5), are dramatically different from those presented for deposits of the volcanic peridotite-associated class (e.g. Kambalda, Nepean, Widgiemooltha).[7,8,9,26] The Se contents at Agnew are very low (providing exceptionally high S/Se values) for each of the dunite, metadunite, serpentinite and massive sulphide in the vicinity of the No. 3 Shoot zone. The ratios are similar only to the Mt Keith serpentinites and talc–carbonate rocks (range *ca* 17 000–44 000) collected from a shallow bulk sample winze. The trend in mean S/Se values across the intrusive body at Agnew is more likely a reflection of zoned sulphur distribution unrelated to serpentinization (as at Mt Keith, Black Swan).[10]

There are a limited number of precious metal and PGE data presented for the No. 1 Shoot zone and its surface gossanous expression,[12,13,18,29] and a small number of analyses for some ore types in the supergene profile indicate that the contents are uniformly low for this deposit (Table 3). Of interest is the frequent excess of Pd content over Pt content in samples analysed from Agnew.

Table 5 S/Se values of some Agnew ore types at more than 800-m vertical depth from the surface (unpublished data provided by Professor D. I. Groves, University of Western Australia)

Rock type	S/Se values	Mean value
Massive sulphide (No. 3 Shoot)	62 100*	
	37 000*	*ca* 50 000
	46 600*	
Poorly mineralized serpentinite	37 000*	
	45 500†	*ca* 45 000
	49 200*	
Partially serpentinized dunite	25 500†	
	29 100†	*ca* 25 000
	21 200†	
Dunite core	29 800‡	*ca* 25 000
	19 800†	

*One sample collected from diamond drill hole WAP 114.
†One sample collected from diamond drill hole WAP 108X.
‡One sample collected from diamond drill hole WAP 110X.

Genesis of Agnew mineralization

Previous model

The genetic aspects of intrusive dunite-associated nickel sulphide deposits occurring in semiconcordant lenses of peridotite to olivinite composition and of komatiitic affinities have been presented in other contributions[14] and provide a general model for the consideration of this deposit.

A purely magmatic model that involves settling of an oxy-sulphide liquid and flowage of heavy immiscible mobile sulphides into a structural trap has been proposed for the Agnew mineralization[1,15,17] based on an interpretation constructed from surface drill-holes and limited underground exposure at the base of the oxide zone (bulk sample winze southeast of the 'bad ground' zone). Martin and Allchurch[15] did not mention or consider in their hypothesis the relationship of any of the three separate disseminated sulphide zones, matrix ores or any other massive sulphide ores other than the basal layer to the Perseverance Ultramafic. The role of deformational and metamorphic processes in modifying the mineralogy, nickel grade and volume of the ores was not discussed.

Such processes have been an important influence on the ores, as indicated by Binns and Groves,[5] who utilized the partition of Fe and Ni in assemblages of forsteritic olivine and the bulk sulphide fraction to confirm constraints on the amphibolite facies metamorphism as 600 ± 50°C and 3–5 kbar. They found a pronounced temperature-dependence in the partition relationship, but owing to a lack of data in definitive nickel sulphide-rich environments did not comment on the genesis of the Agnew mineralization. Their samples were all collected from dunitic ultramafic southeast of the 'bad ground' zone and below the 1230-m level.

Evidence for magmatic model

In the upper levels of Agnew mine all varieties of economic mineralization within or adjacent to the ultramafic body are located close to one marginal contact and by analogy with other deposits of this type[23] this contact is best presumed to mark the stratigraphic base of the ultramafic unit. Furthermore, this facing is supported by the general distribution of disseminated mineralizations located above the massive sulphides. The distribution of metals and sulphur reflects this arrangement of the ore types compatible with magmatic processes of concentration-modified post-emplacement by metamorphic and deformational processes.

Some relocation of the massive sulphide ores has occurred by flow-type mobilization of minerals by plastic flow in response to a variable stress field and, although evidence exists for the preservation of some primary magmatic textures and features in both the ores and their host ultramafics, some other textural variants suggest metamorphic modification of the primary features on all scales. The triangular-textured ore type for one

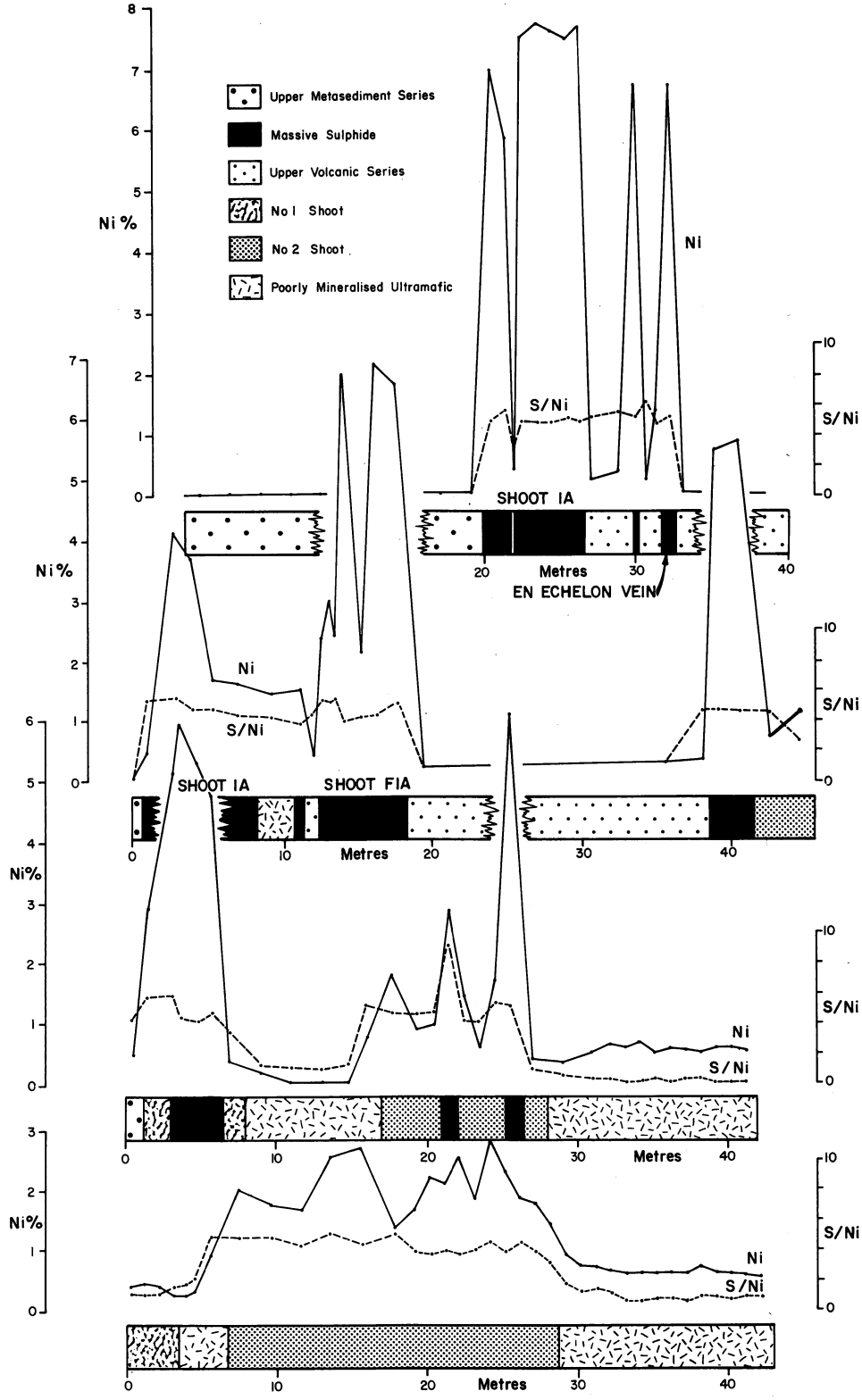

Fig. 12 West–east geochemical profiles (Ni, S/Ni) in diamond drill holes across identified oreshoots and their wallrocks at different levels of Agnew nickel mine. Drill-hole positions for AD80 (top), AD196 (top centre), AD275 (bottom centre) and AD98 (bottom) are shown in Figs. 6 and 8

has been generally accepted to be a product of metamorphic retexturing of a previous magmatic fabric rather than a primary igneous product itself.

Although S/Se values alone cannot be used as a definitive discriminant of nickel sulphide deposit genesis,[28] the high ratios presented for the massive sulphide intersected by diamond drill core at depth in this deposit are at least compatible with a magmatic source for the sulphides.

Similarly, the metal ratios of the different oreshoots presented are similar to the other ores of intrusive dunite-associated affinity, which implies an initial concentration under similar magmatic conditions. Only the marked variation in S/Ni and Fe/Ni values between the shoots suggests a revision to the model and the possible consideration of multiple magmatic episodes of changing composition.

The Perseverance Ultramafic proper, southeast of the 'bad ground' break, may represent the subvolcanic feeder to those magmatic events, itself intrusive into this cosanguineous sequence as a subvolcanic sill. The 'bad ground' is the manifestation of the interface or crush zone between the two magmatic

regimes and the 'Footwall shear' marks a plane of demarcation between two cognate magmatic episodes.

Acknowledgement

Permission to publish the contents of this paper was given by the management of Agnew Mining Company Pty., Ltd., Seltrust Mining Corporation Pty., Ltd., BP Minerals International, Ltd., and Mount Isa Mines, Ltd. Professor D. I. Groves reviewed an early draft and made many constructive suggestions, which improved the quality of the paper. He also provided unpublished data for Table 5, for which I am grateful. J. E. Martin and J. Rowe advised on reorganization of a draft to improve it, and I thank J. Rowe for much assistance in getting to print. Diagrams were drafted by Seltrust Mining Corporation Pty., Ltd. (Drawing Office), and were photographed at the University of Western Australia.

References

1. Allchurch P. D. Perseverance. In *Superficial mineral deposits and exploration geochemistry, Yilgarn Block, Western Australia* Smith R. E. Butt C. R. M. and Bettenay E. eds. *25th Int. geol. Congr., Australia, 1976, Excursion Guide* no. 41C, 1976, 31–5.

2. Archibald N. J. *et al.* Evolution of Archaean greenstone terrains, Eastern Goldfields Province, Western Australia. *Precamb. Res.*, **6,** 1978, 103–31.

3. Barrett F. M. *et al.* Structural history and metamorphic modification of Archean volcanic-type nickel deposits, Yilgarn Block, Western Australia. *Econ. Geol.*, **72,** 1977, 1195–223.

4. Barrett F. M. Groves D. I. and Binns R. A. Importance of metamorphic processes at the Nepean nickel deposit, Western Australia. *Trans. Instn Min. Metall. (Sect. B: Appl. earth sci.)*, **85,** 1976, B252–73.

5. Binns R. A. and Groves D. I. Iron–nickel partition in metamorphosed olivine–sulfide assemblages from Perseverance, Western Australia. *Am. Miner.*, **61,** 1976, 782–7.

6. Binns R. A. Gunthorpe R. J. and Groves D. I. Metamorphic patterns and development of greenstone belts in the eastern Yilgarn Block, Western Australia. In *The early history of the earth* Windley B. F. ed. (New York, etc: Wiley, 1976), 303–13.

7. Ewers W. E. and Hudson D. R. An interpretive study of a nickel–iron sulfide ore intersection, Lunnon Shoot, Kambalda, Western Australia. *Econ. Geol.*, **67,** 1972, 1075–92.

8. Gresham J. J. and Loftus-Hills G. D. The geology of the Kambalda nickel field, Western Australia. *Econ. Geol.*, **76,** 1981, 1373–416.

9. Groves D. I. Barrett F. M. and McQueen K. G. The relative roles of magmatic segregation, volcanic exhalation and regional metamorphism in the generation of volcanic-associated nickel ores of Western Australia. *Can. Mineralogist,* **17,** 1979, 319–36.

10. Groves D. I. and Keays R. R. Mobilization of ore-forming elements during alteration of dunites, Mt. Keith–Betheno, Western Australia. *Can. Mineralogist,* **17,** 1979, 373–89.

11. Hancock W. *et al.* Some ultramafic rocks of the Spargoville area, Western Australia. In *The Archaean rocks* Glover J. E. ed. *Spec. Publ. geol. Soc. Aust.* no. 3, 1971, 269–80.

12. Keays R. R. and Davison R. M. Palladium, iridium and gold in the ores and host rocks of nickel sulfide deposits in Western Australia. *Econ. Geol.*, **71,** 1976, 1214–28.

13, Keays R. R. Ross J. R. and Woolrich P. Precious metals in volcanic peridotite-associated nickel sulfide deposits in Western Australia II: Distribution within the ores and host rocks at Kambalda. *Econ. Geol.*, **76,** 1981, 1645–74.

14. Marston R. J. *et al.* Nickel sulfide deposits in Western Australia: a review. *Econ. Geol.*, **76,** 1981, 1330–63.

15. Martin J. E. and Allchurch P. D. Perseverance nickel deposit, Agnew. In *Economic geology of Australia and Papua New-Guinea, 1: Metals* Knight C. L. ed. (Parkville, Victoria: Australasian Institute of Mining and Metallurgy, 1975), 149–55. (*Monograph Series* no. 5)

16. Martin J. E. and Allchurch P. D. Sampling of the Perseverance nickel deposit. In *Sampling practices in the mineral industries: papers presented at the symposium, Melbourne Branch, 1976* (Parkville, Victoria: Australasian Institute of Mining and Metallurgy, 1976), 63–70. (*Symp. Series* no. 15)

17. Martin J. E. Perseverance nickel deposit. In *Archaean geology and mineral deposits of the Eastern Goldfields* Gee R. D. Groves D. I. and Fletcher C. I. eds. *25th Int. geol. Congr., Australia, 1976, Excursion Guide* no. 42A, 1976, 41–7.

18. McGoldrick P. J. and Keays R. R. Precious and volatile metals in the Perseverance nickel deposit gossan: implications for exploration in weathered terrains. *Econ. Geol.*, **76,** 1981, 1752–63.

19. Nickel E. H. Ross J. R. and Thornber M. R. The supergene alteration of pyrrhotite–pentlandite ore at Kambalda, Western Australia. *Econ. Geol.*, **69,** 1974, 93–107.

20. Nickel E. H. *et al.* Supergene alteration at the Perseverance nickel deposit, Agnew, Western Australia. *Econ. Geol.*, **72,** 1977, 184–203.

21. Oliver R. L. *et al.* Metamorphic olivine in ultramafic rocks from Western Australia. *Contr. Mineral. Petrol.*, **36,** 1972, 335–42.

22. Oliver R. L. and Ward M. A petrological study of serpentinous rocks associated with nickel sulphide mineralisation at Pioneer, Western Australia. Reference 11, 311–9.

23. Porter D. J. and McKay K. G. The nickel sulfide mineralization and metamorphic setting of the Forrestania area, Western Australia. *Econ. Geol.*, **76,** 1981, 1524–49.

24. Ross J. R. and Keays R. R. Precious metals in volcanic-type nickel sulfide deposits in Western Australia, I. Relationship with the composition of the ores and their host rocks. *Can. Mineralogist,* **17,** 1979, 417–35.

25. Ross J. R. and Travis G. A. The nickel sulfide deposits of Western Australia in global perspective. *Econ. Geol.*, **76,** 1981, 1291–329.

26. Seccombe P. K. *et al.* A sulphur isotope study to test a genetic model for Fe–Ni sulphide mineralization at Mt. Windarra, Western Australia. In *Stable isotope developments in the earth sciences* Robinson B. W. ed. *Bull. N.Z. Dep. scient. industr. Res.* 220, 1977, 187–202.

27. Selection Trust Limited. *Annual report to 3 March 1976* (London: The Company, 1976), 44 p.

28. Stanton R. L. *Ore petrology* (New York, etc.: McGraw-Hill, 1972), 713 p.

29. Thornber M. R. Allchurch P. D. and Nickel E. H. Variations in gossan geochemistry at the Perseverance nickel sulfide deposit, Western Australia: a descriptive and experimental study. *Econ. Geol.*, **76,** 1981, 1764–74.

30. Williams I. R. Structural subdivision of the Eastern Goldfields Province, Yilgarn Block. *Ann. Rep. geol. Surv. West. Aust. 1973,* 1974, 53–8.

31. Williams I. R. Eastern Goldfields Province. In *Geology of Western Australia. Mem. geol. Surv. West. Aust.* no. 2, 1975, 33–54.

Mineralogy of platinum group elements in the Kambalda nickel deposits, Western Australia

D. R. Hudson B.Sc.(Hons.), Ph.D., A.M.Aus.I.M.M.
CSIRO Division of Mineralogy, Floreat Park, Western Australia
M. J. Donaldson B.A.(Hons.)
Western Mining Corporation, Ltd., Kambalda, Western Australia

Synopsis

Study of gravity concentrates from the gold-recovery circuit of the Kambalda nickel mill has enabled an assessment to be made of the nature, relative abundance and compositional variability of platinum group element (PGE) minerals and other associated heavy minerals that are present in the Kambalda nickel deposits. The major platinum minerals are sperrylite, $PtAs_2$, and moncheite, (Pt, Pd, Ni)(Te, Bi)$_2$, and the major palladium minerals are sudburyite, (Pd, Pt, Ni)(Sb, Te, Bi), stibiopalladinite, Pd_5Sb_2, and palladoarsenide, Pd_2 (As, Sb), together with a palladium antimonide and a palladium arsenide that have not been fully characterized. Palladian melonites, which contain up to 10 wt% Pd, and palladian nickeline are also important PGE hosts. Sperrylite and sudburyite are by far the most abundant discrete minerals in the gravity concentrates.

Gold occurs as argentian, cuprian and nickeloan–cuprian gold, and as the tellurides calaverite, petzite and auriferous hessite. Silver is present in petzite, hessite and volynskite. Other rare phases contained in the gravity concentrates include native bismuth, altaite, frohbergite, breithauptite, gersdorffite, parkerite, scheelite, tantalite, cassiterite, rutile, bunsenite, gahnite, barite and uvarovite.

Descriptions of *in-situ* occurrences of PGE minerals at Kambalda are rare. Michenerite, PdBiTe, and testibiopalladite, PdSbTe, have been described from a telluride-rich quartz-carbonate vein that intersects massive sulphide ore in Lunnon Shoot. Moncheite has been observed in chalcopyrite-rich stringers, and sudburyite occurs as inclusions in nickeline in a quartz-carbonate veinlet. No discrete PGE minerals have been found within the massive and matrix ore zones in the Kambalda oreshoots, and the geochemical distribution of PGE suggests that the formation of discrete PGE phases may be related to post-magmatic processes—in particular, metamorphic segregation of sulphides, and the interaction of the ore sulphides, containing PGE in solid solution, with younger hydrothermal fluids. This has led to local redistribution of the PGE, with concentration in footwall stringers and veins, and in reaction zones.

Platinum group elements (PGE) are a minor but significant component of magmatic nickel sulphide ores. They are an economically important by-product of many mining operations, being recovered predominantly by chemical separation from sulphide concentrates or matte. The PGE occur as discrete mineral phases in many deposits, but some may also be in solid solution in the Fe and Ni sulphides. The low concentrations of PGE in most Ni ores (<1 ppm), however, make *in-situ* location of PGE minerals extremely difficult, and most studies of this mineral group employ gravity concentration methods and large volumes of crushed and pulverized ore samples.

At Kambalda Ni sulphide ores have been mined since March, 1967, totalling to June, 1982, 15 690 000 t of Ni sulphide ore averaging 3.11% Ni. Ore reserves at June, 1982, were 25 000 000 t at 3.3% Ni. The presence of minor PGE in the ores was recognized early in the development of the deposits, and Western Mining Corporation, Ltd. (WMC), who mine the deposits, are credited for a percentage of the PGE that are largely concentrated in high-grade Ni matte produced from sulphide concentrates at WMC's Kalgoorlie nickel smelter. Further PGE are recovered in some refinery products at WMC's Kwinana nickel refinery, near Perth, but substantial improvements in overall recovery of PGE could still be made. Gold mineralization occurs in close spatial association with many of the nickel oreshoots and in recent years has been recovered by gravity concentration. This study examines the nature and composition of discrete PGE minerals that occur within gravity concentrates from the gold-recovery circuit in the Kambalda nickel concentrator. It is part of a continuing study of PGE mineralogy in Western Australian nickel deposits aimed at improving aspects of exploration, mining and recovery of gold, silver and PGE.

Geological setting of Kambalda deposits

The Kambalda nickel deposits comprise a number of elongate, high-grade sulphide orebodies that occur within a thick sequence of metamorphosed, highly magnesian ultramafic flows (komatiites) of Archaean age. The deposits belong to the volcanic peridotite association of Marston *et al.*[1] and most ores occur at or near the basal contact of a distinctive metaperidotite unit with underlying tholeiitic metabasalt. The geology of the Kambalda nickel field has been described in detail by Gresham and Loftus-Hills.[2] Although most authors[1-4] believe the ores and host rocks to be magmatic in origin, it is widely recognized that postmagmatic events have substantially modified many magmatic features. Barrett *et al.*[5] highlighted the importance of low-amphibolite facies metamorphism and multiphase deformation in the modification of the Ni ores, and this was substantiated by Marston and Kay.[6] Bavinton[7] confirmed a metamorphic grade of low amphibolite facies, and Phillips and Groves[8] documented hydrothermal alteration associated with gold-bearing quartz-carbonate veins. Most ultramafic rocks in the area have been converted to talc–carbonate–chlorite assemblages, and felsic porphyries intrude the entire succession.

Precious metals in Kambalda nickel deposits

Best estimates of average concentration levels of precious metals (PM include the PGE Pt, Pd, Ir, Os, Rh, Ru, together with Au and Ag) in Kambalda ores are derived from monthly composite samples of carted ores from individual production centres. Ross and Keays[9] presented data that represent production from six major oreshoots over an 18-month period, and tonnage-weighted averages of their data are given in Table 1. Also included in Table 1 are the mean values recalculated to levels in 100% sulphides, and a comparison of available data on PM contents of high-grade nickel mattes from the Kalgoorlie nickel smelter. A summary of available data for individual oreshoots at Kambalda was given by Naldrett.[11] The ratios of PM to Ni are approximately constant between ores, 100% sulphides and Ni matte (Table 1), indicating essentially 100% recovery of these metals to the matte. This consistency also supports the average values quoted for ores, although Pt levels may be slightly overestimated (cf. Keays and Davison,[10] who sug-

Table 1 Bulk composition of Kambalda nickel ores and high-grade nickel matte

	Ni wt%	Cu	Co	S	Pt ppb	Pd	Os	Ir	Rh	Ru	Au	Ag
Ni ores*	2.96	0.22	0.07	8.09	326	425	110†	60†	(50)‡	220†	339	1170§
Recalculated to 100% sulphides**	14.45	1.10	0.32	39.95	1630	2104	537††	293††	(240)‡	1074††	1721	5710††
High-grade Ni matte‡‡	72.9	5.6	0.5	19.6	4200	10 900	—	—	1200	4100	5700	24 200

* Tonnage-weighted average of six major oreshoots. From Ross and Keays,[9] Table 1, except where indicated.
† Data from Keays and Davison.[10]
‡ Estimated from levels in Ni matte, assuming 100% recovery.
§ Average of 180 monthly composites of carted ores, 1976–81.
** From Ross and Keays,[9] except where indicated.
†† Recalculated with Ni correction factor.
‡‡ Ni, Cu, Co and S averages of 3 monthly composites, July–September, 1981; Pt, Pd, Au and Ag data averages of 135 matte shipments 1975–81; Rh and Ru averages of 26 matte shipments, 1975–77 (analyses by K.N.S.).

gested <200 ppb Pt in Kambalda ores).

Although the concentration of PGE in Kambalda Ni ores has been systematically studied by sampling bulk ores, mill feeds, and drill core and mine samples, no similar investigation has been undertaken on the mineralogy of PGE. Descriptions of discrete PGE phases, which are believed to occur at low concentration levels and to be very irregularly distributed within the ore environment, are restricted to a few *in-situ* occurrences that have been observed during the routine documentation of mine development.

This study of PGE mineralogy at Kambala has been made possible by the installation of a gravity concentration circuit, which, as well as recovering gold, provides a composite sample of PGE phases from all of the Kambalda oreshoots.

Sampling and concentration techniques

Since 1981 coarse-grained native Au has been recovered in the Kambalda mill from both Ni ore and separately mined Au ore by a combination of flotation and gravity concentration. Flotation concentrates from the Denver cell, which constitute about 40% of total Ni sulphide concentrates produced and represent the coarser-grained, readily floated material, are passed through a gravity circuit that consists of strake and Wilfley tables. Gold is recovered from Wilfley concentrates by amalgamation, leaving a residue that comprises a composite of heavy minerals from all of the producing oreshoots at Kambalda. The residues consist mainly of pentlandite (~60%), together with pyrite (~25%), pyrrhotite (~5%) and magnetite (~10%). Most grains are between 50 and 100 μm in diameter. PGE and other heavy metals are highly enriched in the residues, as are As, Sb, Bi and Te. Analyses of amalgamation residues typical of those used in this study are given in Table 2.

Two techniques were used to further concentrate the heavy minerals in these residues—acid treatment and gravity separation with a Haultain superpanner.

Chemical treatment of gravity concentrates that contain PGE is an established method of removing unwanted phases, including tramp metals and sulphides, arsenides and tellurides of base metals.[12] Concentrated nitric and hydrochloric acids are favoured treatments, but other components can be dissolved with the use of hydrofluoric acid (silicates), hot caustic soda solution (quartz) and cyanide (gold).

Although some losses of PGE minerals do occur, the important platinum minerals sperrylite, $PtAs_2$ and moncheite, $PtTe_2$, are relatively insoluble in both nitric and hydrochloric acids. Other phases, such as sudburyite, PdSb, are attacked more slowly than iron and nickel sulphides and are therefore concentrated during acid treatment.

A number of methods of acid treatment were tried. Most of these involved combination of different strengths and orders of treatment with hydrochloric and nitric acid. Samples were either added to acid or acid was added to samples. The most effective treatment was to use about 1 l of concentrated commercial-grade nitric acid in a 2-l pyrex beaker in a fume hood, the sample being added in 50-g lots; the reaction was allowed to subside before more sample material was added to achieve a total of 500 g. The reaction, particularly during early sample addition, is accompanied by strong boiling and evolution of oxides of nitrogen.

Decomposed sulphides formed a thick greenish-brown precipitate, which was removed by repeated washing and decantation. A further 200 ml of concentrated nitric acid was added and the digestion was completed by standing for one day. Final washing and drying gave dark coloured residues composed of magnetite, chromite and scheelite, with lesser amounts of heavy, resistant minerals, including PGE minerals and gold.

Magnetic minerals were separated by use of a hand magnet. Typical yields, calculated on the basis of a 1000-g sample of

Table 2 Analyses of residue from amalgamation of gravity concentrates, Kambalda gold circuit

Sample no.	Ni wt%	Cu	Co	Cr ppm	Au	Ag	Pb	Zn	As	Te	Bi	Sb
Z17474	19.0	0.50	0.38	2080		550	9050	270	6800			
Z17475	18.6	0.87	0.40	2210		850	14 200	320	13 300			
Z17440	21.7	0.30	0.46	680	2043	175	2650	660	4470	6950	340	
Z14816	9.2	1.30	0.17	2060	1480	310	6000	410	5350		1440	98
Z14817	20.0	0.64	0.39	580	310	700	2200	180	5100		270	27
Z14818	21.0	0.40	0.52	200	150	70	1800	70	4100		240	48
Z14819	6.5	1.05	0.20	1840	1550	350	6650	540	4550		920	52

amalgam residue, are: total residue, 108 g; magnetic residue, 85 g; and non-magnetic residue, 23 g (see Fig. 1). The Frantz Isodynamic Magnetic Separator was used to further subdivide the residues from acid treatments. Standard settings used were: slope, 25–30°; tilt, 15°; current range, 0–1.6 A.

The Haultain superpanner was used to further concentrate residues from acid treatments. Fractions that consisted almost entirely of gold and sperrylite were generated in this way; a gold–sperrylite concentrate (weight 5.9 g) was obtained by panning the non-magnetic acid residues from 1000 g of amalgam residue.

The majority of base and heavy metal sulphides, arsenides, antimonides and tellurides were soluble in concentrated nitric acid. Their identity and abundance were estimated from the heavy mineral concentrates prepared by superpanning amalgam residues and Wilfley table concentrates.

Minerals identified in amalgamation residues

The main minerals that were identified in the gravity concentrates are shown in Fig. 1, together with other heavy minerals that have been described from Kambalda oreshoots. The most abundant PGE minerals are sperrylite, $PtAs_2$, and sudburyite, PdSb, with lesser moncheite, $(Pt,Pd,Ni)(Te,Bi)_2$, and palladoarsenide, $Pd_2(As,Sb)$, together with a palladium antimonide and a palladium arsenide that have not been fully characterized. Palladian melonites with more than 10 wt% Pd and palladian nickeline are also important PGE-bearing minerals. The major morphological and compositional features of the main PGE minerals at Kambalda are described below. Detailed compositional data for these minerals and for the rarer PGE phases will be published later.

Sperrylite was concentrated in samples that had been prepared by either acid treatment or by panning. Fractions that consisted of 40% sperrylite, 50% gold and 10% scheelite were prepared by panning the non-magnetic acid-resistant concentrates from amalgam residues. The concentration of sperrylite in the amalgam residues was estimated at about 0.3% (Fig. 1), but no attempt was made to relate this to the original concentration of sperrylite in ore.

Most grains of sperrylite consist of distorted euhedra and subhedra of complex octahedral habit, with rarer cubic forms (Fig. 2). The grain size ranges from 50–500 μm, with an average of about 200 μm. Many grains are fractured with a splintery to conchoidal fracture surface, but the edges between crystal faces are sharp and generally show no rounding or chipping. This suggests that some grains of sperrylite occurred as inclusions in other grains and that they were liberated during acid treatment rather than during grinding.

Inclusions in sperrylite are common, and were studied to enable a possible paragenesis to be determined. They comprise magnetite, chromite, sphene, calcic amphibole, calcic pyroxene, calcic garnet (both andradite and uvarovite), the carbonates magnesite, siderite and calcite, the sulphides pyrrhotite, pentlandite, chalcopyrite, pyrite and galena, and gold. Inclusions are within the size range <5–40 μm, most being about 10 μm.

Microprobe analyses of sperrylite grains confirm that the composition is stoichiometric $PtAs_2$, with minor contents of

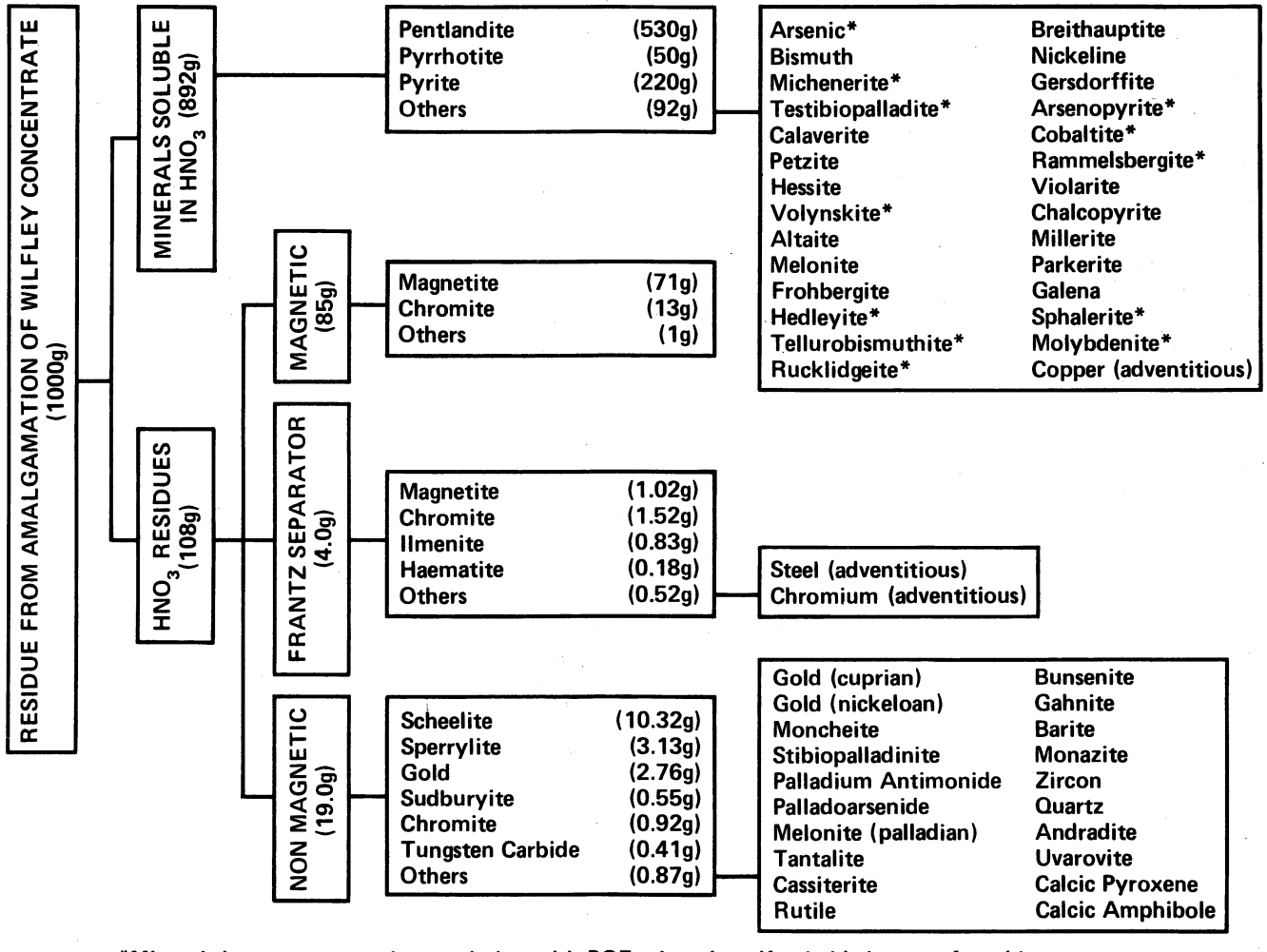

Fig. 1 PGE minerals and associated heavy minerals from Kambalda nickel deposits determined by chemical and physical separation of residues from amalgamation of gravity concentrates from gold circuit of Kambalda nickel mill

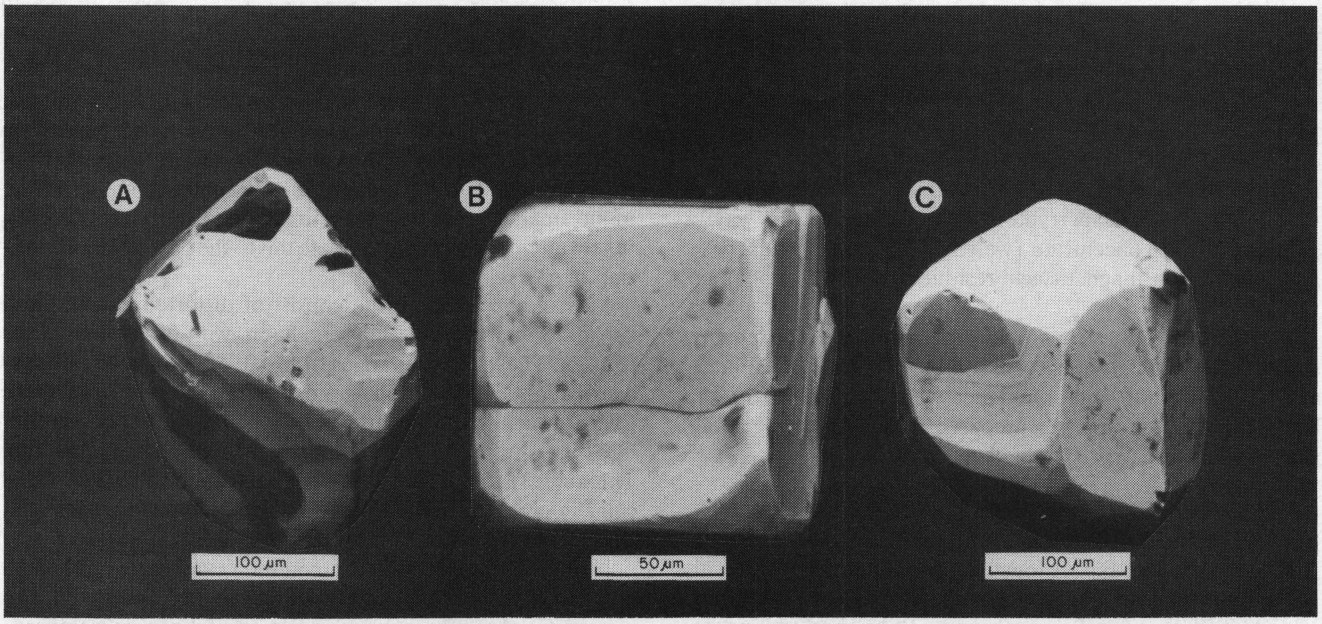

Fig. 2 Backscattered electron image of euhedral crystals of sperrylite separated by nitric acid treatment of heavy mineral residues from gold-recovery circuit of Kambalda nickel mill. Crystals occur as distorted and complex octahedra (*A*) and (*C*) with rarer, complex octahedral modifications of cube (*B*). Calc–silicate and oxide inclusions occur in sperrylite (*A*)

other PGE (Table 3). Rhodium contents are up to 1.44 wt%, but other PGE are less than 0.5 wt%.

Sudburyite, the predominant discrete palladium mineral at Kambalda, comprises about 0.05% of the amalgam residue (Fig. 1). Pd also occurs in solid solution in pentlandite,[13] however, and in melonite and nickeline, and the relative importance of sudburyite as a host for Pd at Kambalda has not been determined.

Table 3 Concentration of minor PGE in Kambalda sperrylite

Wt%	Range	Average	Error
Pd	Nil –0.51	0.13	0.10
Os	Nil –0.50	0.22	0.15
Rh	0.16–1.44	0.52	0.10
Ru	Nil –0.26	0.10	0.05
Ir	0.07–0.44	0.23	0.15

Sudburyite occurs as tabular anhedral grains or as subhedral to euhedral hexagonal plates. It dissolves slowly in nitric acid, and most grains that have been separated in this way have suffered alteration. In polished sections studied in reflected light this alteration appears as a brownish-grey rim, often with a comb-like inner margin, surrounding pale cream grains of sudburyite. Sudburyite occurs in intergrowths with stibiopalladinite and with nickeline.

Electron-microprobe analyses of sudburyite indicate that there is a wide variation in composition, particularly with respect to the degree of substitution of Te and Bi for Sb (Table 4). The Kambalda data suggest that the substitution of Te and Bi occurs in the ratio of 3:1, most analyses lying between PdSb and $Pd_2SbBi_{0.25}Te_{0.75}$ (Fig. 3). This is believed to be a greater range in composition for sudburyite than has previously been reported.[14]

Moncheite is a minor PGE mineral in the amalgam residues, but shows considerable variation in the degree of substitution of Ni for Pt, tending towards palladian melonite, Pd for Pt, tending towards merenskyite, and Bi for Te. Analyses of three representative moncheite grains and one grain of palladian melonite are given in Table 5 and the compositional variation is shown in Fig. 4. The Kambalda analyses suggest that a continuous solid solution may exist between palladian melonite and palladian

Table 4 Compositions of sudburyite from Kambalda

		Sudburyite (35–3A–4)		Bi–Te sudburyite (27–1C–4)	
Wt%	Pd	46.21		41.94	
	Pt	0.43		0.26	
	Ni	0.20		0.17	
	Sb	51.63		32.39	
	Te	0.89		16.06	
	Bi	0.54		9.42	
	As	0.07		0.16	
	Total	99.97		100.40	
At%	Pd	49.66		47.07	
	Pt	0.25	50.3	0.16	47.6
	Ni	0.39		0.35	
	Sb	48.49		31.77	
	Te	0.80	49.7	15.03	52.4
	Bi	0.30		5.37	
	As	0.11		0.25	

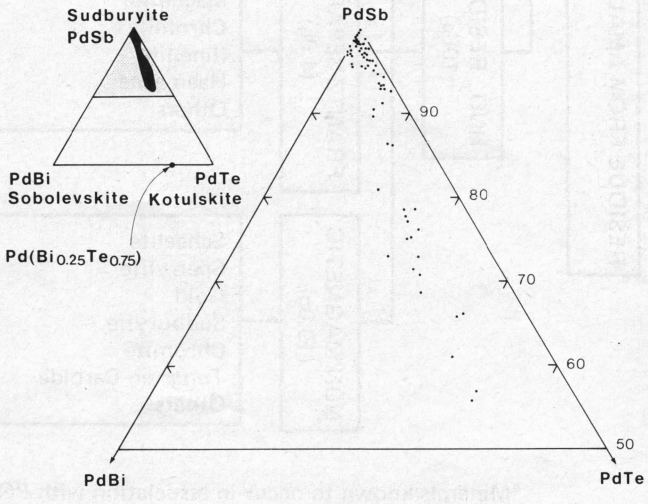

Fig. 3 Compositional variation of sudburyite from Kambalda based on electron-microprobe analyses of 68 grains from amalgam residues. Most analyses fall close to line joining PdSb to $Pd_2SbBi_{0.25}Te_{0.75}$

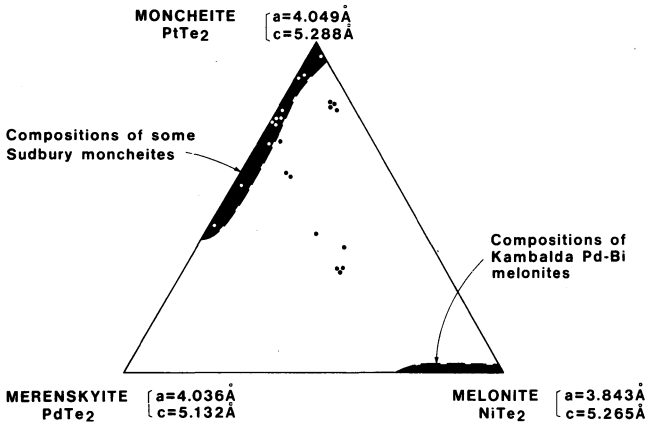

Fig. 4 Compositional variation of moncheite from Kambalda based on electron-microprobe analyses of grains from amalgam residues. Fields of Pd–Bi melonite from Kambalda and moncheite from Sudbury[14] shown for comparison

Occurrence of PGE minerals in ore environment

Distribution of precious metals in ores and host rocks

The distribution of Pd, Ir and Au in contact ores, footwall stringers and sulphide mineral separates was described by Ross and Keays[9] and Keays and co-workers:[13] they found that Pd was enriched in pentlandite concentrates, that Ir was more evenly distributed among pentlandite, pyrrhotite, pyrite and chalcopyrite, and that Au was enriched in pyrite concentrates. Unfortunately, these studies did not include Pt determinations. It was concluded that discrete PGE minerals were unlikely to occur within massive and matrix ores. These studies also showed that Pd and Au contents of massive ores were significantly lower than values in matrix and disseminated ores and bulk carted ore composites, when corrected to 100% sulphides. This was attributed[13] to mobilization of Pd and Au into chalcopyrite-rich footwall stringers, which were shown to contain high, but erratic, levels of these metals, suggestive of the occurrence of discrete PGE minerals.

Table 5 Compositions of moncheite and palladian melonite from Kambalda

		Moncheite (27–1C–24)		Ni–Pd–Bi moncheite (29–5)		Pt–Pd–Bi melonite (29–2)		Pd melonite (35–10–2)	
Wt%	Pt	37.81		26.30		15.38		0.50	
	Pd	0.96		6.34		7.72		9.87	
	Ni	0.83		1.91		6.03		11.39	
	Te	56.44		50.22		65.51		69.08	
	Sb	0.47		0.44		0.58		0.61	
	Bi	1.02		14.34		5.04		7.65	
	Total	97.53		99.55		100.26		99.10	
At%	Pt	29.01		19.46		9.89		0.29	
	Pd	1.35	32.5	8.60	32.8	9.12	31.9	10.64	33.2
	Ni	2.13		4.69		12.90		22.23	
	Te	66.21		56.82		64.47		62.06	
	Sb	0.58	67.5	0.52	67.2	0.60	68.1	0.57	66.8
	Bi	0.73		9.90		3.03		4.20	

moncheite. They are thus different from the nickel-poor merenskyite–moncheite solid solution indicated by the composition of Sudbury moncheites.[14]

Gold occurs as argentian gold, cuprian gold and nickeloan–cuprian gold and as the tellurides petzite, calaverite and auriferous hessite. Electron-microprobe analyses of argentian gold gave a range of silver values from 0.7 to 29.3 wt% Ag, skewed about a median value of 5.1 wt% Ag. This corresponds to a range from $Au_{98.7}Ag_{1.3}$ to $Au_{57.0}Ag_{43.0}$, with a median of $Au_{91.1}Ag_{8.9}$. The variation in silver content is reflected in a colour change from gold, in low-Ag grains, to pale yellow in argentian gold. Copper values were within the range nil to 0.6 wt%, most grains containing less than 0.2 wt%. Ni, Fe, As, Sb and Te were consistently less than 0.2 wt%.

Cuprian gold and nickeloan–cuprian gold are rare metallic phases in the concentrates, with a combined abundance of about 0.03% of the argentian gold. Cuprian gold is pale pink in reflected light and nickeloan–cuprian gold has a bronze colour in rough grains and is pinkish yellow in reflected light. Electron-microprobe analyses suggest two main compositional groups, clustered about $CuAu_4$ and(Cu,Ni)Au, with a typical analysis (wt%) of nickeloan–cuprian gold of 68.7 Au, 0.2 Ag, 19.4 Cu and 10.2 Ni.

Silver occurs predominantly as argentian gold, but is also present as hessite, petzite and, more rarely, as volynskite.

A number of heavy minerals were recognized at Kambalda for the first time as a result of this study. These include native bismuth, native arsenic, parkerite, breithauptite, frohbergite, hedleyite, bunsenite, gahnite, cassiterite and tantalite.

The massive ores are not depleted in Ir, and Keays *et al.*[15] showed that such geochemical separation of Pd and Ir is most probably brought about by hydrothermal processes in which Ir is essentially immobile. Paterson *et al.*[16] documented separation of Pd from Ir in hydrothermally mobilized Ni ores associated with interflow sediments at Kambalda (see also Bavinton and Keays[17]), and Lesher and Keays[18] presented similar PM

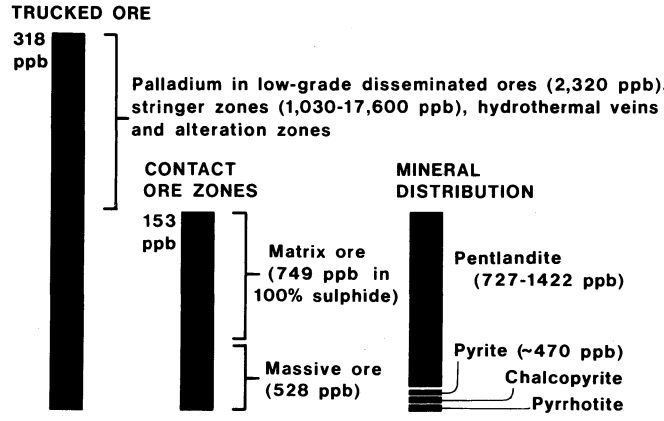

Fig. 5 Distribution of palladium in Lunnon Shoot ores, Kambalda, based on data from Ross and Keays[9] and Keays and co-workers.[13] Pd content of trucked ore (318 ppb) distributed among massive and matrix ores and associated disseminated and stringer zones on basis of contained Ni values. Pd values in brackets for 100% sulphide

data for other mobilized Ni sulphides.

The distribution of palladium in Lunnon Shoot ores is summarized in Fig. 5. About half of the Pd in bulk ore analyses may be contained as discrete PGE minerals in veins and reactions zones, the remainder being contained as finely dispersed microscopic grains or held in solid solution in sulphide minerals, mainly pentlandite, of the massive and matrix ore zones.

Previously reported PGE minerals from Kambalda

Observations of PGE minerals in Kambalda ores are rare. Although several occurrences of tellurides (e.g. altaite, PbTe, calaverite, $AuTe_2$, hessite, Ag_2Te, melonite, $NiTe_2$, tellurobismuthite, Bi_3Te_2, usually associated with native Au), and more common occurrences of arsenides (arsenopyrite, FeAsS, gersdorffite, NiAsS, nickeline, NiAs) have been recorded by WMC geologists, there were only two reports of PGE minerals prior to the present study. Sperrylite was recorded from massive ore at Fisher Shoot,[19] but Hudson and co-workers[20] provided the only detailed description of discrete PGE mineralogy. They described euhedral zoned crystals of michenerite, PdBiTe,–testibiopalladite, Pd(Sb,Bi)Te, associated with other tellurides (hessite, Ag_2Te, rucklidgeite, $(Bi,Pb)_3Te_4$, volynskite, $AgBiTe_2$, and melonite, $NiTe_2$) in a quartz-carbonate–andradite vein that cut massive Ni sulphides in Lunnon Shoot.

Small grains of sudburyite occur within nickeline in a quartz–carbonate vein associated with a massive ore 'pinch-out' in Ken Shoot. Grains of sudburyite are sub-angular in shape and range in size up to 50 μm, but most are smaller than 10 μm. The sudburyite occurs irregularly dispersed within the nickeline and also along grain boundaries, particularly those with gersdorffite. Rare grains of stibiopalladinite have also been observed within the nickeline.

Moncheite has been reported (Professor E. F. Stumpfl, personal communication, 1982) from chalcopyrite-rich stringers beneath the massive sulphide ore zones.

The *in-situ* occurrences of discrete PGE minerals at Kambalda have been from zones of reaction, or from hydrothermal veins, or from mobilized stringers of sulphide. These preliminary results support the suggestion[13] that postmagmatic mobilization of PGE into veins and stringers has been important in controlling the distribution and nature of discrete PGE minerals.

Interaction of telluride-, arsenide- and antimonide-rich hydrothermal veins with massive and matrix nickel ores is also considered an important mechanism for the release of PGE from sulphides and their subsequent crystallization as discrete PGE tellurides, arsenides or antimonides. The michenerite–testibiopalladite occurrence at Lunnon Shoot and the sudburyite occurrence at Ken Shoot are both thought to have formed in this way.

Although no *in-situ* occurrence of sperrylite has been found in this study, the calc–silicate and oxide inclusions suggest that this PGE phase may also have crystallized in postmagmatic hydrothermal environments, such as reaction zones or veins.

Conclusions

A number of discrete PGE minerals are present in the Kambalda nickel sulphide ores and some of these are sufficiently coarse for economic recovery by gravity concentration methods to be considered. The two most important phases are sperrylite and sudburyite, but at this stage it is not clear what proportions of each may be amenable to gravity concentration.

Paragenesis of the PGE minerals has not been firmly established, although limited data show that discrete PGE minerals occur within veins and reaction zones. They appear to have formed by either late magmatic segregation or by subsequent concentration of PGE from Ni sulphide ores during metamorphism and hydrothermal alteration.

Acknowledgement

The generous assistance of Western Mining Corporation, Kambalda, in providing samples of concentrate and access to their mines is gratefully acknowledged. Valuable discussions were held with many of the metallurgical and geological staff at Kambalda during this study, and the encouragement of J. J. Gresham is particularly acknowledged.

Philippa Cromellin provided excellent technical support in the separation, identification and analysis of PGE phases. Figures were drafted by Colin Steel and the manuscript was typed by Irene Piercy.

The study forms part of a project entitled 'Nature, distribution and recovery of platinum group element (PGE) minerals in Western Australian nickel ores' that is jointly sponsored by Western Mining Corporation and The Western Australian Mining and Petroleum Research Institute (WAMPRI).

References

1. Marston R. J. *et al.* Nickel sulfide deposits in Western Australia: a review. *Econ. Geol.*, **76,** 1981, 1330–63.
2. Gresham J. J. and Loftus-Hills G. D. The geology of the Kambalda nickel field, Western Australia. *Econ. Geol.*, **76,** 1981, 1373–416.
3. Ewers W. E. and Hudson D. R. An interpretive study of a nickel–iron sulfide ore intersection, Lunnon Shoot, Kambalda, Western Australia. *Econ. Geol.*, **67,** 1972, 1075–92.
4. Groves D. I. Barrett F. M. and McQueen K. G. The relative roles of magmatic segregation, volcanic exhalation and regional metamorphism in the generation of volcanic-associated nickel ores of Western Australia. *Can. Mineralogist,* **17,** 1979, 319–36.
5. Barrett F. M. *et al.* Structural history and metamorphic modification of Archean volcanic-type nickel deposits, Yilgarn Block, Western Australia. *Econ. Geol.*, **72,** 1977, 1195–223.
6. Marston R. J. and Kay B. D. The distribution, petrology and genesis of nickel at the Juan Complex, Kambalda, Western Australia. *Econ. Geol.*, **75,** 1980, 546–65.
7. Bavinton O. A. The nature of sulfidic metasediments at Kambalda and their broad relationships with associated ultramafic rocks and nickel ores. *Econ. Geol.*, **76,** 1981, 1606–28.
8. Phillips G. N. and Groves D. I. Fluid access and fluid–wallrock interaction in the genesis of the Archaean gold-quartz vein deposit at Hunt mine, Kambalda, Western Australia. In *Gold '82: the geology, geochemistry and genesis of gold deposits* Foster R. P. ed. (Rotterdam: Balkema, 1984), 389–416. (*Spec. Publ. geol. Soc. Zimbabwe* no. 1)
9. Ross J. R. and Keays R. R. Precious metals in volcanic-type nickel sulfide deposits in Western Australia: I, relationship with the composition of the ores and their host rocks. *Can. Mineralogist,* **17,** 1979, 417–35.
10. Keays R. R. and Davison R. M. Palladium, iridium, and gold in the ores and host rocks of nickel sulfide deposits in Western Australia. *Econ. Geol.*, **71,** 1976, 1214–28.
11. Naldrett A. J. Nickel sulfide deposits: classification, composition and genesis. *Econ. Geol. 75th anniversary vol.*, 1981, 628–85.
12. Feather C. E. Mineralogical considerations in the recovery of platinum group minerals from Witwatersrand mines gravity concentrates. *Trans. geol. Soc. S. Afr.*, **81,** 1978, 229–31.
13. Keays R. R. Ross J. R. and Woolrich P. Precious metals in volcanic peridotite-associated nickel sulfide deposits in Western Australia: II, distribution within the ores and host rocks at Kambalda. *Econ. Geol.*, **76,** 1981, 1645–74.
14. Cabri L. J. and Laflamme J. H. G. The mineralogy of the platinum-group elements from some copper–nickel deposits of the Sudbury area, Ontario. *Econ. Geol.*, **71,** 1976, 1159–95.
15. Keays R. R. *et al.* Iridium and palladium as discriminants of volcanic-exhalative, hydrothermal, and magmatic nickel sulphide mineralization. *Econ. Geol.*, **77,** 1982, 1535–47.
16. Paterson H. L. *et al.* Nickeliferous sediments and sediment-associated nickel ores at Kambalda, Western Australia. In *Sulphide deposits in mafic and ultramafic rocks* Buchanan D. L. and Jones M. J. eds (London: IMM, 1984), 81–94.
17. Bavinton O. A. and Keays R. R. Precious metal values from interflow sedimentary rocks from the komatiite sequence at Kambalda, Western Australia. *Geochim. cosmochim. Acta,* **42,** 1978, 1151–63.

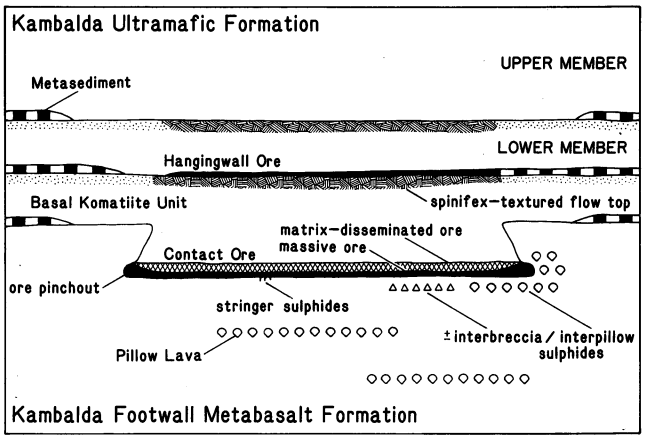

Fig. 1 Schematic sketch of Kambalda oreshoot in cross-section after removal of superimposed structural deformation. Metabasalts comprise both massive and pillowed facies with volcaniclastic flow top breccia horizons; interpillow/interbreccia and hydrothermal vein-type sulphides in this study occur predominantly in metabasalt footwall directly beneath main (basal) contact ore horizon. Not to scale

top breccias. Interstitial spaces are normally filled with metamorphosed basaltic glass and fractured pillow rims, sometimes displaying perlitic devitrification textures, pervasively replaced by calcite ± quartz.

Most contact ores at Kambalda are characterized by the assemblage monoclinic pyrrhotite–pentlandite–pyrite–chalcopyrite–magnetite–ferrochromite, although pentlandite–pyrite–chalcopyrite–magnetite–ferrochromite and pentlandite–pyrite–millerite–chalcopyrite–magnetite–ferrochromite assemblages are present in some shoots.[15] These mineralogical variations correspond to systematic variations of the minor chalcophile elements and PGE (e.g. Cu, Co, Pt, Pd, Ir) with Ni contents (or Fe/Ni ratio) of the sulphide fractions,[6,15] which are interpreted to represent original variations in the compositions of the sulphide melts at different shoots. The distinctive ferrochromites in these ores are considered to be primary chalcophile phases[17] preferentially crystallized at the periphery of the massive sulphide layer at the magmatic stage owing to higher fO_2 at that boundary.[15,16]

All ores have been variably deformed during a complex history of polyphase deformation and lower amphibolite facies regional metamorphism involving an early phase (D_1) of subhorizontal recumbent folding and thrust faulting and later phases (D_2 and D_3) of upright folding and faulting.[8,18] Regional metamorphism is considered to have been syn-D_2/D_3. Although multiple metamorphic peaks have been proposed by some authors,[7,8,9] there is generally little evidence for multiple metamorphism on a regional scale.[19,20] Most local features ascribed to a second metamorphic peak (e.g. dyke alteration, annealed fabrics in ores, K-metasomatism, reaction zones) may be attributed to retrograde metamorphism, which outlasted D_3, and the difficulty of timing or assigning local deformation to one of the recognized major tectonic phases. During peak metamorphism (*ca* 500°C and 2 kb[20]) the ores reverted, at least in part, to metamorphic monosulphide solid solution (mss) plus spinels and pyrite.[21] There is also evidence for considerable late metamorphic addition of sulphur to the ores, probably via the vapour phase.[9,10]

Platinum group elements in contact ore sulphides

As a comparison of the PGE contents of interpillow/interbreccia and vein-type Fe–Ni–Cu sulphides with those of normal contact ores constitutes one of our principal criteria for interpreting their origin, a brief discussion of PGE variations and distributions in the contact ore zone is required.

To establish the average Pd and Ir contents of a typical contact ore zone Keays and co-workers[12] analysed bulked channel samples taken across both massive and matrix ore layers at eleven different localities in the Lunnon Shoot. As summarized in Table 1, they found that both Pd and Ir and Pd/Ir ratios are variable from locality to locality. In addition, analyses of point samples taken across other ore zones revealed that Pd generally increases and Ir decreases from the base of the massive ore layer upwards through the matrix ore layer (see reference 12, Fig. 5). These trends are believed to have been produced by fractionation of the parental sulphide melt at the magmatic stage (when a strong thermal gradient existed over the contact ore zone) and/or by metamorphic differentiation during subsequent metamorphism and deformation of the ores and host rocks.

In comparison, the Pd/Ir ratios of the bulk mined ore (bulk ore composites and mill feed composite in Table 1) are twice those of the contact ore zone taken as a whole and more than three times those of the massive ore zone (Table 1). This difference between the bulk mined ore and the contact ore zone is very important; Keays and co-workers[12] concluded that, during metamorphism, the contact ore zone lost substantial quantities of Pd and other metals, the bulk of which is now in footwall stringers, which are incorporated in ore during mining operations. Keays and co-workers[12] also drew attention to the similarities between the Pd/Ir ratios of the bulk ore samples (*ca* 6.1, which was taken to represent the Pd/Ir ratios of the parental sulphide melts from which the orebodies formed) and those of the spinifex-textured Lunnon 'Metapicrite' (average 8.4, Table 1, which was taken to represent the silicate melt from which the sulphides had separated). Although the Lunnon 'Metapicrite' probably represents a derivative (fractionated) silicate liquid,[18] and not the erupted parental liquid with which the sulphides equilibrated, the similar Pd/Ir ratios of the ores and komatiites support a magmatic origin for the ores.

Although the Ir contents of the contact ore samples are variable (Table 1), all samples contain significant levels of Ir. In fact, the minimum 38.6 ppb Ir value recorded in Table 1 is the lowest value obtained by Keays and co-workers[12] for 76 analyses of a wide range of contact ore samples (see their Table 1).

Interpillow and interbreccia Fe–Ni–Cu sulphides

Field relationships

The metabasalt hosts to interpillow or interbreccia mineralization are identical to unmineralized pillow lavas and flow top breccias elsewhere in the footwall sequence, except that the interstitial spaces are occupied by Fe–Ni–Cu sulphides (Figs. 2, 3 and 4) instead of white carbonate. Some fractured (fragmental) pillow rims may also be present interstitial to mineralized pillow lava (Fig. 3). Transitions from slightly carbonated metahyaloclastite through carbonated metahyaloclastite to mineralized metahyaloclastite have been observed contiguous with a metabasalt–metabasalt ore pinchout (Fig. 5). Both interbreccia and interpillow sulphides are generally found directly beneath or adjacent to normal contact ore horizons (Fig. 2) and rarely extend more than a few metres into the footwall. The massive ore layer may thin dramatically over these sulphide zones, but occurrences of interpillow sulphides beneath otherwise barren metakomatiite/metabasalt contacts are rare and normally restricted to tectonically complex areas. It is significant that interpillow sulphides sometimes occur in the metabasalt *overlying* the contact ore horizons in metabasalt–metabasalt ore pinchouts (see Fig. 4).

One very important locality is the Ken Far East area on the western flank of the Kambalda Dome.[8] Here an interpillow sulphide horizon occurs within the upper pillowed division of a metabasalt flow 15 m beneath the Ken Far East orebody,

Table 1 Metal values and metal ratios of Kambalda carted ore composites, Lunnon contact ore and Lunnon Metapicrite

	Ni, %	Cu, %	Pd, ppb	Ir, ppb	Au, ppb	Ni/Cu	Pd/Ir
*Bulk mined ore composites**	14.3±2.2† (12.0–18.0)	1.12±.12 (.97–1.30)	2056±530 (1615–3041)	—	—	12.7±1.3 (11.4–14.8)	—
*Kambalda mill feed composite***	14.2	.96	1586	258	494	14.8	6.1
Lunnon contact ores‡							
Matrix layer	10.8±1.1 (9.5–12.7)	.93±.61 (.19–2.24)	749±346 (251–1188)	171±82 (38.6–255)	232±236 (41.1–730)	24.2±29.4 (5.59–113)	4.71±3.36 (1.20–12.8)
Massive layer	9.2±1.5 (5.1–11.1)	.53±.59 (.02–1.73)	528±309 (212–1232)	228±42 (174–297)	118±163 (10.8–555)	99.4±147 (2.95–165)	2.29±1.15 (0.89–4.84)
Lunnon metapicrite§	1000±228 ppm (610–1350)	84.3±93.9 ppm (8–263)	9.17±1.90 (6.9–12.1)	1.20±0.29 (0.64–1.59)	4.56±5.40 (0.71–17.6)	40.8±43.4 (3.84–128)	8.42±3.61 (4.34–14.6)

*,**Taken from Ross and Keays:[6] *tonnage-weighted means of 18 four-weekly weighbridge composites for each of six Kambalda oreshoots (Lunnon, Juan, Durkin, Ken, Fisher and McMahon); **one yearly composite of Kambalda total mill feed; analyses by W.M.C. recalculated to 100% sulphides based on S/Ni ratios.

†Data given as mean, standard deviation and range of values.

‡Taken from Keays and co-workers.[12] PGE analyses by R.R.K. recalculated to 100% sulphides based on average sulphur content of Lunnon contact ore (38.8%S).

§Taken from Keays and co-workers.[12] Average of 10 analyses of platy spinifex-textured metakomatiite recalculated volatile-free.

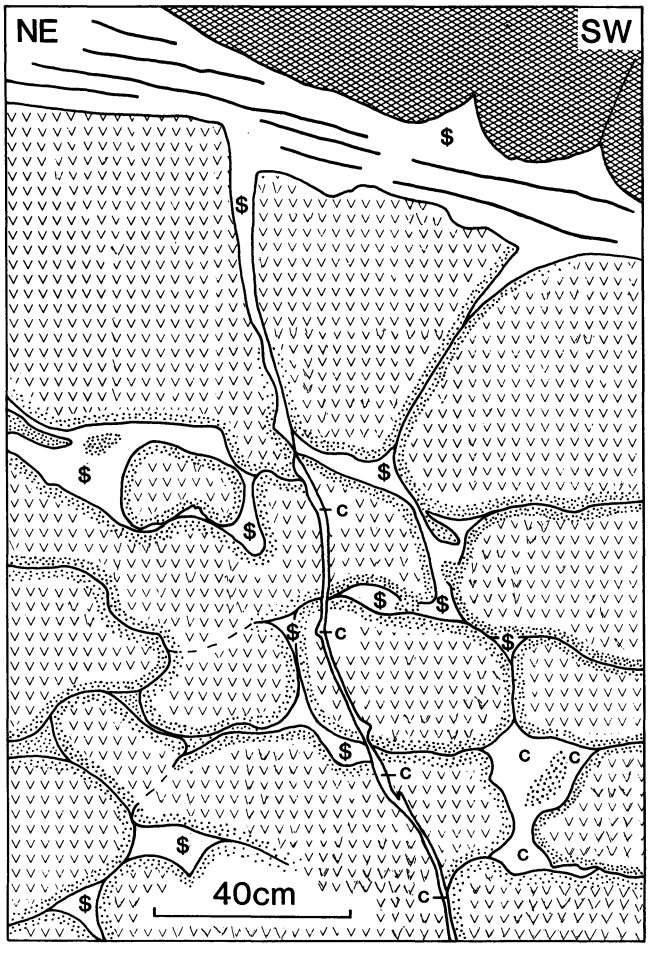

JUAN B 1218 NNW

Fig. 2 Vertical face sketch of interpillow sulphides directly beneath contact ore horizon exposed in Juan B 1218 NNW open stope. Note that interpillow sulphides ($) are physically contiguous with contact ore. Dark, amphibole-rich recrystallized pillow margins are stippled. Some interpillow spaces are filled with calcite ± quartz; this is normal situation away from the ore zone. Legend applies to all figures

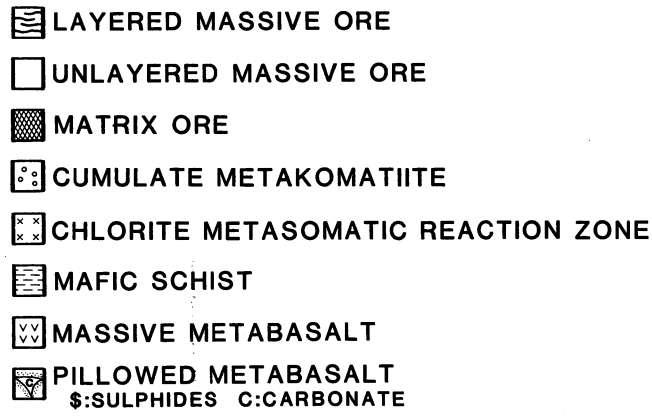

KEN 205 SE RISE

Fig. 3 Vertical face sketch of interpillow sulphides in Ken 205 SE rise showing extensionally fractured pillow margin (stippled at right) interstitial to Fe–Ni–Cu sulphides. Note associated calcite; these relationships are identical to those observed where carbonate exclusively occurs interstitial to pillow lava. Some metabasalt is bleached (carbonated: hachured); other ornamentation as in Fig. 2

apparently separated from the contact ore horizon. This stratigraphic relationship has been used to infer early eruption of sulphides prior to the contact ores.[9] Underground exposure in this area is, however, limited to one margin of the ore horizon and diamond drill hole data indicate an overall inverted mushroom shape for the interpillow sulphide mineralization.[22] As such, the interpillow sulphides cannot be assumed to represent a stratigraphically isolated horizon. In addition, although the metabasalt stratigraphy appears to be intact, much of the metabasalt is strongly foliated, some pillows are flattened with length to

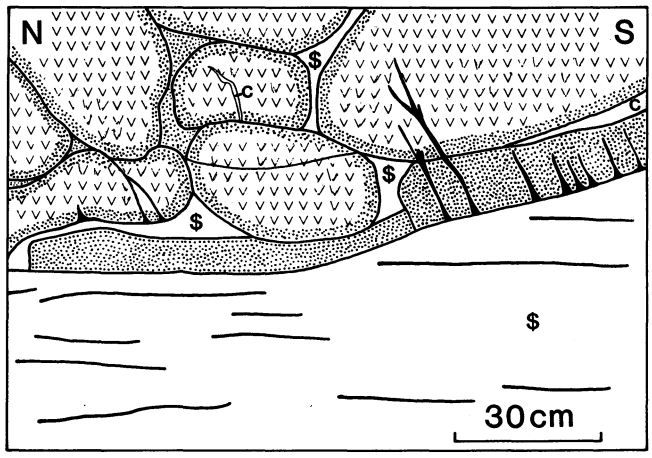

JUAN B 1218 NNW

Fig. 4 Vertical face sketch in same locality as Fig. 2 showing upper contact of contact ore horizon near its margin where massive sulphides are directly overlain by metabasalt (i.e. metabasalt–metabasalt ore pinchout, see Fig. 1). Note presence of interpillow sulphides stratigraphically *above* contact ore and sulphide stringers (black) transgressing basalt. Ornamentation as in Fig. 2

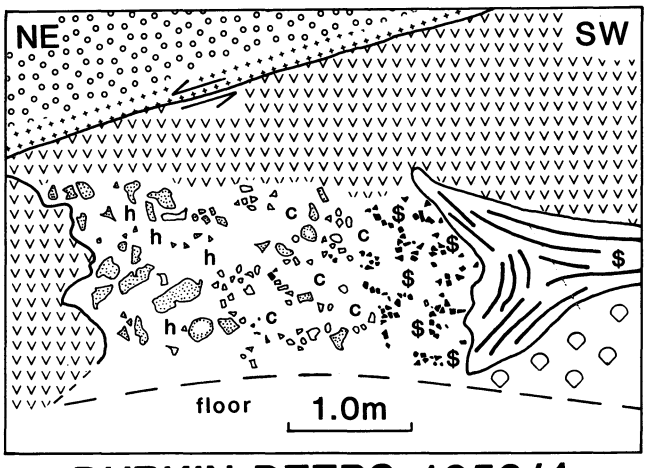

DURKIN DEEPS 1050/4

Fig. 5 Vertical face sketch of pinchout of the contact ore horizon exposed in Durkin Deeps 1050/4 cut and fill stope. Toe of a basaltic lava flow (left) and flow front volcaniclastic breccia (shown schematically) are stratigraphically contiguous with ore horizon (right). Metabasalt above ore pinchout is massive; that below is pillowed. Note that matrix component of breccia changes from metahyaloclastite (h) through white calcite ± quartz (c) to Fe–Ni–Cu sulphides ($) towards ore horizon. Ornamentation as in Fig. 2

width ratios in excess of 10:1 and sulphides exhibit strong deformation fabrics—all indicative of pervasive penetrative deformation in the area.[16] The significance of this is discussed further below.

Mineralogy and geochemistry

Most interpillow and interbreccia sulphide assemblages (Table 2) comprise pyrrhotite–pentlandite ± pyrite ± chalcopyrite with variable carbonate ± quartz, i.e. similar to normal contact ores. Magnetite is rare and ferrochromite is conspicuously absent. Most interpillow/interbreccia sulphides contain abundant fine quartz–carbonate inclusions. Pentlandite normally rims pyrrhotite, or occurs as flames within or along fractures in pyrrhotite. Pyrite–chalcopyrite (if present) form symplectic intergrowths. The relationship between the sulphides and interstitial carbonate in these areas could not be assessed as both have been completely recrystallized during metamorphism and form equilibrium granoblastic textures.

Geochemically, the interpillow and interbreccia sulphides (Table 2) are highly variable, but within the range of Lunnon contact ore compositions (Table 1). They are depleted in ore metals, however, especially Cu and PGE, relative to Kambalda bulk ore composites and mill feed (Table 1). Some of the variation is undoubtedly a result of the point sampling required for this style of mineralization. Chrome and Zn contents and S/Se ratios are also variable, but within the normal range for massive ores.[23]

Vein-type Fe–Ni–Cu sulphides

Field relationships

Several types of hydrothermal carbonate and/or quartz veins within the footwall metabasalt at Kambalda may be distinguished on the basis of their mineralogy, alteration envelopes (or absence of) and timing with respect to deformation. Although several different generations of veins may occur within a single area, three major types of veins have been recognized at Hunt mine on the southwestern flank of the Kambalda Dome:[24] (1) carbonate-rich veins (mainly calcite), averaging <2 cm in thickness, which do not exhibit alteration envelopes and are commonly multiply deformed; (2) late tectonic quartz veins with recrystallized (granoblastic) fabrics, sharp margins and weak wallrock alteration; and (3) late tectonic quartz-rich, gold-related veins with albite–ankerite margins and strong carbonate–albite–pyrite–biotite alteration envelopes; quartz exhibits strongly deformed fabrics.

The Fe–Ni–Cu sulphide–quartz veins examined in this study are also late tectonic and commonly exhibit strongly deformed quartz fabrics and are therefore physically similar to the auriferous quartz veins, but have sharp margins with negligible wallrock alteration (Fig. 6). They are to be further distinguished from rare quartz–carbonate–iron sulphide (pyrite–marcasite)–nickel arsenide (gersdorffite) ± Au veins, which do exhibit strong alteration envelopes. The latter are similar to those characterizing the vein-type arsenical nickel deposit at Mt Martin, Western Australia.[1]

The Fe–Ni–Cu sulphide–quartz veins occur almost exclusively within the footwall metabasalt, either sub-parallel to or steeply transgressing the deformed metakomatiite/ore/metabasalt contact, thinning rapidly into the talc–carbonate metakomatiites. These veins are not an important aspect of the nickel mineralization at Kambalda in terms of abundance and appear to be most common at the Juan Complex. Significantly, both Hunt and Juan occupy hinge positions along the major anticlinal axis of the Kambalda Dome,[8] and it has been suggested that the preferential localization of the hydrothermal veins in the footwall metabasalt may be due to preferential hydraulic fracturing of the more brittle metabasalt during uplift of the Kambalda Dome.[24]

Mineralogy and geochemistry

Most Fe–Ni–Cu sulphide veins are quartz-rich, although albite and/or carbonate are common marginal phases. Veins within the ultramafic rocks are dolomite-rich. Quartz is normally deformed, ranging from bent grains that exhibit undulose extinction to highly deformed grains with fine discontinuous or Boehme deformation lamellae and deformation bands. Albite may be partially retrogressively altered to sericite. Sulphide assemblages comprise pyrrhotite–pentlandite–pyrite ± violarite ± chalcopyrite, and are distinctly more pyrite- and commonly more chalcopyrite-rich than interpillow sulphides. Spinels are conspicuously absent. Pentlandite occupies fractures with chalcopyrite, or occurs as flames within pyrrhotite. Pyrite is commonly coarse-grained and contains numerous peripheral gangue inclusions; some pyrite has replaced pyrrho-

Table 2 Metal values, metal ratios and sulphide assemblages in 13 metamorphically or hydrothermally mobilized magmatic sulphide samples from Kambalda

Sample No.	Location/stope	Type*	Percent sulphides	wt%			ppm					ppb							
				S	Fe	Ni	Cu	Co	Cr	Zn	Se	Pd	Ir	Au	Ni/Cu	Ni/Co	Pd/Ir	S/Se	Assemblage†
95106	Juan B 1218	IPS	82.6	37.30	(52.9)	9.23	3100	1900	670	60	57.5	638	130	57.9	29.8	48.6	4.91	6490	po–pn–(py)–(cp)
95107	Ken Main 205	IPS	63.3	36.86	(50.2)	12.07	1610	1990	4800	110	33.0	1240	136	16.8	75.0	60.7	9.12	11200	po–pn–(mt)–(fc)–(py)
												1580	171	17.4			9.24		
95108	Durkin Deeps 1050	IPS	67.6	39.04	(48.1)	11.07	1.20%	3670	1910	90	39.4	1030	163	93.8	9.24	30.2	6.32	9910	po–pn–py–(sm)–(cp)
												1157	244	89.8			4.74		
95109	Juan B 1218	IPS	39.4	37.61	(53.4)	8.20	4590	1600	1370	330	38.3	226	99.5	19.8	17.9	51.3	2.27	9820	po–pn–(cp)–(mt)
												151	95.7	28.7			1.58		
95110	Juan B 1218	IPS	90.9	38.39	(53.4)	7.87	2310	840	660	30	48.8	117	156	19.9	34.1	93.7	.75	7870	po–pn–(cp)–(mt)
95111	Juan West 916	IPS	41.5	37.49	(54.8)	7.11	3130	1590	1520	240	30.6	1050	153	59.8	22.7	44.7	6.86	12300	po–pn–(cp)
95112	Ken Main NO5	IPS	31.8	37.76	(47.8)	13.18	5660	3590	3270	380	N/A	1429	175	24.2	23.3	36.8	8.17	—	po–pn–vl
95113	Juan Main 1104	IBS	51.5	36.72	(48.8)	13.98	2870	2160	250	170	51.7	427	139	108	48.7	64.7	3.07	7100	po–pn–cp–(py)
95115	Juan B 1118	HQV	50.8	39.78	(48.3)	11.08	3980	4170	330	180	246	72600	(<.08)	675	27.8	26.6	≫	1620	po–pn–py–(cp)
												60800	.35	1160			≫		
95116	Juan Main 1204	HQV	21.1	38.86	(45.3)	12.84	2.35%	1370	190	5210	58.8	1000	1.1	41.7	5.47	93.7	877	6610	po–pn–py–cp–(sm)
												654	1.5	62.1			436		
95117	Juan B 1218	HQV	62.5	42.56	(49.7)	7.12	1860	3870	30	60	113	310	<.03	306	38.3	18.4	≫	3770	po–pn–py–vl–(cp)
95118	Lunnon	HQV	88.5	39.19	(52.2)	8.31	1560	1540	80	30	44.6	571	(.07)	14.5	53.3	54.0	≫	8790	po–pn–vl–py–(sph)–(sm)
	Upper Roll 704											567	.73	12.7			777		
95119	Juan Main 1204	HCV	25.9	35.37	(37.9)	10.42	16.0%	930	190	2160	21.1	298	N/A	3620	0.65	112	—	16800	pn–po–cp–(sph)–(mt)

Notes: All samples are representative hand samples from underground exposures except 95112, which is a split of diamond drill core; analyses recalculated to 100% sulphides based on sulphur contents of samples and relative proportions of assumed stoichiometric sulphide phases determined by quantitative X-ray diffraction technique;[31] sulphur by Leco automatic titrator; Ni, Cu, Co, Cr and Zn by atomic absorption spectrophotometry with routine precision of ± 5–10%; Fe by difference; precious metals and Se by radiochemical neutron activation with estimated accuracy of ± 15% (procedure modified after Crocket and co-workers[32] and Keays *et al.*[33]) See Marston and Kay[9] and Gresham and Loftus-Hills[8] for mine locations; N/A=not analysed; ≫=ratio greater than 999.

*IPS=interpillow sulphides, IBS=interbreccia sulphides, HQV=hydrothermal sulphide–quartz±albite vein, HCV=hydrothermal sulphide–carbonate vein.

†cp=chalcopyrite, fc=ferrochromite, mt=magnetite, pn=pentlandite, po=pyrrhotite, py=pyrite, sm=smythite, sph=sphalerite, vl=violarite.

Metamorphically and hydrothermally mobilized Fe–Ni–Cu sulphides at Kambalda, Western Australia

C. M. Lesher B.Sc., A.M.
Formerly Department of Geology, University of Western Australia, Nedlands, Western Australia (now J. Tuzo Wilson Research Laboratories, University of Toronto-Erindale, Mississauga, Ontario, Canada)
Reid R. Keays B.Sc., Ph.D.
Department of Geology, University of Melbourne, Melbourne, Victoria, Australia

Synopsis

The komatiite-associated Fe–Ni–Cu sulphide mineralization at Kambalda, Western Australia, is generally believed to be magmatic in origin, but a number of postmagmatic processes significantly modified the original distribution, structure, texture, mineralogy and chemistry of the ores. Two important types of mobilized magmatic sulphides are *interpillow/interbreccia sulphides* and *hydrothermal vein-type sulphides.*

Interpillow and interbreccia sulphides occur interstitial to pillowed or volcaniclastic footwall metabasalts beneath or adjacent to the stratiform contact ore horizons. They are mineralogically and compositionally similar to massive ores (and are similarly depleted in PGE relative to the compositions of bulk samples of mined ores), but normally do not contain the distinctive chalcophile ferrochromites characteristic of contact ores. They are interpreted as magmatic sulphides that have been mobilized from the overlying or adjacent massive sulphide layer during peak tectono-metamorphism.

Hydrothermal sulphide–quartz ± albite veins also occur in the footwall metabasalt and contain unannealed deformation fabrics indicative of emplacement during retrograde metamorphism. The high Ni and Pd contents of these sulphides (7–13% Ni, up to 70 ppm Pd) indicate that the metals have been derived from the spatially associated komatiites and/or contact ores, consistent with the Pd depletion previously inferred for massive ores. Very low Ir contents and high Pd/Ir ratios of the vein-type sulphides confirm an aqueous transportation-deposition mechanism; hydrothermal transfer of PGE results in strong decoupling of Pd from Ir.

There appears to be a complete continuum of sulphide mobilization at Kambalda ranging from whole-scale physical dislocation (fault offset ores) and selective mobilization (stringer sulphides) through metamorphic replacement (interpillow/interbreccia sulphides) to hydrothermal dissolution and redeposition (vein-type sulphides).

The type-examples of komatiite-associated nickel deposits[1] occur at the base of the ultramafic lava pile at Kambalda, Western Australia. On the basis of such features as gradational disseminated/matrix/massive sulphide segregation at the base of the host units, distinctive chalcophile ferrochromites in sulphide ores, and ore geochemistry in the light of known and inferred partitioning behaviour with komatiitic magmas, the Fe–Ni–Cu sulphides at Kambalda are generally considered to be magmatic in origin.[2–6] A complex history of polyphase deformation and lower amphibolite facies regional metamorphism[7,8] has, however, resulted in some redistribution and mobilization of the magmatic sulphides, particularly of massive sulphides. Tectonic-metamorphic physical mobilization of sulphides to form footwall stringers, fault offset and tectonic breccia ores[2,7,8,9] plus the introduction of sulphur via the vapour phase during waning metamorphism[10] have been considered important ore-modifying processes.

The aim of this paper is to describe and evaluate two additional types of mobilized magmatic sulphides, which have considerable implications with regard to the importance of postmagmatic processes in sulphide redistribution: (1) Fe–Ni–Cu sulphide mineralization interstitial to pillowed footwall metabasalts, termed *interpillow sulphides,* or interstitial to volcaniclastic flow top breccias, termed *interbreccia sulphides,* and (2) Fe–Ni–Cu sulphides that occur within late metamorphic quartz ± albite ± carbonate veins predominantly within the metabasalt footwall, referred to as *vein-type sulphides.* Interpillow sulphides have been cursorily mentioned by several authors and used as evidence for a volcanic origin for the Kambalda ores in general,[8] or for early eruption of sulphide-rich melts;[9] however, no specific evidence has been given to indicate that these sulphides are in their original stratigraphic positions or if they are actually magmatic. Vein-type sulphides have not been previously documented at Kambalda and should be distinguished from the chalcopyrite-rich sulphide stringers sporadically present in the immediate footwall of many ore-shoots.[2,11,12]

It has recently been appreciated that the platinum group elements (PGE) are of considerable value in distinguishing between primary magmatic, fractionated magmatic and hydrothermal sulphides,[6,12,13] and an evaluation of the decoupling of Pd and Au from Ir during fractionation and hydrothermal mobilization is an important aspect of our interpretation of the formation of interpillow and vein-type Fe–Ni–Cu sulphide mineralization at Kambalda.

Geological setting

The geology of the Kambalda area has recently been reviewed by Gresham and Loftus-Hills.[8] Most of the high-grade Fe–Ni–Cu sulphide mineralization in the area occurs directly on the basal contact of a metakomatiite sequence (Fig. 1) and is termed *contact ore.* Contact ores are normally confined to linear, rarely elliptical, re-entrant embayments in the footwall metabasalt, referred to as 'troughs', in which the lateral margins of the ore horizons are directly overlain by metabasalt forming metabasalt–metabasalt ore pinchouts (Fig. 1).

Contact mineralization normally comprises massive Fe–Ni–Cu sulphides overlain by matrix to disseminated sulphides within the host metakomatiite unit directly overlying the footwall tholeiitic metabasalt.[2,11] All contacts between massive sulphides and less massive sulphides or wallrocks have been loci for ferrochromite crystallization.[14–16] The absence of any basal ultramafic selvedge, or a metasomatic reaction zone that indicates its former presence, has been used to infer that the sulphides were present in segregated layers at the time of emplacement.[3,9] Underground mapping indicates that the footwall metabasalt comprises both pillowed and massive facies commonly forming compound flows 5 to 30 m thick with pillowed upper divisions and massive lower divisions, and massive flows with broken pillow and metahyaloclastite flow

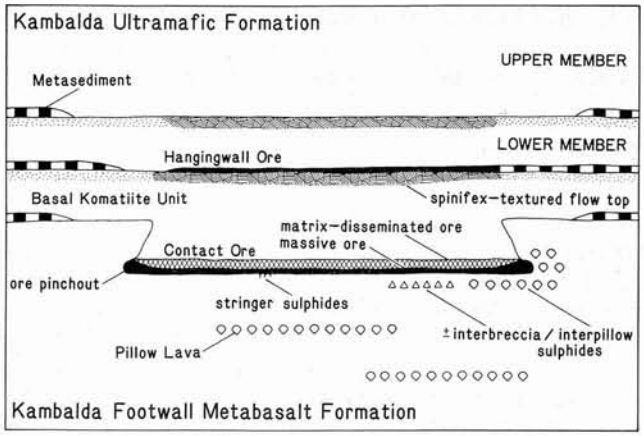

Fig. 1 Schematic sketch of Kambalda oreshoot in cross-section after removal of superimposed structural deformation. Metabasalts comprise both massive and pillowed facies with volcaniclastic flow top breccia horizons; interpillow/interbreccia and hydrothermal vein-type sulphides in this study occur predominantly in metabasalt footwall directly beneath main (basal) contact ore horizon. Not to scale

top breccias. Interstitial spaces are normally filled with metamorphosed basaltic glass and fractured pillow rims, sometimes displaying perlitic devitrification textures, pervasively replaced by calcite ± quartz.

Most contact ores at Kambalda are characterized by the assemblage monoclinic pyrrhotite–pentlandite–pyrite–chalcopyrite–magnetite–ferrochromite, although pentlandite–pyrite–chalcopyrite–magnetite–ferrochromite and pentlandite–pyrite–millerite–chalcopyrite–magnetite–ferrochromite assemblages are present in some shoots.[15] These mineralogical variations correspond to systematic variations of the minor chalcophile elements and PGE (e.g. Cu, Co, Pt, Pd, Ir) with Ni contents (or Fe/Ni ratio) of the sulphide fractions,[6,15] which are interpreted to represent original variations in the compositions of the sulphide melts at different shoots. The distinctive ferrochromites in these ores are considered to be primary chalcophile phases[17] preferentially crystallized at the periphery of the massive sulphide layer at the magmatic stage owing to higher f_{O_2} at that boundary.[15,16]

All ores have been variably deformed during a complex history of polyphase deformation and lower amphibolite facies regional metamorphism involving an early phase (D_1) of subhorizontal recumbent folding and thrust faulting and later phases (D_2 and D_3) of upright folding and faulting.[8,18] Regional metamorphism is considered to have been syn-D_2/D_3. Although multiple metamorphic peaks have been proposed by some authors,[7,8,9] there is generally little evidence for multiple metamorphism on a regional scale.[19,20] Most local features ascribed to a second metamorphic peak (e.g. dyke alteration, annealed fabrics in ores, K-metasomatism, reaction zones) may be attributed to retrograde metamorphism, which outlasted D_3, and the difficulty of timing or assigning local deformation to one of the recognized major tectonic phases. During peak metamorphism (*ca* 500°C and 2 kb[20]) the ores reverted, at least in part, to metamorphic monosulphide solid solution (mss) plus spinels and pyrite.[21] There is also evidence for considerable late metamorphic addition of sulphur to the ores, probably via the vapour phase.[9,10]

Platinum group elements in contact ore sulphides

As a comparison of the PGE contents of interpillow/interbreccia and vein-type Fe–Ni–Cu sulphides with those of normal contact ores constitutes one of our principal criteria for interpreting their origin, a brief discussion of PGE variations and distributions in the contact ore zone is required.

To establish the average Pd and Ir contents of a typical contact ore zone Keays and co-workers[12] analysed bulked channel samples taken across both massive and matrix ore layers at eleven different localities in the Lunnon Shoot. As summarized in Table 1, they found that both Pd and Ir and Pd/Ir ratios are variable from locality to locality. In addition, analyses of point samples taken across other ore zones revealed that Pd generally increases and Ir decreases from the base of the massive ore layer upwards through the matrix ore layer (see reference 12, Fig. 5). These trends are believed to have been produced by fractionation of the parental sulphide melt at the magmatic stage (when a strong thermal gradient existed over the contact ore zone) and/or by metamorphic differentiation during subsequent metamorphism and deformation of the ores and host rocks.

In comparison, the Pd/Ir ratios of the bulk mined ore (bulk ore composites and mill feed composite in Table 1) are twice those of the contact ore zone taken as a whole and more than three times those of the massive ore zone (Table 1). This difference between the bulk mined ore and the contact ore zone is very important; Keays and co-workers[12] concluded that, during metamorphism, the contact ore zone lost substantial quantities of Pd and other metals, the bulk of which is now in footwall stringers, which are incorporated in ore during mining operations. Keays and co-workers[12] also drew attention to the similarities between the Pd/Ir ratios of the bulk ore samples (*ca* 6.1, which was taken to represent the Pd/Ir ratios of the parental sulphide melts from which the orebodies formed) and those of the spinifex-textured Lunnon 'Metapicrite' (average 8.4, Table 1, which was taken to represent the silicate melt from which the sulphides had separated). Although the Lunnon 'Metapicrite' probably represents a derivative (fractionated) silicate liquid,[18] and not the erupted parental liquid with which the sulphides equilibrated, the similar Pd/Ir ratios of the ores and komatiites support a magmatic origin for the ores.

Although the Ir contents of the contact ore samples are variable (Table 1), all samples contain significant levels of Ir. In fact, the minimum 38.6 ppb Ir value recorded in Table 1 is the lowest value obtained by Keays and co-workers[12] for 76 analyses of a wide range of contact ore samples (see their Table 1).

Interpillow and interbreccia Fe–Ni–Cu sulphides

Field relationships

The metabasalt hosts to interpillow or interbreccia mineralization are identical to unmineralized pillow lavas and flow top breccias elsewhere in the footwall sequence, except that the interstitial spaces are occupied by Fe–Ni–Cu sulphides (Figs. 2, 3 and 4) instead of white carbonate. Some fractured (fragmental) pillow rims may also be present interstitial to mineralized pillow lava (Fig. 3). Transitions from slightly carbonated metahyaloclastite through carbonated metahyaloclastite to mineralized metahyaloclastite have been observed contiguous with a metabasalt–metabasalt ore pinchout (Fig. 5). Both interbreccia and interpillow sulphides are generally found directly beneath or adjacent to normal contact ore horizons (Fig. 2) and rarely extend more than a few metres into the footwall. The massive ore layer may thin dramatically over these sulphide zones, but occurrences of interpillow sulphides beneath otherwise barren metakomatiite/metabasalt contacts are rare and normally restricted to tectonically complex areas. It is significant that interpillow sulphides sometimes occur in the metabasalt *overlying* the contact ore horizons in metabasalt–metabasalt ore pinchouts (see Fig. 4).

One very important locality is the Ken Far East area on the western flank of the Kambalda Dome.[8] Here an interpillow sulphide horizon occurs within the upper pillowed division of a metabasalt flow 15 m beneath the Ken Far East orebody,

Table 1 Metal values and metal ratios of Kambalda carted ore composites, Lunnon contact ore and Lunnon Metapicrite

	Ni, %	Cu, %	Pd, ppb	Ir, ppb	Au, ppb	Ni/Cu	Pd/Ir
*Bulk mined ore composites**	14.3±2.2† (12.0–18.0)	1.12±.12 (.97–1.30)	2056±530 (1615–3041)	—	—	12.7±1.3 (11.4–14.8)	—
*Kambalda mill feed composite***	14.2	.96	1586	258	494	14.8	6.1
Lunnon contact ores‡							
Matrix layer	10.8±1.1 (9.5–12.7)	.93±.61 (.19–2.24)	749±346 (251–1188)	171±82 (38.6–255)	232±236 (41.1–730)	24.2±29.4 (5.59–113)	4.71±3.36 (1.20–12.8)
Massive layer	9.2±1.5 (5.1–11.1)	.53±.59 (.02–1.73)	528±309 (212–1232)	228±42 (174–297)	118±163 (10.8–555)	99.4±147 (2.95–165)	2.29±1.15 (0.89–4.84)
Lunnon metapicrite§	1000±228 ppm (610–1350)	84.3±93.9 ppm (8–263)	9.17±1.90 (6.9–12.1)	1.20±0.29 (0.64–1.59)	4.56±5.40 (0.71–17.6)	40.8±43.4 (3.84–128)	8.42±3.61 (4.34–14.6)

*,**Taken from Ross and Keays:[6] *tonnage-weighted means of 18 four-weekly weighbridge composites for each of six Kambalda oreshoots (Lunnon, Juan, Durkin, Ken, Fisher and McMahon); **one yearly composite of Kambalda total mill feed; analyses by W.M.C. recalculated to 100% sulphides based on S/Ni ratios.

†Data given as mean, standard deviation and range of values.

‡Taken from Keays and co-workers.[12] PGE analyses by R.R.K. recalculated to 100% sulphides based on average sulphur content of Lunnon contact ore (38.8%S).

§Taken from Keays and co-workers.[12] Average of 10 analyses of platy spinifex-textured metakomatiite recalculated volatile-free.

JUAN B 1218 NNW

Fig. 2 Vertical face sketch of interpillow sulphides directly beneath contact ore horizon exposed in Juan B 1218 NNW open stope. Note that interpillow sulphides (S) are physically contiguous with contact ore. Dark, amphibole-rich recrystallized pillow margins are stippled. Some interpillow spaces are filled with calcite ± quartz; this is normal situation away from the ore zone. Legend applies to all figures

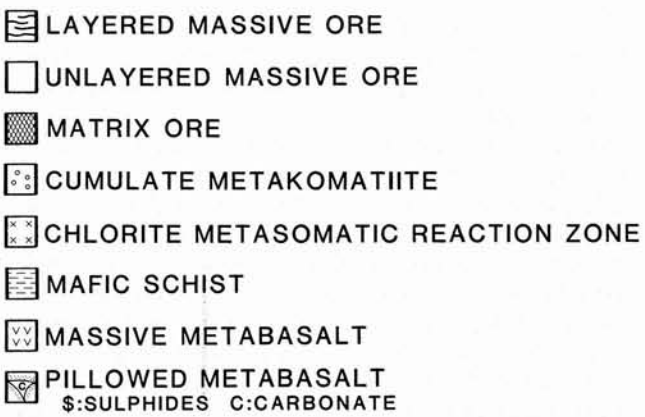

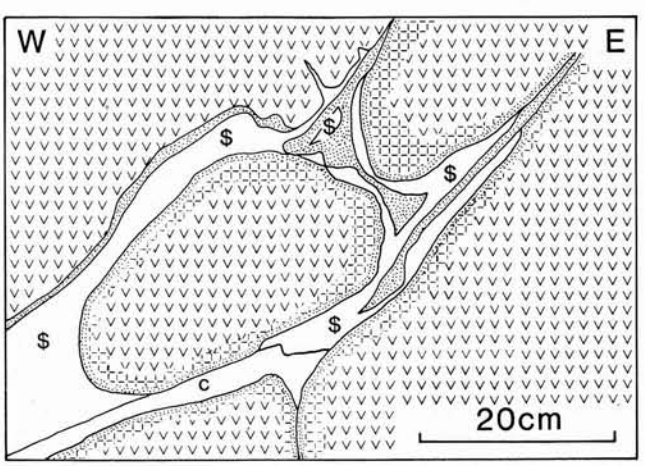

KEN 205 SE RISE

Fig. 3 Vertical face sketch of interpillow sulphides in Ken 205 SE rise showing extensionally fractured pillow margin (stippled at right) interstitial to Fe–Ni–Cu sulphides. Note associated calcite; these relationships are identical to those observed where carbonate exclusively occurs interstitial to pillow lava. Some metabasalt is bleached (carbonated: hachured); other ornamentation as in Fig. 2

apparently separated from the contact ore horizon. This stratigraphic relationship has been used to infer early eruption of sulphides prior to the contact ores.[9] Underground exposure in this area is, however, limited to one margin of the ore horizon and diamond drill hole data indicate an overall inverted mushroom shape for the interpillow sulphide mineralization.[22] As such, the interpillow sulphides cannot be assumed to represent a stratigraphically isolated horizon. In addition, although the metabasalt stratigraphy appears to be intact, much of the metabasalt is strongly foliated, some pillows are flattened with length to

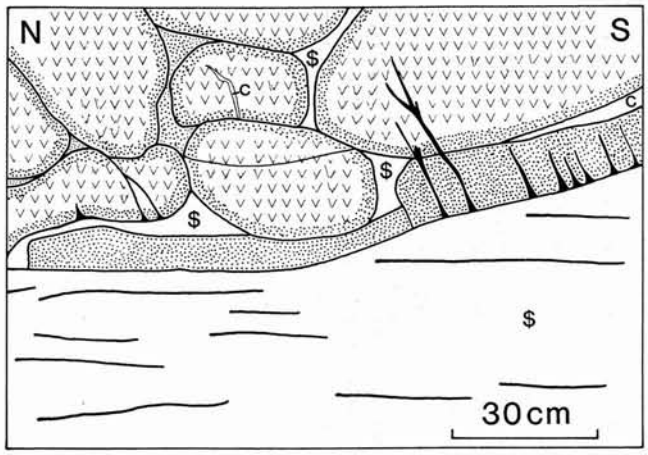

JUAN B 1218 NNW

Fig. 4 Vertical face sketch in same locality as Fig. 2 showing upper contact of contact ore horizon near its margin where massive sulphides are directly overlain by metabasalt (i.e. metabasalt–metabasalt ore pinchout, see Fig. 1). Note presence of interpillow sulphides stratigraphically *above* contact ore and sulphide stringers (black) transgressing basalt. Ornamentation as in Fig. 2

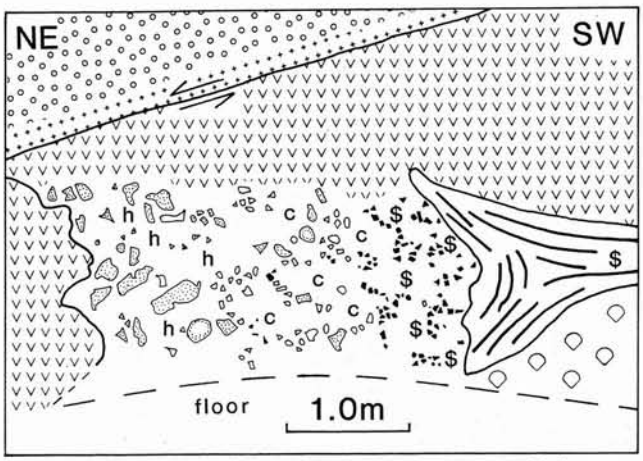

DURKIN DEEPS 1050/4

Fig. 5 Vertical face sketch of pinchout of the contact ore horizon exposed in Durkin Deeps 1050/4 cut and fill stope. Toe of a basaltic lava flow (left) and flow front volcaniclastic breccia (shown schematically) are stratigraphically contiguous with ore horizon (right). Metabasalt above ore pinchout is massive; that below is pillowed. Note that matrix component of breccia changes from metahyaloclastite (h) through white calcite ± quartz (c) to Fe–Ni–Cu sulphides ($) towards ore horizon. Ornamentation as in Fig. 2

width ratios in excess of 10:1 and sulphides exhibit strong deformation fabrics—all indicative of pervasive penetrative deformation in the area.[16] The significance of this is discussed further below.

Mineralogy and geochemistry

Most interpillow and interbreccia sulphide assemblages (Table 2) comprise pyrrhotite–pentlandite ± pyrite ± chalcopyrite with variable carbonate ± quartz, i.e. similar to normal contact ores. Magnetite is rare and ferrochromite is conspicuously absent. Most interpillow/interbreccia sulphides contain abundant fine quartz–carbonate inclusions. Pentlandite normally rims pyrrhotite, or occurs as flames within or along fractures in pyrrhotite. Pyrite–chalcopyrite (if present) form symplectic intergrowths. The relationship between the sulphides and interstitial carbonate in these areas could not be assessed as both have been completely recrystallized during metamorphism and form equilibrium granoblastic textures.

Geochemically, the interpillow and interbreccia sulphides (Table 2) are highly variable, but within the range of Lunnon contact ore compositions (Table 1). They are depleted in ore metals, however, especially Cu and PGE, relative to Kambalda bulk ore composites and mill feed (Table 1). Some of the variation is undoubtedly a result of the point sampling required for this style of mineralization. Chrome and Zn contents and S/Se ratios are also variable, but within the normal range for massive ores.[23]

Vein-type Fe–Ni–Cu sulphides

Field relationships

Several types of hydrothermal carbonate and/or quartz veins within the footwall metabasalt at Kambalda may be distinguished on the basis of their mineralogy, alteration envelopes (or absence of) and timing with respect to deformation. Although several different generations of veins may occur within a single area, three major types of veins have been recognized at Hunt mine on the southwestern flank of the Kambalda Dome:[24] (1) carbonate-rich veins (mainly calcite), averaging <2 cm in thickness, which do not exhibit alteration envelopes and are commonly multiply deformed; (2) late tectonic quartz veins with recrystallized (granoblastic) fabrics, sharp margins and weak wallrock alteration; and (3) late tectonic quartz-rich, gold-related veins with albite–ankerite margins and strong carbonate–albite–pyrite–biotite alteration envelopes; quartz exhibits strongly deformed fabrics.

The Fe–Ni–Cu sulphide–quartz veins examined in this study are also late tectonic and commonly exhibit strongly deformed quartz fabrics and are therefore physically similar to the auriferous quartz veins, but have sharp margins with negligible wallrock alteration (Fig. 6). They are to be further distinguished from rare quartz–carbonate–iron sulphide (pyrite–marcasite)–nickel arsenide (gersdorffite) ± Au veins, which do exhibit strong alteration envelopes. The latter are similar to those characterizing the vein-type arsenical nickel deposit at Mt Martin, Western Australia.[1]

The Fe–Ni–Cu sulphide–quartz veins occur almost exclusively within the footwall metabasalt, either sub-parallel to or steeply transgressing the deformed metakomatiite/ore/metabasalt contact, thinning rapidly into the talc–carbonate metakomatiites. These veins are not an important aspect of the nickel mineralization at Kambalda in terms of abundance and appear to be most common at the Juan Complex. Significantly, both Hunt and Juan occupy hinge positions along the major anticlinal axis of the Kambalda Dome,[8] and it has been suggested that the preferential localization of the hydrothermal veins in the footwall metabasalt may be due to preferential hydraulic fracturing of the more brittle metabasalt during uplift of the Kambalda Dome.[24]

Mineralogy and geochemistry

Most Fe–Ni–Cu sulphide veins are quartz-rich, although albite and/or carbonate are common marginal phases. Veins within the ultramafic rocks are dolomite-rich. Quartz is normally deformed, ranging from bent grains that exhibit undulose extinction to highly deformed grains with fine discontinuous or Boehme deformation lamellae and deformation bands. Albite may be partially retrogressively altered to sericite. Sulphide assemblages comprise pyrrhotite–pentlandite–pyrite ± violarite ± chalcopyrite, and are distinctly more pyrite- and commonly more chalcopyrite-rich than interpillow sulphides. Spinels are conspicuously absent. Pentlandite occupies fractures with chalcopyrite, or occurs as flames within pyrrhotite. Pyrite is commonly coarse-grained and contains numerous peripheral gangue inclusions; some pyrite has replaced pyrrho-

Table 2 Metal values, metal ratios and sulphide assemblages in 13 metamorphically or hydrothermally mobilized magmatic sulphide samples from Kambalda

Sample No.	Location/stope	Type*	Percent sulphides	wt%			ppm					ppb							
				S	Fe	Ni	Cu	Co	Cr	Zn	Se	Pd	Ir	Au	Ni/Cu	Ni/Co	Pd/Ir	S/Se	Assemblage†
95106	Juan B 1218	IPS	82.6	37.30	(52.9)	9.23	3100	1900	670	60	57.5	638	130	57.9	29.8	48.6	4.91	6490	po–pn–(py)–(cp)
95107	Ken Main 205	IPS	63.3	36.86	(50.2)	12.07	1610	1990	4800	110	33.0	1240	136	16.8	75.0	60.7	9.12	11200	po–pn–(mt)–(fc)–(py)
												1580	171	17.4			9.24		
95108	Durkin Deeps 1050	IPS	67.6	39.04	(48.1)	11.07	1.20%	3670	1910	90	39.4	1030	163	93.8	9.24	30.2	6.32	9910	po–pn–py–(sm)–(cp)
												1157	244	89.8			4.74		
95109	Juan B 1218	IPS	39.4	37.61	(53.4)	8.20	4590	1600	1370	330	38.3	226	99.5	19.8	17.9	51.3	2.27	9820	po–pn–(cp)–(mt)
												151	95.7	28.7			1.58		
95110	Juan B 1218	IPS	90.9	38.39	(53.4)	7.87	2310	840	660	30	48.8	117	156	19.9	34.1	93.7	.75	7870	po–pn–(cp)–(mt)
95111	Juan West 916	IPS	41.5	37.49	(54.8)	7.11	3130	1590	1520	240	30.6	1050	153	59.8	22.7	44.7	6.86	12300	po–pn–(cp)
95112	Ken Main NO5	IPS	31.8	37.76	(47.8)	13.18	5660	3590	3270	380	N/A	1429	175	24.2	23.3	36.8	8.17	—	po–pn–vl
95113	Juan Main 1104	IBS	51.5	36.72	(48.8)	13.98	2870	2160	250	170	51.7	427	139	108	48.7	64.7	3.07	7100	po–pn–cp–(py)
95115	Juan B 1118	HQV	50.8	39.78	(48.3)	11.08	3980	4170	330	180	246	72600	(<.08)	675	27.8	26.6	≫	1620	po–pn–py–(cp)
												60800	.35	1160			≫		
95116	Juan Main 1204	HQV	21.1	38.86	(45.3)	12.84	2.35%	1370	190	5210	58.8	1000	1.1	41.7	5.47	93.7	877	6610	po–pn–py–cp–(sm)
												654	1.5	62.1			436		
95117	Juan B 1218	HQV	62.5	42.56	(49.7)	7.12	1860	3870	30	60	113	310	<.03	306	38.3	18.4	≫	3770	po–pn–py–vl–(cp)
95118	Lunnon	HQV	88.5	39.19	(52.2)	8.31	1560	1540	80	30	44.6	571	(.07)	14.5	53.3	54.0	≫	8790	po–pn–vl–py–(sph)–(sm)
	Upper Roll 704											567	.73	12.7			777		
95119	Juan Main 1204	HCV	25.9	35.37	(37.9)	10.42	16.0%	930	190	2160	21.1	298	N/A	3620	0.65	112	—	16800	pn–po–cp–(sph)–(mt)

Notes: All samples are representative hand samples from underground exposures except 95112, which is a split of diamond drill core; analyses recalculated to 100% sulphides based on sulphur contents of samples and relative proportions of assumed stoichiometric sulphide phases determined by quantitative X-ray diffraction technique;[31] sulphur by Leco automatic titrator; Ni, Cu, Co, Cr and Zn by atomic absorption spectrophotometry with routine precision of ± 5–10%; Fe by difference; precious metals and Se by radiochemical neutron activation with estimated accuracy of ± 15% (procedure modified after Crocket and co-workers[32] and Keays *et al.*[33]) See Marston and Kay[9] and Gresham and Loftus-Hills[8] for mine locations; N/A = not analysed; ≫ = ratio greater than 999.

*IPS = interpillow sulphides, IBS = interbreccia sulphides, HQV = hydrothermal sulphide–quartz ± albite vein, HCV = hydrothermal sulphide–carbonate vein.

†cp = chalcopyrite, fc = ferrochromite, mt = magnetite, pn = pentlandite, po = pyrrhotite, py = pyrite, sm = smythite, sph = sphalerite, vl = violarite.

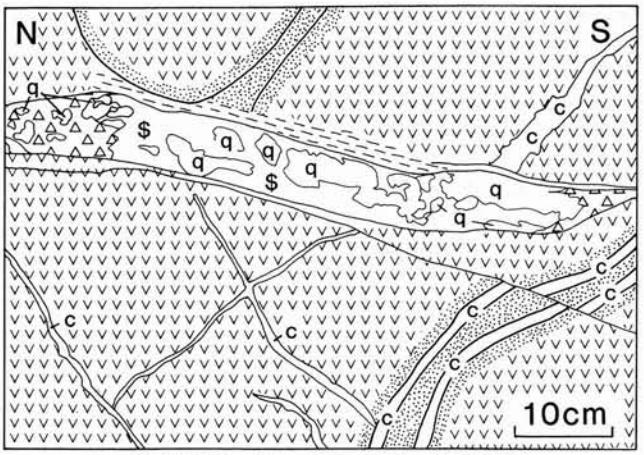

Fig. 6 Floor sketch of hydrothermal quartz–pyrrhotite–pentlandite vein in footwall of Juan B 1218 NNW ore horizon. Note sharp, foliated margins of vein and its crosscutting relationship with pillowed metabasalts (margins stippled). Ornamentation as in Fig. 2

tite—by sulphurization rather than oxidation (no associated magnetite). Sphalerite, when present, is exsolved from chalcopyrite.

Geochemically, the vein-type Fe–Ni–Cu sulphides (Table 2) are highly variable and may be extremely enriched in Au, Cu, Zn and/or Pd. They contain negligible Ir (maximum 1.5 ppb) and have low Cr contents. Sulphur/Se ratios are generally within the normal magmatic range. High Cu is commonly accompanied by high Zn, but Cu/Zn ratios are variable.

Discussion

Vein-type sulphides

Field relationships indicate that these sulphides are of secondary hydrothermal origin. As this is one possible origin for the interpillow/interbreccia sulphides, the vein-type sulphides are discussed first.

The high Ni and Pd contents of the vein-type sulphides provide strong evidence that the metals in them were derived from the spatially associated contact ores and/or ultramafic rocks, which are strongly enriched in these metals.[12] In addition, it has been demonstrated[6,12] that as much as one-half of the original Pd content of the Ni sulphide ores has been lost from the contact ores, probably during deformation and metamorphism. There is, however, no indication of any loss of Ir. The very low Ir contents and high Pd/Ir ratios of the vein sulphides (Table 2) confirm that Pd and the other metals were transferred from the magmatic sulphides to the vein sulphides via an aqueous medium; hydrothermal transfer of the PGE results in a strong decoupling of Pd from Ir.[13] Low Cr contents suggest that Cr was not very soluble in the hydrothermal fluids and the near-magmatic S/Se ratios indicate a reducing fluid or limited opportunity for fractionation of the two elements during transport and deposition.

Fluid inclusions in these veins are very small and difficult to resolve in the deformed quartz. Most primary inclusions have decrepitated, but some samples appear to contain both H_2O and CO_2-rich inclusions possibly representative of eutectic phase separation of a H_2O–CO_2 fluid at higher temperatures (S. Grigson, personal communication, 1982). Carbonation of komatiites and basalts is widespread at Kambalda[3,8,20,24] and sulphur has been highly mobile in the komatiites.[16,25] As such, both HCO_3^- and HS^- may have been important metal complexing ligands in the fluids that formed these veins (see also Phillips and Groves[24]).

As the hydrothermal sulphide veins postdate most wallrock deformation, but contain unannealed deformation fabrics, they are inferred to have been emplaced during retrograde metamorphism. They are therefore very similar and possibly temporally related to the auriferous veins at Hunt mine, although the lack of significant wallrock alteration bordering the Fe–Ni–Cu sulphide–quartz veins indicates either different fluid compositions or much smaller volumes of fluids. The sulphide–quartz veins may be rapidly emplaced features following extensional fracture of the brittle metabasalt rather than major plumbing systems centralized on previously formed deformation zones, such as at Hunt mine.[24]

Interpillow/interbreccia sulphides

There are several possible origins for interpillow and interbreccia sulphides: (1) early-erupted sulphide lavas (see Ross and Hopkins[3]) marking the commencement of komatiitic volcanism, possibly overlapping with basaltic volcanism;[9] (2) downwards percolation of molten sulphides into void spaces[23] or replacement of matrix material by sulphides during emplacement of contact ores; (3) late magmatic emplacement of contact zone sulphides into the footwall, either filling voids or replacing matrix material as suggested for footwall mineralization in Strathcona mine, Sudbury;[26] (4) tectono-metamorphic mobilization of massive contact ores coupled with metasomatic replacement of interpillow/interbreccia matrix material; or (5) hydrothermal mobilization of metals and sulphur from contact ore horizons into footwall positions.

The conspicuous absence of distinctive chalcophile ferrochromites in most ores of this type suggests that they are not original magmatic distributions (models 1–3), because the present interpretation of the distribution of these spinels[15] as related to high f_{O_2} on silicate contacts would suggest that they might be expected to be *more* abundant because of the greater wallrock surface area. In any case, although the Cr contents of these sulphides (250–3300 ppm, excluding 95107, Table 2) are generally similar to that of normal massive ores,[15,23] they are lower than that estimated for the entire ore zone (i.e. original sulphide–oxide liquid) at 4000 ppm.[14] The only sample with a high Cr content and significant spinels (95107, Table 2) shows evidence of an early (D_1?) sub-horizontal deformation and is stratigraphically equivalent to, and within several metres of, the spinel-rich pinchout of the main contact ore horizon. It also has the highest Pd/Ir and Ni/Cu ratios; it probably represents physically mobilized contact sulphides (i.e. fault offset ore).

It is considered unlikely that the interbreccia sulphides are magmatic sulphides introduced during emplacement of the contact ores (model 2), because dense (4.0–4.3 g cm^{-3}) liquid sulphides would be expected to displace metabasalt fragments (*ca* 3.0 g cm^{-3}) in interbreccia ores upwards if introduced into hyaloclastite at the magmatic stage; this is not observed. Most importantly, this model does not explain the rare presence of interpillow sulphides *overlying* ore pinchouts (Fig. 4).

Although the number of samples is limited and comparisons are hampered by the large degree of variation inherent in sulphide ores, the compositional similarity of the interpillow/interbreccia sulphides with Lunnon contact ores and corresponding depletion in PGE relative to bulk mined ores suggest that they are modified magmatic sulphides. In particular, the high Ir contents rule out the possibility that they are hydrothermally mobilized sulphides (model 5). The range of Pd/Ir ratios is not consistent with fractionation of the sulphides at the magmatic stage; late-stage magmatic melts (model 3) would be enriched in Cu and, to a lesser degree, Ni,[11] as well as Pd and Au, but depleted in Ir. For example, footwall mineralization believed to have been produced by migration of a fractionating sulphide melt into the footwall at Strathcona mine contains an average of 700 ppb Pd, but only 4 ppb Ir.[26,27]

Sulphide melts introduced into interpillow spaces by downward percolation or replacement of matrix material during contact ore emplacement (model 2) would similarly fractionate owing to the strong thermal gradient between the contact sulphides at the base of the host komatiite (*ca* 1600°C) and the cold seafloor; such fractionation is not evident. Thus, the geochemistry of the interpillow/interbreccia sulphides argues against the operation of any of models 2, 3 or 5.

The best interpretation of these sulphides that can be made with available data is that they have been physically mobilized from the overlying/adjacent massive sulphide layer during peak tectono-metamorphism (model 4). This accounts for (i) their general restriction to the major ore zones, (ii) thinning of massive contact ores over some such horizons, (iii) rare occurrences *above* the ore pinchouts, (iv) compositional similarity to normal ores (Ni/Cu and Pd/Ir) and (v) the lack of ferrochromites, which would not be dissolved in mss and transported with the ductile sulphide phase. The variable Pd/Ir ratios (Table 2) do, however, indicate some hydrothermal modification of the sulphides either prior or subsequent to mobilization. Replacement of the interstitial matrix (basaltic debris, sedimentary material or carbonate) could be accomplished by a combination of physical and diffusive metamorphic processes involving dissolution of the matrix and physical introduction of sulphides into areas of lower stress, such as the more competent basaltic footwall, during peak tectono-metamorphism. Such selective replacement of matrix material by sulphides has not to our knowledge been previously considered theoretically or experimentally, but a few natural examples may be noted—for example, (1) selective replacement of all but cruciform-twinned andalusite crystals in the pelitic rocks forming the footwall at Creighton mine, Sudbury,[28] (2) selective replacement of matrix interstitial to serpentinized olivines at Alexo mine[29] and (3) partial replacement of cherty, albitic metasediments by massive sulphides at Jan Shoot, Kambalda.[30]

The paucity of pyrite in these interpillow and interbreccia sulphides compared to most massive ores can probably be attributed to the fact that most pyrite in the ore zones is probably due to late metamorphic (i.e. post-deformational) introduction of sulphur along areas of dilatation during retrograde thermal contraction of massive sulphides.[10]

Summary and conclusions

On the basis of their field relationships, mineralogy and geochemistry, the interpillow/interbreccia Fe–Ni–Cu sulphides at Kambalda are interpreted to have been mobilized by tectonic-metamorphic processes from the ductile massive sulphide layer into the more competent footwall metabasalt and to have replaced interstitial matrix material. As such, their present stratigraphic position in the ore zones cannot be used to support genetic models involving early eruption or emplacement of sulphide-rich melts prior to the host komatiitic lavas. Rather, these mobilized sulphides highlight and support previous studies that emphasized the importance of tectonic-metamorphic processes in modifying the distribution, structure, texture, mineralogy and geochemistry of the original magmatic sulphides at Kambalda.

In contrast, vein-type Fe–Ni–Cu sulphides at Kambalda formed by hydrothermal dissolution and redeposition of metals derived from the ores or possibly the komatiite host rocks. Although tectonic-metamorphic mobilization of ores at Kambalda has generally been considered to have involved only limited redistribution over distances of tens of metres,[7,9] the occurrence of hydrothermal vein-type sulphides in some areas raises the possibility that some proportion of the metals in the ores, particularly of Pd and Au, may have been entirely lost from the ore environment. This suggests that even with very careful, long-term sampling of bulk mined ores it may not be possible to *precisely* determine the original precious metal contents in these ores.

Finally, it can be noted that the two types of mobilized magmatic sulphides described in this paper form part of a continuum of ore-mobilizing processes thus far documented at Kambalda, ranging from whole-scale physical dislocation (fault offset ores) and selective (fractional?) mobilization (stringer sulphides) through metamorphic replacement (interpillow–interbreccia sulphides and some metasediment ores) to hydrothermal dissolution and redeposition (vein-type sulphides). As has been emphasized by previous authors, the effects of these processes *must* be considered before applying geochemical, stratigraphic or petrogenetic studies to the magmatic stage.

Acknowledgement

Western Mining Corporation, Ltd. (Kambalda Nickel Operations), granted access to the deposit and kindly performed the AA, sulphur and XRD analyses. The cooperation of J. J. Gresham and M. J. Donaldson at Kambalda was much appreciated. Discussions with D. I. Groves and thoughtful reviews of the manuscript by D. L. Buchanan, M. J. Donaldson, J. J. Gresham and D. I. Groves are gratefully acknowledged. S. Dalglish assisted with the neutron activation analyses and Mrs. P. Denning typed the manuscript. Financial support was provided, in part, from a University of Western Australia Research Scholarship to C.M.L. and grants from the Australian Research Grants Committee and the Australian Institute of Nuclear Science and Engineering to R.R.K.

References

1. Marston R. J. *et al.* Nickel sulfide deposits in Western Australia: a review. *Econ. Geol.*, **76**, 1981, 1330–63.
2. Woodall R. and Travis G. A. The Kambalda nickel deposits, Western Australia. In *Mining and petroleum geology* Jones M. J. ed. (London: IMM, 1970), 517–33. *(Proc. 9th Commonw. Min. Metall. Congr., 1969,* vol. 2)
3. Ross J. R. and Hopkins G. M. F. Kambalda nickel sulphide deposits. In *Economic geology of Australia and Papua New Guinea I. Metals* Knight C. L. ed. (Parkville, Victoria: Australasian Institute of Mining and Metallurgy, 1975), 100–21. (*Monograph series* no. 5)
4. Groves D. I. Barrett F. M. and McQueen K. G. The relative roles of magmatic segregation, volcanic exhalation and regional metamorphism in the generation of volcanic-associated nickel ores of Western Australia. *Can. Mineralogist*, **17**, 1979, 319–36.
5. Naldrett A. J. Partitioning of Fe, Co, Ni and Cu between sulfide liquid and basaltic melts and the composition of Ni–Cu sulfide deposits—a reply and further discussion. *Econ. Geol.*, **74**, 1979, 1520–8.
6. Ross J. R. and Keays R. R. Precious metals in volcanic-type nickel sulfide deposits in Western Australia: I. Relationship with the composition of the ores and their host rocks. *Can. Mineralogist*, **17**, 1979, 417–35.
7. Barrett F. M. *et al.* Structural history and metamorphic modification of Archean volcanic-type nickel deposits, Yilgarn Block, Western Australia. *Econ. Geol.*, **72**, 1977, 1195–223.
8. Gresham J. J. and Loftus-Hills G. D. The geology of the Kambalda nickel field, Western Australia. *Econ. Geol.*, **76**, 1981, 1373–416.
9. Marston R. J. and Kay B. D. The distribution, petrology and genesis of nickel ores at the Juan Complex, Kambalda, Western Australia. *Econ. Geol.*, **75**, 1980, 546–65.
10. Seccombe P. K. *et al.* Sulfide paragenesis and sulfur mobility in Fe–Ni–Cu sulfide ores at Lunnon and Juan Main shoots, Kambalda: textural and sulfur isotopic evidence. *Econ. Geol.*, **76**, 1981, 1675–85.
11. Ewers W. E. and Hudson D. R. An interpretive study of a nickel–iron ore intersection, Lunnon Shoot, Kambalda, Western Australia. *Econ. Geol.*, **67**, 1972, 1075–92.
12. Keays R. R. Ross J. R. and Woolrich P. Precious metals in volcanic peridotite-associated nickel sulfide deposits in Western Australia: II. Distribution within the ores and host rocks at Kambalda. *Econ. Geol.*, **76**, 1981, 1645–74.

13. Keays R. R. *et al.* Iridium and palladium as discriminants of volcanic-exhalative, hydrothermal and magmatic nickel sulfide mineralization. *Econ. Geol.*, **77,** 1982, 1535–47.
14. Groves D. I. *et al.* Spinel phases associated with metamorphosed volcanic-type iron–nickel sulfide ores from Western Australia. *Econ. Geol.*, **72,** 1977, 1224–44.
15. Woolrich P. Cowden A. and Giorgetta N. E. The chemical and mineralogical variations in the nickel mineralization associated with the Kambalda dome, Western Australia. *Econ. Geol.*, **76,** 1981, 1629–44.
16. Lesher C. M. Localization and genesis of komatiite-associated Fe–Ni–Cu sulphide mineralization at Kambalda, Western Australia. Ph.D. thesis, University of Western Australia, 1983.
17. Ewers W. E. *et al.* Crystallization of chromite from nickel iron sulphide melts. *Contr. Miner. Petrol.*, **54,** 1976, 61–4.
18. Archibald N. J. *et al.* Evolution of Archaean greenstone terrains, Eastern Goldfields Province, Western Australia. *Precamb. Res.*, **6,** 1978, 103–31.
19. Binns R. A. Gunthorpe R. J. and Groves D. I. Metamorphic patterns and development of greenstone belts in the eastern Yilgarn Block, Western Australia. In *The early history of the earth* Windley B. F. ed. (New York: Wiley, 1976), 303–13.
20. Bavinton O. A. Interflow sedimentary rocks from the Kambalda ultramafic sequence: their geochemistry, metamorphism and genesis. Ph.D. thesis, Australian National University, 1979.
21. McQueen K. G. Experimental heating and diffusion effects in Fe–Ni sulfide ore from Redross, Western Australia. *Econ. Geol.*, **74,** 1979, 140–8.
22. Nevill M. W. K.N.O. progress report—McMahon complex. Unpublished Western Mining Corp. Report K2501, 1980, 30 p.
23. Groves D. I. and Hudson D. R. The nature and origin of Archaean strata-bound volcanic-associated nickel–iron–copper sulphide deposits. In *Handbook of strata-bound and stratiform ore deposits, volume 9* Wolf K. H. ed. (Amsterdam: Elsevier, 1981), 305–410.
24. Phillips G. N. and Groves D. I. Fluid access and fluid wallrock interaction in the genesis of the Archaean gold-quartz vein deposit at Hunt mine, Kambalda, Western Australia. In *Gold '82: The geology, geochemistry and genesis of gold deposits* Foster R. P. ed. (Rotterdam: Balkema, 1984), 389–416. (*Spec. Publ. geol. Soc. Zimbabwe* no. 1)
25. Lesher C. M. *et al.* Geochemistry of komatiites from Kambalda, Western Australia: I. Chalcophile element depletion—a consequence of sulfide liquid separation from komatiitic magmas. *Econ. Geol.*, **76,** 1981, 1714–28.
26. Keays R. R. and Crocket J. H. A study of precious metals in the Sudbury nickel irruptive ores. *Econ. Geol.*, **65,** 1970, 438–50.
27. Naldrett A. J. *et al.* Compositional variations within and between five Sudbury ore deposits. *Econ. Geol.*, **77,** 1982, 1519–34.
28. Pattison E. Personal communication to R.R.K., 1978.
29. Naldrett A. J. Discussion of papers concerned with sulfide deposits. In *Magmatic ore deposits* Wilson H. D. B. ed. *Econ. Geol. Monograph* 4, 1969, 359–65.
30. Paterson H. L. *et al.* Nickeliferous sediments and sediment-associated nickel ores at Kambalda, Western Australia. In *Sulphide deposits in mafic and ultramafic rocks* Buchanan D. L. and Jones M. J. eds (London: IMM, 1984), 81–94.
31. Hooton D. H. and Giorgetta N. E. Quantitative X-ray diffraction analysis by a direct calculation method. *X-Ray Spectrometry*, **6,** 1977, 2–5.
32. Crocket J. H. Keays R. R. and Hsieh S. Determination of some precious metals by neutron activation analysis. *J. radioanalyt. Chem.*, **1,** 1968, 487–507.
33. Keays R. R. *et al.* The simultaneous determination of 20 trace elements in terrestrial, lunar and meteoritic material by radiochemical neutron activation analysis. *Analyt. chim. Acta*, **72,** 1974, 1–29.

Genesis of komatiite-associated nickel sulphide deposits at Kambalda, Western Australia: a distal volcanic model

C. M. Lesher B.Sc., A.M.
Formerly Department of Geology, University of Western Australia, Nedlands, Western Australia (now J. Tuzo Wilson Research Laboratories, University of Toronto-Erindale, Mississauga, Ontario, Canada)

N. T. Arndt B.Sc.(Hons.), Ph.D.
Abteilung Geochemie, Max-Planck-Institut für Geochemie, Mainz, Federal Republic of Germany

D. I. Groves B.Sc.(Hons.), Ph.D., A.M.Aus.I.M.M.
Department of Geology, University of Western Australia, Nedlands, Western Australia

Synopsis

The Archaean komatiite-associated nickel sulphide deposits at Kambalda, Western Australia, exhibit a number of stratigraphic features that are indicative of a strong volcanic control on ore localization, including (1) a restriction to specific basal cumulate metakomatiite host units, (2) confinement within distinctive synvolcanic embayments in the footwall and (3) variations in the internal structure and composition of overlying and adjacent barren metakomatiite flows and the distribution of interflow metasediments with proximity to the ore zones.

The high magnesium content of the host units (up to 45% MgO volatile-free) in comparison with that of aphyric or spinifex-textured lavas (16–32% MgO) has been considered previously to indicate either magmas/lavas rich in intratelluric olivine or selective accumulation of olivine phenocrysts. The marked linear trend of the oreshoots, basal host units, footwall embayments and the volcanic stratigraphic relationships have been used as evidence for local linear feeding fissures. Rare relict igneous olivine in some host units is, however, demonstrably not intratelluric, and there is no direct or indirect evidence of a proximal eruptive site (e.g. footwall feeders, pyroclastic breccias, ultramafic intrusives) at Kambalda such as at some other deposits of this type. Kambalda is interpreted as a distal rather than proximal volcanic environment.

Emplacement of the komatiite sequence at Kambalda was probably controlled by the locations of a few specific eruptive sites relative to regional topographic gradients and influenced by the topography of the pre-existing volcanic surface. Olivine enrichment in the basal host units occurred by *in-situ* fractionation and cumulus crystallization of olivine during longitudinal lava flow within linear lava conduits, possibly centralized on depressions between non-overlapping footwall basalt flows. The distinctive stratigraphic relationships are attributed to localization of lava conduits along the volcanic pitchline, flanked by more slowly moving parts of the flows. There are analogies with the physical volcanology of Modern basaltic and Proterozoic komatiitic lava flows.

A corollary of this model is that the lava conduits thermally eroded and assimilated sulphidic sediments, contributing additional sulphur to sulphur-saturated komatiites or possibly inducing sulphide separation in originally sulphur-undersaturated komatiites. The latter would account for the restriction of ores to linear cumulate komatiite host units (thermally active lava conduits) and the locally mutually exclusive, but stratigraphically equivalent, relationship between the ores and sulphidic metasediments at Kambalda.

Archaean komatiite-associated nickel deposits,* of which the Kambalda deposits are considered the type examples, have recently been well documented in reviews[1–4] and in special issues of *Canadian Mineralogist* (vol. 17, pt. 2) and *Economic Geology* (vol. 76, no.6). There is a wide variety of field, geochemical and experimental evidence in support of a magmatic origin for the sulphide ores, including (1) a restrictive association with the most magnesian basal units in the sequence, (2) localization within footwall embayments, (3) gradational disseminated/matrix/massive sulphide segregation at the base of the host unit, (4) characteristic chalcophile ferrochromites in sulphide ores and (5) ore geochemistry in the light of known and inferred metal partitioning in mafic–ultramafic systems.

The association of many Western Australian ore deposits with komatiite lava flows and with apparently conformable pillowed footwall metabasalts further indicates a subaqueous volcanic origin. Although there are differences in detail from deposit to deposit, most genetic interpretations[3–10] follow a similar general theme: after a period of basaltic volcanism komatiitic volcanism commenced with the eruption of a pulse of ultramafic magma that contained a very high proportion of intratelluric olivine crystals. This liquid-crystal mush with a very high effective viscosity did not travel far from its eruptive site, being largely confined to, or ponded within, embayments in the footwall. Erupted in advance of the mush or entrained as droplets within it was a previously exsolved immiscible Fe–Ni–Cu sulphide–oxide liquid. As the magma was erupted, the direction of movement changed from vertical to horizontal and the dense, fluid sulphide droplets settled rapidly through the olivine–liquid mush and accumulated in footwall embayments. The loci of such sulphide accumulation have generally been interpreted to be very close to the eruption sites.

The similarity between genetic models proposed for these deposits, however, belies some of the very important differences between them, and also does not take into account the unusual physical properties of komatiite lavas. More detailed studies suggest that a proximal volcanic model that involves lavas rich in intratelluric olivine and mantle-derived sulphides is probably not applicable for all deposits, particularly the type examples at Kambalda. The aims of this paper are to (1) briefly summarize the volcanic features of the well-characterized Kambalda deposits, (2) critically discuss previous genetic models in the light of new data and interpretations, and relevant observations of the physical volcanology of better exposed komatiitic and basaltic lava flows elsewhere, (3) describe the probable physical properties of komatiite lava and (4) intro-

*Although these deposits have been previously referred to as volcanic peridotite-associated deposits, the host units are here recognized as komatiites and named accordingly.

duce a new volcanic-assimilation model for the emplacement of the ores and host komatiites at Kambalda.

This paper represents an amalgamation of ideas developed independently by the authors and presented in part at the Nickel Sulphide Field Conference III Symposium held in Perth, Western Australia, from 23 to 25 May, 1982. More detailed treatments of specific aspects of new data and interpretations summarized here will be published elsewhere.

Volcanic features

Most komatiite-associated nickel deposits in Western Australia, including the Kambalda deposits, occur within the south-central part of the NNW-trending Norseman–Wiluna Greenstone Belt (see Fig. 3 of Groves and co-workers[11]). Compared with flanking areas, the Norseman–Wiluna Belt is characterized by (1) more complex volcanic-sedimentary stratigraphy, (2) abundant komatiites, (3) ubiquitous sulphidic shale or chert and a paucity of oxide-facies BIF, (4) epiclastic sediments containing ultramafic and/or mafic clasts and (5) numerous NNW-trending strike faults and lineaments. It has been interpreted as a volcanically active intracratonic rift zone.[11] Most deposits occur at the base of metakomatiite sequences, normally overlying metabasalt or amphibolite formations, within stratigraphically low mafic–ultramafic sequences. Thus, there appears to be a regional volcanic stratigraphic control on such nickel mineralization (see Fig. 4[11]).

The nickel sulphide ores at Kambalda (Fig. 1) normally occur at the base of the thickest and most magnesian basal units in the ultramafic sequence, localized within distinctive footwall embayments (Fig. 2). This mineralization is referred to as contact ore.[7] Mineralization, however, may occur additionally or exclusively at the base (stratiform) of immediately overlying

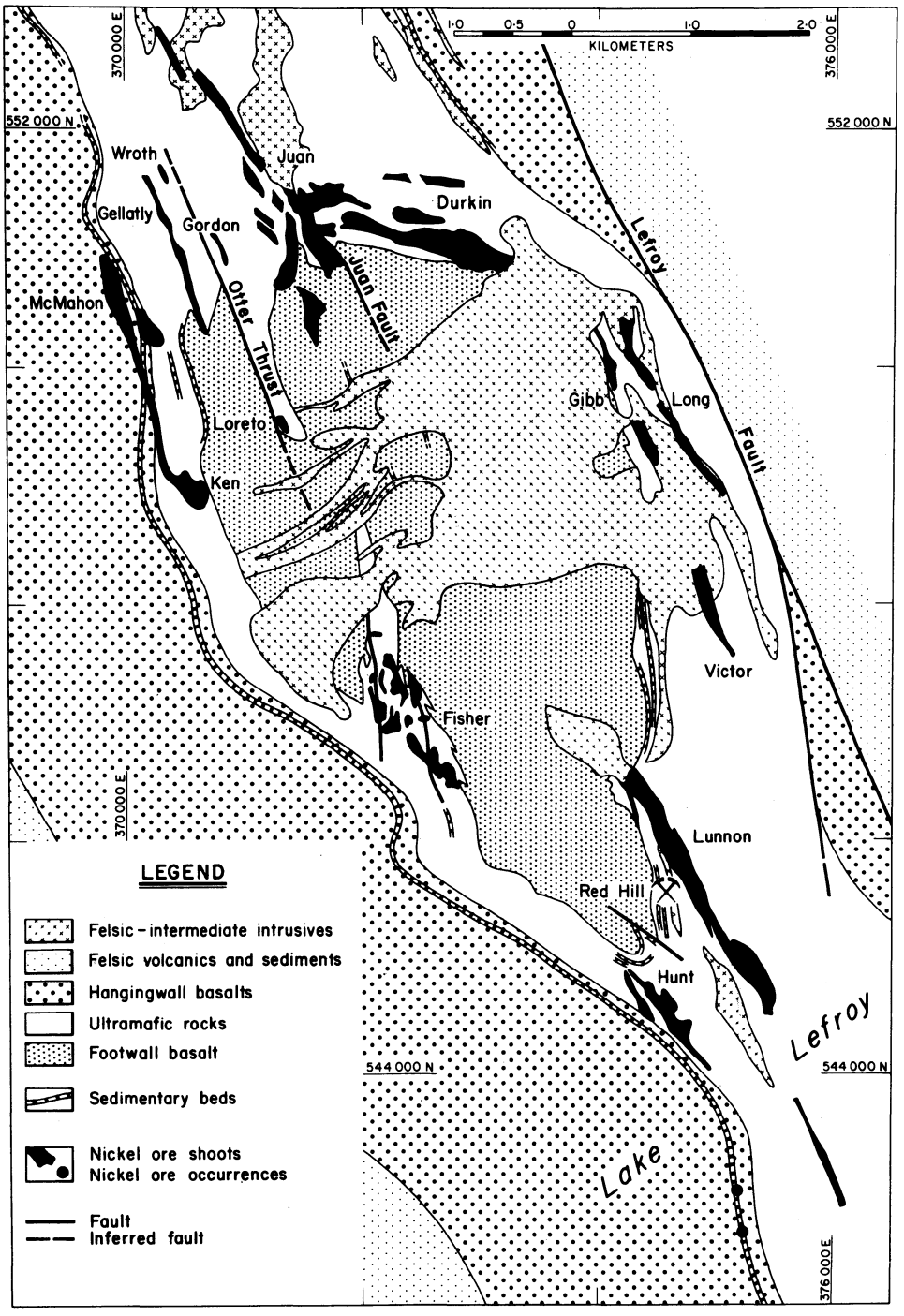

Fig. 1 Solid rock geology of Kambalda Dome showing oreshoots in plan projection. From Gresham and Loftus-Hills[7]

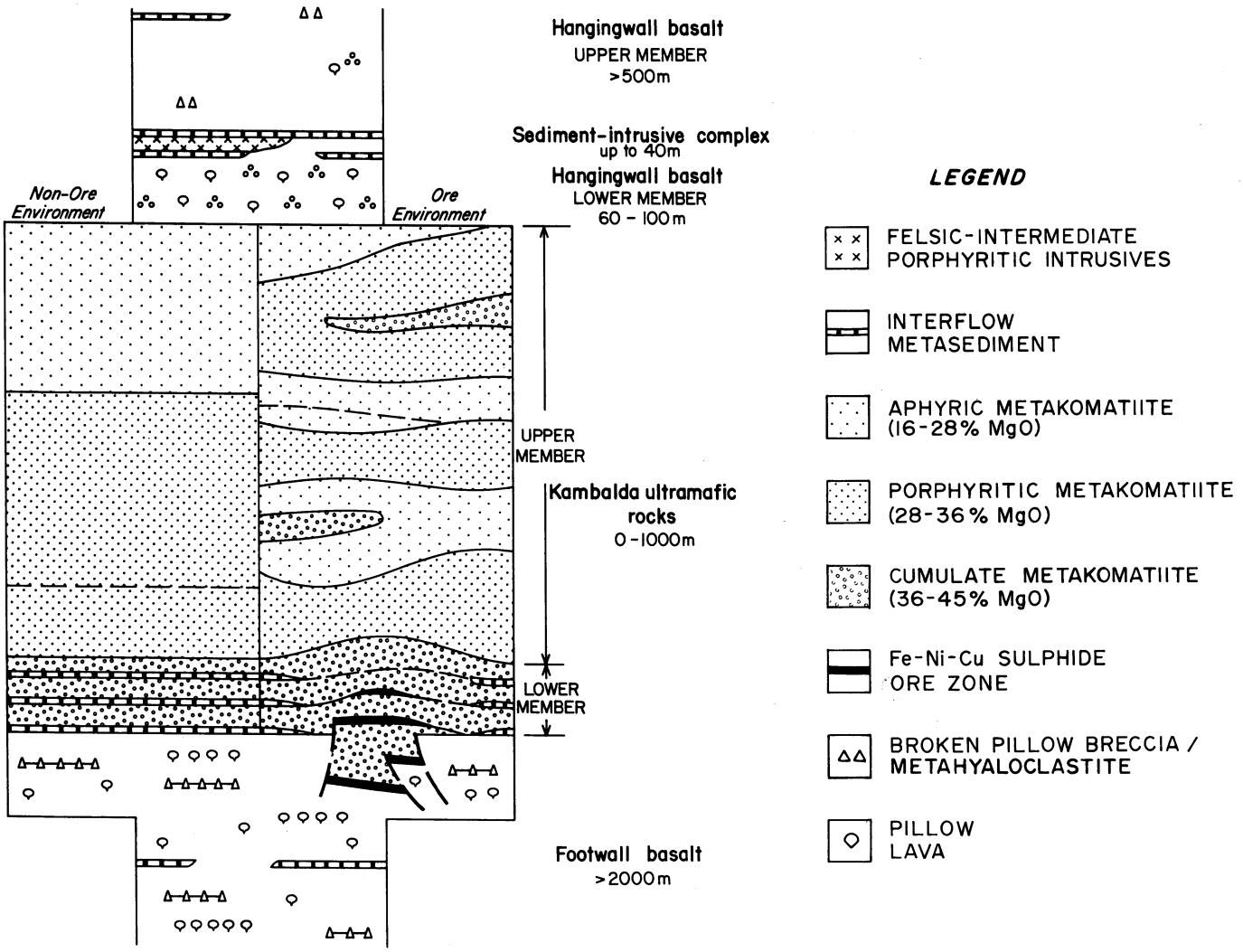

Fig. 2 Diagramatic stratigraphic column of Kambalda sequence at Kambalda Dome illustrating differences between ore and non-ore environments. After Gresham and Loftus-Hills.[7] Note that in text we distinguish between *basal host unit* largely confined to embayment in ore environment and *barren flanking basal unit* in non-ore environments, though no stratigraphic relationship is implied by that distinction

units, or as disseminated blebby sulphides (strata-bound) within the basal host units (hanging-wall ore[7]). The nickel sulphides appear to be associated with the initial stages of komatiitic volcanism. Specific features that suggest a volcanic origin for the Kambalda deposits, as summarized in the following section, include (1) the physical volcanology and stratigraphy of the host komatiite sequence, (2) the internal structure and composition of the distinctive basal host units and (3) the nature of the ore-localizing footwall embayments.

Host komatiite sequence

Interpretation of the internal structure and nature of the host ultramafic sequence at Kambalda is based primarily on diamond drill core logging and, to a certain degree, on comparisons with better exposed volcanic sequences in other Archaean greenstone belts. At Kambalda the ultramafic sequence is made up of multiple and overlapping units with (1) abrupt compositional changes at unit boundaries, (2) chilled margins, (3) flow-top breccias, (4) conformable intercalated metasedimentary horizons, (5) rare (?) pillowed zones and (6) variable degrees of asymmetrical textural and compositional differentiation.* On the basis of this evidence the host ultramafic sequence is considered to comprise a series of ultramafic lava flows.[5,7] Aphyric and spinifex-textured lavas range between 32 and 16% MgO (volatile-free)[12] and from this and other textural and geochemical characteristics may be classified as komatiite. Polymictic ultramafic pyroclastic rocks and intrusive ultramafic bodies are present at Scotia,[9] but are conspicuously absent at Kambalda.

The host komatiite sequence at Kambalda comprises a lower member of thick (10–30 m), highly magnesian (36–45% MgO) flows, with intercalated metasediments, which grades upwards into an upper member dominated by thinner (1–10 m) and less magnesian (16–36% MgO) flows (Fig. 2). Superimposed on these general trends are *lateral* variations in stratigraphic ordering, composition and differentiation of the overlying and adjacent barren komatiite lavas, and distribution of interflow metasediments:[7] near-ore environments are characterized by (1) anomalously thick, highly magnesian basal host units, (2) an absence of interflow metasedimentary horizons, (3) better textural and compositional differentiation in the komatiites and (4) a more 'disordered' sequence, which contains

*The terms differentiation and fractionation have been used synonymously in igneous petrology to describe the formation of a variety of rock compositions from a single parental composition. In this paper the term *differentiation* is used in a primarily internal structural sense to indicate macroscopic textural and/or compositional variations within a single lava flow unit due to the physical–chemical segregation of crystalline and liquid components (e.g. by flowage differentiation, gravity settling and/or fractional crystalization). The term *fractionation* is used in a primarily chemical sense to refer to the progressive evolution of the magmatic liquid (and derivative mineral and whole-rock compositions) undergoing separation of a crystallizing phase. The term *olivine enrichment* indicates that the weighted mean (bulk) composition of the flow unit is enriched in magnesium relative to its aphyric chilled margins by the addition of olivine phenocrysts and/or liquid replenishment and olivine crystallization *in situ*.

some thick, very magnesian units high in the sequence and exhibits poor lateral correlation between even very closely spaced (*ca* 30–50 m) drill-holes. In contrast, away from ore (1) the barren flanking basal units are thinner and less magnesian, (2) interflow metasedimentary horizons are ubiquitous in the lower member, at equivalent stratigraphic levels to the nickel ores, (3) komatiites are generally poorly texturally and compositionally differentiated and (4) the sequence is much more ordered, showing a regular upwards trend to thinner, less magnesian flows, and containing individual or series of flow units that correlate along strike for considerable distances (up to 500 m or more). These stratigraphic variations are displayed within prisms of rock elongate along the length of the linear oreshoots, extending upwards through the barren komatiite sequence above an oreshoot (Fig. 2). Importantly, they suggest a strong volcanogenic control on ore localization.

Basal host units

These units are normally the thickest (average 50 m, but up to 100 m) and most magnesian (generally 40–45% weighted mean MgO) in the host komatiite sequence at Kambalda. In most areas the basal host units are anomalous linear lithological and stratigraphic elements of the komatiite sequence, largely confined to the footwall embayments (Fig. 2). The stratigraphic relationships between the basal host units and the barren flanking basal units are poorly defined, but in most areas the spinifex-textured top of the basal host unit is above the projected level of the embayment margins and the basal host unit is interpreted to laterally overlap the embayment[13] (cf. Fig. 2). Significantly, the thick basal host units at Kambalda are commonly more extensive along plunge than the mineralization, which may range up to 1.5 km (rarely in excess of 2.5 km) in length.[7]

The basal host units at Kambalda are strongly differentiated and olivine-enriched with anomalously thick lower cumulate divisions and relatively thin upper spinifex-textured divisions (Fig. 3). They are compositionally and texturally *gradational*, however, with overlying and adjacent komatiite lavas; on this basis they are interpreted to represent an end-member in a continuum of komatiite lava flows exhibiting compositional and structural variations owing to variable degrees of olivine enrichment and differentiation *in situ* (Fig. 4).

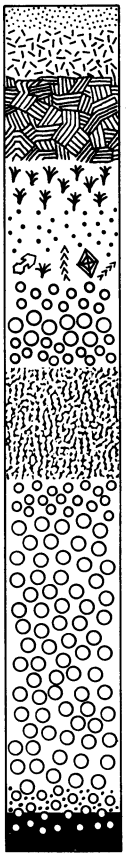

Fig. 3 Schematic structural subdivisions of typical Kambalda basal cumulate komatiite host unit; relative thicknesses of zones very variable and spinifex divisions may be very much thinner. From Lesher[13]

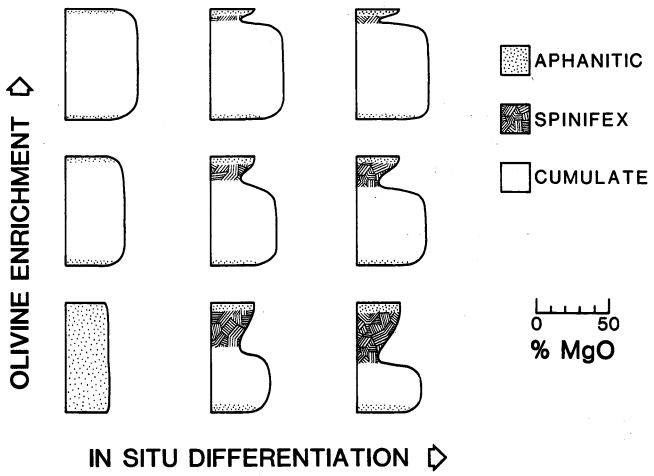

Fig. 4 Variations in internal structure and composition of komatiite lava flows as functions of olivine enrichment and differentiation *in situ*. From Lesher.[13] Width of flow profiles proportional to volatile-free MgO content. Poorly differentiated, unenriched flows may be massive, pillowed or rarely volcaniclastic, are characterized by their uniform composition and dominate upper member in non-ore environments at Kambalda (cf. Fig. 2). Differentiated, unenriched flows are characterized by less magnesian upper spinifex-textured divisions and lower cumulate divisions, have bulk MgO contents similar to their chilled margins and are common in the upper member in ore environments at Kambalda. Poorly differentiated, olivine-enriched flows are characterized by bulk MgO contents greater than their chilled margins and dominate lower member flanking ore zones at Kambalda, including barren flanking basal units (cf. Fig. 2). Differentiated, olivine-enriched flows characterized by anomalously thick lower cumulate divisions and relatively thin upper spinifex-textured divisions; these are the basal cumulate komatiite host units at Kambalda (cf. Fig. 3)

Footwall embayments

Virtually all contact ores at Kambalda are localized within distinctive footwall embayments (Fig. 2). These vary in morphology from shallow, open flexures (e.g. some shoots in the southern part of the Kambalda Nickel Field;[7] cf. Wannaway[8] and Scotia[9]) to more complex re-entrant troughs (e.g. most shoots at the Kambalda Dome[7]). They range from rare elliptical features less than 100 m in length to highly elongate structures commonly up to 1.5 km or more in length; nearly all exhibit a pronounced NNW-trending elongation (Fig. 1) parallel to the regional structural trend.[7,11] They are variably modified by superimposed polyphase deformation, but appear to have originally been 2–30 m in depth.[13] Like the basal host units, some embayments are more extensive along plunge than the mineralization.[7] Metasediments are characteristically absent from the embayments and from a narrow zone that flanks the embayments, but are ubiquitous on the more distant flanking basal contacts (Fig. 2).

Detailed stratigraphic and structural studies[5,7,13] have shown that the footwall embayments that localize most of the Kambalda oreshoots are synvolcanic features, which pre-date emplacement of most of the overlying komatiite sequence. The ubiquitous occurrence of the distinctive olivine-enriched basal cumulate komatiite units within the embayments suggests that the latter were depressions or grabens in the underlying basalt topography, which influenced the emplacement of the komatiite flows.

Evaluation of previous volcanic models

Despite the accumulation of considerably more data (both from grid diamond drilling and mining operations), most recent interpretations of the volcanic features of the Kambalda ores[7] have only modified an earlier interpretation of the Lunnon Shoot;[5] most models include (1) intratelluric olivine-rich magmas/lavas, (2) proximal eruptive sites ± linear feeding fissures and (3) separation ± segregation of sulphide liquids prior to eruption. Each of these fundamental aspects is discussed briefly but critically in the light of additional data and new interpretations.

Olivine enrichment

All basal host units at Kambalda are strongly olivine-enriched—that is, they have weighted mean MgO contents considerably greater than their spinifex-textured zones, which are considered to represent the composition of the magmatic silicate liquid. Mass balance calculations indicate 15–60% olivine enrichment for most host units.[6,13] Although such calculations are only applicable for the vertical section of the host unit analysed, there is no evidence for any appreciable fractionation along the limited (maximum 2.5 km) drilled length of most host units at Kambalda.[7,13] These data have been used previously to demonstrate that these lavas were either very rich in suspended intratelluric olivine on eruption,[3–10] or that they represent preferential accumulation of intratelluric olivine into overflowing lava ponds,[14] topographic depressions,[6,15] or ponded lava flows.[16] These interpretations have generally not been supported by detailed petrographic and geochemical studies, however, because most cumulate komatiites at Kambalda are pervasively serpentinized and metamorphosed. Such studies are, nevertheless, critical as the form and composition of the olivine phenocrysts are critical in distinguishing between (1) allogenic olivine xenocrysts, (2) intratelluric olivine crystals, (3) gravity-settled olivine primocrysts or (4) *in-situ* crystallized cumulus olivine.

Rare relict igneous olivine is preserved at Victor and Durkin Shoots. It is recognized by its igneous textures, light brown colour and relatively high Ca, Ni and Cr contents; in contrast, metamorphically regenerated olivine is easily distinguishable by its porphyroblastic or granoblastic habit, clear colour and negligible minor-element contents[13] (see also Stolz and Nesbitt[10]). Ross and Keays[17] assumed that the brown igneous olivine at Victor Shoot is of intratelluric origin, and used it to develop models for PGE partition coefficients. More detailed study[13] has, however, shown that the olivine in the basal host unit exhibits significant systematic variations in composition (Fo_{91-94}) with stratigraphic height. This suggests that this olivine is not intratelluric; because of the high temperatures and extended period of time available for equilibration, intratelluric olivine should have a relatively uniform composition throughout a single flow unit. The range of olivine composition is, however, precisely that which would be in equilibrium with the range of derivative silicate liquid compositions represented by the overlying fractionated spinifex-textured division (31–16% MgO); this argues against a xenocrystic origin for the olivine.

The textural habits of olivine preserved in the basal host unit at Victor Shoot are also important. The uppermost part of the cumulate division contains granular and polyhedral olivine, which could represent gravity-settled olivine primocrysts or *in-situ* crystallized cumulus olivine. This directly and conformably overlies a zone of branching crescumulate olivine, which must have crystallized *in situ*. Although the lower part of the cumulate division in this unit is pervasively serpentinized, branching crescumulate olivine is present at the very *base* just above the ore zone; crescumulate olivine textures are also preserved within and at the base of the host unit at Durkin Shoot.[13] This is very important because it indicates that if any intratelluric or primocrystic olivine was present in these lavas on emplacement, it was volumetrically unimportant; olivine would settle very rapidly in low-viscosity komatiite liquids and should accumulate near the base of the flow. This is supported by the observed negligible phenocryst contents in the chilled margins of these flows.[5,13] Low suspended olivine contents are also consistent with the calculations of Usselman *et al.*[16] based on a single-stage emplacement, conductive cooling model for the ore segregation profile at the base of these units; high concentrations of phenocrysts ($>$ *ca* 10%) should result in ore profiles without massive ore zones.

The best interpretation of olivine enrichment in these units is that it occurred *in situ* by fractional crystallization of olivine during lava flow—not by accumulation of intratelluric olivine. It is very likely that all Kambalda host units, which show similar chemical profiles to those from Victor and Durkin Shoots, formed in a similar way. It is now recognized that cumulates in many layered intrusions, once attributed to gravitational settling, probably resulted from crystallization *in situ*.[18] The observed compositional and textural variations of olivine at Victor Shoot probably represent variations in the degree of undercooling and rates of nucleation and crystallization within the lava flow profile. Reversals indicate repeated lava influx. Processes by which this olivine enrichment could occur are suggested by additional data relevant to the physical volcanology of these units.

Eruptive sites and physical volcanology

The footwall embayments at Kambalda have been previously interpreted as (1) tectonic grabens that were active during volcanism,[5] (2) volcanic topographic depressions between non-overlapping basalt flows[13] and (3) possibly in the case of some distinctly re-entrant embayments, overlapping of initial linear host komatiite flows by waning basaltic lavas.[19,20] Another possibility is that they are depressions produced by thermal erosion of the basaltic footwall by the flowing komatiite lava.[21,22] A detailed analysis of this problem will be published elsewhere, but features such as (1) an absence of demonstrably early subvertical faults, (2) the geometry of the embayments with respect to plausible deformational mechanisms, (3) contiguous stratigraphy and consistent upward younging in the adjacent metabasalt sequence and (4) the presence of chilled margins (rarely spinifex-textured and normally metasomatically altered) on the re-entrant metabasalt/metakomatiite contacts make the first interpretation very unlikely.[13] The observation that many host units appear to overlap the embayments and the probability that low-viscosity komatiite flows would not form with such high depth:width aspect ratios (see further below) both argue against the third possibility as a general model. The planar, generally conformable nature of the footwall contact,[7] the elliptical shape of some embayments[13] and the lack of any field or geochemical evidence for extensive basalt assimilation present difficulties for the model that the embayments formed by thermal erosion, but some degree of local assimilation and enlargement of the embayments cannot be precluded. The best interpretation of the embayments is that they represent original topographic depressions between non-overlapping footwall metabasalt flows, possibly enlarged by thermal erosion, which have been modified by deformation.

The linear NNW trend of the oreshoots, troughs, basal host units and the distinctive 'disordered' stratigraphy above the oreshoots at Kambalda have been used to infer proximal linear feeding fissures.[5,7] Despite extensive exposure during mining operations, however, no footwall feeders have been identified at Kambalda. In addition, if linear stratigraphic relationships in the overlying komatiite sequence were related to fissure eruption, it would require a fixed eruptive site at each shoot. Again, despite intensive grid diamond drilling centred on the ore-

shoots, no transgressive ultramafic bodies have been identified in the komatiite squence at Kambalda. In contrast, some deposits of this type exhibit direct evidence of the original feeders (e.g. Damba–Silwane and Shangani, Zimbabwe,[23] and Langmuir, Ontario[24]) or indirect evidence for a proximal eruptive site, such as polymictic ultramafic pyroclastic breccias and ultramafic intrusives (e.g. Scotia[9]).

Naldrett and Campbell[15] proposed lateral flow of lavas across the embayments (presumably from eruptive sites to the east or west), but this model is based on riffling and accumulation of intratelluric olivine into the embayments—a process that was discounted above. Furthermore, such a model cannot account for the distinctive komatiite stratigraphy above the ore zones unless the embayments were repeatedly subsiding and ponding komatiites during emplacement of the entire komatiite sequence. Stratigraphic reconstructions[25,26,27] that provide evidence in support of such subsidence are based on equivocal structural interpretations (no early synvolcanic faults have been positively identified[13]) and/or unjustified assumptions concerning the morphology of the komatiite flows (see further below). In addition, the barren flanking basal units at Victor Shoot are more fractionated than the adjacent basal host unit; they have less magnesian chilled margins (<26% MgO) and contain less magnesian olivine (Fo_{91-89}) than the basal host unit (31–28% MgO and Fo_{94-91}, respectively). Thus, the more magnesian basal host unit at Victor Shoot is not related to the less magnesian barren flanking basal units by simple equilibrium olivine accumulation, as required in that model.

Recognizing these problems, Lesher *et al.*[12] suggested that the eruptive sites were at some distance along plunge from the present ore zones (i.e. to the north or south) and that linear stratigraphic relationships were due to linear lava flow constrained by the locations of a few specific eruptive sites relative to local and/or regional topographic gradients. In this context the recent observations of Arndt[28] on the well-exposed basaltic komatiites at Gilmour Island, Hudson Bay, are very relevant. There, detailed mapping of several continuously exposed flows shows them to have an overall lens-like shape with elongate, elevated, flat-topped central portions containing spinifex texture alternating along strike with massive, polyhedrally jointed or pillowed portions (Fig. 5). The spinifex-textured portions are between 20 and 200 m wide, about 15 m high and constitute 50–70% of the total measured strike lengths of the flows. The intervening massive pillowed portions are 60–300 m wide, but only 10–12 m high. The shape of these flows, particularly the 3–5 m relative elevation of the spinifex-textured portions, is best interpreted as a series of lava conduits (spinifex-textured lenses) bounded by adjacent stagnant areas (massive pillowed lava), like levees in modern flows. It can be imagined that the conduits consisted of elastic skins of chilled lava acting as an envelope enclosing lava flowing from its eruptive site to the active flow front. Internal pressure of the flowing lava would have inflated the conduits and maintained their shape during eruption. The facies variations in lava structure are analogous to those deduced at Kambalda; the linear form of the differentiated, olivine-enriched basal host units at Kambalda and absence of feeders are thus consistent with them being lava conduits, which transported lava from a distant eruptive site rather than ponded lavas above a proximal linear feeding fissure (cf. Gresham and Loftus-Hills[7]). This is discussed in more detail below.

Separation, segregation and eruption of sulphide melts

Pre-eruptive separation and segregation of sulphide melts has been proposed to account for the normal occurrence of massive ore conformably overlying the basaltic footwall without any intervening selvedge of ultramafic rock.[5,25] Mechanisms by which dense (*ca* 4.0 g cm^{-3}) molten sulphides could be erupted in advance of the host komatiitic magmas are, however, tenuous. For example, it is doubtful that dense sulphides previously separated and segregated in a subsurface magma chamber[3,25] could be erupted before any of the overlying less dense (*ca* 2.8 g cm^{-3}) silicate magma, even if they were buoyant enough to rise through the crust. Similarly, dynamic flowage segregation of sulphides from a sulphide–silicate magma during vertical transport to the surface[25] is also improbable in view of the low phenocryst content (and lower effective viscosity) inferred above. If mantle-derived, it is more likely that the sulphides were carried upwards as very fine droplets, which separated from, and were entrained in, the komatiitic magma during transport to the sur-

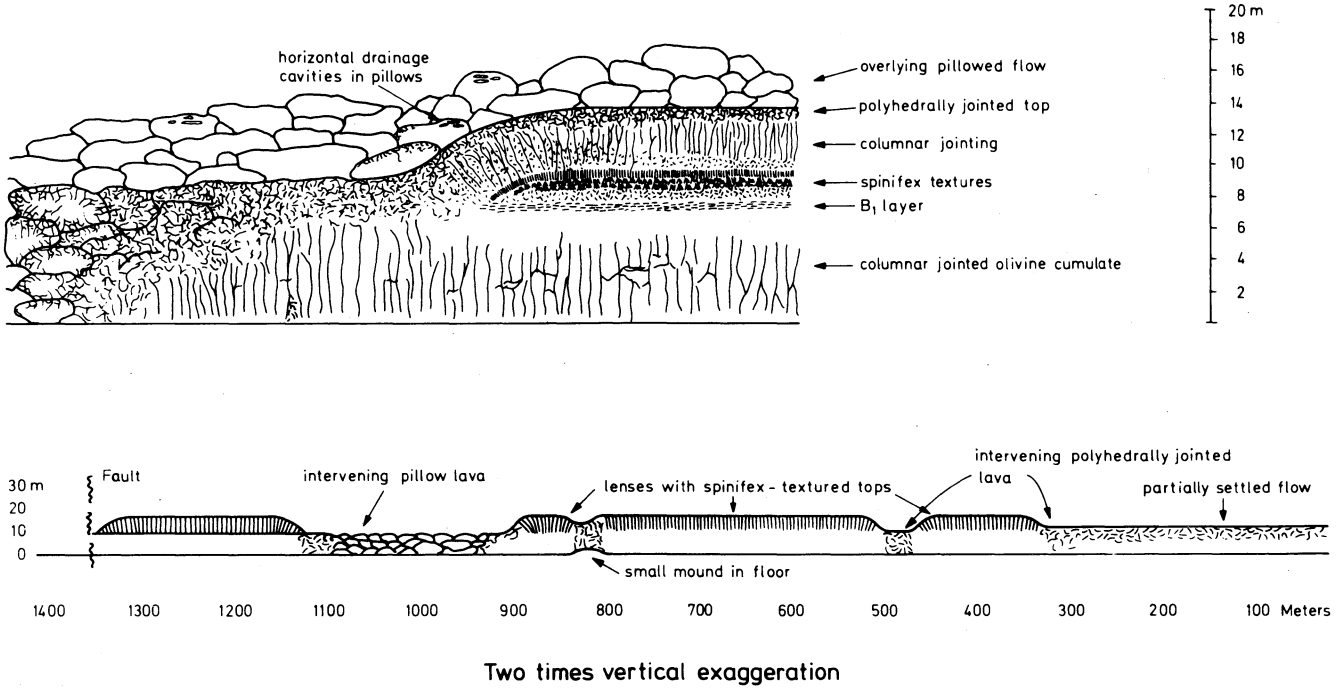

Fig. 5 Internal structure and physical volcanology of basaltic komatiite lavas at Gilmour Island, Hudson Bay. From Arndt.[28] *(a)*, Sketch of termination of spinifex-textured portion of a flow; *(b)*, sketch of measured interval along spinifex-textured flow (see text for further description)

face.[12] As the host lavas probably flowed some distance from their eruptive site(s), there would be ample opportunity for elutriation and gravity segregation of dense, low-viscosity sulphides during emplacement. In any case, if a silicate chill zone initially developed at the base of the flow beneath settling sulphides, the combination of high thermal conductivity of the sulphides and continued influx of high-temperature lava probably resulted in melting of this zone with resultant situation of massive sulphides directly on footwall basalts.

All models that involve eruption of sulphides with the komatiites, however, generate the enigma of why the upper and adjacent portions of the host units and the overlying komatiites are barren of mineralization. Once sulphur-saturated, the lavas should continue to exsolve sulphides as they cool and oxidize during eruption, emplacement and crystallization. This is exacerbated in the case of olivine-enriched units where olivine crystallization and enrichment should also be accompanied by sulphide exsolution and enrichment. Although the stratabound disseminated blebby ores may have exsolved and concentrated in such a manner, these are restricted exclusively to the basal host units; there is negligible disseminated mineralization outside of the major ore zones at Kambalda. There is indirect evidence that all of the magma that now represents the komatiite sequence at Kambalda equilibrated with sulphides prior to eruption,[12] but this does not require that those sulphides were erupted. Significantly, several relevant experimental studies[29,30,31] have documented an apparent negative pressure-dependence on sulphide solubility. It is therefore possible that the parental komatiite magma may have been sulphur-saturated in the source region (or magma reservoir), but sulphur-undersaturated on eruption until the late stages of crystallization. This leads us to an alternative possibility, considered further below, that the sulphides that compose the stratiform ores were not erupted with the komatiites but exsolved during emplacement.

Physical properties of komatiite magmas

Komatiite magmas have unusual physical properties, which probably control their manner of eruption and influence the formation of nickel sulphide deposits. The more important features are a very low viscosity (1–10 g cm^{-1} sec^{-1}), a high density (2.7–2.8 g cm^{-3}), a high liquidus temperature (1500–1600°C), a large interval between the liquidus and solidus (350–450°C), and a high heat content (*ca* 200 cal g^{-1}).[16]

Because of these features, the following predictions can be made.

(1) As the eruption rate of a magma varies inversely with viscosity, komatiites should erupt very rapidly. Furthermore, as komatiites form by relatively high degrees of melting of their mantle source (10–15%, even if a sequential melting process is involved), the volume of melt produced in any melting event should be relatively high. Komatiite lava flows are therefore likely to be large and to erupt and flow rapidly.

(2) Once the low-viscosity, high-density komatiite magma reaches the sea-floor it will form highly mobile flows, which, unless ponded, will travel great distances. These flows will fill depressions or flow down pre-existing valleys. Just as with Modern basaltic lavas,[22] and Proterozoic basaltic komatiites on Gilmour Island (Fig. 5), the flowage is likely to become channelized, most lava transport being confined to central conduits or lava tubes between more stagnant areas that act as levees.

(3) Because of the high heat content and large interval between the liquidus and solidus, the komatiite lava will take a relatively long time to cool and to solidify.

Komatiite volcanism is likely, therefore, to have involved the eruption of very hot, highly fluid lava that flowed rapidly, for long periods, through conduits that probably followed depressions, grabens or valleys in the pre-existing volcanic topography. During this flowage the rocks that underlie the lava conduit are likely to suffer at least some degree of erosion.

Distal volcanic-assimilation model

Given the above physical properties of komatiite lavas and the observed field relationships, especially the linear stratigraphic trends and lack of any evidence for a proximal eruptive site, we conclude that emplacement of the volcanic sequence at Kambalda was controlled by the pre-existing volcanic topography and the unusual properties of flowing komatiite lavas. The basaltic lavas erupted from the southwest rift of Mauna Loa exhibit precisely such a topographic control (Fig. 6) and the volcanic landscape is similar to that envisaged for the footwall embayments at Kambalda. Very low-viscosity komatiitic lavas would, however, be expected to have very much smaller depth:width aspect ratios, especially if erupted into deep water[11] where volatiles would not be exsolved from the lava.

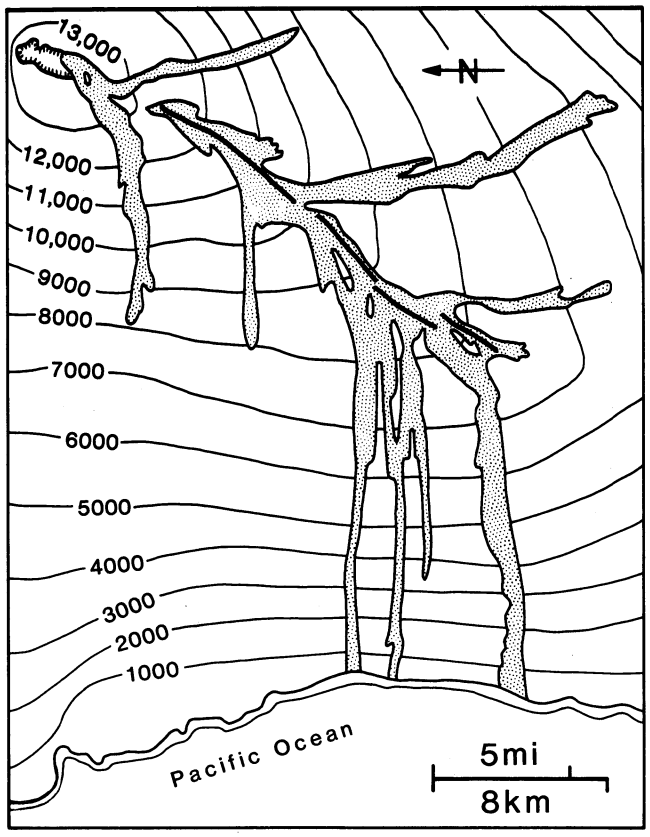

Fig. 6 Portion of southwest rift of Mauna Loa, Hawaii, showing 1949 (nearest crest) and 1950 lava flows. After Macdonald and Finch.[32] Note topographic control on linear form of these basaltic lava flows

It is most likely that the thick, linear basal host units at Kambalda represent actively flowing lava conduits, which were largely confined to the footwall embayments (Fig. 7). The barren flanking basal unit may represent more slowly moving lateral portions of the flow, or possibly lateral overflow from the central conduit, which periodically ruptured. In the first case there would be less lava flow-through and therefore more fractionation *in situ*, and in the second case more opportunity for olivine crystallization and fractionation of the lava prior to emplacement, both accounting for the more fractionated (less magnesian) composition of the barren flanking basal units. Provided that the eruptive site remained fixed relative to the topographic gradient, lava conduits in overlying flows of the sequence would be similarly localized along or near the topographic pitchline (dip direction). Alternatively, or additionally, the flanking flows could act as levees; both would account for the anomalous highly magnesian, better differentiated flows in

the upper member overlying the ore zones (cf. Figs 2 and 7). Thus, the stratigraphic sequence over the ore zones may not be 'disordered' but may represent stacking of lava conduits, much as topographic gradients influence the vertically stacked accumulation of sedimentary debris flows.[33] The predominantly poorly differentiated flows in the flanking sequence (non-ore environment) may represent intervening, more slowly flowing or stagnant portions of the flows, such as observed in Proterozoic komatiites of Gilmour Island (cf. Figs 5 and 7). Importantly, if some host units at Kambalda are lens-shaped with thicker central zones (see Fig. 7) instead of perfectly planar upper surfaces as frequently assumed in stratigraphic reconstructions, the geometry of the sequence may simulate that produced by subsiding synvolcanic faults suggested in some interpretations,[25,26,27] but not actually observed in the footwall sequence.

An important corollary of this model is the possibility of thermal erosion and assimilation beneath flowing, thermally active lava conduits, such as described in other volcanic terrains.[22] Complete analysis of this possibility is beyond the scope of this paper, but some of the implications are relevant not only to ore localization but also to ore genesis and are considered briefly below. The first implication of thermal erosion is that the embayment that originally localized the lava conduit may become enlarged. Although the Kambalda ores are generally considered to conformably overlie the footwall metabasalts,[7] the contact between the two lithologies is normally tectonized and otherwise diffuse and strongly recrystallized.[13] In less deformed areas the ores commonly conform to the convex upper surfaces of pillowed metabasalts, but are rarely transgressive (i.e. intrusive); porous pillowed zones may have been more resistant to thermal erosion owing to hydrothermal circulation

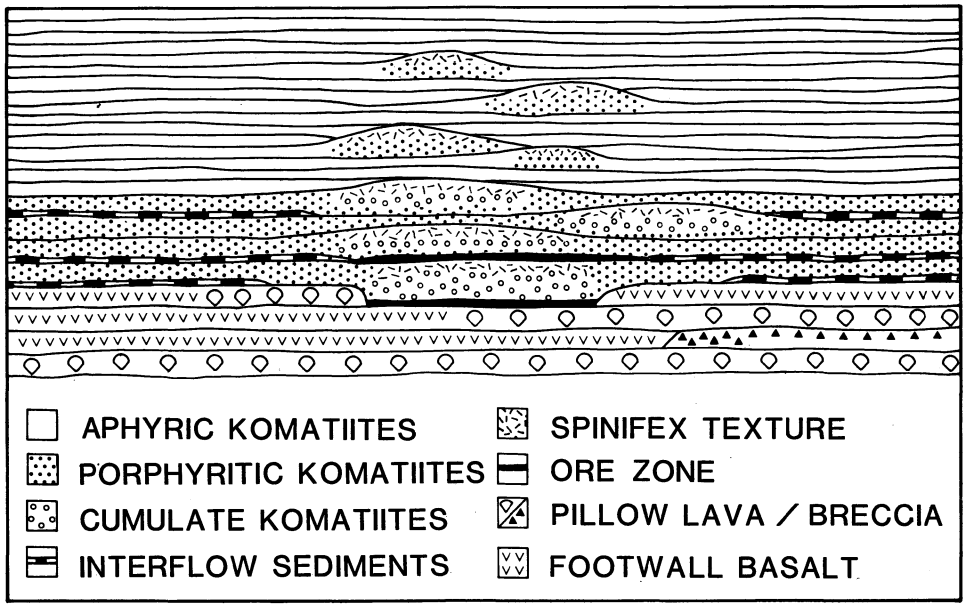

Fig. 7 Schematic interpretative reconstruction of Kambalda ore environment in cross-section after removal of superimposed structural deformation; rock compositions as in Fig. 2. Note localization of contact ore, hanging-wall ore and lava conduits, and absence of sedimentary horizons along (above) inferred topographic pitchline (see discussion in text for further details). From Lesher[13]

Olivine enrichment could have occurred in the active lava conduits by gradual accumulation of gravity-settled primocrysts and/or by *in-situ* fractional crystallization of cumulus olivine. Continuous or periodic flow-through of lava would replenish crystallizing olivine components without producing extensive *in-situ* fractionation of the silicate liquid. Mass balance calculations[13] indicate that the degree of olivine enrichment in the host units could be produced with negligible (1–2% MgO) fractionation along the drilled length of the host unit by flow-through of only 5–10 times the volume of the host unit (i.e. that volume within the embayment). This is consistent with the host units (and embayments) being commonly more extensive along plunge than the ore zones. Repeated influx of lava is also supported by the presence of essentially conformable zones of disseminated blebby sulphide mineralization within the basal host units at Otter,[34] Durkin and Fisher Shoots.[7] This mineralization is spatially separated from the underlying contact ore, is too coarse (up to 1-cm diameter) not to have settled if emplaced with the initial lava pulse, and is too abundant (up to 30% sulphide) to have exsolved *in situ* from a statically emplaced host unit. In addition to the reversals in olivine composition and morphology at Victor Shoot noted above, there is also evidence of compositional zoning in the basal host unit at Otter Shoot[34] and of compositional layering in the basal host unit at Lunnon Shoot[25]—all consistent with periodic or repeated lava influx.

in the footwall. Most embayments at the Kambalda Dome are highly discontinuous troughs with re-entrant margins (see Figs. 3 and 7), compared with the shallow, open flexures that characterize many other deposits of this type (e.g. Wannaway,[8] Scotia[9] and some shoots in the southern part of the Kambalda Nickel Field[7]), and it is uncertain whether this represents variations in original topography of the underlying basalts, enlargement by thermal erosion and/or differences in the style of superimposed deformation. Note that if the volume of komatiite flowing through the overlying conduit was large—a fundamental feature of our model—there would be little geochemical evidence for local assimilation of basaltic material.

A second, and potentially more important, implication is the possibility of selective thermal erosion and assimilation of sulphidic sediments (unconsolidated ?) beneath the thermally active lava conduits. Depending on the degree of sulphur saturation in the komatiite on emplacement, assimilation of sulphur from the sediments (average 7% S^{35}) could induce rapid and localized sulphide exsolution. This would account for (1) the very restricted spatial distribution of the ores, that is, their restrictive association with linear, highly magnesian host rocks (thermally active lava conduits), (2) the stratigraphically equivalent, but locally mutually exclusive relationship between the nickel ores and sulphidic metasediments, (3) the localization of very high-grade magmatic nickel ores at the base of otherwise

commonly barren host units and (4) the results of mass balance calculations[12,13] that indicate that the volume of sulphides in the ore zones is too large to have exsolved from the overlying host unit. The relatively high nickel and PGE contents of the ores suggest that the sulphides equilibrated with a large volume of silicate lava, implicit in our flow-through emplacement model, but minor variations would account for the different massive ore tenors of the oreshoots.[17] The indistinguishable S/Se and sulphur isotopic ratios of the Kambalda ores and metasediments and their paired difference with those of the Windarra ores and sediments[6] are consistent with a major contribution of sedimentary sulphur, but are not definitive because both ores and sedimentary sulphides could have formed independently from the same sulphur source. This assumes that the sulphur in the metasediments was present at the volcanic stage and not introduced during subsequent alteration or metamorphism of the komatiites (see Lesher *et al.*[12] for a discussion of sulphur mobility in the komatiites); the regional distribution of sulphidic shales and geochemical studies of the Kambalda metasediments[35] support the former interpretation.

The contact metasediment has been interpreted previously to overlap and post-date the basal host units,[5,7,35] but in those rare instances where it does overlap the margins of the embayments (see Table 8[7]), it does not occur at recognizable flow boundaries in the komatiite sequence and has probably been faulted into those positions.[13] As was noted above, the basal host unit in most areas apparently overlaps the margins of the embayments and is probably contiguous with the barren flanking basal unit(s) that overlie(s) the contact metasediment (Fig. 7). The contact metasediment is compositionally relatively uniform[35] and this, plus its widespread distribution, suggests that it represents a major time-stratigraphic volcanic hiatus. Our interpretation is that it and the internal sediments were once present on the basalt contact and throughout the lower member of the komatiite sequence, but were subsequently thermally eroded and assimilated beneath the lava conduits, which were localized within and above the embayments. Significantly, the nickel ores at the margins of some stratiform hanging-wall oreshoots do grade laterally into metasediments.[35,36] Contact sediments may have originally preferentially accumulated in the embayments (cf. references 5, 7 and 35), but would have been selectively assimilated beneath the major lava conduit now represented by the anomalously thick, olivine-enriched basal host units. Metasediments do occur beneath the contact ores within the shallower, open embayments at some shoots (e.g. Cruickshank[7] and Scotia deposit[9]); they are highly altered and may represent unassimilated variants, but they are also strongly sheared and it is uncertain whether they are in their original stratigraphic position. We also note that at Widgiemooltha,[8] where two ultramafic cycles are present, only the upper komatiites contain sulphidic metasediments and are mineralized.

This is not an entirely new interpretation: the close spatial association of the nickel ores with sulphidic metasediments or country rocks has been noted by several authors, who considered that the latter may have been the source of sulphur in these deposits.[37,38,39] These models have been criticized by others[6,12,35] on the basis of the lack of any direct evidence for sediment contamination, such as (1) sedimentary xenoliths, (2) anomalous Zn–SiO_2–alkali contents or (3) strong chalcophile element depletion in the host rocks. If assimilation occurred by thermal erosion of poorly consolidated sediments beneath an actively flowing komatiite lava conduit, however, xenoliths are unlikely to be preserved and most of the host unit would crystallize from replenished liquid; only the lowermost part (now mineralized, deformed, metamorphosed, and pervasively metasomatized) would exhibit any evidence of contamination.

Irrespective of the timing and mode of sulphide separation, segregation of the sulphides at the base of the flow could have occurred at almost any stage during emplacement of the host komatiites. Because of their higher thermal conductivity and lower solidus temperature in comparison with the komatiite lava, it is likely that the sulphides would have remained molten during lava emplacement. The ores were initially formed or localized in the embayments and then probably preferentially concentrated in subsidiary topographic features within the embayments. Even if they were erupted with the komatiite magma, it is unlikely that the very low-viscosity molten sulphides ever completely separated from the host komatiite flow during emplacement,[4,5,6,25] as they would rapidly solidify once separated from the komatiite lava and then be remelted as the flow advanced. The present ore profile (disseminated/matrix/massive sulphides) probably formed by gravity segregation and/or flowage differentiation at a later stage once olivine crystallization had commenced in the established lava conduit. Because of the influence of continued flow-through of lava in the conduit, the ore segregation/solidification process would be similar to, but considerably more complex than, the conductive thermal model of Usselman *et al.*[16]

In this genetic model the Kambalda deposits are interpreted as a relatively distal volcanic environment, the linear stratigraphic trends (Fig. 1) representing the vector of lava transport. Thus, an important implication of this model is that the local strike of the sea-floor during komatiite emplacement was roughly east–west, highly oblique to the regional structural trends and the interpreted rift zone. The extensive block faulting in the area (see Fig. 4[11]) prevents determination if the north–south stratigraphic trend was unique; the correspondence between the volcanic pitchline and the regional structural trend may only be fortuitous, but is more likely to represent a fundamental tectonic control, such as differential subsidence along the length of the postulated rift zone.[11] Lack of surface exposure and complex polyphase structural deformation in the area hamper detailed studies of the three-dimensional morphology and physical volcanology of the Kambalda komatiites that might indicate the direction of transport. The entire komatiite sequence is reported to thicken markedly to the north of the Kambalda Dome and thin to zero further to the south,[7] which may indicate lava transport from north to south; unfortunately, structural thickening or thinning cannot be precluded.

Conclusions

The Archaean komatiite-associated nickel deposits at Kambalda, Western Australia, exhibit a number of features that indicate a strong volcanic control on ore emplacement, including (1) a restriction to the south-central part of the Norseman–Wiluna Belt, interpreted to represent a volcanically active intracratonic rift zone, (2) a regional stratigraphic localization within low-level ultramafic sequences, (3) a restriction to specific basal cumulate komatiite host units, (4) confinement within synvolcanic footwall embayments and (5) variations in the physical volcanology of overlying and adjacent barren komatiites with proximity to the ore zones.

Significant variations in olivine composition and the presence of *in-situ* crystallized crescumulate olivine in some basal host units that escaped complete alteration suggest that the basal host units did not form by accumulation of intratelluric olivine phenocrysts, as postulated in previous models, but that olivine enrichment probably occurred by *in-situ* fractional crystallization of olivine during longitudinal lava flow. Continuous or periodic flow-through of lava would replenish crystallizing olivine components without producing extensive fractionation of the silicate liquid until the magma supply ceased.

There is a conspicuous lack of any direct or indirect evidence of a proximal eruptive site (e.g. footwall feeders, pyroclastic breccias, ultramafic intrusives) such as observed in some other deposits of this type. Hence, the linear trend of the oreshoots,

footwall embayments, basal host units and the distinctive stratigraphic sequence over the ore zones at Kambalda are considered to indicate linear lava emplacement controlled by (1) the location of unidentified eruption sites relative to local and/or regional north–south topographic gradients and (2) the local volcanic topography. The olivine-enriched basal host units probably represent actively flowing lava conduits centralized on the footwall embayments. The stratigraphically 'disordered' and laterally 'discontinous', differentiated and olivine-enriched barren komatiites over the ore zones possibly represent similar localization of overlying lava conduits along the same topographic pitchline. The absence of metasediments from the ore zones and, indeed, the presence of the nickel sulphide mineralization may be due to assimilation of sulphidic sediments during thermal erosion by the fixed lava conduits, but this is not implicit to the emplacement model. The poorly differentiated lavas that flank the ore zones probably represent more slowly moving parts of the flows.

Like most previous genetic models, many aspects remain somewhat speculative, being based primarily on fragmentary data and interpretation of a few better preserved or better studied areas and on analogies with better exposed lava piles in other areas. This model is more consistent with the observed field and geochemical relationships documented at Kambalda, however, and represents a fundamental change in the scale and direction of observation from which these deposits may be viewed. From an exploration standpoint this model emphasizes the possible importance of distal dynamic volcanic processes in the localization of the ores and host units rather than proximal static accumulation. A corollary of this model is that the association of the nickel sulphides with highly magnesian basal host units may be due to the coincidence of sulphidic sediments and thermally active komatiite lava conduits. A literature search indicates that most deposits of this type in Western Australia, Canada and Zimbabwe are associated with sulphidic metasediments. Assimilation of country rocks as sulphur sources and/or to induce sulphide saturation has been proposed for virtually every other type of nickel deposit in mafic–ultramafic rocks[2] and perhaps komatiite-associated deposits are no exception. Most importantly, this model predicts that mineralization may be localized at several points along the major lava flow system. The clustering of komatiite-associated nickel deposits along the *ca* 50 km long zone, including the Kambalda–St Ives – Tramways and Spargoville–Widgiemooltha–Pioneer nickel fields, wherever the host sequence has been uplifted and exposed by folding and/or granitoid diapirism (see Fig. 4[11]), may indicate the minimum dimensions of these Archaean komatiitic volcanic systems.

Acknowledgement

C.M.L. is grateful to Western Mining Corporation (Kambalda Nickel Operations) for providing access to the deposit and for sponsoring the field work. We thank M. J. Bickle, I. H. Campbell, M. J. Donaldson, G. D. Loftus-Hills and R. S. J. Sparks for stimulating discussions, J. J. Gresham and M. J. Donaldson for comments on an earlier manuscript, D. L. Buchanan for editorial suggestions, and P. Denning for typing. C.M.L. was supported by a University of Western Australia Research Scholarship.

References

1. Lesher C. M. Donaldson M. J. and Groves D. I. Nickel deposits and their host rocks in the Norseman–Wiluna Belt. In *Regional geology and nickel deposits of the Norseman–Wiluna Belt, Western Australia.* Groves D. I. and Lesher C. M. eds. *Univ. West. Aust. geol. Dep. Extension Service Publ.* no. 7, 1982, B1–63.
2. Naldrett A. J. Nickel sulfide deposits: classification, composition and genesis. *Econ. Geol., 75th anniversary vol.*, 1981, 628–85.
3. Groves D. I. and Hudson D. R. The nature and origin of Archaean strata-bound volcanic-associated nickel–iron–copper sulphide deposits. In *Handbook of strata-bound and stratiform ore deposits, volume 9* Wolf K. H. ed. (Amsterdam: Elsevier, 1981), 305–410.
4. Marston R. J. *et al.* Nickel sulfide deposits in Western Australia: a review. *Econ. Geol.*, **76,** 1981, 1330–63.
5. Ross J. R. and Hopkins G. M. F. Kambalda nickel sulphide deposits. In *Economic geology of Australia and Papua–New Guinea 1. Metals* Knight C. L. ed. (Parkville, Victoria: Australasian Institute of Mining and Metallurgy, 1975), 100–21. (*Monograph Series* no. 5).
6. Groves D. I. Barrett F. M. and McQueen K. G. The relative roles of magmatic segregation, volcanic exhalation and regional metamorphism in the generation of volcanic-associated nickel ores of Western Australia. *Can. Mineralogist,* **17,** 1979, 319–36.
7. Gresham J. J. and Loftus-Hills G. D. The geology of the Kambalda nickel field, Western Australia. *Econ. Geol.*, **76,** 1981, 1373–416.
8. McQueen K. G. Volcanic-associated nickel deposits from around the Widgiemooltha dome, Western Australia. *Econ. Geol.*, **76,** 1981, 1417–43.
9. Page M. L. and Schmulian M. L. The proximal volcanic environment of the Scotia nickel deposit. *Econ. Geol.*, **76,** 1981, 1469–79.
10. Stolz G. W. and Nesbitt R. W. The komatiite nickel sulfide association at Scotia: a petrochemical investigation of the ore environment. *Econ. Geol.*, **76,** 1981, 1480–502.
11. Groves D. I. Lesher C. M. and Gee R. D. Tectonic setting of the sulphide nickel deposits of the Western Australian Shield. In *Sulphide deposits in mafic and ultramafic rocks* Buchanan D. L. and Jones M. J. eds (London: IMM, 1984), 1–13.
12. Lesher C. M. *et al.* Geochemistry of komatiites from Kambalda, Western Australia: I. Chalcophile element depletion—a consequence of sulfide liquid separation from komatiitic magmas. *Econ. Geol.*, **76,** 1981, 1714–28.
13. Lesher C. M. Localization and genesis of komatiite-associated Fe–Ni–Cu sulphide mineralization at Kambalda, Western Australia. Ph.D. thesis, University of Western Australia, 1983.
14. Naldrett A. J. Nickel sulphide deposits—their classification and genesis, with special emphasis on deposits of volcanic association. *Trans. Can. Inst. Min. Metall.*, **76,** 1973, 183–201.
15. Naldrett A. J. and Campbell I. H. Physical and chemical constraints on genetic models for komatiite-related Ni-sulphide deposits. In *Komatiites* Arndt N. T. and Nisbet E. G. eds (London: George Allen and Unwin, 1982), 423–34.
16. Usselman T. M. *et al.* Physical constraints on the characteristics of nickel-sulfide ore in ultramafic lavas. *Can. Mineralogist,* **17,** 1979, 361–72.
17. Ross J. R. and Keays R. R. Precious metals in volcanic-type nickel sulfide deposits in Western Australia. I. Relationship with the composition of the ores and their host rocks. *Can. Mineralogist,* **17,** 1979, 417–35.
18. Irvine T. N. Terminology for layered intrusions. *J. Petrol.*, **23,** 1982, 127–62.
19. Harley D. N. K.N.O. progress report—Juan Shoot. Unpublished Western Mining Corporation Report K2497, 1980.
20. Lesher C. M. Concomitant tholeiitic and komatiitic volcanism as an ore localizing mechanism at Kambalda, Western Australia (abs). *Fifth Aust. Geol. Conv. Abs. Vol.*, **3,** 1981, 74–5.
21. Sparks R. S. J. Personal communication to N.T.A., 1982.
22. Lunar and Planetary Institute. *Basaltic volcanism on the terrestrial planets* (Oxford, etc.: Pergamon, 1981), 1200 p.
23. Williams D. A. C. The association of some nickel sulfide deposits with komatiitic volcanism in Rhodesia. *Can. Mineralogists,* **17,** 1979, 337–49.
24. Green A. H. and Naldrett A. J. The Langmuir volcanic peridotite-associated nickel deposits: Canadian equivalents of the Western Australian occurrences. *Econ. Geol.*, **76,** 1981, 1503–23.
25. Ross J. R. H. Archean nickel sulfide mineralization at Lunnon shoot, Kambalda, Western Australia. Ph.D. thesis, University of California, Berkeley, 1974.
26. Fisher D. The petrology of the Mt. Edwards nickel sulphide deposit, Widgiemooltha, Western Australia. Ph.D. thesis, University of Toronto, 1979.
27. Middleton C. N. K.N.O. progress report—Lunnon shoot. Western Mining Corporation Report K2517, 1980.
28. Arndt N. T. Proterozoic spinifex-textured basalts of Gilmour Island, Hudson Bay. *Pap. geol. Surv. Can.* 81-1A, 1982, 137–42.

29. Helz R. T. Determination of the P–T dependence of the first appearance of FeS-rich liquid in natural basalts to 20 KB (abstr.) *EOS, Trans. Am. geophys. Union.* **58.** 1977, 523.
30. Huang W.-L. and Williams R. J. Melting relations of portions of the system Fe–S–Si–O to 32 kb with implications to the nature of the mantle–core boundary (abstr). In *Lunar and Planetary Science Conference XI.*, 1980, 486–8.
31. Wendlandt R. F. Sulfide saturation of basalt and andesite melts at high pressures and temperatures. *Am. Miner.*, **67,** 1982, 877–85.
32. Macdonald G. A. and Finch R. H. The June 1950 eruption of Mauna Loa. *Volcano Letter* no. 509, 1950, 7 p.
33. Lewis D. W. Laird M. G. and Powell R. D. Debris flow deposits of early Miocene age, Deadman Stream, Marlborough, New Zealand. *Sedim. Geol.*, **27,** 1980, 83–118.
34. Keele R. A. and Nickel E. H. The geology of a primary millerite-bearing sulfide assemblage and supergene alteration at the Otter Shoot, Kambalda, Western Australia. *Econ. Geol.*, **69,** 1974, 1102–17.
35. Bavinton O. A. The nature of sulfidic metasediments at Kambalda and their broad relationships with associated ultramafic rocks and nickel ores. *Econ. Geol.*, **76,** 1981, 1606–28.
36. Paterson H. L. *et al.* Nickeliferous sediments and sediment-associated nickel ores at Kambalda, Western Australia. Reference 11, 81–94.
37. Naldrett A. J. The role of sulphurization in the genesis of iron–nickel sulphide deposits of the Porcupine District, Ontario. *Trans. Can. Inst. Min. Metal.*, **69,** 1966, 147–55.
38. Prider R. T. Nickel in Western Australia. *Nature, Lond.*, **226,** 1970, 691–3.
39. Hopwood T. The significance of pyritic black shales in the genesis of Archean nickel sulphide deposits. Reference 3, 411–67.

Nickeliferous sediments and sediment-associated nickel ores at Kambalda, Western Australia

H. L. Paterson B.Sc., M.Sc.(App.), A.M.Aus.I.M.M.
M. J. Donaldson B.A.(Hons.)
R. N. Smith B.Sc.(Hons.), M.Sc.
M. F. Lenard B.Sc.(Hons.)
J. J. Gresham B.Sc.(Hons.) A.M.Aus.I.M.M.
D. J. Boyack B.Sc., M.Sc.
Kambalda Nickel Operations, Western Mining Corporation, Ltd., Kambalda, Western Australia
Reid R. Keays B.Sc., Ph.D.
Department of Geology, University of Melbourne, Parkville, Victoria, Australia

Synopsis

Albite-rich sedimentary rocks that contain abundant Fe sulphides occur in the lower portion of the ultramafic sequence at Kambalda and their broadly antipathetic relationship to most of the nickel orebodies is well documented. These sediments generally contain less than 0.1% Ni, but nickeliferous equivalents with 0.3 to >6% Ni occur locally in close spatial association with more typical volcanic peridotite-associated massive, matrix and disseminated ores. Nickeliferous sediments have been mined at several locations at Kambalda but, collectively, they constitute less than 2% of the total Kambalda nickel reserve.

The nickeliferous sediments occur both on the ultramafic–footwall basalt contact and within the lower part of the ultramafic sequence, and are usually less than 5 m thick. They are commonly finely laminated rocks with a cherty appearance, composed essentially of layers of albite+quartz±amphibole, alternating with pyrrhotite+pentlandite±pyrite layers. Some contain a minor amount of carbon. The sediments are only of ore grade (>1% Ni) immediately adjacent to massive Fe–Ni–Cu sulphides, which are interpreted as normal magmatic ores on the basis of geochemistry and the presence of distinctive ferrochromites. The nickel content of the sediments decreases to background levels (<0.1%) within about 20 m of the massive sulphides. In most locations the massive sulphides clearly have been emplaced tectonically within or adjacent to the sediments, which are commonly highly deformed. Typical nickeliferous sediments contain about 1% Ni, 0.1% Cu, 0.1% Zn, 400 ppb Pd, <0.2 ppb Ir and 10–200 ppb Au. They have lower Ni/Cu (average 10), higher S/Ni (average 6) and higher S/Se (average 11 200) than associated massive sulphides (average 40, 4.8 and 7400, respectively). The Pd/Ir ratio of the nickeliferous sediments (typically >1000) contrasts markedly with that of associated massive sulphides (average *ca* 16).

The high Pd/Ir values are similar to those which have been reported for hydrothermal Fe–Ni sulphides and barren sulphidic sediments of probable volcanic exhalative origin. They preclude a direct magmatic origin for the sulphides in the nickeliferous sediments, though S/Se and S isotope data indicate a magmatic source for the sulphur. The restriction of nickeliferous sediments to within about 20 m of normal magmatic sulphides and the lack of a widespread Ni dispersion halo suggest local redistribution of originally magmatic Ni. This probably occurred by diffusion and hydrothermal mobilization during deformation and amphibolite-facies metamorphism. Although not totally ruled out, a volcanic exhalative origin for the Ni seems unlikely.

Iron–nickel sulphide deposits at Kambalda, Western Australia, occur at or near the base of an extrusive komatiitic ultramafic sequence that overlies a footwall formation of massive and pillowed tholeiitic metabasalts. The host rocks and ores are of Archaean age (~2800 m.y.) and have undergone relatively low-strain, medium-grade metamorphism (maximum temperature ~520°C[1,2]). The nickel ores are commonly localized in elongate depressions within the footwall metabasalts (contact ores), though some occur at the base of the second or third ultramafic flow unit (hanging-wall ores). Most ores are considered to be of magmatic origin, resulting from extrusion of ultramafic lava and sulphide melt along sea-floor fissures. The orebodies at Kambalda have become known as the type examples of the Volcanic Peridotite-Associated class of nickel deposit.[3]

Thin metasedimentary units occur both at the ultramafic–footwall metabasalt contact and at interflow positions within the lower portion of the ultramafic sequence. There is a general antipathetic relationship between Ni ores and sediments, though there are isolated occurrences in most oreshoots* where sediments and Ni ores are closely associated, and in these locations the sediments may contain in excess of 6% Ni. Nickeliferous metasediments have been mined at several localities, though collectively such ores constitute a very minor proportion (<2%) of the total Kambalda pre-mining nickel ore reserve. Some of these finely laminated nickeliferous metasediments bear similarities to the tuffites associated with volcanogenic massive sulphide deposits and they have been cited as evidence for a volcanic exhalative origin for at least some of the Kambalda nickel ores (e.g. Hutchinson[4]). A similar origin was proposed by Lusk[5,6] for the normal, ultramafic-hosted ore, though this was strongly criticized by Groves *et al.*[7] and Bavinton,[1] both of whom dismissed exhalative processes as unimportant in the formation of most Ni ores. These authors did recognize, however, that the barren sulphidic sediments may include an exhalative component.

The present study was initiated to document the important nickeliferous sediment occurrences at Kambalda in order to evaluate the contribution of exhalative processes to their genesis. If such processes were operative in the formation of the nickeliferous sediments, there would be important implications for current models of Ni sulphide ore genesis by strictly magmatic processes and, consequently, for the erection of exploration models.

Throughout the remainder of this paper the prefix 'meta' is omitted for simplicity, though it is recognized that all rocks discussed have been metamorphosed to lower amphibolite facies conditions. Sediments that contain in excess of 0.3% Ni are defined as *nickeliferous*, whereas those with <0.3% Ni are referred to as *barren* (a cutoff grade of 1.0% Ni is used for mining at Kambalda and the average grade of ore mined is about 3% Ni). Where massive Fe–Ni sulphides are intimately

*'Shoot' is the local term for a cluster of Ni orebodies that are usually mined from a common shaft or decline access.

associated with sediments they are referred to as *sediment-associated massive sulphides* to distinguish them from normal ultramafic-hosted massive ores.

Terminology used for ultramafic rocks in this paper is based on their volatile-free MgO content as defined by Gresham and Loftus-Hills:[8] picrites contain 15–28% MgO, peridotites 28–36% MgO and olivine peridotites more than 36% MgO. Although this nomenclature is used throughout this paper, extensive hydration and carbonation have produced in these rocks mineral assemblages that are dominated by tremolite and chlorite (in picrites), tremolite–antigorite–chlorite or talc–dolomite–chlorite (peridotites), and antigorite–chlorite or talc–magnesite–chlorite (olivine peridotites).

Previous work

The Kambalda interflow sediments have been the subject of numerous detailed studies that covered mineralogical and geochemical aspects as well as their spatial relationships with Ni ores and ultramafic rocks. Hudson[9,10] first pointed out the generally antipathetic relationship between ores and sediments at Lunnon shoot (Fig. 1), and he also documented an occurrence of sediment-associated massive sulphides with in excess of 1% Ni. Ross[11] elaborated on the antipathetic relationship of the sediments and ores at Lunnon shoot and used this relationship to constrain genetic models for the origin of the Fe–Ni sulphide mineralization (see also Ross and Hopkins[12]). He considered the sediments to have formed by a combination of chemical precipitation of silica and clastic sedimentation, possibly related to ultramafic volcanic activity. The first detailed geochemical data on the sediments were presented by Schwann.[13] His study of McMahon shoot sediments included whole-rock major and trace-element analyses of 'black shales' and 'cherts', and he concluded that the sediments were deep-water chemical precipitates.

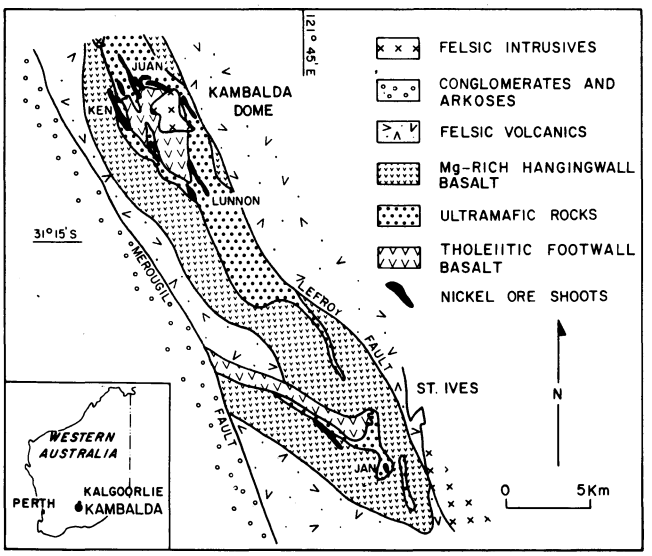

Fig. 1 Geological plan of Kambalda Dome–St. Ives area

The recognition that sediments may be important in the identification of ore environments led to detailed studies of these rocks by Bavinton,[1,2] who documented spatial distribution of sediments around the Kambalda Dome and described their mineralogy and chemical compositions. Specific reports that covered precious metals and rare-earth element (REE) characteristics of the sediments were given by Bavinton and Keays[14] and Bavinton and Taylor,[15] respectively, and S, C, and O isotope data were presented by Donnelly.[16] On the basis of S isotope data and S/Se ratios Bavinton[1,2] concluded that the sulphur in the sediments was of magmatic origin.

Hopwood[17] proposed a genetic model for Kambalda-type Ni ores that involved transport of Ni as carbonyl complexes and an intimate spatial association of ores and sediments. He postulated that the Ni ore originated by the intrusion of ultramafic magma into actively deforming pyritic sediments, and subsequent reaction to form Fe–Ni sulphides. Most of Hopwood's speculations are at variance with common observations at Kambalda, and his model is not generally accepted.

Chapman and Groves[18] (see also Chapman[19]) followed up the work of Bavinton and Keays[14] on the Au content of Kambalda sediments and preferred a volcanic-exhalative origin for the Au, though they stressed the equivocal nature of available data. Groves and co-workers[20,21] summarized available data on cherty sediments within ultramafic flow sequences and suggested an origin that involves predominantly volcaniclastic and exhalative components, probably related to waning basaltic volcanism. They considered the minor Ni-rich sediments to be the result of either limited Ni diffusion from ultramafics into sediments or Ni-rich exhalation.

Sediments within Kambalda ultramafic sequence

The lower portion of the ultramafic sequence (the Lower Member as defined by Gresham and Loftus-Hills[8]) is characterized by the presence of thin sedimentary units that occur both at interflow positions and on the footwall basalt contact. These sediments have been grouped by Bavinton[1] into cherty, carbonaceous and chloritic types, the latter being the least common. (The term 'cherty' is used to describe the physical appearance, rather than the composition, of these rocks.) Both cherty and carbonaceous varieties consist of layers of albite and quartz (with subsidiary chlorite, talc, micas, tremolite and carbonate), separated by thin layers (commonly 1–2 mm) of pyrrhotite with minor pyrite and sphalerite and chalcopyrite. The proportion of sulphides is highly variable, but averages about 20% by volume and commonly increases towards the top of the sediment unit.

Studies of sediment distribution around the Kambalda Dome[1,2] have shown that sediments are far less common in the Lower Member in areas immediately adjacent to the nickel orebodies. Contact sediments are absent from the footwall troughs that host most contact orebodies, and there is commonly a zone of sediment-free contact on both flanks of the trough—the 'void zone' of Bavinton[1] (see also Fig. 9 of Gresham and Loftus-Hills[8]). Similarly, sediments at interflow positions are absent from the prism of ultramafic rocks that overlies almost all major ore positions (Figs. 3 and 6 in Gresham and Loftus-Hills[8]).

Regardless of the appreciable sulphide content of these sediments, they are characterized by extremely low Ni contents. Bavinton[2] listed an arithmetic mean value of 232 ppm Ni for a population of 217 samples collected from the Kambalda Dome and St. Ives areas. He recognized, however, that minor occurrences of nickeliferous sediment were present, and could be grouped into three categories: *(a)* crosscutting, structural relationship between Ni sulphides and associated sediments (Fig. 2*(B)*), *(b)* intimate interlayering of Ni sulphides and sediments (Fig. 2*(C)* and *(D)*) and *(c)* parallel contact between Ni sulphides and sediments with no interlayering. Bavinton[1,2] considered group *(a)* to be a result of tectonic mobilization of normal magmatic ore, but thought that groups *(b)* and *(c)* may represent syngenetic formation of Ni ores and sediments, largely on the basis of fine-scale layering and low Ni tenor of associated massive sulphides.

Nickeliferous sediment occurrences

Although volumetrically and economically unimportant, nickeliferous sediments occur at most of the oreshoots in the Kambalda Dome–St. Ives area (Fig. 1). This study examined occurrences at Juan, Ken, Lunnon and Jan shoots and details of

Table 1 Summary of nickeliferous sediment occurrences

Shoot	Area	Setting	Pre-mined geological ore reserve	Per cent of pre-mined GOR tonnage‡	Strike length, m	Thickness, m	Mineralogy (in decreasing order of abundance)†	Geochemistry					
								Ni in sediment, %	Ni in associated massive ore, %	Nickeliferous sediments			
										S/Ni	Ni/Cu	Pd/Ir	S/Se
Juan	624	Hanging-wall sediment within Juan Fault zone. Nickeliferous where adjacent to normal contact orebody (N5ØC), but less-sulphidic and barren along strike	6000 t @ 2.3%	1	35	up to 4	Ab,Am,Qz,Tc. Po,Pn,Py,Cp	2.0	10	5	11	400–58 000	16 500–49 300
	1216	Contact sediment in structurally complex Juan West underside area. Thick lenses of low-tenor massive sulphide within sediment	6000 t @ 2.5% Ni	1	45	2	Ab,Qz,Am,Bi. Po,Pn,Cp,Py	1.0	4.5	8	9	230–7000	2200–10 200
Ken	404	Hanging-wall sediment in talc–chlorite and picritic ultramafics 20 m above basalt contact	11 000 t @ 1.4%	1	60	1.5	Ab,Qz,Bi,Tc. Py,Vl	0.9	6	16	8	—	—
	901	Contact sediment disrupted by low-angle shears. Reserve figure includes transition to normal sediment-free contact up-dip	64 000 t @ 1.5%	8	100	2	Ab,Qz,Bi,Tc. Po,Pn,Vl,Py	0.7	8	7	8	300–1500	2500–14 800
Lunnon	903	Located on basalt contact to east of main Lunnon trough. Grades to normal ultramafic-associated ore to west; sub-grade to barren sediment contact to east	60 000 t @ 3.2%	1.3	250	2	Qz,Ch,Bi. Po,Pn	0.5–1.0	8	7	5	900–8200*	4700–9400
Jan	702	Hanging-wall sediment at north end of Jan Main (NØ1H) surface. Ni content increases towards NØ1H	1500 t @ 1.2%	1	25	2–3	Ab,Tc,Do,Bi,Ch,Qz, Po,Pn,Vl	1.2	10.4	5	9	—	—
	902	Hanging-wall sediment at north end of Jan Main (NØ1H) surface. Lenses and seams of massive sulphides associated with sediments. Sediments grade into massive sulphides of NØ1H	11 000 t @ 3.5%	1	30	2–3	Ab,Do,Tc,Bi,Ch. Po,Pn,Py,Vl	1.0–6.0	12	15	4	1700–18 000	9500–18 500

* One high Ir sample (13 ppb) has Pd/Ir=16.
† Ab = albite; Am = amphibole; Tc = talc; Do = dolomite; Pn = pentlandite; Cp = chalcopyrite; Qz = quartz; Bi = biotite; Ch = chlorite; Po = pyrrhotite; Py = pyrite; Vl = violarite.
‡ GOR = geological ore reserve, i.e. pre-mining.

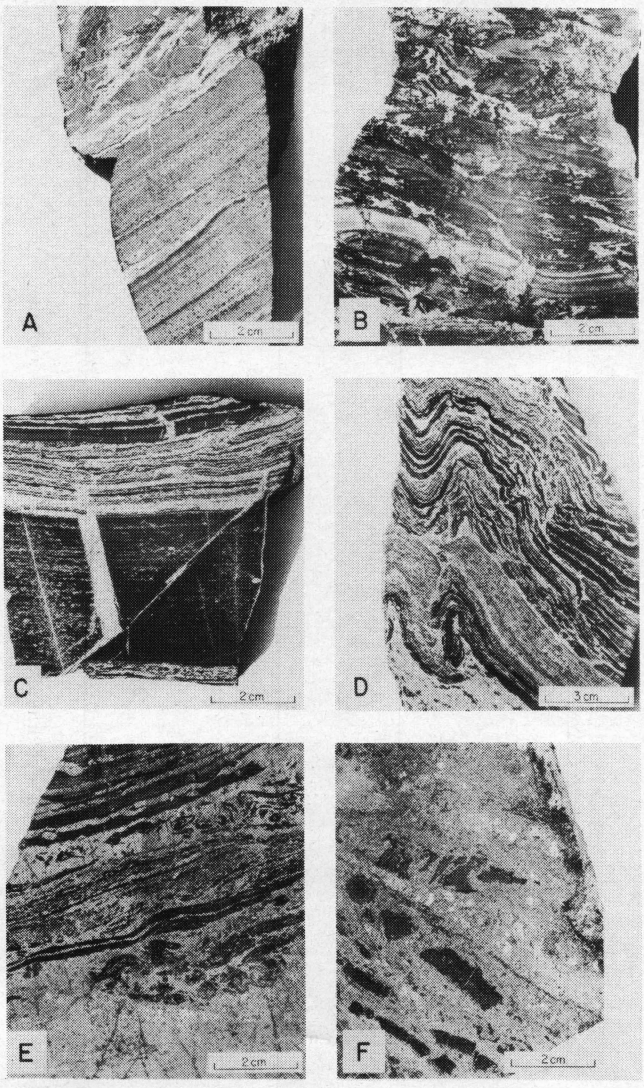

Fig. 2 Photographs of sawn slabs of nickeliferous sediments and associated massive sulphides. *A*, finely laminated nickeliferous sediment (> 1% Ni) directly overlying basalt (not shown), Juan shoot 1216 area. Dark bands are albite-rich; white layers carbonate. Most of remainder of finely banded section is very fine-grained disseminated pyrrhotite in albite + amphibole matrix. Upper section is strongly sheared and brecciated sediment (albite + amphibole + carbonate (white) + sulphides) containing about 1% Ni. *B*, finely banded nickeliferous sediment (1.8% Ni), Juan shoot 624 area. Silicate laminæ (albite + amphibole) approximately parallel, but sulphides (pyrrhotite + pentlandite—trace chalcopyrite) are fracture-filling and generally not contained within lamination. *C*, finely laminated nickeliferous sediment (2.6% Ni), Juan shoot 624 area. Dark areas are largely albite + amphibole; light areas pyrrhotite + pentlandite + chalcopyrite. Thick, near-vertical remobilized vein in centre is chalcopyrite-rich. Note very fine-scale sulphide laminæ and evidence of diffusion of remobilized sulphides (pyrrhotite + pentlandite—formerly mss) into previously barren sediment adjacent to veins. *D*, albitic nickeliferous sediments from Jan shoot, 902 area. Highly contorted, interlaminated albite and sulphides. Note silicate fragments in sulphide-rich layer at bottom and considerable brecciation within individual layers. *E*, contact between massive Fe–Ni sulphide lens and nickeliferous sediment, Jan shoot 902 area. Interface between these rock types marked by zone about 5 cm wide of strong brecciation. *F*, massive Fe–Ni sulphides (10% Ni) with included fragments of albitic sediment (dark). Pentlandite grains are coarse and many are distinguishable as light, highly reflecting patches. Patches of fine-grained pyrite occur at bottom right and top left. Finely laminated nickeliferous sediments grade into massive ores through transition zones such as that depicted. Jan shoot 902 area

individual localities are summarized in Table 1. Mineralogical and chemical data for these occurrences are summarized in Tables 2, 3 and 4.

Juan shoot

Juan shoot is a major contact ore position on the northwest flank of the Kambalda Dome (Fig. 1). Details of the shoot geology and a typical cross-section were given by Gresham and Loftus-Hills.[8] Although sediments are comparatively rare in the mine area, Juan is host to two nickeliferous sediment occurrences.

On the 6 level (624 area) a sulphide-rich sediment lies within the Juan Fault zone—close to where the Juan Fault terminates a major contact orebody (Fig. 3). A thin unit of peridotitic ultramafic separates the sediment from the footwall basalt, and the whole sequence is now overturned. The intervening peridotitic ultramafic and the footwall basalt contain lenses, streaks and irregular patches of massive and disseminated Fe–Ni sulphides that reflect the complex kinematic history of the Juan

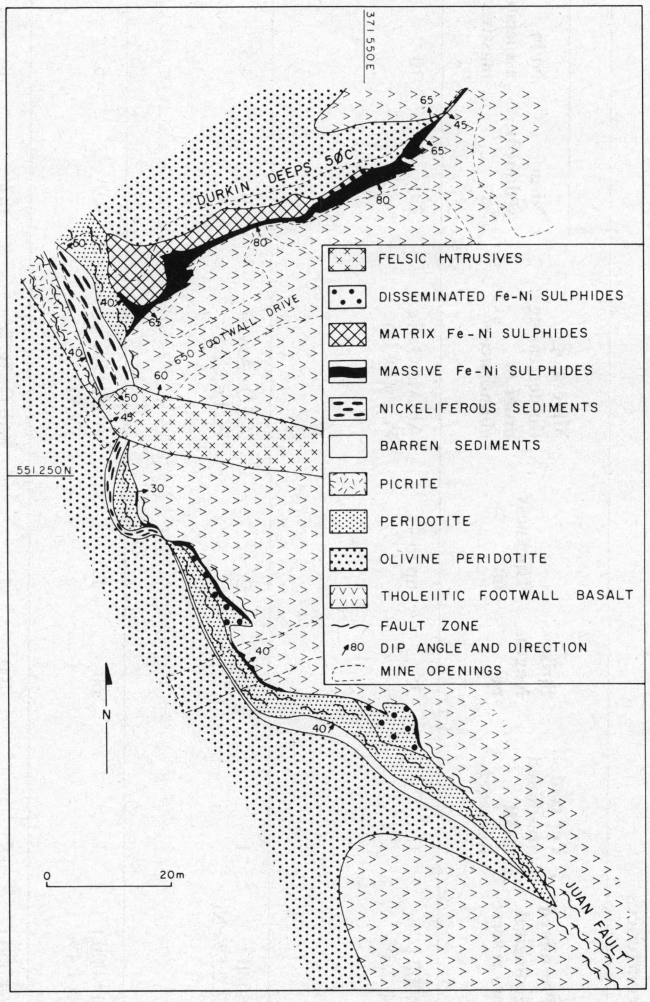

Fig. 3 Geological plan of part of 6 level, Juan shoot, showing relationship of nickeliferous sediments to normal contact ores

Fault. The sediment grades along strike from a barren, pale grey non-sulphidic variety to a strongly sulphidic black type (Fig. 2 *(B)* and *(C)*) that shows abundant folds on all scales of observation. A feature of this sediment is the presence of sulphide nodules of unknown origin. Grade distribution is consistent at around 2% Ni, but no massive sulphide lenses are present within the sediment. Both nickel grade and total sulphide content decrease along strike away from the fault-juxtaposed contact orebody (i.e. to the southeast).

On the 12 level (1216 area) a sediment on the footwall basalt contact contains lenses up to 1 m thick of massive Fe–Ni sulphides with 4–6% Ni. The sediment and its associated massive ore are overlain by a coarse-grained amphibole–chlorite rock, which, in turn, is overlain by sheared peridotite. The area is

strongly deformed, and in part of the 1216 area the sediment is repeated by faulting. The peridotitic ultramafics are strongly sheared parallel to the sediment. A fracture cleavage has developed in the sediment at about 70° to the layering, and pyrrhotite and chalcopyrite have been remobilized on to the cleavage surfaces. Nickel in the sulphidic sediments (Fig. 2 *(A)*) decreases away from the lenses of massive ore, and the erratic grade distribution (due largely to variations in total sulphide content) requires that mining above the 1% cutoff grade must be restricted to areas where there are massive sulphide lenses within the sedimentary section. The sediment-associated massive ore is of lower tenor than normal Juan ultramafic-hosted massive ore, which averages 10–12% Ni. The 1216 sediment has been exposed for about 100 m and, of this strike length, about 45 m includes massive sulphide. At the northern end of the exposure the massive sulphide occurs at the top of the sediment and is directly overlain by sheared peridotite in a more normal ultramafic association.

Ken shoot

Ken shoot consists of a group of contact orebodies that lie close to the crossfold axis on the west flank of the Kambalda Dome (Fig. 1). Gresham and Loftus-Hills[8] summarized the main features of the shoot in their Table 8. Ore is associated with sediments on both flanks of the main contact ore trough, but no sediments are present within the trough.

On the upper, east flank of the trough at the 4 level (404 area) two lenses of nickeliferous sediments and associated massive sulphides occur within the ultramafic sequence. These sediments converge up-dip and approach the footwall basalt, and at the 3 level the nickeliferous sediments lie on the basalt contact. Strong shearing of the footwall basalt and the ultramafic rocks adjacent to the sediments indicates that the latter have been displaced into their present hanging-wall position by faulting. Pyrite is the predominant sulphide in the sediments, but pentlandite and violarite are present in the more sulphidic varieties. Supergene alteration has obliterated many of the original chemical and mineralogical characteristics of this ore.

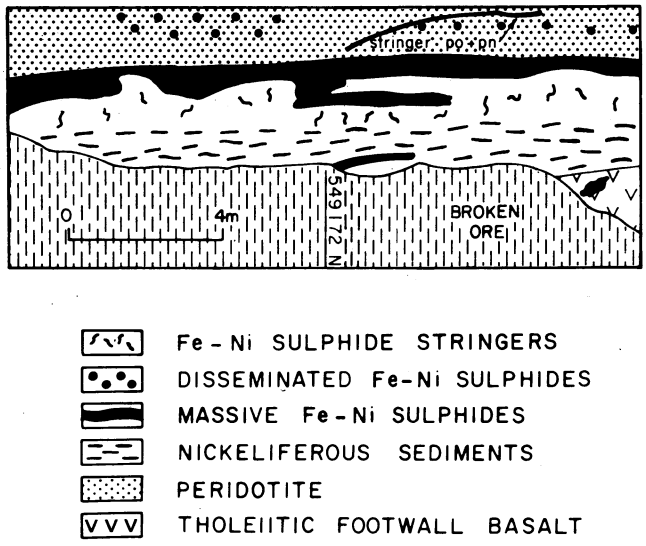

Fig. 4 Face sketch, Ken shoot 901 area, showing relationship between nickeliferous sediment and sediment-associated massive sulphides

On the 9 level (901 area) massive and matrix Fe–Ni sulphides overlie a contact nickeliferous sediment on the lower, west flank of the main contact ore trough (Fig. 4). The sediment lenses out up-dip near the lip of the ore trough. Repeated low-angle thrusting has formed several thin basalt wedges, which are separated by massive ore. Massive sulphides that overlie the sediments are highly deformed breccias with abundant silicate and carbonate inclusions. Fold noses, boudins and rolled rock fragments are recognizable, and the sulphides have been redistributed into irregular lenses in both the hanging-wall ultramafics and in the footwall basalt.

Lunnon shoot

Situated on the southeast flank of the Kambalda Dome (Fig. 1), Lunnon shoot is characterized by a gently plunging ribbon-like trough of contact ore bounded to the west by a steeply dipping normal fault and to the east by a series of stepped contacts produced by reverse faulting (see Table 8[8]). The uppermost of these steps is sediment-covered in part, and nickeliferous sediment has been mined in the 903 stope above the 9 level on this contact (Fig. 5*(A)*).

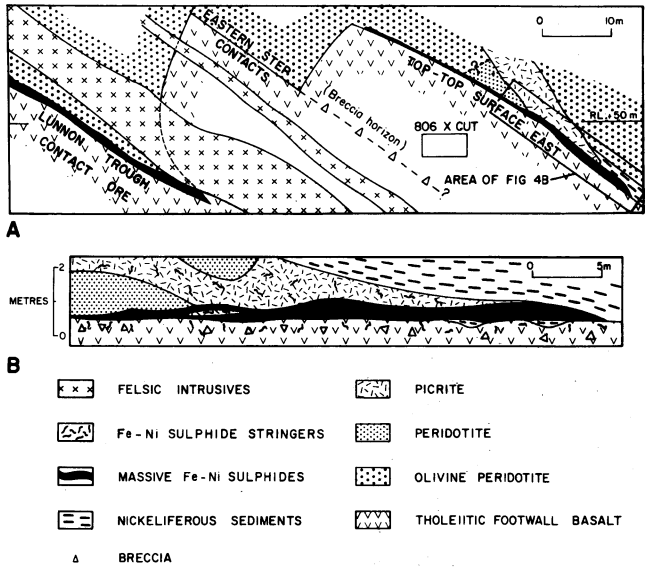

Fig. 5 Geological cross-sections, Lunnon shoot 903 area: *A*, relationship of sediment-associated ore to normal Lunnon Trough contact ore and *B*, detail of portion of Fig. 5*(A)*

In this area a thin, discontinuous sediment overlies the pillowed footwall basalt, possibly occupying shallow depressions in the basalt surface (Fig. 5 *(B)*). This sediment is overlain by a layer of massive sulphide up to 2 m thick that is of similar tenor to that of normal contact massive ore at Lunnon shoot. Sediment also overlies the massive ore, separated in places by a thin picritic ultramafic unit. To the east, where the massive sulphides lens out, the upper sediment lies directly on the footwall basalt contact and is 5–10 m thick.

The sediment beneath the massive sulphides has a higher sulphide content and is richer in nickel than the overlying sediment. Sediments in areas with no associated massive sulphides are barren (<0.1% Ni).

Jan shoot

Jan shoot is located in the St. Ives area 24 km SSE from Kambalda (Fig. 1). The Kambalda sequence of footwall basalt, extrusive ultramafic rocks and sediments is isoclinally folded with axial surfaces dipping steeply to the east (see Table 8[8]). Most ore at Jan occurs in the hanging-wall at the base of the second, third or fourth ultramafic flow unit. Sulphidic sediments also occur at these interflow positions and are nickeliferous where they are in contact with the oreshoots. The Jan shoot occurrences of nickeliferous sediment are of interest in that they exhibit by far the highest grades yet encountered at Kambalda for this ore type.

The major ore surface at Jan (Jan Main) occurs at the base of the third ultramafic flow unit. Sedimentary rocks associated with Jan Main are of two types: (1) albite-rich, locally carbona-

ceous sediments flank the margins of the oreshoot, though on some mine levels they are poorly developed or completely absent. Irregular pod-like bodies of albitic sediment also occur within the Jan Main orebody. (2) Soft, chloritic sediments generally less than 1 m thick form the northern margin of Jan Main between the 11 and 12 levels. They contain zones of orientated pyrrhotite-rich stringers that locally assay up to 2% Ni, but are sub-grade at minimum mining width (1.6 m).

Nickeliferous albitic sediments on the northern margin of Jan Main have been mined on the 7 and 9 levels. The Jan Main ore and the sediments overlie the spinifex-textured biotitic ultramafic flow top of the previous flow unit, and a thin layer of sheared ultramafic separates the sediment from the thick overlying olivine peridotite.

On the 9 level (902 area) the sediments (Fig. 6) are typically grey, banded rocks with alternating sulphide (pyrrhotite–pentlandite) and albite–dolomite layers (Fig. 2 *(D)*). The sediments lens out to the north and merge with the massive and matrix ore of Jan Main surface to the south. On the 9 level the sediment is nickeliferous for most of its 25-m strike length, but on the 7 level the nickel values drop to less than 0.3% a few metres distant from the Jan Main ore (though the sulphide content of the sediment remains high).

In addition to the thin layers of sulphide that are an integral part of these unusual sediments, the Jan 902 nickeliferous sediment also hosts lenses of massive sulphide up to 0.5 m thick close to the junction with Jan Main (Fig. 2 *(E)*). The junction is complex, both massive ore and sediment becoming brecciated (Fig. 2*(F)*), and nickeliferous sediments grading into massive sulphides as the relative proportion of sulphide increases over a distance of a few metres. At the junction the sediment becomes indistinguishable from the massive ore.

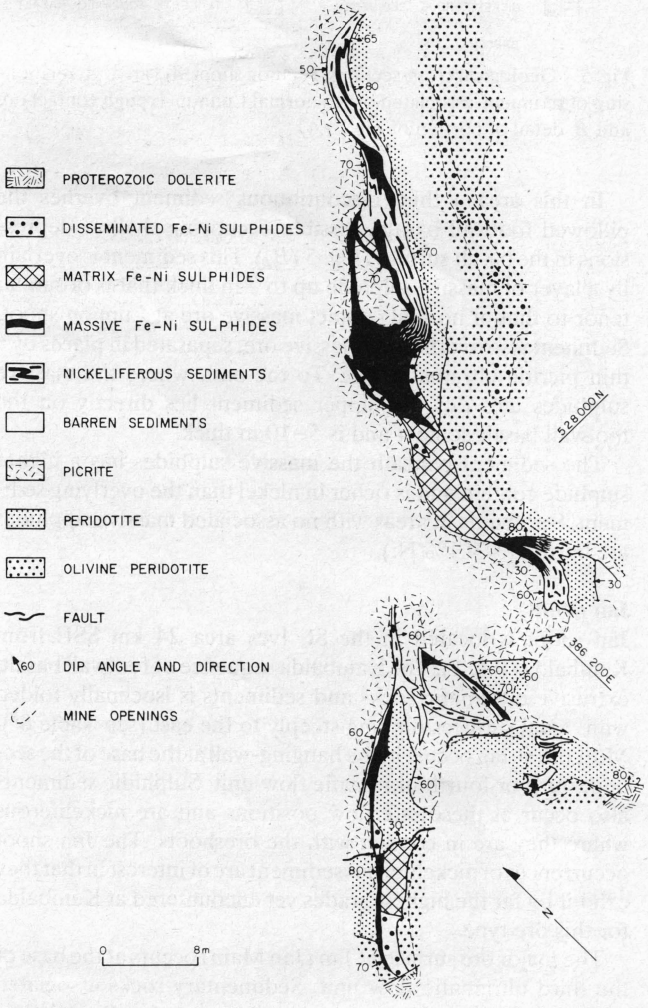

Fig. 6 Geological plan of 902/1 cut-and-fill stope, Jan shoot

Features of nickeliferous sediments and sediment-associated massive sulphides

General description

The nickeliferous sediments are superficially similar to normal, barren sediments (see description by Bavinton[1,2] and Bavinton and Keays[14]). They are quite variable in appearance, depending on the colour and composition of the non-sulphide fraction, and on the thickness and spacing of the sulphide layers.

A typical sample from Jan 902 is strongly layered, approxi-

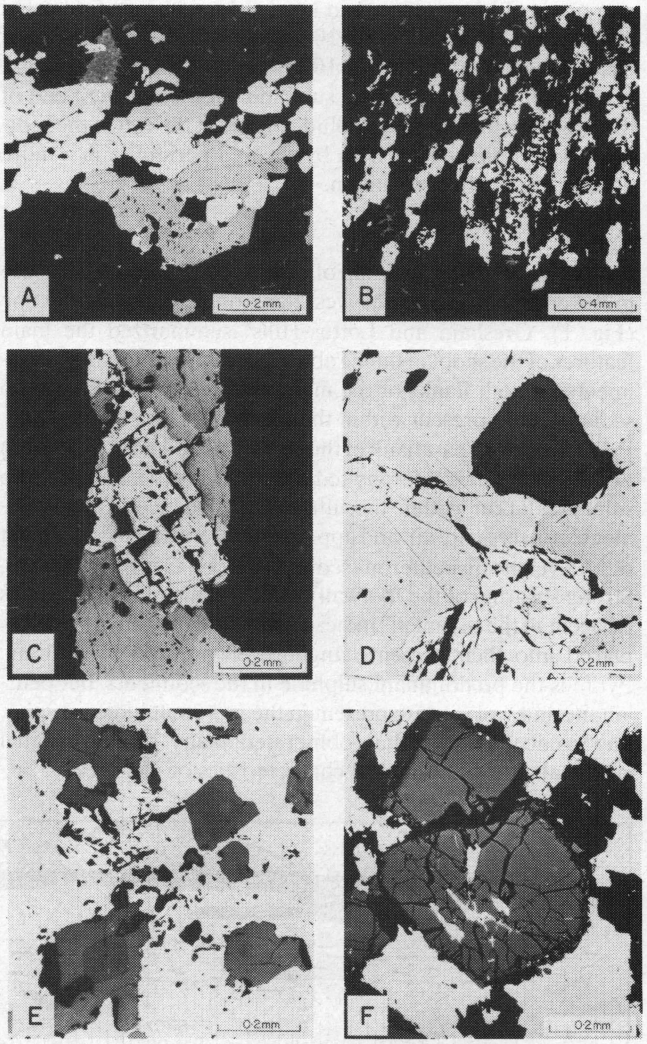

Fig. 7 Photomicrographs of nickeliferous sediments and associated massive sulphides. *A*, fine lamella of pyrrhotite (grey) and subhedral pyrite (white) in nickeliferous sediment (0.7% Ni) composed largely of albite, quartz, calcite and biotite. Pyrite is not common in the sediments, but in this case it forms a substantial part of a single layer in otherwise pyrrhotite-rich rock. Juan shoot 1216 area. *B*, strong cleavage developed at high angle to layering (horizontal) in single sulphidic layer of quartz-rich nickeliferous sediment (1.6% Ni) from Lunnon shoot. Pyrrhotite grey; pentlandite white with cleavage pits. *C*, coarse-grained pentlandite grain (light grey, with cleavage pits) in pyrrhotite; cross-cutting remobilized vein in nickeliferous sediment, Juan shoot 1216 area. Approximately constant pentlandite:pyrrhotite ratios (1:3) in sulphide lamellæ, massive sulphide lenses and remobilized veins suggest that single monosulphide solid solution existed formerly in all situations. *D*, euhedral ferrochromite (dark grey) in sediment-associated massive sulphides. Pyrrhotite grey and pentlandite white, with cleavage pits. Juan shoot 1216 area. *E*, zoned spinels in sediment-associated massive sulphides, Lunnon shoot 903 area. Dark core of spinels ferrochromite; rims magnetite. Pentlandite white; pyrrhotite light grey. Note fine exsolution lamellæ of pentlandite in pyrrhotite. *F*, fractured ferrochromites infilled with chalcopyrite; sediment-associated massive sulphides, Jan shoot 902 area. Severe fracturing of normally resistant ferrochromite testifies to intense local deformation of these ores

mately 30% sulphides (by volume) occurring as bands 0.5–2 mm thick spaced 2–5 mm apart (Fig. 2*(D)*). At hand specimen scale the sulphide layers are continuous (Fig. 2 *(A)* and *(D)*), but microscopically they are ragged, irregular and commonly discontinuous (Fig. 7*(A)* and *(B)*). Some sulphide layers are boudinaged and small-scale folds are present (Fig. 2*(B)* and *(D)*). Chalcopyrite may be concentrated near fold noses. The silicate layers vary from pale grey to black in colour, and alternations of these colours result in a layering within the silicate bands. Sulphides are commonly remobilized into crosscutting veinlets and stringers (Fig. 2*(C)*). Thicker layers (from 1 cm up to 0.5 m) of massive sulphides occur parallel to the overall banding, and these commonly contain folded and boudinaged remnants of albitic sediment (Fig. 2*(E)* and *(F)*).

Sediment-associated massive ores are similar in appearance to normal ultramafic-hosted ores, though they rarely show the prominent mineralogical banding that is seen in much of the Kambalda massive sulphide ore. The sediment-associated massive ores are commonly brecciated, especially close to the contact with the sediments, and alignment of silicate inclusions and fragments of sediment imparts a fabric that is not shown by the sulphides (Fig. 2 *(F)*).

Mineralogy

The mineralogy of the sediments is dominated by albite, with lesser proportions of carbonate, quartz, amphibole, talc, chlorite and biotite (Table 2). Grain size is generally fine, so the high albite content gives the silicate portion a cherty appearance. The black colour of some sediments is due to minor carbon.[2]

Lunnon shoot sediments differ from the others that are listed in Table 2 in their relatively high quartz and low albite content, and this reflects a regional spatial variation that was documented by Bavinton.[1,2] Sulphide layers consist of pyrrhotite, with minor pyrite, pentlandite (locally altered to violarite) and chalcopyrite (Fig. 7*(C)*). Similarly, the principal mineralogical difference between nickeliferous sediments and the barren sediments described by Bavinton[2] is the important presence of pentlandite in the former. In most other respects the two types are indistinguishable.

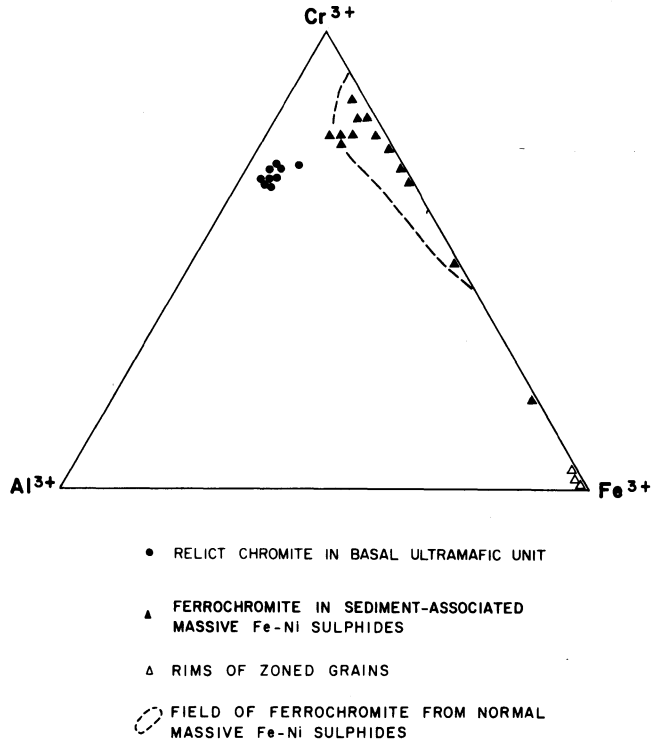

Fig. 8 Composition of spinels in ores and ultramafic rocks from Kambalda in terms of Cr^{3+}–Al^{3+}–Fe^{3+}. Field of ferrochromites from normal massive Fe–Ni sulphides from Groves *et al.*[29]

The massive sulphides are pyrrhotite-rich, pentlandite occurring as coarse-grained aggregates and as fine exsolution lamellæ in pyrrhotite. Chalcopyrite occurs in symplectite-like intergrowths with pyrite, and as concentrations in pressure shadows around silicate inclusions. Fine-grained gersdorffite/cobaltite occurs as a rare accessory. A feature of the massive sulphides is the occurrence of euhedral spinels (Fig. 7*(D)*, *(E)* and *(F)*). Analysis of these grains shows them to be ferro-

Table 2 Averaged XRD modal mineralogy of nickeliferous sediments and sediment-associated massive sulphides (wt %)*

	n	Pn	Po	Py	Vl	Cp	Tc	Ch	Bi	Am	Qz	Ab	Do	Ca
Juan 624														
Nickeliferous sediments	5	6	24	2	1	0	3	0	0	14	1	48	0	1
Juan 1216														
Nickeliferous sediments	18	3	25	0	0	0	1	1	6	9	6	44	1	3
Massive sulphides	8	18	76	0	3	1	tr	tr	1	0	0	1	0	0
Ken 901														
Nickeliferous sediments	7	3	9	0	0	0	1	2	16	0	15	45	1	8
Massive sulphides	10	15	47	7	9	0	5	5	8	0	0	0	0	0
Lunnon 903														
Ni sediments above mass. sulphides	10	6	17	0	0	0	0	15	17	0	31	7	0	7
Ni sediments below mass. sulphides	6	6	18	0	0	0	0	12	10	12	36	1	0	3
Massive sulphides	8	31	66	0	3	tr	1	0	0	0	0	0	0	0
Jan 902														
Ni sediments adjacent to mass. sulphides	3	8	24	1	1	0	7	0	0	0	3	52	3	0
Ni sediments distant from mass. sulphides	3	5	26	0	0	0	4	3	3	0	0	46	13	0
Averages														
Nickeliferous sediments	52	5	20	1	1	0	2	6	8	5	14	32	1	3
Massive sulphides	26	21	62	3	5	0	2	1	3	0	0	0	0	0
Barren sediments	243†	0	13	5	0	9	2	5	6	8	27	28	1	6

* n = number of samples; Pn = pentlandite; Po = pyrrhotite; Py = pyrite; Vl = violarite; Cp = chalcopyrite; Tc = talc; Ch = chlorite; Bi = biotite; Am = amphibole; Qz = quartz; Ab = albite: Do = dolomite; Ca = calcite.
Quantitative XRD mineralogy determined by method of Hooton and Giorgetta.[22]
† Average of 203 'grey, siliceous' sediments and 40 'black, carbonaceous' sediments from Bavinton.[2]

chromites, though the rims of zoned grains are commonly magnetite (Fig. 8). The ferrochromites in sediment-associated massive sulphides are similar in composition to those of spinels in normal massive sulphide ore, and are readily distinguishable (chemically) from the relict chromites that occur within the basal ultramafic unit (Fig. 8).

Chemistry

Analytical data for nickeliferous sediments and sediment-associated massive sulphides are summarized in Table 3. Compositional fields for barren and nickeliferous sediments, sediment-associated massive ores and normal ultramafic-hosted massive ores are summarized in Ni+Co–Cu–Zn and S–Fe–Ni+Co plots (Fig. 9). It is clear from both plots that the nickeliferous sediments occupy a position intermediate between barren sediments and massive ores. Individual samples of nickeliferous sediment show considerable disparity in chemistry—mainly because of variations in total sulphide content. The high nickel content of the Jan shoot samples (Table 3), however, readily distinguishes this area from the other occurrences that were studied. The Cu content, though variable, is generally higher in the nickeliferous sediments than in normal ores, Ni/Cu usually being less than the Kambalda average of about 15. Similarly, Zn content is higher in the nickeliferous sediments than in normal ores, but is similar to levels in the barren sediments. Samples from the Juan 1216 area are relatively enriched in Ag, but the reason for this is not clear.

Nickeliferous sediments at Juan and Jan shoots are Na-rich and K-poor, whereas those at Ken shoot are rich in both Na and K (Table 4). Lunnon shoot sediments, which are quartz-rich, are low in Na content but contain moderate K levels. This chemistry clearly reflects the albite and biotite contents of the sediments. Thallium contents are low, but relatively higher in the Lunnon and Ken shoot sediments where Tl correlates with K. This probably results from Tl substitution for K in biotite.

Palladium and Au contents of the sulphide fraction of the nickeliferous sediments are high relative to normal Kambalda massive ores, though the Ir contents are very low (Fig. 10), which results in extremely high Pd/Ir ratios. The S/Se ratios of the nickeliferous sediments are broadly similar to, though marginally lower than, those in massive sulphides and barren sediments (Fig. 11).

Relative to normal Kambalda massive ores, the sediment-associated massive ores are characterized by higher S/Ni ratios (reflecting the higher pyrrhotite/pentlandite ratio, Table 3). Copper and Zn proportions are higher than in normal massive ores (Fig. 9). Iridium and Au contents are similar to those for normal massive ores (Fig. 10), but Pd levels are significantly higher. The S/Se ratios are lower (Fig. 11).

Table 3 Averaged geochemical data for nickeliferous sediments and sediment-associated massive sulphides

	n	Ni,%	Cu,ppm	Co,ppm	Cr,ppm	Ag,ppm	Fe,%	Zn,ppm	As,ppm	S,%	S/Ni	Ni/Cu
Nickeliferous sediments												
Juan 624	8	1.82	1890	205	525	4	15.6	3620	4	10.7	4.9	11.2
Juan 1216	22	1.03	1550	380	130	8	12.4	1680	2	8.1	8.2	9.3
Ken 404	6	1.27	1670	225	120	3	20.9	590	9	13.0	12	9.4
Ken 901	7	0.74	1070	190	105	3	6.4	170	15	3.9	6.5	8.0
Lunnon 903—above mass. sulphides	10	0.98	1080	325	115	4	9.0	1640	5	4.7	4.8	9.1
Lunnon 903—below mass. sulphides	7	1.60	3480	530	245	3	16.8	350	2	8.8	4.3	4.6
Jan 702	1	1.18	2220	220	100	2	13.3	2930	2	10.6	9.1	5.3
Jan 902—adjacent to mass. sulphides	8	4.43	5320	690	1170	4	22.2	700	61	15.6	3.5	19
Jan 902—distant from mass. sulphides	5	2.27	2170	270	175	4	17.9	190	2	11.7	5.0	11.5
Average	74	1.67	2100	360	290	5	14.6	1340	15	9.1	6.4	11
Sediment-associated massive sulphides												
Juan 1216	9	4.56	3000	2315	340	22	46.2	345	3	31.6	7.4	34
Ken 901	7	7.81	5230	2220	230	na	43.5	55	11	34.1	4.6	38
Lunnon 903	8	8.39	3650	1450	150	5	49.7	100	5	33.2	4.0	32
Jan 702	1	11.40	720	1610	400	4	41.1	20	6	33.2	2.9	158
Jan 902	6	12.06	4650	1720	360	5	44.7	100	21	32.8	2.7	24
Average	31	7.95	4530	1930	365	12	45.6	160	9	32.9	4.9	41
Data for comparison												
Typical Kambalda massive sulphides	12		8000	2000	400	5	44	40	8	37	2.5	15
Barren sediments (Bavinton[2])	186	0.04	498	114	156		9.6	1485		6.7	170	0.7

Analysis by atomic absorption spectrometry (AAS) following HF digestion, except S (Leco furnace) and As (AAS following hydride generation).

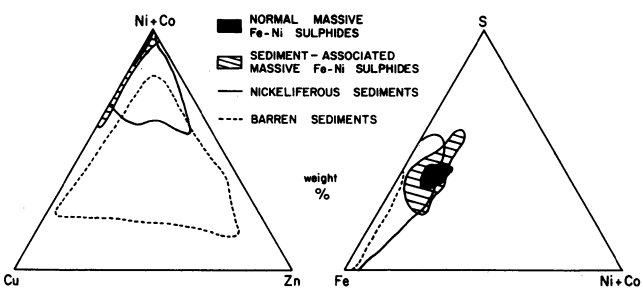

Fig. 9 Composition of sediments and massive Fe–Ni sulphides from Kambalda in terms of Ni+Co–Cu–Zn and S–Fe–Ni+Co

Discussion

Origin of barren interflow sediments at Kambalda

Bavinton[1,2] considered the barren sediments to comprise an exhalative component, local mafic and ultramafic detritus, and felsic detritus from some unspecified distant source. Sulphur isotope data[16] and S/Se ratios[21] indicate a magmatic source for the sulphur in the sediments, and an exhalative origin for the barren sulphides is suggested on the basis of high Pd/Ir ratios.[14,26] Recent unpublished work at Kambalda has demonstrated that komatiitic magmas may fractionate to produce an end product with 2–4% Na_2O. Although this sodic fraction may exhale with other volatile components to contribute to albitic sediment formation, Groves and co-workers[21] considered the sediments to be related more to exhalations associated with waning basaltic volcanism—a view consistent with

Table 4 Na_2O, K_2O and Tl contents of selected nickeliferous sediments and associated massive and remobilized ores

Sample number	Shoot and area	Na_2O,%	K_2O,%	Tl,ppb
Nickeliferous sediments				
Z9770	Juan 1216	3.11	1.00	1360
Z9777		n.a.	n.a.	326
Z9795		6.55	0.16	336
Z9796		4.75	0.11	450
Z15303	Juan 624	2.62	0.02	279
Z15306*		2.75	0.20	649
Z17101	Ken 901	1.13	2.11	1500
Z17103		5.52	2.76	1170
Z17105		7.56	1.53	1260
Z17111		8.30	1.32	1290
Z9638	Lunnon (upper)	0.36	2.71	1090
Z9640		0.43	2.37	1080
Z9635	Lunnon (lower)	0.26	1.57	1730
Z17130*	Jan 902 (adjacent)	6.97	0.09	161
Z17148*		3.88	0.04	139
Z17121	Jan 902 (distant)	5.83	0.17	425
Z17123		4.91	0.33	555
Sediment-associated massive sulphides				
Z9767	Juan 1216			649
Z9778				101
Z9791				359
Z9794				154
Z17099	Ken 901			97
Z17104				201
Z17108				231
Z17112				259
Z9633	Lunnon 903			35
Z9641				18
Z9646				52
Z17134	Jan 902			968
Z17138				152

n.a. = not analysed. Na_2O, K_2O by AAS, Tl by NAA (see Table 5).
*Minor 'carbon' residue after acid digestion.

the local occurrence of albitic sediments within the footwall basalts.[8] Bavinton[2] has attributed the enrichment in sulphur of Kambalda sediments relative to other Western Australian Archaean sediments to a combination of exhalative and sea-floor leaching processes.

For the purpose of this discussion we interpret the generally albite-rich, finely laminated sulphidic sediments as predominantly of volcanic exhalative origin, directly related to komatiitic and/or basaltic volcanism, but with some detrital component.

Relationship between nickeliferous and barren sediments

The nickeliferous sediments are mineralogically and chemically similar to barren interflow sediments, except for the important presence of pentlandite in the former. The geochemical differences between the two sediment types largely reflect the presence of Ni and its associated elements (Cu, Co, Cr, Pd). Zn, Ag, Au and Ir contents are similar in both rock types, as are S/Se ratios. In the northern part of the Kambalda Dome and at Jan shoot barren and nickeliferous sediments are predominantly composed of albite and pyrrhotite, but at Lunnon shoot both sediment types are quartz- and pyrrhotite-rich (cf. Bavinton[1]).

Barren sediments are known to occur throughout most of the Kambalda region and they usually display an antipathetic relationship with magmatic nickel sulphide orebodies. Nickeliferous sediments are known only where sulphidic sediments

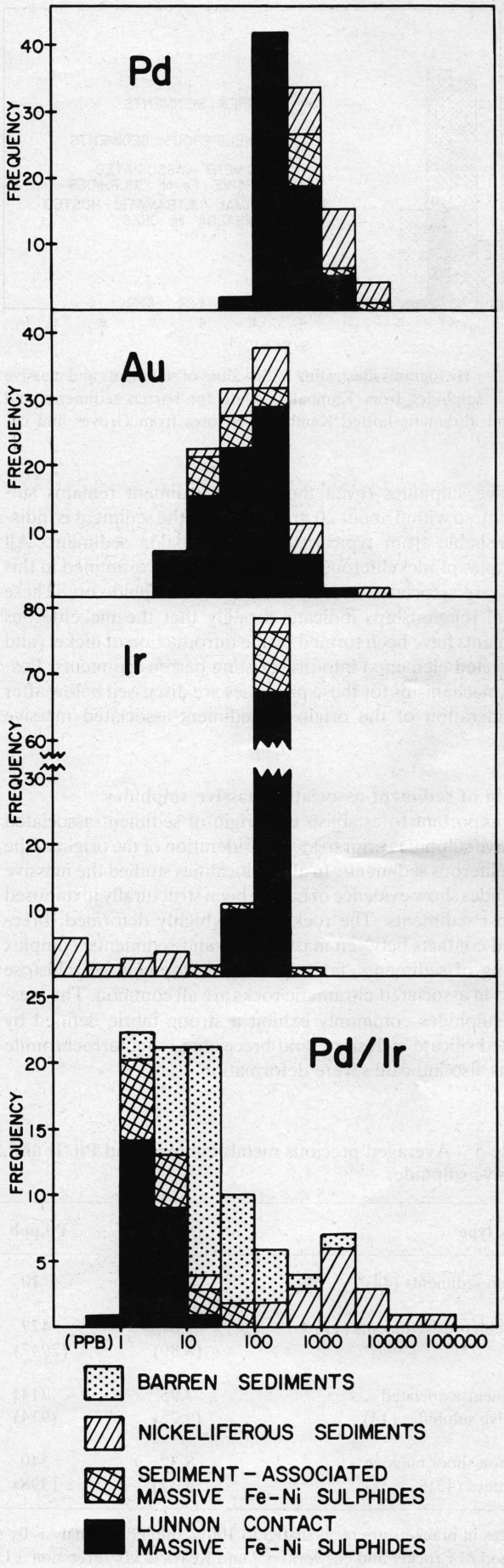

Fig. 10 Histograms illustrating contents of Pd, Au and Ir in sediments and massive Fe–Ni sulphides from Kambalda

have been juxtaposed against massive sulphides. The nickel grade of the sediments is seen to diminish rapidly away from the

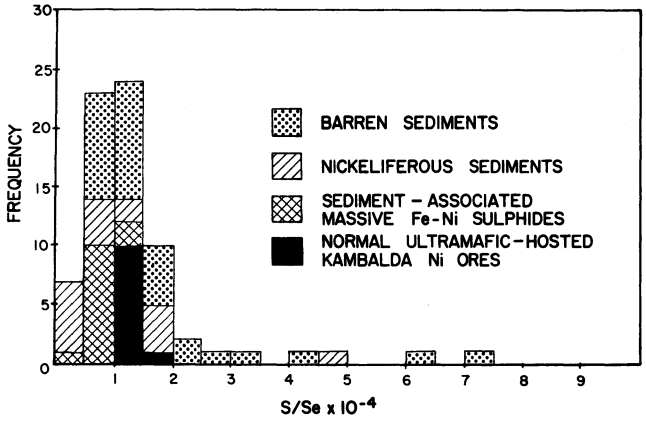

Fig. 11 Histograms illustrating S/Se values of sediments and massive Fe–Ni sulphides from Kambalda. Data for barren sediments and normal ultramafic-hosted Kambalda Ni ores from Groves and co-workers[21]

massive sulphides (even though the sediment remains sulphidic), so within about 20 m along strike the sediment is indistinguishable from typical, barren Kambalda sediment. All examples of nickeliferous sediment that were examined in this study are associated with normal massive sulphide ore. These spatial relationships indicate strongly that the nickeliferous sediments have been formed by the introduction of nickel (and associated elements) into pre-existing barren sediments. Possible mechanisms for these processes are discussed below after consideration of the origin of sediment-associated massive ores.

Origin of sediment-associated massive sulphides

It is important to establish the origin of sediment-associated massive sulphides prior to any consideration of the origin of the nickeliferous sediments. In all the localities studied the massive sulphides show evidence of having been structurally juxtaposed against sediments. The rocks are all highly deformed: brecciated contacts between massive ores and sediments, complex folding of sediments, faulting and development of schistose zones in associated ultramafic rocks are all common. The massive sulphides commonly exhibit a strong fabric defined by aligned silicate inclusions, and brecciated relict ferrochromite grains also indicate severe deformation.

Despite their unusual association within or adjacent to sediments, and their complex deformational history, the sediment-associated massive sulphides are mineralogically and geochemically similar to normal ultramafic-associated massive sulphides. They are composed predominantly of pyrrhotite and pentlandite with minor pyrite and chalcopyrite. Importantly, ferrochromites of distinctive composition (Fig. 8) are common and locally abundant. Although sulphide textures and compositions represent re-equilibration to below 300°C (cf. Groves *et al.*[27]), ferrochromites of this composition are thought to have formed either by crystallization directly from an oxysulphide melt (e.g. Ewers *et al.*[28] and Groves *et al.*[29]) or by metamorphism of igneous Al-rich chromite (cf. Evans and Frost[30]). Their presence in the sediment-associated massive sulphides is therefore regarded as strong evidence for a magmatic origin.

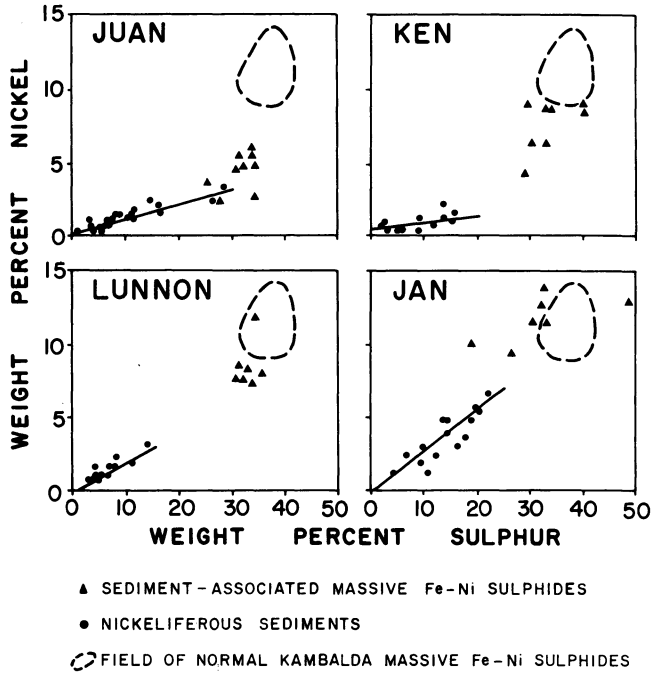

Fig. 12 Ni–S plots of nickeliferous sediments and sediment-associated massive Fe–Ni sulphides from Juan, Ken, Lunnon and Jan shoots

Table 5 Averaged precious metals contents and Pd/Ir and S/Se ratios for barren and nickeliferous sediments and associated massive sulphides

Rock type	Ni,%	Pd,ppb	Ir,ppb	Au,ppb	Pd/Ir	S/Se
Barren sediments (44)*	0.06	10	0.3	146	33	16 800†
Nickeliferous sediments (17)	1.67 (8.89)	427 (2947)	1.2** (9.1)	136 (458)	6730	11 200
Sediment-associated massive sulphides (14)	7.95 (9.25)	714‡ (914)	169 (201)	56 (69)	16	7 435
Lunnon shoot massive sulphides (43)§	8.32 (9.37)	340 (398)	167 (191)	62 (73)	2	12 900†

Figures in brackets are recalculated to 100% sulphides. Analysis by neutron activation analysis (NAA) at University of Melbourne after method of Crocket and co-workers[24] and Keays *et al.*[25] Precision ±15%.[23]

* From Bavinton and Keays.[14]

† Averages quoted by Bavinton;[2] derived from Groves and co-workers.[21]

‡ Excludes one high value (6910 ppb).

§ From Keays and co-workers[23] (average of Lunnon shoot data in their Table 1).

** Strongly influenced by one high value (13.6 ppb); most are <0.2 ppb.

The chemical composition of sediment-associated massive sulphides is similar in most respects to normal ultramafic-hosted massive ores, though Ni tenor is lower in some occurrences (Figs. 9 and 12) and As and Zn contents are significantly higher (Table 3). The Ir and Au contents of sediment-associated massive sulphides are similar to levels reported for normal ultramafic-associated massive sulphides from Lunnon shoot.[27] Palladium is erratically distributed in sediment-associated massive sulphides and although the average Pd value is higher than in Lunnon shoot ultramafic-hosted massive sulphides (Table 5), this is largely influenced by a few extreme values. Palladium contents in sediment-associated massive ore at Lunnon shoot are very similar to the data of Keays *et al.*[26] for normal contact ores (Fig. 13).

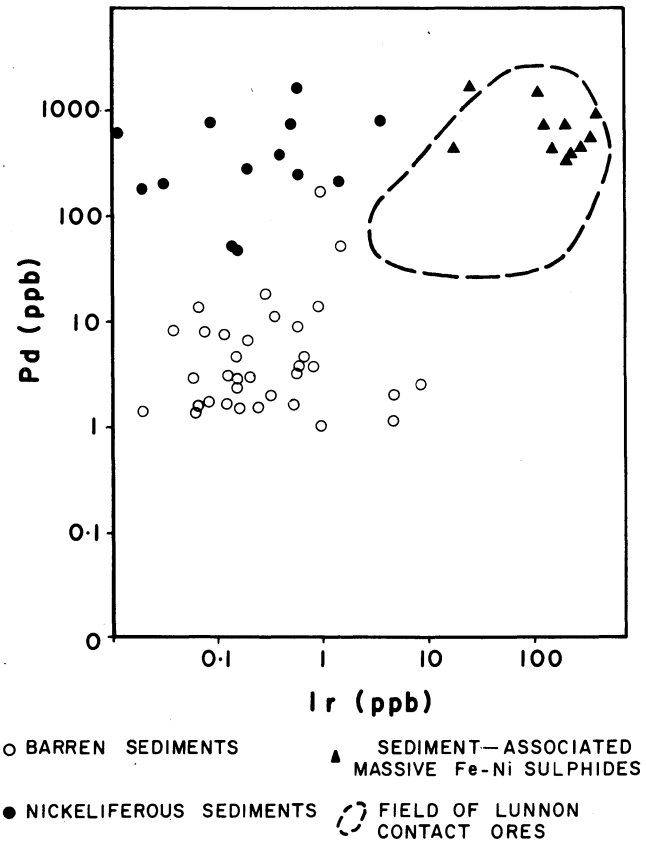

Fig. 13 Pd–Ir plot of sediments and massive Fe–Ni sulphides from Kambalda. Field of Lunnon contact ores from Keays and co-workers[23]

The normal, ultramafic-hosted massive Ni ores at Kambalda are considered by most workers to be of magmatic origin, based on field relationships, mineralogy (e.g. ferrochromite), chemical compositions (including precious metals), and S isotope and S/Se data.[8,21,23] The similarities between the sediment-associated massive sulphides and normal Kambalda massive sulphides are strongly indicative of a common magmatic origin. The partial assimilation of sediments that are commonly Fe sulphide-rich and contain high levels of Zn would result in the slightly lower Ni tenor and elevated Zn contents of some sediment-associated massive ore.

Origin of nickeliferous sediments

As has previously been indicated, the nickeliferous sediments are similar in most respects to barren sulphidic sediments at Kambalda. The vast majority of the sediments are barren, nickeliferous varieties being found only adjacent to lenses of massive Fe–Ni sulphides. The formation of nickeliferous sediments is therefore a local, specific process rather than a general process associated with all sediment formation. The close mineralogical and chemical similarities between barren and nickeliferous sediments suggest a common origin for both rock types, yet the spatial relationships of the latter group suggest strongly that they were formed by post-depositional addition of Ni (and some associated elements) to formerly barren sulphidic sediments. We have therefore considered five possible origins for the Ni in the nickeliferous sediments.

Magmatic

Addition of Ni at the magmatic stage is unlikely for several reasons. The nickeliferous sediments are finely banded rocks that contain sulphide laminæ that commonly range from less than 1 mm to several millimetres in thickness. The non-sulphide layers are unlikely to be truly magmatic (though they may be derived ultimately from a magmatic source) and it is difficult to conceive a mechanism of injecting magmatic sulphides to form fine laminæ that extend for tens of metres. The most compelling arguments against a direct magmatic origin for the Ni, however, are the extremely low Ir contents and very high Pd/Ir ratios (Fig. 10). The sediments are enriched in Pd in comparison with most normal massive ores, but generally contain less than 10 ppb Ir, even when recalculated to 100% sulphides (Fig. 10). Normal magmatic ores have Pd/Ir ratios less than 10, whereas in nickeliferous sediments this ratio averages more than 1000. Keays and co-workers[23] demonstrated limited fractionation of Pd and Ir between the various sulphide minerals in Kambalda ores, and magmatic fractionation of these elements has been postulated[31,32] (see also Naldrett *et al.*[33] and Naldrett[34]). Pyrite is enriched in Ir relative to pentlandite (Table 6[23]), but even complete separation of these phases by magmatic (or metamorphic) processes could not achieve the extreme Pd/Ir ratios observed in the nickeliferous sediments. The extreme depletion of Ir in the nickeliferous sediments is unknown in any magmatic ore environment (e.g. Table 2[34]), but, as is shown below, is characteristic of Ni sulphides in hydrothermal veins.[26]

Exhalative

The setting of interflow sediments being lateral equivalents of ore and becoming nickeliferous adjacent to major ore positions is broadly analogous to that of the tuffite horizons associated with exhalative massive sulphide deposits (e.g. Franklin and co-workers[35]). Similar ore–sediment relationships have been described by Stanton.[36] The cherty appearance of the Kambalda sediments is also consistent with this analogy.

Kambalda barren sediments, thought to be largely exhalative in origin, have higher Pd/Ir ratios than massive, magmatic Ni–Fe sulphides (Fig. 10); this is consistent with the known geochemical characteristics of Ir—in particular, its extreme insolubility (e.g. Bavinton and Keays[14]). (The limited data of Crocket and co-workers[37] suggest that modern exhalative sediments forming on the East Pacific Rise are also depleted in Ir relative to Pd and Au levels in the basic source rocks.) The even higher Pd/Ir ratio of nickeliferous sediments and their very low Ir contents (Fig. 10) are also consistent, therefore, with an exhalative origin.

The restriction of nickeliferous sediments to within about 20 m of normal magmatic massive ores, however, and the lack of any appreciable Ni halo around these occurrences are unlikely in an exhalative environment unless the massive ore is itself exhalative, and this possibility has been rejected in the foregoing discussion. Extensive geochemical haloes are characteristic of many volcanic exhalative ores, such as the Kuroko deposits in Japan[38] and the Rosebery deposit, Tasmania[39,40] (see also Thurlow and co-workers[41] and Franklin and co-workers[35]). No such zonation occurs in the Kambalda sediments[1,2] and elements typical of exhalative deposits (e.g. Ag, As, Tl) are not noticeably enriched in the nickeliferous sediments. Moreover, most exhalative deposits overlie interpreted source rocks, and they commonly have extensive alteration

pipes associated with them.[35] Although it is possible that the underlying ultramafic rocks and ores were the source of Ni for the hanging-wall nickeliferous sediments, it is important to note that many of the nickeliferous (and barren) sediments occur at the base of the ultramafic pile. Furthermore, the distinctive alteration pipes of exhalative deposits do not occur with either hanging-wall or contact nickeliferous sediments.

Remobilization

Remobilization or physical injection of sulphides into sediments during metamorphism and deformation has clearly been important at several scales of observation. For example, lenses of massive ore up to about 1 m × 4 m have been injected into sediments with highly brecciated contacts at Jan shoot (Fig. 6), and minor crosscutting veins of either pyrrhotite and pentlandite or chalcopyrite-rich sulphides (Fig. 2 *(B)* and *(C)*) are common. These lenses of remobilized massive ore have Pd/Ir ratios similar to those of the normal massive ore. Physical remobilization of massive sulphides is well documented throughout the Kambalda mines. Although this process has been locally important, it cannot be invoked to explain the delicate, millimetre-scale layering of Fe–Ni sulphides in the nickeliferous sediments (Fig. 2). The almost total absence of Ir and extreme Pd/Ir values of these fine sulphide layers also preclude an origin by simple remobilization of normal magmatic ore. The complete absence of ferrochromite or chromite within the nickeliferous sediments supports this contention.

Diffusion

Diffusion of elements in solid materials may occur by ionic substitution or grain boundary movements (e.g. Stanton[42]) and Ewers[43] demonstrated that Ni diffuses rapidly in pyrrhotite at elevated temperatures. This process is likely therefore to have been operative where massive Fe–Ni sulphides were in direct contact with Fe sulphide-rich layers in sediments, the sulphide layers acting as channelways for the diffusing elements. Relative diffusion rates for other elements are unknown, but they may be expected to be broadly similar to Ni. Palladium has been added to the sediments together with Ni, yet it is clear that Ir did not diffuse with other elements. One explanation for this is that Ir (and Os) is considerably more siderophile than Pd and Ni and would have been present as an Ir–Os alloy in the massive sulphide ores at the sulphur activity prevailing during metamorphism (see Fig. 11[23]). This suggests that Ir would remain immobile in the metallic state, whereas Ni and Pd would be free to diffuse as complex ions. Iridium (and Os) is characterized by its extreme insolubility in most fluids (possibly also attributable to its metallic state), and it is this property that contrasts it with the other platinum group elements. The lack of Ir enrichment in the nickeliferous sediments suggests strongly that some form of fluid transport was involved.

Hydrothermal

Hydrothermal transport has been suggested as the cause of extremely high Pd/Ir ratios (and very low Ir contents) in Ni-rich sulphide veins at Nullagine, Western Australia,[26] and similar extreme Pd/Ir values occur in interpreted hydrothermal Ni–Fe sulphide veins at Kambalda.[44] Hydrothermal alteration is also associated with gold-bearing veins (containing quartz, carbonate ± tellurides ± sulphides ± arsenides) in the Kambalda area. Although Ni is not normally regarded as a 'hydrothermal' element, it is clear that some Ni is mobilized by hydrothermal fluids. An occurrence of pentlandite rimming gold in a quartz–carbonate–gold vein adjacent to Hunt shoot Fe–Ni sulphides clearly demonstrates that Ni can be transported by hydrothermal solutions—in this case at temperatures between 350 and 450°C.[45] It is therefore probable that diffusion and/or hydrothermal transport have been responsible for redistribution of Ni from massive, magmatic Fe–Ni sulphides to formerly barren sulphidic sediments that have been tectonically juxtaposed.

These sulphidic sediments would also act as sinks for the large quantities of Pd lost from the contact ore zone sulphides during metamorphism. Ross and Keays[46] and Keays and coworkers[23] have demonstrated that possibly as much as one-half of the original Pd contents of the magmatic sulphide melts that formed the Ni orebodies was lost from these ore zones during deformation and metamorphism. Fig. 13 clearly shows that Pd, but not Ir, has been added to sediments that were already high in Pd/Ir in comparison with magmatic massive ores. Fig. 12 further shows that, with the possible exception of Ken shoot, which has suffered some supergene alteration, the composition of the sulphides in the sediments is related to the composition of adjacent massive ore: the S/Ni ratio of the nickeliferous sediments is approximately constant regardless of sulphide content, and is similar to, but marginally lower than, the S/Ni ratio of associated massive sulphides for each shoot. This is shown by the narrow spread of data points about the computed regression lines shown in Fig. 12 and the trend of these lines towards the fields of the associated massive ores.* For example, the slope of the computed regression lines ($r > 0.9$ for all except Ken shoot data) varies for each shoot, as does the S/Ni of associated massive sulphides. This implies a uniform composition of the sulphide fraction of massive ores and sediments in each shoot, which is substantiated by the calculated Ni contents in 100% sulphides presented in Table 5. A uniform composition in terms of Fe, Ni and S would be expected if equilibrium were attained between barren sediments and adjacent massive Fe–Ni sulphides during metamorphism, as a monosulphide solid solution (mss) of fixed Fe:Ni ratio (depending on bulk composition of system) would be the stable phase.[47,48] Barrett *et al.*[49] have shown that the massive pyrrhotite–pentlandite ± pyrite ores would have largely reverted to an mss (± pyrite) during amphibolite-facies metamorphism, and the relationships shown in Fig. 12 indicate that such equilibrium was attained, at least over limited distances. At Jan shoot sediments distant from massive ore have higher S/Ni values than those adjacent to it and plot below the regression line of Fig. 12. In all situations investigated in this study nickeliferous sediments grade into barren sediments about 20 m away from massive ores. The equilibration between barren sulphidic sediments and magmatic Ni ores was apparently achieved by two-way transfer of component elements. Assimilation of barren sulphidic sediments by massive ore lenses (as evidenced by trails and inclusions of sediment within the latter) resulted in elevated Zn contents and S/Ni ratios of the sediment-associated massive sulphides, and Ni and associated elements were introduced into the sediments. Relative abundances of sediments (pyrrhotite-rich) and massive ores controlled final Fe:Ni (and therefore S/Ni) ratios. At Jan shoot massive Ni ores were apparently more abundant than associated sediments, so Ni tenor was not significantly influenced by Fe dilution, whereas at Juan the reverse applied. The fact that Ir was not added to the sediments with the other elements (Ni, Cu, Pd, etc.) suggests that hydrothermal transport was the predominant mechanism to have been involved.

Although there is no obvious Ni depletion halo in massive sulphides adjacent to nickeliferous sediments, previous studies of massive Fe–Ni sulphides at Kambalda have indicated that they are strongly depleted in Pd and Au (and to a lesser extent Cu) relative to their associated matrix sulphides, whereas Ir is

*These regression lines are computed for samples with more than 0.3% Ni. In detail, such plots would tail off at low Ni values to a point approximating the Ni and S levels in barren sediments (0.04% Ni, 6.7% S quoted by Bavinton[1]).

undepleted.[23,46] The limited data that are available[23,44] indicate enrichment of Cu, Pd, and Au in footwall stringers, relative to adjacent contact ores, whereas there is no associated enrichment in Ir. The similar element distribution patterns in the sulphide stringers and nickeliferous sediments indicate that hydrothermal mobilization of many ore elements was common in the Kambalda environment.

Conclusions

Nickeliferous sediments are of minor importance as a source of Ni at Kambalda, but it is important to clarify their origin as, superficially, they are similar to some volcanic exhalative base-metal bearing sediments. This study has shown that the nickeliferous sediments at Kambalda are of very limited areal extent, and are always intimately associated with massive Fe–Ni sulphides that are clearly of magmatic origin. This close association, unusual for sediments and ores at Kambalda, has in most cases been brought about by structural juxtaposition during deformation and metamorphism of the rocks. All ore environments at Kambalda (including those with sediment-associated ore) show evidence of considerable structural complexity.

The geochemistry of the nickeliferous sediments—in particular, their Pd and Ir contents—precludes a direct magmatic origin: clearly, they have not been formed by magmatic sulphide melts penetrating the sediments, or by late physical remobilization of sulphides either as pyrrhotite and pentlandite or as monosulphide solid solution. Although the laterally extensive barren interflow sediments are probably largely of exhalative origin, the restriction of nickeliferous sediment occurrences to the immediate environs of tectonically juxtaposed massive magmatic sulphides argues against an exhalative origin for the nickel in these unusual sediments.

We favour an origin by local redistribution of most ore elements from normal magmatic Fe–Ni sulphide ores through a combination of hydrothermal transport and solid-state diffusion during amphibolite-facies metamorphism. Tectonic juxtaposition of massive Ni-rich sulphides with barren Fe sulphide bearing sediments has resulted in an interchange of elements across a zone of high chemical potential. Such local redistribution of ore components represents just part of a wide spectrum of remobilization features associated with the Kambalda nickel deposits.

Acknowledgement

Numerous geologists have been involved with this study since its inception in 1980—in particular, C. N. Middleton, W. E. Bannister, E. N. Sharpe and D. S. Clarke. Additional mapping and data from new exposures at Juan were provided by K. Johnson and A. Cowden. We are indebted to R. E. Perkin, R. Gregory and S. Jones for drafting the figures, to L. Mitchell, who supervised the XRD work and assisted with manipulation of analytical data, and to C. Furstner, who prepared the photographic plates. We have also benefited from discussions with D. R. Hudson. This study was supported in part by Australian Institute of Nuclear Science and Engineering and Australian Research Grants Scheme grants to RRK. We are indebted to Miss S. Dalglish for technical assistance and to Ms. S. Nation who patiently typed and edited the manuscript. The permission of Western Mining Corporation, Ltd., to publish this paper is gratefully acknowledged.

References

1. Bavinton O. A. Interflow sedimentary rocks from the Kambalda ultramafic sequence: their geochemistry, metamorphism and genesis. Ph.D. thesis, Australian National University, Canberra, 1979, 196 p.
2. Bavinton O. A. The nature of sulfidic metasediments at Kambalda and their broad relationships with associated ultramafic rocks and nickel ores. *Econ. Geol.*, **76**, 1981, 1606–28.
3. Marston R. J. *et al.* Nickel sulfide deposits in Western Australia: a review. *Econ. Geol.*, **76**, 1981, 1330–63.
4. Hutchinson R. Contributed discussion. In *Seminar on sea-floor hydrothermal systems* Goldie R. and Bottrill T. J. *Geosci. Canada*, **8**, 1981, 93–104.
5. Lusk J. A possible volcanic-exhalative origin for lenticular nickel sulfide deposits of volcanic association, with special reference to those in Western Australia. *Can. J. Earth Sci.*, **13**, 1976, 451–8.
6. Lusk J. A possible volcanic-exhalative origin for lenticular nickel sulfide deposits of volcanic association, with special reference to those in Western Australia: reply. *Can. J. Earth Sci.*, **13**, 1976, 1651–3.
7. Groves D. I. *et al.* A possible volcanic-exhalative origin for lenticular nickel sulfide deposits of volcanic association with special reference to those in Western Australia: a discussion. *Can. J. Earth Sci.*, **13**, 1976, 1646–50.
8. Gresham J. J. and Loftus-Hills G. D. The geology of the Kambalda nickel field, Western Australia. *Econ. Geol.*, **76**, 1981, 1373–416.
9. Hudson D. R. Sediment–ore relationships at Lunnon shoot. Unpublished preliminary report, C.S.I.R.O., 1972, 28 p.
10. Hudson D. R. Evaluation of genetic models for Australian sulphide nickel deposits. In *Australasian Institute of Mining and Metallurgy Annual Conference, Newcastle 1972* (Parkville: Australasian IMM, 1972), 59–68.
11. Ross J. R. Archaean nickel sulfide mineralization, Lunnon shoot, Kambalda, Western Australia. Ph.D. thesis, University of California, Berkeley, 1974, 283 p.
12. Ross J. R. and Hopkins G. M. F. Kambalda nickel sulphide deposits. In *Economic geology of Australia and Papua New-Guinea, I: Metals* Knight C. L. ed. (Parkville, Victoria: Australasian Institute of Mining and Metallurgy, 1975), 100–21. *(Monograph Series* no. 5)
13. Schwann P. B. An introductory study of the Kambalda sediments. Undergraduate dissertation, Western Australia Institute of Technology, 1975, 36 p.
14. Bavinton O. A. and Keays R. R. Precious metal values from interflow sedimentary rocks from the komatiite sequence at Kambalda, Western Australia. *Geochim. cosmochim. Acta*, **42**, 1978, 1151–63.
15. Bavinton O. A. and Taylor S. R. Rare earth element geochemistry of Archaean metasedimentary rocks from Kambalda, Western Australia. *Geochim. cosmochim. Acta*, **44**, 1980, 639–48.
16. Donnelly T. H. A reconnaissance study of stable isotope ratios in Archaean rocks from the Yilgarn Block, Western Australia. *J. geol. Soc. Australia*, **24**, 1978, 409–20.
17. Hopwood T. The significance of pyritic black shales in the genesis of Archaean massive nickel sulphide deposits. In *Handbook of stratabound and stratiform ore deposits, volume 9: regional studies and specific deposits* Wolf K. H. ed. (Amsterdam: Elsevier, 1981), 411–67.
18. Chapman D. G. and Groves D. I. A preliminary study of the distribution of gold in Archaean interflow sulphidic metasediments, Yilgarn Block, Western Australia. In *Gold mineralization* Glover J. E. and Groves D. I. eds. *Univ. West. Aust. Geol. Dep. Extension Service Publ.* 3, 1979, 76–88.
19. Chapman D. G. Gold distribution and content of sulphide-rich interflow metasediments in the Eastern Goldfields, Western Australia. M.Sc. thesis, University of Western Australia, 1981, 110 p.
20. Groves D. I. Barrett F. M. and McQueen K. G. Geochemistry and origin of cherty metasediments within ultramafic flow sequences and their relationship to nickel mineralization. In *Archaean cherty metasediments: their sedimentology, micropalaeontology, biogeochemistry, and significance to mineralization* Glover J. E. and Groves D. I. eds. *Univ. West. Aust. Geol. Dep. Extension Service Publ.* 2, 1978, 57–69.
21. Groves D. I. Barrett F. M. and McQueen K. G. The relative roles of magmatic segregation, volcanic exhalation and regional metamorphism, in the generation of volcanic-associated nickel ores of Western Australia. *Can. Mineralogist*, **17**, 1979, 319–36.
22. Hooton D. H. and Giorgetta N. E. Quantitative X-ray diffraction analysis by a direct calculation method. *X-ray Spectrometry*, **6**, 1977, 2–5.
23. Keays R. R. Ross J. R. and Woolrich P. Precious metals in volcanic peridotite-associated nickel sulfide deposits in Western Australia II: Distribution within the ores and host rocks at Kambalda. *Econ. Geol.*, **76**, 1981, 1645–74.
24. Crocket J. H. Keays R. R. and Hsieh S. Determination of some precious metals by neutron activation analysis. *J. radioanalyt. Chem.*, **1**, 1968, 487–507.

25. Keays R. R. *et al.* The simultaneous determination of 20 trace elements in terrestrial, lunar and meteoritic material by radiochemical neutron activation analysis. *Analyt. chim. Acta,* **72,** 1974, 1–29.
26. Keays R. R. *et al.* Iridium and palladium as discriminants of volcanic-exhalative, hydrothermal and magmatic nickel sulfide mineralization. *Econ. Geol.,* **77,** 1982, 1535–47.
27. Groves D. I. *et al.* Sphalerite compositions from Western Australian nickel deposits, a guide to equilibria below 300°C. *Econ. Geol.,* **70,** 1975, 391–6.
28. Ewers W. E. *et al.* Crystallization of chromite from nickel–iron sulphide melts. *Contr. Mineral. Petrol.,* **54,** 1976, 61–4.
29. Groves D. I. *et al.* Spinel phases associated with metamorphosed volcanic-type iron–nickel sulfide ores from Western Australia. *Econ. Geol.,* **72,** 1977, 1224–44.
30. Evans B. W. and Frost B. R. Chrome-spinel in progressive metamorphism—a preliminary analysis. *Geochim. cosmochim. Acta,* **39,** 1975, 959–72.
31. Chyi L. L. and Crocket J. H. Partition of platinum, palladium, iridium and gold among coexisting minerals from the deep ore zone, Strathcona mine, Sudbury, Ontario. *Econ. Geol.,* **71,** 1976, 1196–205.
32. Keays R. R. and Crocket J. H. A study of precious metals in the Sudbury nickel irruptive ores. *Econ. Geol.,* **65,** 1970, 438–50.
33. Naldrett A. J. *et al.* The composition of Ni-sulfide ores, with particular reference to their content of PGE and Au. *Can. Mineralogist,* **17,** 1979, 403–16.
34. Naldrett A. J. Nickel sulfide deposits: classification, composition, and genesis. *Econ. Geol. 75th anniversary vol.,* 1981, 628–85.
35. Franklin J. M. Lydon J. W. and Sangster D. F. Volcanic-associated massive sulfide deposits. *Econ. Geol. 75th anniversary vol.,* 1981, 485–627.
36. Stanton R. L. Petrochemical studies of the ore environment at Broken Hill, New South Wales: 3—banded iron formations and sulphide orebodies: constitutional and genetic ties. *Trans. Instn. Min. Metall. (Sect. B: Appl. earth sci.),* **85,** 1976, B132–41.
37. Crocket J. H. MacDougall J.D. and Harriss R.C. Gold, palladium and iridium in marine sediments. *Geochim. cosmochim. Acta,* **37,** 1973, 2547–56.
38. Tono N. Minor element distribution around Kuroko deposits of northern Akita, Japan. In *Geology of Kuroko deposits* Ishihara S. *et al.* eds (Tokyo: The Society of Mining Geologists of Japan, 1974), 399–420. *(Min. Geol., Tokyo, Special Issue* no. 6)
39. Smith R. N. Trace element distributions within some major stratiform orebodies. B.Sc.(Hons) thesis, University of Melbourne, 1973, 132 p.
40. Smith R. N. Precious and volatile metal distributions in the ores and host rocks of the Rosebery sulphide deposit, Tasmania. M.Sc. thesis, University of Melbourne, 1975, 171 p.
41. Thurlow J. G. Swanson E. A. and Strong D. F. Geology and lithogeochemistry of the Buchans polymetallic sulfide deposits, Newfoundland. *Econ. Geol.,* **70,** 1975, 130–44.
42. Stanton R. L. *Ore petrology* (New York, etc.: McGraw-Hill, 1972), 713 p.
43. Ewers W. E. Nickel–iron exchange in pyrrhotite. *Proc. Australas. Inst. Min. Metall.* no. 241, 1972, 19–25.
44. Lesher C. M. and Keays R. R. Metamorphically and hydrothermally mobilized Fe–Ni–Cu sulphides at Kambalda, Western Australia. In *Sulphide deposits in mafic and ultramafic rocks* Buchanan D. L. and Jones M. J. eds (London: IMM, 1984), 62–9.
45. Phillips G. N. and Groves D. I. Fluid access and fluid-wallrock interaction in the genesis of the Archaean gold-quartz vein deposit at Hunt mine, Kambalda, Western Australia. In *Gold '82: the geology, geochemistry and genesis of gold deposits* Foster R. P. ed. (Rotterdam: Balkema, 1984), 389–416. (*Spec. Publ. geol. Soc. Zimbabwe* no. 1)
46. Ross J. R. and Keays R. R. Precious metals in volcanic-type nickel sulphide deposits in Western Australia, I: Relationship with the composition of the ores and their host rocks. *Can. Mineralogist,* **17,** 1979, 417–35.
47. Naldrett A. J. Craig J. R. and Kullerud G. The central portion of the Fe–Ni–S system and its bearing on pentlandite exsolution in iron–nickel sulfide ores. *Econ. Geol.,* **62,** 1967, 826–47.
48. Kullerud G. Yund R. A. and Moh G. H. Phase relations in the Cu–Fe–S, Cu–Ni–S, and Fe–Ni–S systems. In *Magmatic ore deposits* Wilson H. D. B. ed. *Econ. Geol. Monograph* 4, 1969, 323–43.
49. Barrett F. M. *et al.* Structural history and metamorphic modification of Archaean volcanic-type nickel deposits, Yilgarn Block, Western Australia. *Econ. Geol.,* **72,** 1977, 1195–223.

Windarra nickel deposits, Western Australia

M. L. Schmulian B.Sc., M.Sc.
Western Mining Corporation, Ltd., Windarra, Western Australia

Synopsis

The Windarra nickel deposits display many of the characteristics that typify Archaean volcanic peridotite-associated nickel sulphide ores of Western Australia. The Fe–Ni–Cu sulphide mineralization, which comprises dominantly disseminated sulphides, occurs at the base of a differentiated ultramafic volcanic pile grading upwards from massive meta-peridotitic flows to thin, locally spinifex-textured meta-picritic units. The entire mafic–ultramafic belt has been subjected to mid-amphibolite-facies metamorphism. The ore-bearing ultramafic is immediately underlain by dominantly sulphide-facies banded iron formation (BIF), which commonly contains nickel sulphides adjacent to its contact with mineralized ultramafic. BIF-hosted ores are formed both by physical remobilization of ultramafic-hosted sulphides and by migration of Ni and Cu into pre-existing iron sulphides.

At Mt. Windarra the mineralization comprises eight steeply dipping, steeply plunging elongate oreshoots, which display a marked parallelism with major and minor fold structures in the underlying BIF. Seven of the shoots occur at or close to the base of the ultramafic pile, and are hosted by at least three overlapping flows. The zone of overlap occurs at the northern end of each flow, where picritic ultramafic, representing a dominantly liquid portion of the flow, occupies the basal contact. A gross south–north ultramafic flow direction is inferred. The eighth shoot occurs in a stratigraphically higher position within the ultramafic sequence.

At South Windarra at least two overlapping mineralized flows occupy the basal contact, the ore zone having a strike extent three to four times its downdip extent. There is no obvious structural control to the mineralization.

The Mt. Windarra and South Windarra nickel deposits are located 260 km NNE of Kalgoorlie in the eastern portion of the Yilgarn Block (Fig. 1). The Mt. Windarra deposit was discovered by Poseidon N.L. in 1969 as a result of a surface prospecting programme,[8] and 14 km to the south at South Windarra (Fig. 2) a consortium that comprised Union Oil Development Corporation, Australian Hanna, Ltd., and Homestake Iron Ore Co. of Australia, Ltd., located economic sulphide mineralization beneath transported overburden in

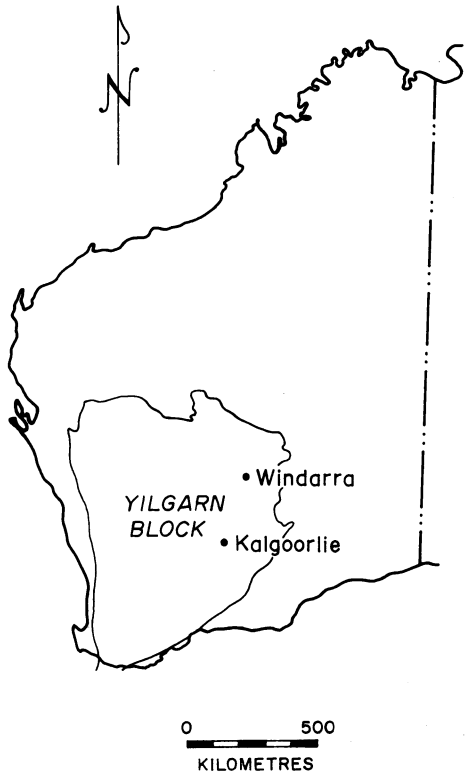

Fig. 1 Location plan

early 1971. The tenements that cover both deposits are now held by Western Mining Corporation, Ltd., which is currently mining only the Mt. Windarra deposit. The ore is concentrated on site, the concentrates being transported by road and rail to Western Mining Corporation's smelter near Kalgoorlie. The project is also mining and treating gold ore at Lancefield mine, 15 km southeast of Mt. Windarra (Fig. 2).

The discovery of the deposits has been summarized by Robinson and co-workers,[8] and a more complete account of their geological setting was given by Roberts.[7] Aspects of the structural and metamorphic history of the area have been covered by Barrett *et al.*[1] and Seccombe *et al.*[11] discussed the implications of sulphur isotope data on ore genesis. The object of the present contribution is to update previous descriptions of the Windarra deposits and to summarize current thoughts on the nature of the ore environment.

Regional geology

The Mt. Windarra and South Windarra nickel deposits occur close to the exposed base of a dominantly north–south-trending Archaean greenstone belt. The deposits lie on the steep eastern limb and the flatly south-plunging nose, respectively, of a regional structure termed the Mt. Margaret anticline (Fig. 2). The entire belt has been subjected to mid-amphibolite-facies metamorphism,[1,7] tholeiitic metabasalts being typified by blue-green hornblende–albite±almandine, and rare pelites by biotite–muscovite–staurolite–almandine. Throughout this contribution, however, the prefix 'meta-' has been omitted, and appropriate igneous and sedimentary terminology has been adopted.

The Fe–Ni–Cu sulphide mineralization occurs at the base of a thick sequence of mafic and ultramafic volcanics, in contact with a prominent underlying banded iron formation (BIF). At Mt. Windarra the ore is in contact with a thin (2–25 m) iron formation ('inter-BIF') separated from the main basal BIF by a barren peridotite 3–45 m thick ('corridor ultramafic').

The core of the Mt. Margaret anticline is occupied by a major intrusive granitoid pluton that has locally stoped out the main BIF. Mafic–ultramafic and BIF xenoliths thought to be stratigraphically equivalent to the Windarra sequence occur within the granitoid 8 km west of South Windarra at Woodline Well. In addition, a number of remnants of an apparently older mafic–ultramafic sequence occur as xenoliths within the granitoid, west of the main Windarra BIF. A granitoid pluton to the east of Mt. Windarra coalesces with the 'footwall' granitoid mass north of the mine area, resulting in a wedge-shaped termination of the

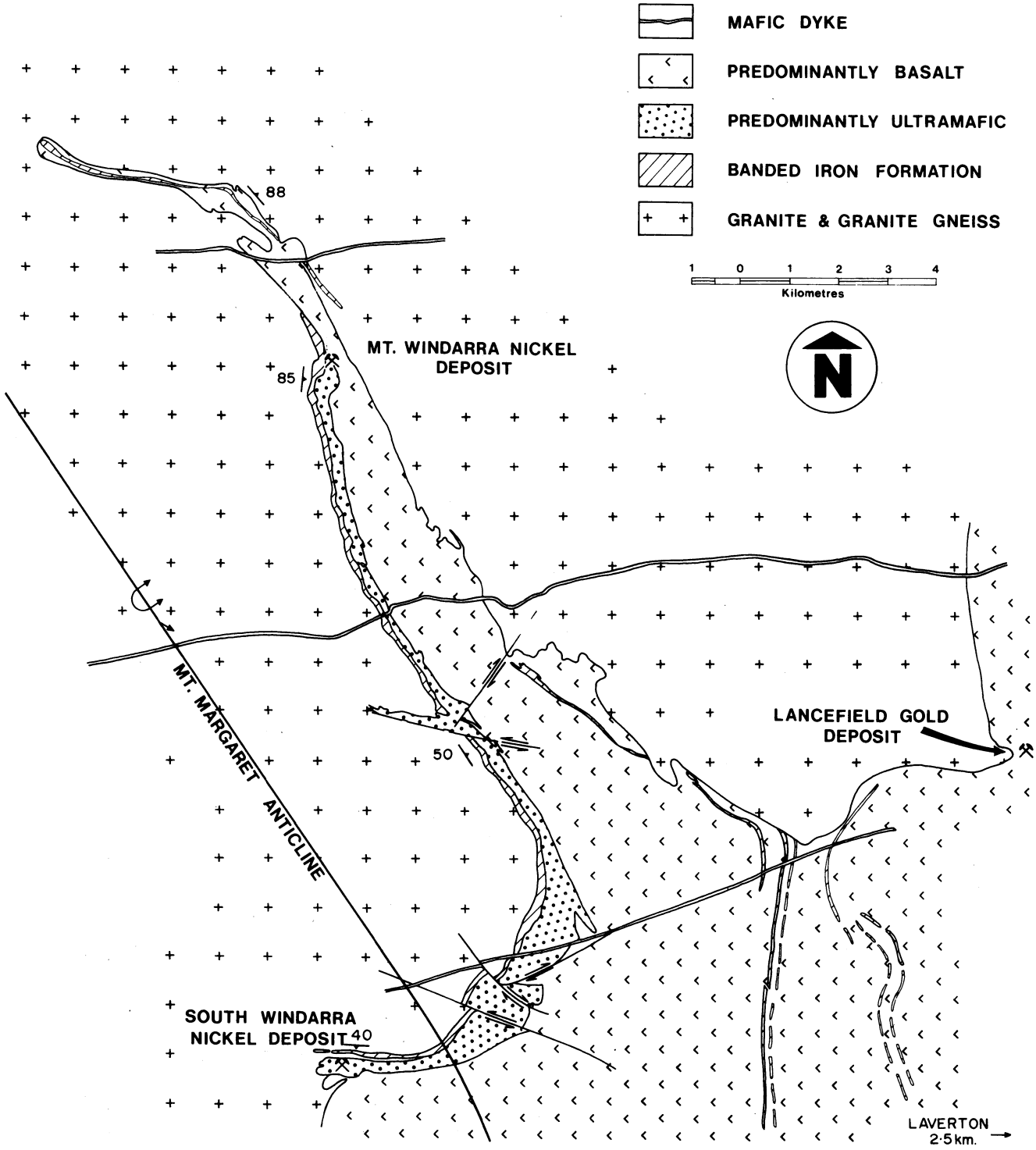

Fig. 2 Generalized geological plan of Windarra greenstone belt

Windarra belt north of Mt. Windarra. Further south the full thickness of the sequence is preserved and a series of major BIF units forms prominent marker horizons within the sequence. Much of the gold mineralization within the region is closely associated with these upper BIFs, but no gold mineralization has been located within or adjacent to the Windarra BIF.

Mt. Windarra

The Mt. Windarra orebody is located close to the northern extremity of the preserved portion of the east limb of the Mt. Margaret anticline at the base of a thick ultramafic pile. The orebody comprises eight distinct, steeply dipping oreshoots, generally separated by a series of steeply plunging dextral 'dragfolds'* (Fig. 3).

The orebody is exploited by an underground decline mine that uses trackless diesel equipment, and has been in production since mid-1974. Production was temporarily halted in mid-1978, full production being resumed during 1981. Ore milled to June, 1982, totalled 1 909 100 t with an average of 1.71% Ni. Diluted ore reserves at June, 1982, were estimated at 6 652 000 t at 1.60% Ni.

Stratigraphy

The stratigraphic sequence at Mt. Windarra is summarized in

*As used here 'dragfold' is a colloquial mine term rather than a strictly correct technical description.

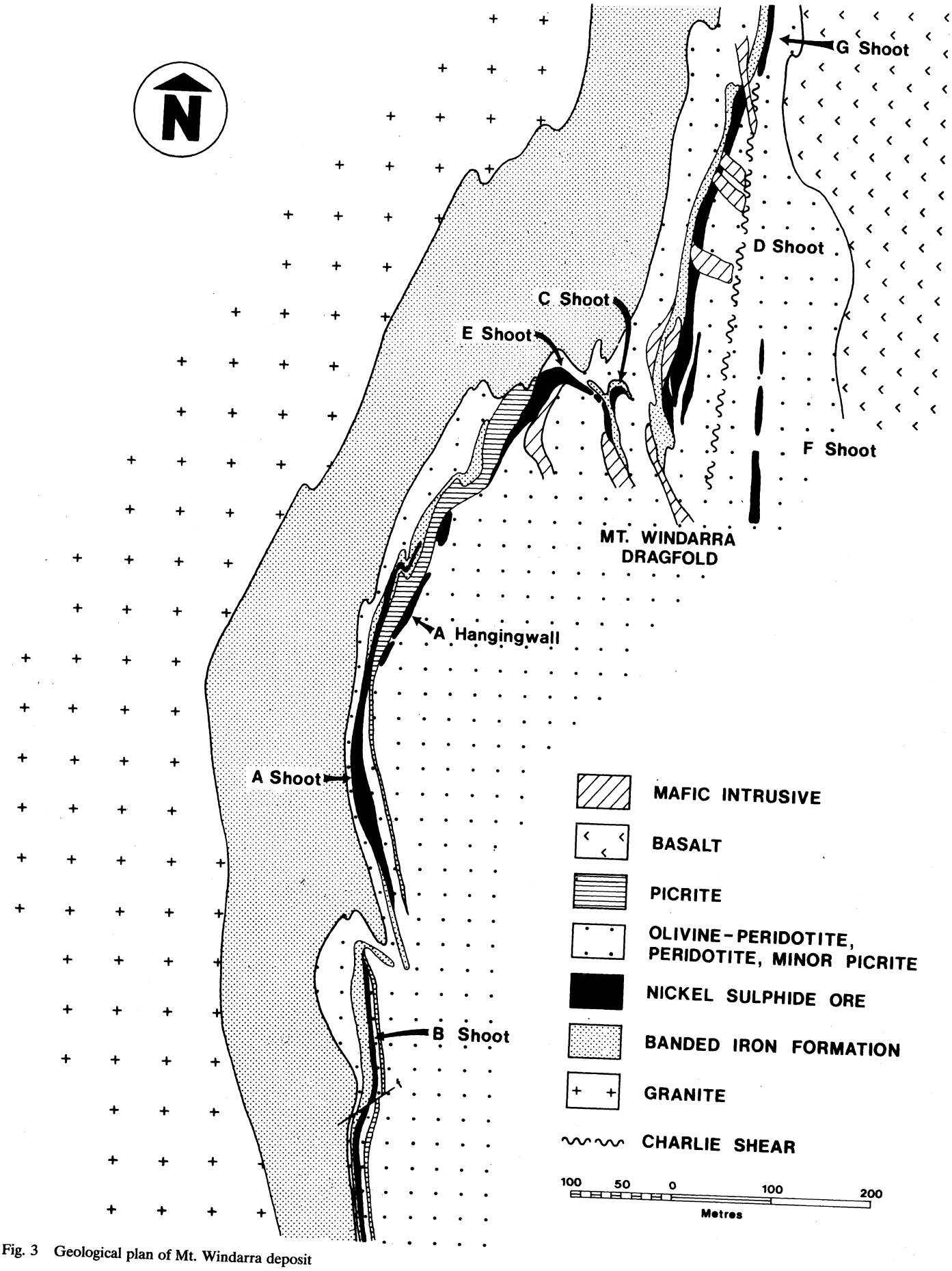

Fig. 3 Geological plan of Mt. Windarra deposit

Table 1 Summary of Mt. Windarra stratigraphy

Informal mine name	Description	Approximate thickness, m
Intrusives	Main BIF intruded by granitoid (granitic gneiss in part); metadolerites and quartz-feldspar porphyries ('felsites') intrude Windarra ultramafic sequence and overlying basalts	
Hanging-wall basalts	Komatiitic and tholeiitic metabasalts (amphibolites) and occasional metapicrite (tremolite–chlorite), with minor intercalated metasediments, particularly at base[5]	5000+
Windarra ultramafic sequence	Flow sequence comprising metaolivine peridotite (serpentinite and talc–magnesite), metaperidotite (talc–chlorite–dolomite, serpentine–chlorite–tremolite) and metapicrite (tremolite–chlorite). Fe–Ni–Cu sulphides at base of sequence, and within sequence (*F* shoot) associated with discontinuous intercalated metasediment (quartz–amphibole–pyrite)	300
Inter-BIF	Layered cherty metasediment (quartz –pyrite ± actinolite ± feldspar ± biotite); feldspathic quartzite	0–50
Corridor ultramafic	Metaperidotite (talc–chlorite–magnesite)	5–50
Main BIF	Layered Metasediments (quartz–pyrite ± pyrrhotite ± grunerite ± magnetite ± almandine ± biotite)	80–150

Table 1, the detailed geological relationships being shown in Figs. 3 and 4.

Main BIF

This horizon is 80–150 m thick, and comprises both clastic and banded chemical sediments, the latter being regarded by Drake[3] as metamorphosed carbonate-facies and sulphide-facies BIF. The rocks are extremely siliceous and contain variable amounts of grunerite, actinolite, magnetite, albite, chlorite, pyrite and pyrrhotite. Clastic rocks are best developed at various localities between Mt. Windarra and South Windarra, where they comprise quartz grits and conglomerates. Granular quartz-feldspar rocks in the mine area may represent metamorphosed feldspathic sandstones.

Corridor ultramafic

This barren ultramafic unit is 3–45 m thick and has a bulk composition of peridotite to olivine–peridotite. It now comprises a talc–chlorite–dolomite metamorphic assemblage and is devoid of relict igneous textures. It displays an asymmetric decrease in MgO content towards its upper margin, but it is uncertain whether this represents a flow top or the top of a differentiated sill. The unit is present in the Mt. Windarra area, and at various localities south of the deposit, but is absent at South Windarra.

Inter-BIF

This siliceous sediment forms the immediate footwall to the nickel mineralization and also represents an important host to the Fe–Ni–Cu sulphides. The inter-BIF is generally 2–15 m thick, but is subject to both marked structural thickening and thinning in the hinge zones of dragfolds. As with the main BIF, the inter-BIF comprises a variety of sedimentary types dominated by banded sulphidic chert (quartz–pyrite) and feldspathic quartzite. It is distinguished from the main BIF by the absence of grunerite—a characteristic constituent of the main sedimentary horizon. Individual sediment horizons vary considerably in thickness and lateral extent, chert units displaying greater continuity than coarser-grained horizons. Slumping and scour structures and graded bedding are present in some of the finer banded units.

Main ultramafic sequence

The Fe–Ni–Cu sulphide mineralization occurs at the base of a sequence of differentiated ultramafic flows 100–300 m thick. The ultramafic pile shows an overall decrease in MgO content with increasing stratigraphic height. Overlying high-magnesium basalts grade upwards into tholeiitic basalts. Thick (10–30 m) olivine–peridotite (talc–magnesite or serpentinite) units in the basal portion of the sequence are capped by largely untextured picritic (tremolite–chlorite) zones 1–2 m thick, whereas thinner (5–10 m) peridotite units in the upper portion of the sequence display spinifex-textured picritic tops. The ultramafic sequence is interpreted as a volcanic pile that comprises olivine–peridotite flows with upper picritic chill zones, indicative of an east-facing sequence.

Dwyer[4] has documented complete flows that comprise flow-top breccia, random spinifex texture, sheaf spinifex texture, skeletal zone and basal cumulate zone. The interlayering of picritic ultramafics, possible high-magnesium basalts and tholeiitic basalts in the upper portion of the ultramafic sequence provides further evidence for this being a flow sequence.

In the area immediately south of the Mt. Windarra dragfold a thick picrite unit is in direct contact with the inter-BIF (Fig. 3). This picritic material is interpreted as being a liquid-rich portion of the *A* shoot flow to the south, and appears to be laterally equivalent to the well-developed flow top that caps the differentiated ore-bearing flow (Figs. 3 and 4). The high effective viscosity of the olivine crystal mush, which formed the olivine-enriched base of the *A* shoot flow, resulted in this material having a more restricted areal extent than the less viscous liquid-rich lava. A similar situation exists at the north end of *B* shoot, where a thin picritic unit occupies the basal position (Fig. 3).

The basal ultramafic contact is therefore occupied by at least three overlapping flows, each of which contains concentrations of Fe–Ni–Cu sulphides at its base. The *B* shoot mineralization is hosted by the lowermost flow, succeeded by the *A* shoot flow and the third flow, hosting the *A* hanging-wall, *E*, *C*, *D* and *G* shoot mineralization.

A hanging-wall is the term that is used for mineralization at the base of the third flow where this flow overlaps the *A* shoot flow at the northern extremity of the *A* shoot mineralization. This zone of overlap extends further north into the Mt. Windarra dragfold hinge zone, so *E* shoot and portions of *C* shoot are underlain by the picritic northern extremity of the *A* shoot flow (Fig. 3). The proportion of low-magnesium ultramafic also increases towards the downdip margin of *A* shoot, which implies a south–north and downdip ultramafic flow direction.

F shoot, which lies east of *D* shoot, appears to occur at the base of a stratigraphically higher flow, analogous to the hanging-wall mineralization at Lunnon Shoot, Kambalda,[9] but is associated with a discontinuous BIF horizon and apparent thrust slices of basalt. Dwyer,[4] postulated that *F* shoot represents a structurally emplaced equivalent of *D*–*G* shoot mineralization, but direct evidence for this is lacking.

The thick overlying mafic pile comprises dominantly tholeiitic basalts (cf. Hallberg[6]) that are now represented by strongly foliated amphibolites. The contact zone between the ultramafic and mafic sequences is gradational and contains units of high-magnesium basalt interfingered with picritic and tholeiitic flows. In the mine area this transition zone is around 50 m thick,

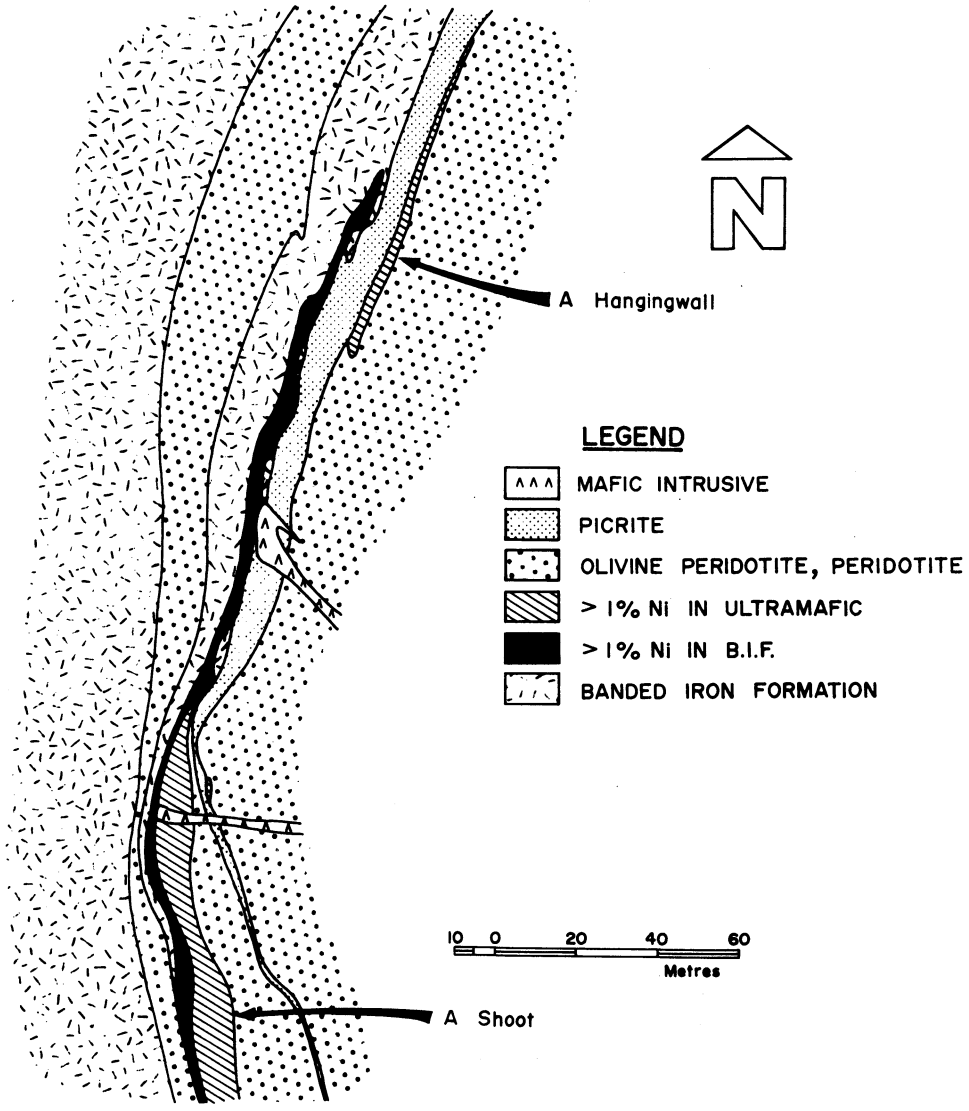

Fig. 4 Plan showing relationship between *A* shoot and *A* hanging-wall mineralization

but south of the mine, where the volume of high-magnesium ultramafic rocks decreases rapidly, the transition zone is up to 400 m in thickness. Here low-magnesium ultramafics (tremolite–chlorite ± plagioclase rocks with 18–24% MgO) are irregularly interfingered with zones of high-magnesium basalt (hornblende–chlorite–plagioclase ± quartz, 10–18% MgO) and occasional higher-magnesium ultramafics (talc–chlorite–magnesite rocks). Contacts are gradational over short distances (10–50 cm), with no obvious flow textures in the ultramafic units. The high-magnesium basalts commonly contain zones of flattened felsic 'ocelli', and are locally pillowed.

The mafic–ultramafic transition zone comprises rocks that appear to represent a complete gradation from tholeiitic basalts to olivine peridotites, and it is therefore difficult to envisage separate magma sources for the interfingered mafic and ultramafic flow units.

Iron–nickel–copper sulphide mineralization

The Fe–Ni–Cu sulphide oreshoots at Mt. Windarra, as defined by the 1% Ni cutoff, are up to 20 m thick, with a strike length of 50–350 m and a known downdip extent of up to 900 m (Fig. 5). The oreshoots comprise both massive and disseminated ore within the ultramafic, and massive, breccia and stringer ore within the inter-BIF. Disseminated sulphides represent the dominant ore type, massive sulphides, commonly at the base of the sulphide zone, being irregularly distributed and generally of limited lateral extent. The tenor of disseminated and massive sulphides within ultramafic rocks is 10–19% Ni, and is commonly higher in disseminated ore than in massive sulphides. BIF-hosted ore, which occurs most frequently towards the margins of oreshoots, particularly *A* shoot, is of highly variable nickel tenor (2–10% Ni). This suggests that this ore formed by physical mobilization of Fe–Ni–Cu sulphides into the BIF during tectono-metamorphism and/or by diffusion of nickel into pre-existing iron sulphides. Trace-element and sulphur isotopic data that bear on such processes were discussed by Seccombe *et al.*,[11] who concluded that diffusion of nickel from the overlying ultramafic unit is the dominant mechanism of BIF-hosted ore formation, particularly in undeformed sedimentary ores.

Pyrrhotite, pentlandite, pyrite and chalcopyrite are the major sulphide phases—in decreasing order of abundance. The pyrrhotite:pentlandite ratio varies from unity in disseminated ore to up to 8:1 in iron-rich BIF-hosted ore. Within the supergene zone, which extends from the base of the oxidized zone, at a depth of around 40 m, to a vertical depth of 60–90 m, pyrite and violarite are the dominant sulphide phases. The transition zone, where violarite and pentlandite coexist, extends to a vertical depth of up to 180 m.[7]

Mean Ni:Cu ratios vary from 8.4:1 in *A* shoot to 19.5:1 in *F* shoot (Table 2). A decrease in chalcopyrite content from *A* shoot to *F* shoot is accompanied by an increase in pentlandite:pyrrhotite ratios, the tenor of ultramafic-hosted ore varying from around 10% Ni in *A* shoot to 19% Ni in *F* shoot. The Ni:Cu ratios would appear to confirm a common origin for *C, D*

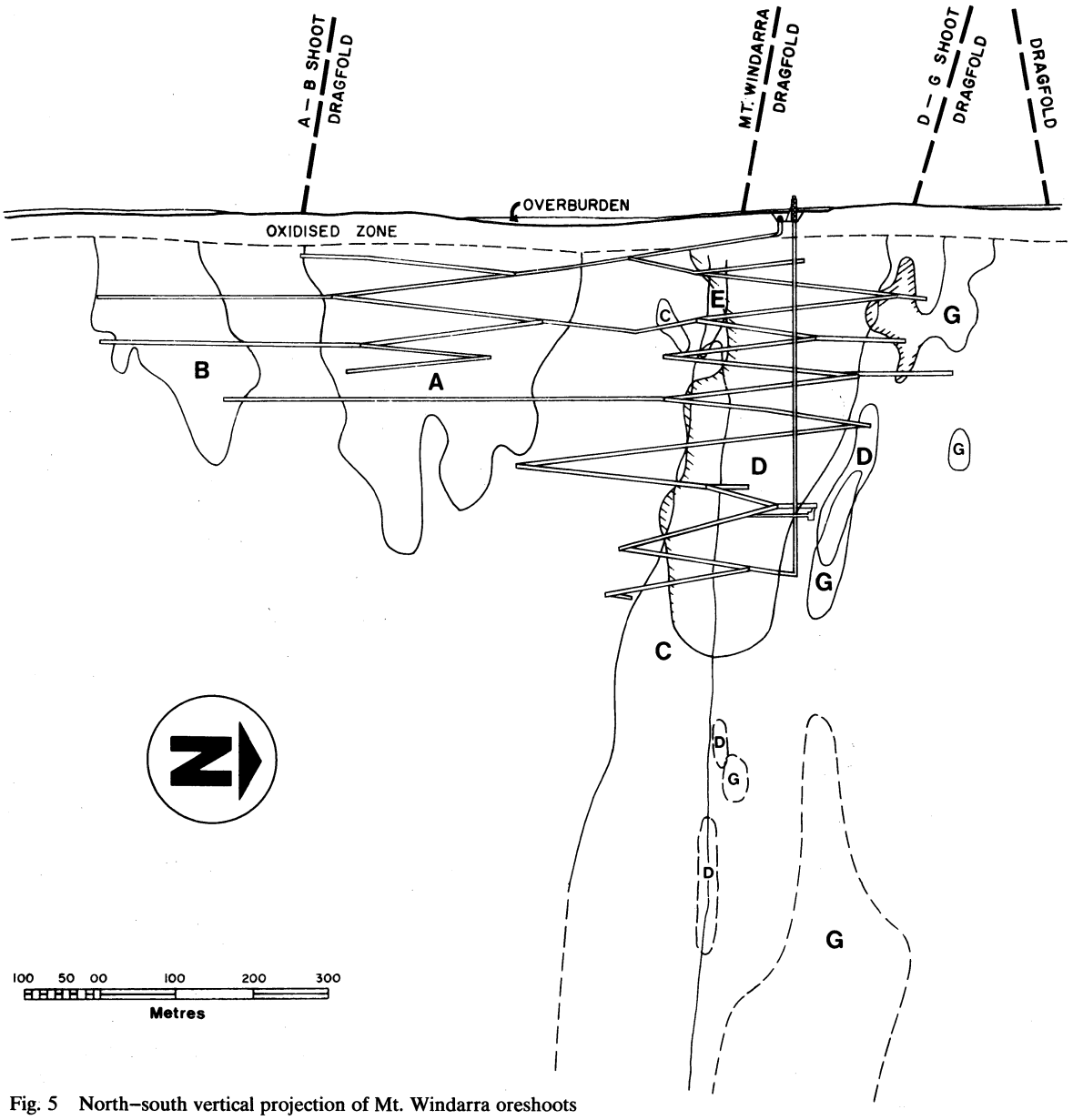

Fig. 5 North–south vertical projection of Mt. Windarra oreshoots

and *G* shoots, at the same time suggesting that the *E* shoot and *A* hanging-wall ores may be related to individual separate flows. Ni:Cu ratios within individual shoots can be extremely variable, in *E* shoot varying from 8.4:1 to 12.2:1 within different portions of the ore zone. The markedly different bulk metal ratios in *F* shoot would appear to indicate that this mineralization is related to a magmatic event quite distinct from that which generated the underlying mineralization.

There is an extremely close spatial relationship between Fe–Ni–Cu sulphides and highly magnesian ultramafic rocks, the ultramafic-hosted sulphides dying out where picritic material occupies the basal contact. Remobilized low-tenor BIF-hosted ores may be present in these areas. The restrictive association of Fe–Ni–Cu sulphides and rocks of the highest normative olivine content, in the absence of an obvious structural trap, suggests that this association is a physical one. The high effective viscosity of an olivine crystal mush would enable this material to entrap and transport immiscible sulphides, subsequent settling concentrating the sulphides at the base of the flow. If sulphides had been extruded as a separate sulphide flow, as postulated for Kambalda by Ross and Hopkins,[9] sulphides would occur on the contact where the contact position was occupied by both crystal mush (olivine–peridotite) and liquid (picrite) portions of the flow.

Table 2 Bulk Ni/Cu ratios for Mt. Windarra oreshoots based on 1% Ni cutoff

Shoot	Ni/Cu
A	8.4
A hanging-wall	11.6
B	9.6
C	12.3
D	12.9
E	10.7
F	19.5
G	12.6

In *A* shoot around 40% of the total volume of ore (at a 1% cutoff) is hosted within BIF. This sediment-hosted ore occurs at the base of the southern and central portions of the ore zone and comprises the entire northern 'tail' of the shoot. This northern mineralization comprises up to 80% sulphide, and is commonly highly deformed and brecciated, containing irregular sediment inclusions. It has been widely termed breccia ore.[1,7,11] This horizon is locally separated from the barren overlying picritic ultramafic by a sulphide-poor quartz–albite ± biotite sediment, and appears to be an along-strike equivalent of a barren

quartz–pyrite sediment unit. It is conceivable that considerable movement may have taken place along the breccia ore horizon, accompanied by physical injection of Fe–Ni–Cu sulphides. Isotopic data do not clearly indicate either a wholly magmatic or wholly sedimentary origin for the breccia ores,[11] and geological relationships favour both diffusion of nickel into pre-existing sulphides and physical remobilization of magmatic sulphides.

Sediment-hosted ores in other areas (principally *C* and *D* shoots) are unbrecciated along-strike equivalents of nickel-free sulphide-facies BIF, with no evidence for sulphide enrichment within the ore zone. Sulphur isotope data, which show a comparatively wide range and slightly negative mean $\delta^{34}S$ value, are consistent with a sedimentary origin for these sulphides.[11] The selective occurrence of nickel sulphides within rocks that contain pre-existing iron sulphides would further imply that the relatively undeformed sedimentary ores were generated purely by diffusion of nickel and copper from adjacent ultramafic-hosted ores. Barrett *et al.*[1] suggested that this process occurred early in the metamorphic history of the deposit, followed by the reversion of sulphides to mss and the subsequent exsolution of the observed sulphide minerals from mss.

Structure

A series of steeply south-plunging dextral dragfolds controls the disposition of the oreshoots at Mt. Windarra (Figs. 3 and 5). These folds, particularly the main Mt. Windarra dragfold, are concentric folds[2] characterized by marked pinching and swelling of the BIF horizons. This has resulted in a highly irregular and discontinuous distribution of the inter-BIF in the complex hinge zones of the folds. Fold axial surfaces are frequently intruded by dolerite dykes, which commonly terminate against the main BIF. Major shear zones, of which the most prominent is termed 'Charlie' shear, extend from the fold hinge zones into the ultramafic pile (Fig. 3).

'Charlie' shear is an ultramylonite zone, generally 1–3 m wide, east of *D* shoot in a position that may in part be coincident with the top of the mineralized flow. It appears to represent a zone of stress relief that separates the eastern part of the mafic–ultramafic sequence, which was unable to fully accommodate the dragfold movement, from the underlying tightly folded portion of the sequence. Tensional openings between 'Charlie' shear and the inter-BIF have been filled by tabular, sub-vertical and, more rarely, sub-horizontal dolerite intrusions. The lack of shearing on the east and west termini of these dolerites and the absence of faulted extensions suggest that the dolerites have not been truncated by faulting. The lower portion of the ultramafic sequence, particularly in the southern (*B* shoot) area, has been cut by numerous irregular quartz-feldspar porphyry ('felsite') intrusives. Intrusives appear to both pre- and post-date the major period of deformation, and are commonly boudinaged and folded in high-strain zones. The high-strain regime at Mt. Windarra is evidenced by the strong pervasive foliation in the overlying basalt (amphibolite) sequence. This foliation has a general north–south strike in the mine area, with a steep westerly dip.

There is a marked parallelism between individual oreshoots and the major structural elements, the northern and southern limits of most shoots being defined by the steeply plunging dragfolds (Figs. 3 and 5). The folded *E* and *C* shoots are enclosed within the Mt. Windarra dragfold, but the increase in the strike length of *C* shoot at depth, apparently at the expense of *D* shoot, suggests that *C* and *D* shoots may have been a single south-plunging sheet subsequently folded and dislocated by the more steeply plunging Mt. Windarra dragfold.

South Windarra

The South Windarra deposit occurs broadly at the same stratigraphic position as the mineralization at Mt. Windarra, although the inter-BIF and underlying corridor ultramafic are locally missing from the sequence. The ore lies close to, or in direct contact with, the main BIF, which dips south at 40–45°. The orebody was mined in an open-cut operation between June, 1974, and January, 1978, when mining was suspended. A total of 2 057 500 t of ore grading 1.47% Ni has been mined, leaving an *in-situ* ore reserve of 2 561 000 t at 1.03% Ni. The mineralization occurs over a strike length of around 1300 m and comprises two major primary lenses further subdivided by crosscutting dolerite intrusives, which commonly terminate against the main BIF as at Mt. Windarra. The ore is up to 25 m thick, but thins rapidly at depth and appears to die out at around 300 m below surface.

The degree of deformation is considerably less at South Windarra than at Mt. Windarra, and major fold structures are absent. Only minor amounts of mobilized BIF-hosted ore are present; disseminated ore predominates over massive sulphides, which commonly occur at the base of the ore zone. The primary sulphide assemblage is similar to that at Mt. Windarra, with the exception of a lower chalcopyrite content, resulting in a mean Ni:Cu ratio of approximately 22:1. A large proportion of the ore occurs in the supergene pyrite–violarite zone.

Santul[10] has documented a 350-m thick ultramafic volcanic pile that comprises spinifex-textured flow units 5–25 m thick, underlain by massive mineralized flows. The basal ore-bearing flow, 25–45 m thick, is confined to the strongly mineralized western portion of the deposit. A second massive mineralized unit overlies the basal flow in the west, but is in direct contact with the main BIF in the eastern portion of the deposit (J. H. Cleghorn, personal communication). A third untextured flow contains sub-economic basal Fe–Ni–Cu sulphide mineralization—directly analogous to the internal hanging-wall mineralization at Kambalda.[9]

As a result of lower strain primary igneous textures are somewhat better preserved than those at Mt. Windarra. The basal ultramafic consists dominantly of serpentinite with local talc–magnesite zones. Laths of serpentinized metamorphic olivine are common within the mineralized units, and trains of magnetite grains form rims to original serpentinized olivines.[10]

The sequence is cut by a 10–20 m thick, steeply dipping, north–south-trending transgressive ultramafic body. This is a low-magnesian ultramafic with a MgO content of around 15–22% (volatile-free); it is even less magnesian than the thin spinifex-textured units.[10] It was regarded by Santul[10] as a late differentiate of the ultramafic magma, but transects both the main BIF and underlying granitoid and therefore appears to post-date the main Windarra ultramafic volcanic sequence.

The ultramafic pile is cut by numerous feldspar porphyry (felsite) dykes and lenses, generally orientated either north–south or northwest–southeast. These intrusives both pre- and post-date the intrusion of dolerites and post-date the transgressive ultramafic body.

The overlying mafic sequence at South Windarra contains a higher proportion of high-magnesium basalt than that at Mt. Windarra, and includes extremely coarse-grained amphibolites, some of which contain large almandine porphyroblasts.

Acknowledgement

The contribution to the understanding of the Windarra geology made by past and present mine geologists is gratefully acknowledged. In particular, the author has benefited from discussions with C. T. Reddell, J. R. Simmonds, D. J. Boyack and T. E. Craske.

References

1. Barrett F. M. *et al.* Structural history and metamorphic modification of Archean volcanic-type nickel deposits, Yilgarn Block, Western

Australia. *Econ. Geol.*, **72,** 1977, 1195–223.
2. Davidson D. E. Structural mapping project Mt. Windarra BIF. Unpublished WMC Report, 1977, p. 9.
3. Drake J. R. The structure and petrology of banded iron formations at Mt. Windarra, Western Australia. B.Sc. thesis, University of Western Australia, 1972, p. 93.
4. Dwyer J. R. Mt. Windarra stratigraphic project. Unpublished WMC Report, 1977, p. 8.
5. Goss B. J. Regional exploration project, Windarra. Final report. Unpublished WMC Report no. K2363, 1977, p. 47.
6. Hallberg J. A. Geochemistry of Archaean volcanic belts in the Eastern Goldfields region of Western Australia. *J. Petrol.*, **13,** 1972. 45–56.
7. Roberts J. B. Windarra nickel deposits. In *Economic geology of Australia and Papua New Guinea 1. Metals* Knight C. L. ed. (Parkville, Victoria: Australasian Institute of Mining and Metallurgy, 1975), 129–43. *(Monogr. Series* no. 5)
8. Robinson W. B. Stock E. C. and Wright R. The discovery and evaluation of the Windarra nickel deposits, Western Australia. In *Western Australia conference 1973* (Parkville, Victoria: Australasian Institute of Mining and Metallurgy, 1973), 69–90. (*Conf. Series* no. 2)
9. Ross J. R. and Hopkins G. M. F. Kambalda nickel sulphide deposits. Reference 7, 100–21.
10. Santul J. The geology, geochemistry and mineralization of the South Windarra nickel ore deposit, W.A. B.Sc. thesis, University of Adelaide, 1975, p. 42.
11. Seccombe P. K. *et al.* A sulphur isotope study to test a genetic model for Fe–Ni sulphide mineralization at Mt. Windarra, Western Australia. In *Stable isotope developments in the earth sciences* Robinson B. W. ed. *Bull. N.Z. Dep. scient. ind. Res.* 220, 1977, 187–202.

Sulphide–silicate reactions as a guide to Ni–Cu–Co mineralization in central Maine, U.S.A.

J. F. H. Thompson B.A., M.Sc., Ph.D.
Formerly Department of Geology, University of Toronto, Toronto, Ontario, Canada (now B.P. Minerals Australia, Boulder, Western Australia)
A. J. Naldrett B.A., M.Sc., Ph.D.
Department of Geology, University of Toronto, Ontario, Canada

Synopsis

Synorogenic mafic intrusions are a common feature of the northern Appalachians. Two sulphide-bearing intrusions in central Maine that have been investigated revealed a number of important features that illustrate sulphide–silicate interaction that relates to magmatic sulphides.

The Moxie Pluton is a large mafic intrusion emplaced during the Devonian Acadian orogeny. The Katahdin gabbro is a small mafic body that is probably genetically and temporally related to the Moxie Pluton. Both intrusions were formed by the intrusion of variably fractionated magmas into irregular chambers and feeder zones. The southern half of the Moxie Pluton contains three small sulphide accumulations, whereas the Katahdin gabbro hosts a large, predominantly massive, sulphide body. Textural evidence clearly documents the magmatic origin of these sulphides.

The three Moxie Pluton sulphide bodies are located at or very close to the intersection between the intrusion and the sulphide-bearing Hildreths Formation. Sulphur assimilation, suggested by this relationship, is supported by the isotopically light ($\delta^{34}S = -8$ to -25) and the selenium-poor (S/Se = 25 000–48 000) character of the Moxie sulphides and correlation with the Hildreths Formation sulphides ($\delta^{34}S = -25$, S/Se = 25 000–48 000). Isotopically light sulphur ($\delta^{34}S = -20$ to -21) and high S/Se ratios indicate that the majority of sulphur in the Katahdin sulphide body was also derived from an unexposed country rock source. The volume of sulphide in this example illustrates the potential efficiency of the sulphur assimilation process—so efficient in this case that marked dilution of the economic chalcophile elements resulted from the addition of so much external sulphur.

The three Moxie Pluton sulphide occurrences are all impoverished in Ni and Cu (1.87–0.44% Ni; 0.72–0.32% Cu in massive sulphide), but contain normal Co contents (0.22–0.13%) relative to typical magmatic sulphides. The Katahdin sulphides show a greater Ni and Cu impoverishment (0.2% Ni; 0.1% Cu in massive sulphide) with similar Co (0.17%). The Ni content of the Moxie Pluton olivines document the fractional removal of sulphides during crystallization of the host magma, which resulted in the progressive depletion of the chalcophile metals in this magma. Modelling that involved the fractional crystallization of the magma coupled with the fractional removal of a specified proportion of sulphide has successfully duplicated the Moxie Pluton sulphide compositions. A similar magmatic model has been postulated for the Katahdin sulphides with a greater degree of sulphide fractionation. This latter model is again supported by extremely low Ni/forsterite ratios in olivines, though the compositional range is insufficient to document fractionation. These magmatic models are not unique, but they provide a relatively constrained and consistent explanation for the sulphide compositions.

The Ni contents of olivines are the most important indicator of sulphide–silicate interaction in mafic magmas and have exploration potential. They provide a means of assessing the timing and extent of sulphur saturation in an intrusion and are a guide to the Ni content of a sulphide accumulation in equilibrium with olivine. In the Maine examples they provide strong evidence of the magmatic origin of the sulphide accumulations and justification for magmatic modelling.

Nickel–copper–cobalt sulphide ores are associated with mafic and ultramafic host rocks and are generally accepted to have formed in the magmatic environment as a result of the separation of an immiscible sulphide liquid.[26] The composition of the sulphide ores will reflect a number of parameters—in particular, the composition of the magma with which the immiscible sulphide liquid equilibrated. Conversely, under the right circumstances the silicate chemistry may reflect the sulphide segregation process, the resultant changes in silicate chemistry having applications for exploration. To understand the potential of these processes it is important to determine the timing of sulphur saturation and the separation of immiscible sulphides. The original source of sulphur is, therefore, an important control in terms of sulphur saturation.

Much of the understanding of magmatic sulphide deposits, implicit in the statements above, has been derived from recent experimental work. The experimental work may be divided into three areas: (1) the determination of the partition and exchange distribution coefficients of chalcophile elements between sulphide and silicate liquids (e.g. MacLean and Shimazaki,[22] and Rajamani and Naldrett[34]) and between sulphide and olivine (Boctor[2]); (2) experimental studies in silicate systems—for example, the distribution of Fe and Mg between olivine and silicate liquid (Roeder and Emslie[36]) and the distribution of Ni between olivine and silicate liquid (Duke,[9] Irvine and Kushiro,[17] Mysen, [25] Arndt[1] and Leeman and Lindstrom[19]); and (3) experimental determinations on the solubility of sulphur in mafic magmas (e.g. Haughton and co-workers,[15] Shima and Naldrett[37] and Buchanan and Nolan[5]).

The results of these experimental studies have provided sufficient data for the modelling of the fractional crystallization of mafic and ultramafic magmas under sulphur-saturated and undersaturated conditions.[8,10] This modelling has predicted the effects that sulphide segregation may have on silicate chemistry. The experimental work has been used also to model the sulphide composition of several deposits by varying the ratio of the amount of silicate magma to the amount of sulphide liquid with which it equilibrates[7] and combining this parameter with the degree of sulphide fractional segregation.[28,29,30]

A series of mafic intrusions that host magmatic sulphides is located in central Maine, northeastern United States. These occurrences provide the opportunity to investigate the source

of sulphur, the extent of sulphide–silicate interaction and the relevance of magmatic models in the determination of the sulphide composition. The successful application of such magmatic models provides natural examples of theoretical magmatic processes and has important implications for exploration.

Moxie Pluton and Katahdin gabbro

Mafic intrusions are known throughout the Caledonian Appalachian orogenic belt. These intrusions have a number of features in common—in particular, their synorogenic age of emplacement. Two belts of such intrusions are recognized in the northern part of the Appalachians.[41] The coastal Maine belt extends northeast from Maine into New Brunswick and the central Maine belt extends southwest towards New Hampshire. Magmatic Ni–Cu sulphide occurrences are found associated with a number of these intrusions in both belts (Fig. 1).

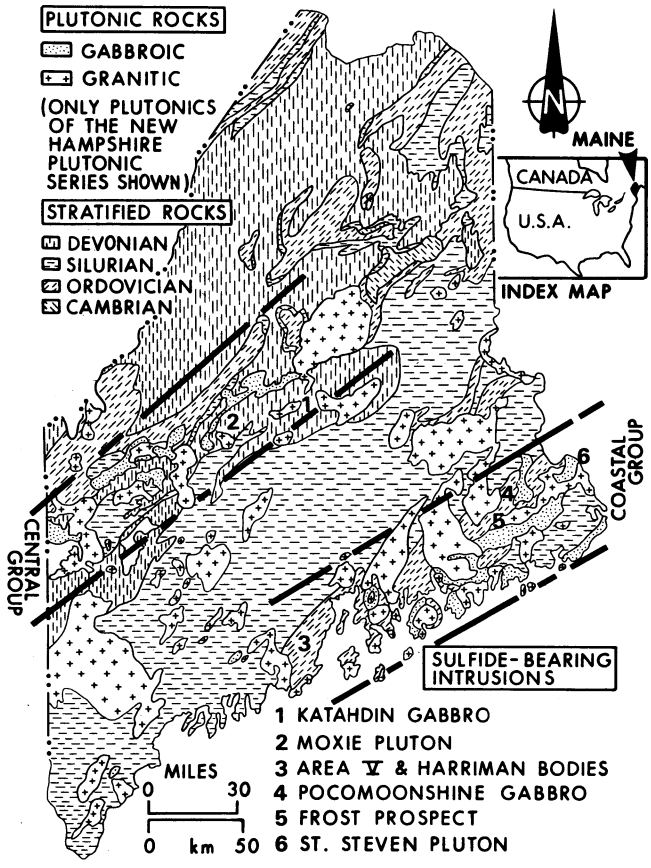

Fig. 1 General geology of Maine indicating two belts of Acadian mafic intrusions and magmatic sulphide occurrences

This study is concerned with the Moxie Pluton and the informally named Katahdin gabbro, both of which are located within the central belt. The southwestern half of the Moxie Pluton contains three small sulphide showings close to the southeast contact of the pluton. These showings were investigated by a number of mining companies and the U.S. Geological Survey between 1950 and 1970. The most extensive programme was carried out by Exxon Minerals. The Katahdin gabbro contains an enormous pyrrhotite body. The limonitic gossan that overlies this body was worked for iron ore between 1843 and 1890, the deposit being named the Katahdin iron works. Subsequently, the pyrrhotite body has been investigated for its Fe, S, Ni, Cu and Co potential, the most recent work having been carried out by the Superior Mining Company.

Moxie Pluton

The Moxie Pluton is an irregularly shaped mafic intrusion that extends for more than 70 km in length and varies in width from 2 to 8 km. The intrusion was emplaced during the Acadian orogeny, indicated by contact aureole porphyroblasts overgrowing Acadian F_1 structures and being deformed by F_2 and later structures.[32] A single biotite K–Ar age determination yielded a result of 393 m.y.[43] A broad contact aureole is present around most of the intrusion, with the progressive development of biotite, andalusite, andalusite + cordierite, sillimanite and sillimanite + K-feldspar towards the intrusion. Partial melting may be present locally. The mineralogy indicates pressures between 2 and 2.9 kb, with temperatures in excess of 650°C at the contact of the intrusion.[41] Contact relations are complex with screens of country rock, irregular brecciation and intrusion on the contact, the incorporation of xenoliths and the chaotic disruption of the country rock all being common features.

Various parts of the pluton have been mapped and the petrology has been discussed in general terms by Visher,[42] Espenshade and Boudette[12] and Espenshade.[11] These studies outlined broad differentiation from dunitic rocks in the southwest to gabbros and diorites in the northeast. The present study has been concentrated on the southwestern half of the pluton, which contains the three sulphide occurrences. The petrology of this part of the intrusion is shown in Fig. 2 in terms of the lithological variation and the olivine and orthopyroxene compositions. This half of the intrusion may be divided into three parts—two broad lobate areas connected by a narrow zone. The sulphide showings—Big Indian Pond, Burnt Nubble and Black Narrows—are located in the narrow section (Fig. 2).

The lobe south of Pleasant Pond contains a considerable amount of olivine adcumulate (dunite), the most primitive olivine compositions (Fo_{86-88}) being present in the intrusion. The contacts between the areas of dunite and olivine–plagioclase

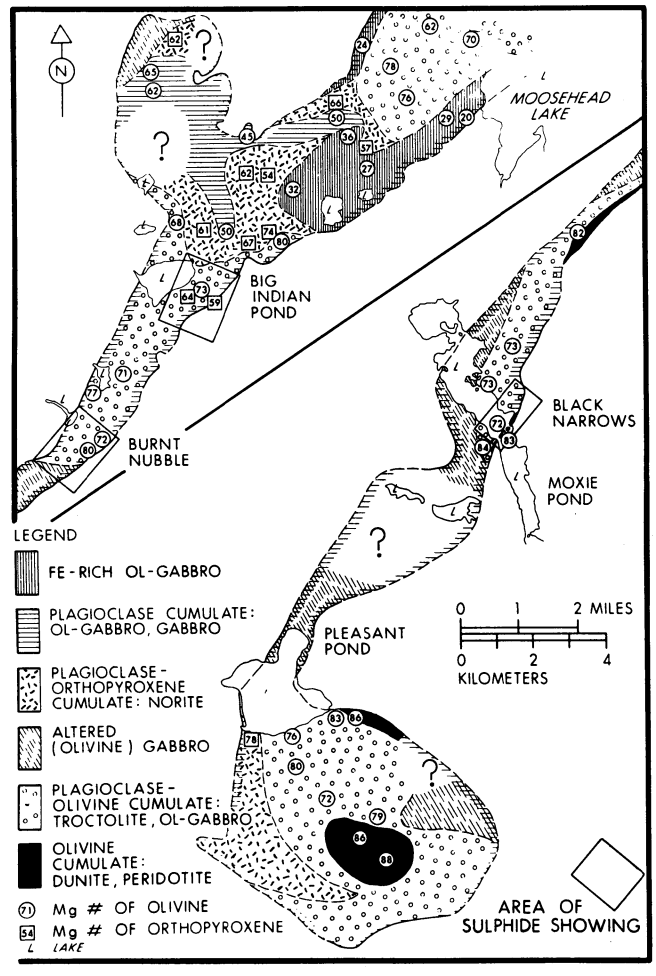

Fig. 2 Geology of Moxie Pluton with representative compositions of olivines and orthopyroxenes

cumulates are rarely exposed, and an irregular rock type distribution is apparent. The south shore of Pleasant Pond reveals a more regular variation, olivine cumulates passing in a westerly direction into olivine–plagioclase cumulates and orthopyroxene–plagioclase cumulates. The narrow part of the intrusion between Pleasant Pond and Big Indian Pond contains a considerable amount of altered olivine gabbro. In less altered sections olivine and orthopyroxene cumulates are present on the southeast contact, passing into olivine–plagioclase cumulates towards the northwest. North of Big Indian Pond orthopyroxene–plagioclase and olivine–plagioclase cumulates outcrop with a progressive increase in the Fe content of these minerals towards the north. This trend reverses west of Moosehead Lake with the reappearance of more primitive olivine–plagioclase cumulates. In addition, Fe-rich olivine gabbro outcrops on both margins of the pluton, the unit appearing to crosscut less fractionated lithologies (Fig. 2).

There is a marked lack of layering features within the intrusion and the cryptic variation shown in Fig. 2 and described above is highly irregular. Post-crystallization deformation and alteration effects account for part of this variation and are most apparent in the narrow part of the intrusion. This is supported by the structural interpretation of palaeomagnetic results.[33]

The form of the pluton prohibits detailed comparisons with other mafic intrusions. The full range of mineral variation demonstrated at Moxie is, however, typical of many classic mafic intrusions, and the pluton shows the same trend of Fe enrichment and Si depletion as is exhibited by such bodies as the Bushveld Complex. The most primitive olivines at Moxie would have been in equilibrium with a magma of relatively high Mg/Fe ratio that could have been derived, with minor modification, from a mantle source region.

Katahdin gabbro

The Katahdin gabbro is a small elliptical mafic intrusion with dimensions of 4.5 km north–south and 1.5 km east–west. The intrusion is poorly exposed and sampling is largely restricted to diamond drill holes. The Katahdin gabbro intrudes the Devonian Seboomook Formation. The exact relationship between emplacement and the Acadian orogeny is not clear. The intrusion does, however, cut Acadian structures and is, itself, clearly deformed, which suggests temporal correlation with the Moxie Pluton. Contact metamorphosed country rocks are present around the margin of the body, but a mineral zoned aureole is absent, possibly because of retrogressive metamorphism within the aureole of the felsic Onawa Pluton to the west.

The intrusion consists predominantly of three rock types—olivine–plagioclase cumulates, orthopyroxene–plagioclase cumulates and pegmatitic gabbro. No regular layering was observed in drill core. A distinct marginal facies is present with an increased component of primary hydrous phases, micropegmatite and diffuse but generally rounded sulphide blebs.

The variation of the mineral chemistry is shown in Fig. 3 in terms of the olivine and orthopyroxene compositions. This demonstrates a Fe-enriched trend towards the centre of the intrusion based on the limited drill-hole intersections. A similar but weaker trend is indicated by the anorthite content of plagioclases.[41] The range of mineral compositions is considerably less than that in the Moxie Pluton. There is, however, sufficient chemical and textural overlap to suggest that the two intrusions are genetically related. This, however, implies fractionation of the Katahdin magma prior to injection.

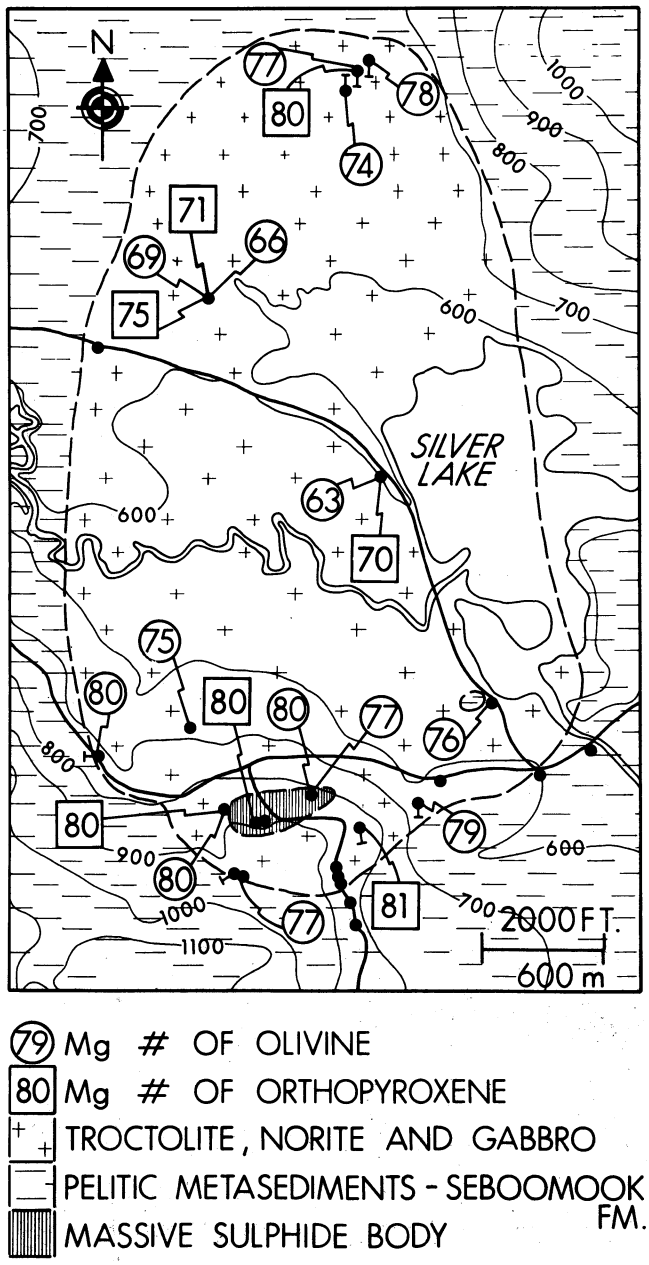

Fig. 3 Olivine and orthopyroxene compositions in Katahdin gabbro

Sulphides in Moxie Pluton and Katahdin gabbro

Moxie Pluton

Three individual sulphide showings are present on or close to the southeast contact of the Moxie Pluton (Fig. 2). In addition, the majority of the more primitive cumulates contain up to 2% interstitial sulphide, particularly in the southern lobe of the intrusion. The most significant accumulation of sulphides occurs at Big Indian Pond. Exxon Minerals skeleton drill sections from Big Indian Pond and Burnt Nubble were sampled, but sampling at Black Narrows was limited to surface outcrop around the shores and islands of Moxie Pond. The general features of the three sulphide occurrences are described in Table 1. The major difference between the three is the host rock composition, Black Narrows being hosted largely by forsteritic olivine cumulates and Burnt Nubble and Big Indian Pond by similar and rather more fractionated olivine–plagioclase cumulates.

In all three localities the sulphide predominantly occupies an interstitial position to the magmatic silicates. This is demonstrated in a sample from Big Indian Pond (Fig. 4). This texture is most simply interpreted to be the result of the crystallization of an immiscible sulphide liquid that accumulated interstitially to cumulus igneous silicates and demonstrates the magmatic origin of these occurrences. The only exception to this texture is at Black Narrows, where rounded sulphide blebs are present in more altered and amphibole-rich host rocks. Sulphide blebs have been described in other sulphide deposits[27] and inter-

Table 1 Characteristics of three Moxie Pluton sulphide occurrences

	Black Narrows	Burnt Nubble	Big Indian Pond
Host rocks	Olivine cumulate–altered ol–plag cumulate	Olivine–plag cumulate	Olivine–plag cumulate
Composition	$01:Fo_{83-84}$	$01:Fo_{72-79}$ $Plag:An_{80-92}$	$01:Fo_{72-76}$ $Plag:An_{86-93}$
Size	Extends over approx. 500 m along contact	Patchy over 600 m along contact	Irregular area 1000 m × 200 m approx. 400 m from contact
Sulphide–silicate texture	Interstitial to cumulus olivine; subspherical blebs in altered and amphibole-rich rocks	Interstitial to cumulus olivine and plagioclase	Interstitial to cumulus olivine and plagioclase
Sulphide mineralogy	Pyrrhotite+pentlandite+ chalcopyrite+violarite +mackinawite	Pyrrhotite+pentlandite+ chalcopyrite+ mackinawite	Pyrrhotite+pentlandite+ chalcopyrite+ mackinawite

preted on the basis of a magmatic origin. The texture at Black Narrows is ambiguous, however, and may relate to alteration; serpentinization and chloritization are both present and secondary alteration of the sulphides is apparent in places. There is, however, sufficient preservation to indicate the primary magmatic origin of the majority of the sulphides and the restricted extent and degree of alteration has not modified the sulphide chemistry throughout the deposit. Burnt Nubble and Big Indian Pond are essentially unaltered.

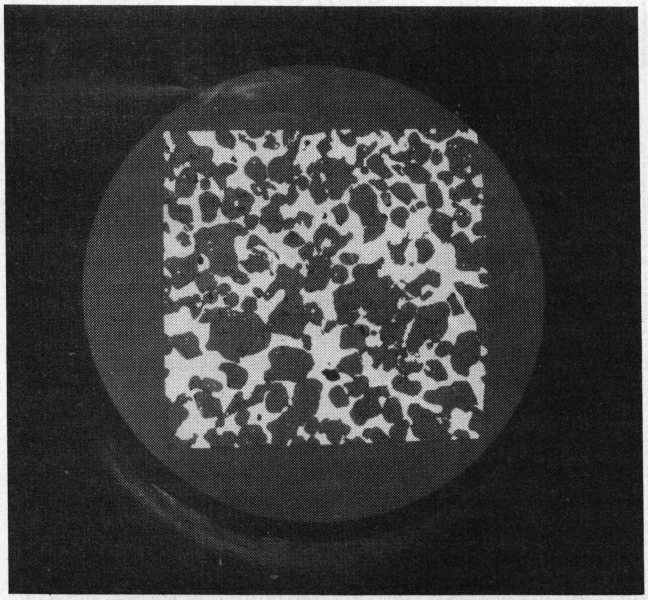

Fig. 4 'Net-textured' sulphide in polished section from Big Indian Pond. Sulphide interstitial to olivine grains. Polished section 2 cm across

Limited fresh outcrop and drill core reduced the number of samples available for analysis. All the samples were analysed for Ni, Cu and Co and several samples were analysed for a number of other elements, including Se, Zn, As, Sb, Au and the PGE. The levels of all the elements are low and fall below detection limits in many cases—in particular, the platinum group elements (PGE). As a result this paper will only attempt to explain quantitatively the Ni, Cu and Co data, some qualitative explanation being given of the general sulphide elemental abundances. The mean Ni, Cu and Co data for 100% sulphide calculated from the original analyses for each Moxie occurrence are shown in Table 2, where they are compared with the range of values found in Sudbury deposits (Sudbury deposits were chosen for comparison on the basis of their mafic host rock lithologies). Despite the limited amount of data, the following points emerge: (1) the Ni and Cu contents of these sulphides are uniformly low in comparison with the Sudbury deposits; (2) the Co content is similar to that in the Sudbury deposits; (3) the Ni contents of the three localities are significantly different (97.5% confidence level), the Burnt Nubble Ni and Cu contents being lower than the other two; and (4) the Cu/(Cu + Ni) ratio of Black Narrows is significantly lower (99% confidence level) than the similar ratios at Burnt Nubble and Big Indian Pond.

The low Ni/Co and Ni/(Ni + Fe) ratios merely reflect the depleted Ni contents of these sulphides. The Zn content of these sulphides is relatively typical of magmatic sulphides and the PGE and Au values are extremely low.[41]

Katahdin

The Katahdin gabbro contains a large sulphide body towards its southern margin (Fig. 3). The body constitutes in excess of 200 000 000 ton of largely massive (>75%) pyrrhotite. In addition, sulphides are found throughout the host intrusion, locally concentrated in minor zones. Pyrrhotite is the dominant sulphide phase throughout, with minor amounts of chalcopyrite and pentlandite, the latter mineral being cobalt-rich (up to 32 wt%).

Sulphides throughout most of the intrusion occur in a typical interstitial magmatic relationship. Sulphides in the marginal mafic rocks occur as diffuse clots and blebs and may represent large immiscible sulphide droplets preserved in the chilled and apparently volatile-rich contact zone. Three textural variations are distinguished within the massive sulphide body: (1) the massive pyrrhotite commonly contains euhedral olivine, plagioclase and rare chromite grains, which may occur as small chains or as isolated mineral grains; (2) with an increasing silicate content a distinct foliation is present in the rock owing to the planar arrangement of elongate 'fragments' of silicate; and (3) at low sulphide contents interstitial magmatic textures are preserved.

Variable amounts of alteration are present throughout the intrusion, including the sulphide body. Rare samples show sulphide–silicate alteration with remobilization of sulphide and minor amounts of silicate replacement. These processes are quantitatively insufficient to provide a mechanism for either generating the original sulphide body or concentrating the sulphides in their present position. It is concluded, therefore, that

Table 2 Mean sulphide metal contents and ratios of three Moxie Pluton sulphide occurrences and Katahdin sulphide body. Two sets of values shown for latter body derived from results of this study and Superior Mining Company assay data. Compositions compared with 'typical' Sudbury data from Naldrett.[26] Standard errors of mean shown in brackets

	Moxie Pluton			Katahdin		
	Black Narrows	Burnt Nubble	Big Indian Pond	This study	Superior assay data	'Typical' Sudbury
n	10	5	8	8	84	—
Ni	1.87 (0.41)	0.44 (0.04)	0.84 (0.08)	0.152 (0.015)	0.209 (0.004)	3.5–6.0
Cu	0.72 (0.22)	0.32 (0.07)	0.65 (0.11)	0.097 (0.022)	0.103 (0.003)	3.5–4.5
Co	0.22 (0.04)	0.13 (0.01)	0.16 (0.01)	0.091 (0.003)	0.178 (0.004)	0.15–0.22
Cu/Cu+Ni	0.28	0.42	0.44	0.37	0.33	0.3–0.5
Ni/Co	8.50	3.40	5.30	1.66	1.18	20.35
Ni/Ni+Fe	0.031	0.007	0.014	0.0024	0.0034	0.05–0.08

the sulphides throughout the intrusion accumulated as an immiscible sulphide liquid in the magmatic environment, late magmatic remobilization accounting for the textures and position of the massive sulphide body. The mean Ni, Cu and Co data for 100% sulphide from eight samples collected for this study are compared with the mean Superior Mining Company assay data, also converted to 100% sulphide, and the typical range of values of Sudbury deposits (Table 2). Although the eight samples examined are not totally representative in relation to the assay data, both sets of data clearly indicate the extremely depleted Ni and Cu and relatively normal Co contents of these sulphides in comparison with the Sudbury range. Normal Zn values and extremely low levels of PGE and Au relative to Sudbury were encountered[41] and are consistent with the observations on the Moxie Pluton.

Source of sulphur

Moxie Pluton

Mining companies that worked in the vicinity of the Moxie Pluton sulphide occurrences noted the presence of a sulphide-bearing country rock at or close to the contact of the Moxie Pluton at all three mineralized localities. The relationship between this country rock, the Hildreths Formation, and the Moxie Pluton is shown in Fig. 5, which is drawn on the basis of limited outcrop and aeromagnetic studies.[3,4,24] Fig. 5 demonstrates the very strong spatial correlation between sulphide

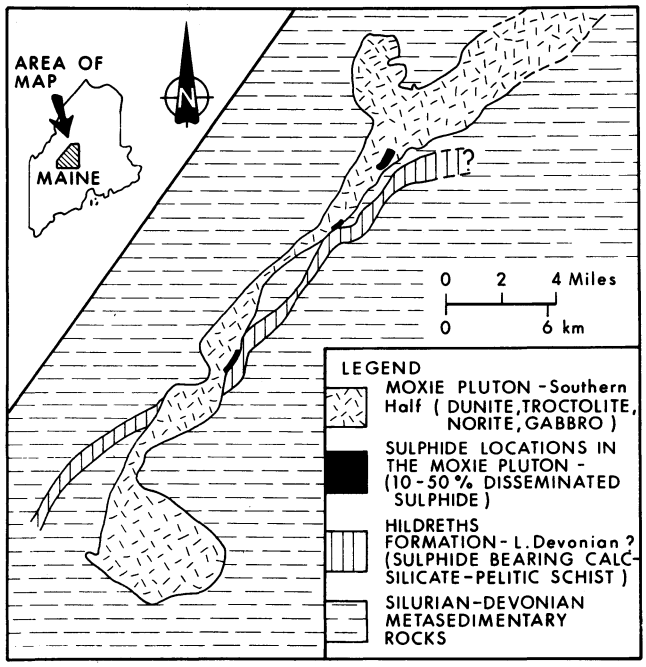

Fig. 5 Relationship between Hildreths Formation and Moxie Pluton as indicated by outcrop and aeromagnetic investigations

mineralization and the presence of the Hildreths Formation and suggests that at least a component of sulphur in the intrusion may have been derived from this formation. Sulphur isotope analyses (Fig. 6) clearly support this inference. The light isotopic character of the sulphur in all three localities is clearly non-magmatic and correlates with the isotopic character of sulphur in the Hildreths Formation. The range of values at the different localities suggests that the largest proportion of country rock sulphur was assimilated at Burnt Nubble and the least amount at Big Indian Pond.

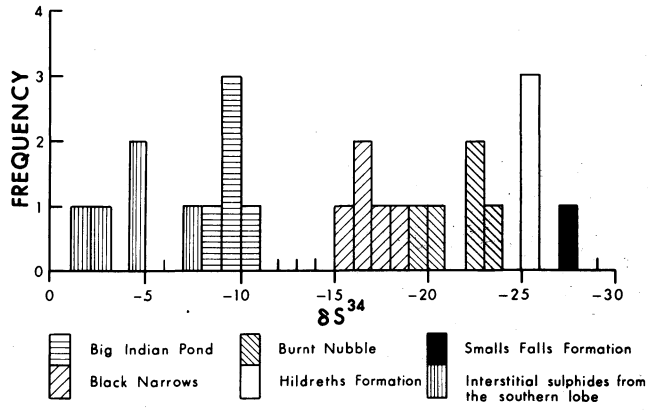

Fig. 6 Sulphur isotope results from Moxie Pluton sulphide occurrences and interstitial sulphides from southern lobe compared with results from Hildreths Formation

The Hildreths Formation is a pyrite-bearing banded pelite and laminated calc–silicate. Close to the intrusion the formation undergoes a number of changes: (1) the rock is contact metamorphosed and mechanically disrupted, competent calc–silicate fragments floating in a pelitic matrix; (2) xenoliths of the Hildreths Formation are included in the intrusion; (3) the modal sulphide content decreases from around 10 to 5% or less; and (4) the sulphide mineralogy becomes pyrite–pyrrhotite with additional minor amounts of magnetite.

On the basis of these observations, temperature–pressure conditions indicated by the contact aureole silicate mineralogy and theoretical determination of the expected range of oxygen and sulphur fugacities in the magma and country rock, Thompson[41] suggested a sulphur assimilation mechanism that involved the thermal breakdown of pyrite and the diffusion of H_2S into the magma. The available evidence supports a sulphur-specific mechanism. Xenolith content is insufficient to provide the major sulphur source and shows no local relationship to sulphide content. In addition, petrographic observations indicate that the xenoliths did not contribute greatly to the process.[41]

Sulphur isotope analyses of minor interstitial sulphides from the southern lobe of the Moxie Pluton, also shown in Fig. 6, cover a range of slightly negative values. The least negative values correspond to the most primitive olivine cumulates in

this part of the intrusion, which suggests that the original magma may have been virtually sulphur-saturated with primary magmatic sulphur. Sulphur may have been assimilated to the southern lobe, which gave rise to the more negative isotopic values. This sulphur could have been derived from a second sulphide-bearing country rock—the Smalls Falls Formation—the presence of which at depth in the vicinity of the pluton is indicated by regional structure.

Katahdin

The strong evidence for sulphur assimilation at the Moxie Pluton raises the question of whether a similar origin also applies to the Katahdin sulphides. Sulphur isotope analyses from sulphides in a number of places throughout the Katahdin

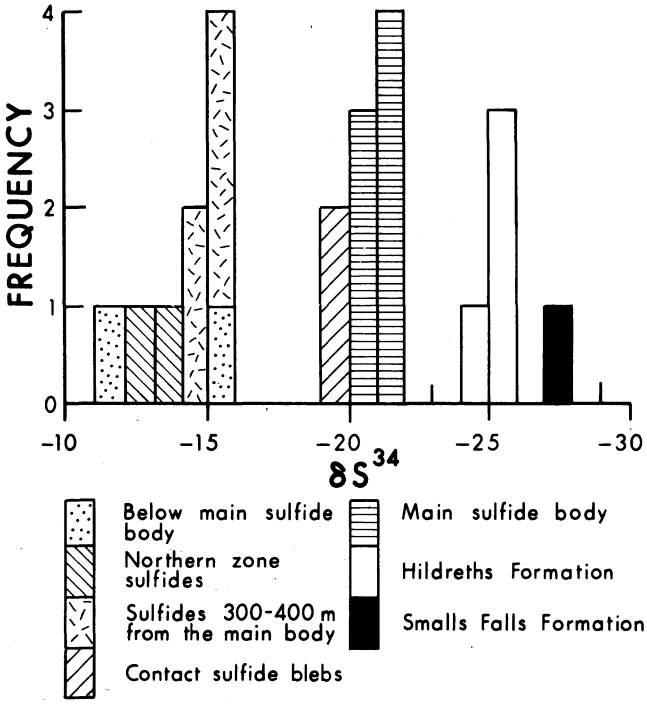

Fig. 7 Sulphur isotope results from sulphides throughout Katahdin gabbro compared with results from Hildreths and Smalls Falls Formations

gabbro are shown in Fig. 7. The very light isotopic character, particularly in the main sulphide body, is clearly non-magmatic and correlates well with the sulphur isotopic composition of sulphides from the Hildreths and Smalls Falls Formations. Although neither of these formations outcrops around the Katahdin gabbro, both may be present at depth. Sulphur assimilation at depth is indicated independently by the presence of sulphide blebs in the marginal gabbro that also contains isotopically light sulphur (Fig. 7) and suggests sulphur saturation prior to intrusion.

Discussion

Sulphur assimilation is clearly documented in the Moxie Pluton, supported by field relations and sulphur isotope analyses. Rigorous modelling of the assimilation mechanism is not possible because of the numerous uncertainties about the variables that are involved in the model—in particular, the diffusivities of the sulphur-bearing species. The volume of sulphide in the Katahdin gabbro demands assimilation of a mass of sulphur between 1.2×10^{11} and 9.8×10^{11} kg.[41] This requires removal of 50% of the pyrite from a typical 500-m thick sulphide-bearing unit intersected by the intrusion, sulphur removal occurring over a distance of between 125 and 2200 m, depending on the dip of the formation. This indicates the relative efficiency of the assimilation process.

The sulphur isotope data have been compared with S/Se

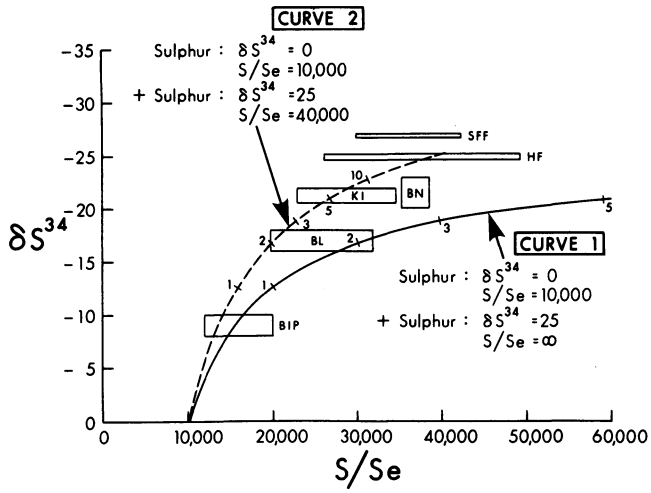

Fig. 8 Plot of S/Se ratios against sulphur isotopic composition of Moxie Pluton sulphide occurrences: Big Indian Pond (BIP), Burnt Nubble (BN), Black Narrows (BL); Katahdin sulphide body (Kl); Hildreths Formation (HF) and Smalls Falls Formation (SFF). Region of analyses for each occurrence given by box. Ideal calculated mixing curves shown and described in text

ratios for the three Moxie Pluton sulphide occurrences and the Katahdin sulphide body (Fig. 8). Magmatic S/Se ratios commonly fall below 10 000 (cosmic abundance = 7000[44]), whereas sedimentary sulphides have higher S/Se ratios. The resultant contrasting geochemical behaviour of S and Se has been described previously.[14,20] S/Se ratios of the sulphides from these examples and the sedimentary formations all fall above 10 000 and are shown as a range compared with the range of $\delta^{34}S$ values in Fig. 8.

Two ideal mixing curves are also shown in Fig. 8: curve 1 was constructed on the basis of the addition of sulphur alone of the isotopic composition of the Hildreths Formation, and curve 2 was constructed by adding sulphur of the same isotopic composition and selenium with a S/Se ratio of 40 000—the mean composition of the Hildreths Formation. Both curves assume an initial magmatic $\delta^{34}S = 0$ and S/Se = 10 000. In theory this approach should provide a means to distinguish between the assimilation of sulphur alone and sulphur + selenium, though in this case the scatter in the observed S/Se ratios is too great to allow any firm conclusion to be drawn. Calculation of the mixing curves does, however, provide an estimate of the proportion of sulphur added to a component of original magmatic sulphur at the different localities under these model conditions. Our conclusions are that the proportions of non-magmatic sulphur are 33–41% at Big Indian Pond, 64–71% at Black Narrows and 80–91% at both Burnt Nubble and Katahdin.

Ni contents of olivine

Igneous olivines typically contain a certain amount of nickel that varies systematically with the forsterite content of the olivines, thereby providing a potential indicator of fractionation. Experimental studies have shown that nickel partitions into olivine relative to the silicate magma, though the degree of partitioning is dependent on *T*, *P* and melt composition.[1,9,17,19,25] The chalcophile nature of nickel results in the strong partitioning of nickel into sulphide relative to silicate liquid[34] and into sulphide relative to olivine.[2] As a result the presence of sulphide in a mafic intrusion that crystallizes olivine should have an effect on the nickel content of the olivine, depending on the amount of sulphide that precipitates.

The nickel contents of olivine were determined by electron microprobe by use of wavelength-dispersive analysis. Thompson[41] indicated detection limits below 100 ppm NiO and precision better than 75 ppm. Major-element concentrations were

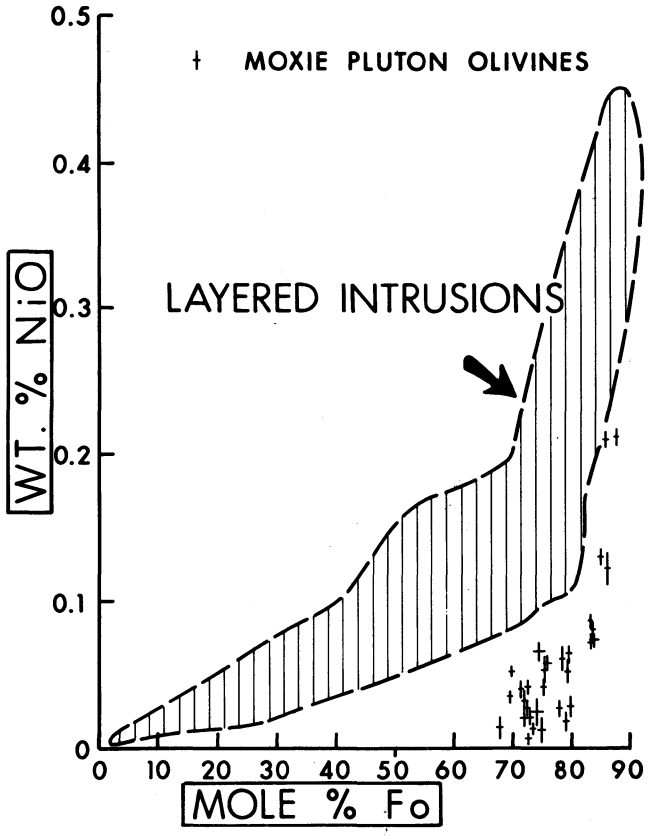

Fig. 9 Composition of Moxie Pluton olivines compared with typical layered intrusions (Simkin and Smith[39]). Error bars represent one standard deviation

determined by EDA microprobe techniques.

The compositions of the Moxie Pluton olivines are illustrated in terms of their NiO and forsterite content in Fig. 9. The area that is occupied by olivines from mafic layered intrusions is also shown for comparison (data from Simkin and Smith[39]). This plot demonstrates the marked depletion of the Moxie Pluton olivines, nickel contents dropping rapidly from values around 2200 ppm NiO at Fo_{88} in the most primitive olivine cumulates of the southern lobe to values typically well below 1000 ppm NiO for less forsteritic olivines. The low Ni/forsterite ratios and the apparent fractionation trend of rapidly decreasing NiO with decreasing forsterite results from the fractional removal of sulphide, as indicated by the presence of minor magmatic sulphides throughout the intrusion. The composition of the Katahdin olivines is shown in a similar diagram (Fig. 10), the areas occupied by layered intrusions and the Moxie Pluton being shown for comparison. The Katahdin olivines are extremely depleted, Ni/forsterite ratios falling below those in the Moxie Pluton and, thus, demanding the interaction of the crystallizing Katahdin magma with larger volumes of sulphide. The range of Katahdin olivine composition does not document fractional crystallization and the uniform low Ni/forsterite ratios throughout the intrusion suggest that at least partial equilibration of sulphide liquid and silicate magma was achieved prior to intrusion. This is consistent with the evidence indicating early sulphur assimilation and sulphur saturation.

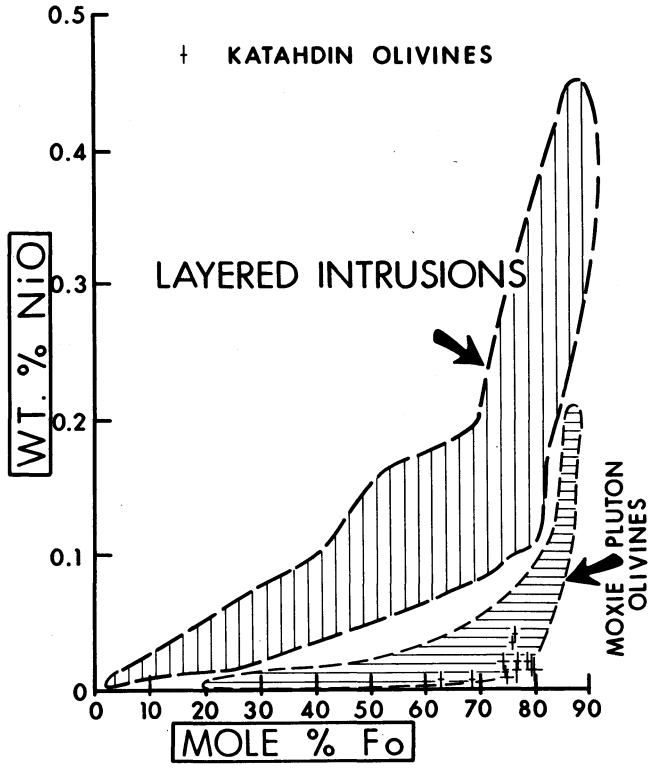

Fig. 10 Composition of Katahdin gabbro olivines compared with typical layered intrusions[39] and Moxie Pluton. Error bars represent one standard deviation

Magmatic models

Any magmatic model for the Moxie and Katahdin intrusions and their sulphides must attempt to explain the low nickel and copper contents of the sulphides, the low Ni/forsterite ratio and the role of sulphur assimilation. Two types of magmatic processes have been invoked to explain a number of magmatic sulphide deposits in the past—the fractional segregation of variable amounts of sulphide and batch equilibration of sulphide at varying magma to sulphur ratios.[28-30] Both processes apply in the context of the Moxie Pluton and the Katahdin gabbro.

Moxie Pluton

Two magma compositions have been selected from different tectonic environments (Table 3) and assigned arbitrary Ni, Cu and Co contents. The magma compositions were constrained only by the need to crystallize olivine more forsteritic than Fo_{88} according to the Roeder and Emslie[36] relationship. Fractional crystallization of these magma compositions was simulated by an adapted version of the Duke[8] computer program. Modifications (by J. M. Duke) include the fractional crystallization of plagioclase with the appearance of plagioclase in the model set

Table 3 Two magma compositions selected for modelling fractional crystallization by computer simulation

	I	II
SiO_2	49.10	49.17
TiO_2	1.50	0.82
Al_2O_3	13.50	15.58
Fe_2O_3	1.60	—
FeO	9.00	8.82*
MnO	0.15	0.15
MgO	12.80	11.40
CaO	7.90	12.01
Na_2O	3.03	1.87
K_2O	1.03	0.11
P_2O_5	0.36	—
Ni, ppm	350 (364)	350 (257)
Cu, ppm	80 (N.D.)	80 (82)
Co, ppm	50 (56)	50 (52)

I, Adapted from primitive continental tholeiite composition.[13]
II, Primitive MORB composition used by Duke.[8]
Ni, Cu and Co values not those designated in analyses and arbitrarily set at these values. Original values shown in brackets.
*Total Fe as FeO.

at the point in the crystallization of the magma at which olivine reached the composition of Fo_{80} (consistent with petrographic observations). Pyroxenes do not appear to be an important liquidus phase and were excluded from this model. The results of the computer-simulated fractional crystallization of these magmas are shown in Fig. 11 in terms of the Ni content of olivines relative to their forsterite content. Crystallization was modelled by the fractionation of olivine + plagioclase alone and also by the fractionation of olivine + plagioclase + sulphide at olivine to sulphide ratios of 100:1 and 50:1.

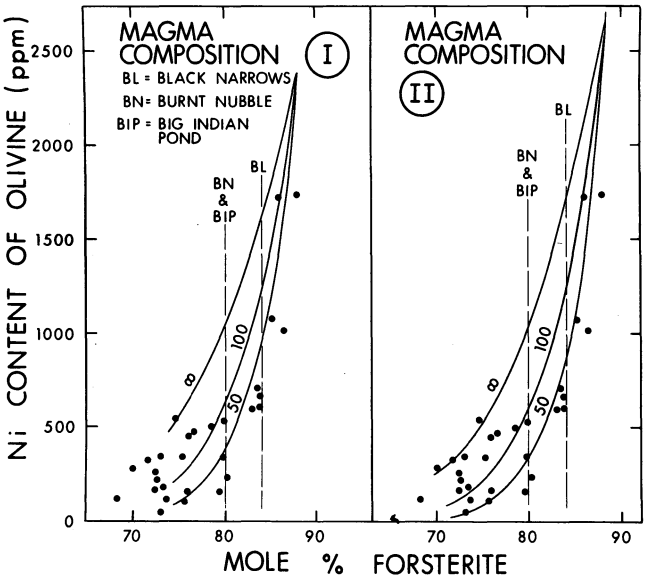

Fig. 11 Computed fractionation of mafic magma in terms of its olivine composition, fractionation being carried out at three olivine to sulphide ratios. Moxie Pluton olivine compositions shown: position of the three sulphide occurrences shown as indicated by their olivine compositions

The composition of the Moxie Pluton olivines is shown in Fig. 11: although representative of a range of values, they all fall consistently within the area predicted by sulphide fractional removal from these magmas. A perfect match between olivine composition and a single curve representative of a specific olivine/sulphide ratio is not to be expected because of the variability of olivine analyses and the simplification involved in a computer-simulated fractional crystallization of a single mass of magma. The complex form of both intrusions is interpreted to have resulted partially from multiple injection[41]—a process not accounted for in the computer modelling.

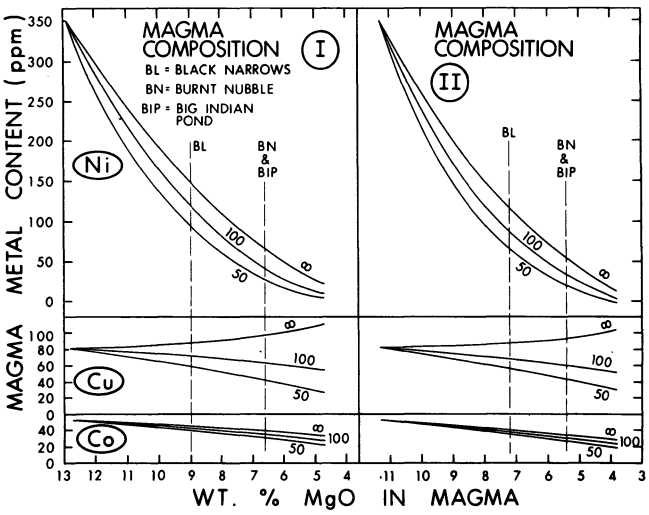

Fig. 12 Computed fractionation of mafic magma in terms of its Ni, Cu and Co contents. Three Moxie Pluton sulphide occurrences shown as indicated in Fig. 11

Table 4 Range of silicate magma metal contents (ppm) indicated for three Moxie Pluton sulphide occurrences by fractional crystallization models

	Black Narrows	Burnt Nubble and Big Indian Pond
Ni	75–150	25–65
Cu	50–80	40–80
Co	34–40	27–35

The composition of the silicate magma that is undergoing the model fractional crystallization is indicated in Fig. 12. The ranges of silicate magma metal contents in equilibrium with the olivine composition at the three sulphide localities are derived from this diagram and listed in Table 4.

Sulphur isotope analyses and S/Se ratios from the three Moxie Pluton sulphide occurrences suggest a variable component of assimilated sulphur at the different localities (Fig. 8). If equilibration between the resultant immiscible sulphide liquid and the silicate magma was restricted, variable magma to sulphide ratios would result that showed some correlation to the proportion of assimilated sulphur. Campbell and Naldrett[7] predicted the effects of varying the magma to sulphide ratio according to the relationship

$$Y_i = \frac{X_{i(o)} \cdot D_i^{Sul/Sul} \cdot (R+1)}{(D_i^{Sul/Sil} + R)}$$

where Y_i is the chalcophile metal content of the sulphide, $X_{i(o)}$ the initial metal content of the sulphide, R the magma to sulphide ratio and $D_i^{Sul/Sil}$ the sulphide–silicate partition coefficient for the metal, i. This relationship is valid for sulphide precipitating with sulphur of magmatic origin. For the addition of sulphur the relationship is modified:

$$Y_i = \frac{X_{i(o)} \cdot D_i^{Sul/Sul} \cdot (R)}{(D_i^{Sul/Sil} + R)}$$

Varying magma to sulphide ratios have been applied to the Moxie Pluton to generate the observed sulphide compositions from the predicted metal contents of the silicate magma shown

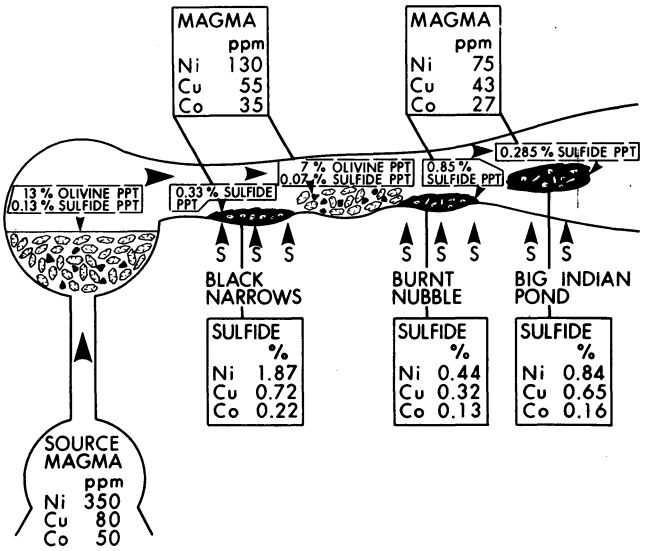

Fig. 13 Summary magmatic model for Moxie Pluton sulphide occurrences. Model involves two phases of olivine + sulphide fractionation and use of particular magma to sulphide ratios at individual sulphide occurrences, set to generate indicated sulphide compositions

in Table 4. The combined use of these two processes is schematically summarized in Fig. 13. According to this model, the magma is intruded and undergoes olivine + sulphide removal, generating a silicate magma with a depleted chalcophile metal content. This depleted magma then equilibrates with additional sulphide at Black Narrows at a magma to sulphide ratio set specifically to generate a sulphide composition close to that observed. The magma undergoes a second phase of olivine + sulphide removal, further depleting the chalcophile metal content. The magma composition equilibrates with sulphide at Burnt Nubble and Big Indian Pond—again at specific magma to sulphide ratios set to generate the sulphide compositions close to those observed at these localities. The magma to sulphide ratios are indicated by the amount of sulphide that precipitates. The lowest magma to sulphide ratio is indicated at Burnt Nubble and the highest at Big Indian Pond, which is consistent with the suggested variable volume of assimilated sulphur indicated by sulphur isotopes and S/Se ratios.

The sequence of events outlined in Fig. 13 is one example of a magmatic model suitable for the generation of the observed sulphide compositions. A number of variations could have been included. The existing model is, however, consistent with the following observations: (1) the general trend of fractionation within the southern half of the Moxie Pluton; (2) the ubiquitous presence of small amounts of sulphide in the early cumulates; (3) the low Ni/forsterite ratios of the olivines and the observed olivine fractionation; (4) the degree of fractionation at the different sulphide localities (this is indicated by the olivine compositions, the appearance of plagioclase at Burnt Nubble and Big Indian Pond (Table 1) and the lower Cu/(Cu+Ni) ratio of the Black Narrows sulphides (Table 2)); (5) the depleted Ni and Cu contents of the sulphides and the relatively typical Co content; and (6) the very low Ni and Cu contents of the Burnt Nubble sulphides.

The magmatic processes that are involved in this model have a greater influence on the sulphide Ni and Cu contents than that of Co because of the higher and similar partition coefficients of the former elements.[34] It is expected, therefore, that these processes will have an even greater effect in reducing the PGE and Au contents of these sulphides owing to their very strong chalcophile tendencies. The extremely low levels of these elements are qualitatively consistent with these models. Conversely, Shimazaki and MacLean[38] suggested a sulphide–silicate partition for zinc close to one, and thus magmatic sulphide–silicate interaction should not influence the sulphide zinc content. Again, the zinc contents of the Moxie Pluton sulphides are consistent with these arguments.

Katahdin gabbro

The limited range of mineral compositions in the Katahdin gabbro prohibits the development of a fractional crystallization model. The particularly unusual sulphide composition of the Katahdin sulphide body does, however, demand an earlier phase of sulphide removal. The particularly low Ni and Cu contents and the relatively high Co content cannot be generated by a single batch equilibration event unless the magma Co content was higher than its Ni content. This would also demand an unreasonably low magma to sulphide ratio even in comparison with the volume of sulphide present in this intrusion. Thus, sulphide fractional removal at depth, with subsequent batch equilibration, is postulated and schematically shown in Fig. 14.

In the model a magma of the same composition as that which was used for the Moxie Pluton undergoes fractional crystallization with the removal of olivine + sulphide. The olivine to sulphide ratio (20:1) is considerably lower than that invoked for the Moxie Pluton and results in the removal of a large proportion of the chalcophile metals and the generation of a magma with higher Co than Ni. This magma then undergoes batch

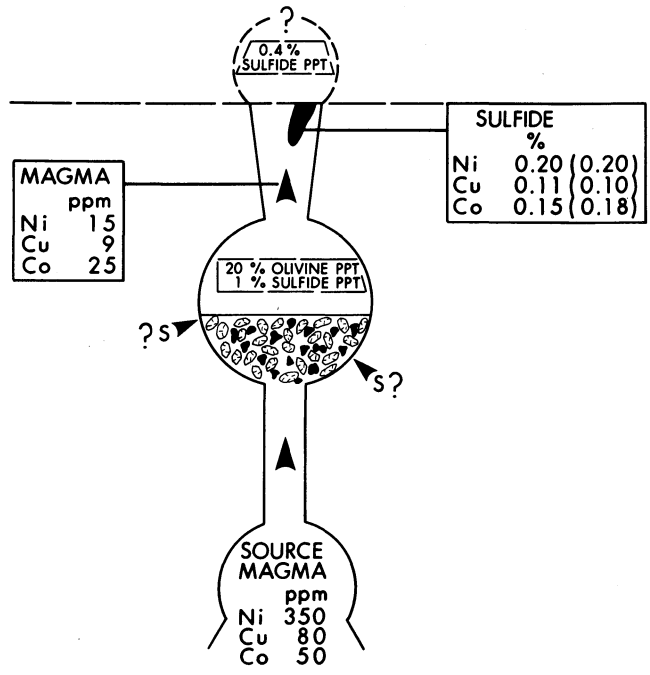

Fig. 14 Possible magmatic model for Katahdin sulphide body involving olivine + sulphide fractionation at depth and batch equilibration. Values shown in brackets are mean values of Katahdin sulphide body from assay data

equilibration—again at a specified magma to sulphide ratio—these sulphides segregating to form the sulphide body of a composition close to that which is observed. The magma to sulphide ratio that has been assumed for the batch equilibration (250:1) is reasonable in terms of volume of sulphide present in this small intrusion. As with the Moxie Pluton, this is just one of a number of possible magmatic models. The model is, however, constrained by the particularly unusual (low Ni and Cu, high Co) sulphide composition and is consistent with the following: (1) the very low Ni/forsterite ratios in olivine indicating crystallization from a Ni-depleted magma: the range of NiO contents (70–400 ppm) suggests equilibration with magmas of Ni contents between 5 and 40 ppm as determined from the partition coefficient for nickel between olivine and silicate liquids—a range consistent with the model; (2) the evidence indicating fractional crystallization at depth, i.e. the lower forsterite content of the most primitive olivines compared with those of the Moxie Pluton; and (3) the evidence favouring sulphur assimilation and sulphide saturation at depth.

Implications for exploration

The sulphide occurrences that have been described in this paper represent documented examples of magmatic sulphides. The considerable compositional variability between the sulphide occurrences is attributed to their having formed under different and unusual circumstances. These circumstances have had a marked effect on the composition of the host silicate magmas. The understanding of these sulphide accumulations and their relationship to their host rocks has both local and general exploration significance.

Sulphur assimilation

The relationship between sulphide mineralization in the Moxie Pluton and the Hildreths Formation is clearly important. Sulphur assimilation has been documented in a number of other sulphide-bearing mafic intrusions, e.g. the Duluth complex[23,35] the Bushveld intrusion[6,21] and the Noril'sk deposits.[18,40] Together, these deposits constitute a major resource of magmatic Ni–Cu–Co–PGE. Naldrett and Macdonald[31] emphasized the importance to exploration of consideration of the

source of sulphur and the potential reaction of mafic magmas with supracrustal rocks. The Moxie Pluton examples illustrate localized assimilation that has failed to generate significant sulphide accumulations. The Katahdin sulphide body, however, demonstrates the potential efficiency of this process. Unfortunately, in this case it has been shown that assimilation of excess sulphur in the Katahdin gabbro has effectively diluted the original chalcophile metal content of the magma to such an extent that the Ni + Cu concentrations of the resulting mineralization are sub-economic. The sulphur assimilation process is, however, clearly a viable means of generating economic magmatic sulphides and the relationship between mafic intrusions and sulphur-bearing supracrustal rocks should be considered during exploration.

Ni content olivines

The Ni content olivines have been used extensively in this study to determine the extent and timing of sulphide–silicate interaction. In addition, the understanding of the effects of sulphide–silicate interaction through the Ni content of olivines provides a means of assessing the potential of a mafic intrusion to host magmatic sulphides. Low olivine Ni/forsterite ratios indicate a low magma chalcophile metal content. This may have three implications: (1) if the Ni/forsterite ratio is uniformly low, the intrusion is an unlikely host for economic magmatic sulphides; (2) if sulphides are not present associated with the olivines, it is likely that sulphides may have accumulated at a lower stratigraphic level within the intrusion; and (3) a localized region of low Ni/forsterite ratios may indicate the presence of a hidden sulphide body in that part of the intrusion.

The Moxie Pluton illustrates these points, the evidence suggesting that higher-tenor sulphides may occur only within the more primitive rocks of the southern lobe. This suggestion is, in itself, an illustration of the power of the Ni/forsterite ratios of olivine. A limited number of olivine compositions throughout a mafic intrusion is all that is required to assess the possibility of sulphide saturation, but more detailed analytical work is needed to assess the potential of individual areas within the intrusion.

Table 5 Relationship between mean Ni content of sulphides in central Maine occurrences and Ni content of magma and olivine in equilibrium with sulphide. Predictions made with use of simple Nernst partition coefficients shown. Observed olivine Ni contents shown for comparison

	Ni (sulphide), determined	Ni (magma), predicted	Ni (olivine), predicted	Ni (olivine), observed
Black Narrows	18700	68	612	260–700
Burnt Nubble	4400	16	144	160–170
Big Indian Pond	8400	31	275	160–320
Katahdin	2000	7	65	70–170

$D_{Ni}^{Sul/Sil} = 275.$[34]
$D_{Ni}^{Ol/Sil} = 9.$[1]

The Ni content of olivines has another important use: it is possible to calculate the predicted nickel contents of the silicate magma and olivine, in equilibrium with this magma, from the mean sulphide composition by use of simple partition coefficients. For the Moxie Pluton and Katahdin sulphide bodies there is a marked correlation between predicted and observed values (Table 5). Similar results are obtained by use of the Ni partition coefficient between olivine and sulphide.[2] This relationship may be applied in reverse. The measured Ni content of olivines should indicate the potential Ni content of sulphides in equilibrium with these olivines. Clearly, very low Ni contents in olivine severely limit the potential Ni grade of any magmatic sulphide accumulation associated with those olivines, assuming that the olivine compositions represent equilibrium with sulphide under magmatic conditions. This may provide a simple and cheap means of assessing the overall economic potential and, if a number of olivine compositions are determined, the degree of homogeneity within a sulphide body. In either case a number of olivine determinations should be obtained in and around the sulphides to provide a statistically representative sample and the clearest indication of the potential.

Conclusions

The most important findings of this study are summarized below.

(1) Synorogenic mafic intrusions represent an important class of mafic rocks in the Appalachian–Caledonian orogenic belt. Many of these intrusions contain variable amounts of sulphide.

(2) The Moxie Pluton is a complex and irregular mafic body intruded during the Acadian orogeny. Layering features and regular differentiation are absent, but the full compositional range illustrates a fractionation trend similar to those of other mafic intrusions.

(3) The Katahdin gabbro is compositionally and texturally similar to the Moxie Pluton, though it represents a restricted range of fractionation.

(4) Both intrusions were formed by the injection of variably fractionated magmas into irregular magma chambers and feeder zones.

(5) The southern half of the Moxie Pluton contains three small sulphide accumulations, and the Katahdin gabbro contains an enormous sulphide body. Textural evidence indicates the magmatic origin of these sulphides. The composition of these sulphides is, however, highly impoverished in Ni and Cu relative to other magmatic sulphide deposits. In contrast, the Co contents are typical.

(6) Field relations, isotopically light sulphur and high S/Se ratios demonstrate that the majority of sulphur in the Moxie Pluton sulphide occurrences was derived by local assimilation from the Hildreths Formation. Similar sulphur isotopes and S/Se ratios from the Katahdin sulphides demand a similar sulphur source at depth.

(7) The Ni/forsterite ratios in olivines from both intrusions are low and suggest sulphide–silicate interaction during the crystallization of the magmas. The range of olivine compositions in the Moxie Pluton indicates the fractionation of sulphide and is suitable for computer-simulated modelling.

(8) Internally consistent magmatic models that involve sulphide fractional crystallization and batch equilibration adequately explain the Moxie Pluton and Katahdin gabbro sulphide compositions.

(9) The determination of olivine compositions in a mafic or ultramafic intrusion provides a means of assessing the role of sulphides during crystallization and the potential for that intrusion to host economic sulphides.

(10) The Ni content of olivines may also provide a means of determining the Ni grade of sulphides in equilibrium with these olivines by the application of experimental partition data.

(11) The correlation between the observed Ni content of olivines and those predicted from the sulphide composition by use

of experimental partitioning data is further justification for magmatic modelling. Calculated natural exchange partition coefficients for Fe and Ni between sulphide and olivine fall in the range from 4 to 11.[41] These are slightly lower than the value that was experimentally determined by Boctor,[2] but they are sufficiently close to add more weight to the magmatic arguments presented in this paper.

Acknowledgement

We thank the Superior Mining Company for granting permission to study and sample the Katahdin Iron Works drill core. In particular, we thank Paul Lapierre and also acknowledge the late Berkeley Wycoff, who helped initiate the project and provided enthusiastic support in the early stages of the research. We also thank Exxon Minerals, the Scott Paper Company and the International Paper Company, which granted permission to study and sample Big Indian Pond and Burnt Nubble drill core and map the Moxie Pluton in these areas.

Research support was provided by Geological Society of America research grants 2745-80, 2547-79 and 2401-78 to the senior author and by National Research Council of Canada operating grant A4244 to the second author.

References

1. Arndt N. T. Partitioning of nickel between olivine and ultrabasic and basic komatiite liquids. *Yb. Carnegie Instn Wash.*, **76,** 1976–77, 553–7.
2. Boctor N. Z. Partitioning of nickel between olivine and iron monosulfide melts. *Yb. Carnegie Instn Wash.*, **80,** 1980–81, 356–9.
3. Bromery R. W. and Natof N. W. Aeromagnetic map of the Forks quadrangle, Piscataquis and Somerset Counties, Maine. *Geophys. Invest. Map U.S. geol. Surv.* GP-485, 1964.
4. Bromery R. W. *et al.* Aeromagnetic map of the Greenville quadrangle and parts of the Sebec Lake quadrangle, Piscataquis and Somerset Counties, Maine. *Geophys. Invest. Map U.S. geol. Surv.* GP-335, 1963.
5. Buchanan D. L. and Nolan J. Solubility of sulfur and sulfide immiscibility in synthetic tholeiitic melts and their relevance to Bushveld-Complex rocks. *Can. Mineralogist,* **17,** 1979, 483–94.
6. Buchanan D. L. *et al.* The genesis of sulfide mineralization in a portion of the Potgietersrus Limb of the Bushveld Complex. *Econ. Geol.*, **76,** 1981, 568–79.
7. Campbell I. H. and Naldrett A. J. The influence of silicate : sulfide ratios on the geochemistry of magmatic sulfides. *Econ. Geol.*, **74,** 1979, 1503–6.
8. Duke J. M. Computer simulation of the fractionation of olivine and sulfide from mafic and ultramafic magmas. *Can. Mineralogist,* **17,** 1979, 507–14.
9. Duke J. M. Distribution of the period four transition elements among olivine, calcic clinopyroxene and mafic silicate liquids: experimental results. *J. Petrol.*, **17,** 1976, 499–521.
10. Duke J. M. and Naldrett A. J. A numerical model of the fractionation of olivine and molten sulfide from komatiite magma. *Earth Planet. Sci. Letters,* **39,** 1978, 255–66.
11. Espenshade G. H. Geology of the Moxie Pluton in the Moosehead Lake—Jo-Mary Mountain area, Piscataquis County, Maine. *Bull. U.S. geol. Surv.* 1340, 1972, 40 p.
12. Espenshade G. H. and Boudette E. L. Geology and petrology of the Greenville quadrangle, Piscataquis and Somerset Counties, Maine. *Bull. U.S. geol. Surv.* 1241-F, 1967, 60 p.
13. Frey F. A. Green D. H. and Roy S. D. Integrated models of basalt petrogenesis: a study of quartz tholeiites to olivine melilitites from southeastern Australia utilizing geochemical and experimental petrological data. *J. Petrol.*, **19,** 1978, 463–513.
14. Hatton H. Geochemistry of selenium: formation of ferroselite and selenium behavior in the vicinity of oxidizing sulfide and uranium deposits. *Geochim. cosmochim. Acta,* **41,** 1977, 1665–78.
15. Haughton D. R. Roeder P. L. and Skinner B. J. Solubility of sulfur in mafic magmas. *Econ. Geol.*, **69,** 1974, 451–67.
16. Hoffman E. L. *et al.* The determination of all the platinum group elements and gold in rocks and ore by neutron activation analysis after preconcentration by a nickel sulphide fire-assay technique on large samples. *Anal. chim. Acta,* **102,** 1978, 157–66.
17. Irvine T. N. and Kushiro I. Partitioning of Ni and Mg between olivine and silicate liquids. *Yb. Carnegie Instn Wash.*, **75,** 1975–76, 668–75.
18. Kovalenker V. A. Gladyshev G. D. and Nosik L. P. Isotopic composition of sulfide sulfur from deposits of Talnakh ore node in relation to their selenium content. *Int. Geol. Rev.*, **17,** 1975, 725–34.
19. Leeman W. P. and Lindstrom D. J. Partitioning of Ni^{2+} between basaltic and synthetic melts and olivine—an experimental study. *Geochim. cosmochim. Acta,* **42,** 1978, 801–16.
20. Leutwein F. Selenium, 34. In *Handbook of geochemistry* Wedepohl K. H. ed. (Berlin: Springer-Verlag, 1972), II-3, 34A–O.
21. Liebenberg L. The sulfides in the layered sequence of the Bushveld Igneous Complex. Ph.D. thesis, University of Pretoria, 1968.
22. MacLean W. H. and Shimazaki H. The partition of Co, Ni, Cu, and Zn between sulfide and silicate liquids. *Econ. Geol.*, **71,** 1976, 1049–57.
23. Mainwaring P. R. and Naldrett A. J. Country-rock assimilation and the genesis of Cu–Ni sulfides in the Water Hen intrusion, Duluth Complex, Minnesota. *Econ. Geol.*, **72,** 1977, 1269–84.
24. Mattick R. E. Aeromagnetic and generalized geological map of the Bingham quadrangle, Somerset County, Maine. *Geophys. Invest. Map U.S. geol. Surv.* GP-499, 1965.
25. Mysen B. O. Nickel partitioning between upper mantle crystals and partial melts as a function of pressure, temperature and nickel concentration. *Yb. Carnegie Instn Wash.*, **75,** 1975–76, 622–8.
26. Naldrett A. J. Nickel sulfide deposits: classification, composition, and genesis. *Econ. Geol. 75th anniversary vol.*, 1981, 628–85.
27. Naldrett A. J. A portion of the system Fe–S–O between 900 and 1080°C and its application to sulfide ore magmas. *J. Petrol.*, **10,** 1969, 171–201.
28. Naldrett A. J. and Duke J. M. Platinum metals in magmatic sulfide ores. *Science,* **208,** 1980, 1417–24.
29. Naldrett A. J. *et al.* The composition of Ni-sulfide ores, with particular reference to their content of PGE and Au. *Can. Mineralogist,* **17,** 1979, 403–15.
30. Naldrett A. J. *et al.* Compositional variation within and between five Sudbury ore deposits. *Econ. Geol.*, **77,** 1982, 1519–34.
31. Naldrett A. J. and Macdonald A. J. Tectonic settings of Ni–Cu sulphide ores. In *The continental crust and its mineral deposits* Strangway D. W. ed. *Spec. Pap. geol. Ass. Can.* 20, 1980, 633–57.
32. Newell W. R. Stratigraphy, structure and petrology of the Bingham quadrangle, west central Maine. M.Sc. thesis, Syracuse University, 1978.
33. Pfann H. D. Paleomagnetically determined structure of the Moxie Pluton in west-central Maine. *Geol. Soc. Am. Abstr.*, **10,** no. 2 1978, 80.
34. Rajamani V. and Naldrett A. J. Partitioning of Fe, Co, Ni and Cu between sulfide liquid and basaltic melts and the composition of Ni–Cu sulfide deposits. *Econ. Geol.*, **73,** 1978, 82–93.
35. Ripley E. M. Sulfur isotopic studies of the Dunka Road Cu–Ni deposit, Duluth Complex, Minnesota. *Econ. Geol.*, **76,** 1981, 610–20.
36. Roeder P. L. and Emslie R. F. Olivine–liquid equilibrium. *Contr. Miner. Petrol.*, **29,** 1970, 275–89.
37. Shima H. and Naldrett A. J. Solubility of sulfur in an ultramafic melt and the relevance of the system Fe–S–O. *Econ. Geol.*, **70,** 1975, 960–7.
38. Shimazaki H. and MacLean W. H. An experimental study on the partition of zinc and lead between the silicate and sulfide liquids. *Mineral. Deposita,* **11,** 1976, 125–32.
39. Simkin T. and Smith J. V. Minor-element distribution in olivine. *J. Geol.*, **78,** 1970, 304–25.
40. Tarasov A. V. Structural control of copper and nickel mineralization in Noril'sk I deposit. *Int. Geol. Rev.*, **12,** 1970, 933–41.
41. Thompson J. F. H. The intrusion and crystallization of mafic magmas, central Maine and genesis of their associated sulfides. Ph.D. thesis, University of Toronto, 1982.
42. Visher G. S. The geology of the Moxie Pluton, west-central Maine. Ph.D. thesis, Nothwestern University, 1960.
43. Faul H. *et al.* Ages of intrusion and metamorphism in the northern Appalachians. *Am. J. Sci.*, **261,** 1963, 1–19.
44. Cameron A. G. W. A new table of abundances of the elements in the solar system. In *Origin and distribution of the elements* Ahrens L. H. ed. (Oxford: Pergamon, 1968), 125–43.

Nickel sulphide mineralization in the Lick Fork prospect, Virginia, U.S.A.

Walter Wrightson Jr. B.S., M.S.
Jackson and Associates, Knoxville, Tennessee, U.S.A.
Kula C. Misra B.Sc., M.Tech., Ph.D.
Department of Geological Sciences, University of Tennessee, Knoxville, Tennessee, U.S.A.

Synopsis

The Lick Fork prospect shows appreciable nickel sulphide mineralization in a narrow, steeply dipping, layered sequence of metamorphosed hornblende peridotite, gabbro and hornblende gabbro, intrusive into the Pedlar Formation (charnockitic pyroxene granulite) of the Virginia Blue Ridge Complex (Precambrian). Rocks of the intrusion have equilibrated to granulite-facies metamorphism, as indicated by pervasive polygonal texture of silicate aggregates, development of biotite- and hornblende-preferred orientation, compositional equilibration of the silicate minerals, the Mg–Fe^{2+} (orthopyroxene–clinopyroxene) distribution coefficients (average 0.57), $(MgO + FeO + Fe_2O_3)/Al_2O_3$ ratios in orthopyroxenes, and Ti contents and Al(IV)/Al(VI) ratios of hornblendes.

The sulphides, consisting of pyrrhotite–pentlandite (with up to 4 wt% Co)–chalcopyrite–pyrite–marcasite–violarite–bornite–mackinawite, are virtually restricted to the ultramafic unit of the intrusion and constitute 20–30% of the samples of hornblende peridotite studied. Although the basal accumulation of the sulphides may suggest magmatic segregation, sulphide–silicate textures typical of sulphide liquid immiscibility are not present, even in the sparsely mineralized gabbro units. On the other hand, the transgressive and relict textures are strongly suggestive of replacement of the silicate minerals by sulphides. These include chalcopyrite ± pyrrhotite ± pentlandite (violarite) ± pyrite ±magnetite veins crosscutting silicates, sulphide penetration into silicates at silicate–sulphide contact zones, rounding of silicate grains against sulphide matrix, and islands of silicate minerals (olivine, hornblende, pyroxene, biotite) in sulphide masses. Metamorphic mobilization of pre-existing sulphides is a possibility, but involvement of post-metamorphic, hydrothermal fluids is suggested by the following features: paucity of annealing and deformation textures in the sulphides, replacement of metamorphic and deformed silicates, lack of differential sulphide mobilization and the common occurrence of sulphides along grain boundaries and triple junctions of polygonal silicate aggregates. The consistent association between sulphides and hydrothermal alteration products of silicates suggests that they are cogenetic. The hydrothermal fluids may have merely mobilized and concentrated the pre-existing, disseminated, magmatic sulphides, or there may have been significant addition of sulphides during this process. This question cannot be resolved unequivocally with the existing data.

The Lick Fork nickel (–cobalt) prospect consists of pyrrhotite–pentlandite–chalcopyrite mineralization in a small, 'layered' ultramafic–mafic intrusion, which is located in a high-grade (granulite-facies) metamorphic terrain of Precambrian age (Fig. 1). The intrusion is one of the very few gabbroic bodies in the Southern Appalachians with appreciable nickel sulphide mineralization. In terms of ore localization and mineralogy this occurrence appears somewhat similar to the nickel sulphide mineralization in many differentiated gabbroic intrusions, but the silicate–sulphide textural relations in the Lick Fork rocks are not characteristic of magmatic segregation of an immiscible sulphide–oxide melt. The main objective of this paper is to document the metamorphism and hydrothermal alteration of the host rocks and to relate the present distribution of sulphides to these postmagmatic processes.

Previous work

The Lick Fork deposit was mined prior to the Civil War for its iron contained in the pyrrhotite for production of 'copperas'. Subsequently, the property has been developed intermittently as a potential nickel orebody by Virginia Nickel Company, and since 1942 by individual owners. An open adit bears testimony to the past mining activity; the two shafts mentioned by Watson[47] have since been filled up.

Watson[47] emphasized an igneous origin for the rocks associated with the deposit—a dyke composed of ore-bearing 'gabbro' and a hanging-wall unit of 'olivine diabase', and intrusive into the surrounding 'pyroxene syenite'. Ross[42] considered the country rock to be quartz monzonite, which was recrystallized to granodiorite near the contact with the dyke, and the dyke to be composed of pyroxenite, pyroxene gabbro and mica-

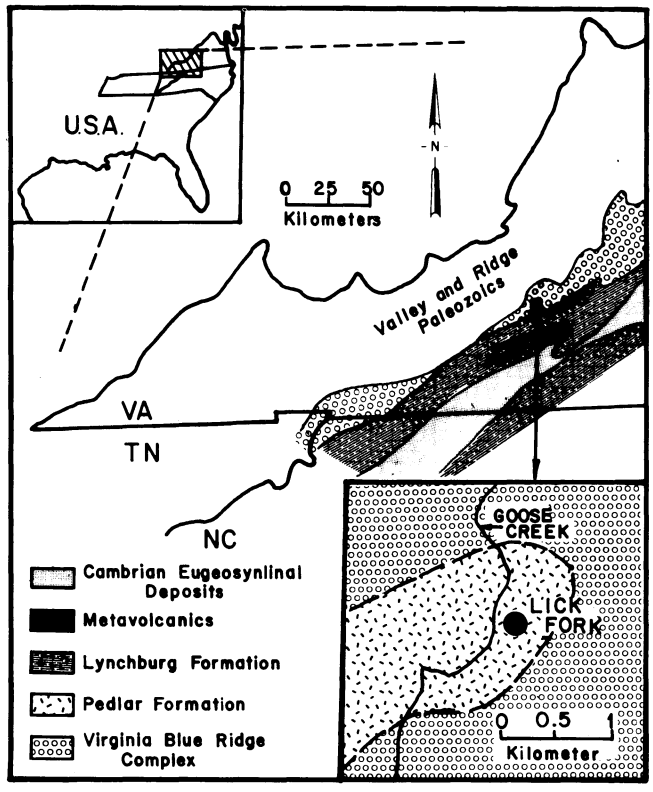

Fig. 1 Location map of Lick Fork Ni–Co prospect, Floyd Co., Virginia, and general geology of surrounding area. Regional geology of Blue Ridge belt in Virginia adapted from King and Beikman[29] and Milici and co-workers[34]

bearing pyroxene gabbro. According to him, the sulphide mineralization, mainly contained in the pyroxenite unit, resulted from hypogene processes associated with the dyke rocks. Recently, Craig and Higgins[11] discussed the violarites from this deposit. Based on the similarity of sulphide–silicate textures with those in disseminated ores of larger nickel sulphide deposits, such as that at Sudbury, Ontario, they suggested that the Lick Fork sulphides possibly formed from an immiscible sulphide melt.

Geologic setting

The Lick Fork nickel–cobalt sulphide deposit is hosted by a small mafic–ultramafic intrusion, which is located in the Blue Ridge belt of the southern Appalachians at the northeast corner of Floyd County, southwestern Virginia (37° 05′ N: 80° 12′ 30″ W) (Fig. 1). The intrusion occurs in a Precambrian high-grade (granulite-facies) metamorphic terrain, which has been mapped as the 'Virginia Blue Ridge Complex'[34] or 'Orthogneiss'.[29] The Blue Ridge Complex forms the older Precambrian crystalline basement in southwestern Virginia. To the northwest of the complex lie Palaeozoic sediments of the Valley and Ridge belt; rocks to the southeast of the complex include the younger Precambrian Lynchburg Formation (a stratified sequence of metasedimentary and metavolcanic rocks) and metavolcanics (probably equivalent of the Catoctin Greenstone), and a Cambrian sequence of eugeosynclinal deposits. The country rocks in the immediate vicinity of the intrusion consist of metamorphosed pyroxene syenite of charnockitic affinity (Pedlar Formation[7]) and gneisses of varying mineralogy, which may be correlatives of the Lovingston and Marshall Formations.[7] The Pedlar Formation is a hypersthene-bearing rock of felsic composition, characterized by granoblastic texture and foliation marked by pyroxene-rich streaks. The silicate assemblage comprises quartz, perthitic orthoclase, albite-rich plagioclase, orthopyroxene, and accessory biotite, zircon and garnet. The feldspar is partially sericitized, and the pyroxene is commonly altered to amphibole and epidote.

Lick Fork intrusion

Rock types

The Lick Fork body consists of three rock types: (1) hornblende peridotite, characterized by the presence of both olivine and hornblende, (2) gabbro, characterized by the absence of both olivine and hornblende, and (3) hornblende gabbro, characterized by the absence of olivine. Although the rocks of the intrusion as well as the enclosing rocks (alkali pyroxene syenite) have been metamorphosed, the igneous terminology is used throughout this paper for the sake of simplicity.

Field relations

The intrusion is exposed in an open adit (approximately 8 m × 6.5 m × 9 m) facing the Lick Fork Creek, and consists of almost vertical layers of ultramafic and mafic lithologies, which give it the appearance of a differentiated dyke (Figs. 2 and 3). Most of the samples used in this study were collected from the walls of this adit, mainly across the northern face (Fig. 3); some were also collected from the mine dumps. The geometry of the adit is not conducive to determination of the actual thickness of the intrusion, but Watson[47] mentioned a thickness of 8–10 m. The trend of the intrusion is parallel to the strike of foliation in the enclosing pyroxene syenite (N10°W), but the dip of the units is transgressive to the dip of syenite foliation (65°). The Lick Fork rocks usually show a weak but distinct foliation marked by preferred orientation of biotite. In addition, the hornblende gabbro often contains a gneissose banding owing to alternation of felsic-rich and mafic-rich streaks of about 3 cm across, and very localized preferred orientation of hornblende. Both the foliation and banding are conformable to the foliation in pyroxene syenite. The intrusive nature of the Lick Fork body is, however, clearly evidenced by the presence of numerous apophyses of peridotite and gabbro in the pyroxene syenite. Slickensides along the hanging-wall contact of the Lick Fork body and the

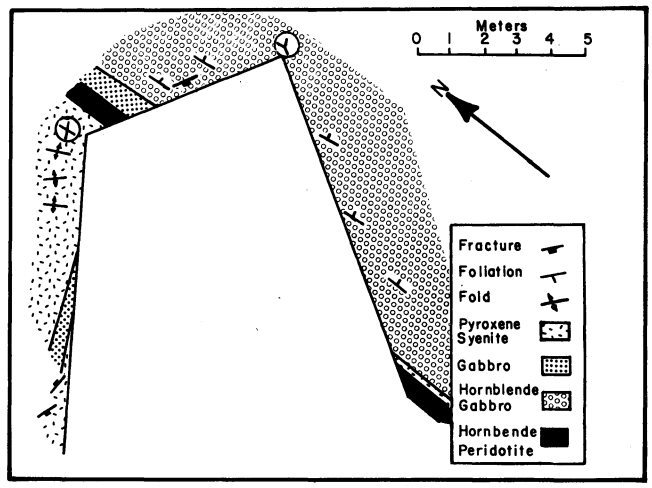

Fig. 2 Geological plan of Lick Fork adit

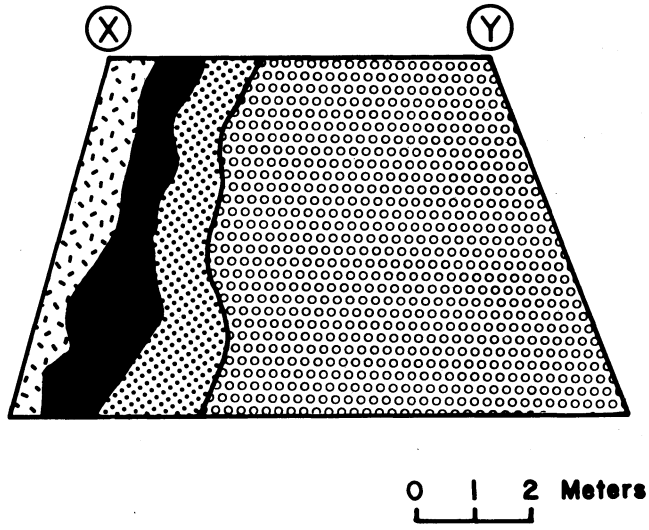

Fig. 3 North Face of Lick Fork adit (symbols for rock types as in Fig. 2)

pyroxene syenite suggest the presence of faulting. A fault contact is also supported by the fact that the pyroxene syenite at the contact is intensely sheared, as observed in thin sections.

Silicate petrology

The major 'primary' silicate minerals common to all the three lithologies include clinopyroxene (Cpx), orthopyroxene (Opx) and biotite (Bt). Modal analyses (Fig. 4) show a distinct variation in mineralogy among the lithologies. Olivine (Ol) is restricted to the hornblende peridotite. The plagioclase (Plag) content decreases significantly from the gabbro to the hornblende gabbro (there is no plagioclase in the hornblende peridotite), whereas there is a systematic increase in the clinopyroxene content from the hornblende peridotite to the hornblende gabbro. Hornblende (Hb), a major constituent of the hornblende peridotite and hornblende gabbro, is absent in the gabbro.

All the rocks of the intrusion are characterized by a dominantly polygonal-granoblastic texture of the major silicate minerals—hornblende, clinopyroxene, orthopyroxene and plagioclase (Fig. 5(*a*) and (*b*)). Development of foliation is limited to the local occurrence of mafic- and felsic-rich streaks

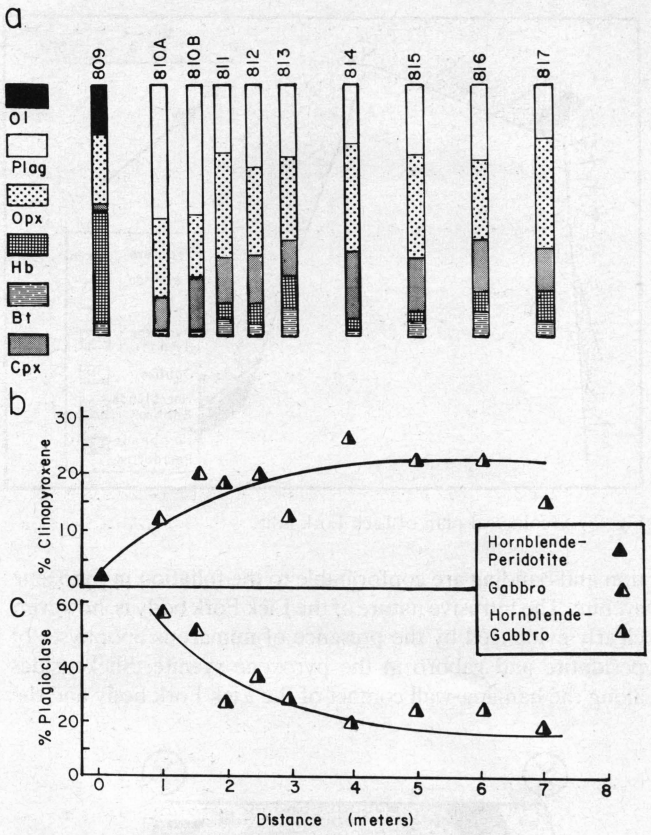

Fig. 4 Variation in silicate mineralogy across Lick Fork intrusion (North face, Fig. 3): (*a*) modal % silicates; (*b*) modal % clinopyroxene; (*c*) modal % plagioclase. Hydrothermal alteration of silicate phases not considered for modal analysis

in the gabbro and hornblende gabbro, and a crude, microscopic-scale, preferred orientation of biotite laths, especially in the hornblende gabbro (Fig. 5(*c*)). Occasionally, prisms of hornblende also show a dimensional preferred orientation in the hornblende gabbro.

Much of the olivine is altered to serpentine; the relict olivine at the core of large serpentinized grains shows an average composition of Fo_{77} without any zoning. The colour of hornblende varies from green-brown in the hornblende peridotite to brown in the hornblende gabbro, probably related to a corresponding variation in Ti from about 1.2 to more than 2 wt% of TiO_2. The hornblende is of two textural varieties without any discernible compositional difference between them—'primary' hornblende (Fig. 5(*a*)), which is polygonal, strongly pleochroic and deformed (undulose extinction), and 'secondary' hornblende, an alteration product of clinopyroxene, which may rim pyroxene grains or occur along their cleavage planes. The hornblende compositions form a fairly tight cluster, the average Mg/(Mg + Fe) ratio varying from 0.79 in the hornblende peridotite to about 0.75 in the hornblende gabbro. The clinopyroxene compositions ($Wo_{42-47}En_{40-45}Fs_{7-17}$) fall within the augite field of the pyroxene quadrilateral (Fig. 6). Inclusions of green spinel (pleonaste) as small, orientated platelets in clinopyroxene are abundant in the hornblende peridotite. As with the clinopyroxene, no compositional zoning was detected in individual grains of orthopyroxene, but there is a considerable difference in

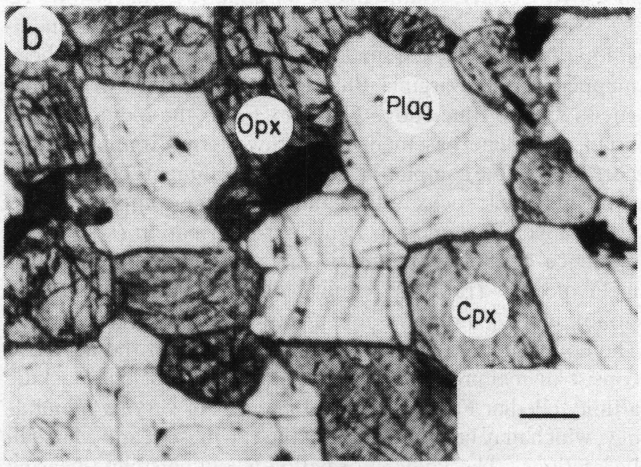

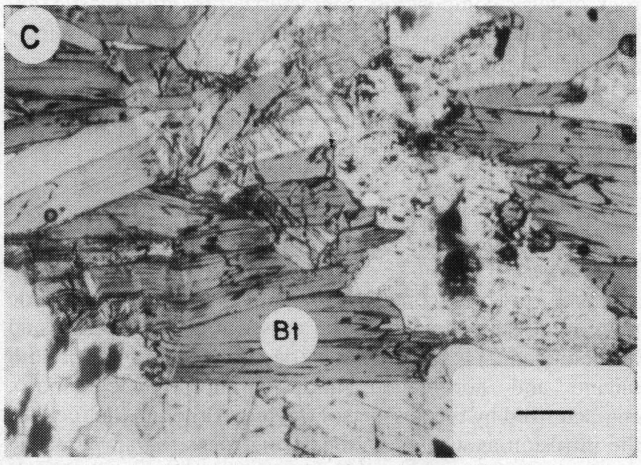

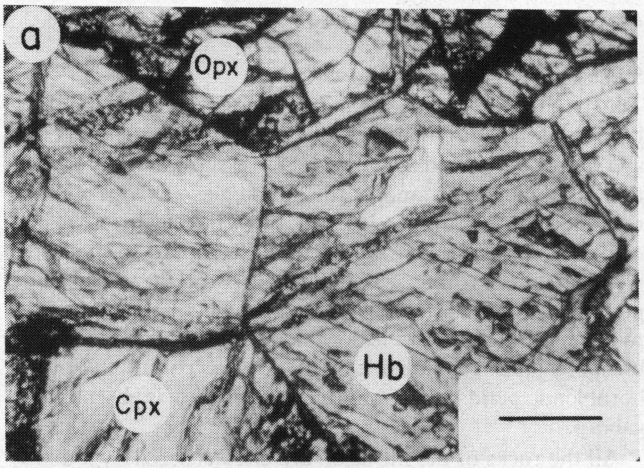

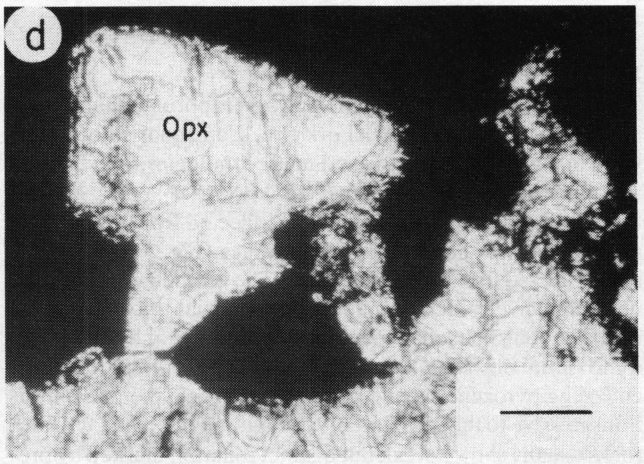

Fig. 5 Textures and mineralogies of Lick Fork rocks. (*a*) Hornblende (Hb)–clinopyroxene (Cpx)–orthopyroxene (Opx) polygonal aggregate with close to 120° triple-junction points, hornblende peridotite; (*b*) plagioclase (Plag)–orthopyroxene (Opx)–clinopyroxene (Cpx) polygonal aggregate, gabbro; (*c*) crude biotite (Bt) foliation, hornblende gabbro; (*d*) residual island of orthopyroxene (Opx), with discontinuous alteration rim, in sulphide matrix (black), hornblende peridotite. Transmitted plane-polarized light; scale bar, 0.1 mm

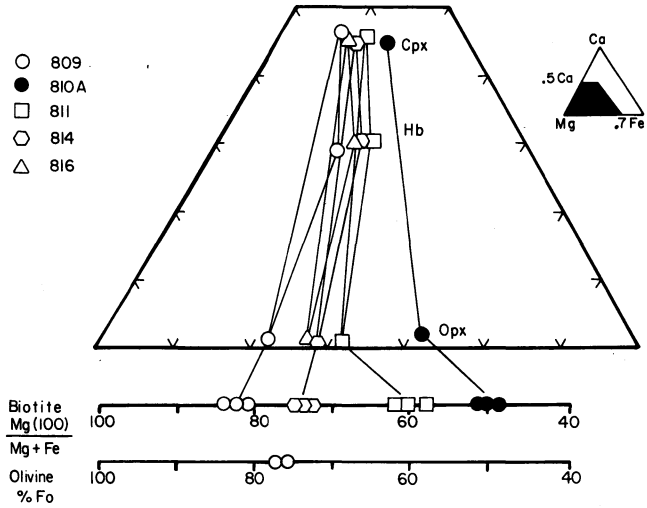

Fig. 6 Compositions (mole %) of orthopyroxene, clinopyroxene, hornblende, olivine, and biotite in Lick Fork hornblende peridotite (809), gabbro (810A) and hornblende gabbro (811, 814, 816), plotted in Ca–Mg–Fe ternary

orthopyroxene composition among the lithologies, from En_{77} in the hornblende peridotite to En_{60} in the gabbro. Ca content is consistently low for all orthopyroxenes (maximum Wo_1). Both orthopyroxene and clinopyroxene grains show extensive alteration to chlorite and mica at the margins, especially when they are in contact with sulphides (Fig. 5(*d*)). Biotite is reddish brown in colour, and in thin sections shows ample evidence of deformation in the form of undulose extinction, bent cleavage and kink bands. The deformation of the biotite laths appears to be more severe in the hornblende peridotite. There is a wide variation in the composition of biotite, especially in respect of TiO_2 content (peridotite, 2.4; gabbro, 2.9; hornblende gabbro, 45–5 wt%) and Mg/(Mg + Fe) ratio (periodotite, 0.85; gabbro, 0.52; hornblende gabbro, 0.60–0.75). Plagioclase compositions in the gabbro and hornblende gabbro range from An_{61} to An_{40} (Fig. 7). Although plagioclase composition varies in a

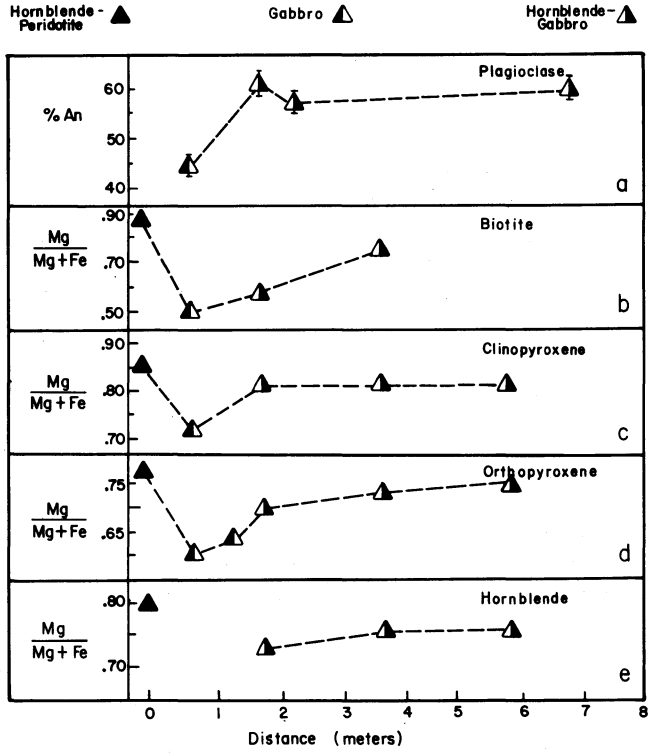

Fig. 7 Compositional variations in coexisting silicate minerals across Lick Fork intrusion (North face, Fig. 3)

single sample, presumably because of its widespread sericitic alteration, no compositional zoning was detected in individual grains. Twin lamellae in plagioclase are generally spindle-shaped, suggesting deformation.[13] The plagioclase is often clouded with a fine, rod-shaped inclusion. X-ray diffraction and energy dispersive methods were employed to determine the nature of this phase, but no positive identification could be made. Such clouded texture has been interpreted by Spry[45] as indicative of progressive metamorphism of feldspar phases. Also, associated with the clouded plagioclase are minute opaque inclusions, probably a spinel phase.

A plot of the Mg/(Mg + Fe) ratios of the mafic phases (hornblende, clinopyroxene, orthopyroxene, biotite) and the An% of plagioclase across the trend of the intrusion illustrates noticeable variations among the three lithologies (Fig. 7). The pronounced 'dip' for the gabbro in the Mg/(Mg + Fe) ratio and An% profiles is, however, not consistent with normal differentiation trends. These profiles, as well as the modal clinopyroxene and plagioclase variations (Fig. 4), suggest that either the Lick Fork body is a multiple intrusion or the original differentiation trends have been obscured by subsequent metamorphism.

Metamorphism

Whatever were the conditions of magmatic crystallization, the intrusion has undergone high-grade (granulite-facies) metamorphism. The many lines of evidence, both textural and compositional, which lead to this interpretation are discussed below.

As was mentioned earlier, the rocks of the intrusion show weak but distinct foliations—a granulitic fabric due to parallel felsic streaks in the gabbros and a poorly developed preferred orientation of biotite in all the lithologies—which are parallel to the foliation in the country rocks. Another feature that is sug-

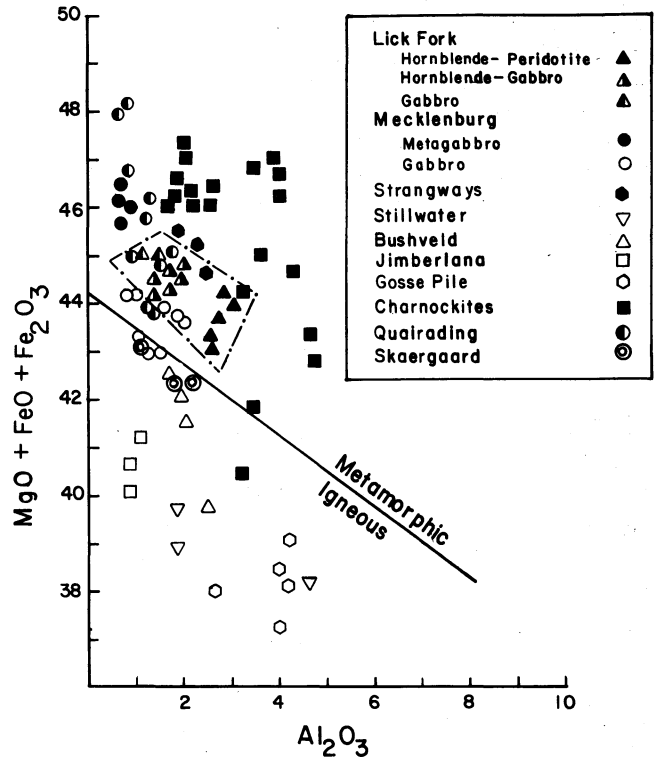

Fig. 8 Composition (wt% oxides, MgO + FeO + Fe_2O_3 versus Al_2O_3) of orthopyroxenes from Lick Fork intrusion compared with orthopyroxenes from Mecklenburg gabbro–metagabbro,[23] Strangways granulites,[48] Stillwater Complex,[46] Bushveld Complex,[1] Skaergaard Complex,[6] Jimberlana intrusion,[8] Gosse Pile ultramafic intrusion,[37] Quairading granulites[12] and charnockites from Madras[24] and Kondapalli.[32] Boundary between igneous and metamorphic fields taken from Bhattacharyya[4]

gestive of metamorphic recrystallization is the ubiquitous presence of polygonal textures in all three lithologies. This texture is most pronounced in the coarse-grained hornblende aggregates, in which triple junction points with 120° dihedral angles are the rule rather than the exception (Fig. 5(*a*)). Similar 'foam' textures are also common in single-phase aggregates of orthopyroxene and clinopyroxene, however, as well as in polyphase aggregates involving hornblende, pyroxene, olivine and plagioclase (Fig. 5(*b*)). A further indication of metamorphism is provided by lack of compositional zoning in the silicates. Apparent equilibrium among different assemblages in terms of the compositions of their mafic phases is illustrated by non-intersecting tie-lines (Fig. 6).

Composition of orthopyroxene

Bhattacharyya[4] proposed that orthopyroxenes from igneous rocks (excluding volcanic rocks) and metamorphic rocks occupy different fields in a wt% ($MgO + FeO + Fe_2O_3$) versus Al_2O_3 plot, separated by a line defined by the equation ($MgO + FeO + Fe_2O_3$) + 0.775 (Al_2O_3) = 44.04. The validity of this demarcation is borne out by additional data from several well-established igneous and metamorphic complexes (Fig. 8). The Lick Fork orthopyroxenes clearly fall in the metamorphic field.

Mg–Fe^{2+} distribution coefficient (K_d) for coexisting orthopyroxene–clinopyroxene

From available analytical data on coexisting orthopyroxene–clinopyroxene pairs in igneous and metamorphic rocks Kretz[31] concluded that K_d values for igneous pyroxene pairs (0.65–0.86) are quite distinct from high-grade metamorphic pyroxene pairs (0.51–0.65). Despite the lack of a reliable K_d temperature calibration curve[22] and the continuing debate about the best model for the intracrystalline Mg–Fe^{2+} distribution in pyroxenes,[15,43] the general validity of the empirical approach is supported by pyroxene compositions from a wide variety of igneous and metamorphic complexes reported by many workers.[12,38,43] This is also evident from the K_d plot (Fig. 9), which includes some additional data. The K_d for the Lick Fork pyroxenes varies from 0.480 to 0.653 (average 0.570), so almost all the values lie within the range for metamorphic pyroxenes. The reliability of this interpretation is enhanced by the fact that the Lick Fork pyroxenes show a wide variation in Mg/Fe ratios instead of one cluster.[12]

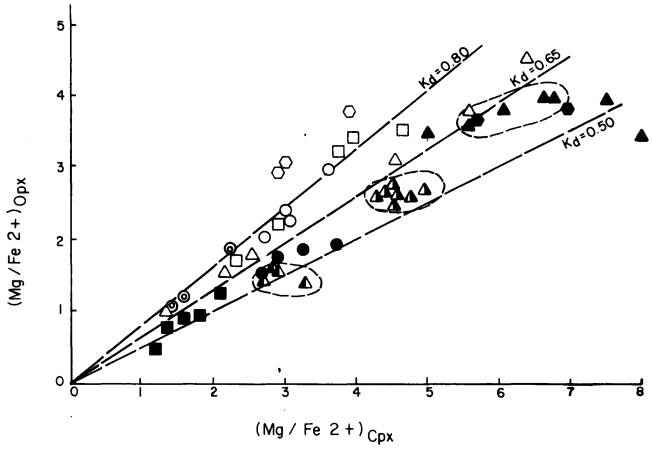

Fig. 9 $K_d^{Mg\text{-}Fe^{2+}}$ (orthopyroxene–clinopyroxene) for Lick Fork intrusion compared with K_d values from other igneous and metamorphic rocks (symbols as in Fig. 8)

Recently, Jen and Kretz[26] have shown that the Fe^{2+}–Mg distribution between orthopyroxene and clinopyroxene in granulite-facies rocks from India, Australia and the Adirondacks in North America fits a curve with $K_D(Fe^{2+}\text{–}Mg) = 1.80$, except

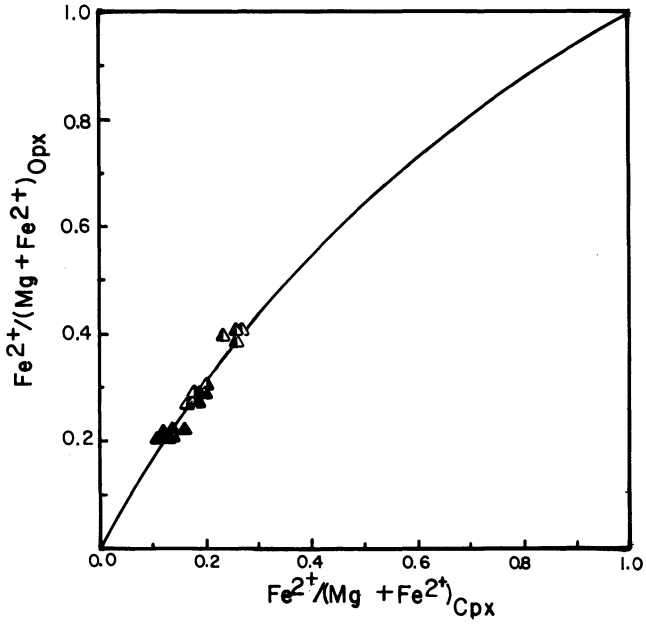

Fig. 10 $K_D^{Fe^{2+}\text{-}Mg}$ (orthopyroxene–clinopyroxene) for Lick Fork lithologies compared with $K_D = 1.80$ curve for granulite-facies rocks. After Jen and Kretz[26]

for a slight decrease in K_D above $X_{Fe}^{cpx} = 0.58$. The close correspondence of the Lick Fork pyroxenes to this curve (Fig. 10) suggests granulite-facies metamorphism for the Lick Fork rocks.

Composition of hornblende

Many workers have noted an increase in the Ti content of hornblende with increasing metamorphic grade,[5,10,40] which is believed to be a consequence of rising temperature. From a

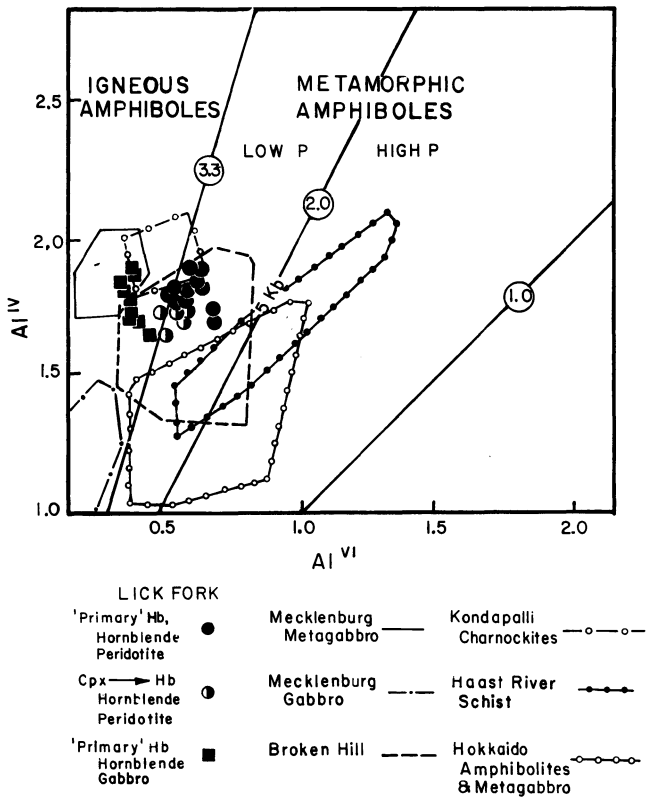

Fig. 11 Al(IV)–Al(VI) plot (after Fleet and Barnett[17]) for hornblendes from Lick Fork rocks compared with hornblendes from Mecklenburg gabbro–metagabbro,[23] Broken Hill granulites,[5] Kondapalli chronockites,[33] Haast River schists[10] and Hokkaido amphibolite–metagabbro complex[19]

compilation of Ti contents of hornblendes from rocks of different metamorphic facies Raase[40] showed a systematic variation in the maximum possible Ti (cations on the basis of 23 oxygen) in hornblende of the different facies: greenschist–amphibolite transition facies, 0.08; lower-grade amphibolite facies, 0.13; higher-grade amphibolite facies, 0.21; and hornblende–granulite facies, 0.30. The Ti contents in the Lick Fork hornblendes show a considerable range (0.08–0.15 in hornblende peridotite; 0.22–0.32 in hornblende gabbro), apparently due to variation in the whole-rock composition,[40] but the maximum Ti (0.32) is consistent with granulite-facies metamorphism of the Lick Fork rocks.

From a compilation of Al(IV) and Al(VI) contents of hornblende in selected igneous and metamorphic rocks Fleet and Barnett[17] proposed that Al(IV)/Al(VI) $\simeq$ 3.3 may define a limiting boundary for the field of unaltered igneous amphibole and Al(IV)/Al(VI) = 2.0, roughly equivalent of the 5-kbar line of Raase,[40] an approximate boundary between low- and high-pressure assemblages. They used the Al(IV)/Al(VI) ratios to confirm that Frood mine (Sudbury Complex, Canada) green hornblende is igneous, whereas the blue-green hornblende is metamorphic. On such a Al(IV)–Al(VI) plot (Fig. 11) the Lick Fork hornblende compositions straddle the igneous–metamorphic boundary, though most of them fall in the field for the Broken Hill rocks.[5] The ambiguity presented by this plot, which is also evident from hornblende compositions for the Mecklenburg metagabbro[23] and the Kondapalli charnockites[33] as well as from the data compiled by Kostyuk and Sobolev,[30] is not a case against the metamorphic nature of the Lick Fork amphiboles. It merely points out that the Al(IV)/Al(VI) ratios do not provide an unequivocal discrimination between igneous and metamorphic amphiboles. Although the Al(IV)/Al(VI) ratio of metamorphic hornblende is a function of temperature and pressure (Al(IV) increasing with increasing temperature of equilibration and Al(VI) increasing with increasing pressure of equilibration), it is significantly dependent on the whole-rock composition,[2,7] particularly on the availability of charge-balancing cations in M (Ti, Fe^{3+}) and A (Na, K) sites. Owing to the uncertainty in computation of Fe^{3+} from electron-microprobe analyses, we have made no attempt to calculate Fe^{3+} or A (Na, K) for the Lick Fork hornblendes. The low Al(IV) compositions (Fig. 11), however, show good inverse correlation with Ti contents.

None of the criteria discussed above can be claimed to be universally applicable. Although pervasive polygonal texture is often considered to be diagnostic of metamorphic rocks,[45] such a texture has been observed in cumulate rocks of layered igneous intrusions, such as the Stillwater Complex.[25] Compositional equilibration may have been achieved owing to slow magmatic crystallization, pyroxene and hornblende compositions are certainly affected by whole-rock chemistry, and empirical discriminant diagrams may not work in certain cases. The collective evidence provided by different lines of approach discussed above does, however, support the interpretation that the Lick Fork intrusion is metamorphosed, probably to granulite-facies conditions.

Sulphide mineralization

Distribution

The bulk of the sulphides in the Lick Fork intrusion is confined to the hornblende peridotite unit, without a discernible concentration in any particular part of the unit. Watson[47] observed sulphide concentrations up to 50% of the rock mass in this unit and estimated an average grade of 'not less than 1.75% Ni' for the ore. In specimens collected from this unit the sulphides constitute 20–30% of the rock by volume, and often show a net texture with occluded grains of primary and altered silicates. A small proportion of the sulphides occurs as stringers cutting across silicate grains and aggregates. In contrast, only traces of sulphides are found in the gabbro and hornblende gabbro units of the intrusion and in the adjacent pyroxene syenite; in these units the sulphides occur as disseminations, often associated with hydrous alteration products of the primary mafic silicates.

Mineralogy

Sulphide minerals in the hornblende peridotite include, in decreasing order of abundance, pyrrhotite (po), marcasite (ms), violarite (vl), chalcopyrite (cp), pentlandite (pn) and pyrite (py), with trace amounts of bornite and mackinawiite. The hornblende gabbro contains essentially the same sulphide assemblage, but the sulphides of the gabbro and pyroxene syenite comprise mainly pyrrhotite, with some chalcopyrite. The sulphides have been subjected to supergene alteration; this is evidenced by the appearance of goethite, which occurs as rims around sulphide minerals and in fractures (sometimes associated with siderite) trangressive to the silicates, marcasite and violarite.

Electron-microprobe analysis of the various sulphide phases showed no systematic compositional differences that can be correlated with the silicate assemblages of the different host rocks. The pyrrhotite is of the hexagonal variety (47.5 $\pm$ 0.5 at% Fe), although the presence of monoclinic pyrrhotite in these rocks has been reported by Craig and Higgins.[11] Pyrrhotite frequently alters to marcasite, whereas pentlandite alters to violarite (Fig. 13(*b*)). The textures and compositions of pentlandite and violarite[49] are very similar to those reported by Misra and Fleet[35] for the po–pn–py–ms–vl assemblages in various nickel sulphide deposits. Craig and Higgins[11] proposed that the Fe-rich violarites may have altered from pyrrhotite, but we found no textural evidence to support this interpretation. The small amount of pyrite is found as irregularly distributed patches and tiny corroded islands in po–pn aggregates, and as fine veinlets, often associated with magnetite, traversing silicates. The pyrite is stoichiometric, with about 0.4 wt% Ni (comparable with the Ni content of pyrrhotite) and undetectable Co (in contrast, pentlandite and violarite contain up to 4 wt% Co). Much of the chalcopyrite occurs as stringers in the silicates; some is associated with pyrrhotite.

Oxide minerals comprise about 2–5% (by volume) of the hornblende peridotite and gabbro, but occur only in trace amounts in hornblende gabbro. The oxide minerals include green spinel (pleonaste), magnetite (mt), ilmenite (ilm), hematite, rutile and goethite. Green spinel is restricted to the peridotite, where it is interstitial to the primary silicates. A representative wt% analysis of green spinel is as follows: FeO, 23.49; MgO, 10.16; MnO, 0.54; NiO, 0.09; Al_2O_3, 47.43; Cr_2O_3, 11.21; TiO_2, 0.02; and Fe_2O_3, 7.15. Ilmenite is the dominant oxide phase in the gabbro, occurring as euhedral crystals with exsolved lamellae of hematite. In the hornblende peridotite ilmenite is found as blebs in magnetite, whereas in the hornblende gabbro it commonly rims biotite; in both the lithologies rutile forms asterisks in biotite. Magnetite occurs in three different associations—with pyrrhotite as stringers and along grain boundaries, with green spinel as rims and as exsolved (?) blebs, and with serpentine as a product of serpentinization of olivine. Magnetite formed by serpentinization is enriched in Cr (3.86% Cr_2O_3), whereas that associated with pyrrhotite is very low in Cr (0.13% Cr_2O_3; cf. 2–6% Cr_2O_3 for magmatic magnetite in the Sudbury Complex[18]). All the magnetites are low in Ti ($<$ 0.3% TiO_2) and Ni ($<$ 0.20% NiO).

Textures

As was mentioned earlier, a large proportion of the sulphides in the Lick Fork intrusion is confined to the hornblende peridotite unit. Therefore, the textures described and documented below are predominantly from the hornblende peridotite unit, though

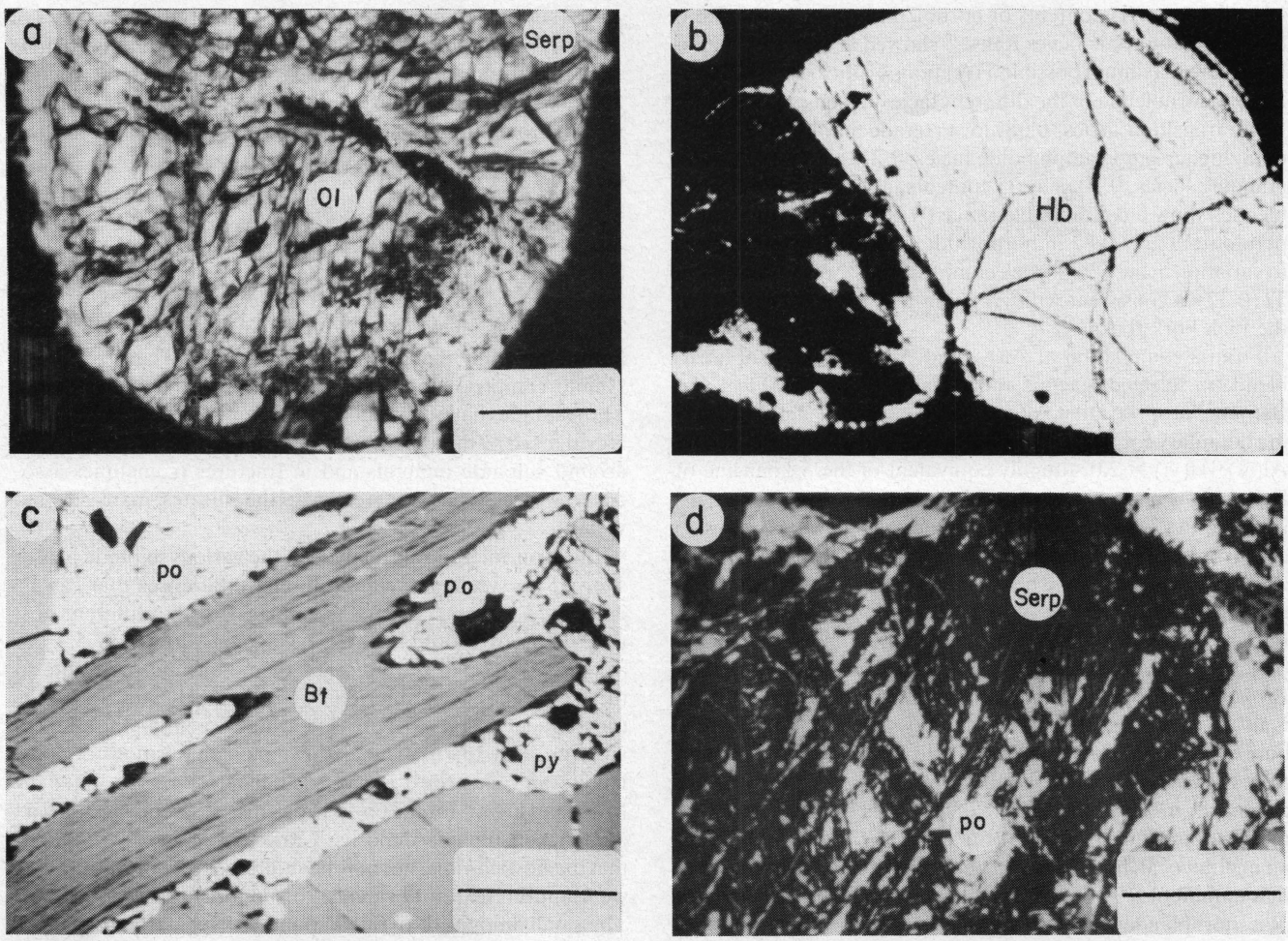

Fig. 12 Textures of Lick Fork nickel sulphide ores in hornblende peridotite. (*a*) Rounded island of serpentinized (Serp) olivine (Ol), with sulphide veinlets, in sulphide matrix (black), transmitted light, partially crossed nicols; (*b*) rounded island of polygonal hornblende (Hb) in sulphide matrix (black), with remnants of one almost completely replaced crystal, transmitted light; (*c*) sulphide (pyrrhotite–pyrite) penetration along biotite (Bt) cleavage, reflected light; (*d*) pyrrhotite (po)–serpentine (Serp) intergrowth, reflected light; scale bar, 0.1 mm

similar textures are also present in the gabbro units.

The sulphides are characterized by a paucity of textures that are considered typical of immiscible sulphide segregation—bleby or globular sulphides[44] and interstitial sulphide masses moulded by the surrounding silicate crystals.[38] In contrast, the sulphide–silicate textures, especially for the serpentinized olivine and pyroxenes, are dominated by transgressive and irregular boundary relationships.

The observed textures are strongly suggestive of replacement of silicate minerals and aggregates by sulphides. Examples of such textures include the following: (1) rounding of silicate grains against sulphide matrix, especially of olivine, often with penetration of sulphides into the silicates (Fig. 12(*a*) and (*b*)); (2) unsupported, residual islands of silicate minerals (olivine, pyroxene, hornblende, biotite) aggregates in sulphide matrix, usually with corroded margins (Figs. 5(*d*), 12(*a*) and (*b*)); (3) veining of silicate crystals by sulphides (which include chalcopyrite, pyrrhotite, pyrite, pentlandite/violarite), with or without associated magnètite (Fig. 13(*a*) and (*b*)); and (4) penetration of sulphides along weak crystallographic planes of silicate minerals, sometimes resulting in an orientated sulphide intergrowth texture (Fig. 12(*a*), (*c*) and (*d*)).

Such textures in other nickel sulphide assemblages have been interpreted to be due to replacement of pre-existing silicates.[3,16,36,39] In Lick Fork all the primary mafic silicate minerals appear to be prone to replacement, though to varying degrees. The susceptibility of a silicate phase to replacement seems to be related to its hydrothermal alteration. The hornblende and biotite are often unaffected, except for stringers and veinlets of sulphides, and show sharp and smooth contacts against sulphides (Figs. 12(*c*) and 13(*a*)). On the other hand, sulphides are intimately intergrown with the alteration envelope around the pyroxene and olivine, and they often penetrate into the relatively unaltered cores (Figs. 5(*d*) and 12(*a*)). Considering the ease with which olivine is replaced by sulphides,[3,36] it is possible that much of the space now filled with sulphides was originally occupied by olivine.

Origin

The concentration of the sulphides in the ultramafic unit of the Lick Fork intrusion (the unit now forms the hanging-wall owing to overturning by folding or faulting) would seem to suggest that the sulphides represent magmatic segregation of an immiscible sulphide (–oxide) melt. The absence of typical magmatic textures suggests, however, that if such sulphides were present, they have been modified beyond recognition by later metamorphism and/or hydrothermal alteration.

Recrystallization/mobilization of pre-existing sulphides during high-grade metamorphism of the Lick Fork intrusion is evidenced by such features as concentration of magnetite along pyrrhotite grain boundaries and occasional polygonal pyrrhotite aggregates. Some of the pyrrhotite may also have been produced by metamorphism of pyrite. The bulk of the pyrrhotite occurs, however, as anhedral aggregates without any recrystallization or deformation fabric. The preferred orientation of biotite and hornblende and the pronounced polygonal fabric of the hornblende–pyroxene aggregates indicate that these minerals were recrystallized during metamorphism. Therefore, their replacement by sulphides must have been later than the peak of metamorphism. This conclusion is further corroborated by the

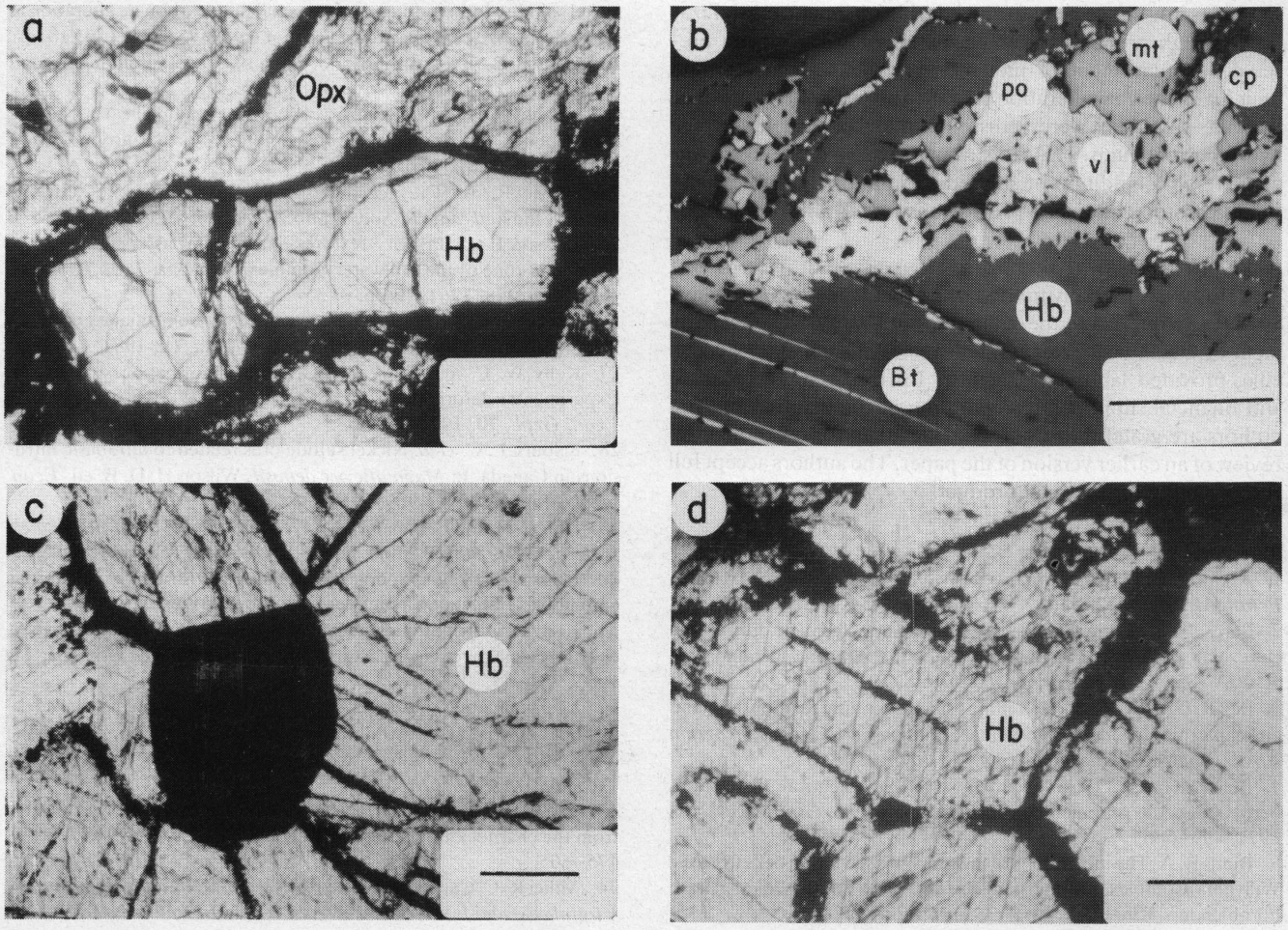

Fig. 13 Textures of Lick Fork nickel sulphide ores in hornblende peridotite. (*a*) Hornblende (Hb) veined by sulphides (black), transmitted light; (*b*) vein of pyrrhotite (po)–violarite (vl)–chalcopyrite (cp)–magnetite (mt) across hornblende (Hb) and biotite (Bt), and pyrrhotite along biotite cleavage, reflected light; (*c*) sulphides (pyrrhotite–marcasite–chalcopyrite–magnetite) (black) at triple-junction point of hornblende (Hb) aggregate, with tentacles (magnetite, with minor chalcopyrite and pyrrhotite) along and across hornblende grain boundaries, transmitted light; (*d*) sulphides (pyrrhotite–pentlandite–chalcopyrite) (black) concentrated along grain boundaries and cleavages of polygonal hornblende aggregate, transmitted light; scale bar, 0.1 mm

presence of textures strongly suggestive of preferential replacement of annealed hornblende aggregate at triple junctions and along grain boundaries (Fig. 13(*c*) and (*d*)). Also, the overall mineralogy of the sulphide stringers and veins in silicates and the large sulphide patches is the same (Fig. 13(*b*)); metamorphic mobilization should have produced selective migration of more easily deformable sulphide phases, such as chalcopyrite and pyrrhotite.[9,27] Thus, most of the observed features cannot be accounted for by solid-state metamorphic mobilization of sulphide constituents.

Kilburn *et al.*[28] have described a progressive sequence of textural modifications in nickel sulphide ores from Canada owing to later serpentinization. Sulphide–serpentine intergrowth textures are common in Lick Fork ores (Fig. 12(*d*)), but there is no clear evidence (such as veining of sulphides by serpentinite) that serpentinization was later than the emplacement of sulphides. On the contrary, some textures are suggestive of serpentine replacement by sulphides (Fig. 12(*a*)). In any case, the intimate association of the sulphides with serpentine and other secondary silicates and the frequent penetration of sulphides into the primary silicates do suggest a genetic relationship between hydrothermal alteration and the present disposition of sulphides. The hydrothermal fluids may have served merely as an agent for redistributing the pre-existing magmatic sulphides, but it is also possible that the fluids contributed to the volume of sulphides in the Lick Fork intrusion. Based on replacement textures, such hydrothermal fluids have been considered to be the source for disseminated nickel sulphide mineralization in the ultramafic rocks of Ungava peninsula, Canada,[39] and Bulong Complex, Western Australia,[36] and in the quartz diorite of Frood mine, Ontario.[16] On the other hand, from a study of some altered Archaean dunites in Western Australia, Groves and co-workers,[21] Groves and Keays[20] and Donaldson[14] argued that the hydrothermal fluids redistributed the magmatic disseminated sulphides, but this was accompanied by a significant addition of sulphides (S from the fluid, Fe and/or Ni from olivine). A similar model is compatible with several critical features of the Lick Fork sulphide mineralization: (1) pervasive replacement textures involving metamorphic silicate minerals; (2) intimate association of sulphides with hydrothermal alteration of silicate minerals, with some replacement of the alteration products by sulphides; (3) relatively high proportion of sulphides in the hornblende peridotite unit, but without typical magmatic textures; and (4) extensive hydrothermal alteration of the hornblende peridotite unit, which had an original abundance of olivine and now contains almost all of the sulphides. The role of the hydrothermal fluids as a possible source of additional sulphur (or sulphides), however, cannot be adequately evaluated from the available data.

Conclusions

The Lick Fork deposit is an example of the problems involved in interpretation of nickel sulphide mineralization in mafic–ultramafic bodies that have been subjected to high-grade metamorphism and hydrothermal alteration. Compositions and textures of silicate phases of the host rocks provide clues to their igneous parentage and subsequent modification, but those of the sulphides are less diagnostic. Considering the lithologies of the Lick Fork intrusion, some amount of immiscible

sulphides must have been formed during magmatic crystallization, though primary magmatic textures have not been preserved. Replacement of metamorphic silicate minerals and their hydrothermal alteration products provides clear evidence that the sulphides were redistributed by post-metamorphic hydrothermal fluids. This redistribution may have been accompanied by the addition of sulphides; additional chemical and sulphur isotope data may provide answers to this problem.

Acknowledgement
This study was partially funded by a grant from the Geological Society of America to the senior author (W. W.).The Department of Geological Sciences, University of Tennessee, Knoxville, provided laboratory facilities for research, and clerical and financial support for preparation of the manuscript. The authors are grateful to Dr. D. L. Buchanan for his thoughtful review of an earlier version of the paper. The authors accept full responsibility for the final product.

References

1. Atkins F. B. Pyroxenes of the Bushveld Intrusion, South Africa. *J. Petrol.*, **10,** 1969, 222–49.
2. Bard J. P. Composition of hornblendes formed during the Hercynian progressive metamorphism of the Aracena metamorphic belt (SW Spain). *Contr. Miner. Petrol.*, **28,** 1970, 117–34.
3. Bell R. C. and Fleet M. E. Sulfide–silicate textural relationships and nickel partitioning in the Rensy mine, southwestern Quebec. *Program Abstr. geol. Ass. Miner. Ass. Can.*, **5,** 1980, 42.
4. Bhattacharyya C. An evaluation of the chemical distinctions between igneous and metamorphic orthopyroxenes. *Am. Miner.*, **56,** 1971, 499–506.
5. Binns R. A. The mineralogy of metamorphosed basic rocks from the Willyama Complex, Broken Hill district, New South Wales, part I: hornblendes. *Mineralog. Mag.*, **35,** 1965–66, 306–26.
6. Brown G. M. Pyroxenes from the early and middle stages of fractionation of the Skaergaard intrusion, East Greenland. *Mineralog. Mag.*, **31,** 1956–58, 511–43.
7. Brown W. R. Geology and mineral resources of the Lynchburg quadrangle, Virginia. *Bull. Va geol. Surv.* 74, 1958, 97 p.
8. Campbell I. H. and Borley G. D. The geochemistry of pyroxenes from the lower layered series of the Jimberlana Intrusion, Western Australia. *Contr. Miner. Petrol.*, **47,** 1974, 281–97.
9. Clark B. R. and Kelly W. C. Sulfide deformation studies: I. Experimental deformation of pyrrhotite and sphalerite to 2000 bars and 500°C. *Econ. Geol.*, **68,** 1973, 332–52.
10. Cooper A. F. and Lovering J. F. Greenschist amphiboles from Haast River, New Zealand. *Contr. Miner. Petrol.*, **27,** 1970, 11–24.
11. Craig J. R. and Higgins J. B. Cobalt- and iron-rich violarites from Virginia. *Am. Miner.*, **60,** 1975, 35–8.
12. Davidson L. R. Variation in ferrous iron–magnesium distribution coefficients of metamorphic pyroxenes from Quairading, Western Australia. *Contr. Miner. Petrol.*, **19,** 1968, 239–59.
13. Deer W. A. Howie R. A. and Zussman J. *An introduction to the rock-forming minerals* (London: Longmans, 1966), 528 p.
14. Donaldson M. J. Redistribution of ore elements during serpentinization and talc–carbonate alteration of some Archean dunites, Western Australia. *Econ. Geol.*, **76,** 1981, 1698–713.
15. Fleet M. E. Mg, Fe^{2+} site occupancies in coexisting pyroxenes. *Contr. Miner. Petrol.*, **47,** 1974, 207–14.
16. Fleet M. E. Origin of disseminated copper–nickel sulfide ore at Frood, Sudbury, Ontario. *Econ. Geol.*, **72,** 1977, 1449–56.
17. Fleet M. E. and Barnett R. L. Al^{IV}/Al^{VI} partitioning in calciferous amphiboles from the Frood mine, Sudbury, Ontario. *Can. Mineralogist,* **16,** 1978, 527–32.
18. Gasparrini E. and Naldrett A. J. Magnetite and ilmenite in the Sudbury Nickel Irruptive. *Econ. Geol.*, **67,** 1972, 605–21.
19. Grapes R. H. Hashimoto S. and Miyashita S. Amphiboles of a metagabbro–amphibolite sequence, Hidaka metamorphic belt, Hokkaido. *J. Petrol.*, **18,** 1977, 285–318.
20. Groves D. I. and Keays R. R. Mobilization of ore-forming elements during alteration of dunites, Mt. Keith–Betheno, Western Australia. *Can. Mineralogist,* **17,** 1979, 373–89.
21. Groves D. I. Hudson D. R. and Hack T. B. C. Modification of iron–nickel sulfides during serpentinization and talc–carbonate alteration at Black Swan, Western Australia. *Econ. Geol.*, **69,** 1974, 1265–81.
22. Hensen B. J. Pyroxenes and garnets as geothermometers and barometers. *Yb. Carnegie Instn Wash.*, **72,** 1973, 527–34.
23. Hermes O. D. Petrochemistry of coexistent mafic silicates from the Mecklenburg gabbro–metagabbro complex, North Carolina. *Bull. geol. Soc. Am.*, **81,** 1970, 137–63.
24. Howie R. A. The geochemistry of the charnockite series of Madras, India. *Trans. R. Soc. Edinb.*, **62,** 1955, 725–68.
25. Jackson E. D. Primary textures and mineral associations in the ultramafic zone of the Stillwater Complex, Montana. *Prof. Pap. U.S. geol. Surv.* 358, 1961, 106 p.
26. Jen L. S. and Kretz R. Mineral chemistry of some mafic granulites from the Adirondack region. *Can. Mineralogist,* **19,** 1981, 479–91.
27. Kelly W. C. and Clark B. R. Sulfide deformation studies: III. Experimental deformation of chalcopyrite to 2000 bars and 500°C. *Econ. Geol.*, **70,** 1975, 431–53.
28. Kilburn L. C. *et al.* Nickel sulfide ores related to ultrabasic intrusions in Canada. In *Magmatic ore deposits* Wilson H. D. B. ed. *Econ. Geol. Monograph* 4, 1969, 276–93.
29. King P. B. and Beikman H. M. *Geologic map of the United States: scale 1 : 2 500 000* (Reston, Va.: U.S. Geological Survey, 1974).
30. Kostyuk E. A. and Sobolev V. S. Paragenetic types of calciferous amphiboles of metamorphic rocks. *Lithos,* **2,** 1969, 67–81.
31. Kretz R. Distribution of magnesium and iron between orthopyroxene and calcic pyroxene in natural mineral assemblages. *J. Geol.*, **71,** 1963, 773–85.
32. Leelanandam C. Chemical study of pyroxenes from the charnockitic rocks of Kondapalli (Andhra Pradesh), India, with emphasis on the distribution of elements in coexisting pyroxenes. *Mineralog. Mag.*, **36,** 1967–68, 153–79.
33. Leelanandam C. Chemical mineralogy of hornblendes and biotites from the charnockitic rocks of Kondapalli, India. *J. Petrol.*, **11,** 1970, 475–505.
34. Milici R. C. Carlisle T. S. Jr. and Wilsom J. W. In *Geologic map of Virginia: scale 1:500 000* Calver J. L. and Hobbs C. R. B. eds (Charlottesville, Va.: Division of Mineral Resources, 1963).
35. Misra K. C. and Fleet M. E. Chemical composition and stability of violarite. *Econ. Geol.*, **69,** 1974, 391–403.
36. Moeskops P. G. and Davis G. R. Unusual sulphide replacement textures in altered olivine-rich rocks of the Bulong Complex near Kalgoorlie, Western Australia. *Mineralog. Mag.*, **41,** 1977, 473–9.
37. Moore A. C. The mineralogy of the Gosse Pile ultramafic intrusion, central Australia II: pyroxenes. *J. geol. Soc. Aust.*, **18,** 1971, 243–58.
38. Naldrett A. J. and Kullerud G. A study of the Strathcona mine and its bearing on the origin of the nickel–copper ores of the Sudbury district, Ontario. *J. Petrol.*, **8,** 1967, 453–531.
39. Philpotts A. R. Textures of the Ungava nickel ores, Canada. *Can. Mineralogist,* **6,** 1961, 680–8.
40. Raase P. Al and Ti contents of hornblende, indicators of pressure and temperature of regional metamorphism. *Contr. Miner. Petrol.*, **45,** 1974, 231–6.
41. Ray S. and Sen S. K. Partitioning of major exchangeable cations among orthopyroxene, calcic pyroxene and hornblende in basic granulites from Madras. *Neues Jb. Miner. Abh.*, **114,** 1970, 61–88.
42. Ross C. S. Origin of the copper deposits of the Ducktown type in the Southern Appalachian region. *Prof. Pap. U.S. geol. Surv.* 179, 1935, 165 p.
43. Saxena S. K. Mg^{2+}–Fe^{2+} order–disorder in orthopyroxene and the Mg^{2+}–Fe^{2+} distribution between coexisting minerals. *Lithos,* **4,** 1971, 345–54.
44. Skinner B. J. and Peck D. L. An immiscible sulfide melt from Hawaii. Reference 28, 310–22.
45. Spry A. *Metamorphic textures* (Oxford: Pergamon, 1969), 350 p.
46. Wager L. R. and Brown G. M. *Layered igneous rocks* (Edinburgh: Oliver & Boyd, 1968), 588 p.
47. Watson T. L. The occurrence of nickel in Virginia. *Trans. Am. Inst. Min. Engrs,* **38,** 1907, 683–97.
48. Woodford P. J. and Wilson A. F. Chemistry of coexisting pyroxenes, hornblendes and plagioclases in mafic granulites, Strangways Range, Central Australia. *Neues Jb. Miner. Abh.*, **128,** 1976, 1–40.
49. Wrightson W. Jr. Petrogenesis of the Lick Fork Ni–Co prospect, Floyd Co., Virginia. M.S. thesis, University of Tennessee, Knoxville, 1981, 111 p.

Cu–Ni–PGE mineralization in the marginal series of the Early Proterozoic Koillismaa layered igneous complex, northeast Finland

Tuomo Alapieti Ph.D.
Tauno Piirainen Ph.D.
Department of Geology, University of Oulu, Oulu, Finland

Synopsis

The Koillismaa layered igneous complex is the result of igneous activity that occurred 2436±5 m.y. ago. Its crystallization took place in three separate but connected magma chambers, the total volume of which is estimated at more than 2000 km³. These chambers were located partly in a feeder system within Archaean granitoids and partly in an unconformity between these granitoids and Early Proterozoic supracrustal rocks. The composition of the parental magma that initially filled the chambers is thought to have been that of a relatively MgO-rich tholeiite.

Sulphides and platinum-group minerals are mainly concentrated in the marginal series of the western part, where they are encountered over a distance of 25 km. This marginal series is an originally nearly horizontal series of rock types that displays a reversed differentiation trend, grading inwards from gabbroic to ultramafic rocks, followed by rocks of the layered series. The chilled margin is not encountered anywhere in its original position at the contact, probably as a consequence of magmatic erosion, but remnants are to be found in the form of elongated xenoliths. Partly melted siliceous fragments from gneissic country rock typical of the lower part of the marginal series indicate pronounced contamination.

Chalcopyrite, pentlandite and pyrrhotite±pyrite are the predominant sulphides. The accessory sulphide minerals include covellite, violarite, marcasite, mackinawite, sphalerite and argentian pentlandite. Platinum-group minerals are represented by froodite, michenerite, merenskyite and sperrylite. Other accessories that have been identified are electrum and native copper and gold. The mean of the Cu/(Cu+Ni) ratio in the mineralizations is 0.67 and Pt/(Pt+Pd) 0.31.

It is suggested that the sulphide phase was formed in the marginal series as the solubility of sulphur in the basic magma was lowered by contamination, possibly assisted by some other factors. The sulphur isotope data support the juvenile origin of the sulphur.

The bedrock of Finland is principally Archaean and Proterozoic in age. The Archaean areas are composed of granitoids, 2800–2600 m.y. in age, and occasional narrow greenstone belts. Discordantly on top of the Archaean bedrock there occur in eastern and northern Finland Proterozoic conglomerates, quartzites, limestones, mica schists and various basic volcanic and intrusive rocks. In the western part of the country the Archaean rocks are no longer present, and the Proterozoic rocks are represented by metaturbidites and metavolcanics, which would appear to be 'floating' on younger granitoids about 1900–1800 m.y. old.

Five separate magmatic phases can be recognized within the geological evolution of the Proterozoic in Finland, the ages of which are approximately 2400, 2100, 1900, 1800 and 1600 m.y. The genesis of these formations favours an explanation that involves plate tectonics, in which the first of these dates represents the possible rift phase, the second the beginning of subduction and the last three the syn-orogenic, late orogenic and post-orogenic plutonisms in the Svecokarelian orogeny.

Whatever the origin of the bedrock of Finland, however, it is clear that the geological evolution of the Proterozoic began here with the extensive intrusion and eruption of basic magmas. In the Koillismaa area alone (Fig. 1) the amount of basic magma that went into the formation of the layered igneous complex is estimated at a minimum of 2000 km³.[1] This intrusive complex, however, only comprises about one-third of all exposed Early Proterozoic layered intrusions in northern Finland, so the whole volume of magma must have been much greater than that mentioned above. The most prominent of these intrusions, which are located outside Koillismaa, are those of Kemi, Penikat, Suhanko and Koitelainen.

The chromium ore in the Kemi intrusion, which has been mined since 1968, and the vanadium ore of Mustavaara in the Koillismaa area, which has been mined since 1976, are the most significant ore deposits in the Early Proterozoic layered intrusions of Finland. Other potential horizons of economic interest are the chromitite layer in the Koitelainen intrusion, which occurs in the anorthositic zone in the upper part of the layered series,[7] and the low-grade, disseminated PGE-bearing Cu–Ni sulphide occurrences to be found in many major and minor intrusions of northern Finland.

The largest sulphide occurrences of this kind are found within the marginal series of the Koillismaa complex, where they can be followed for some 25 km. These occurrences began to interest prospecting organizations as early as the 1950s. In the following decade Outokumpu Oy initiated an extensive ore exploration programme in this area, geological mapping, geophysical surveys and diamond drilling being undertaken. These investigations culminated in pilot-plant tests, but as the results were discouraging, the work was terminated in the summer of 1968. Later, however, the investigations were continued, mainly by the Koillismaa Research Project, initiated by the University of Oulu in 1971, the purpose of which was to study basic magmatism and related metallogeny in the Koillismaa area.[9,10] The prospecting companies have also recently resumed exploration to some extent, even though any economically exploitable occurrences have yet to be found.

Koillismaa layered igneous complex

The Koillismaa layered igneous complex (subsequently referred to as the Koillismaa complex) is taken here to refer to the Early Proterozoic layered basic–ultrabasic igneous rocks 2436±5 m.y. in age located in the Koillismaa district of northeastern Finland, beginning in the west with the hill of Syöte and continuing in the east to the hill of Näränkävaara and across the border into the Soviet Union (Fig. 1). The Koillismaa complex consists of two exposed intrusions—the eastern or Näränkävaara intrusion, and the western intrusion, together with a hidden 'dyke' that connects them, which may well itself be a layered intrusion (Fig. 2). These two intrusions and the connecting 'dyke' together represent three original magma chambers that were initially linked together and were located partly within the Archaean basement complex some 2700 m.y.

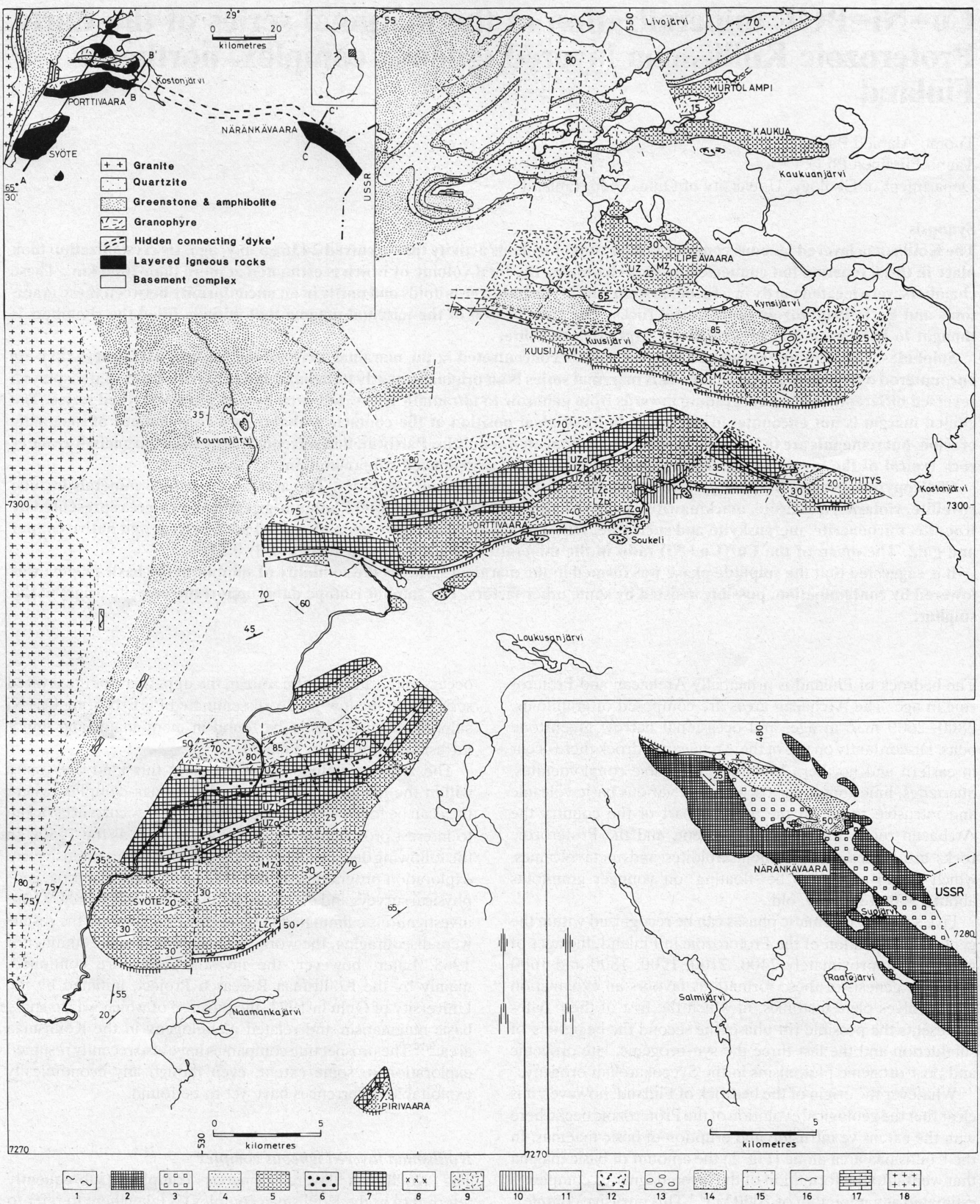

Fig. 1 General geological map and index map of the Koillismaa layered igneous complex: 1, marginal series; 2, peridotite; 3, pyroxenite; 4, gabbronorite with intercumulus plagioclase; 5, norite and gabbronorite with cumulus plagioclase; 6, magnetite gabbro; 7, leucogabbro and anorthosite; 8, quartz diorite and granodiorite; 9, granophyre; 10, contact-metamorphic granitoid; 11, Archaean granitoids; 12, Archaean mafic and ultramafic extrusive and intrusive rocks; 13, conglomerate; 14, Proterozoic greenstones and amphibolites; 15, quartzite, 16, mica schist; 17, dolomite; 18, granite

in age and partly between this basement and the Early Proterozoic supracrustal rocks.[1,2,3]

The western intrusion originally formed a more or less sheet-like body 1–3 km thick (Figs. 2 and 3). Later tectonic events during the Svecokarelidic orogeny broke the intrusion into a number of tilted blocks. Dips in the four southernmost blocks are towards the north and in the more northerly blocks towards the south or southwest, so the present overall form is that of a broad, interrupted synclinal formation. The blocks, from south to north, are those of Pirivaara, Syöte, Porttivaara, Kuusijärvi, Lipeävaara, Kaukua and Murtolampi (Figs. 1–3).

The eastern Näränkävaara intrusion would seem to have

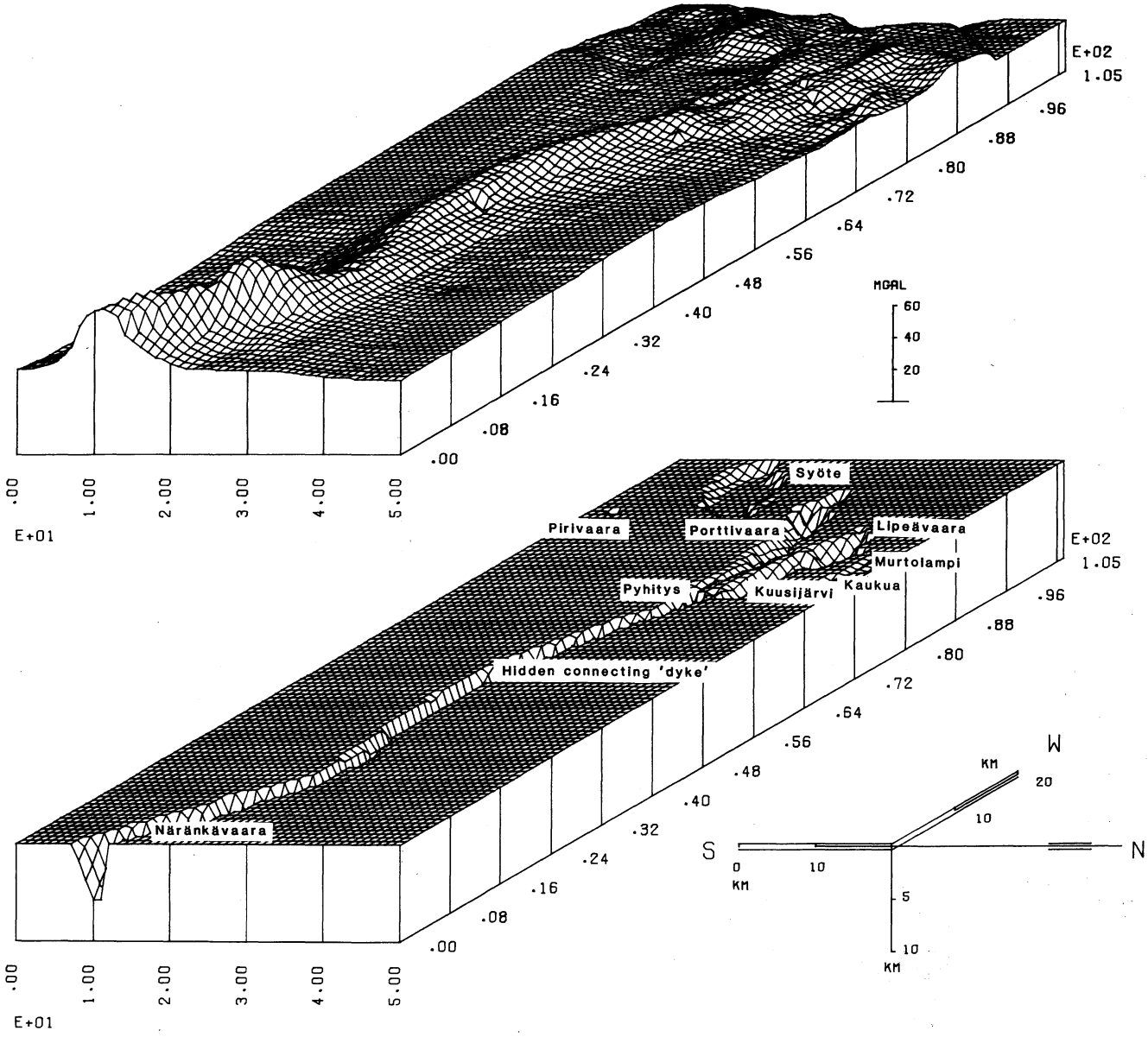

Fig. 2 Perspective block diagrams of gravity field (top) and Koillismaa complex (bottom) seen from east. Latter depicted negatively and thus lower plot shows present-day basement of Koillismaa complex

retained practically its original form, having been, as it is now, an elongated layered intrusion with roughly triangular cross-sections (Figs. 1–3). Its outer contacts are steep and its layering is sub-horizontal in the upper parts, but apparently steeper at greater depths. The feeder channel, which supplied the whole Koillismaa complex, was situated mainly just below the Näränkävaara intrusion and the connecting 'dyke'.

Data for the connecting 'dyke' are limited and mainly based on geophysical investigations,[4] according to which the upper surface of the 'dyke' is at an average depth of about 1.4 km below the present erosional surface, and the anomalous mass is about 3 km wide and very deep, descending almost vertically and at the same time becoming narrower (Fig. 2). Its strike is indicated on the present bedrock surface by a narrow 'vein' of conglomerate about 25 km long, the fragments of which are derived from the surrounding gneisses. At its western end the connecting 'dyke' bifurcates into two branches, the more southerly of which is exposed at the hill of Pyhitys in the western end of the Porttivaara block (Fig. 1).

The crystallization conditions in the three original magma chambers were different, and this led, in turn, to characteristic trends of fractionation in each of the chambers resulting in specific rock types in different parts of the complex. One distinct feature that they all have in common, however, is that the marginal series shows reversed fractionation in comparison with the layered series. This feature is also found in Jimberlana and Muskox.[6,11]

The marginal series of the Näränkävaara intrusion is exposed at the northern border of the northwest tip of the intrusion (Fig. 1). The main rock type here is a heterogeneous metagabbroid, which borders on to granitoids to the north.[3] In view of the considerable vertical dimension of the Näränkävaara intrusion the proportion of the marginal series must be very much larger at greater depths than it is in outcrop.

The exposed portion of the layered series of the Näränkävaara intrusion is made up of a basal zone of ultramafic cumulates, the lowermost parts of which are composed of olivine (–chrome spinel) cumulates with only small amounts of intercumulus material (Fig. 4). These rocks are then followed in the stratigraphy by olivine–bronzite (–chrome spinel), bronzite, bronzite–augite and bronzite cumulates, followed again by olivine–bronzite (–chrome spinel) cumulates, in ascending order. The ultramafic cumulates are then overlain by the zone of gabbroic rocks and later differentiates. These rocks are, first, bronzite–augite±olivine heteradcumulates with poikilitic plagioclase as the significant intercumulus phase, and then

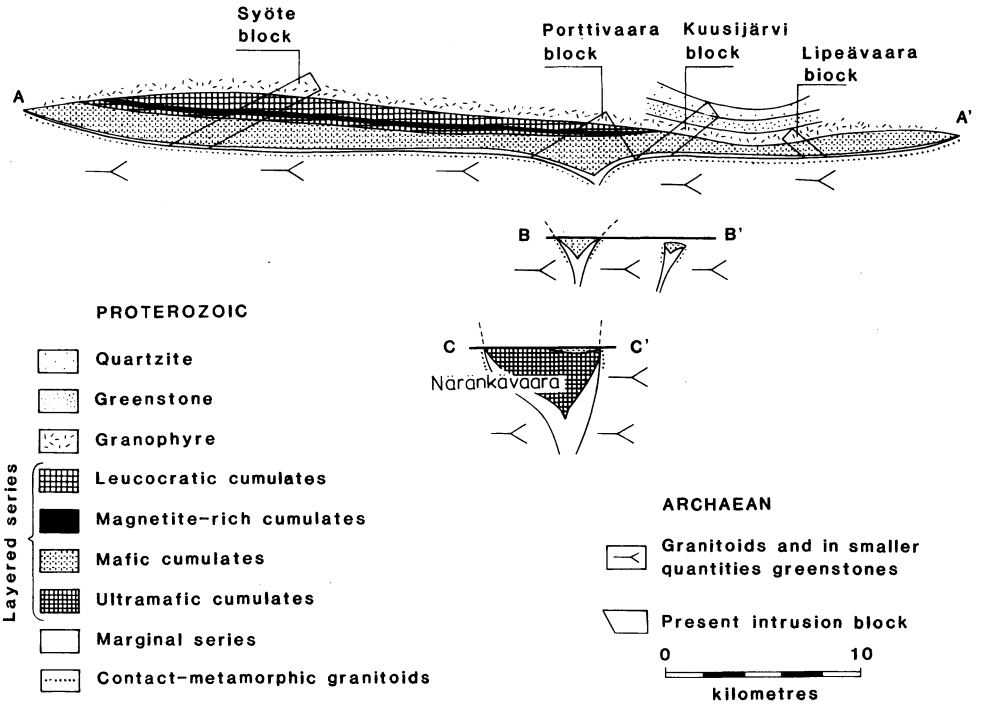

Fig. 3 Schematic cross-sections of Koillismaa complex during period preceding Svecokarelidic movements (profiles *A–A'*, *B–B'* and *C–C'* also shown in Fig. 1)

plagioclase–hypersthene–augite and plagioclase–augite cumulates, the last mentioned containing relatively abundantly intercumulus quartz.

The fractionation trends for ferromagnesian silicates in the Näränkävaara layered series are restricted, and are predominantly Mg-rich in composition (Fig. 4). The anorthite content of plagioclases also varies over a relatively narrow range of between An_{54} and An_{68}, except in the dioritic rocks, where values fall below An_{30}. The minerals of the spinel group in contrast have a wide range of compositions intermediate between the chromites and titanomagnetites, forming a complete iron–titanium–chromium solid solution series rarely found in any layered intrusion.

Everywhere in the western intrusion the marginal series

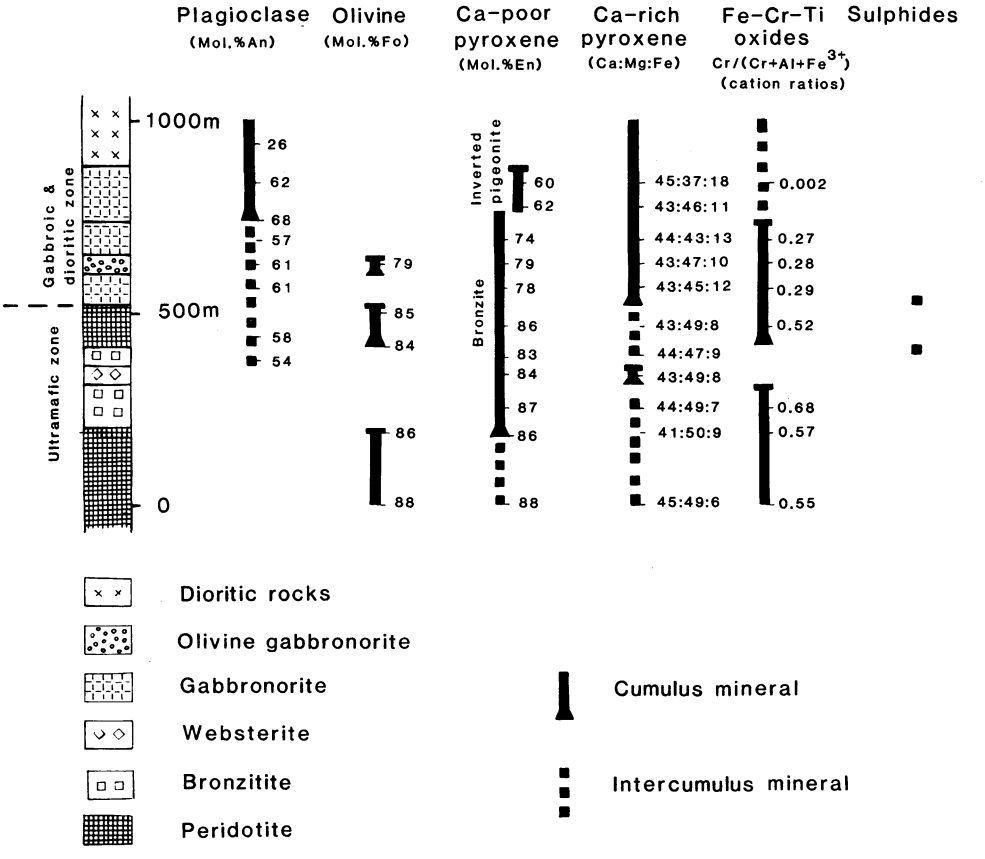

Fig. 4 Stratigraphic sequence and cryptic variation in minerals in eastern part of Koillismaa complex (Näränkävaara intrusion). Cumulus minerals indicated by solid lines and intercumulus minerals by broken lines. Stratigraphic section covers one-sixth of vertical extent of intrusion

separate the discrete intrusion blocks from the underlying basement complex. This sequence varies in thickness from 50 to 200 m, and its rock types are heterogeneous, containing diffuse streaks and veinlets of granitic material from the underlying basement complex.

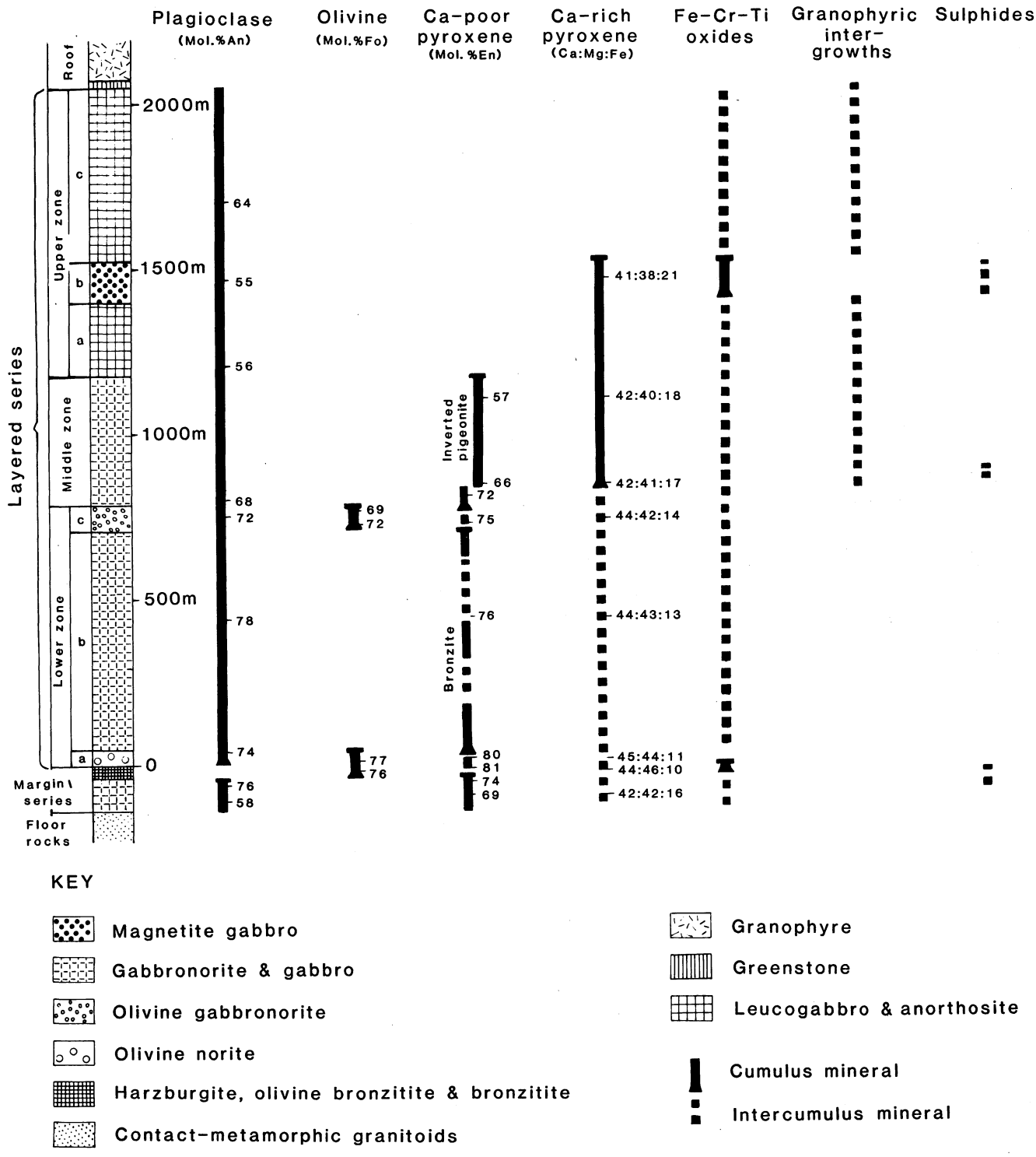

Fig. 5 Stratigraphic sequence and cryptic variation in minerals in western part of Koillismaa complex (Porttivaara block). Cumulus minerals indicated by solid lines and intercumulus minerals by broken lines

The layered series in the western intrusion consists of three mineralogically quite distinct zones—the lower, middle and upper (Fig. 5). Geophysical investigations suggest, however, that the lower zone may be underlain in places by further hidden layers, which should be regarded as constituting a fourth zone. Olivine is a significant cumulus phase in the lower zone, together with plagioclase and sometimes also with bronzite. In the middle zone olivine is absent and is replaced by augite as a cumulus mineral, together with plagioclase and inverted pigeonite. In the Porttivaara and Syöte blocks the middle zone in places also contains PGE-bearing Cu–Ni sulphide enrichments (Fig. 5) in connexion with mottled gabbro, the mottled appearance of this rock being due to those minerals which are late in crystallizing, being concentrated in discrete, light-coloured clusters, into which the sulphides have also aggregated. In the upper zone, which is divided into three distinct sub-zones, the lower and upper parts are plagioclase-rich

cumulates, grading in places into anorthosites, whereas the middle sub-zone is composed of magnetite gabbros in which titaniferous magnetite is a constituent cumulus mineral that coexists with plagioclase and augite. The fine-grained, dust-like chalcopyrite inclusions are typical of the uralitized augite grains in this sub-zone. The upper zone of the western intrusion is then overlain by the thick layer of relatively homogeneous granophyre that conformably caps the layered series. This rock type is commonly porphyritic or microphyric, showing subhedral phenocrysts of albite with granophyric intergrowths of quartz and alkali-feldspar in the matrix. Biotite and hornblende, probably of metamorphic origin, occur as mafic minerals.

In the layered series of the western intrusion, as in the Näränkävaara intrusion, the fractionation trends for ferromagnesian silicates and plagioclase feldspars are also restricted (Fig. 5). The minerals of the spinel group are, in contrast to those at Näränkävaara, represented by titaniferous magnetite only. In certain layers, however, these oxides can be quite chromium-rich.

The various gabbroic rocks are dominant in the exposed western part of the connecting 'dykes'. The nature of these rocks suggests that the whole 'dyke' would be a transition between the eastern and western intrusions.[1] Verification of this conclusion would, however, need additional investigations and, in particular, more borehole data.

Marginal series and sulphide mineralization

Only the marginal series of the western intrusion blocks is considered here—in the other parts of the Koillismaa complex the marginal series is very poorly exposed and the sulphide occurrences are mainly concentrated in the western blocks.

The marginal series of the western blocks is in contact downwards with granite gneisses, in which the original gneissic texture is often preserved, even in the immediate vicinity of the contact itself. A chilled margin is not encountered anywhere at the contact with the basement, probably as a consequence of magmatic erosion, but remnants of it are to be found in the form of xenoliths further away from the contact. The representative analysis from this fine-grained rock type, which also gives some indications of the nature of the primary magma of the western intrusion, is presented in Table 1.

Table 1 Representative analysis of fine-grained rock type from Koillismaa marginal series with C.I.P.W. norms

SiO_2	51.84	C.I.P.W. norms		
TiO_2	0.45			
Al_2O_3	14.60	Quartz		1.28
Fe_2O_3	1.43	Orthoclase		0.78
FeO	6.11	Albite		23.69
MnO	0.12	Anorthite		26.88
MgO	9.65	Wollastonite	di	6.59
CaO	8.60	Enstatite	di	4.38
Na_2O	2.80	Ferrosilite	di	1.73
K_2O	0.13	Enstatite	hy	19.70
Cr	0.021	Ferrosilite	hy	7.80
V	0.005	Magnetite		2.08
Ni	0.017	Ilmenite		0.85
Cu	0.006	Chromite		0.05
Co	0.005			
Zn	0.006			

The lowest part of the marginal series is occupied by heterogeneous gabbronorite with diffuse inclusions of partly melted granitoid fragments indicative of pronounced local contamination (Fig. 6). The volume of these fragments diminishes further away from the contact, and the rock grades to a homogeneous, medium-coarse grained gabbronorite, and this, in turn, to bronzitite, olivine–bronzitite and harzburgite, which are then followed discordantly by the more feldspathic rocks of the layered series. Typical features in all rock types of the marginal series are the originally nearly horizontal layering and primary igneous textures.

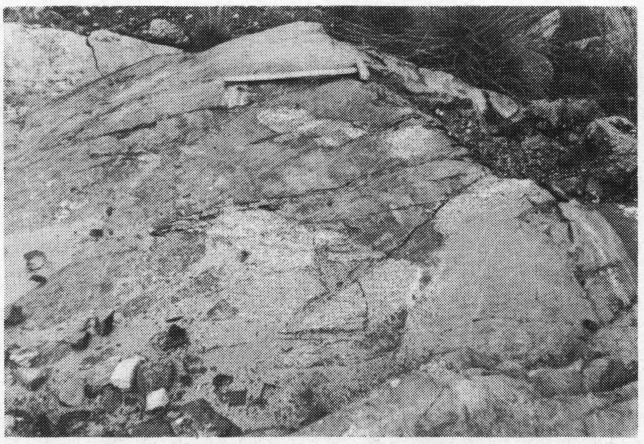

Fig. 6 Granitoid inclusions in mafic rocks of Porttivaara marginal series

The primary minerals in the marginal series are plagioclase, olivine, Ca-poor and Ca-rich pyroxenes and, to a lesser extent, Fe–Cr–Ti oxides. Subhedral grains of plagioclase and Ca-poor pyroxene and poikilitic grains of augite occur in the gabbronorites. The texture is the same in the pyroxenites with respect to pyroxenes, whereas plagioclase is now generally absent or, when it occurs, it is poikilitic. In the harzburgite olivine is euhedral and both pyroxenes are usually anhedral in texture. The change in the abundance of the minerals is accompanied by a change in mineral composition, ferromagnesian silicates becoming more magnesian, the plagioclase more calcic and the oxide minerals more chromium-rich from the outer contact upwards, until the trends are reversed in the layered series (Figs. 5 and 7). These reversed trends, shown by the variation in composition of a relatively small number of the above-mentioned primary minerals, are also confirmed by several semiquantitative microprobe analyses of the inhomogeneous uralites.

The sulphide minerals in the marginal series are largely concentrated in the homogeneous, usually quite coarse-grained gabbronorite at the top of gabbroic rocks (Fig. 7), where they are present as a disseminated phase, occurring as rounded blebs of various sizes interstitial to silicates. Highest concentrations are found in the Porttivaara, Kuusijärvi and Lipeävaara intrusion blocks, where the total amount of nickel and copper can exceed 1% by weight, and that of platinum and palladium can exceed 1 ppm (Fig. 8). Sulphides are also present in places in the ultramafic rocks, especially in pyroxenites, where they particularly occur as a fine-grained, chalcopyrite-predominant dissemination in the uralite grains. They also occur in the heterogeneous, strongly contaminated gabbronorite, where they are generally associated with siliceous fragments. The mineralization does not, however, continue into the contact-metamorphic granitoids below the marginal series.

The sulphides consist of chalcopyrite, pentlandite, pyrrhotite and, in places, pyrite. Microprobe analyses of these minerals are shown in Table 2. The accessory and secondary minerals include mackinawite, sphalerite, argentian pentlandite, millerite, covellite, violarite and marcasite. The platinum-group minerals, which occur mainly as tiny inclusions in sulphide, particularly chalcopyrite and pyrrhotite grains, are represented by froodite, michenerite, merenskyite and sperrylite. Other accessories identified are hessite, electrum, native copper and gold.

The concentrations of the elements in each sample shown in the histograms in Fig. 8 have been recalculated to characterize

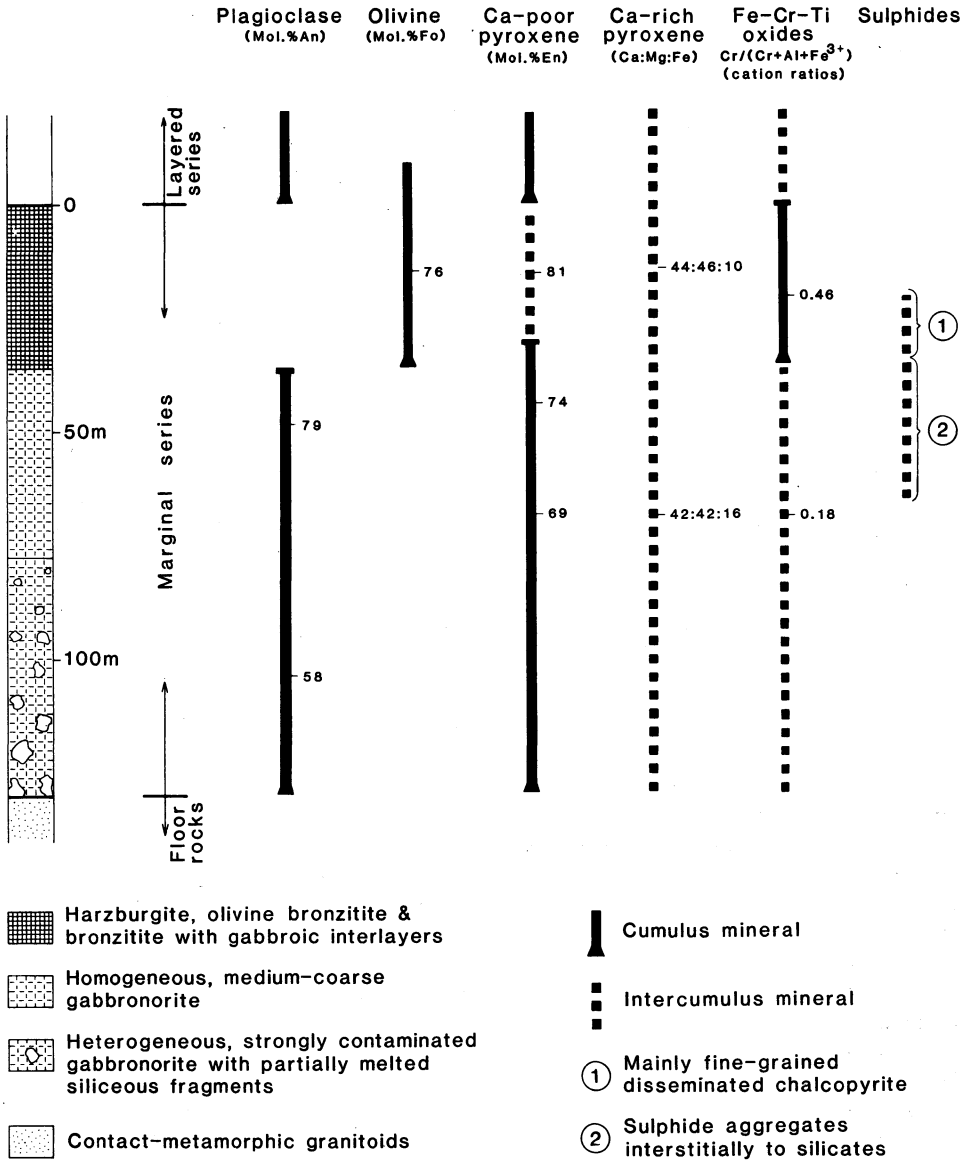

Fig. 7 Stratigraphic sequence and cryptic variation in minerals in marginal series of western part of Koillismaa complex

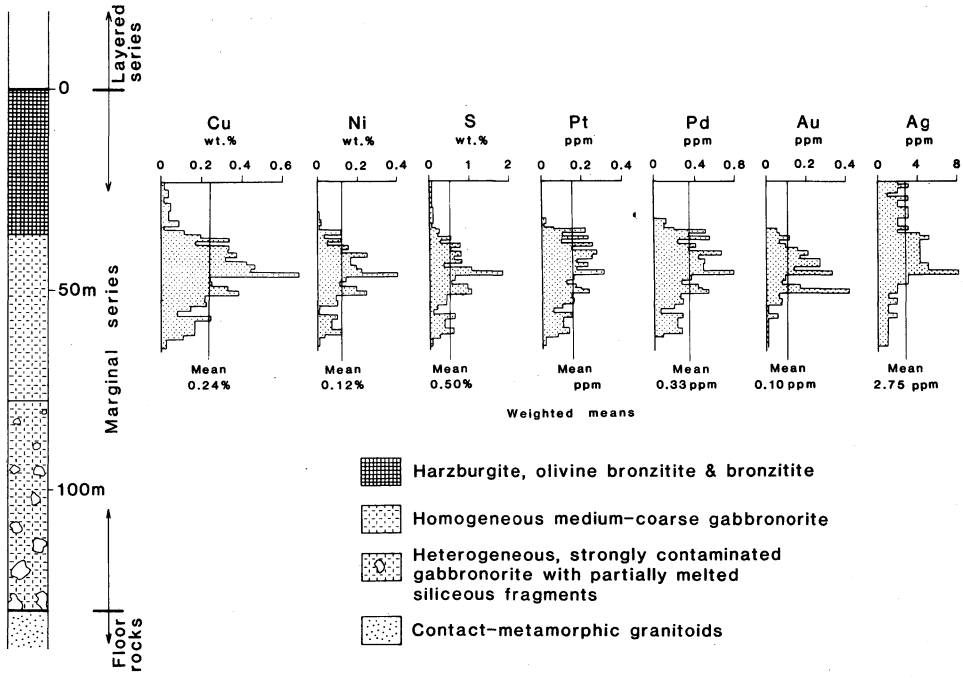

Fig. 8 Vertical variation in Cu, Ni (determined by selective bromine methanol leach), S, Pt, Pd, Au and Ag in drill-hole section (Pso-7) in Koillismaa marginal series. Analytical data from Lahtinen[5]

Table 2 Microprobe analyses of sulphides in marginal series of Porttivaara intrusion block (analyses carried out at Institute of Electron Optics, University of Oulu)

	1	2	3	4	5	6	7	8
Zn	n.d.	0.01	n.d.	n.d.	0.02	0.03	0.02	n.d.
Cu	n.d.	n.d.	33.8	33.2	0.01	n.d.	0.01	0.44
Ni	35.2	38.5	0.02	0.02	0.78	0.47	0.06	0.03
Co	0.61	0.95	0.03	0.04	0.05	0.04	1.21	2.14
Fe	31.0	28.7	30.6	30.6	59.1	59.5	47.0	44.5
S	33.4	32.2	35.1	35.1	38.9	40.0	52.6	51.5
Total	100.21	100.36	99.55	98.96	98.86	100.04	100.90	98.61

1 and 2, pentlandite; 3 and 4, chalcopyrite; 5 and 6, pyrrhotite; 7 and 8, pyrite; n.d., not detected.

the variation in composition of the sulphide fraction in the marginal series (Fig. 9). These calculations are based on the assumption that the sulphide fraction present in these rocks contains 37% by weight sulphur, which probably closely approximates to the true value in the paragenesis chalcopyrite–pentlandite–pyrrhotite±pyrite. The recalculated analyses indicate that the metal contents in the sulphide fraction vary almost sympathetically with one another, and that the highest values are encountered in the upper parts of the mineralization. The concentration of copper and nickel in the sulphide fraction is, generally speaking, high, the weighted means (weighted by the length of the sample) being 17.7% and 8.9% by weight, respectively. The content of precious metals is also relatively high, the weighted mean for platinum being 10.7, for palladium 24.4, for gold 7.10 and for silver 204 ppm.

ultramafic and gabbroic rocks. On the basis of the Cu/Ni and Pd/Pt ratios the sulphide mineralization in the Koillismaa marginal series resembles the Noril'sk ore (cf. Naldrett and Cabri[8]) in spite of the different geological settings of these two formations. When the Cu/(Cu+Ni) ratio is compared with the MgO content of the proposed parental magma (Table 1) the accordance is similarly apparent.

The values for the sulphur isotope composition vary between +1.3 to +2.0‰ (Fig. 10), and are therefore similar to mantle-derived sulphides.

Discussion

It cannot be stated for certain what the nature of the primary liquid that initially filled the Koillismaa magma chambers was. An indication is provided, however, by the fine-grained rock type from the marginal series represented in Table 1, which corresponds in composition to a tholeiitic basalt and is characterized by a relatively high MgO content and low TiO_2. This rock is slightly quartz-normative in character, which is probably a reflection of minor salic contamination.

The Koillismaa magma reached its present location by passing through a long, narrow feeder channel opening out into the Archaean basement and forming the Näränkävaara intrusion and connecting 'dyke' with their roughly triangular cross-sections. This magma then also began to intrude along the practically horizontal unconformity between the basement and the overlying Early Proterozoic supracrustal rocks at the western end of the same feeder to form the extensive, sheet-like western intrusion.

One consequence of the rapid cooling of the basic magma was the formation of a fine-grained chilled margin. As magma emplacement continued, however, this broke up and became

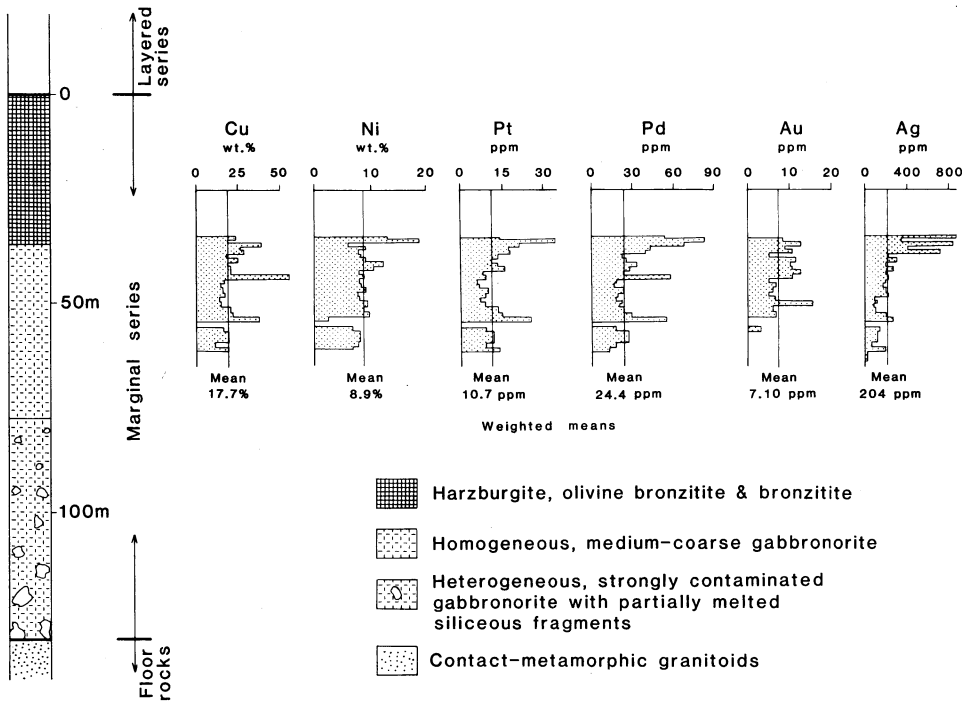

Fig. 9 Vertical variation in Cu, Ni, S, Pt, Pd, Au and Ag of calculated sulphide fraction in drill-hole section (Pso-7) in Koillismaa marginal series. Analytical data from Lahtinen[5]

The sulphide mineralization is characterized as a whole by the predominance of copper over nickel and of palladium over platinum, the concentration ratio for both metal pairs exceeding 2:1 (Fig. 10). The highest values for the Cu/Ni ratio (>30) are recorded in the ultramafic rocks, where the sulphides are chiefly composed of fine-grained chalcopyrite. The Pd/Pt ratio is also highest in the same rock type, even though the maximum value, about 6, is now closer to the boundary between the eroded and is now only encountered as xenoliths located some distance from the contact. While the magma, which was close to being saturated with sulphur, was still in a state of movement granitoid fragments of the salic country rocks became incorporated in it, melting either totally or partially and giving rise to pronounced local contamination. At the same time the more coarse-grained rocks began to crystallize at the base of the western intrusion, resulting in the marginal series, which shows

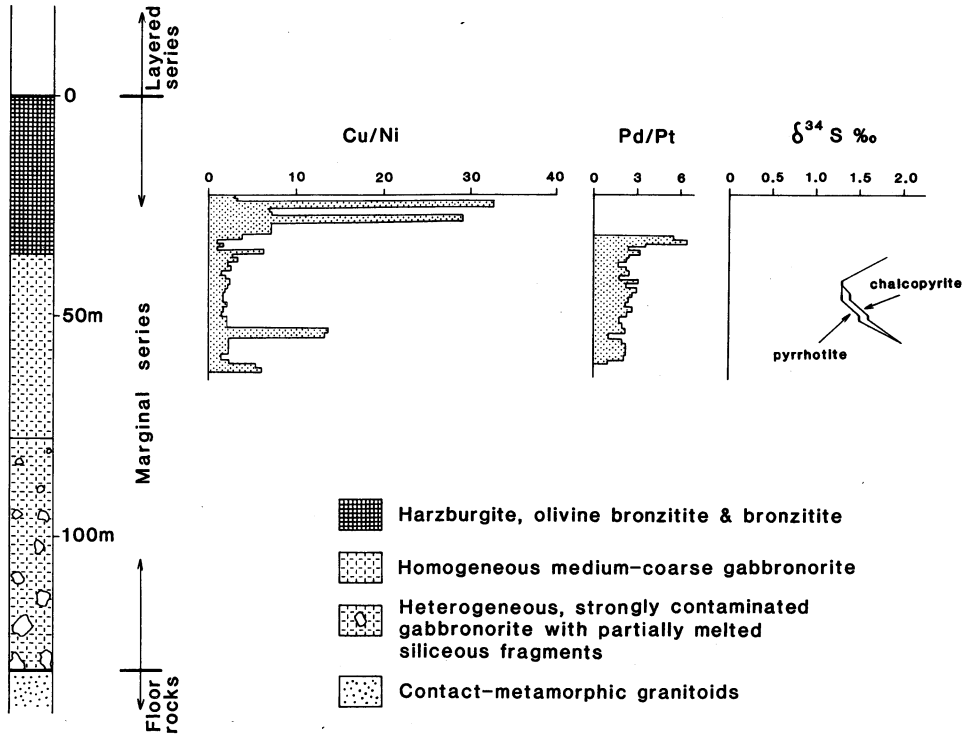

Fig. 10 Vertical variation in Cu/Ni and Pd/Pt ratios and sulphur isotope composition in drill-hole section (Pso-7) in Koillismaa marginal series. Analytical data from Lahtinen[5]

reversed fractionation in comparison with the layered series. During crystallization, the solubility limit for sulphur was exceeded and, in consequence, the separation of the immiscible Cu–Ni–Fe sulphide liquid from the silicate melt took place. Salic contamination is believed to have had an essential role in this process. The sulphide liquid formed was conspicuously copper-rich, and also nickel and precious metal contents were relatively high. The sulphur in the liquid was obviously completely juvenile in origin, as is shown by the isotope data, and, thus, no secondary sulphur has been introduced into the magma.

The sulphide mineralization thus formed was mainly concentrated in the homogeneous, coarse-grained gabbronorite below the ultramafic rocks, where the sulphides are chiefly composed of fine-grained chalcopyrite inclusions in the uralite grains, possibly as a consequence of the later regional metamorphism. In the strongly contaminated lower part of the marginal series the sulphide mineralization is poorly developed and the separate sulphide grains are generally aggregated around siliceous fragments.

Acknowledgement

The authors thank Jarmo Lahtinen, Lapin Malmi, for permission to use his analytical data concerning the element variation in a drill-hole section. Furthermore, the authors wish to express their gratitude to Dr. D. L. Buchanan, Royal School of Mines London, for his constructive criticism of the manuscript and to Dr. Sheila Hicks, University of Oulu, for correction of the English text.

References

1. Alapieti T. The Koillismaa layered igneous complex, Finland—its structure, mineralogy and geochemistry, with emphasis on the distribution of chromium. *Bull. geol. Surv. Finl.* 319, 1982, 116 p.
2. Alapieti T. Hugg R. and Piirainen T. Structure, mineralogy and chemistry of the Syöte section in the Early Proterozoic Koillismaa layered intrusion, northeastern Finland. *Bull. geol. Surv. Finl.* 299, 1979, 43 p.
3. Alapieti T. *et al.* The ultramafic and mafic intrusion at Näränkävaara, northeastern Finland. *Rep. Invest. geol. Surv. Finl.* no. 35, 1979, 31 p.
4. Hjelt S.-E. *et al.* Regional interpretation of magnetic and gravimetric measurements, based on combinations of dipping prisms and plates. *Geol. För. Stockh. Förh.*, **99**, 1977, 216–25.
5. Lahtinen J. PGE-bearing copper–nickel occurrences in the marginal series of the Early Proterozoic Koillismaa layered intrusion, northern Finland. *Rep. Invest. geol. Surv. Finl.* In press.
6. McClay K. R. and Campbell I. H. The structure and shape of the Jimberlana Intrusion, Western Australia, as indicated by an investigation of the Bronzite Complex. *Geol. Mag.*, **113**, 1976, 129–39.
7. Mutanen T. A new type of platinum-bearing chromite ore in the Koitelainen mafic layered intrusion, northern Finland. In *Third international platinum symposium, Pretoria, South Africa, abstracts of papers* Pretorius D. A. ed. (Johannesburg: Economic Geology Research Unit, University of the Witwatersrand, 1981), 28–9.
8. Naldrett A. J. and Cabri L. J. Ultramafic and related mafic rocks: their classification and genesis with special reference to the concentration of nickel sulfides and platinum-group elements. *Econ. Geol.*, **71**, 1976, 1131–58.
9. Piirainen T. *et al.* The marginal border group of the Porttivaara layered intrusion and related sulphide mineralization. *Bull. geol. Soc. Finl.* no. 49, 1977, 125–42.
10. Piirainen T. *et al.* Koillismaan malmikriittisten alueiden tutkimusprojektin loppuraportti 1976. English summary: The report of the Koillisma Research Project. *Rep. Invest. geol. Surv. Finl.* no. 18, 1978, 51 p.
11. Smith C. H. Notes on the Muskox Intrusion, Coppermine River area, District of Mackenzie. *Pap. geol. Surv. Can.* 61-25, 1962, 16 p.

Ni–Cu sulphide deposits in Vietnam

Le Thac Xinh
Nguyen Van Chu
General Department of Geology, Hanoi, Vietnam

Synopsis

In northern Vietnam Ni–Cu sulphide deposits associated with ultramafic rocks are located in several continental rift zones of Permo-Triassic age. In recent years a number of ultramafic bodies have also been discovered in southern Vietnam, but detailed work on sulphide occurrences within these bodies has still to be undertaken.

A brief description is given of some Ni–Cu sulphide deposits that are located in the northern part of the country. Of the deposits that have been examined in any detail, those in the Takhoa region are of the greatest economic interest. Ni and Ni–Cu sulphide bodies have, however, also been found in association with the ultramafic rocks.

Location of Ni–Cu sulphide-bearing ultramafic complexes

Although mafic and ultramafic bodies are widely distributed in the north of Vietnam (Fig. 1), Ni–Cu sulphide mineralization is found only in those which are associated with rift zones of Permo-Triassic age. The largest ultramafic complexes in northern Vietnam belong to the Nui Nua group of rocks in

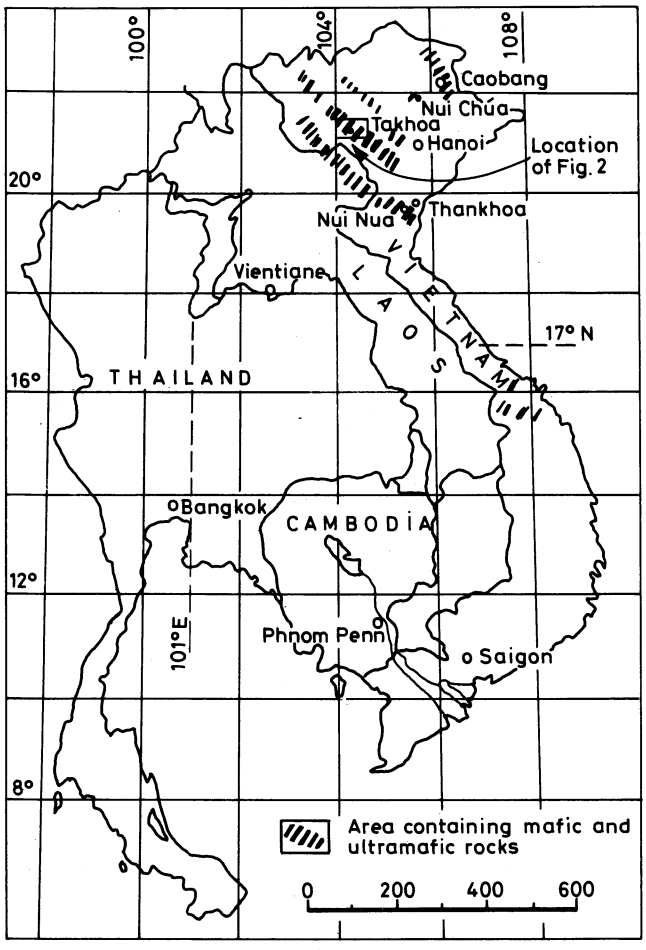

Fig. 1 Location of ultramafic rocks in Vietnam

Thankhoa Province. These do not, however, contain Ni sulphide mineralization, though chromite is present in the rocks and Ni laterites have formed at the surface. The mafic intrusions that are associated with the Nui Nua Complex also contain ilmenite ore. The main deposits of Ni and Ni–Cu sulphide are located in the Takhoa region of the Da River rift zone (Figs. 1 and 2), but some non-economic occurrences of Ni sulphide have been found in mafic and ultramafic rocks of the Caobang Complex, which is located in the Caobang rift zone near the northern border.

Geological setting of Takhoa region

Located in northwestern Vietnam inside the Da River rift zone, the Takhoa region contains abundant ultramafic bodies of various sizes (Fig. 2). In addition to the ultramafic rocks, a system of northwest–southeast-trending diabase dykes has intruded the region. The Da River fracture zone has a similar trend and has been considered as the boundary of the South China and Indochina plates.[1-3]

Structurally, the Takhoa region consists of a pitching anticline of Devonian formations overlain by Permian and Triassic basaltic flows with limestone intercalation. Lower and Middle Devonian terrigenous sediments were locally metamorphosed into mica schist, gneiss and hornfels.

Mafic and ultramafic rocks intruded into Devonian formations and, in turn, they were penetrated by a granitic pegmatite 105 m.y. in age. Similar age relationships have been established between ultramafic and mafic rocks with mafic lavas hosting Permian and Triassic fossil-bearing interflow sediments. The dykes and ultramafic and mafic intrusives have been considered to represent the roots of the overlying mafic lavas. The conclusion is that the ultramafic Ni–Cu-bearing rocks in the regions were emplaced during rifting of the continental crust during Permo-Triassic time.[3]

The ultramafic rocks consist of dunite, peridotite and pyroxenite, most of which have been altered to serpentine, tremolite and phlogopite rocks.

Mineralization

Almost all of ultramafic rocks in the Takhoa region contain some Ni and Ni–Cu sulphide mineralization in the form of disseminated ore that is found near the base of the intrusion, such as those of Banfuc, Bantrang and Hôngngai. Dyke-like Ni–Co sulphide bodies have also been found on the margins of the ultramafic massives in the surrounding Devonian rocks at the Banfuc and Banmong deposits.

Banfuc deposit

The Banfuc deposit consists of an elipsoid 940 m long and 440 m wide with a total area of 0.248 km^2 (Figs. 3 and 4). The rocks consist of serpentinite and serpentinized dunite, the upper part of the body being completely serpentinized. Antigorite dominates over chrysotile; phlogopite, chlorite and chrome spinel are also present. In the lower part of the intrusion relict olivine grains have been preserved. The body has been intruded by granitic pegmatite veins.

Two types of sulphide ore have been recognized.

Dyke-type Ni–Cu sulphide ore

The orebody is located at a distance of 20–100 m outside the ultramafic rocks body (dip 70–90°). It is 640 m in length and reaches depths of 450 m. The massive ore is 0.2–5 m thick and

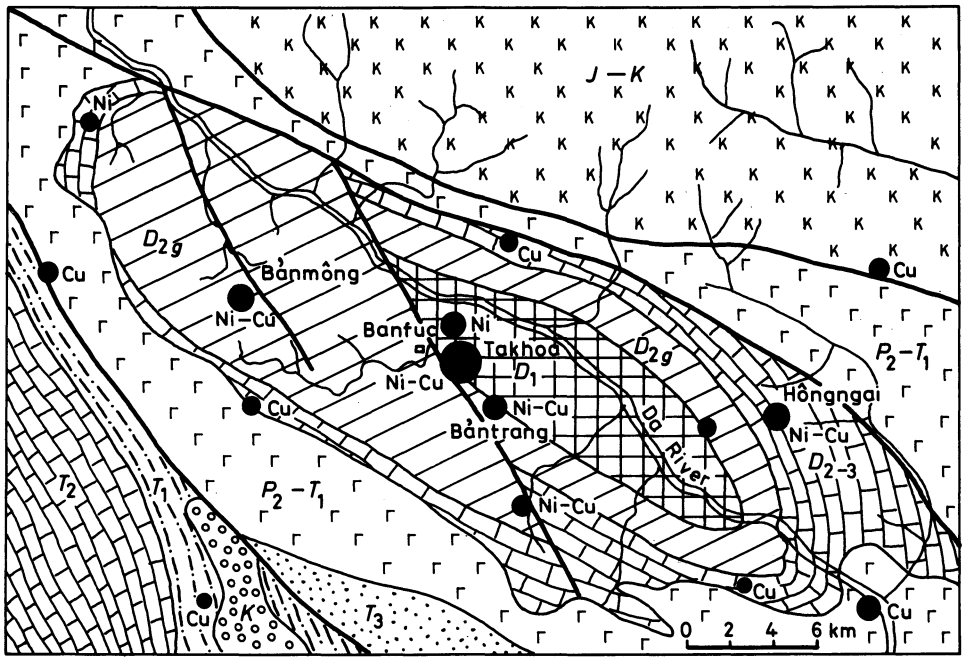

Fig. 2 Mineral map of Takhoa Region: D_1, Lower Devonian (sericite schist, mica schist, quartzite); D_{2g}, Givetian (sericite schist, sandstone, chert); D_{2-3}, Middle–Upper Devonian (limestone); $P_2–T_1$, Upper Permian–Lower Triassic (basalt porphyrite); T_1, Lower Triassic (sandstone, shale); T_2, Middle Triassic (limestone); T_3, Upper Triassic (conglomerate, sandstone, shale, coal); $J–K$, Jurassic–Cretaceous (acidic–mafic volcanic rocks); K, Cretaceous (conglomerate, sandstone, shale)

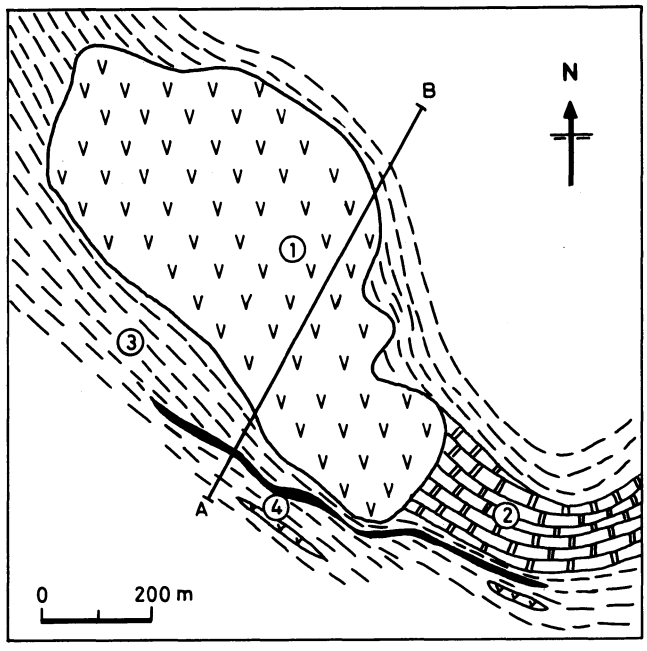

Fig. 3 Geological map of Banfuc deposit: 1, ultramafic rocks; 2, marble; 3, schist; 4, dyke-type orebody

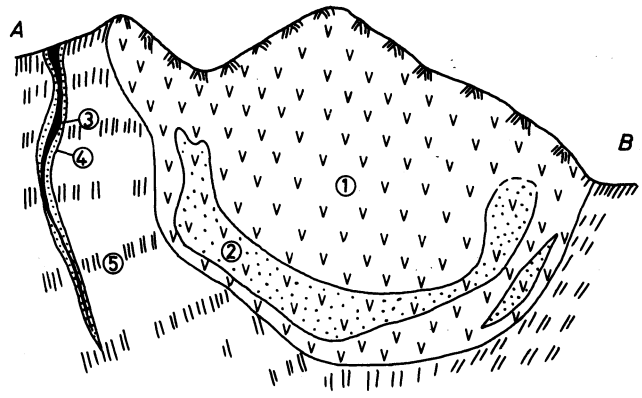

Fig. 4 Cross-section $A–B$; 1, ultramafic rocks; 2, disseminated Ni sulphide ore; 3, massive Ni–Cu sulphide ore; 4, disseminated Ni–Cu sulphide ore; 5, schist

that of the surrounding disseminated ore varies between 0.6 and 19 m.

Sulphide from the massive ore consists mainly of pyrrhotite, pentlandite and chalcopyrite. Analytical data reveal Ni/Cu = 3, Ni/Co = 30, 0.75–1.63% Cu, 0.49–4.78% Ni, 24.98% S, 0.02–0.20% Co and 0.004% Se.

Besides the above-mentioned minerals, the disseminated ore that surrounds the massive ore contains the following additional phases: pyrite, sphalerite, galena, niccolite, skutterudite, rammelsbergite, violarite, quartz and chlorite. Analytical data show Ni/Cu = 2/3, Ni/Co = 40/1, 0.75% Cu, 0.49% Ni, 0.021% Co, 0.005% Se, 0.0001% Te and 0–0.05 g/t Pt.

Ni sulphide disseminated ore in ultramafic rocks

Low-grade Ni sulphide ore is concentrated at or near the base of the ultramafic intrusion. The major mineral phases are pentlandite, pyrrhotite, chalcopyrite and magnetite. In addition, chalcopyrite, pyrite, niccolite, cubanite, galena and sphalerite occur as small veins. Analytical data reveal 0.1% Cu, 0.7% Ni and 0.02% Co. Se, Te, Pt, Au, Ag are present in trace amounts. The thickness of the orebody varies from 1 to 36.7 m.

Genesis

The dyke-type ore is considered[4] as the product of injection of immiscible sulphide liquid segregated from an ultramafic magma into a fracture zone. The disseminated ore present in the ultramafic rocks is considered to be the product of sulphide segregation from the host magma, which settled at the base of the body. Metamorphic activity crystallization of the magma may also have played some role in enrichment of the ore.

Acknowledgement
The authors are very grateful for assistance from their colleagues in the preparation of this paper, which is published by kind permission of the Heads of the General Department of Geology.

References

1. Le Thac Xinh. Metallogenic epoch in North Vietnam. *Georeview, Hanoi,* 1978. (Vietnamese text)
2. Le Thac Xinh, Mine and Geology College, Hanoi. Report (1979) on Indochina metallogenic epoch in North Vietnam. (Vietnamese text)
3. Le Thac Xinh. Mineralization of the continental rifting epoch in North Vietnam. In *Proceeding of IV GEOSEA Conference, Manila, 1981* (Manila: Geological Society of the Philippines, in press).
4. Ha Phat Vinh, General Department of Geology, Hanoi. Report (1963) on prospecting of Banfuc Ni–Cu deposit. (Vietnamese text)

Aspects of nickel metallogeny of Southern Africa

E. C. I. Hammerbeck D.Sc.
Geological Survey of South Africa, Pretoria, South Africa

Synopsis

Geological controls and constraints in space and time define the milieu of the nickel deposits of Southern Africa. Primary, magmatic deposits are of two types, e.g. synvolcanic or syntectonic deposits confined to certain orogenic domains, and those related to intracratonic, post-orogenic magmatism, e.g. the Great Dyke, the Bushveld Complex and the Insizwa intrusion. Epigenetic and supergene deposits form a separate, unrelated group and are of minor economic importance.

The metallogenic evolution of syntectonic nickel deposits is particularly well illustrated in the Zimbabwean Province, where the relationships between Archaean greenstone development and nickel mineralization are best illustrated. Volumetrically subordinate, nickel-poor greenstones in the 3500 m.y. old Sebakwian Group are followed by more common komatiite development in the Lower Greenstones (3000 m.y.), and, finally, by very significant komatiites with important nickel mineralization in the 2700 m.y. old Upper Greenstones of the Bulawayan Group.

Comparable nickel mineralization is not known in the Kaapvaal Province, in spite of ubiquitous komatiitic magmatism of the Onverwacht Group (3500 m.y.) and other greenstone sequences. No komatiitic rocks younger than about 3200 m.y. are known in this region, orogenic activity in the Kaapvaal tectonic province having ceased at about 3100 m.y., whereas the Zimbabwe Province remained tectonically active until at least 2600 m.y.

The tectonic environment, host-rock petrology and mode of emplacement, as well as some details of the nickel mineralization, are the parameters employed to classify the Southern African magmatic nickel deposits. A rating of the deposits is introduced that reflects the original resources of the deposit, its average nickel content, its mining history and potential to facilitate ready comparison with and assessment of the nickel deposits listed in the classification, as well as some important nickel deposits worldwide.

Much new information and fresh perspectives on Southern African geology have become available in recent years, largely as a result of the efforts of the South African Committee for Stratigraphy and its working groups, as well as research carried out under the international geodynamics programme. Results of the former work were published by SACS,[1] whereas Tankard *et al.*[2] provided a new synthesis of the geological history of Southern Africa. Likewise, under the auspices of the *IGCP 161 project* knowledge of the nickel deposits of the subcontinent has proliferated. Recent reviews of the latter aspect were provided by Williams,[3] Von Gruenewaldt,[4] Clutten and co-workers[5] and Hammerbeck.[6]

For details on the geology in general, as well as on the geographical distribution of the individual nickel deposits of Southern Africa in particular, the interested reader is referred to the above-mentioned literature. In addition, the recently published mineral map of South Africa and some neighbouring territories[7] provides an overall metallogenic setting of some of the nickel deposits that are discussed. This paper is designed to be complementary to the above nickel reviews in that an attempt is made to classify the nickel deposits in the light of recently devised international classification schemes and to map out their tectonic and metallogenic framework.

Some geological controls and constraints in space and time

Geological setting

The development of favourable geological domains of primary nickel deposits in Southern Africa must be viewed, first, against the recurrence of basic to ultrabasic magmatism throughout the geological history of the subcontinent, and, second, against the tectonic framework of the area. In Table 1 the stratigraphic position of nickel deposits in the main nickel-bearing areas, as well as those orogenic cycles marked by important syntectonic or synvolcanic basic to ultrabasic magmatism, is shown. The geological framework of Southern Africa comprises a number of structural provinces, which were recently redefined by Tankard *et al.*[2] Of these, the Kaapvaal, Zimbabwe, Limpopo and Namaqua Provinces are of special interest as far as nickel is concerned (see Fig. 1).

Nickel in orogenic domains of Southern Africa

In contrast to the more or less coeval Zimbabwe and Limpopo Provinces, nickel mineralization in the Kaapvaal Province is rather conspicuous by its absence—not only in the Barberton Sequence but also in the Gravelotte, Giyani, Pietersburg, Kraaipan, Marydale and other Archaean greenstone belts—in spite of ubiquitous komatiitic magmatism. Anhaeusser[8] stressed the almost total confinement of komatiitic basalts and peridotites to Archaean greenstone belts. These terrains have evolved over an enormous time-span of 1000 m.y., i.e. from approximately 3500 to 2500 m.y. ago. Ultrabasic magmatism is a very important facet of these greenstones, accounting, for instance, for

Table 1 Stratigraphic and tectonic setting of nickel deposits in Southern Africa

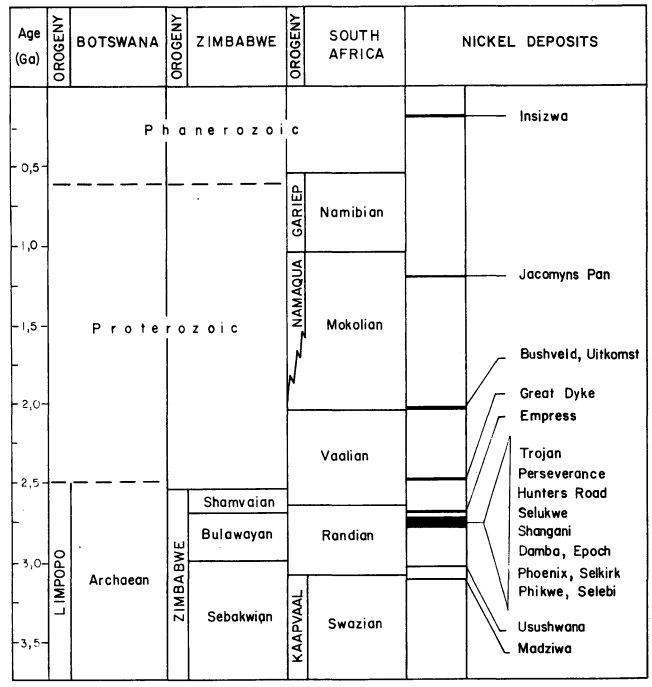

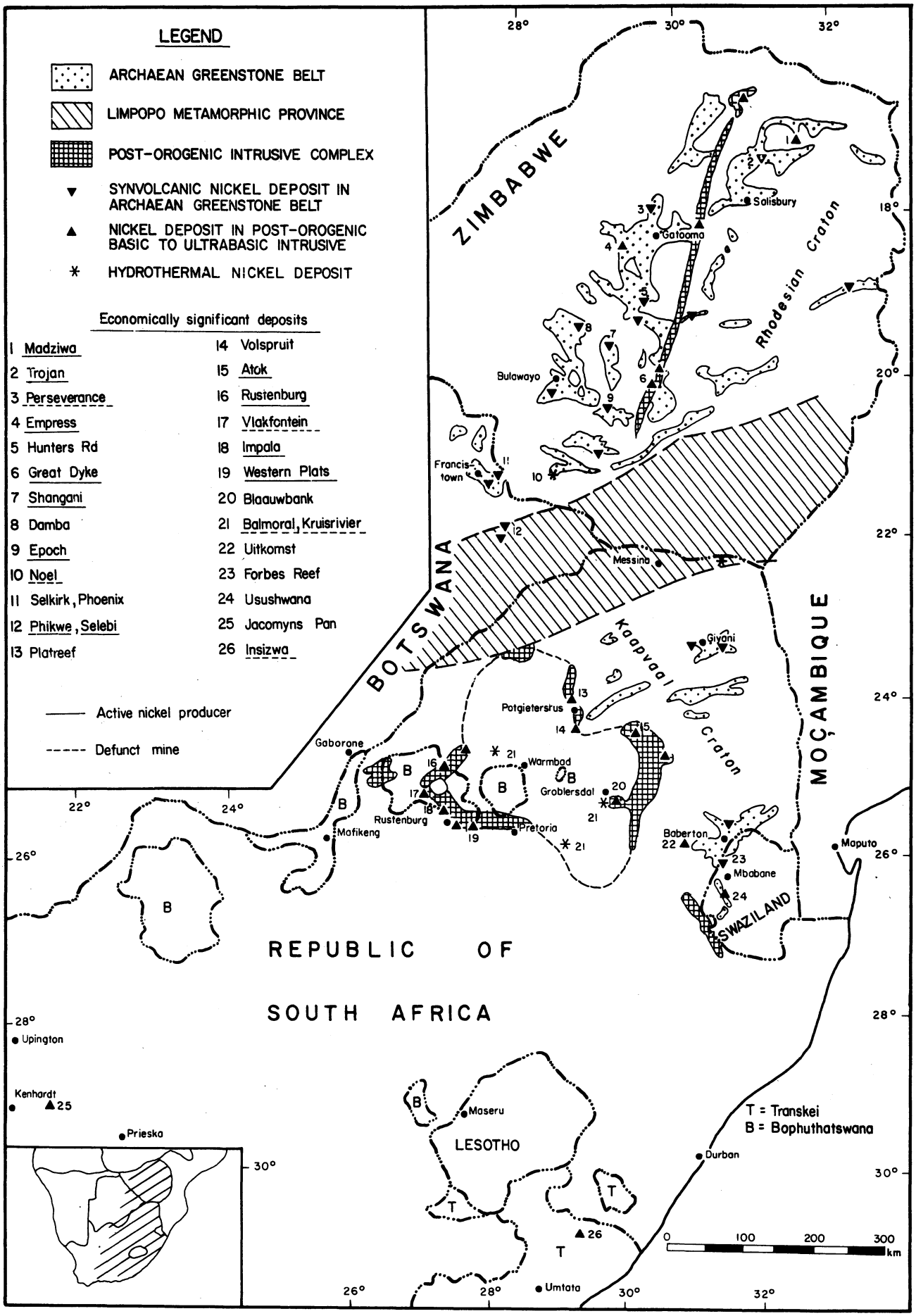

Fig. 1 Nickel deposits of Southern Africa. From Hammerbeck[6]

more than 90% by volume of the Onverwacht Group of the Barberton Sequence. The Onverwacht komatiites and related ultrabasics are dated at 3500 m.y. and represent one of the most significant accumulations of ultrabasic volcanics in the world.[9] According to Anhaeusser,[8] all greenstone belts consist of a lower, largely volcanic, and an upper sedimentary cycle. Compared with the Barberton Sequence, the evolutionary history of the Zimbabwe greenstone terrain was much more prolonged. In the Sebakwian Group—the oldest rocks (*ca* 3500 m.y.) in the Zimbabwe Province—greenstones are very subordinate to granite–gneiss in volume. Only in the Bulawayan Group are greenstones ubiquitous. Here a bimodal spatial development of ultrabasic magmatism is observed, the Lower Greenstones of uncertain age, and the Upper Greenstones, dated 2700–2800 m.y.[10,11] These Upper Greenstones are of special interest because of their important nickel mineralization. Wilson[10] discounted the applicability of the Barberton model to the Zimbabwe Province, as propounded by Anhaeusser,[12] the main reason being the two greenstone cycles developed in the Bulawayan Group.

Sebakwian greenstones of the Zimbabwean Province are comparable in age with those of the Kaapvaal craton, but are vastly subordinate in volume. Moreover, the Zimbabwean Bulawayan greenstones have no known counterpart in space and time on the Kaapvaal craton[10]—a very important fact as far as nickel mineralization in the Archaean greenstone belts of Southern Africa is concerned.

Another significant difference is that orogenic activity in the Kaapvaal Province ceased much earlier than in the Zimbabwe and Limpopo Provinces (Table 1). As a result, intracratonic sedimentation together with concomitant tholeiitic magmatism ensued on the Kaapvaal craton from about 3100 m.y. onwards, whereas the Zimbabwe and Limpopo Provinces remained tectonically active until at least 2600 m.y.

The exact age and spatial relationships of the basic magmatism with which the nickel–copper deposits of Phikwe–Selebi are associated remain uncertain. These intrusions are assigned to the Baines Drift Metamorphic Suite, which is believed to be coeval with the Upper Greenstone of the Bulawayan Group, as preserved in the Tati and Matsitama schist belts, outside the high-grade Limpopo Province.[2] Lithologically, however, these rocks also compare favourably with the 3200 m.y. Messina Suite of the Beit Bridge Complex. Nevertheless, there is no doubt that the tectonic setting of the Phikwe, Selebi and related basic intrusions forms an integral part of the Limpopo orogeny.

The Namaqua Province comprises a large, heterogeneous group of tectonically reworked medium- to high-grade metamorphic rocks, covering a large tract of land in the northwestern Cape Province and southern South West Africa. Detailed descriptions of the present status of knowledge on this very complex geology have been provided.[1,2] Syntectonic basic and ultrabasic magmatism is relatively rare in this orogenic domain. The best-known example is the large cluster of more than 700 bodies collectively known as the Okiep basic intrusions, some of which are mineralized with copper and gave rise to the substantial industry of the O'okiep Copper District. Metamorphosed basic intrusions are also known farther east near Pofadder,[13] the Kakamas–Keimoes area[14] and the area between Keimoes and Prieska Poort.[1] Of all these basic intrusions, only one on Jacomyns Pan and the adjoining Hartebeest Pan east of Kenhardt is known to carry significant low-grade nickel mineralization.[15]

Nickel in post-orogenic domains

The Usushwana Complex, emplaced into the 3000 m.y. old Pongola Sequence cover rocks on the Kaapvaal craton, represents the oldest (~2900 m.y.) example of a nickel-bearing, post-orogenic intrusion in Southern Africa.[16,17]

Large-scale post-orogenic magmatism occurred during the Early Proterozoic on the cratonized Zimbabwean and Kaapvaal Shields, giving rise to the Great Dyke (2500 m.y.) and Bushveld Complex (2000 m.y.), respectively. Several styles of low-grade nickel mineralization can be recognized in the Bushveld Complex, the most important of which are in the stratiform Merensky Reef, and in the Platreef, which represents sulphide concentrations near the floor of the complex.[6] Owing to the association of nickel with economic concentrations of platinum-group metals in these two settings, the Bushveld Complex constitutes one of the largest exploitable nickel repositories in the world, though of rather low grade.

The youngest important basic to ultrabasic magmatic activity with a bearing on nickel mineralization in Southern Africa took place during the early Jurassic, approximately 1000 m.y. after the Namaqua metamorphic event. Karoo lava flows of the 'Flood Basalt' type[22] and concomitant emplacement of dolerite sheets and dykes occurred over vast areas of the subcontinent, but nickel mineralization of economic interest is known only from the substantial layered intrusion at Insizwa in the Transkei.[18]

Epigenetic and supergene mineralization

A number of small hydrothermal and superficial nickel deposits are known in Southern Africa. Although clearly of limited economic significance, the different geological environments of these deposits are of interest.

Hydrothermal nickel-bearing deposits are characterized by particularly varied and complex mineral assemblages, the best-known examples of which are the Ag–Co–Ni–Bi–U–As deposits of the Cobalt district in Canada and of the Erzgebirge in Eastern Germany.[19] In Southern Africa hydrothermal nickel deposits are found in Archaean greenstone belts in Zimbabwe, where they were exploited in a number of workings at Noel[3] and possibly in Swaziland at Forbes Reef, though the origin of this low-grade deposit remains uncertain.[20] For this reason this deposit has been provisionally included in the classification of magmatic nickel deposits (Table 2). At the former locality nickel is present in the form of cloanthite and niccolite; gersdorffite is the predominant nickel mineral at Forbes Reef. 'Cobalt'-type hydrothermal deposits are present in the Bushveld Complex, near Rooiberg, at Balmoral, in the Kruisrivier area, and at the old Albert silver mine.[6] Typical hydrothermal nickel ores, such as gersdorffite and niccolite, are present at some deposits, and cobaltiferous ores are more conspicuous at Kruisrivier and Balmoral.

Nickeliferous laterite and garnierite are of minor economic importance in Southern Africa. Large resources of birbiritic laterite, with approximately 1% nickel, are known from the Great Dyke, Zimbabwe (J. G. Stagman, personal communication), whereas some 20 000 000 t of such material of similar grade is present near Potgietersrus in the Bushveld Complex (S. A. de Waal—see discussion in Hammerbeck[6]). In addition, a number of small surficial deposits are known in some greenstone belts—at Barberton, Lusinzi and Nkandla.[21]

Classification of nickel deposits

Present classification schemes

Nickel deposits are being classified according to a variety of parameters. The earliest form is a distinction simply between sulphide ores and secondary deposits, but this fails to express the complexities in various geological settings in which the sulphide ores may be found.

To overcome this problem the IGCP Working Group 161 has adopted a classification that reflects, in essence, a classification of basic to ultrabasic magmatism.[22] This scheme succeeds in expressing the variety of nickel deposits on a global

Table 2 Classification of magmatic nickel deposits of Southern Africa

Geological environment				Host rock of ore zone			Nickel deposit			
Tectonic setting		**Stratigraphic unit**	**Age, m.y.**	**Petrological affiliation**	**Rock type**	**Mode of emplacement and morphology**	**Ni, %**	**Ni:Cu (bulk)**	**Rating***	**Deposit name**
Orogenic domain (syntectonic/ synvolcanic)	Kaapvaal Province	Onverwacht Group	3500	Komatiitic (?)	Talc carbonate schist		0.11	1.0–1.3	3.4.4	Forbes Reef
				Komatiitic	Serp., talc carb.	Volcanic; lava	0.68	up to	3.3.1	Trojan
					Serp., talc carb. Peridotite	flows	0.3	20	3.3.2	Damba
					Peridotite	Intrusive; mushroom shaped	0.8		3.2.1	Shangani
					Peridotite	Intrusive; layered	0.64	up to 20	3.3.1	Epoch
					Serpentinite	Intrusive	0.7		3.3.2	Hunters Rd.
	Zimbabwe Province	Bulawayan Group	2700–2800	Komatiitic	Serpentinite	Intrusive; lenticular	1.0	2.5	3.2.3	Perseverance
					Peridotite	Intrusive	2.5		4.1.4	Selukwe
						Veins in shear zones	2.1	2.6	3.1.4	Phoenix
					Amphibolite	Intrusive; faulted	0.5–1.2	1.1–2.0	4.2.4	Selkirk, Tekwane
				Tholeiitic	Peridotite, gabbro	Intrusive; dyke	0.72	1.3	3.2.1	Empress
		Sebakwian		Tholeiitic	Meta-pyroxenite, Meta-gabbro	Intrusive; podiform	0.61		3.2.1	Madziwa
	Limpopo Province	Baines Drift Suite	2800(?)	Tholeiitic	Amphibolite	Uncertain; disrupted conformable body or layered intrusion	0.95–1.22	1.0–1.3	3.2.1	Phikwe
					Amphibolite		0.73-0.91	0.5-0.6	3.3.1	Selebi
					Amphibolite		0.86	0.9	4.1.2	Selebi North
	Namaqua Province	Keimoes Suite	1200	Tholeiitic(?)	Biotite–tremolite schist, hypersthenite	Intrusive	0.25	1.5	3.3.4	Jacomyns Pan
Post-orogenic or anorogenic domain (intracratonic)	Pongola	Usushwana	2900	Tholeiitic	Gabbro	Intrusive; layered	0.16	0.4	4.4.4	Embo, Maloya
	Post-Zimbabwe	Great Dyke	2500	Tholeiitic	Pyroxenite	Intrusive; sheet-like	0.25	1.25	1.3.4	Hartley, Wedza
	Transvaal Basin	Bushveld Complex	2000	Tholeiitic	Feldspathic pyroxenite	Intrusive; sheet-like	0.18	2.0	1.4.1	Merensky Reef
					Harzburgite, pyroxenite	Intrusive	Variable	2.0	1.3.2	Platreef
					Pyroxenite	Intrusive sheet-like	0.24	2.0	1.4.4	Volspruit PGE
					Gabbro-norite	Intrusive; sheet-like	0.22		1.4.4	Grass Valley
					Harzburgite Bronzitite	Intrusive; pipes, veins	Variable	1.0	3.2.3	Vlakfontein
		Bushveld Satellite intrusion	2000	Tholeiitic	Pyroxenite, gabbro	Intrusive; layered sill	0.1–0.7		3.3.2	Uitkomst
	Karoo Basin	Karoo dolerite	200	Tholeiitic	Picrite	Intrusive; layered	Variable	0.3–1.6	4.1.3	Insizwa

*See text for explanation of rating system.

scale, and highlights favourable geological environments with known nickel deposits, as well as potentially favourable areas without known mineralization. At the same time, however, it incorporates certain aspects that have little genetic significance as far as nickel is concerned. For instance, the distinction between large sheet-like complexes, such as the Bushveld, and dyke-like complexes, such as the Great Dyke, seems not to be warranted, as Worst[23] has already pointed out that the latter in reality comprises four sheet-like layered intrusions. Moreover, the fact that some nickel deposits occur in large, and others in small, layered intrusions is probably of minor metallogenic significance.

The nickel deposits of Western Australia are classified according to their petrological associations.[24] This very practical scheme facilitates a classification by means of parameters that are easy to determine, such as the MgO content of the host rocks and the Ni:Cu ratio of the sulphide ores. The differentiation between intrusive dunite associated (IDA) and volcanic peridotite associated (VPA) deposits is, however, less straightforward in that both types are of synvolcanic affiliation,[22] and the distinction depends on interpretation of field relationships.

Classification of Southern African deposits

Three types of nickel deposits may be recognized—primary magmatic nickel–copper sulphides, hydrothermal vein-type deposits and laterite deposits. In the Southern African context

only the magmatic ores are of economic importance and these are dealt with in detail in Table 2. The proposed scheme takes cognizance of the most important genetic concepts of the classifications referred to above, and should be seen as an attempt to synthesize characteristic features peculiar to the local, Southern African circumstances and not as a classification of nickel deposits *per se.*

The salient parameters that are employed are the geological environment of the magmatic event, details about the host rock of the ore zone and, finally, information on the nickel deposit as such, combined with a rating of deposits based on size of the deposit, ore grade and economic potential.

Two structural domains are recognized. The orogenic domain comprises syntectonic basic to ultrabasic magmatism and includes the synvolcanic category in Naldrett's classification,[22] whereas the post-orogenic or anorogenic domain represents nickel deposits in basic to ultrabasic intrusions emplaced into the stable platform cover.

The information on the host rocks permits an assessment of the geological milieu of the magmatic nickel deposits—in a similar fashion to the Western Australian classification. Komatiitic suites are distinguished from the tholeiitic suites, both of which host important nickel mineralization. Information such as whether the magmatism is of extrusive or intrusive nature, and the morphology of the host-rock body, has a bearing on the style of nickel mineralization, and has been used in both Naldrett's and Marston's classifications.

Characteristics of the orebody, i.e. massive, matrix or disseminated sulphides, the nickel content of the ores and their characteristic Ni:Cu ratios are standard parameters that are used to describe nickel deposits.

Rating of nickel deposits

In addition to the above parameters, a rating, based on worldwide data on nickel deposits, is given that reflects the original resources of the deposit, its average nickel content and its mining history and potential to facilitate ready comparison and assessment of the nickel deposits listed in Table 2. The proposed rating comprises three digits, each ranging from 1 to 4, to portray the following information.

The *first digit* signifies the pre-mining nickel resources (contained metal), subdivided into four classes, i.e. (1) very large: >2 000 000 t; (2) large: 500 000–2 000 000 t; (3) medium: 25 000–500 000 t; and (4) small: <25 000 t. The size classification is adopted from the legend of the USGS *Metallogenic map of North America;*[25] this classification has also been used in the mineral map of South Africa and some neighbouring territories,[7] but it does not make provision for very large deposits. An additional class of deposits thus seemed desirable for the proposed rating scheme. If the given size categories were to be extrapolated exponentially, only deposits with in excess of 10 000 000 t of nickel would be classed as very large: as only Sudbury would answer this qualification, it is considered too stringent and the 2 000 000-t parameter is therefore arbitrary, having been chosen to define a few other very large deposits, in addition to Sudbury.

The *second digit* denotes the average nickel content of the ores (in mass per cent) according to four categories: (1) >1.5% Ni; (2) 0.8–1.5% Ni; (3) 0.25–0.8% Ni; and (4) <0.25% Ni.

As far as grouping the nickel values is concerned, the 0.8% limit was chosen in compliance with the global assessment of nickel resources by Ross and Travis.[26] The 0.25% Ni and 1.5% Ni values were chosen arbitrarily to achieve a reasonable spread in a rating of deposits listed by these authors and to be able to discriminate between various Southern African deposits (Table 2).

The *third digit* represents a statement on the mining status and potential of the deposits: (1) significant present or recent production (primary or by-product); high economic resource potential; (2) significant unmined economic or near-economic resource; (3) important past production; small or uncertain resource potential; and (4) low grade and sub-economic; alternatively, insignificant past production; small or uncertain resource potential.

Assessing the mining status and potential of a deposit may be open to some ambiguity in that it depends to some extent on personal interpretation under changing circumstances. In this classification emphasis has been placed on present potential economic importance.

Southern African nickel deposits in world perspective

The Archaean nickel deposits of Southern Africa appear to be constrained in time and space by a very definite age limit of approximately 3000 m.y. This is borne out by the confinement of the synvolcanic deposits to the Upper Greenstones of the Bulawayan Group (2700–2800 m.y.) in Zimbabwe and their virtual total absence in older environments both in the Zimbabwe and Kaapvaal Provinces, in spite of the ubiquitous komatiitic magmatism of the Onverwacht Group (3500 m.y.) on the Kaapvaal craton. No komatiitic rocks younger than about 3200 m.y. are known in this region, orogenic activity in the Kaapvaal tectonic province having ceased at about 3100 m.y., whereas the Zimbabwe Province remained tectonically active until at least 2600 m.y.

The upper time limitation on the presence of nickel in komatiites seems not to be peculiar to Southern Africa. In Western Australia, by way of comparison, some 96% of nickel resources are found in rocks of komatiitic affiliation in the Norseman–Wiluna belt of the Yilgarn Block (2700–2800 m.y.), whereas only minor nickel occurrences in gabbroid intrusions are known in the Pilbara Block, the age of which exceeds 3200 m.y.[24] Similar conditions obtain in Canada, where Archaean volcanic peridotite-associated nickel deposits, notably those of Langmuir, are confined to the 2700 m.y. old Abitibi greenstone belt.[27]

The syntectonic nickel deposits of Zimbabwe and Botswana are mostly hosted in komatiitic host rocks, which are either comparable with the VPA or IDA classes in Western Australia. Trojan and Damba are probably of the VPA type and have Ni:Cu ratios of up to 20, which compares well with a range of 7 to 19 for the VPA deposits of Western Australia. Most of the intrusive, komatiitic nickel deposits in Zimbabwe are comparatively rich in copper and consequently have low Ni:Cu ratios, e.g. 1.1 to 20 (Table 2), compared with 19 to 70 for the Western Australian IDA deposits.[24]

The Great Dyke, Bushveld Complex, Insizwa and other igneous complexes of Southern Africa represent intrusions in cratonic areas,[22] and are comparable with the 'gabbroid associated' class of Marston *et al.*[24] With the exception of massive ores at Insizwa and Vlakfontein (in the Bushveld Complex), these deposits are generally marked by disseminated sulphides. These intrusions have counterparts in the Stillwater and Duluth Complexes of the U.S.A.

In the Great Dyke disseminated nickel mineralization is found in the Hartley and Wedza Complexes, i.e. those sections where the intrusion was emplaced into the nickeliferous Bulawayan greenstone belt. Intriguing questions remain as to whether the nickel mineralization in the Great Dyke could have been remobilized from the Bulawayan greenstones, and if such a link indeed exists, whether a primary nickel source could be surmised in the floor rocks of the Bushveld Complex.

The komatiitic syntectonic deposits are characterized by relatively high ore grades, but small resources in comparison with the very large, low-grade orebodies in the intracratonic, tholeiitic intrusions. This distinction is borne out by the classification of magmatic nickel deposits of Southern Africa (Table 2), and exemplified by the proposed rating scheme. The latter

is, however, primarily aimed at facilitating easy comparison of nickel deposits according to size, ore grade and economic potential. If this rating is applied to some of the world's important nickel deposits, these would be rated as follows: Sudbury, Canada (1.1.1); Oktyabr'skiy, U.S.S.R. (1.1.1); Agnew, Western Australia (2.1.1); Mount Keith, Western Australia (2.3.2); Noril'sk, U.S.S.R., (2.4.1); Kambalda–St. Ives, Western Australia (2.1.1); Mt. Windarra, Western Australia (3.1.1); Wigie 3, Western Australia (4.2.4); Marbridge, Canada (4.1.3); Duluth, U.S.A. (1.4.4), according to data furnished by Ross and Travis,[26] Marston *et al.*[24] and Groves and Lesher.[28]

Southern Africa constitutes a nickel province of major importance; with a total nickel production of about 60 000 t in 1980 this region ranks as the third nickel producer in the Western world.[6] A wide variety of deposits are found on this subcontinent, and this is borne out by a diverse nickel-mining industry. Whereas primary nickel and nickel–copper producers in Zimbabwe and Botswana contribute some 60% of the above production, most of these deposits do not match comparable, important deposits in Canada and Western Australia as far as size and economic potential are concerned. About 40% of the production is derived as a by-product from the winning of platinum-group metals in the Merensky Reef of the Bushveld Complex. Although the grade is very low in comparison with the komatiite-hosted deposits, and the economic potential is tied to the fortunes of the platinum industry, the Merensky Reef, together with the yet unmined Platreef, represents one of the world's largest, long-term nickel resources.

References

1. South African Committee for Stratigraphy (SACS). *Stratigraphy of South Africa, part 1: lithostratigraphy of the Republic of South Africa, South West Africa/Namibia and the Republics of Bophuthatswana, Transkei and Venda* Kent L. E. comp. *Handbk geol. Surv. S. Afr.* no. 8, 1980, 690 p.
2. Tankard A. J. *et al. Crustal evolution of southern Africa: 3.8 billion years of earth history* (New York: Springer, 1982), 523 p.
3. Williams D. A. C. The association of some nickel sulphide deposits with komatiitic volcanism in Rhodesia. *Can. Mineralogist,* **17,** 1979, 337–49.
4. Von Gruenewaldt G. A review of some recent concepts of the Bushveld Complex, with particular reference to sulphide mineralization. *Can. Mineralogist,* **17,** 1979, 233–56.
5. Clutten J. M. Foster R. P. and Martin A. Nickel mineralization in Zimbabwe. *Episodes,* no. 2 1981, 10–15.
6. Hammerbeck E. C. I. A review of nickel in southern Africa. In *Proceedings twelfth congress of the Council of Mining and Metallurgical Institutions, Johannesburg, 1982* Glen H. W. ed. (Johannesburg: South African Institute of Mining and Metallurgy, 1982), vol. 1, 83–94.
7. Martini J. E. J. and Hammerbeck E. C. I. *Mineral map of the Republics of South Africa, Transkei, Bophuthatswana, Venda and Ciskei and the Kingdoms of Lesotho and Swaziland, 1:1 000 000* (Pretoria: Geological Survey of South Africa, 1981).
8. Anhaeusser C. R. The relationship of mineral deposits to early crustal evolution. *Econ. Geol. 75th anniversary vol.,* 1981, 42–62.
9. Viljoen M. J. Viljoen R. P. and Pearton T. N. The nature and distribution of Archaean komatiite volcanics in South Africa. In *Komatiites* Arndt N. T. and Nisbet E. G. eds (London, etc.: George Allen and Unwin, 1982), 53–79.
10. Wilson J. F. A preliminary reappraisal of the Rhodesian Basement Complex. In *A symposium on mineral deposits and the transportation and deposition of metals* Anhaeusser C. R. Foster R. P. and Stratten T. eds. *Spec. Publ. geol. Soc. S. Afr.* no. 5, 1979, 1–23.
11. Nisbet E. G. *et al.* Komatiites in Zimbabwe. Reference 9, 97–104.
12. Anhaeusser C. R. Archean metallogeny in southern Africa. *Econ. Geol.,* **71,** 1976, 16–43.
13. Joubert P. The gneisses of Namaqualand and their deformation. *Trans. geol. Soc. S. Afr.,* **77,** no. 3 1974, 339–45.
14. Von Backström J. W. The geology of an area around Keimoes, Cape Province, with special reference to phacoliths of charnockitic adamellite-porphyry. *Mem. geol. Surv. S. Afr.* 53, 1963, 218 p.
15. Attridge R. L. The Jacomyns Pan copper–nickel occurrence, Kenhardt district, northern Cape. *Spec. Publ. geol. Soc. S. Afr.* In press.
16. Winter P. E. The Usushwana Igneous Complex. *Bull. geol. Surv. Swazild* no. 5, 1965, 29 p.
17. Hunter D. R. The geology of the Usushwana Complex in Swaziland. In *Symposium on the Bushveld Igneous Complex and other layered intrusions. Spec. Publ. geol. Soc. S. Afr.* no. 1, 1970, 645–60.
18. Scholtz D. L. The magmatic nickeliferous ore deposits of East Griqualand and Pondoland. *Trans. geol. Soc. S. Afr.,* **39,** 1936, 81–210.
19. Stanton R. L. *Ore petrology* (New York, etc.: McGraw-Hill, 1972), 713 p.
20. Davies D. N. The nickel–tungsten–gold deposits at Forbes Reef. *Bull. geol. Surv. Swazild* no. 4, 1964, 45–50.
21. Hammerbeck E. C. I. and Vermaak C. F. Nickel. In *Mineral resources of the Republic of South Africa, fifth edition* Coetzee C. B. ed. *Handbk geol. Surv. S. Afr.* no. 7, 1976, 177–81.
22. Naldrett A. J. Nickel sulfide deposits: classification, composition and genesis. *Econ. Geol. 75th anniversary vol.,* 1981, 628–85.
23. Worst B. G. The Great Dyke of Southern Rhodesia. *Bull. geol. Surv. Sth. Rhod.* no. 47, 1960, 234 p.
24. Marston R. J. *et al.* Nickel sulfide deposits in Western Australia: a review. *Econ. Geol.,* **76,** 1981, 1330–63.
25. United States Geological Survey. *Preliminary metallogenic map of North America: contribution to the Metallogenic Subcommission, Commission of the Geological Map of the World* (Washington, D.C.: The Survey, 1980).
26. Ross J. R. and Travis G. A. The nickel sulfide deposits of Western Australia in global perspective. *Econ. Geol.,* **76,** 1981, 1291–329.
27. Green A. H. and Naldrett A. J. The Langmuir volcanic peridotite-associated nickel deposits: Canadian equivalents of Western Australian occurrences. *Econ. Geol.,* **76,** 1981, 1503–23.
28. Groves D. I. and Lesher C. M. Regional geology and nickel deposits of the Norseman–Wiluna Belt, Western Australia. *Univ. West. Aust. geol. Dep. Extension Service Publ.* no. 7, 1982, 234 p.

Role of contamination in the precipitation of sulphides in the Platreef of the Bushveld Complex

D. L. Buchanan Ph.D., D.I.C., M.I.M.M.
Mining Geology Division, Department of Geology, Royal School of Mines, Imperial College, London, England
J. E. Rouse M.Sc., M.N.Z.I.C.
British Geological Survey, London, England

Synopsis

During the emplacement of the Bushveld Complex in the Potgietersrus area magma reacted with the original floor rocks—Archaean granite or Malmani dolomite and overlying Penge banded ironstone or sedimentary rocks of the Pretoria Series. The complex sequence of sulphide-rich mafic rocks that formed along the contact is known as the Platreef. Associated with the sulphide mineralization are important concentrations of platinum-group metals, copper and nickel. Xenoliths of Malmani dolomite have been incorporated into the Platreef and previous work has suggested that anhydrite is likely to have been present in the dolomite. The sedimentary-derived sulphur thus introduced into the magma exercised an important control on the formation of the sulphides.

Petrographic studies on the Platreef rocks from the Tweefontein area indicate that the original magma reacted with the banded ironstone to form iron-rich pyroxenites. In the Turfspruit area, to the south, the footwall rocks consist of sediments of the Timeball Hill Series. Original argillaceous rocks have been metamorphosed to cordierite-, corundum- and spinel-bearing hornfelses. Graphite was present in the contact zone in both the Tweefontein and Turfspruit areas. Anhydrite-bearing hornfels rocks are also present on Turfspruit.

The Platreef rocks that overlie the corundum- and spinel-bearing hornfelses on Turfspruit are peridotitic, and pyroxenites are present in areas underlain by cordierite-bearing hornfels. The absence of orthopyroxene in the peridotite is probably indicative of low silica activity in the original magma. The pyroxenites have, however, undergone silica contamination from the underlying more siliceous cordierite hornfels.

Carbon isotope studies indicate that the graphite in the Tweefontein and Turfspruit samples represents organic material originally associated with the footwall sediments. Sulphur isotope determinations on the anhydrite-bearing floor rocks indicate that this phase is clearly of sedimentary origin and was probably derived from an evaporitic unit within the carbonate sequence. This provides firm support for a model of ore genesis that involved the introduction of additional sulphur into the Bushveld magma. Isotope studies on sulphides associated with the banded ironstone and graphite indicate that these units were not the source of additional sulphur. Experimental studies predict, however, that a magma contaminated with iron- and carbon-rich material would have a high sulphur-carrying capacity. Where additional sulphur is available the magma would achieve saturation early in its crystallization history and precipitate an immiscible sulphide phase. Experimental work has also shown that sulphide precipitation can be triggered by the introduction of salic material into a magma close to sulphur saturation. This mechanism probably played a role in the control of the sulphide mineralization in the Turfspruit area.

In the Potgietersrus limb of the Bushveld Complex, South Africa (Fig. 1), sulphide mineralization is associated with the intrusive contact between a sequence of Bushveld pyroxenitic gabbros up to 120 m thick and floor rocks of either Archaean granite or Transvaal Supergroup sediments (Fig. 2). These sediments consist of Malmani dolomite and overlying Penge banded ironstone or sedimentary rocks of the Pretoria Series.

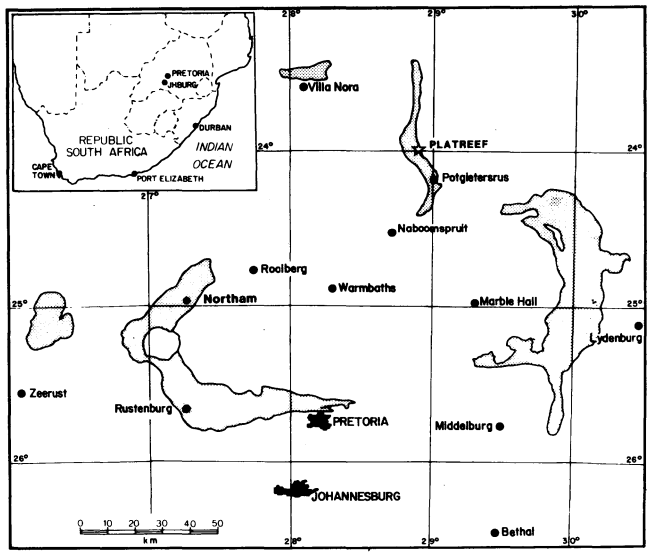

Fig. 1 Locality plan showing distribution of mafic phases of Bushveld Complex

Xenoliths of floor rocks have been incorporated into the pyroxenitic gabbros to form a complex sequence of rock types that together make up the Platreef. Whole-rock values of up to 0.5 and 1.3 wt% copper and nickel, respectively, have been obtained in borehole intersections through the Platreef zone, and values of up to 28 ppm platinum-group metals have been reported for these rocks.

In a previous study[1] it was shown that the silicate phases in the Platreef were equivalent in composition to the Merensky Reef, but marked departures are present where reaction took place between the original Bushveld magma, the footwall and footwall xenoliths. Particular attention was given in the previous study to the role of the Malmani dolomite in controlling the distribution of the sulphide mineralization. In the present study the effect is examined of multiple contamination from dolomite together with banded ironstone and graphitic sediments.

Geology and petrography

In the Tweefontein area the Bushveld is in contact with Malmani dolomite and the overlying Penge banded ironstone. The previous study[1] was undertaken mainly on material from borehole TN12, drilled in the northern part of the farm Tweefontein. This borehole intersected banded ironstone at the base of the Platreef. In outcrop the banded ironstone forms resistant ridges and is present as a prominent hill to the southeast of Tweefontein into which a series of vertical shafts and adits was excavated in the 1920s. These were developed to expose sulphide mineralization on the contact between the Platreef, footwall hornfels units and banded ironstone; the general geology

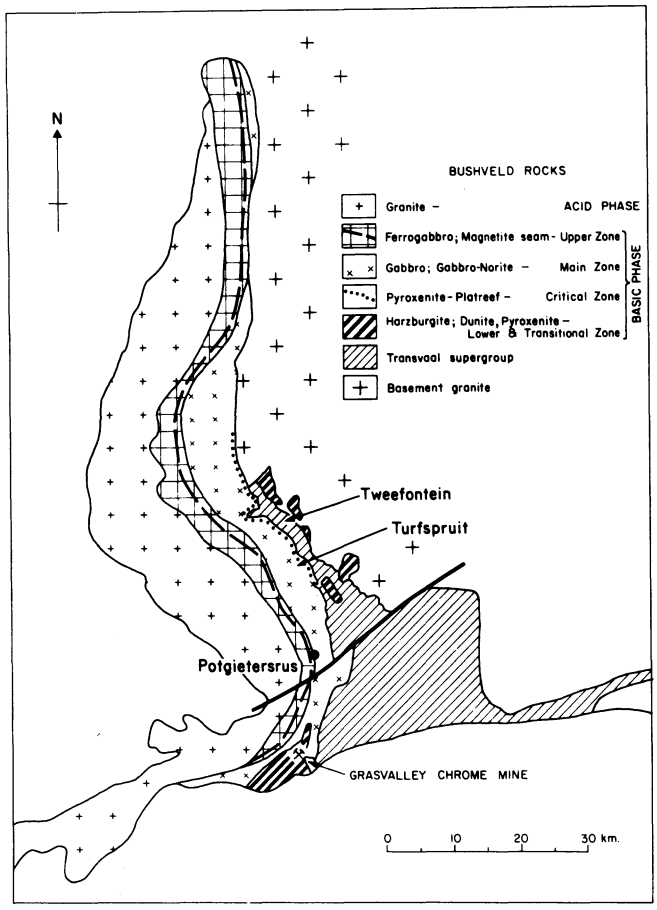

Fig. 2 Map showing regional geology of Potgietersrus limb of Bushveld Complex. Unornamented area to west consists of cover of younger sedimentary rocks of Waterberg Supergroup

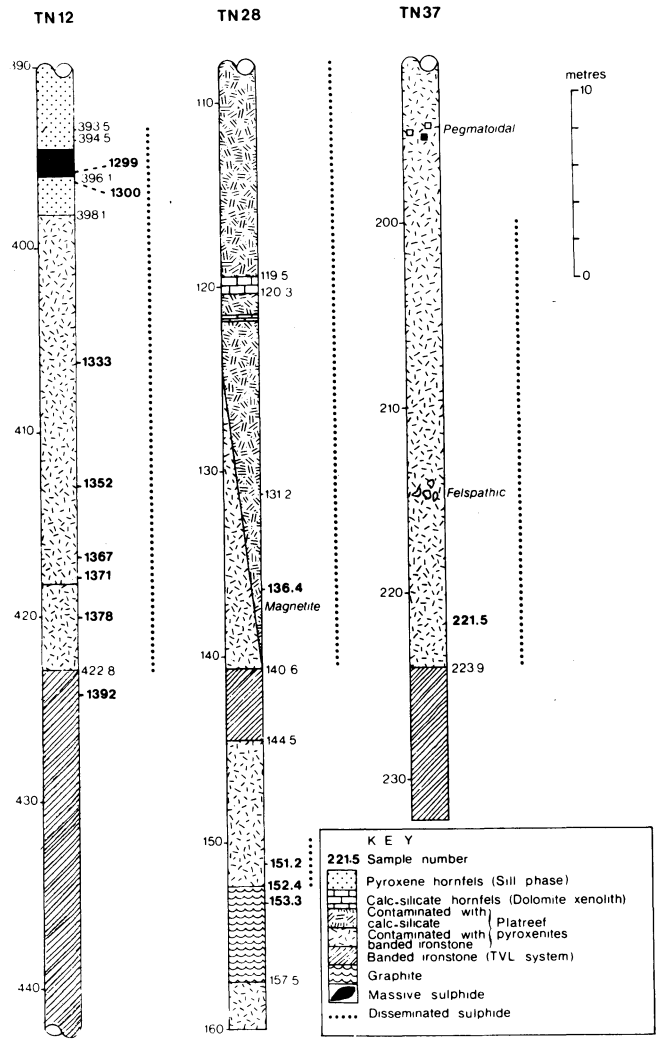

Fig. 3 Logs of intersections through base of Platreef in boreholes drilled in Tweefontein area showing petrography associated with banded ironstone together with position of samples examined in this study. Numbers to left of borehole columns represent depth, m

of the area has been described by Wagner.[2] Two boreholes drilled near the Tweefontein Hill (boreholes TN28 and TN37) intersected this contact. Borehole TN28 also intersected a 5-m zone of pyroxenite that contained up to 20 wt% graphite. Summary logs of boreholes TN12, TN28 and TN37 are given in Fig. 3.

Graphite was also intersected in boreholes drilled on the farm Turfspruit, which is located immediately to the south of Tweefontein (Fig. 2). The footwall rocks in the area consist of aluminous argillaceous shales of the Timeball Hill Series, which also contain dolomite horizons. Graphite is present both in the footwall to the Platreef (borehole TS18), where it forms up to 81 wt% of the rock and in a hornfels xenolith located in the norites above the Platreef (borehole TS19), where it forms up to 67 wt% of the rock. Summary logs of both boreholes, together with an additional borehole drilled in the area (borehole TS21), are given in Fig. 4.

One of the boreholes drilled on the Turfspruit–Tweefontein boundary (borehole TS9) intersected hornfelses immediately below the Platreef that contain up to 50 vol% of anhydrite, and material from this borehole was included in the study. Detailed mapping of the area in the vicinity of borehole TS9 has not yet been undertaken and the exact nature of the footwall sequence is not known.

Between the banded ironstone present at the top of the Malmani dolomite and the normal Platreef on Tweefontein there is an intersection up to 25m thick, between 398.1 and 422.8 m in the case of borehole TN12 (Fig. 3), of a coarse-grained sulphide-rich pyroxenite with only minor amounts of plagioclase. Gradational contacts exist between the banded ironstone and the pyroxenite, whereas in borehole TN28 the banded ironstone has been detached from the footwall and the graphite-rich zone is present in the underlying pyroxenite. In thin section the pyroxenites are seen to contain inverted pigeonite, whereas the banded ironstone is characterized by an assemblage of pyroxene, magnetite and quartz, and displays recrystallization textures.

The Platreef rocks in boreholes TS19 and TS21 (Fig. 4) are pyroxenitic, whereas in borehole TS18 they are predominantly peridotites. Cordierite hornfels forms the footwall in boreholes TS18 and TS21, though bladed crystals of corundum, together with porphyroblasts of alumina-rich spinel, are also present immediately below the contact of the Platreef in borehole TS18. Cordierite hornfels is present as xenoliths in the Platreef as well as in the overlying norites in borehole TS19. These rocks were clearly derived from sediments of the Timeball Hill Series. Graphite in both boreholes TS18 and TS19 is associated with the cordierite hornfels units, though graphite is also present in the peridotites at the base of the Platreef in borehole TS18. The pyroxene in this part of the Platreef is partially replaced by amphibole.

Xenoliths of dolomite within the Platreef were intersected in boreholes TS21 and TN28, and dolomite forms the footwall to the Platreef in borehole TS19. These rocks have been metamorphosed to calc-silicate hornfelses that, characteristically, contain salite, the apple-green high-calcium pyroxene. Platreef rocks in close proximity to the xenoliths are normally altered to serpentinites.

Quantitative analysis of mineral phases

To obtain insight into the crystallization history of the rocks of

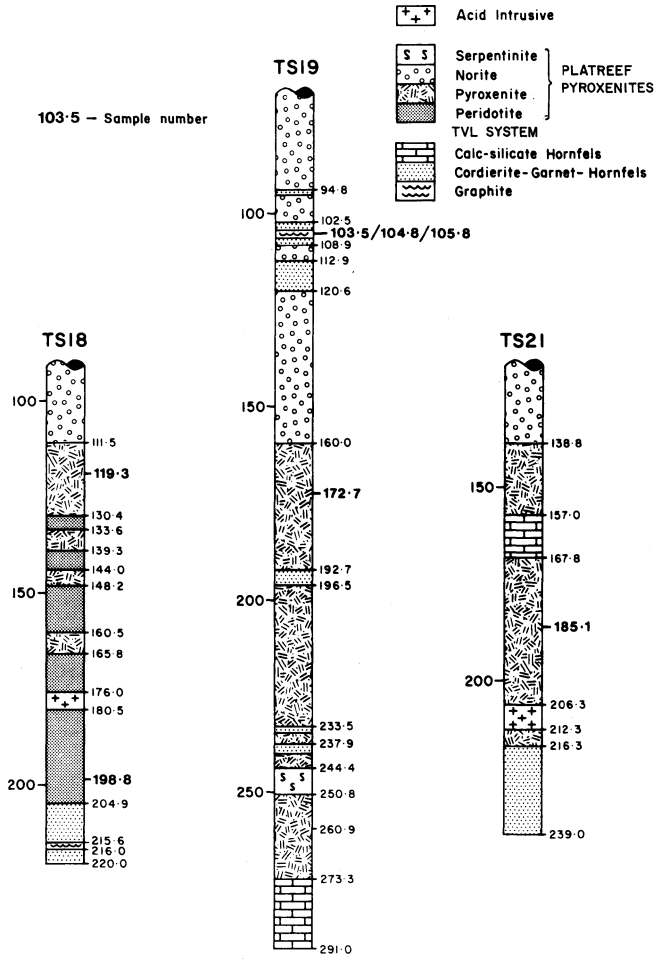

Fig. 4 Logs of boreholes drilled in Turfspruit area showing petrography and position of samples examined in this study. Numbers to left of borehole columns represent depth, m

the Tweefontein and Turfspruit areas a study of the pyroxene, plagioclase and olivine phases was undertaken on samples from all of the boreholes. Sample positions are indicated in Figs. 3 and 4. The mineral chemistry was established by use of the electron microprobe and the analytical data that were obtained from the pyroxene phases were recalculated in terms of Ca, Mg and Fe end-members (Fig. 5). In addition, the compositional field for the Merensky Reef (and uncontaminated Platreef) has been plotted in Fig. 5 together with the fractionation trend in Ca-rich pyroxenes from the Upper Zone of the normal Bushveld sequence. A pyroxene pair from the Upper Zone has also been plotted to establish the orientation of tie-lines for primary magmatic minerals.

It is immediately apparent from Fig. 5 that the pyroxenites associated with the banded ironstones are characterized by pyroxenes that display extreme iron enrichment. The most iron-rich samples are those associated with material that contains magnetite and quartz (sample TN12-1392) and remnant banding (sample TN12-1378). There is no systematic iron-enrichment trend with stratigraphic position and the orientation of the tie-line between pyroxene pairs in sample TN12-1352 is at variance with that expected for primary magmatic minerals. Both these features are normally indicative of non-equilibrium with the original magma. Pyroxenes associated with graphite in borehole TN28 (samples TN28-152.4 and TN28-153.3) also show iron enrichment when compared with normal Platreef.

The composition of the Ca-poor pyroxene coexisting with anhydrite (sample TS9-129) is plotted in Fig. 5. As can be seen, the pyroxene is relatively magnesium-rich in comparison with the field of uncontaminated Platreef, which suggests that the sample represents metamorphosed dolomite. The presence of Ca-rich anhydrite would preclude the crystallization of Ca-rich pyroxene normally present in calc-silicate hornfelses. An example of the effect of dolomite contamination on the composition of Ca-rich pyroxenes is given by sample TN28-136.4 (Fig. 5), which contains 24.4 wt% CaO—significantly more than other Ca-rich pyroxenes analysed in the study.

As can be seen from Fig. 5, the Ca-rich pyroxene present in the peridotite intersected in borehole TS18 (sample TS18-198.8) together with the Ca-poor pyroxene from the overlying pyroxenite (sample TS18-119.3) both have compositions that are normally associated with uncontaminated Platreef. Samples from boreholes TS19 and TS21 containing pyroxene pairs show moderate iron enrichment in comparison with the field of uncontaminated Platreef. The iron enrichment is, however, significantly less than that shown by pyroxenes associated with the banded ironstones. In addition, the orientation of the tie-lines is the same as that established from normal Bushveld pyroxenes of similar composition.

Olivine of composition Fo_{26} is present in sample TN12-1371. The extreme iron enrichment of the pyroxenites associated with the banded ironstone is therefore also reflected in the coexisting olivine. The olivine in the peridotitic Platreef intersected in borehole TS18 has a composition of Fo_{71} (sample TS18-198.8), which is within the range expected for uncontaminated Platreef and close to the value of Fo_{76} established in olivine-bearing Platreef on Tweefontein.[1]

Plagioclase in sample TN12-1333 has a composition of An_{77},

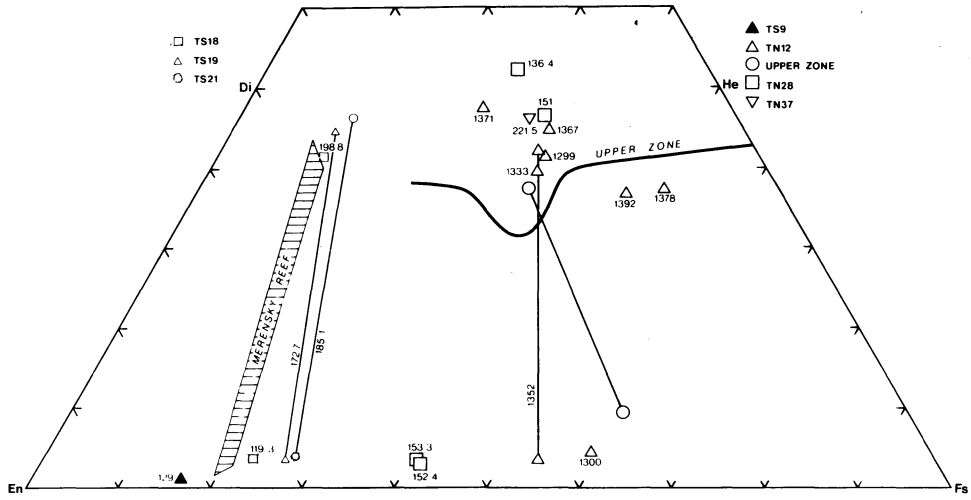

Fig. 5 Microprobe analyses of pyroxenes plotted on enstatite–diopside–hedenbergite–ferrosalite quadrilateral. Sample locations shown in Figs. 3 and 4

and compositions within the range An_{72}–An_{78} were obtained from the Platreef intersected in boreholes drilled on Turfspruit. These are within the range normally associated with the Platreef rocks.

Contamination of Platreef by iron and silica

The most reasonable explanation for the iron enrichment in the Tweefontein boreholes is that the original Platreef magma reacted with, and assimilated, a significant volume of the footwall banded ironstone. The variability in the composition of the pyroxenes, together with evidence of non-equilibrium, suggests that the mechanism by which contamination took place was not accompanied by complete homogenization of the magma.

Because of the crosscutting relationship of the Bushveld with the floor rocks, the banded ironstone in the Turfspruit area is found 500 m below the footwall contact. This field relationship, together with the far more modest degree of iron enrichment in pyroxene pairs present in samples from boreholes TS19 and TS21, and evidence that equilibrium had been achieved, suggest that conditions different from those encountered on Tweefontein apply to the Turfspruit area. The absence of orthopyroxene in the olivine-bearing peridotite intersected in borehole TS18 (sample TS18-198.8) is probably indicative of low silica activity in the original magma. The reverse situation in the equivalent Platreef rocks intersected in boreholes TS19 and TS21 could therefore be accounted for by an increase in the silica activity of the magma according to the reaction

$$(Mg,Fe)_2SiO_4 + SiO_2 \leftrightharpoons 2(Mg,Fe)SiO_3$$

Olivine — Pyroxene

This could be achieved through the introduction of additional silica from the footwall. In the case of borehole TS18 it is possible that the alumina-rich footwall present below the Platreef, consisting of corundum- and spinel-bearing hornfels, proved to be less siliceous than the cordierite hornfels intersected in borehole TS21. In addition, xenoliths of footwall material are present within the Platreef in boreholes TS19 and TS21, but absent from borehole TS18. It is therefore possible that the iron-enrichment trends present in the pyroxene pairs in samples from boreholes TS19 and TS21 were formed in response to salic contamination of the original magma by the footwall sediments.

Isotope geochemistry

Background

In the previous investigation[1] sulphur isotope determinations were undertaken on sulphides from samples of Platreef associated with a calc-silicate xenolith. These gave a range of $\delta^{34}S$ values of from +6.3 to +9.2‰. As the $\delta^{34}S$ values for primary magmatic Bushveld sulphides fall in the range −0.6 to +3.5‰, the isotope geochemistry clearly indicates a contribution of non-magmatic sulphur to the original Bushveld magma. The results of carbon and oxygen isotope determinations on unaltered Malmani dolomite were consistent with rocks deposited in an evaporitic environment during the Precambrian. Anhydrite, normally associated with evaporitic sequences, is likely to have been preserved in the Malmani dolomite when it was incorporated as xenoliths into the Bushveld magma, though sulphur in present-day samples occurs mainly as pyrite. Values of sea water $\delta^{34}S$ during the Precambrian are not well characterized owing to the paucity of sulphate-containing evaporites from this period. The few values available would suggest evaporites of the Archaean–Proterozoic period have $\delta^{34}S$ of about +20‰—not very different from that of today. A single sample of Malmani dolomite, free of pyrite but containing 190 ppm SO_4^{2-}, gave a $\delta^{34}S$ value of +7.09‰. The evidence from the previous study suggested, therefore, that the sulphide mineralization in contaminated Platreef has been derived from the combined influence of a sulphur-rich Merensky Reef type magma and the incorporation of additional sulphur from anhydrite-bearing Malmani dolomite. In view of the model proposed it was encouraging subsequently to find anhydrite in borehole TS9 and a follow-up isotope study on this material was clearly required.

Modern limestones deposited under shallow marine conditions generally have $\delta^{13}C$ values close to 0‰ and Precambrian limestones were probably not very different. Carbon isotopes established on carbonate in the Malmani dolomite[1] fall in the range 0 to −2.8‰, which is consistent with their proposed depositional environment.

The $\delta^{13}C$ isotopic composition of most Phanerozoic kerogens lies within the range −20 to −30‰. Most samples of Precambrian organic carbon, now represented by graphite and other forms of reduced carbon, have isotopic ratios within the same range.[3] The presence of graphite in association with the Platreef is significant, as it could represent the existence of primitive plant life in the pre-Bushveld sedimentary sequence. This would act as a reductant when incorporated into the original magma. Alternatively, the graphite might represent reduced CO_2 from the dolomite or be mantle-derived. In the latter case values of −2 to −10‰ could be expected.[4] A programme of carbon isotope determinations was undertaken to help to establish the source of the original carbon.

Pyrrhotite is normally associated with the graphite in the material from Tweefontein and Turfspruit. In view of the role sedimentary-derived sulphur is considered to play in controlling the formation of the sulphides in the Platreef, it was also decided to undertake a programme of sulphur isotope determinations on these sulphides. This would establish whether the original sulphur is associated with the pre-Bushveld sediments or whether it is derived from mantle sources.

The results obtained from the programme of isotope determinations are given in Table 1. Data from the previous study[1] together with new results have been plotted in Fig. 6.

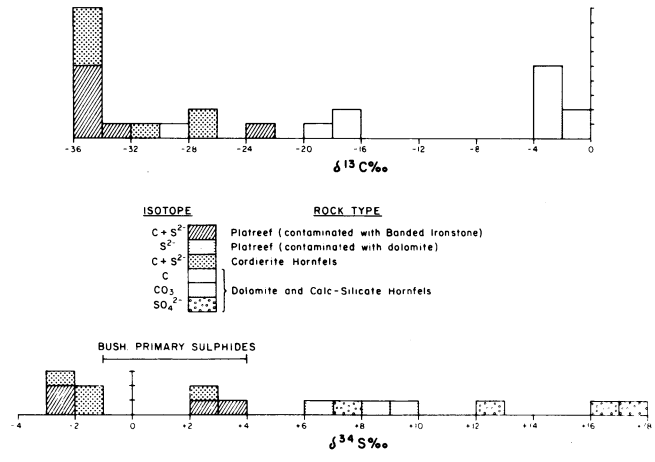

Fig. 6 Histogram of carbon and sulphur isotope data taken from Table 1 and Buchanan *et al.*[1]

Sulphur istopes

The $\delta^{34}S$ values obtained from the anhydrite-bearing material (sample TS9-129) gave values of +16.4 and +17.1% (Table 1) and are therefore consistent with values expected for anhydrite associated with evaporitic sequences. These values are also significantly heavier than the range of $\delta^{34}S$ values obtained from Platreef contaminated with dolomite, which fell in the range +6 to +10‰. A heavy mineral concentrate prepared from sample TS9-129 was shown by semi-quantitative XRD techniques to contain about 70% pyrite, 20% anhydrite and 10% pyroxene. The concentrate gave a $\delta^{34}S$ value of +12‰,

Table 1 Sulphur and carbon isotope data from sulphide, anhydrite and graphite (sample number refers to borehole and depth in metres; most locations plotted in Figs. 3 and 4)

Sample no.	Sulphur-bearing phase	$\delta^{34}S$,‰	Graphite, wt%	$\delta^{13}C$,‰ PDB
TN12-1295	Pyrrhotite	+2.74		
TN12-1352	Pyrrhotite	+3.69		
TN28-152.4			12.7	−35.3
TN28-153.3A	Pyrrhotite vein	−2.16	1.4	−23.7
	Disseminated pyrrhotite	−2.44	15.0	−34.7
			18.6	−35.2
TN28.153.3B			15.4	−34.0
TN28-153.3C			16.0	−35.1
TN28-153.3D			19.6	−32.8
TS9-129	Anhydrite + pyroxene	+16.4		
	Anhydrite (100%)	+17.1		
	Anhydrite (20%), pyrite (70%)	+12.4		
TS18-215.6(I)			32.0	−34.0
TS18-215.6(II)			74.0	−34.3
TS18-216.0(I)			75.0	−34.1
TS18-216.0(II)	Pyrrhotite	+2.0	81.0	−34.1
TS19-103.5	Pyrrhotite + pentlandite	−1.1	63.0	−30.2
TS19-104.8	Pyrrhotite	−2.42	67.0	−27.5
TS19-105.8	Pyrrhotite	−1.81	20.0	−26.6

which suggests a value of +10‰ for the pyrite. Taking, therefore, a difference of 7‰ $\delta^{34}S$ between the anhydrite and pyrite phases in this sample, it can be estimated by extrapolation of experimental studies of sulphate–sulphide isotopic equilibrium fractionation[5] that the sulphate and sulphide were in isotopic equilibrium at temperatures in excess of 700°C. Isotopic exchange would be expected to cease once the melting point of pyrite had been reached. It should be noted that the work of Fincham and Richardson[6] on silicate melts has shown that sulphide and sulphate species coexist over only a very narrow range of partial pressures of oxygen, anhydrite being normally associated with strongly oxidized melts. The pyrite and anhydrite in sample TS9-129 may not, therefore, be in equilibrium with each other. Fincham and Richardson's work was, however, carried out at 1500°C and may not be directly applicable to the magma temperatures of about 1100°C that are thought to be associated with Bushveld rocks. Although it is possible that the anhydrite in sample TS9-129 represents oxidized pyrite, the original sulphur is clearly of sedimentary origin and it is reasonable to suggest that the anhydrite has been derived from an evaporitic unit within the carbonate rocks. The values obtained clearly provide firm support for a model of ore genesis that involved the introduction of sedimentary-derived sulphur into the original Bushveld magma.

Sulphur isotope analysis of sulphides associated with the iron-rich pyroxenites intersected in boreholes TN12 and TN28 gave $\delta^{34}S$ values that fall in the range −3 to +4‰. Sulphides associated with graphite and cordierite hornfels intersected in boreholes TS18 and TS19 fall in a similar range. As primary Bushveld sulphides fall in the range −1 to +4‰, the results obtained on sulphides from the iron-rich pyroxenites and hornfels units suggest that the original sulphur was predominantly mantle-derived. The banded ironstones and Pretoria Series sediments were not, therefore, a source of significant additional sulphur in the magma.

Carbon isotopes

Values of $\delta^{13}C$ from graphite intersected in boreholes TN28, TS18 and TS19 fall in the range −22 to −36‰, a high proportion of the samples falling in the range −34 to −36‰. There is some degree of overlap with data obtained in the previous study,[1] where $\delta^{13}C$ values for organic carbon in dolomite range from −16 to −30‰. $\delta^{13}C$ values obtained on samples of dolomite in the range −16 to −20‰ are probably of normal marine origin, the original organic material perhaps having been derived from Archaean algal mats. Samples that fall predominantly at the very light end of the range are, however, associated with metamorphosed argillaceous sediments and the Platreef rocks. Although the ^{13}C depletion could, perhaps, be due to secondary fractionation of carbon originally derived from the carbonate rocks by the thermal metamorphic effect of the Bushveld or fractionation of mantle-derived carbon, the low values obtained may also be due to the influence of methane-producing bacteria. Schoell and Wellmer[7] have studied graphite samples from the Archaean Superior Province of Canada, where samples associated with sulphidic and oxidic iron formations give $^{13}C/^{12}C$ within the range of Phanerozoic kerogens. They have, however, reported three samples that show significant depletion in the heavy isotope with ^{13}C values between −35 and −43‰. The formation of methane by bacteria and its utilization by methanotrophic organisms is the only geochemical process known to bring about appreciable ^{13}C depletion (typical $\delta^{13}C$ values are around −60 to −80‰).[7]

The obvious conclusion to be derived from the carbon isotope data is that the graphite in the Tweefontein and Turfspruit samples represents original organic material. The most likely source is the Timeball Hill series sediments, which are characterized by carbonaceous horizons (N. J. Beukes, personal communication).

Controls on formation of magmatic sulphides

The results of experimental modelling of silicate–sulphide systems at high temperature are summarized in Fig. 7. The sulphur-carrying capacity of a silicate melt can be increased by adding iron or a reductant, or by reducing the silica content. Clearly, a magma contaminated with banded ironstone and organic material would have a high sulphur-carrying capacity. Where additional sulphur is introduced it would be expected that the magma would achieve saturation early in its crystallization history and precipitate an immiscible sulphide. Provided that the magma was equally rich in the economically important transition elements such as nickel, copper, cobalt and the platinum-group metals, important ore zones would develop.

The Platreef in the Tweefontein area has been contaminated

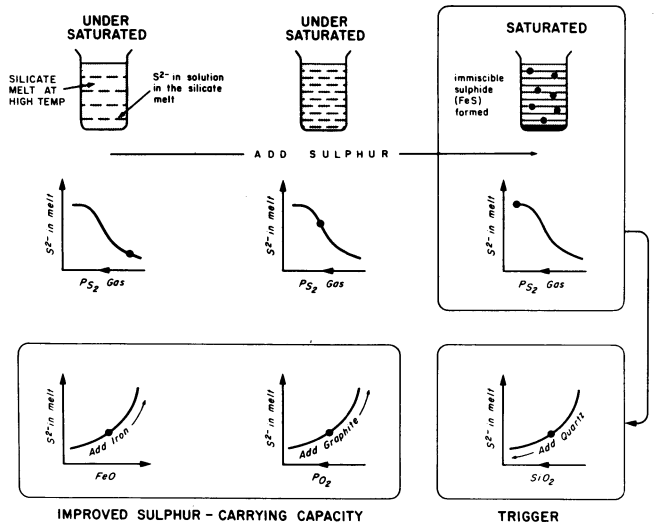

Fig. 7 Diagrammatic summary of results obtained from experimental studies reported in Buchanan and Nolan[8] and Naldrett.[9] It is important to note difference between sulphur as a gas (S_2) and sulphur in solution in silicate melt (S^{2-}) and sulphur combined with iron in immiscible sulphide phase (FeS). Only after silicate melt becomes saturated with S^{2-} does immiscible sulphide form. Saturation can be achieved by adding sulphur into system, usually as S_2 (sulphidization), and is represented by plateau on sulphur solubility curves. Absolute value of sulphur in solution in silicate melt at saturation is influenced by FeO and SiO_2 contents of silicate melt as well as partial pressure of oxygen

with both banded ironstone and organic material, xenoliths of dolomite providing additional sulphur to the original magma. The occurrence of significant sulphide mineralization associated with the Platreef in this area is, therefore, entirely consistent with the experimental predictions.

It also follows that a magma close to saturation could become saturated on the introduction of additional silica into the system. Although the Platreef in the Turfspruit area was not contaminated by banded ironstone, there is evidence that silica was introduced into the magma in association with argillaceous sediments that contained organic material. Dolomite xenoliths and the presence of anhydrite in the footwall suggest that sedimentary-derived sulphur was also introduced into the magma in this area. The association of sulphide mineralization in the Platreef of the Turfspruit area is again consistent with experimental predictions.

Acknowledgement

The authors would like to thank the management of Johannesburg Consolidated Investment Co. for permission to publish this paper and for the provision of access to borehole material. They would also like to thank the Director, British Geological Survey (NERC), for permission to publish the results of the isotope work. The assistance of Miss J. Hurdley and R. Curtis in preparing and analysing heavy mineral concentrates is also much appreciated. The first author is indebted to J. W. J. Davenport, J. A. White and Dr. M. J. Viljoen of JCI for invaluable discussions and assistance in the field. They are both grateful to Dr. D. J. Vaughan for his many helpful comments.

References

1. Buchanan D. L. *et al.* The genesis of sulfide mineralization in a portion of the Potgietersrus limb of the Bushveld Complex. *Econ. Geol.*, **76,** 1981, 568–79.
2. Wagner P. A. *The platinum deposits and mines of South Africa* (Edinburgh: Oliver and Boyd, 1929), 326 p.
3. Baur M. E. Diversity in Precambrian microbial communities. *J. geol. Soc. Lond.*, **140,** 1983, 5–12.
4. Wedepohl K. H. ed. *Handbook of geochemistry, volume II, part I* (Berlin, etc.: Springer, 1969), 586 p.
5. Friedman I. and O'Neil J. R. Compilation of stable isotope fractionation factors of geochemical interest. *Prof. Pap. U.S. geol. Surv.* 440KK, 1977, 12 p.
6. Fincham C. J. B. and Richardson F. D. The behaviour of sulphur in silicate and aluminate melts. *Proc. R. Soc.*, **A223,** 1954, 40–62.
7. Schoell M. and Wellmer F. W. Anomalous ^{13}C depletion in early Precambrian graphites from Superior Province, Canada. *Nature, Lond.*, **290,** 1981, 696–9.
8. Buchanan D. L. and Nolan J. Solubility of sulfur and sulfide immiscibility in synthetic tholeiitic melts and their relevance to Bushveld-Complex rocks. *Can. Mineralogist,* **17,** 1979, 483–94.
9. Naldrett A. J. Nickel sulfide deposits: classification, composition and genesis. *Econ. Geol. 75th anniversary vol.*, 1981, 628–85.

Geology and mineralization at Trojan nickel mine, Zimbabwe

L. R. Chimimba B.Sc.
Trojan Nickel Mine, Ltd., Bindura, Zimbabwe

Synopsis

The Trojan nickel deposit occurs within a pile of ultramafic lavas subjected to a lower amphibolite grade of metamorphism. The lavas form part of the Upper Greenstones (Bulawayan Group) of the Mazoe greenstone belt.

The nickel mineralization occurs as disseminated, massive and near-massive sulphides. The massive and near-massive ore occurs along the basal contact of the serpentinite units and is overlain by the more abundant disseminated ore, which occurs within the serpentinite. The main sulphide minerals are pyrrhotite, pentlandite and chalcopyrite. Minor amounts of millerite and pyrite are present. The Ni : Cu ratio in all three types of ore averages 15 : 1.

The intercumulus nature of sulphides in the near-massive ore and similar textures occasionally seen in the disseminated ore indicates a magmatic origin of the mineralization. The basal position of the near-massive and massive ore suggests that the sulphides settled out under gravity during the emplacement and crystallization of a peridotitic magma. The deposit has been deformed and some of the primary massive ore has been remobilized into veins and breccias. The disseminated mineralization now occurs mainly as blebs of sulphides intergrown with silicate minerals or as stringers of sulphides between foliation planes in the serpentinite.

The Trojan nickel deposit is situated in the southern part of the Mazoe greenstone belt 90 km north of Harare (formerly Salisbury) (Fig. 1). It lies within the Upper Greenstones of the Bulawayan Group. Trojan is one of five operating nickel mines in Zimbabwe: three (Trojan, Shangani and Epoch) are situated within the same ultramafic lava sequence[1] and two (Empress and Madziwa) are associated with mafic intrusions.

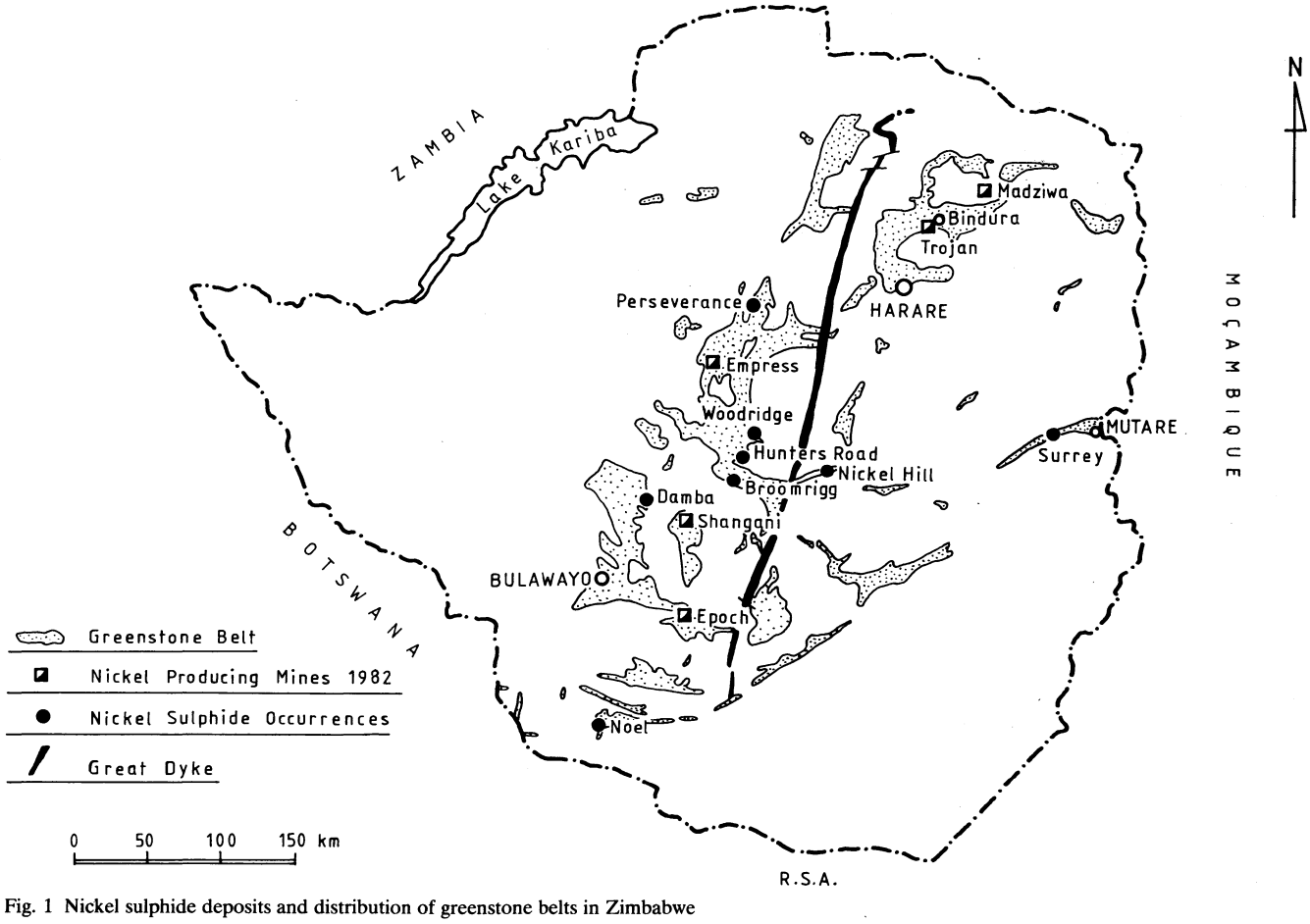

Fig. 1 Nickel sulphide deposits and distribution of greenstone belts in Zimbabwe

The first indication of nickel in the area, in the form of nickel staining in serpentinites in a road-cutting, was found in 1956. Following this discovery a local prospector intersected one of the large orebodies in an adit. Follow-up soil geochemical sampling and drilling by Anglo American Corporation proved the viability of the deposit and the first concentrates were sent to the smelter, situated within the mine complex, in 1968. Current production is 82 000 t/month and ore reserves of 13 000 000 t at an average grade of 0.67% Ni give a mine life of approximately 12 years.

Geological work at the mine in its early days was of a routine nature and it was not until 1979 that a detailed study of the underground and surface mapping was undertaken. This paper presents the preliminary findings of this mapping.

Geological setting of Trojan nickel deposit

The base of the greenstone sequence of the Mazoe greenstone belt, which is locally intruded by granites of the composite Chindamora batholith, is known as the Iron Mask formation.

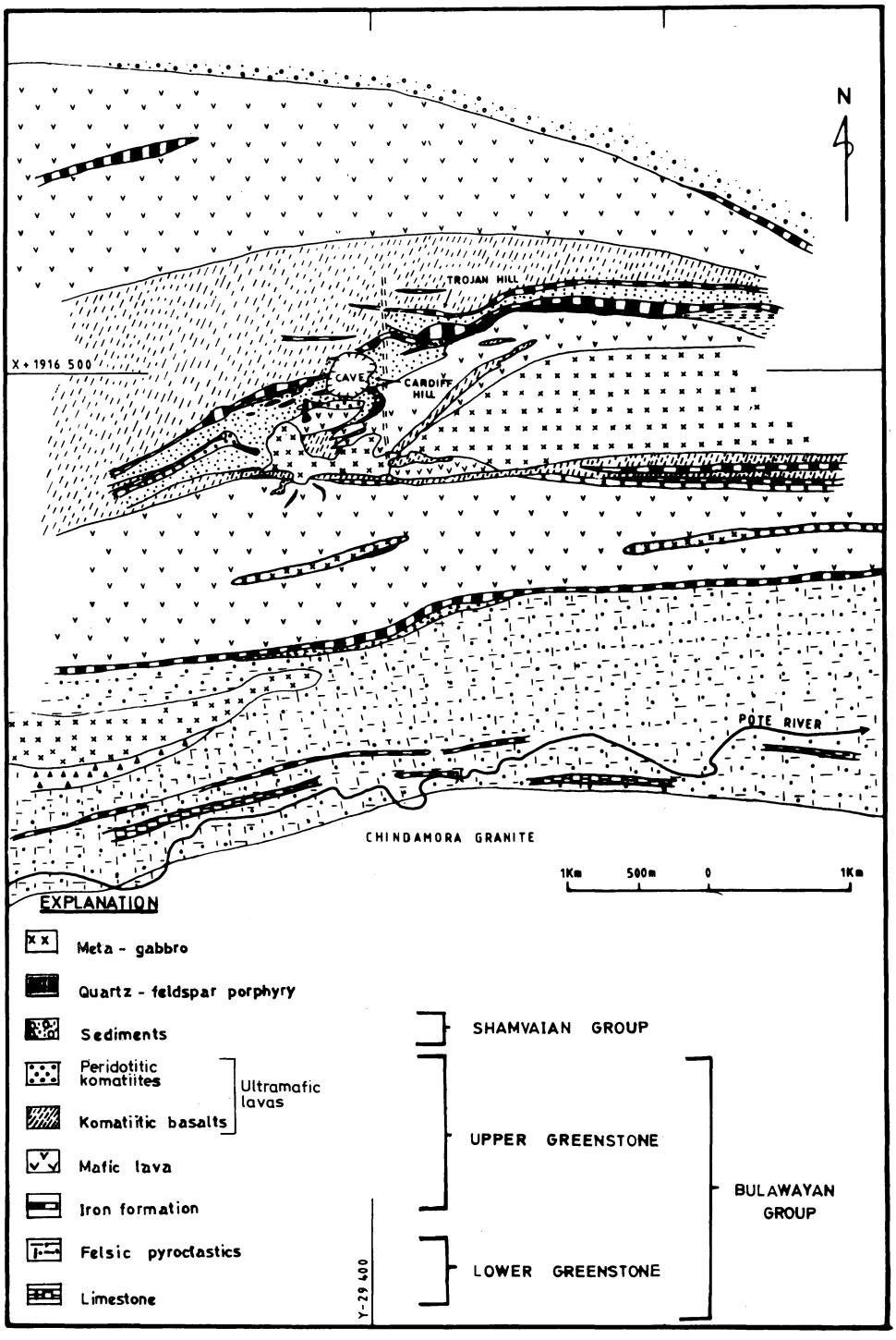

Fig. 2 Plan showing geological setting of Trojan nickel deposit

This formation probably forms part of the Lower Greenstones.[2] The rocks are essentially felsic pyroclastics with minor intercalations of banded iron formation (Fig. 2). They are disconformably overlain by a bimodal pile of ultramafic and mafic lavas within which the Trojan orebodies are situated. Intercalated with these lavas are very minor bands of felsic lava and banded iron formation. This sequence is considered to be part of the Upper Greenstones of the Bulawayan Group.[1,2] The whole succession has been intruded by gabbroic rocks, a quartz-feldspar porphyry and dolerite dykes. Sedimentary rocks of the Shamvaian Group lie unconformably above the ultramafic–mafic pile.

The strike of rocks of the Mazoe greenstone belt follows the outline of the Chindamora granite, and in the area under discussion the rocks strike east–west and dip steeply north. Evidence from the mine suggests that the rocks are folded and that the lithological sequence exposed is probably a result of the folding and not the true stratigraphy. The rocks have been subjected to a lower amphibolite grade of metamorphism.

The following more detailed descriptions relate only to the Upper Greenstones of the Bulawayan Group.

Mafic lavas

Fine-grained mafic rocks are abundant in the south and to the north of the mine (Fig. 2). In the extreme south these rocks disconformably overlie rocks of the Iron Mask formation. Further north from this contact the rocks are interlayered with ultramafic horizons. The rocks are moderately foliated and in places pillowed, the pillows showing a younging direction to the north. The fine grain size and presence of pillows suggest that the rocks are lavas. These rocks are composed of green hornblende, plagioclase (An_{35}–An_{55}), quartz and biotite. They are veined by quartz–calcite assemblages.

Ultramafic lavas

The ultramafic rocks at Trojan are subdivided into two types: one consists principally of tremolite, talc and chlorite, whereas the other, which hosts the orebodies, contains serpentine (antigorite), talc and olivine with minor chlorite and tremolite.

To the south of the mine the tremolite-rich rocks are interlayered with the mafic flows and to the north they overlie and in part are intercalated with the serpentine-rich rocks that host the nickel mineralization.

The tremolitic ultramafites occur in two forms—one strongly cleaved and pale grey and the other undeformed and dark grey. The latter often has relict spinifex texture suggestive of flows and in some areas these cleaved and massive tremolitic assemblages are interlayered as apparent cyclic units some 20–30 m thick. The cleaved portions are the more ultramafic, basal portions of flows, but lack of complete exposure makes the determination of the younging direction impossible. The relict pyroxene spinifex is now pseudomorphed by amphibole and is recognizable in thin section by the characteristic ladder texture and 'hollow' interior of the amphibole needles. Geochemical data (Fig. 3) suggest that these rocks are komatiitic basalts.[3]

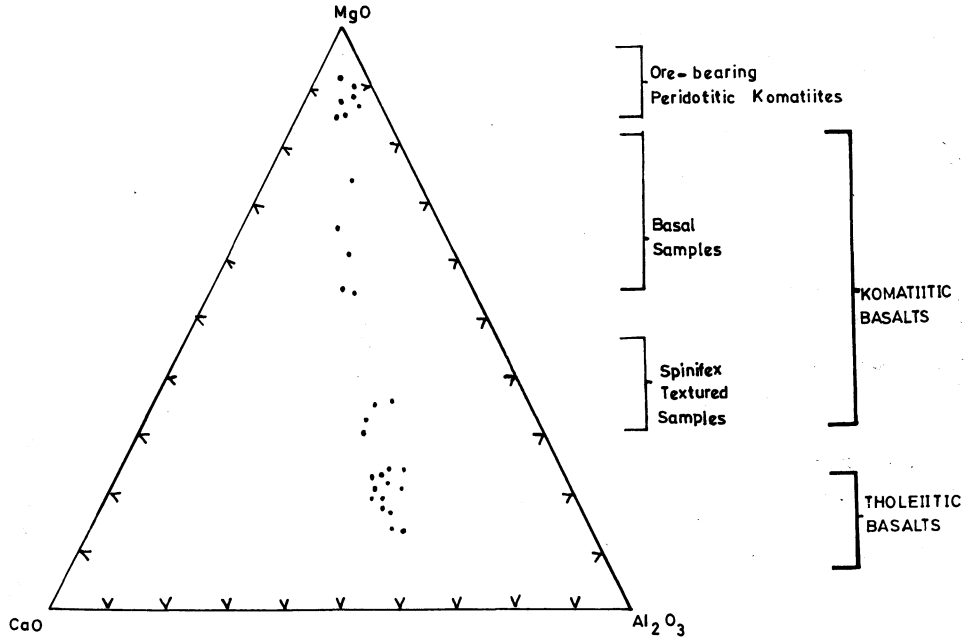

Fig. 3 MgO–CaO–Al_2O_3 plot of compositions of mafic and ultramafic rocks at Trojan mine

Serpentinites are developed at Cardiff Hill (Fig. 2), where the mine is located, and extend westwards for approximately 2 km. They are also developed at Trojan Hill, which lies to the northeast of Cardiff Hill, and extend eastwards from this hill for about 3 km. The intercalation of banded iron formation and, in places, of spinifex-textured komatiitic basalts with the serpentinites suggests that these serpentinites are probably extrusive rocks.

The serpentinites are mostly massive and only exhibit a strong foliation along the margins of the bodies where tremolite and chlorite become conspicuous. They consist of antigorite, talc, magnesite and olivine in varying proportions with accessory tremolite and chlorite. The olivine, now largely pseudomorphed by talc and antigorite, occurs as very coarse equidimensional to elongate crystals. The elongate crystals commonly lie with long axes parallel to regional strike and produce a texture that resembles banding. The coarse, dark equidimensional olivine is sparsely disseminated throughout a pale, talcose matrix and forms a colourful rock with a 'spotted dog' texture. Crystals of both the elongate and granular olivine contain inclusions, mainly of magnetite and tremolite, and because of this, their lack of the brown colour and pleochroism typical of magmatic olivine and their coarse grains, which are atypical of lavas, these olivine crystals are considered to be of metamorphic origin. Geochemically (Fig. 3) the serpentinites are peridotitic komatiites.

Felsic and intermediate rocks

In the Upper Greenstones around Trojan mine felsic and intermediate rocks have only limited distribution. A tuff horizon 30–40 m thick occurs at Trojan and Cardiff Hills (Fig. 2) associated with an iron formation and separates the sequence of interlayered mafic lavas and komatiitic basalts to the south from the ore-bearing peridotitic komatiites. Minor tuff beds are also developed elsewhere.

The tuffs are pale grey to grey and strongly cleaved. The intermediate variety is composed of actinolite, biotite, chlorite and quartz. Dark lenticular pods (1–2 mm), composed mainly of cryptocrystalline quartz and biotite with long axes parallel to the foliation, are regarded as lapilli. Felsic tuffs are composed of fine-grained sutured quartz, feldspar, sericite and cordierite.

A thin unit of felsic lava 40–50 m thick, situated to the east of Trojan Hill (Fig. 2), is on the same stratigraphic horizon as the tuffs. This rock consists of quartz, feldspar and biotite and is often porphyritic.

Iron formations

The iron formations in sequences around Trojan consist largely of thin layers of dark banded chert (2–15 m) and occur intercalated with the ultramafic, mafic and felsic rocks. Minor pyrrhotite and pyrite are interbedded with the cherts. Actinolite, plagioclase and biotite assemblages are commonly present and often form distinct bands of tuffaceous character within the iron formations.

Intrusive rocks

The volcanic rocks of the Upper Greenstones are intruded by dolerite, gabbroic rocks and a quartz-feldspar porphyry. The quartz-feldspar porphyry is situated immediately to the south of the ore-bearing serpentinites at Trojan and Cardiff Hills (Fig. 2), where it is associated with the felsic tuffs and an iron formation that it in part intrudes.

Minor occurrences of the porphyry are also found about 800 m west of Cardiff Hill associated with a tuff horizon between two serpentinite units (Fig. 2). The porphyry is a grey, medium-

to coarse-grained rock with a well-developed mineral lineation pitching west at shallow angles. The rocks are composed of green hornblende, cummingtonite, plagioclase (An_{25}–An_{50}), almandine, quartz and minor biotite. Quartz and plagioclase are present as phenocrysts and the amphiboles and garnet as porphyroblasts. The plagioclase phenocrysts are commonly strongly sericitized.

Coarse-grained amphibolites (meta-gabbro) situated to the south and southwest of the mine (Fig. 2) transgress the mafic lavas and komatiitic basalts. The rocks are massive and porphyritic and are composed of green hornblende, chlorite, plagioclase and quartz. Higher up in the sequence similar and possibly related coarse amphibolites composed essentially of actinolite with minor quartz and feldspar occur as sills intrusive into the ore-bearing serpentinites to the west of Cardiff Hill (Fig. 2).

A north–south-striking dolerite dyke cuts across the whole lava sequence and also intrudes the meta-gabbro.

Mine geology

Mine sequence

Underground exposures show the same rock sequence as that found on surface (Fig. 4). Pillowed mafic lavas situated to the south of the mine are separated from the overlying serpentinites by a 5-m thick iron formation. Thinner iron formations, which peter out towards the east, are interlayered with the serpentinites higher up in the sequence. Komatiitic basalts are confined to the northwest portion of the mine, where relict pyroxene spinifex is developed. The meta-gabbro, quartz-feldspar porphyry and dolerite found on surface are also present in the mine.

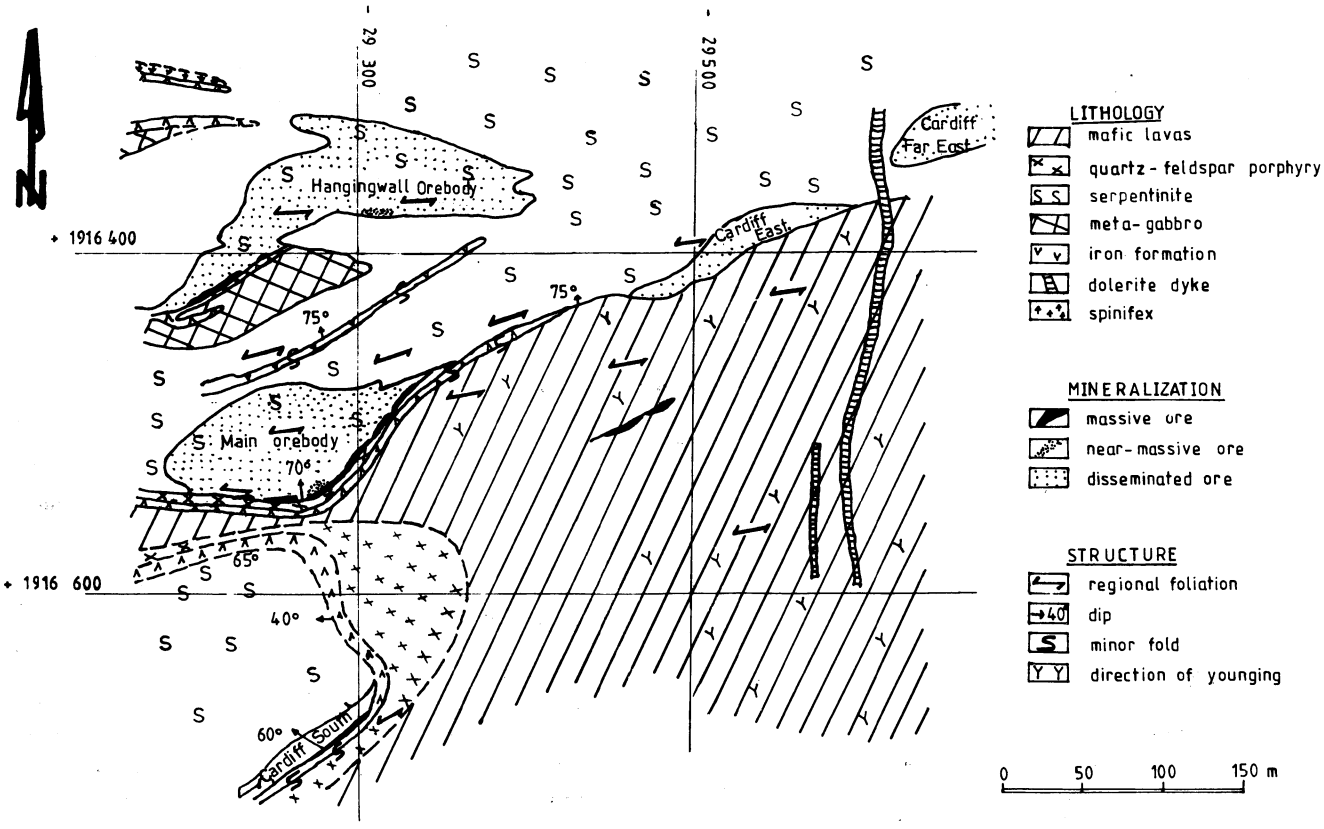

Fig. 4 Plan of 7 level showing distribution of orebodies

Structure

Two cleavages have been recorded in rocks at Trojan. An earlier penetrative fabric strikes approximately east–west and dips 75° north, and a later spaced cleavage has two principal strike directions, 110° and 070°, but with a dip of 65° north (Fig. 5). The two cleavages are best developed in the tremolite–talc–chlorite-rich rocks and in tuffs. In the massive rock types, such as mafic lavas, mata-gabbro, serpentinites and felsic lavas, the two cleavages cannot be distinguished because of their similar orientations and only a regional foliation trending subparallel to lithological contacts is present. In certain localities the spaced cleavage is developed in the banded iron formation.

In the quartz-feldspar porphyry a strong mineral lineation lies within the northerly dipping cleavage and pitches to the west at low angles.

Minor folds with contrasting orientations have been recorded in the iron formations and the quartz-feldspar porphyry sill. Axes of both folds lie within the northerly dipping cleavage, the earlier set pitching gently to the east and the later set pitching at intermediate angles to the west (Fig. 5). The dominant penetrative cleavage is considered to be axial planar to the early set of folds ($F1$) and this cleavage has subsequently been folded by the westerly plunging later set of folds ($F2$). The younger spaced cleavage, which cuts across the folded penetrative cleavage, is considered to be axial planar to the $F2$ folds. In the southwestern portion of the mine a synclinal fold plunges westwards at approximately 40° (Fig. 4). The similar orientation of this fold with the $F2$ minor folds suggests that both folds are probably of the same deformation, but the relationship between this synclinal fold and the folding in the whole area is equivocal and this problem has yet to be solved. It is considered that the folding (both $F1$ and $F2$) has caused some repetition of the stratigraphy.

The quartz-feldspar porphyry sill at the base of the serpentinite sequence has been strongly deformed in addition to the minor folding (Fig. 6). The quartz-feldspar porphyry now occurs as a series of rounded slices projecting into the overlying serpentinite. Exposures along the footwall of one of these slices

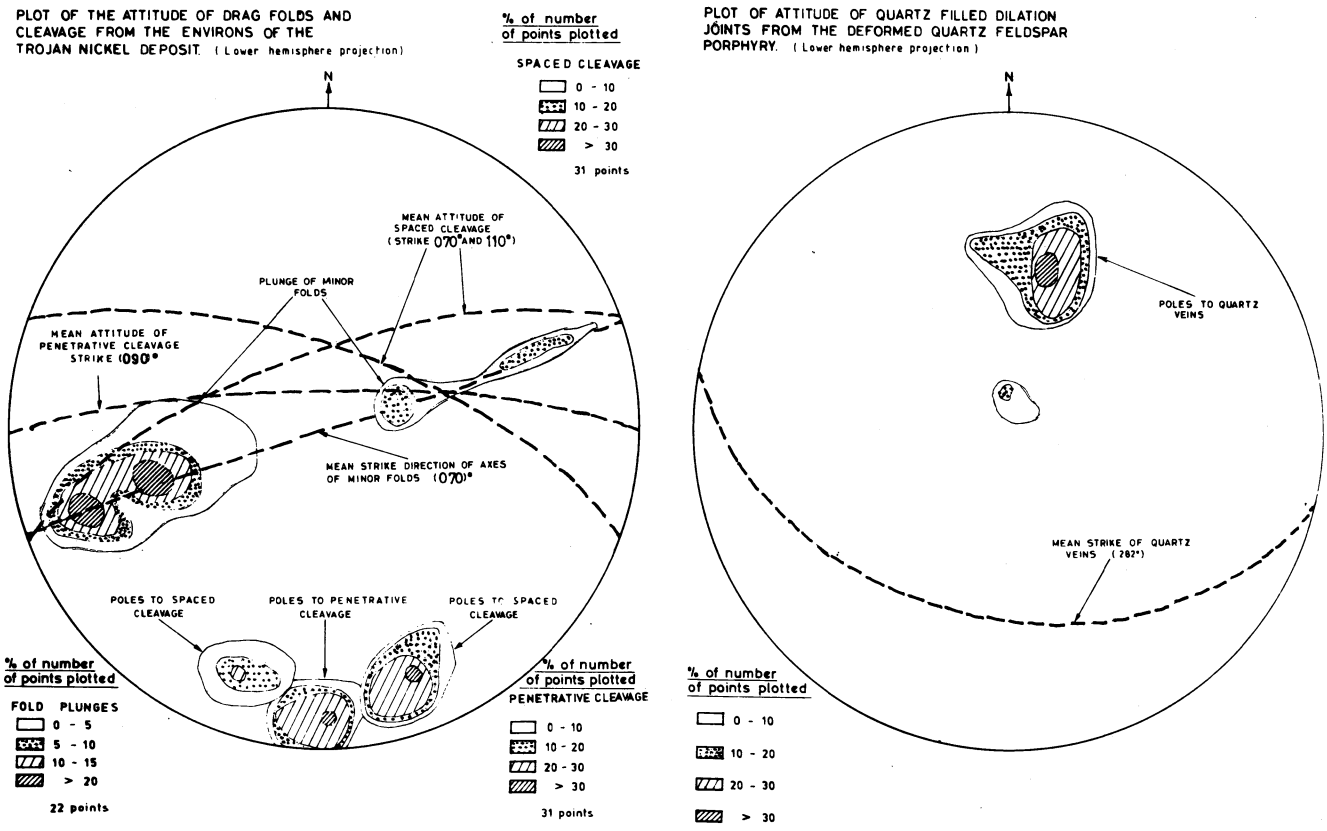

Fig. 5 Stereographic projections showing orientation of minor structures at Trojan

shows that the underlying iron formation has been deformed together with the porphyry and that the deformation occurred along a well-defined discontinuity in the iron formation (Fig. 6). Several of these discontinuities in the iron formation appear to have been active as sinistral faults, which resulted in a series of slices of the porphyry being thrust into the overlying less competent serpentinite as solid intrusions. The stress pattern that gave rise to these tear faults is not readily reconcilable with the broadly north–south stress associated with the *F*1 and *F*2 folding.

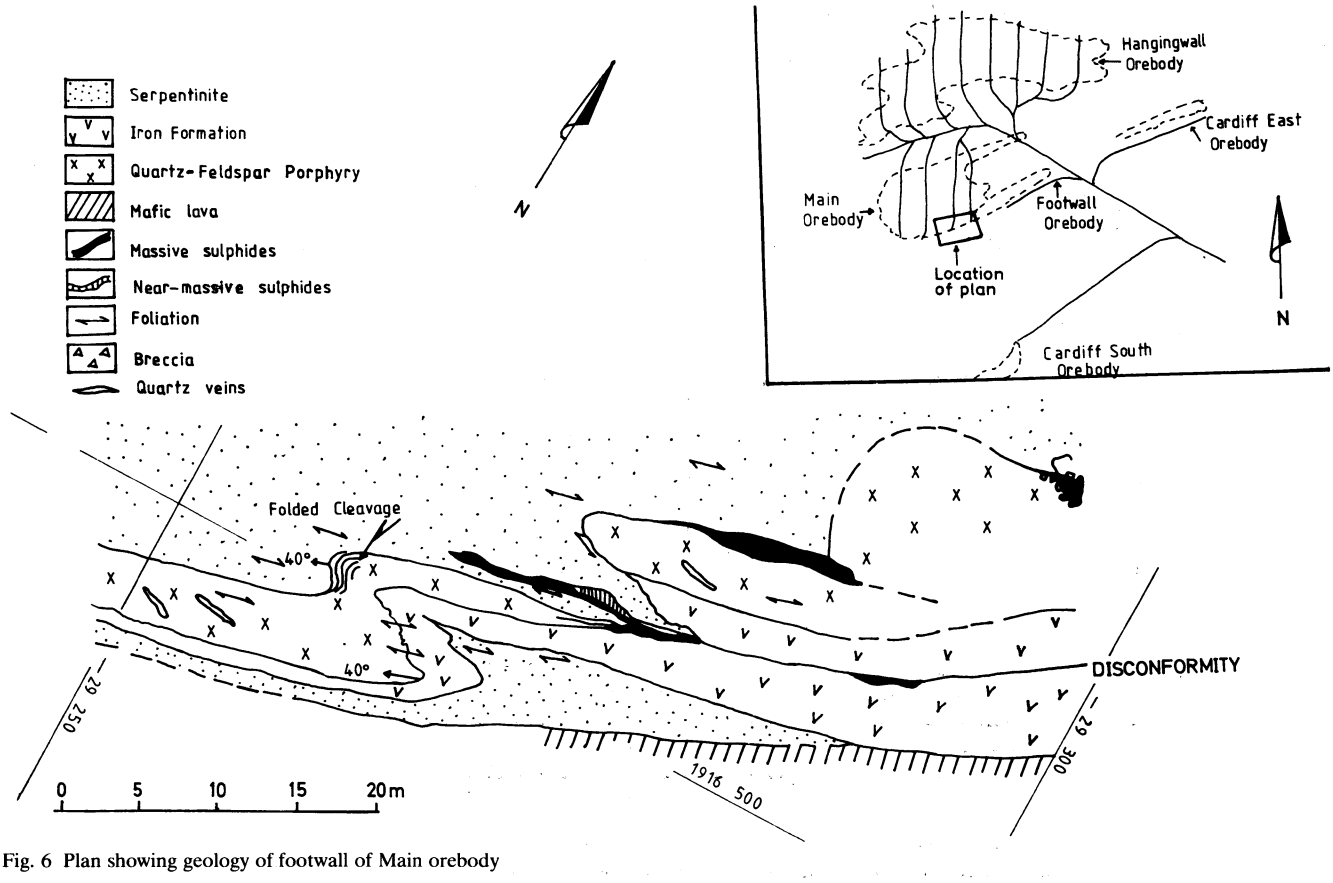

Fig. 6 Plan showing geology of footwall of Main orebody

Numerous dilatation quartz veins occur in the deformed quartz-feldspar porphyry and occasionally in the underlying mafic lavas. The fractures strike at 282° and dip at intermediate angles to the south (Fig. 5). Consideration of the stress pattern suggests that these joints were formed during the thrust slicing. It is likely, therefore, that the dilatation quartz veins and the faults were formed during the same brittle deformation episode, which probably post-dates the two phases of folding.

Metamorphism

Mineral assemblages in the ultramafic, mafic and felsic rocks together define the peak-metamorphic grade at Trojan as lower amphibolite facies. The assemblage in the mafic lavas of green hornblende and plagioclase (An_{35}–An_{55}) suggests a temperature of at least 500°C.[4] The assemblage in the quartz-feldspar porphyry of green hornblende, cummingtonite, plagioclase (An_{25}–An_{50}) and almandine garnet and the presence of cordierite in the felsic tuffs suggest a temperature again of at least 500°C and a possible pressure of 3–4 kbar.[4]

The coexisting assemblages in the ultramafic rocks are tremolite–chlorite–talc, antigorite–talc–chlorite, talc–magnesite–chlorite and metamorphic olivine–antigorite–talc–chlorite. The metamorphic olivine crystals have been extensively altered to antigorite by retrogressive metamorphism and only the cores of the coarse crystals remain fresh. In serpentinites the metamorphic reaction involving the disappearance of brucite and incoming of forsterite occurs at about 450°C.[4] The assemblage forsterite–talc becomes stable at about 600°C. The meta-

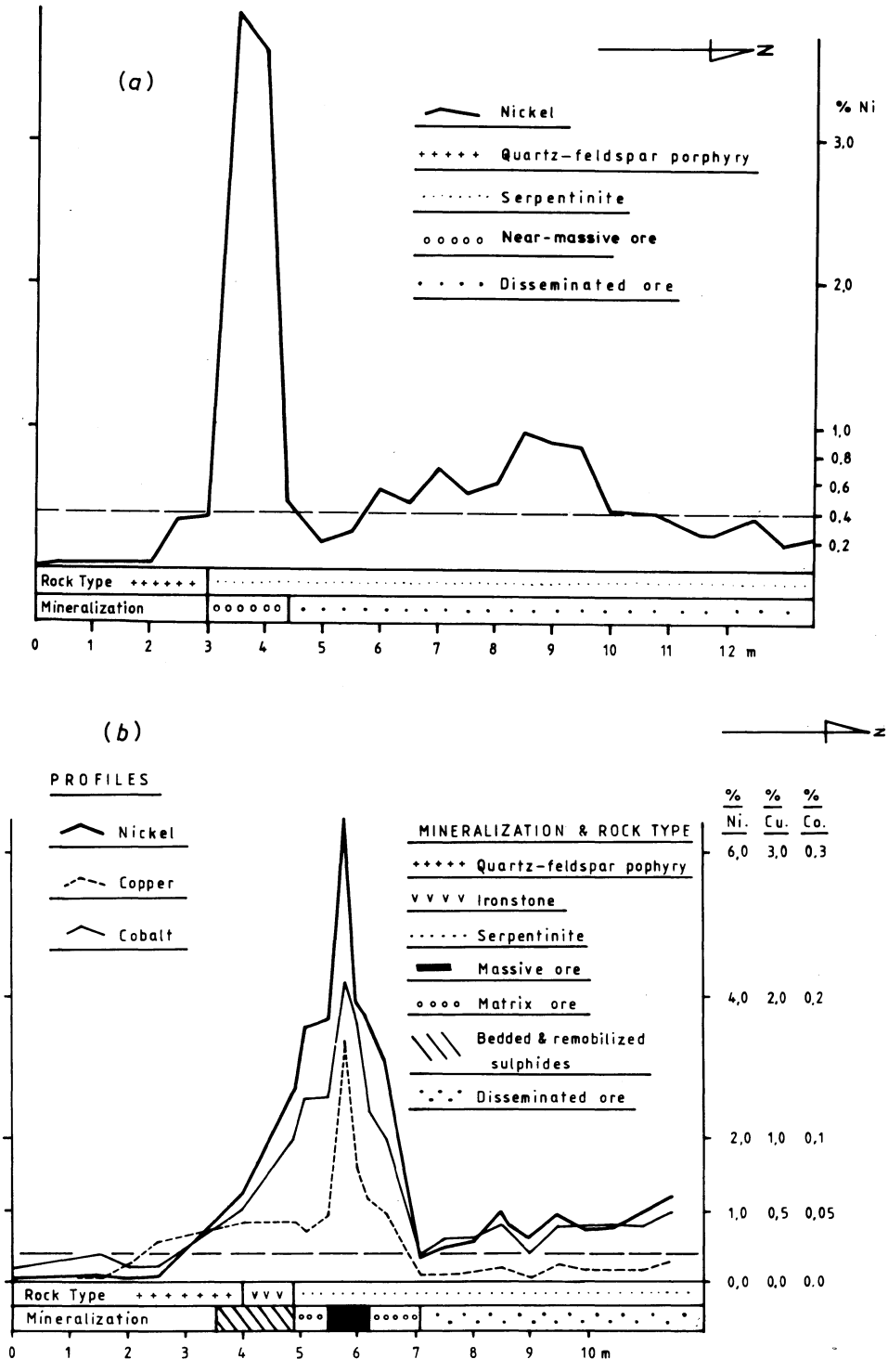

Fig. 7 Nickel profile along drill-hole through Main orebody (drill-hole 11.0.32) (*a*) and nickel, copper and cobalt profiles along drill-hole through footwall of Main orebody (drill-hole 13.0.6) (*b*)

morphic assemblages in rocks at Trojan, therefore, define a peak metamorphism under P–T conditions of 500–600°C and 3–4 kbar.

Mineralization

Three types of nickel sulphide ore are found at Trojan—massive ore, near-massive (matrix) ore and disseminated ore. The massive and near-massive ore are situated towards the base of the ultramafic units and are overlain by the disseminated ore. The two major orebodies (defined by the 0.4% total nickel cutoff)—the Main and Hangingwall—(Fig. 4), hosted by thick (60 m) serpentinite units, contain all three types of mineralization (see Figs. 7 and 8). The massive and near-massive ores occupy a narrow and discontinuous zone along the footwall of both orebodies, the remaining part of these orebodies being occupied by disseminated ore. These two orebodies are separated by a wedge-shaped unmineralized serpentinite (average 0.20% Ni). In the east a narrow (10–15 m) zone of disseminated sulphides is situated close to the contact with the mafic lavas and in the same serpentinite unit as the Main orebody, with which it merges on certain levels. This ore zone constitutes the Cardiff East orebody. The Cardiff Far East orebody, also of disseminated sulphides, lies further away from the contact with the mafic lavas and is regarded as an extension of the Hangingwall orebody. On the southern limb of the synclinal fold in the southwest part of the mine is the Cardiff South orebody, which has a narrow zone of massive ore along the footwall that is overlain by a thicker zone of disseminated nickel sulphide.

Ore types

Massive ore at Trojan occurs as a layer of sulphides up to 1 m thick along the basal contact between the mineralized serpentinite and the underlying iron formation or quartz-feldspar porphyry. It also forms a cement in the brecciated margins of the porphyry, and veins in joints in the mafic lavas immediately below the ultramafic sequence. The sulphide veins in the mafic lavas are narrow (10–30 cm) and uneconomic. The massive sulphide layers between the quartz-feldspar porphyry and the mineralized serpentinite are restricted to the troughs between adjacent slices of the sill, which were formed during the tear faulting (Fig. 6).

The massive sulphide layers often show mineral segregation. Thin bands (1 cm) or coarse rounded aggregates (1–2 cm) of pentlandite often occur within massive pyrrhotite. The pentlandite bands are broadly parallel to the strike of lithological contacts and regional foliation. The massive ore commonly con-

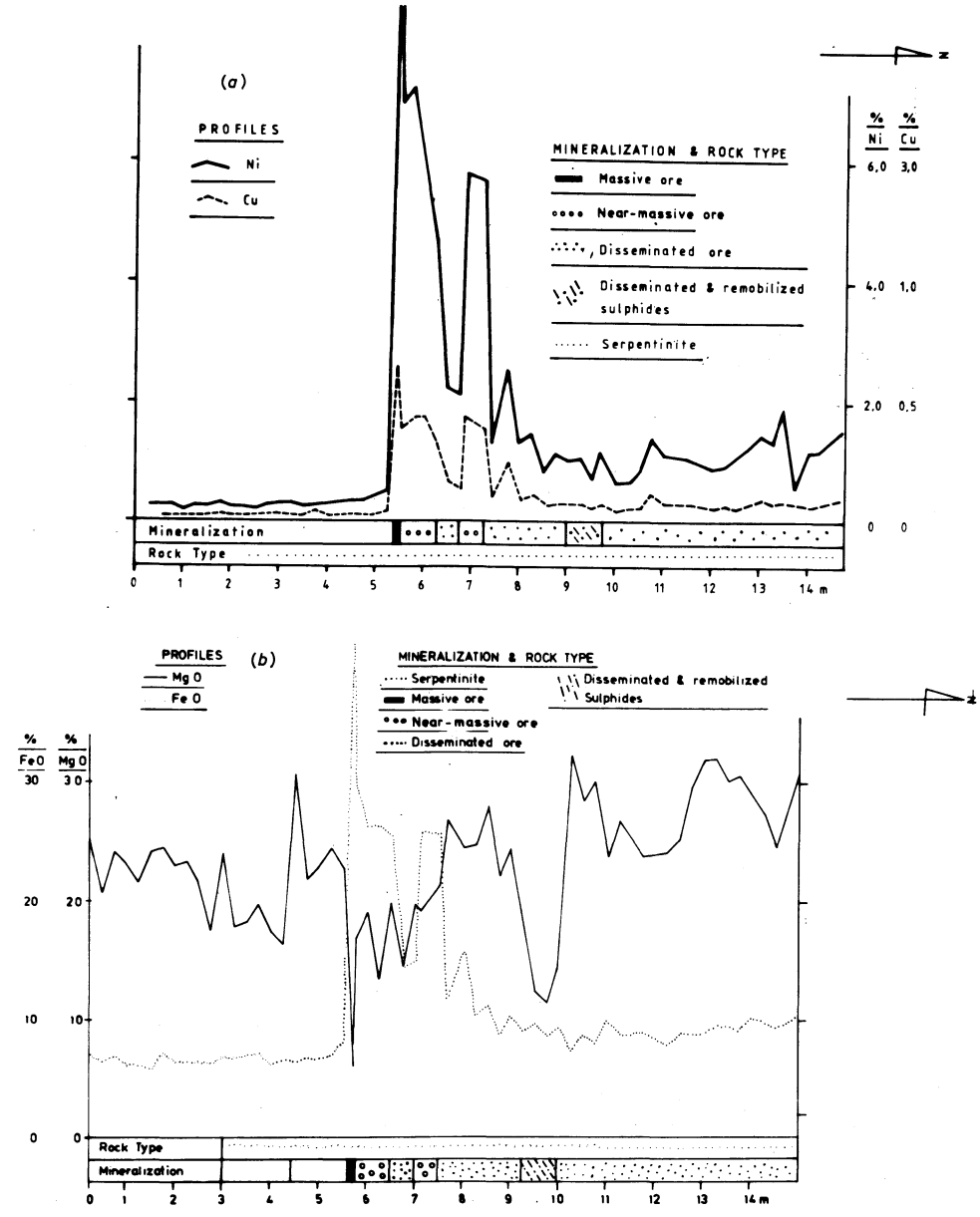

Fig. 8 Nickel and copper profiles (*a*) along drill-hole through footwall of Hangingwall orebody (drill-hole 13.3.6) and (*b*) MgO and FeO profiles along drill-hole shown in (*a*)

tains inclusions of contorted amphibolite or quartz stringers lying parallel to the massive layers.

The massive ore generally occurs as a coarse mosaic of pyrrhotite, pentlandite and chalcopyrite with occasional pyrite. Pyrrhotite is the most abundant sulphide and pentlandite and chalcopyrite are commonly interstitial to the coarse grains of pyrrhotite. The boundaries between the sulphide grains are commonly planar, but the sulphides may show irregular intergrowth and flames of pentlandite occur within the coarse pyrrhotite crystals.

The near-massive (matrix) ore occurs as densely disseminated sulphides (30–50% sulphide) in lenticular serpentinite pods at the base of the mineralized serpentinite units. The ore has a sharp contact against the overlying disseminated ore. Rarely, there is a thin layer of massive ore at the base of the near-massive ore (Figs. 7 and 8). The pods vary in size, but attain maximum dimensions of 30 m long, 30 m wide and 10 m thick.

The sulphides are found as aggregates crudely outlining large (0.5 cm) equidimensional areas of antigorite or talc, which probably represent pseudomorphs of original olivine crystals. This texture indicates original coarse olivine with intercumulus sulphides. Metamorphic recrystallization of the silicates and sulphides has, however, resulted in the interfingering of the silicate and sulphide minerals. The sulphide minerals that are present are, in order of abundance, pyrrhotite, pentlandite and chalcopyrite.

Disseminated sulphides form the bulk of the Trojan ore. The sulphides are often found as discrete blebs up to 5 mm across in serpentinite. The blebs are usually composite patches of pyrrhotite, pentlandite and chalcopyrite. Minor amounts of millerite and pyrite and of the arsenides niccolite, cobaltite, maucherite and gersdorffite are also present.

In sheared serpentinite the sulphides often take the form of elongate blebs between the foliation planes. The disseminated sulphides in both the massive and sheared serpentinites are commonly intergrown with fibrous and lamellar silicates (antigorite and talc) to give spiky and lamellar textures.

Geochemistry

Massive ore at Trojan averages 10% Ni and 0.8% Cu. The near-massive and disseminated ores average 4% Ni and 0.65% Ni, respectively. The Ni : Cu ratio for the Trojan ores (15 : 1) is similar to that in other nickel deposits associated with extrusive peridotitic komatiites, such as Nepean (15 : 1), Kambalda (13 : 1), Windarra (10 : 1) and Scotia (12 : 1).[5]

Geochemical profiles through the ore zones intersected by a diamond drill are shown in Figs. 7 and 8. Nickel shows maximum concentration in the massive and near-massive ore and in the disseminated ore decreases away from the footwall. Cobalt and copper correlate well with the nickel distribution.

Invariably, the nickel and copper profiles across the complete sequence of massive, near-massive and disseminated ore at Trojan show a marked low immediately above the near-massive ore zone (Fig. 7). This zone of low nickel is commonly sheared and pale green, as opposed to the grey colour of the rest of the serpentinite. It is composed of tremolite, talc and chlorite and from the MgO profile along a borehole through this zone (Fig. 8 (*b*)) it is thought that it represents a metapyroxenite selvage and that this selvage is situated above a complete, but thin, sequence of massive, near-massive and disseminated ore. Thus, the selvage defines the margin of a thin ultramafic lava flow very rich in sulphides. Normally, the selvage occurs immediately above the near-massive or massive ore, and this feature is considered to be evidence that the sulphide-rich ores were riffled out of a thick moving flow that was completely displaced by another lava flow that gave rise to the selvage zone along its base and to the overlying disseminated ore.

Genesis of Trojan nickel mineralization

The features that characterize the mineralization and regional setting of the Trojan nickel deposit have been recognized in other nickel deposits associated with Archaean komatiitic sequences in Zimbabwe, Canada and Western Australia. In all cases the mineralization is associated with peridotitic bodies that occur as shallow intrusions or lava flows. The mineralization is commonly controlled by syndepositional structures and the massive and near-massive ore occurs towards the base of the ultramafic bodies, the disseminated mineralization decreasing upwards.

In the near-massive ore at Trojan the sulphides form a matrix partly or completely surrounding pseudomorphs of olivine. This feature suggests that the sulphides form part of the intercumulus phase that surrounded cumulus olivine crystals and that the mineralization is of magmatic origin. The sulphide blebs in the disseminated ore, which in places also partly enclose silicate crystals, are considered as evidence of immiscible sulphide caught up in the main mass of the peridotitic magma during crystallization.

The basal position of the near-massive ore and possibly of the massive ore in the serpentinites provides evidence for the magmatic segregation of the sulphides under gravity during the emplacement and crystallization of the peridotitic body. A notable feature at Trojan is, however, the close association of most of the massive ore with a competent lithology, such as an iron formation or quartz-feldspar porphyry on the footwall contact of the mineralized serpentinite. Very little massive ore is present where mineralized serpentinite immediately overlies unmineralized serpentinite. This feature suggests that the massive sulphide has been remobilized and is structurally controlled. The remobilized massive ore could have been derived from original magmatic massive sulphide or from the near-massive and disseminated ore.

Further evidence for the remobilization of the massive ore at Trojan is the occurrence of this type of ore in low-pressure troughs within the deformed quartz-feldspar porphyry intrusive (Fig. 6), in joints in the mafic lavas and as a cement in brecciated quartz-feldspar porphyry. A tentative explanation for the occurrence of the massive ore in breccias is that the quartz-feldspar porphyry magma melted sulphides as it was forcibly injected at the base of the mineralized serpentinite. On cooling and crystallization the porphyry developed contraction cracks along its margins into which the molten sulphide was injected, giving rise to the breccia-type structure.

Evidence of remobilization of sulphides in the disseminated ore occurs as sulphide blebs elongated parallel to and situated along foliation planes in sheared serpentinite and as the spiky or lamellar intergrowths between the sulphides and metamorphic silicate assemblages in the serpentinite. The latter textures indicate simultaneous recrystallization[6] of the silicates and sulphide minerals. The origin of the banding or layering in the massive ore at Trojan is unclear. Similar mineral segregation has been recorded at Shangani,[6] where the banding is regarded as evidence for magmatic segregation. Barrett and co-workers[5] described bands of pyrrhotite and pentlandite in massive ore at the Nepean nickel deposit in Australia, which they suggested to be of tectonic origin. Studies of fabrics in the massive ore at Trojan have not been done, but since the banding has been recorded in ores that are clearly remobilized it is likely that the structure is of tectonic origin. Whatever mechanism is proposed for the mineral banding, it should take into account the origin of the rounded aggregates or spots of massive pentlandite found in the massive ore.

Clearly, deformation and metamorphism have had a profound effect on the nickel mineralization at Trojan. There are, however, features within the deposit that can only be explained by a primary magmatic origin for the deposit. The features that

are compatible with a magmatic origin for the ore are the intercumulus nature of the sulphides in the near-massive ore, the basal position of the near-massive ore and the ordered sequence of massive, near-massive and disseminated ore upwards from the footwall of the mineralized serpentinite unit, the decrease in nickel content from the footwall to the hanging-wall of the disseminated ore, and the high Ni/Cu ratio, similar to that of other deposits in Archaean komatiitic sequences.

Acknowledgement
This paper has benefited from discussions with J. M. Clutten, Chief Divisional Geologist, AACS, and A. Martin, Department of Geology, University of Zimbabwe. The paper is published with the kind permission of the management of the Bindura Nickel Corporation and Anglo American Corporation Services, Ltd., Zimbabwe.

References

1. Clutten J. M. Foster R. P. and Martin A. Nickel mineralization in Zimbabwe. *Episodes*, no. 2 1981, 10–15.
2. Wilson J. F. A preliminary reappraisal of the Rhodesian Basement Complex. In *A symposium on mineral deposits and the transportation and deposition of metals* Anhaeusser C. R. Foster R. P. and Stratten T. eds. *Spec. Publ. geol. Soc. S. Afr.* no. 5, 1979, 1–23.
3. Arndt N. T. Naldrett A. J. and Pyke D. R. Komatiitic and iron-rich tholeiitic lavas of Munro Township, Northeast Ontario. *J. Petrol.*, **18,** 1977, 319–69.
4. Winkler H. G. F. *Petrogenesis of metamorphic rocks* (New York, etc.: Springer, 1976), 334 p.
5. Barrett F. M. Groves D. I. and Binns R. A. Importance of metamorphic processes at the Nepean nickel deposit, Western Australia. *Trans. Instn Min. Metall. (Sect. B: Appl. earth sci.)*, **85**, 1976, B252–73.
6. Viljoen M. J. and Bernasconi A. The geochemistry, regional setting and genesis of the Shangani–Damba nickel deposits, Rhodesia. Reference 2, 67–98.

Name index

Subject index